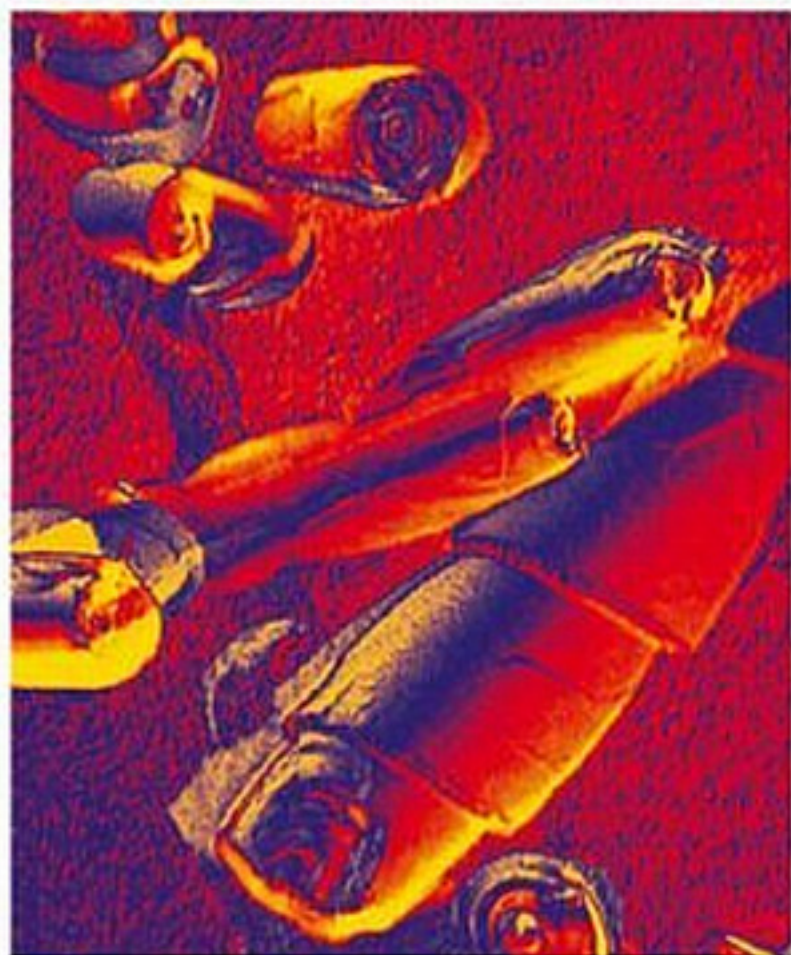


Edited by Challa Kumar

WILEY-VCH

Biological and Pharmaceutical Nanomaterials



nls 

Contents

	Preface	<i>XIV</i>
	List of Contributors	<i>XVII</i>
I	DNA-based Nanomaterials	1
1	Self-assembled DNA Nanotubes	3
	<i>Thom LaBean and Sung Ha Park</i>	
1.1	Introduction	3
1.2	DNA Nanotubes Self-assembled from DX Tiles	4
1.3	3DAE-E DX Tile Nanotubes	5
1.4	DAE-O DX Tile Nanotubes	9
1.5	TX Tile Nanotubes	11
1.6	4 × 4 Tile Nanotubes	14
1.7	6HB Tile Nanotubes	16
1.8	Applications	18
1.9	Summary and Perspectives	19
	References	20
2	Nucleic Acid Nanoparticles	23
	<i>Guy Zuber, Bénédicte Pons and Andrew W. Fraley</i>	
2.1	Introduction	23
2.2	The Chemical and Physical Properties of Therapeutic DNA	25
2.3	Preparation of Nucleic Acid Nanoparticles: Synthesis and Characterization	27
2.3.1	Rationale	27
2.3.2	Synthesis, Characterization and Optimization of Surfactants	31
2.3.3	Organization of the Surfactant–DNA Complexes	35
2.3.4	Quantification of the Stability of Surfactant–DNA Complexes	35
2.4	DNA Functionalization for Cell Recognition and Internalization	37
2.4.1	Strategies for Functionalization	37
2.4.2	Intercalation	38
2.4.3	Triple Helix Formation with Oligodeoxyribonucleotides	39

2.4.4	Peptide Nucleic Acids (PNAs)	41
2.4.5	Interactions of DNA with Fusion Proteins	42
2.4.6	Agents that Bind to the Minor Groove	43
2.5	DNA Nanoparticles: Sophistication for Cell Recognition and Internalization	43
2.5.1	Preparation of DNA Nanoparticles Enveloped with a Protective Coat and Cell Internalization Elements	43
2.5.2	Biomedical Application: Cell Targeting and Internalization Properties of Folate–PEG-coated Nanoparticles	46
2.6	Concluding Remarks	46
	References	47
3	Lipoplexes	51
	<i>Sarah Weisman</i>	
3.1	Introduction	51
3.2	DNA Lipoplexes	51
3.2.1	Composition	51
3.2.2	Nanostructure and Microstructure	52
3.2.2.1	Equilibrium Morphology	52
3.2.2.2	Nonequilibrium Morphology	55
3.2.2.3	Lipoplex Size	57
3.2.3	Lipofection Efficiency	57
3.2.3.1	<i>In Vitro</i>	57
3.2.3.2	<i>In Vivo</i>	59
3.3	ODN Lipoplexes	60
3.4	siRNA Lipoplexes	62
	Acknowledgments	62
	References	62
4	DNA–Chitosan Nanoparticles for Gene Therapy: Current Knowledge and Future Trends	68
	<i>Julio C. Fernandes, Marcio José Tiera and Françoise M. Winnik</i>	
4.1	Introduction	68
4.2	Chitosan as a Carrier for Gene Therapy	69
4.2.1	Chitosan Chemistry	69
4.2.2	General Strategies for Chitosan Modification	71
4.2.3	Chitosan–DNA interactions: Transfection Efficacy of Unmodified Chitosan	71
4.3	Modified Chitosans: Strategies to Improve the Transfection Efficacy	79
4.3.1	The Effects of Charge Density/Solubility and Degree of Acetylation	79
4.3.2	Improving the Physicochemical Characteristics of the Nanoparticulate Systems: Solubility, Aggregation and RES Uptake	80

4.3.3	Targeting Mediated by Cell Surface Receptors	81
4.3.4	Hydrophobic Modification: Protecting the DNA and Improving the Internalization Process	83
4.4	Methods of Preparation of Chitosan Nanoparticles	84
4.4.1	Complex Coacervation	84
4.4.2	Crosslinking Methods	86
4.4.2.1	Chemical Crosslinking	86
4.4.2.2	Ionic Crosslinking or Ionic Gelation	86
4.4.2.3	Emulsion Crosslinking	87
4.4.2.4	Spray Drying	88
4.4.2.5	Other Methods	89
4.5	DNA Loading into Nano- and Microparticles of Chitosan	91
4.6	DNA Release and Release Kinetics	93
4.7	Preclinical Evidence of Chitosan–DNA Complex Efficacy	95
4.8	Potential Clinical Applications of Chitosan–DNA in Gene Therapy	97
4.9	Conclusion	99
	Acknowledgments	99
	References	99
II	Protein & Peptide-based Nanomaterials	115
5	Plant Protein-based Nanoparticles	117
	<i>Anne-Marie Orecchioni, Cécile Duclairoir, Juan Manuel Irache and Evelyne Nakache</i>	
5.1	Introduction	117
5.2	Description of Plant Proteins	118
5.2.1	Pea Seed Proteins	119
5.2.2	Wheat Proteins	119
5.3	Preparation of Protein Nanoparticles	120
5.3.1	Preparation of Legumin and Vicilin Nanoparticles	121
5.3.2	Preparation of Gliadin Nanoparticles	122
5.4	Drug Encapsulation in Plant Protein Nanoparticles	124
5.4.1	RA Encapsulation in Gliadin Nanoparticles	124
5.4.2	VE Encapsulation in Gliadin Nanoparticles	125
5.4.3	Lipophilic, Hydrophilic or Amphiphilic Drug Encapsulation	126
5.5	Preparation of Ligand–Gliadin Nanoparticle Conjugates	127
5.6	Bioadhesive Properties of Gliadin Nanoparticles	129
5.6.1	<i>Ex Vivo</i> Studies with Gastrointestinal Mucosal Segments	130
5.6.2	<i>In Vivo</i> Studies with Laboratory Animals	131
5.7	Future Perspectives	135
5.7.1	Size Optimization	135
5.7.2	Immunization in Animals	136
5.8	Conclusion	137
	References	137

6	Peptide Nanoparticles	145
	<i>Klaus Langer</i>	
6.1	Introduction	145
6.2	Starting Materials for the Preparation of Nanoparticles	146
6.3	Preparation Methods	148
6.3.1	Nanoparticle Preparation by Emulsion Techniques	148
6.3.1.1	Emulsion Technique for the Preparation of Albumin-based Microspheres and Nanoparticles	148
6.3.1.2	Emulsion Technique for the Preparation of Gelatin-based Microspheres and Nanoparticles	151
6.3.1.3	Emulsion Technique for the Preparation of Casein-based Microspheres and Nanoparticles	153
6.3.2	Nanoparticle Preparation by Coacervation	154
6.3.2.1	Complex Coacervation Techniques for the Preparation of Nanoparticles	154
6.3.2.2	Simple Coacervation (Desolvation) Techniques for the Preparation of Nanoparticles	155
6.4	Basic Characterization Techniques for Peptide Nanoparticles	159
6.5	Drug Targeting with Nanoparticles	161
6.5.1	Passive Drug Targeting with Particle Systems	163
6.5.2	Active Drug Targeting with Particle Systems	163
6.5.3	Surface Modifications of Protein-based Nanoparticles	164
6.5.4	Surface Modification by Different Hydrophilic Compounds	164
6.5.5	Surface Modification by Polyethylene Glycol (PEG) Derivatives	165
6.5.6	Surface Modification by Drug-targeting Ligands	166
6.5.7	Different Surface Modification Strategies	168
6.6	Applications as Drug Carriers and for Diagnostic Purposes	169
6.6.1	Protein-based Nanoparticles in Gene Therapy	170
6.6.2	Parenteral Application Route	172
6.6.2.1	Preclinical Studies with Protein-based Particles	172
6.6.2.2	Clinical Studies with Protein-based Particles	172
6.6.3	Topical Application of Protein-based Particles	174
6.6.4	Peroral Application of Protein-based Particles	175
6.7	Immunological Reactions with Protein-based Microspheres	175
6.8	Concluding Remarks	176
	References	176
7	Albumin Nanoparticles	185
	<i>Juan Manuel Irache and Socorro Espuelas</i>	
7.1	Introduction	185
7.2	Serum Albumin	186
7.3	Preparation of Albumin Nanoparticles	187
7.3.1	“Conventional” Albumin Nanoparticles	188
7.3.1.1	Preparation of Albumin Nanoparticles by Desolvation or Coacervation	189

7.3.1.2	Preparation of Albumin Nanoparticles by Emulsification	192
7.3.1.3	Other Techniques to Prepare Albumin Nanoparticles	193
7.3.2	Surface-modified Albumin Nanoparticles	193
7.3.3	Drug Encapsulation in Albumin Nanoparticles	194
7.4	Biodistribution of Albumin Nanoparticles	196
7.5	Pharmaceutical Applications	198
7.5.1	Albumin Nanoparticles for Diagnostic Purposes	198
7.5.1.1	Radiopharmaceuticals	198
7.5.1.2	Echo-contrast Agents	199
7.5.2	Albumin Nanoparticles as Carriers for Oligonucleotides and DNA	199
7.5.3	Albumin Nanoparticles in the Treatment of Cancer	201
7.5.3.1	Fluorouracil and Methotrexate Delivery	201
7.5.3.2	Paclitaxel Delivery	202
7.5.3.3	Albumin Nanoparticles in Suicide Gene Therapy	203
7.5.4	Magnetic Albumin Nanoparticles	204
7.5.5	Albumin Nanoparticles for Ocular Drug Delivery	205
7.5.5.1	Topical Drug Delivery	205
7.5.5.2	Intravitreal Drug Delivery	205
7.6	Concluding Remarks	207
	References	208
8	Nanoscale Patterning of S-Layer Proteins as a Natural Self-assembly System	219
	<i>Margit Sára, D. Pum, C. Huber, N. Ilk, M. Pleschberger and U. B. Sleytr</i>	
8.1	Introduction	219
8.2	General Properties of S-Layers	220
8.2.1	Structure, Isolation, Self-Assembly and Recrystallization	220
8.2.2	Chemistry and Molecular Biology	221
8.2.3	S-Layers as Carbohydrate-binding Proteins	223
8.3	Nanoscale Patterning of S-Layer Proteins	224
8.3.1	Properties of S-Layer Proteins Relevant for Nanoscale Patterning	224
8.3.2	Immobilization of Functionalities by Chemical Methods	225
8.3.3	Patterning by Genetic Approaches	226
8.3.3.1	The S-Layer Proteins SbsA, SbsB and SbsC	226
8.3.3.2	S-Layer Fusion Proteins	228
8.4	Spatial Control over S-Layer Reassembly	241
8.5	S-Layers as Templates for the Formation of Regularly Arranged Nanoparticles	242
8.5.1	Binding of Molecules and Nanoparticles to Functional Domains	242
8.5.2	<i>In Situ</i> Synthesis of Nanoparticles on S-Layers	244
8.6	Conclusions and Outlook	244
	Acknowledgments	245
	References	245

III	Pharmaceutically Important Nanomaterials	253
9	Methods of Preparation of Drug Nanoparticles	255
	<i>Jonghwi Lee, Gio-Bin Lim and Hesson Chung</i>	
9.1	Introduction	255
9.2	Structures of Drug Nanoparticles	257
9.3	Thermodynamic Approaches	257
9.3.1	Lipid-based Pharmaceutical Nanoparticles	258
9.3.2	What is a Lipid?	259
9.3.3	Liquid Crystalline Phases of Hydrated Lipids with Planar and Curved Interfaces	260
9.3.4	Oil-in-water-type Lipid Emulsion	261
9.3.5	Liposomes	261
9.3.6	Cubosomes and Hexosomes	262
9.3.7	Other Lipid-based Pharmaceutical Nanoparticles	263
9.4	Mechanical Approaches	264
9.4.1	Types of Processing	264
9.4.2	Characteristics of Wet Comminution	266
9.4.3	Drying of Liquid Nanodispersions	267
9.5	SCF Approaches	270
9.5.1	SCF Characteristics	270
9.5.2	Classification of SCF Particle Formation Processes	271
9.5.3	RESS	272
9.5.4	SAS	273
9.5.5	SEDS	274
9.6	Electrostatic Approaches	275
9.6.1	Electrical Potential and Interfaces	275
9.6.2	Electrospraying	277
	References	280
10	Production of Biofunctionalized Solid Lipid Nanoparticles for Site-specific Drug Delivery	287
	<i>Rainer H. Müller, Eliana B. Souto, Torsten Göppert and Sven Gohla</i>	
10.1	Introduction	287
10.2	Concept of Differential Adsorption	289
10.3	Production of SLN	292
10.4	Functionalization by Surface Modification	294
10.5	Conclusions	298
	References	299
11	Biocompatible Nanoparticulate Systems for Tumor Diagnosis and Therapy	304
	<i>Mostafa Sadoqi, Sunil Kumar, Cesar Lau-Cam and Vishal Saxena</i>	
11.1	Introduction	304

11.2	Nanoscale Particulate Systems and their Building Blocks/ Components	305
11.2.1	Dendrimers	305
11.2.2	Buckyballs and Buckytubes	307
11.2.3	Quantum Dots	309
11.2.4	Polymeric Micelles	310
11.2.5	Liposomes	310
11.3	Biodegradable Nanoparticles	312
11.3.1	Preparation of Nanoparticles	313
11.4	Biodegradable Optical Nanoparticles	314
11.4.1	Optical Nanoparticles as a Potential Technology for Tumor Diagnosis	314
11.4.2	Optical Nanoparticles as a Potential Technology for Tumor Treatment	315
11.5	Optical Imaging and PDT	317
11.5.1	Optical Imaging	317
11.5.1.1	Fluorescence-based Optical Imaging	317
11.5.1.2	NIR Fluorescence Imaging	317
11.5.1.3	NIR Dyes for Fluorescence Imaging	318
11.5.2	PDT	318
11.5.2.1	Basis of PDT	319
11.5.2.2	Photosensitizers for PDT	320
11.5.3	ICG: An Ideal Photoactive Agent for Tumor Diagnosis and Treatment	320
11.5.3.1	Clinical Uses of ICG	320
11.5.3.2	Structure and Physicochemical Properties of ICG	321
11.5.3.3	Binding Properties of ICG	321
11.5.3.4	Metabolism, Excretion and Pharmacokinetics of ICG	322
11.5.3.5	Toxicity of ICG	322
11.5.3.6	Tumor Imaging with ICG	322
11.5.3.7	PDT with ICG	323
11.5.3.8	Limitations of ICG for Tumor Diagnosis and Treatment	324
11.5.3.9	Recent Approaches for Improving the Blood Circulation Time and Uptake of ICG by Tumors	325
11.5.3.10	Recent Approaches for ICG Stabilization <i>In Vitro</i>	326
11.6	PLGA-based Nanoparticulate Delivery System for ICG	327
11.6.1	Rationale of Using a PLGA-based Nanoparticulate Delivery System for ICG	327
11.6.2	<i>In Vivo</i> Pharmacokinetics of ICG Solutions and Nanoparticles	331
11.7	Conclusions and Future Work	336
	References	338
12	Nanoparticles for Crossing Biological Membranes	349
	<i>R. Pawar, A. Avramoff and A. J. Domb</i>	
12.1	Introduction	349

12.2	Cell Membranes	350
12.2.1	Functions of Biological Membranes	351
12.2.2	Kinetic and Thermodynamic Aspects of Biological Membranes	352
12.3	Problems of Drugs Crossing through Biological Membranes	354
12.3.1	Through the Skin	354
12.3.1.1	Mechanical Irritation of Skin	355
12.3.1.2	Low-voltage Electroporation of the Skin	355
12.3.2	Through the BBB	357
12.3.2.1	Small Drugs	359
12.3.2.1.1	Limitations of Small Drugs	359
12.3.2.2	Peptide Drug Delivery via SynB Vectors	360
12.3.3	GI Barrier	360
12.3.3.1	Intestinal Translocation and Disease	361
12.4	Nanoparticulate Drug Delivery	362
12.4.1	Skin	363
12.4.1.1	Skin as Semipermeable Nanoporous Barrier	363
12.4.1.2	Hydrophilic Pathway through the Skin Barrier	363
12.4.2	Solid-Lipid Nanoparticles (SLN) Skin Delivery	364
12.4.2.1	Chemical Stability of SLN	364
12.4.2.2	<i>In Vitro</i> Occlusion of SLN	365
12.4.2.3	<i>In Vivo</i> SLN: Occlusion, Elasticity and Wrinkles	365
12.4.2.4	Active Compound Penetration into the Skin	365
12.4.2.5	Controlled Release of Cosmetic Compounds	365
12.4.2.6	Novel UV Sunscreen System Using SLN	366
12.4.3	Polymer-based Nanoparticulate Delivery to the Skin	366
12.4.4	Subcutaneous Nanoparticulate Antiepileptic Drug Delivery	366
12.4.5	Nanoparticulate Anticancer Drug Delivery	367
12.4.5.1	Paclitaxel	368
12.4.5.2	Doxorubicin	368
12.4.5.3	5-Fluorouracil (5-FU)	369
12.4.5.4	Antineoplastic Agents	369
12.4.5.5	Gene Delivery	369
12.4.5.6	Breast Cancer	370
12.4.6	Nanofibers Composed of Nonbiodegradable Polymer	370
12.4.6.1	Electrostatic Spinning	371
12.4.6.2	Scanning Electron Microscopy	371
12.4.6.3	Differential Scanning Calorimetry (DSC)	371
12.5	Nanoparticulate Delivery to the BBB	371
12.5.1	Peptide Delivery to the BBB	372
12.5.1.1	Peptide Conjugation through a Disulfide Bond	373
12.5.2	Biodegradable Polymer Based Nanoparticulate Delivery to BBB	373
12.5.3	Nanoparticulate Gene Delivery to the BBB	374
12.5.4	Mechanism of Nanoparticulate Drug Delivery to the BBB	375
12.5.5	Nanoparticulate Thiamine-coated Delivery to the BBB	376
12.5.6	Nanoparticle Optics and Living Cell Imaging	376

12.6	Oral Nanoparticulate Delivery	378
12.6.1	Lectin-conjugated Nanoparticulate Oral Delivery	379
12.6.2	Oral Peptide Nanoparticulate-based Delivery	380
12.6.3	Polymer-Based Oral Peptide Nanoparticulate Delivery	381
12.6.3.1	Polyacrylamide Nanospheres	381
12.6.3.2	Poly(alkyl cyanoacrylate) PACA Nanocapsules	381
12.6.3.3	Derivatized Amino Acid Microspheres	382
12.6.4	Lymphatic Oral Nanoparticulate Delivery	382
12.6.5	Oral Nanosuspension Delivery	383
12.6.6	Mucoadhesion of Nanoparticles after Oral Administration	384
12.6.7	Protein Nanoparticulate Oral Delivery	384
	References	385
	Index	394

Preface

While the recently published first volume of the *NtLS* series, *Biofunctionalization of Nanomaterials*, dealt with approaches to tailoring nanomaterials to be useful in biomedical applications, this second volume of the series, which I am pleased to present to you herewith, focuses on nanomaterials derived from biologically and pharmaceutically important substances. Twelve chapters describe in depth the various nanotechnological aspects behind using DNA, proteins, peptides, chitosan, lipoplexes, lipids and drugs. DNA is the most important and well studied biological molecule which itself is in the nano size regime. One of the attractive features of products containing DNA is the potential for producing materials of biological nature. Although DNA-based nanotechnology is currently in its infancy, it is likely to impact future applications in industrial segments such as electronics, sensors, medicine, and many other fields. The book has four chapters on DNA based nanomaterials. It begins with a chapter entitled *Self-Assembled DNA Nanotubes*, which is a contribution from the laboratories of Thom LaBean and Sung Ha Park from Duke University, USA, on self-assembled one-dimensional (1D) DNA nanotubes with unique design schemes and characteristics. In this chapter, approaches to assembly of artificially designed tiles, DX, TX, 4×4, and 6BH branched-junction tiles to form 1D DNA nanotubes have been described. The second chapter illuminates on the importance of development of effective nucleic acid nanocarriers and provides approaches to prepare DNA nanoparticles containing a single DNA molecule (the minimal particle size possible) as well as their characterization and properties. This chapter, *Nucleic Acid Nanoparticles*, presented by Guy Zuber and co-workers from the Genetic Chemistry Laboratory of Illkirch University, France, reviews strategies for synthesis of DNA nanoparticles and possibilities to functionalize them with cancer cell targeting elements. Mixing DNA with cationic lipids leads to spontaneous self assembly of ordered aggregates known as lipoplexes whose size can range from around 100 nm to several microns depending on preparation conditions. The third chapter, *Lipoplexes*, written by Sarah Weisman from Technion Israel Institute of Technology in Haifa, Israel, gives an overview of the current state of knowledge about lipoplexes, with special attention to their microscopic structure, and the relationships between structure and gene delivery efficiency. Julio C. Fernandes and co-workers from the Medical Faculty of Montreal University, Canada, brought out an exhaustive review on DNA-Chitosan polyplexes presented

in the fourth chapter, *DNA-chitosan Nanoparticles for Gene Therapy: Current Knowledge and Future Trends*. In addition to the basic concepts, the chapter provides information on different procedures to obtain nano- and micro DNA-chitosan particles and their clinical application as non-viral vectors in gene therapy.

Switching gears from DNA to proteins, the book provides a further four chapters on different facets of peptide and protein based nanomaterials. Proteins are a class of natural molecules that have unique functionalities and potential applications in both biological as well as material fields. Nanomaterials derived from proteins, especially protein nanoparticles, are biodegradable, metabolizable and can also be easily amenable for surface modification and covalent attachment of drugs and ligands. In the fifth chapter, Anne-Marie Orecchioni and co-workers from the Laboratory of Galenic Pharmacy of Rouen University, St. Etienne du Rouvray, France, provide an exhaustive account of plant based proteins, their synthesis and applications. This particular chapter, *Plant Protein-based Nanoparticles*, not only provides information on conventional plant protein nanoparticles but also describes 'decorated' (*i.e.*, conjugated) storage protein nanoparticles. Continuing on a similar theme, Klaus Langer from the Biocenter of Frankfurt on Main University, Germany, provides a comprehensive account in chapter six, *Peptide Nanoparticles*, on preparation techniques for peptide and protein-based nanoparticles with focus on their application in drug delivery. Narrowing down from a broad perspective on protein nanoparticles described in chapters two and three, chapter seven has the title *Albumin Nanoparticles*, indicating a review on a specific protein, Serum Albumin, which is extremely important in physicochemical, immunochemical and drug delivery applications. In this chapter, Juan Manuel Irache and Socorro Espuelas from the Galenics Center of Navarra University in Pamplona, Spain, summarize preparation and main applications of albumin nanoparticles for pharmaceutical purposes. Chapter eight, *Nanoscale Patterning of S-Layer Proteins as a Natural Self-Assembly System*, by Margit Sára and co-workers from the Center for Nanobiotechnology of the Agricultural University of Vienna, Austria, provides a survey of the general principles of crystalline bacterial cell surface layer (S-layer) proteins and fusion proteins which are being exploited as building blocks and templates for generating functional nanostructures at the meso- and macroscopic scale for both life and non-life science applications.

Pharmaceutical research and development has recently moved into a new direction thanks to the possibility of obtaining nanoformulation of drugs, *i.e.* formulation of drugs using nanoparticles. Keeping in tune with this trend a separate chapter specifically on drug nanoparticles has been included in this volume. Chapter nine, *Preparation Methods of Drug Nanoparticles* by Jonghwi Lee and co-workers from the Department of Nano Materials Science at Sejong University in Seoul, Korea, describe methods of preparation of drug nanoparticles, their characterization and advantages over conventional methods. In addition, chapter ten provides a review on Solid-Lipid Nanoparticles delineating the concept of differential protein adsorption as the concept of functionalization of SLN via surface modification from a practical point of view. In this chapter entitled *Production of Biofunctionalized Solid Lipid Nanoparticles for Site-specific Drug Delivery*, Rainer H. Müller and

co-workers from the Department of Pharmaceutical Technology of Free University Berlin, Germany, review methods used for the functionalization of solid lipid nanoparticles by modification of their surface characteristics followed by examples for their application in site-specific drug delivery. Mostafa Sadoqi and co-workers from the Physics Department of St John's University at Jamaica, USA, discuss near-infrared dye (NIR) indocyanine green (ICG) loaded PLGA drug nanoparticles and their application in cancer diagnosis and therapy in chapter eleven, *Biocompatible Nanoparticulate Systems for Tumor Diagnosis and Therapy*. Finally, since membrane transport plays an important role in cellular and subcellular pathways, including multidrug resistance (MDR), cellular signaling and cell-cell communication, an exclusive chapter, placed in twelfth position, discusses general information on cell membranes and the problems encountered by drugs when trying to cross them, and why drug nanoparticles are preferred. This chapter, *Nanoparticles for Crossing Biological Membranes*, is presented by Rajendra P. Pawar, A. Avramoff and Abraham J. Domb from the Department of Medicinal Chemistry of the Hebrew University of Jerusalem, Israel.

I do hope that the information that has been painstakingly accumulated by several researchers in this second volume will help in furthering better understanding of the nanosystems derived from biological materials, leading to new and potent applications. I am very grateful to all the authors for their excellent presentation of their topics, providing timely inputs and corrections in making the second volume a reality. I am always thankful to my employers, family, friends and Wiley-VCH publishers for their continued support and encouragement. Finally, my special thanks to you, the readers, for making attempts to utilize the knowledge base provided in this book. I look forward to receiving your comments and suggestions.

Baton Rouge, September 2005

Challa S. S. R. Kumar

I

DNA-based Nanomaterials

1

Self-assembled DNA Nanotubes

Thom LaBean and Sung Ha Park

1.1

Introduction

DNA, well-known as the predominant molecule for the storage of genetic information in biology and biochemistry, has also been recognized as a useful building material in the field of nanotechnology [1–3]. DNA provides basic building blocks for constructing functionalized nanostructures with four major features: molecular recognition, self-assembly, programmability and predictable nanoscale geometry. The limitations of conventional methods of top-down fabrication make bottom-up self-assembled nanostructures using DNA molecules a fascinating and attractive technique for near-term nano/biotechnologies. Recently, self-assembled DNA nanostructures utilizing branched DNA tiles have been reported on (a) various artificial geometrical structures like one- (1-D) and two-dimensional (2-D) periodically patterned structures [4–14], and three-dimensional (3-D) polyhedra [15, 16], and (b) functionalized lattices such as mechanical devices [17–23], molecular computers [24–30] and scaffolds for organizing other functionalized molecules [31–33]. DNA nanostructures are created via self-assembly during the slow annealing of aqueous solutions of carefully designed single-strand DNA, thereby facilitating hybridization of complementary nucleotide sequences, and the formation of double-strand domains and Holliday junction-like crossover points.

In this chapter, we review recent results on self-assembled 1-D DNA nanotubes with unique design schemes and characteristics. DNA nanotubes are characterized by (a) a high aspect ratio, (b) a long, narrow central channel and (c) DNA sidewalls. The 1-D nanotubes are typically made from rolled-up sheets of DNA lattice containing tiles with a variety of motifs: double-crossover (DX) [34], triple-crossover (TX) [35] and four four-arm junctions (4×4) [36]. Schematic drawings of four distinct DNA tile motifs which have been used for constructing complex 1-D DNA nanotubes are shown in Fig. 1.1.

The DNA tiles shown in Fig. 1.1 have each been shown to form large two-dimensional lattice sheets up to 10 μm on an edge, as well as nanotubes formed by lattices which curl and close upon themselves. Superstructure morphology

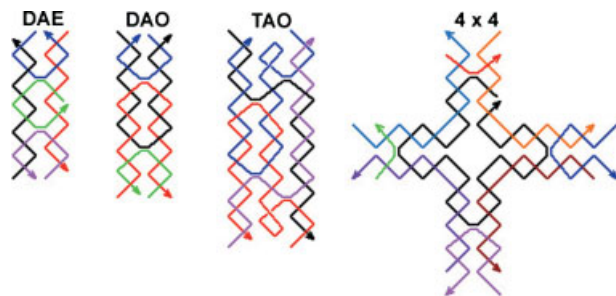


Fig. 1.1. Four distinct DNA motifs for constructing complex 1-D DNA nanotubes. The structures DAE, DAO and TAO are named by acronyms describing their basic characteristics. Names begin with “D” for DX (two helical domains) and “T” for TX (three helical domains). The second character indicates the relative orientations of their two double-helical domains. Here, “A” stands for antiparallel and indicates that, upon crossing over, the strands

change direction of propagation along the helical axes. The third character refers to the number of helical half-turns between cross-overs, “E” for an even number and “O” for an odd number. The 4×4 tile contains four four-arm branched junctions pointing in four directions (north, south, east and west in the tile plane). Arrows indicate simplified strands running from 5' to 3'.

(sheet versus tube) is controlled in these tiling systems by a variety of means, including counterion concentration, lattice corrugation schemes and disulfide bridge formation. As explained in detail below, curled lattice DNA nanotubes have been observed with either stacked, circular layers of tiles or with spirally wound, chiral configurations. DNA nanotubes have also been intentionally constructed by stacking six-helix bundle (6HB) tiles one on top the other to form tubes with only a single tile per layer and a single double-helix diameter channel through the center [37].

1.2 DNA Nanotubes Self-assembled from DX Tiles

Recently, several varieties of nanotubes constructed from DX tiles have been reported [10–12]. Two distinct types of nanotubes made from DNA DX complexes are DAE-E and DAE-O (where the final letter in the acronym indicates the even/odd parity of helical half-turns between neighboring strand-exchange points within inter-tile joints). DAE-E DX tile nanotubes have diameters between 7 and 20 nm and lengths as long as 50 μm with a persistence length of around 4 μm ; they can be programmed to display a variety of patterns. The DAE-O tile lattice can form ribbon structures many micrometers in length and 40–250 nm in width after hybridization.

1.3 DAE-E DX Tile Nanotubes

The construction and characterization of programmable DAE-E nanotubes displaying several tiling schemes as well as the kinetics of their assembly have been studied and reported [10, 11]. DX tiles were first described over 10 years ago [34]. DNA tiles can be thought of as having two parts: (a) a central core of duplex DNA (illustrated by rectangles in Fig. 1.2) and (b) four single-stranded sticky ends which allow it to bind to other tiles (shown protruding from the tile corners). In this first case, the tile core is made up of five oligonucleotides strands that form two double-helical domains held in rigid orientation with parallel axes by a pair of strand-exchange crossover points (Fig. 1.3a). In the study, two different sequence assignments were made to yield two different cores, which the authors called RE and SE [10]. Given an appropriate set of sticky ends, a single core yields a single tile and the unique sequences for sticky end allows the interactions between tiles to be

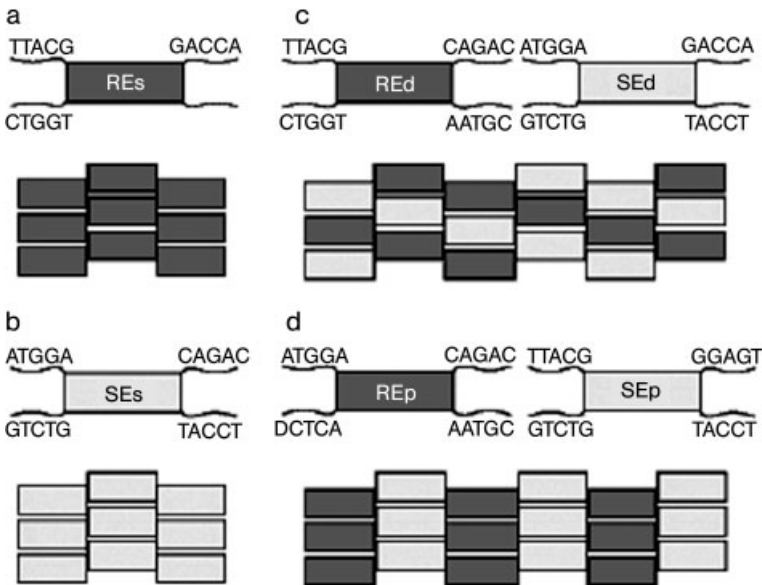


Fig. 1.2. Schematics of lattices utilizing DAE-E tiles. (a) Top: a single REs tile, based on the RE core and carrying four sticky ends. Bottom: complementarity between sticky ends directs the tiles to form a regular lattice. (b) A single SEs tile, based on a different core, SE, and its lattice. (c) Two tiles, REd and SEd, which assemble into a lattice with diagonal stripes; alone each tile could assemble into a linear strip. (d) Another pair of tiles, REp and SEp, cannot assemble independently, but together can form a lattice with stripes perpendicular to the long axis of the tiles. Note: lowercase letters “s”, “d” and “p” denote a particular choice of sticky ends and were chosen to represent the pattern generated by the tile set in which they appear: single tile type, diagonally striped or perpendicularly striped lattice. (From Ref. [10].)

programmed (Fig. 1.2). Figure 1.2(c and d) shows how tile sets have been used to create lattices with stripes either diagonal to or perpendicular to the long axis of the tiles. The authors viewed a set of tiles as a program for the construction of a particular structure including a diagonally striped or perpendicularly striped lattice.

In this system, hybridization of complementary sticky end pairs determines whether or not a set of tiles will form a lattice, but the set of sticky ends does not determine whether the lattice will be flat or curved. Curvature is profoundly affected by the choice of lattice symmetry as shown in Fig. 1.3(c–e). The symmetries depicted in Fig. 1.3(c and d) are compatible with flat lattice sheets since deviations

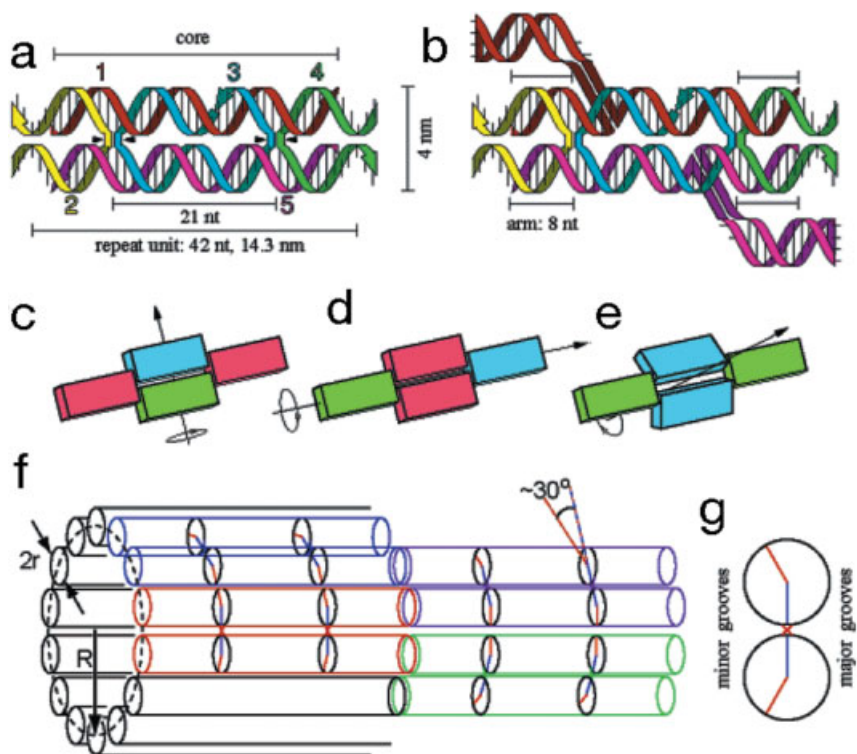


Fig. 1.3. (a) Structure of a DAE-E tile showing numbered strands and their paths through the complex. Tiles contain five single strands with 5-nt sticky ends on strands 2 and 4. (b) Tile structure with hairpins (8-nt stem, 4-nt loop) on strands 1 and 5 between nt 14 and 15 from their 5'-ends. Molecular models suggest that these hairpins attach underneath the molecule, as depicted here; in a tube they would be on the outside. (c and d) Two in-plane rotational symmetries that, if satisfied by a patch of tiles, encourage molecular strain to balance, resulting in a flat sheet. (e) A rotational symmetry, satisfied by DAE-E molecules, that permits curvature. (f) Heptagonal tube of radius R . In each tile, two cylinders of radius r represent the double helices. Black circles mark crossover points. Blue and orange lines connect the position of phosphate backbones to the center of a helix. The smaller angle between the blue and orange lines defines the minor groove. (g) Cross-section of the red tile from (f) at a crossover point. (From Ref. [10].)

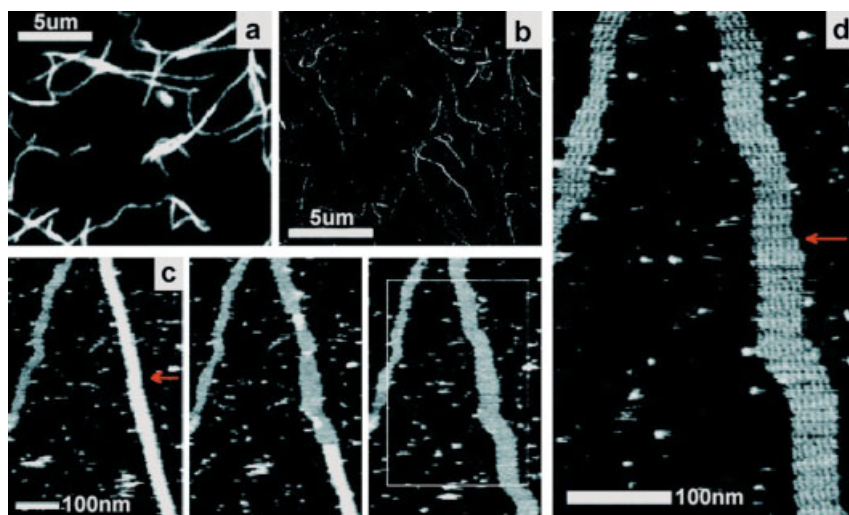


Fig. 1.4. Microscopic images of nanotubes. DNA filaments visualized by (a) fluorescence microscopy and (b) AFM. The solution in (a) contains FAM-labeled REp + SEp and in (b) contains REp + SEp. (c) A time series of AFM images indicates that filaments are tubes (REp + SEp). (Left panel) A thick filament (closed tube) runs the length of the image. Heights of closed tubes suggest they are flattened onto the substrate. An already-open

tube is seen on the left. (Center panel) The tube opens progressively from the top, revealing a one-tile-thick lattice. (Right panel) The fully opened tube resembles the lattice on the left. An arrow marks a discrete change in tube width before opening and in the number of tiles after opening, suggesting a defect in the tile lattice. (d) At greater magnification, individual tiles are resolved. (From Ref. [10].)

from planar geometry can be compensated for; thus, molecular strain that could cause curvature may be balanced by symmetric molecular strain elsewhere. Other possible lattice symmetries, such as the one depicted in Fig. 1.3(e), are compatible with intentionally curved lattices and the formation of DNA nanotubes.

DNA nanotubes constructed according to RE- and SE-core tiles were examined by atomic force microscopy (AFM) and by fluorescence microscopy using fluorescein (FAM)-labeled strands. Characterization by AFM showed parallel and diagonal striped patterns, as expected, providing proof that the structural programming functioned properly. AFM studies also revealed that nanotubes flatten out on the mica substrate and were abraded by the AFM tip from double-layer to single-layer structures by imaging repeatedly at the same place on the sample (Fig. 1.4). The dynamic character of the interactions of nanotubes and lattices with mica was seen by re-imaging a sample by AFM under solution over the course of several hours, and observing tubes coming to and diffusing away from the surface. Fragments of lattice were often left on the mica when a nanotube diffused away. For this reason, the dimensions of the filaments were difficult to measure using surface-based AFM.

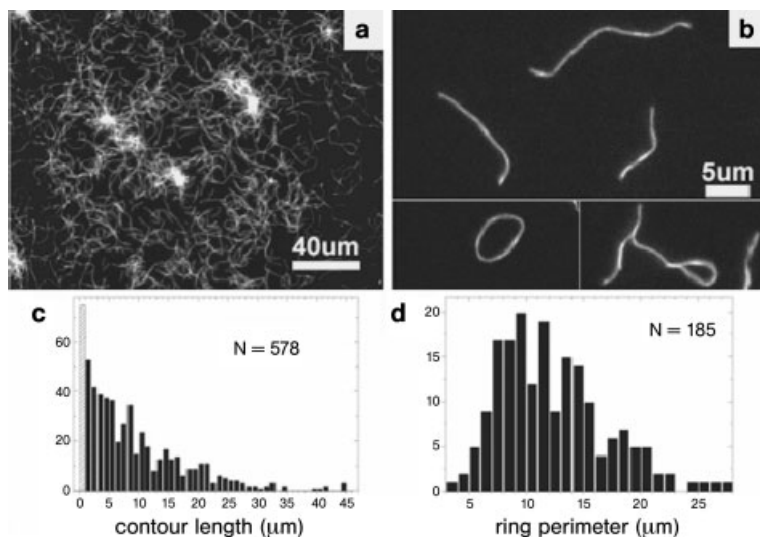


Fig. 1.5. Experimental determination of nanotube persistence length. (a) Epifluorescence image of 400 nM solution of FAM-labeled SEs tubes. Tubes were observed diffusing freely in and out of the focal plane. (b) As (a), but diluted to 40 nM. Occasionally, rings (left) and looped structures (right) are found. (c) Histogram of linear tube lengths

with an average of around 7 μm ; approximately 10% are over 15 μm long, consistent with an exponential distribution. Some tubes of around 50 μm were observed. (d) Circularized tubes averaged 12 μm in perimeter with a unimodal distribution. The ring shown is typical; most rings are free of kinks that would indicate local weakness. (From Ref. [10].)

Fluorescence microscopy was used to measure the length and stiffness of DAE-E nanotubes in solution. At the highest concentration (400 nM tiles) the density of tubes was too high to identify individuals and clump-like aggregates were common (Fig. 1.5a). Upon 10-fold dilution, single tubes were well dispersed and occasionally a ring or frayed bundle was seen (Fig. 1.5b). Only short tubes were observed directly following annealing and tube lengths continued to increase until about 16 h later when the distribution appeared to stabilize (at which point data were collected; Fig. 1.5c). The mean tube length was around 7 μm with a small proportion of tubes with lengths up to 50 μm being observed.

Tube stiffness was inferred from the distribution of ring perimeters by assuming that the rate of ring formation for a tube of length L is approximately proportional to the fraction of time that the ends of the tube are colocalized at equilibrium. Over brief intervals in which the length distribution does not change significantly, this ring closure probability can be calculated a function of tube length L and persistence length p . Under these conditions, the distribution of ring perimeters should be the product of the distribution of tube lengths and the ring closure probability. The mean perimeter distance was around 12 μm . Using the distributions of Fig. 1.5(c and d), the persistence length was calculated to be $3.85 \pm 0.35 \mu\text{m}$.

Rothemund *et al.* performed the most thorough examination of the program-

mability and structural properties of DNA nanotubes [10]. They were able to identify the tile faces hidden inside and exposed outside the tubes, and drew important conclusions regarding the placement of hairpins on tiles and their effects on lattice stability. A subset of the authors went on to study the breaking and joining reactions among SE tile nanotubes and concluded that the growth of DNA tile nanotubes to multimicron length occurs through joining or fusion of preformed nanotubes rather than by sequential addition of individual tiles [11].

1.4 DAE-O DX Tile Nanotubes

A similar system of DNA tiles which was originally designed to form 2-D flat lattice using DAE-O tiles (Fig. 1.6a) was also observed to form nanotubes either with flat ring layers or with spiral layers producing a range of chiral tubes (Figs. 1.6a and 1.7) [12]. As with the study described above, DX tiles (this time of the DAE-O variety) with the four single-stranded sticky ends on each tile were arranged such that α and β tiles tessellate as shown in Fig. 1.6(b). The β tiles contained a 5'-biotinylated strand to enable streptavidin binding to be used as an observable marker. Hybridization was accomplished by cooling the solution by a linear gradient from 96 °C to room temperature over the course of 96 h.

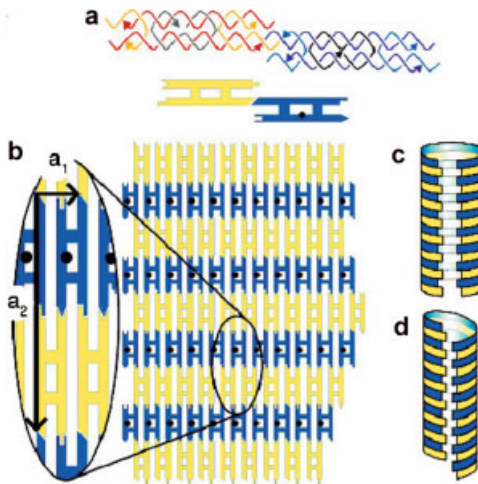


Fig. 1.6. Self-assembly of DAE-O tiles into sheets and tubes. (a) Structure of the DX tiles: colored arrows indicate simplified strands running 5' to 3'. The 6-nt single-stranded sticky ends on the α tile are complementary to those on the β tile (represented schematically by complementary shapes). A 5' biotin label on

the β tile is shown as a black dot. (b) The α and β tiles can tessellate to form extended 2-D arrays. The 2-D sheets curl and close upon themselves to form tubes, producing either alternating rings (c) or nested helices (d) of α and β tiles. (From Ref. [12].)

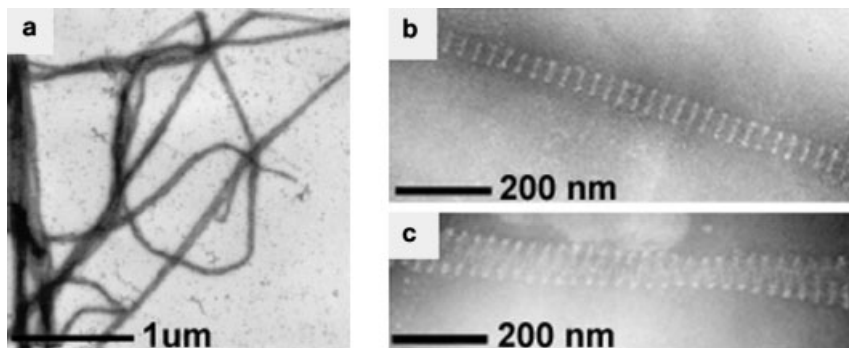


Fig. 1.7. Transmission electron micrographs of negatively stained DNA nanotubes and arrays. White features correspond to points of heavy metal stain exclusion where protein labels are bound to the β tiles. (From Ref. [12].)

In a standard $1 \times$ TAE/Mg²⁺ buffer, containing 20 mM Tris–acetate, pH 8.3, supplemented with 12.5 mM MgCl₂, the tiles form ribbon structures many micrometers in length and 40–250 nm in width after hybridization (Fig. 1.7a). Higher magnification reveals transverse streptavidin bands with a periodicity of 31 ± 2 nm (Fig. 1.7b and c), consistent with the designed 2-D array structure with the long axis of the tiles aligned along the long axis of the ribbons. A natural explanation for the parallel edges of these structures is that arrays of tiles curl and close upon themselves to form tubes. Unambiguous evidence for the formation of tubes is provided by micrographs such as Fig. 1.7(c) in which lines of streptavidin labels zigzag across a ribbon. In all such cases the line is continuous where it changes direction at the edge of the ribbon, proving they represent helical (spiral) tubes with a structure such as that illustrated in Fig. 1.6(d). Mixed superstructure morphologies (tubes and sheets) were observed in buffer with higher salt concentrations.

The authors point out that, as with carbon nanotubes [38], the structure of a DNA nanotube may be characterized by the indices (m, n) of the wrapping vector $\mathbf{c} = m\mathbf{a}_1 + n\mathbf{a}_2$ where \mathbf{a}_1 and \mathbf{a}_2 are basis vectors shown in Fig. 1.6(b), and the tube is formed from a sheet by joining equivalent points separated by \mathbf{c} . For nonhelical tubes $n = 0$ (Fig. 1.7b); $n = 1$ where all labels lie on a single helix (Fig. 1.7c). The short dimensions of the tiles are not resolved (the streptavidin labels are larger than the tile width); assuming $\mathbf{a}_1 = 4$ nm, then $m \sim 40$ (Fig. 1.7c). It is likely that tube diameters are determined by nonequilibrium processes, since once a tube has closed, an activation barrier prevents further lateral growth. Tube formation reduces the free energy of a tile array by satisfying all inter-tile bonds except those at the ends of the tube. Intrinsic curvature of the array would facilitate tube formation; however, the odd number of helical half-turns along the arms joining cross-over points on adjacent tiles means that in this system the intrinsic curvatures of α and β tiles are opposed.

1.5

TX Tile Nanotubes

DNA nanotubes composed of TX tiles have also been constructed and characterized [14]. TX tiles modified with thiol-containing double-stranded DNA stems projected out of the tile plane were used as the basic building blocks. TX nanotubes display a constant diameter of around 25 nm and have been observed with lengths up to 20 μm . In this section, we present high-resolution images of the constructs (TX nanotubes) and experimental evidence of their tube-like nature. DNA nanotubes represent a potential breakthrough in the self-assembly of nanometer-scale circuits for electronics layout because they can be targeted to connect at specific locations on larger-scale structures and can subsequently be metallized to form nanometer-scale metallic wires (see Section 2.6).

TX nanotube self-assemblies were formed from two DNA tile building blocks, a TAO (tile A) and a TAO + 2J (tile B) as shown in Fig. 1.8(a). The B tile contains two extra double-stranded DNA stems, which form junctions with the central helix of the tile such that they project out of the tile plane, with one stem protruding on each side of the tile. The B tiles used here are modified by the replacement of the loop on one protruding stem with a blunt end containing two thiol groups, one on a 3' and the other on a 5' strand terminus. Figure 1.8(b, right) shows a section of the proposed structure of the nanotubes with B tile layers alternating with A tile layers, double-stranded DNA helix axes aligned parallel with the tube axis, and thiol groups are located inside the tubes. Imaging of TX AB flat lattice sheets (Fig. 1.8c, left) demonstrates lattice fragments with widely varying dimensions and often with uneven edges. On the other hand, DNA nanotubes (Fig. 1.8c, right) exhibit uniform widths of around 25 nm for lengths of up to 20 μm .

Figure 1.9(a) shows a typical AFM image (tapping mode in air) of the TX nanotube. Stripes perpendicular to the long axis of the filaments are clearly visible and indicate closed ring structures in successive layers rather than a spiral structure, which would have given stripes with a noticeable diagonal slant. Figure 1.9(b) shows a high-resolution AFM image (tapping mode in buffer) of the TX nanotube in which one can discern three gaps and four tiles in some of the layers. The gaps and tiles are arrayed parallel with the axis of the flattened tube.

Burial of the sulfur moieties within the tubes makes logical sense because disulfide bridges are preferred structures formed by thiol groups under physiologic-like solution conditions such as those used here. The formation of disulfide bonds between neighboring B tiles would cause the lattice to curve and form tubes. The possible existence of free thiols on the outer surface of the nanotubes was probed by using two different gold reagents with reactivity toward sulfur: monomaleimido Nanogold (Nanoprobes, Yaphank, NY) and fresh colloidal gold nanoparticles. The monomaleimido Nanogold failed to react with the tube surfaces, whereas the colloidal gold displayed the interesting reactivity shown in Fig. 1.9(d and e). With very low background levels of unbound gold, the bound gold particles showed a very high probability of attachment to the ends of nanotubes and not to the outer surface anywhere else along the length of the tubes. The indication is that sulfur

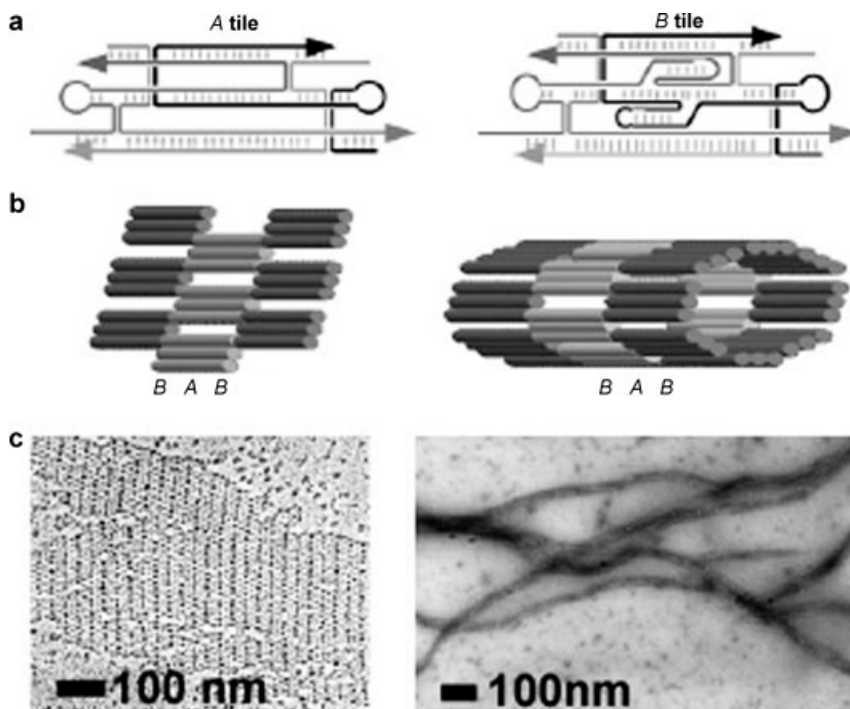


Fig. 1.8. (a) Schematic drawings showing the strand traces through the two tile types used in the constructions. Oligonucleotides are shown in different shades of gray and with arrowheads marking the 3'-ends. Short vertical hash marks indicate base pairing within double-helical regions; paired vertical lines represent crossover points. The central helices of both tile types are terminated with T₄ loops. Two extra stem-loops (2J) on the central helix of the B tile are designed to protrude, one into and one out of the tile plane. (b) (Left) Cartoon of a section of TAO flat lattice constructed from A and B tiles. Tubes repre-

sent double-helical regions; for simplicity, the 2J stem-loops on the B tiles are not shown. (Right) Cartoon model of a section of TAO nanotube shown with eight tiles per layer of tube. (c) (Left) TEM image of platinum rotary shadowed TAO lattice. The B tiles appear darker than the A tiles, having picked up more platinum on their protruding 2J stem-loops; alternating stripes of A and B tiles are clearly visible with approximately the expected distance of 28 nm. (Right) TEM image of negative-stained TAO nanotubes. (From Ref. [14].)

which is buried within the tubes is exposed to some extent at the open ends of the nanotubes and available for binding with gold. This observation, in addition to offering evidence of the location of the thiol groups, may also be exploited in future work on targeted binding or formation of electrical contacts with the ends of TX nanotubes. Final evidence of the involvement of disulfide bridges in TX nanotube formation was provided by annealing the DNA in the presence of the reducing agent dithiothreitol and observing a complete lack of tubes.

Figure 1.10 shows a series of *in situ* zoomed images showing a TX nanotube being converted to a flat lattice by the physical effect of the AFM tip. The series of

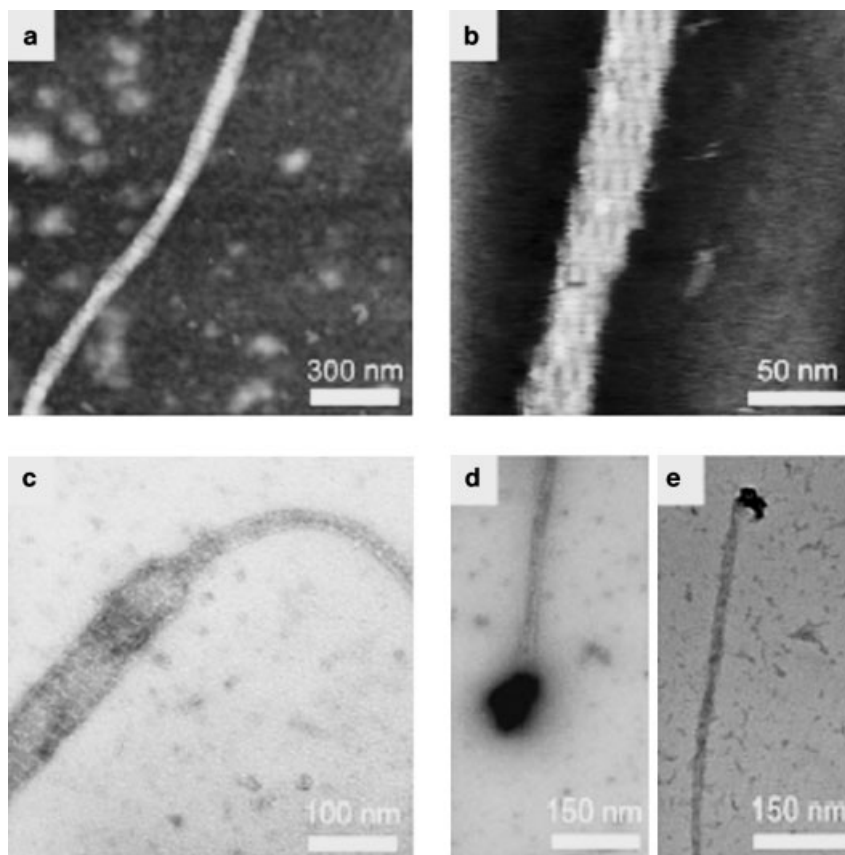


Fig. 1.9. (a) AFM image of a TAO nanotube taken by tapping mode in air. The *B* tile layers are visible as brighter stripes (because of increased height) oriented perpendicular to the long axis of the tube. (b) High-resolution image of a nanotube taken by tapping mode under buffer. Single-helix holes between adjacent tiles are visible as darker patches in

several layers. (c) TEM image of a negative-stained sample, showing a section of a nanotube that appears to have split into a flat lattice. (d and e) Negative-stained TEM images of TAO nanotubes with gold nanoparticles attached to the ends, apparently by interaction with thiol sulfurs partially exposed at the tube termini. (From Ref. [14].)

images was collected by repeatedly re-imaging the same nanotube under buffer with an AFM. The high-resolution image in Fig. 1.10(d) shows the detailed nanostructure of the completely torn open DNA nanotube with alternating layers of *A* and *B* tiles clearly discernible. Whole tiles have been scratched away from the opening nanotube by the force of the AFM tip and therefore the tile layers no longer contain all of the tiles that were present in the nanotube. A few layers are seen that still contain six tiles. The combination of the high-resolution AFM images (Fig. 1.9b and 1.10d) provides supporting evidence for the model in which individual tile layers in intact nanotubes contain eight tiles.

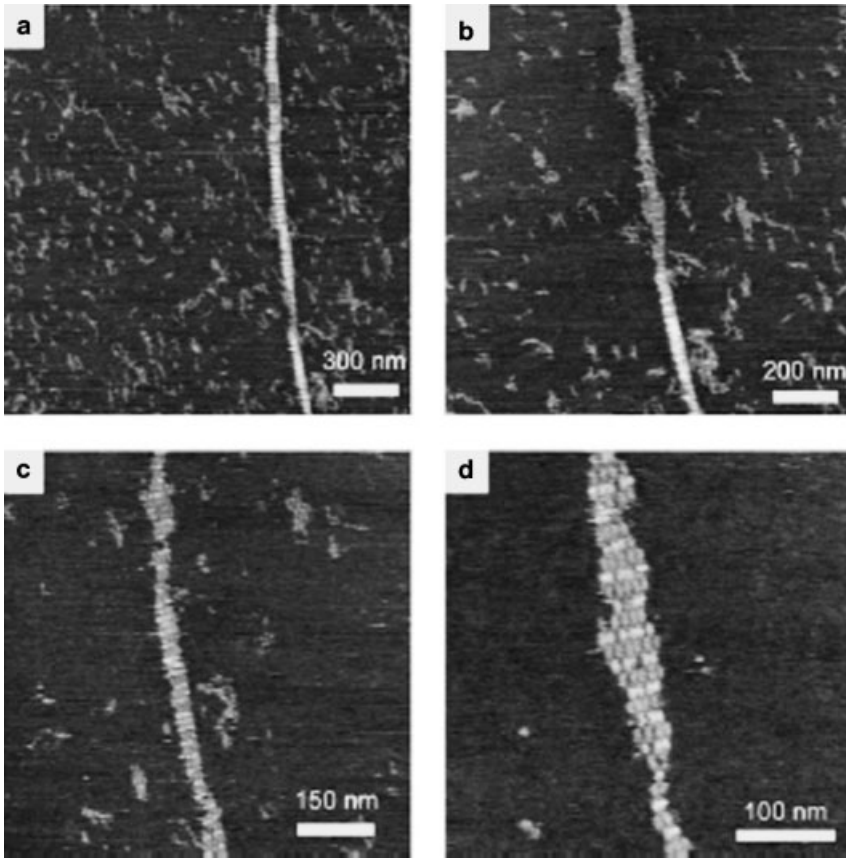


Fig. 1.10. A series of AFM images captured by repeatedly re-imaging and zooming in on the same nanotube, which appears mostly tube-like in (a), with increasing wear-and-tear through (b) and (c) until a section of unfolded tube becomes a single-layer, flat lattice (d) displaying stripes composed of lighter (higher) B tiles and darker (shorter) A tiles. (From Ref. [14].)

1.6

4 × 4 Tile Nanotubes

More complicated 1-D tube-like structure utilizing 4 × 4 tiles has also been reported [36]. Programmable self-assembly of this DNA nanostructure results in a uniform width nanoribbon which displays periodic square cavities. The 4 × 4 DNA tile (Fig. 1.11a) contains four four-armed DNA branched junctions pointing in four directions – north, south, east and west in the tile plane. It is composed of nine strands, with one of the strands participating in every junction. Bulged T₄ loops are placed at each of the four corners inside the tile core in order to decrease the probability of stacking interactions between adjacent four-arm junctions and

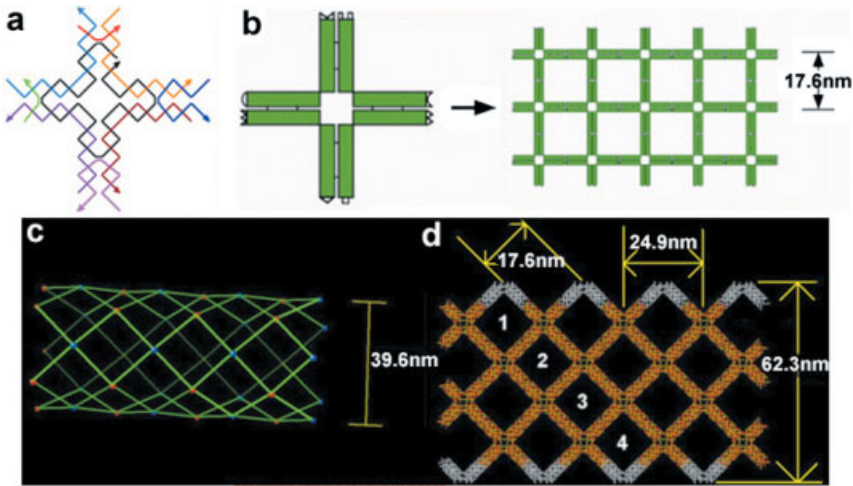


Fig. 1.11. Self-assembly of DNA nanoribbons using the 4×4 DNA tile. (a) The 4×4 tile strand structure. The tile contains nine oligonucleotides, shown as simplified backbone traces in different colors. Each four-arm junction is oriented in four directions. The black strand participates in all four junctions and contains T_4 loops connecting adjacent junctions. (b) Left: double-helical domains are illustrated as rectangles and paired rectangles represent four-arm junctions. Watson–Crick complementary sticky ends are shown as matching geometric shapes. Right: designed structure of the self-assembled lattice. There are four full helical turns between tile centers

so the tiles will be oriented in the same direction in the lattice. (c) Schematic model of the proposed 4×4 nanotube. (d) Overhead view of a tube squashed onto the mica substrate and forming a ribbon with four diagonal square cavities with a width of around 62.3 nm. Note the saw-tooth edge formed by folding one row of 4×4 tiles along a diagonal running through their most flexible region, the T_4 loops between adjacent arms. The jagged edges along with the 45° diagonal containing four cavities are typically observed in high-resolution AFM images of the ribbons. (From Ref. [36].)

allow the arms to point to four different directions. Characterization of structure formation by nondenaturing gel electrophoresis and thermal transition analysis (see Fig. 1.13 below) shows that the 4×4 tile structure is stable and well behaved.

Constructions following the design shown in Fig. 1.11(b) produce a high preponderance of uniform width ribbon structures. In this design the distance between adjacent tiles is an even number of helical half-turns (four full turns) so that the identical face of each tile points toward the same lattice face. Figure 1.12 shows four AFM images of the nanoribbons with lengths of up to around $20 \mu\text{m}$ and a typical uniform width of around 60 nm. The regularity of the periodic cavities is striking, as well as the observation that some of the nanoribbons revealed a single-layer, flat grid lattice unrolled at the open end of the ribbon (see Fig. 1.12d). This observation strongly suggests that the ribbon structure results from tube-like structures which flatten when the sample is deposited on mica. The AFM image height profile clearly shows that the nanoribbon structure has two layers compared to the flat lattice. Also, the edges of the ribbon appear slightly higher, about 0.12 nm,

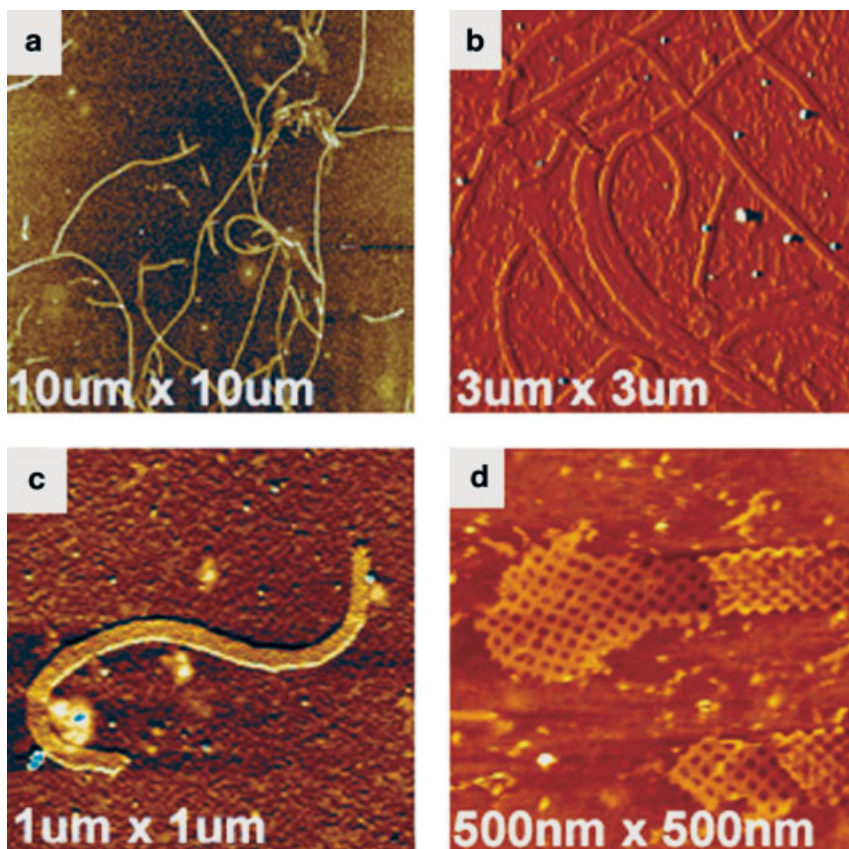


Fig. 1.12. AFM images of 4×4 nanoribbons at various scan sizes. (From Ref. [36].)

than the middle, indicating a finite radius of curvature for the squashed tube structure. The formation of tube-like lattices could be due to the fact that each component tile is oriented in the same direction in the designed lattice planes, and therefore any incidental curvature resident in each tile could accumulate and cause circularization of the lattice. This hypothesis is supported by the AFM analysis and by subsequent experiments showing that corrugation schemes where tiles are flipped in the lattice plane to compensate for tile curvature form large flat lattice sheets.

1.7

6HB Tile Nanotubes

Very recently, a new strategy for the creation of hollow DNA nanotubes was described which made use of tiles that are intrinsically 3-D and formed from a rigid

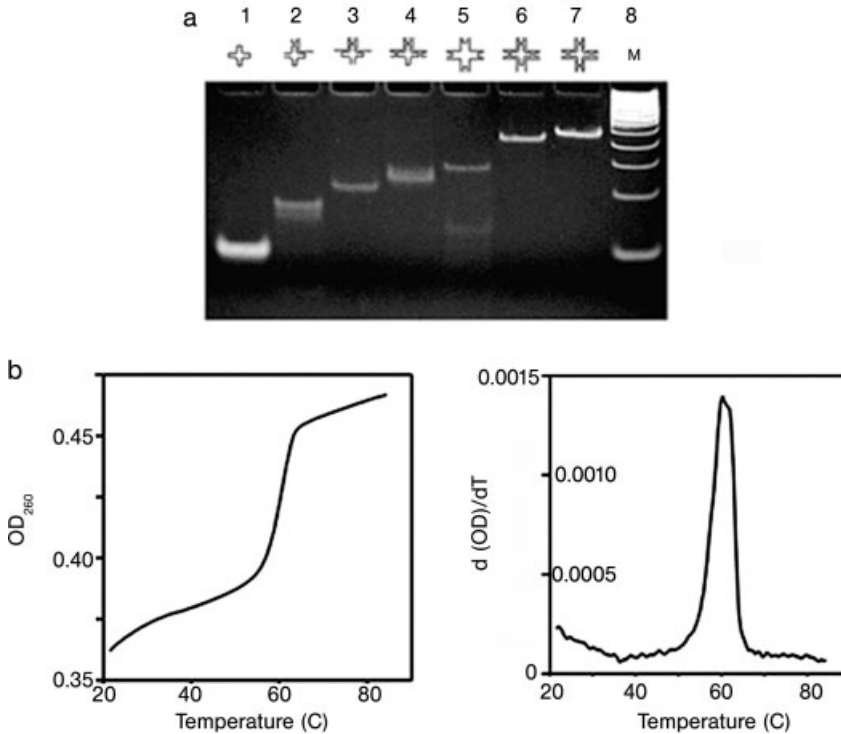


Fig. 1.13. Characterization of the 4×4 tile structure using nondenaturing electrophoresis and thermal transition experiments. (a) An 8% polyacrylamide gel (ethidium bromide stained) showing association complexes between various equimolar combinations of the 4×4 DNA complex component strands. Equimolar mixtures at $1 \mu\text{M}$ concentration per included strand were annealed and run on the gel at room temperature. Strands included in the annealings are indicated in the drawing above each lane. Lane 8 contains a 50-bp DNA ladder size marker. The 4×4 complex runs as a single band on nondenaturing gels, without

any higher-molecular-weight byproducts (from unexpected base pairings between two or more complexes) or lower-molecular-weight byproducts (from dissociated complex), indicating the 4×4 tile complex is a stable structure in the buffer used. (b) Thermal transition profile. The left panel shows the relative change in optical density at 260 nm as a function of temperature. The right panel shows the first derivative of the 4×4 complex melting data. The results show that the 4×4 complex melts cooperatively, as a single transition, with $T_m \sim 60^\circ\text{C}$. (From Ref. [36].)

cluster of double-helical domains with a single-helix width pore running down through its entire length [37]. The 6HB (shown schematically in Fig. 1.14) contained six double helices with each pair of neighboring domains linked by strand exchange at each of two crossover points. With complementary pairs of sticky ends appended to each end of the helices, the tiles were induced to assemble into long 1-D arrays with lengths up to around $15 \mu\text{m}$. These are the first described DNA nanotubes with perfectly designed widths and tube layers made up of single tiles.

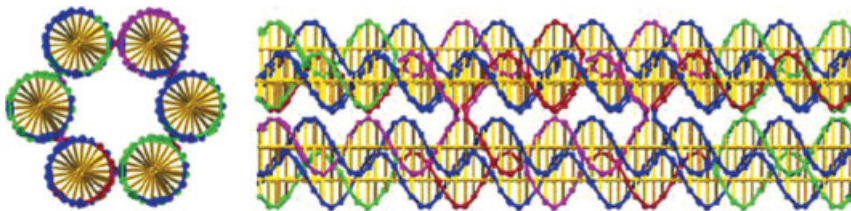


Fig. 1.14. Cross-sectional and transverse views of the 6HB tile model. The cross-sectional view emphasizes the cylindrical hole through the center of the tile (From Ref. [37].)

1.8 Applications

Self-assembled 1-D nanotubes made from artificially designed tiles show great promise for applications that range from fabrication of nanoelectronic devices to biological studies. Electrical transport in bare DNA molecules has been recognized as an interesting research field for last few decades. Although some of the conductivity experiments of DNA molecules had been shown superconducting [39] or semiconducting [40] properties, DNA molecules mostly show insulating characteristic [41]. The DNA molecule's poor conductivity prevents its direct use in electronic nanodevices. Thus, properly designed DNA lattices can serve as a precisely controllable and programmable scaffold for organizing functionalized nanomaterials in the design and construction of functionalized electronic nanodevices. Nanometer-scale fabrication with reliable DNA-templated metallic nanowires is an example demonstration of DNA's scaffolding capability. Several varieties of DNA tile nanotubes have been shown to be useful templates for the specific chemical deposition of metal for nanowire formation.

Until now, mostly natural λ DNA molecules have been used as a template for fabricating various metallic nanowires such as silver [42], gold [43], palladium [44, 45], platinum [46] and copper [47]. More complex and uniform width 1-D nanotubes can also serve as templates for highly conductive metallic nanowires. One example is shown in Fig. 1.15. Here, 4×4 nanoribbons have been metallized with silver using a novel electroless chemical deposition technique [36] and demonstrated electrical measurements through silver nanowires. The resulting nanowires have been characterized by scanning electron microscopy (SEM) and AFM. The metallized nanoribbons have heights of 35 ± 2 nm, widths of 43 ± 2 nm and lengths of up to about 5 μm . The current–voltage curve of the metallic silver 4×4 nanoribbon shows linear behavior and the resistance of this sample is around 200 Ω as measured between the two central contacts at a bias voltage of 0.1 V (Fig. 1.15c). This number corresponds to a bulk resistivity of $2.4 \times 10^{-6} \Omega\text{m}$. This nanowire is easily reproducible and has markedly higher conductivity than previously reported double-helix DNA-templated silver nanowires [42]. Other potential uses of DNA nanotubes are inspired by analogy with the roles of nanotubes and nanowires in living cells, e.g. as structural supports for the cytoskeleton, as tracks for

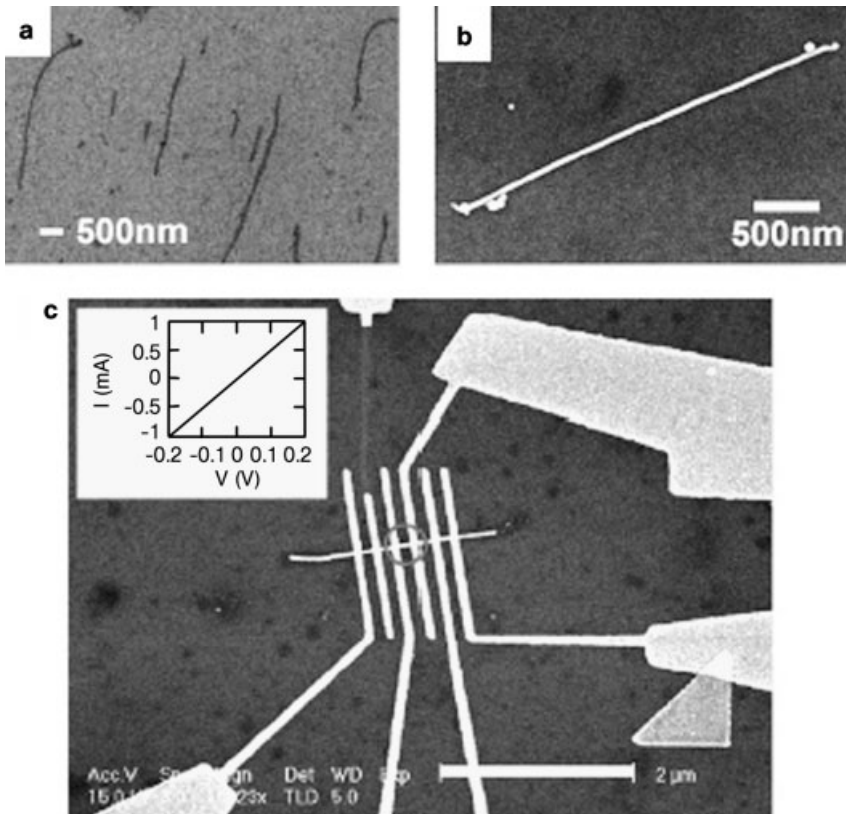


Fig. 1.15. Metallization and a conductivity measurement of metallized 4×4 nanoribbons. (a) SEM image of nonmetallized 4×4 nanoribbons. (b) SEM image of silver-seeded silver nanoribbon. The change in the signal contrast between (a) and (b) is apparent. (c) SEM image of the actual device (scale bar: $2 \mu\text{m}$). (Inset) Current–voltage curve of the metallic silver 4×4 nanoribbon. (From Ref. [36].)

the transport of microscopic cargo and as moving parts for cellular motility. DNA nanotubes may eventually be engineered to mimic all these functions.

1.9 Summary and Perspectives

DNA-based nanotechnology is currently being developed as a general assembly method for nanopatterned materials that may find use in electronics, sensors, medicine and many other fields. In this chapter, we have described a novel assembly of 1-D nanotubes made from artificially designed tiles, DX, TX, 4×4 and 6BH branched junction tiles. Nanotubes, consisting of DAE-E tiles, range from 7 to

20 nm in diameter, grow as long as 50 μm with a persistence length of around 4 μm , and can be programmed to display a variety of patterns. DAE-O DX tiles can form sheets or ribbons with periodic banding controlled by salt concentration. TX nanotubes display a constant diameter of around 25 nm and have been observed with lengths up to 20 μm . Tube formation is controlled by disulfide bonds between tiles augmented with thiol moieties. The 4×4 DNA nanoribbon contains four four-armed DNA branched junctions pointing in four directions. The formation of tube-like lattices is due to the fact that each component tile is oriented in the same direction in the designed lattice plane, and therefore any incidental curvature resident in each tile can accumulate and cause circularization of the lattice. The 1-D arrays of 6HB tiles form DNA nanotubes with one tile per tube layer and represent the smallest possible hollow DNA nanotube. Nanotubes formed from DNA tile lattices have been used as metallization templates for the formation of conductive nanowires. Utilizing DNA molecules as scaffolds for making functionalized nanowires offers certain advantages such as site-specific alignment and massive, parallel self-assembly for future electronic nanodevices. It has also been pointed out that DNA nanotubes, by analogy with cellular microtubules, might be useful as tracks along which artificial bionanomachines might transport molecular cargo [10, 12].

References

- 1 SEEMAN, N. C., DNA in a material world, *Nature* **2003**, 421, 427–431.
- 2 XU, J., LABEAN, T. H., CRAIG, S. L., DNA-based structures and their applications in nanotechnology. In *Supramolecular Polymers 2*, CIFERRI, A. (Ed.), Taylor & Francis, Boca Raton, FL, **2005**, pp. 445–480.
- 3 SEEMAN, N. C., Nucleic acid nanostructures and topology, *Angew. Chem. Int. Ed.* **1998**, 37, 3220–3238.
- 4 SEEMAN, N. C., Nucleic-acid junctions and lattices, *J. Theor. Biol.* **1982**, 99, 237–247.
- 5 SEEMAN, N. C., *De novo* design of sequences for nucleic acid structural engineering, *J. Biomol. Struct. Dyn.* **1990**, 8, 573–581.
- 6 SEEMAN, N. C., WANG, H., YANG, X., LIU, F., MAO, C., SUN, W., WENZLER, L., SHEN, Z., SHA, R., YAN, H., WONG, M. H., SA-ARDYEN, P., LIU, B., QIU, H., LI, X., QI, J., DU, S. M., ZHANG, Y., MUELLER, J. E., FU, T., WANG, Y., CHEN, J., New motifs in DNA nanotechnology, *Nanotechnology* **1998**, 9, 257–273.
- 7 LIU, F., SHA, R., SEEMAN, N. C., Modifying the surface features of two-dimensional DNA crystals, *J. Am. Chem. Soc.* **1999**, 121, 917–922.
- 8 WINFREE, E., LIU, F., WENZLER, L. A., SEEMAN, N. C., Design and self-assembly of two-dimensional DNA crystals, *Nature* **1998**, 394, 539–544.
- 9 MAO, C., SUN, W., SEEMAN, N. C., Designed two-dimensional DNA Holliday junction arrays visualized by atomic force microscopy, *J. Am. Chem. Soc.* **1999**, 121, 5437–5442.
- 10 ROTHEMUND, P., EKANI-NKODO, A., PAPADAKIS, N., KUMAR, A., FYGENSON, D. K., WINFREE, E., Design and characterization of programmable DNA nanotubes, *J. Am. Chem. Soc.* **2004**, 126, 16344–16352.
- 11 EKANI-NKODO, A., KUMAR, A., FYGENSON, D. K., Joining and scission in the self-assembly of nanotubes from DNA tiles, *Phys. Rev. Lett.* **2004**, 93, 2683011–2683014.

- 12 MITCHELL, J. C., ROBIN-HARRIS, J., MALO, J., BATH, J., TURBERFIELD, A. J., Self-assembly of chiral DNA nanotubes, *J. Am. Chem. Soc.* **2004**, *126*, 16342–16343.
- 13 LI, H., PARK, S. H., REIF, J. H., LABEAN, T. H., YAN, H., DNA-templated self-assembly of protein and nanoparticle linear arrays, *J. Am. Chem. Soc.* **2004**, *126*, 418–419.
- 14 LIU, D., PARK, S. H., REIF, J. H., LABEAN, T. H., DNA nanotubes self-assembled from triple-crossover tiles as templates for conductive nanowires, *Proc. Natl Acad. Sci. USA* **2004**, *101*, 717–722.
- 15 ZHANG, Y., SEEMAN, N. C., The construction of a DNA truncated octahedron, *J. Am. Chem. Soc.* **1994**, *116*, 1661–1669.
- 16 SHIH, W. M., QUISPE, J. D., JOYCE, G. F., A 1.7-kilobase single-stranded DNA that folds into a nanoscale octahedron, *Nature* **2004**, *427*, 618–621.
- 17 MAO, C., SUN, W., SHEN, Z., SEEMAN, N. C., A DNA nanomechanical device based on the B–Z transition, *Nature* **1999**, *397*, 144–146.
- 18 YURKE, B., TURBERFIELD, A. J., MILLS, A. P., SIMMEL, F., NEUMANN, J. L., A DNA-fueled molecular machine made of DNA, *Nature* **2000**, *406*, 605–608.
- 19 YAN, H., ZHANG, X., SHEN, Z., SEEMAN, N. C., A robust DNA mechanical device controlled by hybridization topology, *Nature* **2002**, *415*, 62–65.
- 20 TURBERFIELD, A. J., MITCHELL, J. C., DNA fuel for free-running nanomachines, *Phys. Rev. Lett.* **2003**, *90*, 1181021–1181024.
- 21 SHEN, Z., YAN, H., WANG, T., SEEMAN, N. C., Paranemic crossover DNA: a generalized Holliday structure with applications in nanotechnology, *J. Am. Chem. Soc.* **2004**, *126*, 1666–1674.
- 22 PENG, L., PARK, S. H., REIF, J. H., YAN, H., A two-state DNA lattice switched by DNA nanoactuator, *Angew. Chem. Int. Ed.* **2003**, *42*, 4342–4346.
- 23 YIN, P., YAN, H., DANIELL, X. G., TURBERFIELD, A. J., REIF, J. H., A unidirectional DNA walker that moves autonomously along a track, *Angew. Chem. Int. Ed.* **2004**, *43*, 4906–4911.
- 24 ADLEMAN, L., Molecular computation of solutions to combinatorial problems, *Science* **1994**, *266*, 1021–1024.
- 25 WINFREE, E., Algorithmic self-assembly of DNA: theoretical motivations and 2D assembly experiments, *J. Biomol. Struct. Dyn.* **2000**, *11*, 263–270.
- 26 MAO, C., LABEAN, T. H., REIF, J. H., SEEMAN, N. C., Logical computation using algorithmic self-assembly of DNA triple crossover molecules, *Nature* **2000**, *407*, 493–496.
- 27 BENENSON, Y., PAZ-ELIZUR, T., ADAR, R., KEINAN, E., LIVNEH, Z., SHAPIRO, E., Programmable and autonomous computing machine made of biomolecules, *Nature* **2001**, *414*, 430–434.
- 28 RAVINDERJIT, B., CHELYAPOV, N., JOHNSON, C., ROTHMUND, P., ADLEMAN, L., Solution of a 20-variable 3-SAT problem on a DNA computer, *Science* **2002**, *296*, 499–502.
- 29 DWYER, C., POULTON, J., TAYLOR, R., VICCI, L., DNA self-assembled parallel computer architectures, *Nanotechnology* **2004**, *15*, 1688–1694.
- 30 ROTHMUND, P., PAPADAKIS, N., WINFREE, E., Algorithmic self-assembly of DNA Sierpinski triangles, *PLOS Biol.* **2004**, *2*, 2041–2053.
- 31 NIEMEYER, C. M., BURGER, W., PEPLIES, J., Covalent DNA–streptavidin conjugates as building blocks for novel biometallic nanostructures, *Angew. Chem. Int. Ed.* **1998**, *37*, 2265–2268.
- 32 STORHOFF, J. J., MIRKIN, C. A., Programmed materials synthesis with DNA, *Chem. Rev.* **1999**, *99*, 1849–1862.
- 33 BAKER, S. E., CAI, W., LASSETER, T. L., WEIDKAMP, K. P., HAMERS, R. J., Covalently bonded adducts of deoxyribonucleic acid oligonucleotides with single-wall carbon nanotubes, *Nano Lett.* **2002**, *2*, 1413–1417.
- 34 FU, T., SEEMAN, N. C., DNA double-crossover molecules, *Biochemistry* **1993**, *32*, 3211–3220.
- 35 LABEAN, T. H., YAN, H., KOPATSCH, J., LIU, F., WINFREE, E., REIF, J. H., SEEMAN, N. C., Construction, analysis,

- ligation, and self-assembly of DNA triple crossover complexes, *J. Am. Chem. Soc.* **2000**, *122*, 1848–1860.
- 36 YAN, H., PARK, S. H., FINKELSTEIN, G., REIF, J. H., LABEAN, T. H., DNA-templated self-assembly of protein arrays and highly conductive nanowires, *Science* **2003**, *301*, 1882–1884.
- 37 MATHIEU, F., LIAO, S., KOPATSCHEK, J., WANG, T., MAO, C., SEEMAN, N. C., Six-helix bundles designed from DNA, *Nano Lett.* **2005**, *5*, 661–665.
- 38 DRESSELHAUS, M. S., DRESSELHAUS, G., EKLUND, P. C., *Science of Fullerenes and Carbon Nanotubes*, Academic Press, New York, **1996**.
- 39 KASUMOV, A., KOCIK, M., GUERON, S., REULET, B., VOLKOV, V. T., KLINOV, D. V., BOUCHIAT, H., Proximity-induced superconductivity in DNA, *Science* **2001**, *291*, 280–282.
- 40 PORATH, D., BEZRYADIN, A., DE VRIES, S., DEKKER, C., Direct measurement of electrical transport through DNA molecules, *Nature* **2000**, *403*, 635–638.
- 41 STORM, A., VAN NOORT, J., DE VRIES, S., DEKKER, C., Insulating behavior for DNA molecules between nanoelectrodes at the 100 nm length scale, *Appl. Phys. Lett.* **2001**, *79*, 3881–3883.
- 42 BRAUN, E., EICHEN, Y., SIVAN, U., BEN-YOSEPH, G., DNA-templated assembly and electrode attachment of a conducting silver wire, *Nature* **1998**, *391*, 775–778.
- 43 PATOLSKY, F., WEIZMANN, Y., LIUBASHEVSKI, O., WILLNER, I., Au-nanoparticle nanowires Based on DNA and polylysine templates, *Angew. Chem. Int. Ed.* **2002**, *41*, 2323–2327.
- 44 RICHTER, J., MERTIG, M., POMPE, W., MONCH, I., SCHACKERT, H., Construction of highly conductive nanowires on a DNA template, *Appl. Phys. Lett.* **2001**, *78*, 536–538.
- 45 DENG, Z., MAO, C., DNA-templated fabrication of 1D parallel and 2D crossed metallic nanowire arrays, *Nano Lett.* **2003**, *3*, 1545–1548.
- 46 FORD, W. E., HARNACK, O., YASUDA, A., WESSELS, J., Platinated DNA as precursors to templated chains of metal nanoparticles, *Adv. Mater.* **2001**, *13*, 1793–1797.
- 47 MONSON, C. F., WOOLLEY, A. T., DNA-templated construction of copper nanowires, *Nano Lett.* **2003**, *3*, 359–363.

2

Nucleic Acid Nanoparticles

Guy Zuber, Bénédicte Pons and Andrew W. Fraley

2.1

Introduction

Primarily located in a cell's nucleus, 2'-deoxyribonucleic acid (DNA) provides the cell with the ability to store and copy the genetic information required for the synthesis of proteins that are in charge of all chemical transformations underlying the cell's metabolism. DNA is composed of four 2'-deoxynucleotides connected into a polymer via 5'-3' phosphodiester, where the sequence of the nucleotides allows the encoding of genetic information. The composition and position of heterocyclic functional groups provide a specific arrangement of hydrogen bond donors and acceptors enabling a nucleotide to hydrogen bond (or base pair) with a second nucleotide exhibiting a complementary donor/acceptor arrangement. This allows two strands of DNA to anneal in a sequence-dependent manner, where 2'-deoxyadenosine pairs with 2'-deoxythymidine and 2'-deoxyguanosine pairs with 2'-deoxycytidine, and thus further facilitates a mechanism for DNA replication and RNA transcription. Cellular DNA typically conforms to a B-form helix as first proposed in 1953 by Watson and Crick [1], where the two strands are antiparallel with the hydrophobic bases in the center of the helix and the negatively charged hydrophilic sugar-phosphate backbone on the outside (Fig. 2.1).

Although DNA is composed of only four monomers, prior to the 1970s DNA remained difficult to analyze as the typical eukaryotic cell contains nearly 3×10^9 bp of a linear double helix with an extended length of approximately 1 m [2]. Today, nucleic acids are readily manipulated by specific enzymes, produced in large quantities and progress in automation has enabled the sequencing of entire genomes, including the human genome.

Such progress coupled with an increase in the understanding of the molecular mechanisms and genetic implications underlying many diseases has triggered the hope that nucleic acids could treat disease at the source. However, many hurdles remain that must be overcome in order for gene therapy to be of practical use in the clinic. Gene therapy implies the administration of a foreign DNA fragment into a host with subsequent delivery into the nuclei of selected organ cells, where cellular machineries can, in turn, employ the new DNA for production of thera-

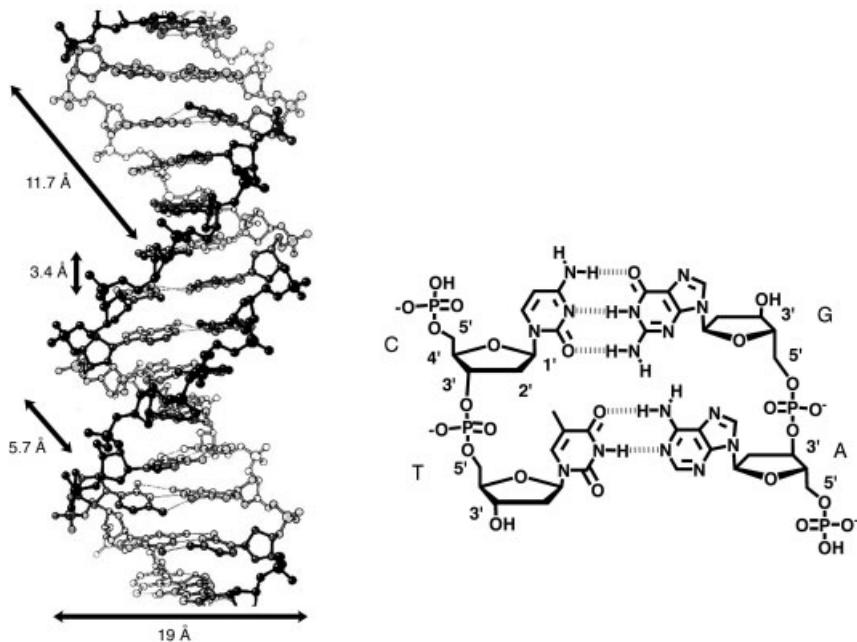


Fig. 2.1. Molecular and chemical structure of the DNA double helix. Self-complementation of the helical strands is based on the guanine (G)–cytosine (C) and adenine (A)–thymine (T) Watson–Crick base pairs.

peptic proteins. Although this method is simple in theory, naked DNA is unable to navigate the route from the needle to the nuclei and thus requires other elements to facilitate delivery into the correct cell nucleus while inhibiting the degradation of therapeutic DNA.

Viruses are natural supramolecular assemblies with gene delivery properties. Their diversity and efficiency fulfill most requirements for gene delivery in the clinic [3], but they do have drawbacks [4, 5]. They are by definition infectious and parasitic, and viral shell proteins are understood to elicit adverse immune responses from the host [6]. The production and exploitation of even weakened viral particles has risks because mass production largely exceeds recombination and mutation frequencies. The chance of producing an undesirable and harmful virus increases, and thus can present a significant risk [7]. One alternative is the development of synthetic vectors that interact with DNA in abiotic systems to form virus-like nanoparticles [8]. The requirements for safe DNA transportation into the nucleus have been set by studies on the fate and trafficking of viruses or drug delivery systems at the animal and cellular levels [9]. *In vitro*, gene delivery is predominantly concerned with barriers presented by the cell itself. In an animal, the delivery systems must also be concerned with supracellular barriers that restrict the size of the drug delivery system to less than 100 nm in diameter. Larger par-

ticles introduced in the body intravenously encounter all the blood constituents and cannot cross the blood vessel walls. They are eliminated by hepatic or renal uptake. Local administration, if possible, could circumvent the circulation problems, but particles still encounter barriers in the form of the extracellular matrix that prevent cell accessibility to low-mobility particles. Ligand-mediated cellular uptake might be size dependent as well. It was shown, for instance, that glycolipid-containing liposomes with a size of 30–70 nm were effectively taken up by the asialoglycoprotein receptor *in vitro* and *in vivo*, whereas 90-nm particles were not [10]. The next step, intracellular trafficking and nuclear import, is also a size-restricted process. It was shown by measuring cytoplasmic diffusion of microinjected fluorescent DNA that DNA molecules larger than 1 kbp are essentially immobile. Finally, assisted nuclear pore crossing through nuclear pore complexes (gates between the cytosol and the nucleus) was reported to be restricted to particles up to 39 nm. An ideal vector must interact with a plasmid in such a way to: (a) form particles of minimal size, (b) protect the DNA from nuclease degradation, (c) provide efficient circulation properties in the host, (d) mediate cell-specific internalization, (e) allow mobility in the cytosol and (f) favor intracellular routing into the nucleus, where the genetic material must be effectively liberated from carrier molecules (Fig. 2.2).

The development of effective nucleic acid carriers must consider the above properties, while accounting for the chemical and physical properties of the therapeutic DNA. Section 2.2 gives an overview of the chemical and physical properties of therapeutic DNA. Section 2.3 presents an approach to prepare DNA particles containing a single DNA molecule (the minimal particle size possible) as well as their characterization and properties. Section 2.4 presents strategies for the functionalization of DNA particles and Section 2.5 presents an example of how to prepare DNA nanoparticles with cancer cell targeting elements.

2.2

The Chemical and Physical Properties of Therapeutic DNA

DNA administered into an animal (*in vivo*) must physically contact the surface of a target cell before cellular uptake can occur. The stability, size and charge of the therapeutic DNA coupled with the organization of host tissues into specialized organs seriously complicates the accessibility of targeted cells.

First, native DNA in the blood stream is subjected to fast degradation. Upon injection into a mouse vein, plasmid DNA is removed from the circulation and degraded within a few minutes by hepatic clearance at a rate almost identical to the hepatic plasma flow rate (1.6 mL min^{-1}) [11]. The delivery of DNA in either *in vivo* or *in vitro* systems is further impeded by the immense mass of DNA that must be delivered (Fig. 2.3). Not only is a gene almost 20 times heavier than the protein it encodes, additional sequences must be added to enable *in vivo* handling and production. To facilitate cellular activity the gene is then cloned into a plasmid, which contains accessory sequences for expression in mammalian cells or cloning into

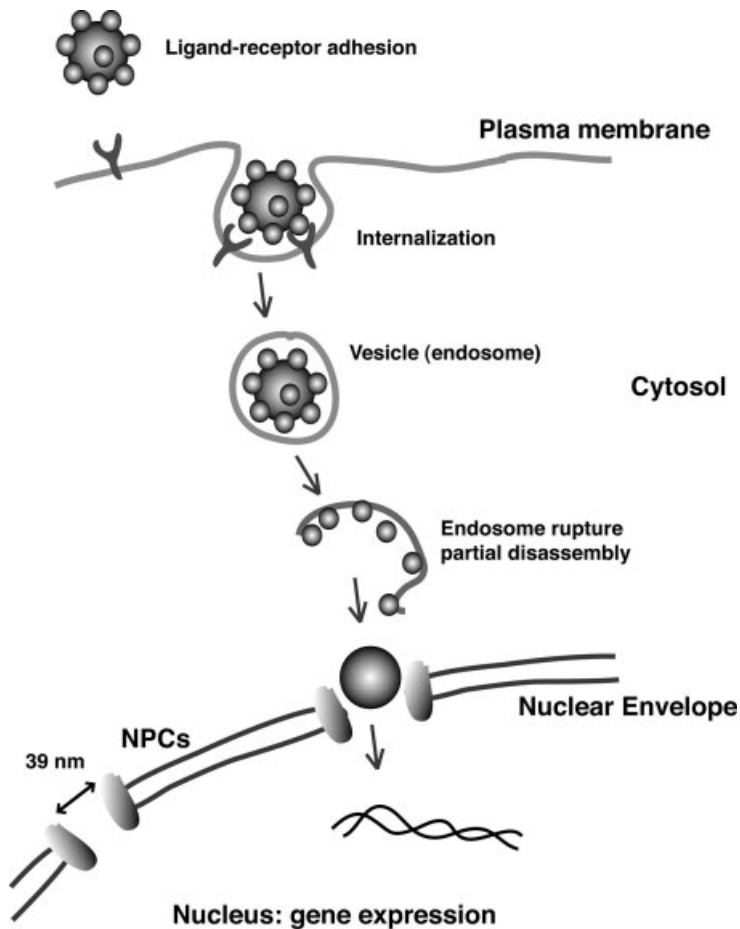


Fig. 2.2. Intracellular pathway for gene delivery. NPC: nuclear pore complexes.

bacteria. Typically, a recombinant plasmid is circular and around 5000 bp in length, with a molar mass of more than 3 MDa. Finally, the polyanionic character of the DNA deoxyribose–phosphate backbone prevents not only passive diffusion across cellular membranes consisting of hydrophobic lipid bilayers, but also the folding of the plasmid into a compact and globular tertiary structure. DNA prefers to exist in a stiff helix that occupies a large volume, which considerably limits mobility [12], particularly in the dense cytoplasm packed with intertwined filaments [13]. Foreign DNA entering fast dividing cells in culture is more readily expressed as it is possible that free and intact DNA plasmids, sitting immobile in the cytoplasm, are transported with chromosomes during mitosis and become incidentally sequestered in the nuclei of daughter cells after reconstruction of the nuclear membrane [14].

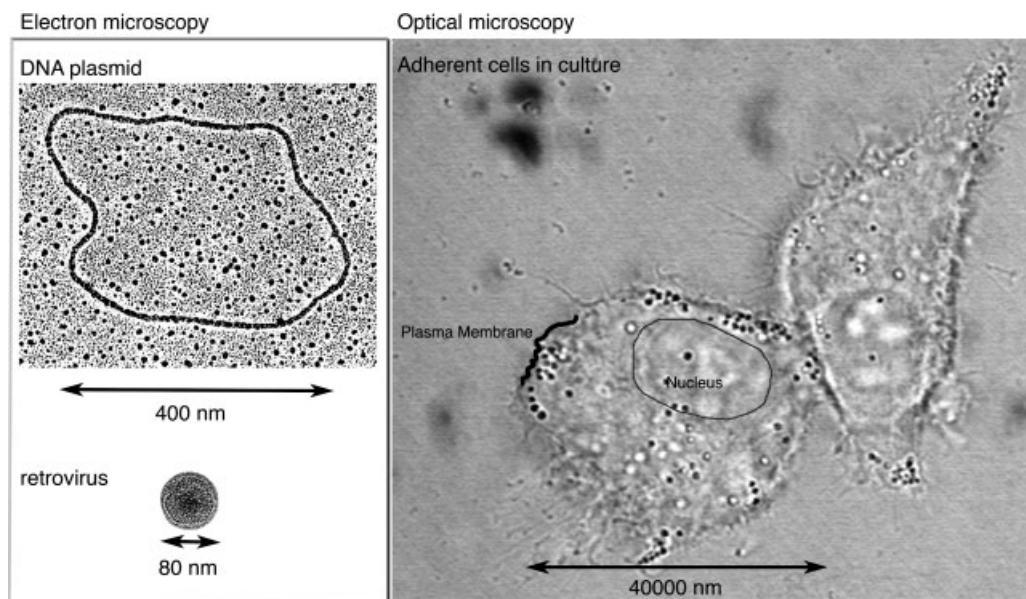


Fig. 2.3. Comparison of sizes of a plasmid, a virus and a cell. The length of a plasmid and its worm-like behavior in solution, as represented by electron microscopy, greatly limits its diffusion properties. The natural polymer is rather degraded. Optical microscopy shows an epithelial cell in culture.

For its expression, the gene must contact the cell, cross the plasma membrane, diffuse into the cytoplasm and go into the nucleus without being degraded. Its condensation in specialized assemblies such as 80-nm viral particles greatly improves its biodistribution and transport into the cell nuclei.

Theoretically, both *in vivo* biodistribution and intracytoplasmic trafficking of a plasmid into a given nucleus is improved by the condensation of a single plasmid molecule. By calculation, the volume occupied by a plasmid corresponds to a sphere approximately 25 nm in diameter. Single plasmid condensation into minimal size particles may even permit gene delivery into nondividing cells as nuclear localization signal peptide (NLS) sequences derived from the viral SV40 large tumor antigen assist the entry of macromolecules as large as 39 nm in diameter into the nucleus through nuclear pore complexes [15].

2.3

Preparation of Nucleic Acid Nanoparticles: Synthesis and Characterization

2.3.1

Rationale

Condensation of the worm-like DNA polymer into a dense particle does not only enhance chemical stability, but additionally improves the dynamic properties of

the polymer with a 10^4 – 10^5 decrease in the effective volume [16]. To give a macroscopic example, a firemen's hose is best transported and handled in a condensed state around a reel, even though the reel adds weight to the system. The compaction of naked DNA into a dense particle is a highly unfavorable process due to the electrostatic repulsion of the charged phosphodiester groups distributed every 7 Å along the backbone. The increase in electrostatic repulsion and competition with other anions could be annihilated by additive effects of Coulomb's interactions using polycationic polymers [16] or cationic surfaces obtained by aggregation of cationic amphiphiles into bilayers or micelles [17]. Although the number and variety of cationic agents are infinite, the formation of DNA condensates is almost entirely driven by electrostatic contributions. Fast kinetic associations of cationic materials with the long DNA polymer typically yield the entrapment of several DNA plasmids and detailed mechanistic studies indicated that DNA condensation proceeds through folding rather than winding. Overall, the nature of the cationic vector dictates the supramolecular organization of the complexes, whereas the stoichiometry and incubation conditions (temperature, ionic forces) impact the final sizes of the DNA condensates [18]. Structural investigations using atomic force microscopy [19, 20] or electron microscopy [21] showed that DNA–cationic polymer complexes display a toroidal or spherical structure of 40–100 nm in diameter. Interaction of DNA with cationic lipid organized in bilayers produces DNA sandwiched into lamellar phases (Fig. 2.4). On the other hand, DNA–cationic lipid complexes adopt an inverted hexagonal phase structure in the presence of DOPE, a lipid well known to induce an inverted hexagonal phase in solution because of its conical shape (Fig. 2.4) [22]. The large contribution of electrostatic interactions also impacts on the colloidal stabilities of these particles. Additional aggregation occurs when ionic surfaces become shielded by other ions (such as physiological conditions) or when the vector/DNA charge ratio approaches the isoelectric point [23, 24]. For transfection into cultured cells, large and positive complexes are advantageous because they sediment onto cells and enter cells by adhesion to ubiquitously expressed anionic receptors present on the cell membranes [25]. Cationic DNA nanoparticles are currently being evaluated for clinical applications [26, 27]. Covalent conjugation of a layer of polyethylene glycol (PEG) onto surfaces greatly enhances the stability and lifespan of biomaterials in the bloodstream [28] or in nasal mucosa [29] by its hindrance and inertness. Inclusion of cell-targeting motifs has further been demonstrated to improve gene delivery to tumors [30] or to liver [31]. Covalent prosthetic groups may interfere with proper DNA condensation [32], complicating these modifications. Theoretically, drastic improvements could be achieved by lowering further the size of the delivery systems to the minimal size (a particle containing a single plasmid) [33].

Cationic detergents, such as cetyltrimethylammonium bromide (CTAB) (see Fig. 2.9 below), have been reported to condense DNA plasmids into homogeneous particles consisting solely of a single plasmid [34]. The formation of these complexes is governed by electrostatic interactions between a single surfactant cationic head and the DNA phosphate group. This initial bimolecular adhesion is immediately followed by aggregation of the surfactant in a highly cooperative manner, leading

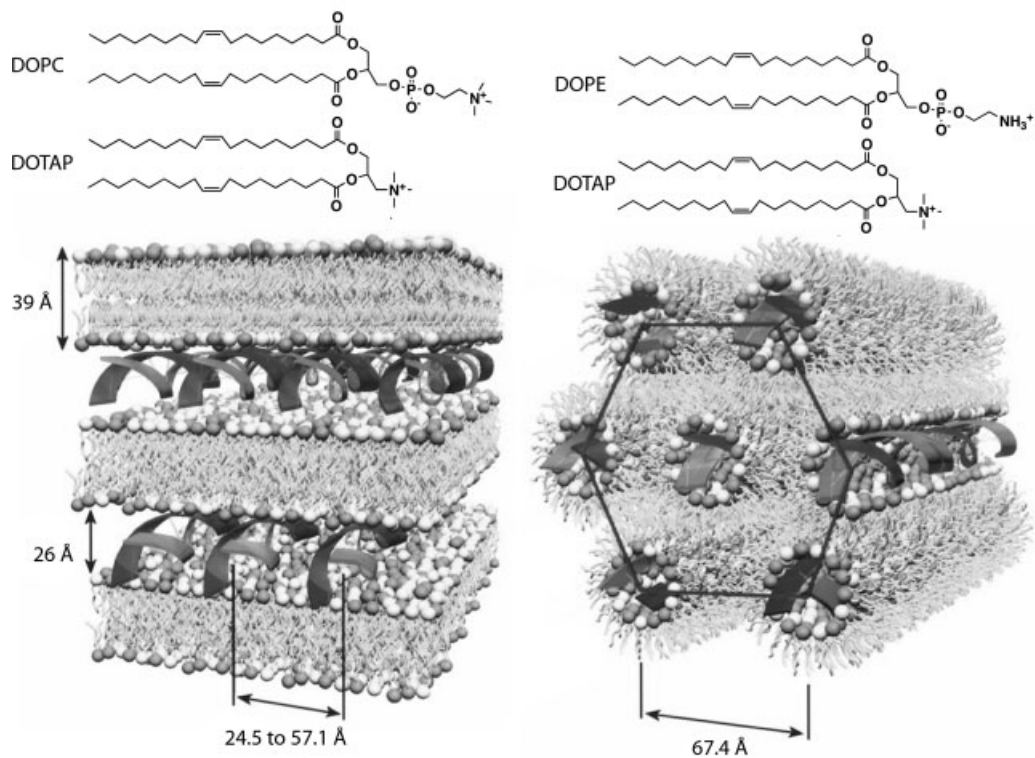


Fig. 2.4. Structure of DNA–cationic lipid complexes in lamellar and inverted hexagonal phases. The inverted hexagonal phase is a consequence of the high content of DOPE (70%) in the lipid phase. (Adapted from Ref. [22].)

to single DNA plasmid collapse. However, fast equilibration between monomeric surfactants and micelle domains produces a fast destabilization of surfactant–DNA complexes upon dilution or addition to cellular bilayer membranes.

An appealing solution to this problem is to combine the favorable features of cationic surfactants for DNA condensation and cationic lipids for assembly stability. The chemical transformation of a cationic detergent into an amphiphile within a DNA–vector complex should lead to stable and monomolecular DNA particles. A chemical transformation of this type must remain inert toward the proximal DNA plasmid to ensure the integrity of genetic information. The air-oxidation of two thiols into a disulfide is a suitable answer and has the additional benefit that thiol-based cationic detergents are readily synthesized.

The proof of this concept was demonstrated by Blessing et al. using a cationic detergent containing a cysteine and a C_{10} alkyl chain ($C_{10}CysG^+$) (Fig. 2.5) [35, 36]. A plasmid was first condensed with a cationic detergent having a free thiol. The concentration of the detergent was kept slightly below its critical micellar con-

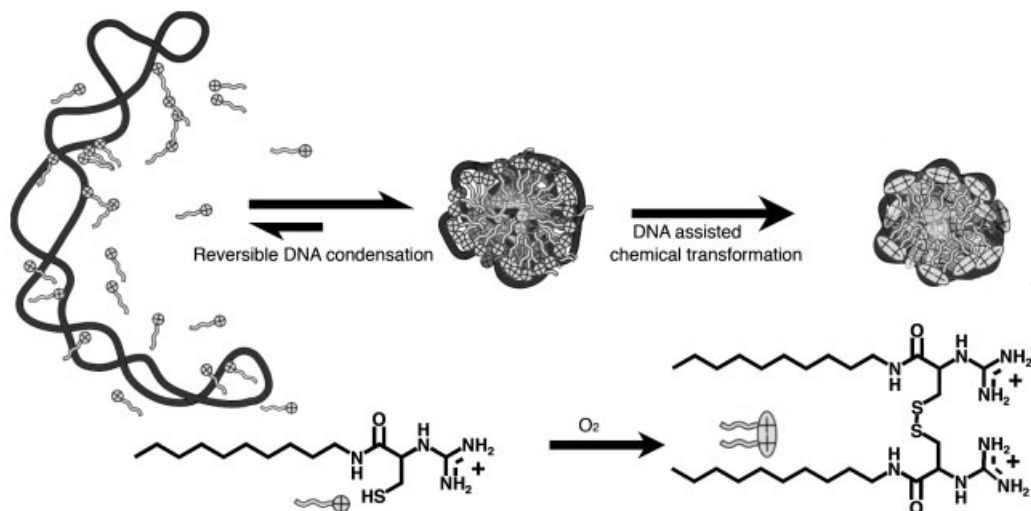


Fig. 2.5. Formation of stable 25 nm diameter globular assembly containing a single DNA plasmid. The plasmid is condensed by a thiol-containing detergent (C₁₀CysG⁺) and the resulting particles are stabilized by template-assisted oxidation of the thiol functions into disulfides.

centration to protect polycationic surfaces from micelle formation and the entrapment of more than one plasmid. Under these conditions, individual phosphate neutralization of the plasmid yields favorable hydrophobic association of detergent molecules into micelle–DNA complexes and the increased concentration of thiol groups around the collapsed DNA polymer in turn favors intracomplex detergent dimerization. According to this theory, oxidative detergent dimerization is expected to be prone to a template effect from the DNA. Kinetic studies confirm this theory – an enhanced thiol oxidation rate was observed in the presence of plasmid DNA (Fig. 2.6).

Upon dimerization of the detergent C₁₀CysG⁺, single plasmids of 5.6 kbp are condensed into a homogeneous population of spherical liponucleic assemblies with a mean diameter of 25 ± 4 nm as determined by transmission electron microscopy. A rough calculation using the volume occupied by a plasmid of 5.6 kbp and 1.1×10^4 detergent molecules (the charge equivalent) yields a spherical assembly with a diameter of 28 nm, confirming monomolecular collapse of the plasmid into a single particle. Moreover, diameters of particles resulting from detergent-mediated aerobic collapse of supercoiled pCMVLuc (5.6 kbp) as well as linear phage λ (48 kbp) and phage T4 (166 kbp) were measured by laser light scattering (Fig. 2.7). Particle diameters plotted against the cubic root of the number of DNA base pairs fit a straight line crossing the origin. Since the volume of a sphere varies as the cube of its size, this result provides further evidence of DNA monomolecu-

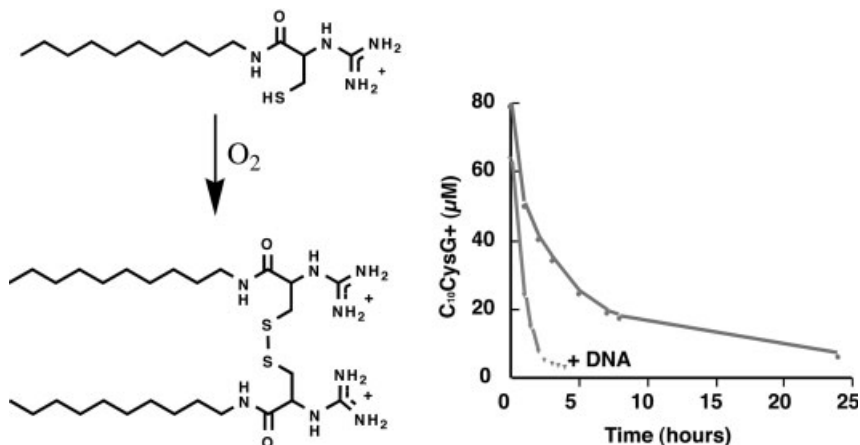


Fig. 2.6. Oxidation of C₁₀CysG⁺ occurs faster in the presence of template DNA.

lar collapse. Interestingly, the ζ potentials of (C₁₀CysG⁺)₂-DNA complexes were found to be negative (-45 to -40 mV) at the isoelectric point. This particular property may be explained by the fact that the DNA backbone constitutes the interface between the aqueous phase and a frozen micellar core. A negative ζ potential also suggests that charge repulsion of the nanoparticles may account for the observed colloidal stability. Unfortunately, this short-chain cysteine detergent C₁₀CysG⁺ and its corresponding gemini cysteine-lipid proved unsatisfactory for biological applications, but led to further investigation of novel amphiphiles.

2.3.2

Synthesis, Characterization and Optimization of Surfactants

The design of a dimerizable detergent must be tuned so the critical micellar concentration for its monomeric form exceeds the DNA phosphate concentration to elicit monomolecular plasmid collapse. Additionally, once oxidized, the gemini surfactant must also exhibit a low solubility to enable stability in biological conditions. Exploration of dimerizable detergents with the above qualities was accomplished by preserving the cysteine as the reactive agent, but with modification to the polar head group and hydrocarbon chain length. Solid-phase synthesis is well adapted for this investigation and provides a mean for the preparation of a large number of different surfactants (Fig. 2.8) [37].

Fortunately, knowledge of surfactant behavior reduces the possible molecules to only a small quantity (Fig. 2.9). Changing the polar head group to ornithine (two positive charges) or spermine (four positive charges) increases both DNA affinity and detergent solubility (e.g. the critical micellar concentration), while lengthening the hydrocarbon chain, in turn, favors an increase in surfactant association and off-

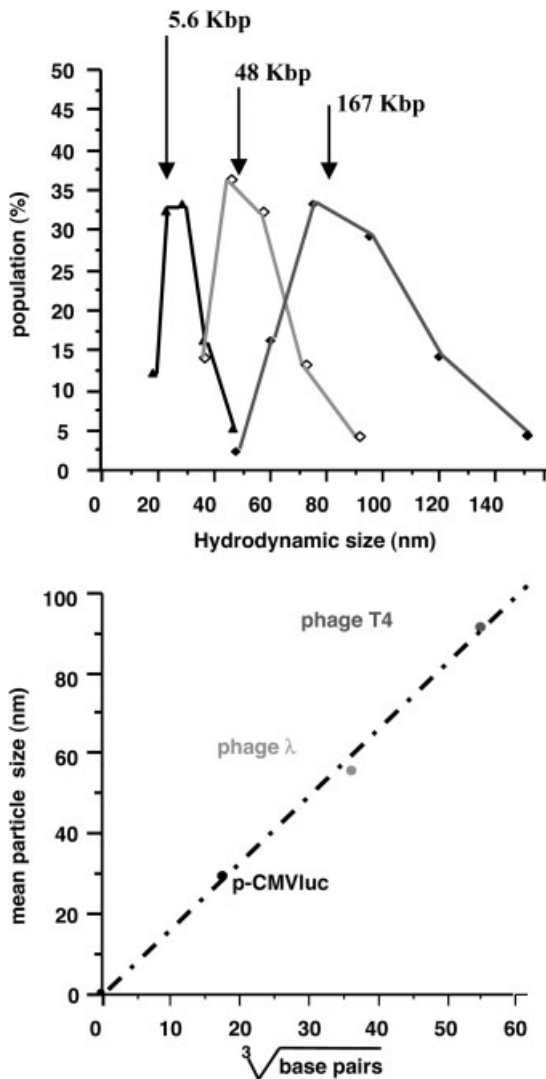


Fig. 2.7. Particle sizes vary as the cubic root of the DNA size, adding more evidence to DNA monomolecular collapse. Particle diameters were determined by light scattering.

sets the increase in solubility (Table 2.1). Typical plasmid concentrations for gene delivery experiments are in the 10–50 μM range, suggesting that C_{14}CO (critical micellar concentration = 45 μM) is the most likely surfactant/gemini lipid candidate for effective monomolecular plasmid condensation [38].

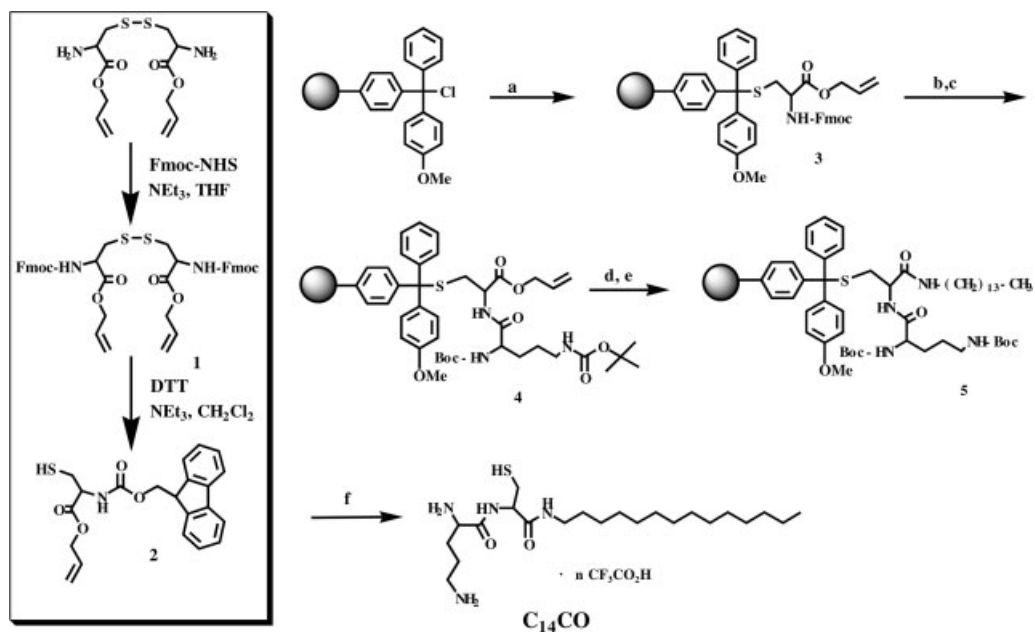


Fig. 2.8. Solid support synthesis of the cationic detergent $C_{14}CO$. Inset: preparation of protected cysteine. (a) **2**, DIEA, CH_2Cl_2 ; (b) 20% piperidine, DMF; (c) Bis-Boc-ornithine,

PyBOP, DIEA, DMF; (d) $Pd(PPh_3)_4$, $CHCl_3$ /AcOH/*N*-methylmorpholine (37:2:1); (e) tetradecylamine, PyBOP, DIEA, DMF; (f) TFA. (Adapted from Ref. [37].)

Validation of the $C_{14}CO$ detergent for stable DNA nanoparticle formation was accomplished by employing a circular 5.6-kbp DNA plasmid with the surfactant at 1/1 charge ratio close to the isoelectric point. The complexes stabilized via DNA-templated air oxidation of the free thiol groups. A gel-retardation assay was used to assess complex formation between plasmid DNA and cationic surfactant (Fig. 2.10). Upon application of an electrical field, molecules or complexes move through the agarose gel at a rate proportional to their charge, but inversely proportional to their volume. Examination of the DNA particle cohesion by agarose gel electrophoresis resulted in a single band with an increase in electrophoretic mobility with respect to the naked plasmid. This result provides evidence that these particles are highly stable in an electric field, where reversible electrostatic interactions would easily be destroyed. Charge neutralization of the DNA phosphate groups and an increase in molecular mass due to the addition of the surfactants should yield a slower migration. However, when one considers that naked DNA tends to move through agarose gel in a snake-like motion, the compaction of the plasmid into a small globular structure can speed migration as there is less entanglement with the gel matrix [37].

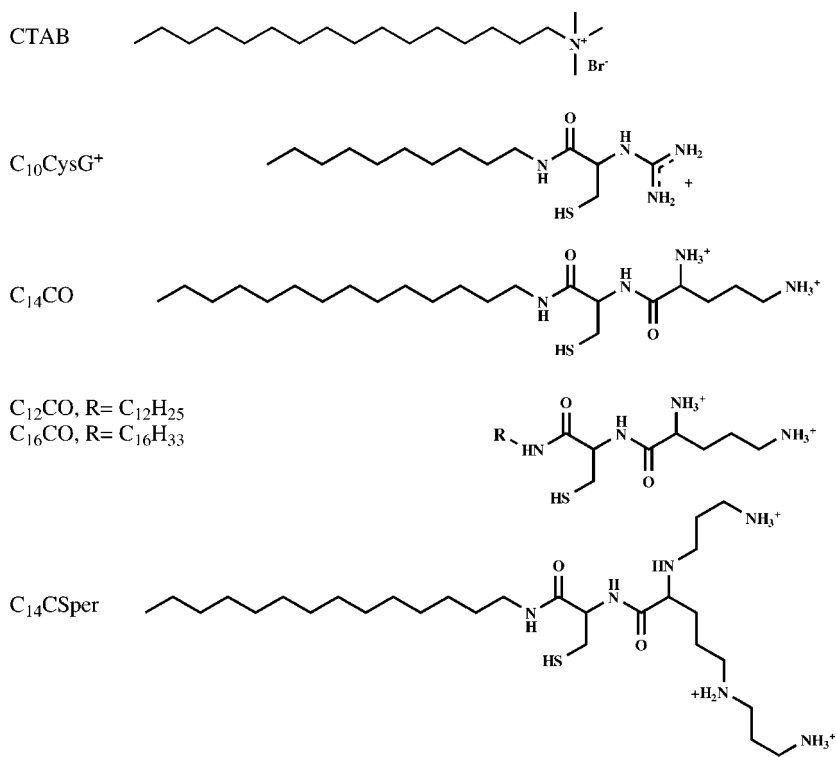


Fig. 2.9. Structure of cationic surfactants.

Tab. 2.1. Parameters describing the stabilities of surfactant–DNA complexes

	<i>Critical micellar concentration (μM)^[a]</i>	<i>Critical aggregation concentration (μM)^[a]</i>	<i>ΔG ($kJ mol^{-1}$)^[b]</i>
CTAB	250	5	−28.0
$C_{10}CysG^+$	100	2.5	−29.5
$(C_{10}CysG^+)_2$		0.4	−33.6
$C_{14}CO$	45	1	−31.9
$(C_{14}CO)_2$		0.0001	−45.8
$C_{12}CO$	100		
$C_{16}CO$	20		
$C_{14}Csper$	150		

^aThe critical micellar concentration and the critical aggregation concentration are measured in HEPES 20 mM, pH 7.4.

^b ΔG is the free energy associated with the binding of the surfactant to DNA. Data adapted from Ref. [40].

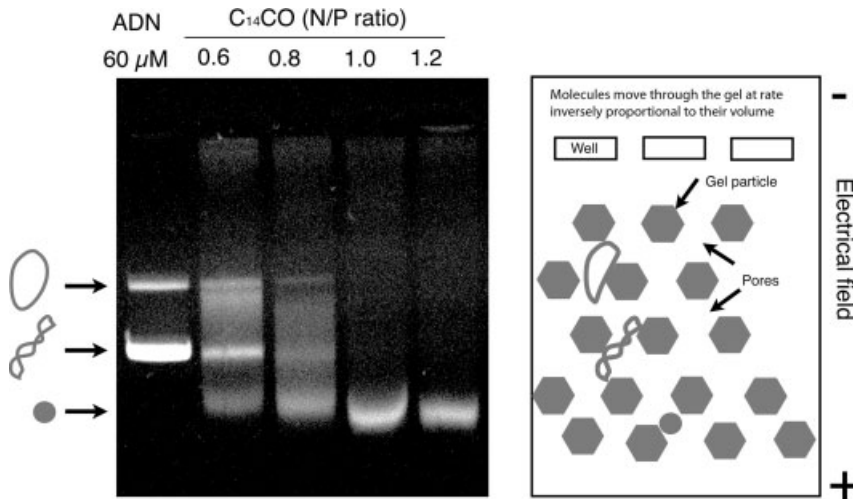


Fig. 2.10. Agarose gel electrophoresis of $(C_{14}CO)_2$ -plasmid complexes and schematic explanation of the difference in mobility.

2.3.3

Organization of the Surfactant–DNA Complexes

Lipid/surfactant domain stabilities can be further evaluated from examination of morphologies within the lipid phase of DNA complexes. The presence of order within DNA particles indicates strong DNA packing and, by extension, quasi-irreversible amphiphile aggregation. Transmission electron microscopy of oxidized $(C_{10}CysG^+)_2$ -DNA complexes resulted in a homogeneous population of nearly spherical objects that do not display an internal orderly structure (Fig. 2.11). In contrast, oxidized $(C_{14}CO)_2$ -DNA particles appeared as a population of 25 nm diameter spheroids that display variable texture from one particle to another. The irregular particle texture appears to be a consequence of close DNA packing induced by quasi-irreversible $(C_{14}CO)_2$ associations into tubes. A similar ultrastructure was observed previously with lipoplexes formed with another polycationic lipid (Transfectam) [39].

2.3.4

Quantification of the Stability of Surfactant–DNA Complexes

Association of detergents/amphiphiles with a plasmid can further be characterized by determination of the critical aggregation concentration [40]. The critical aggrega-

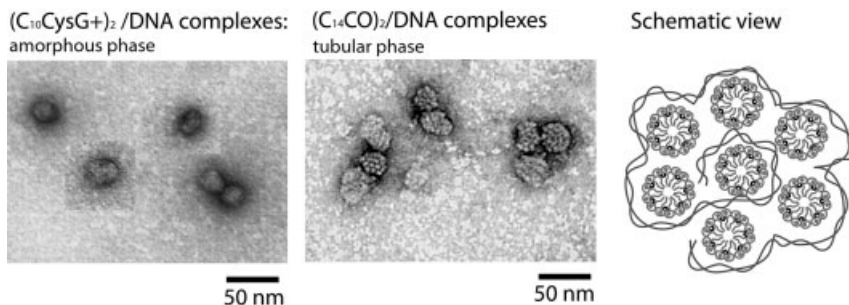


Fig. 2.11. Morphology of surfactant–plasmid complexes. Observation was performed by electron microscopy and complexes were stained with uranyl acetate.

gation concentration corresponds to the concentration of free surfactant necessary to initiate the formation of a micelle like domain on the DNA template. This value depends both on the affinity of the cation for DNA phosphate and the ability of the lipid chain to form micellar structures (characterized by the critical micellar concentration). Using fluorescence quenching of the DNA intercalating agent YOYO-1 upon DNA condensation, critical aggregation concentrations of 1, 2.5 and 5 μM were obtained for C_{14}CO , $\text{C}_{10}\text{CysG}^+$ and CTAB, respectively. These values followed the same trend as the critical micellar concentration, but shifted to lower values (by a factor of 40–50), highlighting the critical role played by electrostatic interactions in the DNA condensation around micelle domains. The stabilities of the gemini surfactant after DNA-assisted oxidation could be also quantified by determination of their critical aggregation concentration. The critical aggregation concentration of the dimeric surfactant $(\text{C}_{10}\text{CysG}^+)_2$ is still in the micromolar range and is reduced only by a factor of 3 by comparison to the critical aggregation concentration of the corresponding monomer. On the contrary, the critical aggregation concentration of the dimeric $(\text{C}_{14}\text{CO})_2$ falls in the nanomolar range and is dramatically reduced by a factor of 10^3 by comparison to the critical aggregation concentration of the monomeric C_{14}CO .

One critical aspect in the use of surfactants for gene therapy is the stability of the DNA–surfactant complexes during dilution in the cell culture medium and in the presence of cellular plasma membranes. External and internal leaflets of the plasma lipid bilayer are modeled by using either neutral or anionic lipid vesicles. Surfactant displacement from DNA complexes into bilayers induces, in turn, DNA decondensation that can be easily monitored using fluorescence probes (Fig. 2.12). With CTAB–DNA and $(\text{C}_{10}\text{CG}^+)_2$ –DNA complexes, the addition of anionic lipid vesicles, and to a lower extend neutral lipid vesicles, leads to almost complete DNA decondensation. In contrast, the addition of both types of vesicles to $(\text{C}_{14}\text{CO})_2$ –DNA particles is unable to induce DNA release, confirming the stabilities of these particles and their putative biomedical applications.

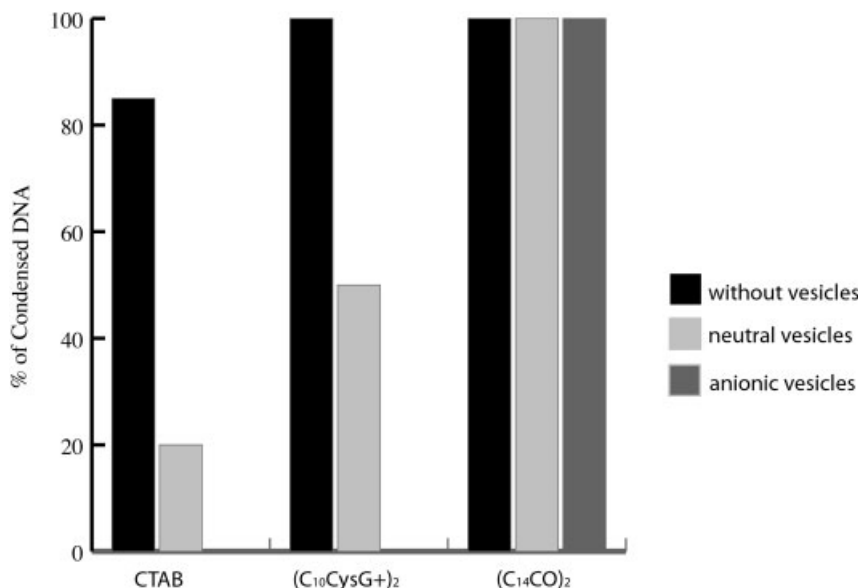


Fig. 2.12. Stability of surfactant–DNA complexes upon interactions with bilayer membranes. (Adapted from Ref. [40].)

2.4

DNA Functionalization for Cell Recognition and Internalization

2.4.1

Strategies for Functionalization

Preparation of nanometric DNA vehicles with the minimal size is necessary, but not sufficient, for gene delivery. (C₁₄CO)₂–DNA nanoparticles have overall negative surfaces and are unable to anchor to cell membranes. As a consequence, they do not transfect cells. The use of such scaffolds requires various components for cell-specific internalization. The decoration of surfactant–DNA complexes with components can be accomplished by anchorage within the hydrophilic surfactant core of a lipid bearing a selected ligand or by anchorage to DNA itself. Characterization of stabilized micelle–DNA complexes indicates that the plasmid is at the surface of the particles, which allow possible anchorage to DNA.

The view that DNA is only a polyanionic polymer is in reality a gross oversimplification. Multiple factors such as base stacking, Watson–Crick hydrogen bonding and sugar conformation enable two negatively charged strands of DNA to anneal into the classical B-form helical duplex (Fig. 2.13). The DNA helical structure affords the binding of other molecules by three common motifs. Without disrupting the Watson–Crick base pairing, planar aromatic molecules are able to intercalate between base pairs. The availability of hydrogen bond donors and acceptors in the major groove allows for triple helix formation via Hoogsteen base pair formation.

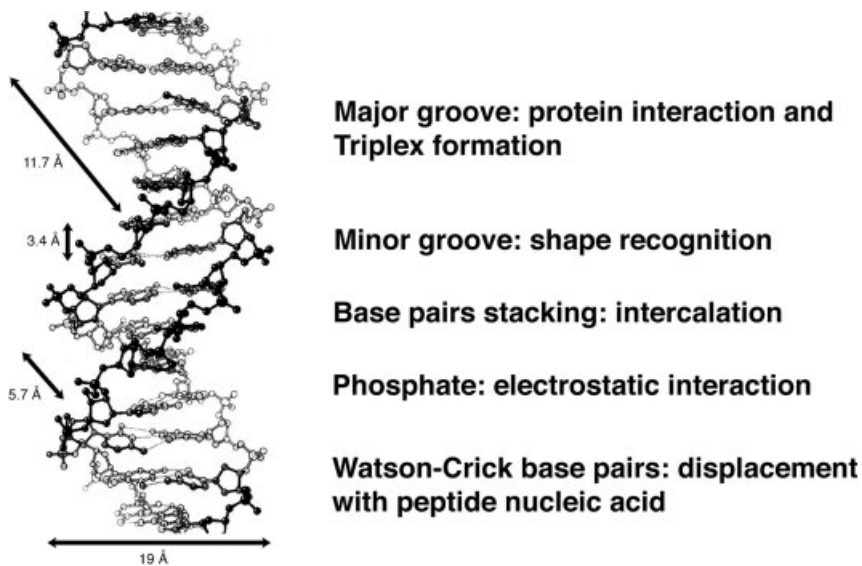


Fig. 2.13. DNA recognition by molecules may use (a) the major groove with formation of Hoogsteen base pairs, (b) the phosphate backbone by electrostatic interaction, (c) the minor groove by shape recognition or (d) base pair stacking with intercalation. Alternatively, one strand could be invaded with polymer forming novel Watson–Crick base pairs.

Likewise, the shallow minor groove enables binding of small molecules such as distamycin or Hoechst 33258 [41].

2.4.2

Intercalation

Several planar aromatic small molecules are able to intercalate into the DNA duplex [2]. Intercalation occurs generally where the base-pair stacking association is higher and produces a sequence preference binding in between stacked 5'-GC-3' base pairs. The affinity of a single intercalator is relatively weak (in the micromolar range). Kinetic analysis indicates that intercalation is in the millisecond range and is preceded by fast diffusion binding at the outside of the double helix, presumably by interaction in the minor groove. Dimerization of two intercalating agents increases the stability of intercalation to where bis-intercalators are able to be used to fluorescently tag DNA duplexes for cellular trafficking studies [42].

The quasi-irreversible properties of intercalation have been exploited to functionalize plasmids with transferrin, a protein that is understood to facilitate cellular entry via receptor-mediated endocytosis (Fig. 2.14) [43]. Human transferrin tethers two identical carbohydrate chains attached by *N*-glycosylation to asparagines 413 and 611, where the glycans are composed of a mannotriosidodi-*N*-acetylchitobiose core bearing two *N*-acetylneuraminy-*N*-acetylglucosamine units. The glycans do

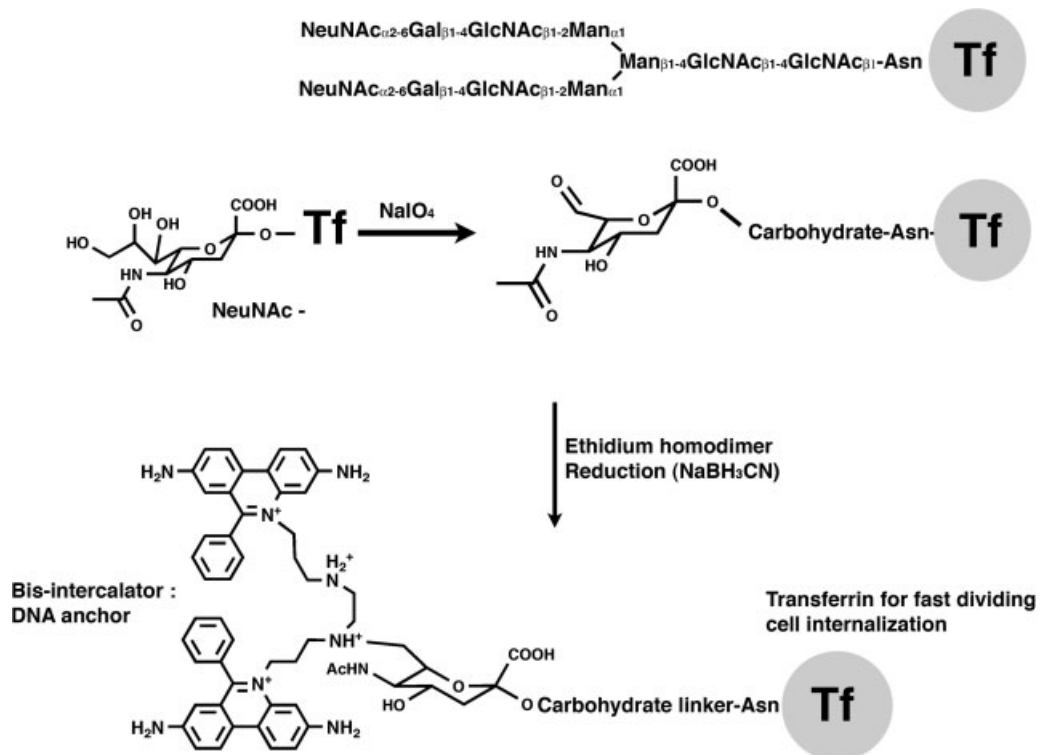


Fig. 2.14. Selective conjugation of a strong DNA binding intercalator to the two glycosylation sites of transferrin (Tf). (Adapted from Ref. [43].)

not have any known involvement or influence on cell surface receptor binding and thus have the potential for exploitation as spacers for the site-specific attachment of nucleic acid-binding domains. Within the sugar chain, the terminal *N*-acetyl neuraminic acid has vicinal diols that are readily oxidized by sodium periodate, producing a transferrin displaying aldehyde groups. Reductive amination of the aldehydes with a bis-intercalating ethidium homodimer results in a new transferrin covalently linked to a DNA high-affinity anchor. Although anchorage efficiency was not fully characterized, DNA–transferrin conjugate complexes were observed to enter cells by endocytosis, presumably after transferrin binds to its corresponding cellular membrane receptor.

2.4.3

Triple Helix Formation with Oligodeoxyribonucleotides

In 1987, Claude Hélène's and Peter Dervan's research groups simultaneously demonstrated that oligodeoxyribonucleotides form stable sequence-specific triple

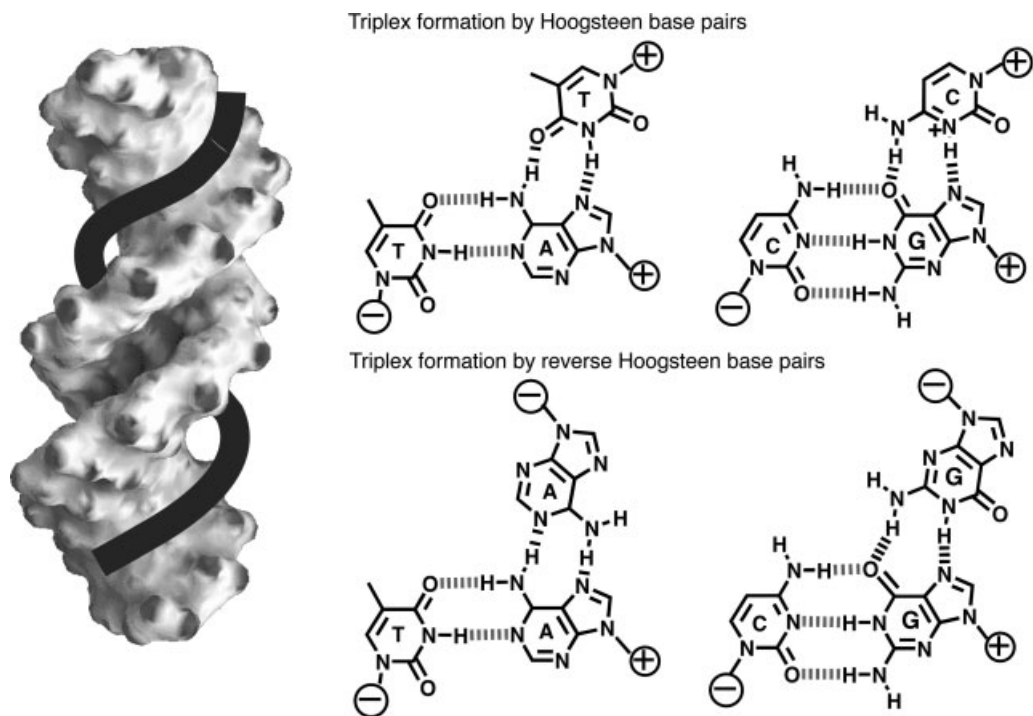


Fig. 2.15. DNA recognition from the major groove by triple helix formation with an oligonucleotide forming Hoogsteen or reverse Hoogsteen base pairs.

helices in the major groove of DNA duplexes under conditions close to physiological conditions [44, 45]. DNA triplex formation obeys specific rules imposed by structural constraints; consequently, only a few sequences are viable targets for triplex formation. (Fig. 2.15).

Specifically, homopurine tracts are required for the third strand homopyrimidine to bind via Hoogsteen hydrogen bonds. This binding motif yields the third strand in a parallel orientation to the homopurine strand in the duplex. Additionally, homopurine stands can specifically bind with homopurine tracts in an antiparallel fashion by forming reverse Hoogsteen-type hydrogen bonds between the same nucleobase (recognition of dG by dG and dA by dA) [46]. Thermodynamic and kinetic parameters indicate that selected triplex-forming oligonucleotides of about 20 nucleotides have high affinities for their corresponding duplex targets. In particular, a 24 mer homopurine sequence coupled to the NLS forms a stable triplex with a target duplex at intracellular potassium concentrations with a residence time of 24 h (Fig. 2.16) [8].

DNA third strand–NLS conjugates have further been exploited to functionalize plasmids specifically cloned with several triplex host sequences. Although cova-

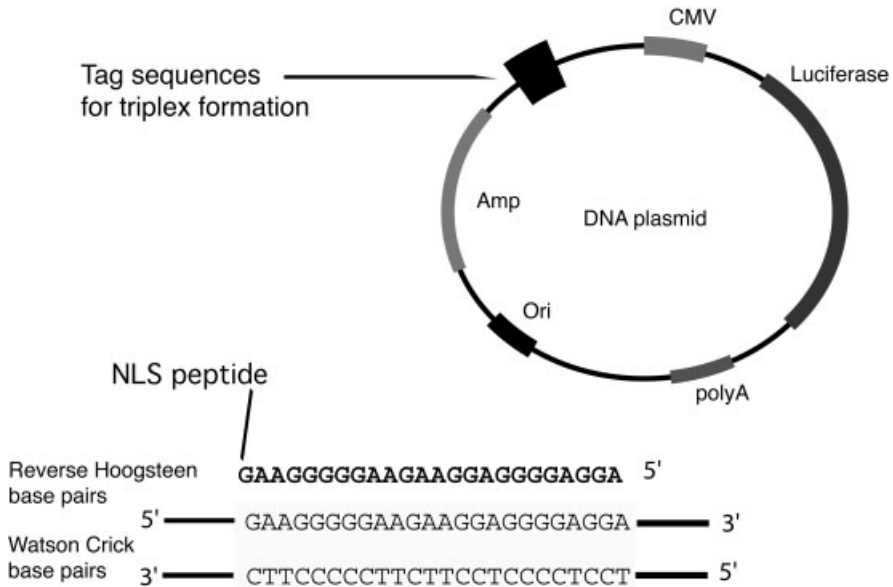


Fig. 2.16. Conjugation of a NLS peptide (–PKKKRV–) to a plasmid by triple helix formation. The system requires the preparation of the plasmid with tags for triplex formation in unread regions of the plasmid.

lently functionalized plasmids are not the ideal constructs for gene delivery, triple helix formation may provide a mechanism to sequence specific covalent attachment to plasmids at unread sequences [47]. Covalent sequence-specific peptide conjugation employing triplex formation was accomplished using a psoralen–DNA–peptide conjugate. After triplex formation, the psoralen was in the correct location to adduct formation of a site-specific peptide–DNA conjugate by UV activation.

2.4.4

Peptide Nucleic Acids (PNAs)

A PNA is an oligonucleotide analog in which the phosphodiester–sugar backbone is replaced by a polyamide composed of a repeating *N*-(2-aminoethyl)-glycine unit (Fig. 2.17). The nucleobases are attached to the polyamide through methylene carbonyl linkers to produce a polymer remarkably isomorphic in terms of geometry and spacing in comparison to native oligonucleotides. The neutrality of the polyamide favors hybridization to target DNA sequences compared to the charge repulsion of native duplex formation. Plasmid denaturation and annealing in the presence of PNA enables sequence specific PNA hybridization via Watson–Crick base pairing and displacement of the complement strand.

Branden et al. conjugated a NLS peptide to a PNA strand that hybridized to 11

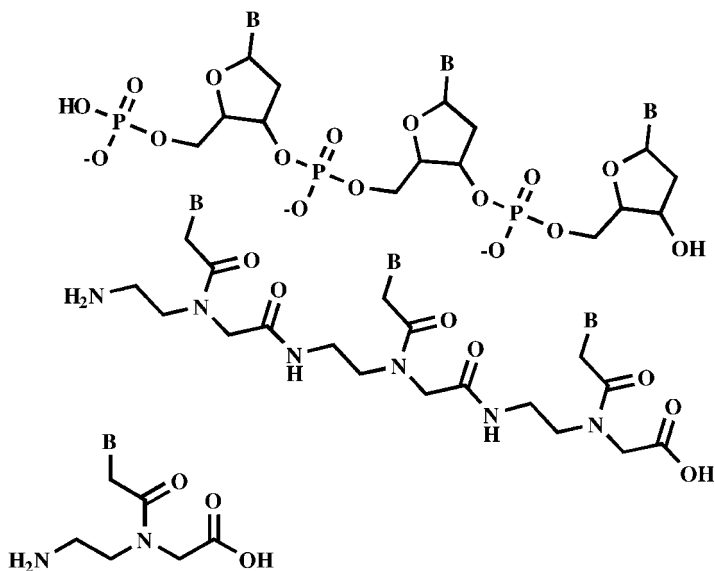


Fig. 2.17. Size comparison between a natural DNA strand and its isomorphous “peptide nucleic acid” based on a *N*-(2-aminoethyl)glycine backbone. B: nucleobase.

sites previously cloned into a plasmid containing the gene for the green fluorescent protein (GFP). The NLS–PNA conjugates were docked by a heat-induced denaturation of the plasmid (hybridization by strand displacement), and the (NLS–PNA)₁₁–plasmid complexes were delivered into cells using polyethylenimine (PEI) or a cationic lipid formulation. Transfection efficiency was increased 8-fold with respect to the untagged plasmid [48]. Recently, Vaysse et al. reported the employment of a NLS–PNA conjugate for strand invasion at room temperature via a triple-helix motif [49]. Unfortunately, delivery of stable plasmid–NLS–PNA complexes by cationic lipids has not significantly improved gene delivery efficiency when compared to plasmid–PNA complexes lacking NLS peptides. Apart from nuclear targeting, PNAs have also been used to tether transferrin to plasmids [50], where condensation of a plasmid–transferrin–PNA complex with the proton sponge PEI enhanced enzymatic expression of the luciferase gene, a standard reporter, about 4-fold over the plasmid–PEI complex. Competition studies using excess free transferrin resulted in lower transfection, suggesting that DNA–transferrin–PNA–PEI complexes mediated this improvement by binding to the transferrin receptor.

2.4.5

Interactions of DNA with Fusion Proteins

Recent progress in biotechnology has enabled the design and production of a variety of fusion proteins, where either whole or subunits of differing proteins have

been cloned together to produce a chimeric protein. Chimeric proteins including cell-anchorage domains, fusogenic peptides, NLS sequence or DNA condensation/recognition elements have been prepared and evaluated as gene delivery agents [51]. Unfortunately, most of the time, *in vitro* reconstruction of viral particles from protein and nucleic acid does not lead to single DNA condensation or nanometric nucleic acid particles [52], but rather to precipitates. Immune response induced by proteins in the host seriously limits the large-scale utilization of exogenous protein [6]. Nonetheless, host-derived protein (as in the case of transferrin) or protein that could be buried within the particles when immune effectors are present, but exposed in the cytoplasm to assist in passage through nuclear pores, could be used. In one study, the fusion between the TetR protein and the NLS peptide exploited the high affinity of the TetR to bind to a short palindromic DNA sequence and the nuclear import capacities of the NLS peptide [49]. Similar to the previous experiment (Fig. 2.16), binding sites for the fusion protein were cloned into a plasmid for NLS anchorage. Gel-shift assays resulted in a lower electrophoretic mobility of the plasmid in the presence of the fusion protein, providing evidence that the TetR protein retains the ability to bind with DNA when conjugated to the NLS peptide. In addition, improved cationic lipid-mediated delivery was observed in mitosis-arrested cell cultures, suggesting that intracellular trafficking to the nucleus mediated by the NLS peptide is improved.

2.4.6

Agents that Bind to the Minor Groove

The high sequence specificity of PNA, triplex forming oligodeoxynucleotides and proteins to corresponding DNA sequences requires cloning of a target or tag sequence into a nonfunctional section of the plasmid. This hinders not only the target sequence, but further limits the number of elements present on the DNA plasmid. Agents that bind to the minor groove such as distamycin or bisbenzimidazole may overcome the need for tag sequences as they bind with less sequence specificity. Although bisbenzimidazole or distamycin binds in the DNA minor groove with high affinity to AATT sites (dissociation constants in the nanomolar range), they also ramp along the DNA minor groove. Additionally, linking several DNA minor groove binding modules by aliphatic spacers increases DNA duplex affinity and interaction time, but with degenerated sequence selectivity [53].

2.5

DNA Nanoparticles: Sophistication for Cell Recognition and Internalization

2.5.1

Preparation of DNA Nanoparticles Enveloped with a Protective Coat and Cell Internalization Elements

The necessity of DNA protection from aggressive media, such as the blood, demands, at first, particles to be coated with multiple elements. Among the above-

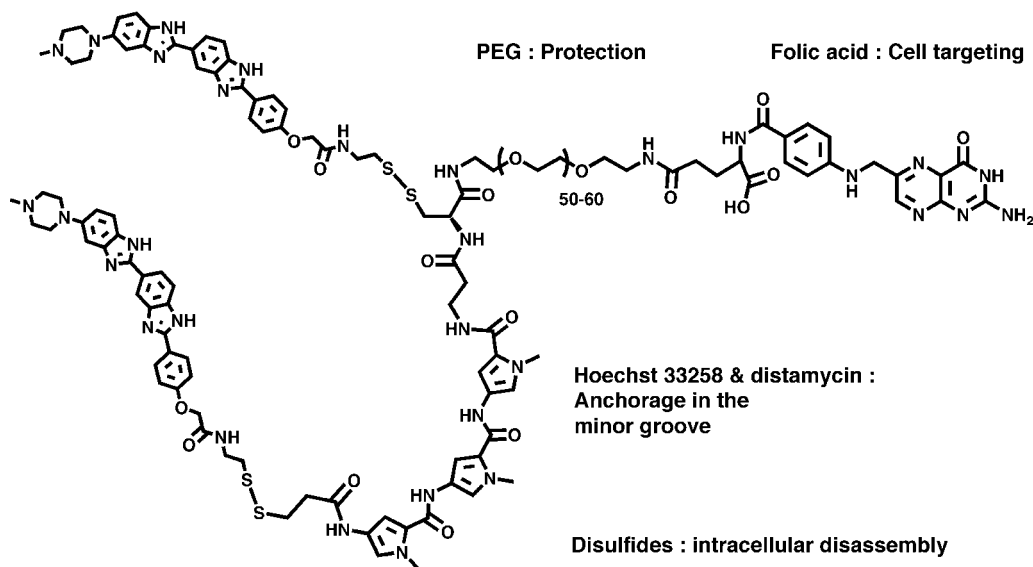


Fig. 2.18. Structure of the DNA anchor 1.

mentioned possible DNA anchors, minor groove agents may prove to be the best choice for noncovalent functionalization of the DNA plasmid with the cell-targeting element. Zuber et al. prepared a minor groove binding anchor (Fig. 2.18, 1) to equip plasmid with folic acid for cell internalization through the folate receptor and PEG to protect the plasmid from degradation in the bloodstream [54].

A distamycin analog and two bisbenzimidazoles were linked by disulfide bond formation, as the presence of disulfide bonds permits the reversion of the anchorage in the cytoplasm by oxidation from glutathione, an intracellular reducing agent. Disulfide bridge cleavage should in turn lead the dissociation of the prosthetic group from the plasmid and therefore facilitate a higher level of expression.

The interaction of 1 with a plasmid of 5.5 kbp was analyzed by agarose gel electrophoresis (Fig. 2.19). Plasmid mobility was reduced and a decrease in ethidium bromide staining was observed in a concentration-dependent manner, suggesting that 1 effectively binds with the plasmid. To test the reversion of the binding in the cytoplasm, glutathione was added to the plasmid–1 complex in solution, resulting in almost complete restoration of plasmid electrophoretic mobility and ethidium bromide staining. The presence of the still-retarded plasmid in lane 4 suggests that some residual bisbenzimidazoles bind to the plasmid; nevertheless, the binding studies indicate the feasibility of release in the cytoplasm.

A PEG–folic acid coat of nanometric DNA particles should not only enhance stability, but further provide cell-targeting and internalization properties. The preparation of monomolecular DNA particles by condensation with lipid-based detergents as previously described in this chapter was accomplished with 1/1 charge equiva-

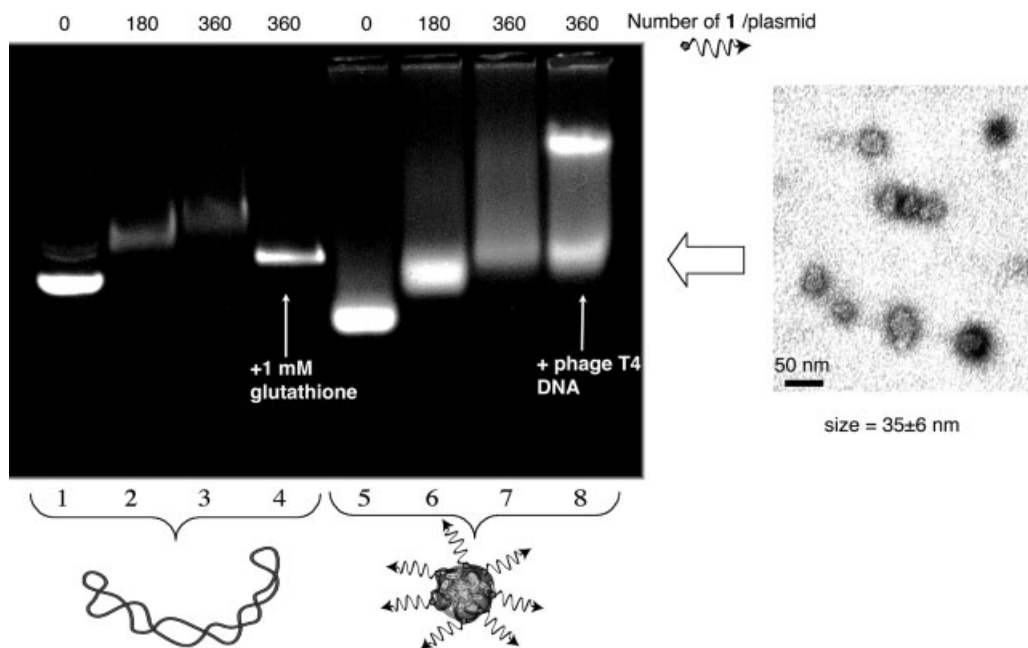


Fig. 2.19. Agarose gel electrophoresis shows complex formation between DNA plasmid, the cationic detergent C₁₄CO and compound **1**. Plasmid was mixed with increasing amount of **1** as indicated. Lane 4: DNA-**1** complexes were incubated with glutathione for release test. Lanes 5–8: nanometric DNA-(C₁₄CO)₂ particles were prepared as described in

Fig. 2.4. After overnight incubation, coverage was effected simply by addition of **1** to the particles. Lane 8: a 1-h incubation of the complexes with excess DNA does not displace the anchor. Transmission electron microscopy image of the final DNA-C₁₄CO-**1** complexes shows monomolecular DNA condensation into compact particles. (Adapted from Ref. [54].)

lents of the cationic detergent C₁₄CO to the plasmid (see Fig. 2.4). After oxidation of the detergent thiols to disulfides, the electrophoretic mobility of the particles through agarose gel was observed to be faster than the corresponding naked DNA (Fig. 2.19). While addition of the PEG-folic acid coat somewhat decreased electrophoretic mobility, competition experiments with excess DNA confirmed quasi-irreversible binding of **1** with the plasmid. Finally, PEG-folate-enveloped DNA particle morphology was observed by transmission electron microscopy. Complexes appeared as a homogeneous population of compact spherical particles with an average diameter of 35 nm. Assuming full DNA association, enveloped particles prepared as in Fig. 2.11 (lane 7) are coated with around 360 molecules of the PEG-folate conjugate, which corresponds to approximately one PEG polymer every 10 nm. This polymer density is sufficient for polymer overlapping onto the surface (termed “weakly overlapping mushroom regime”), [55] and hence should provide both stealth delivery properties and folate receptor-binding properties to the particles.

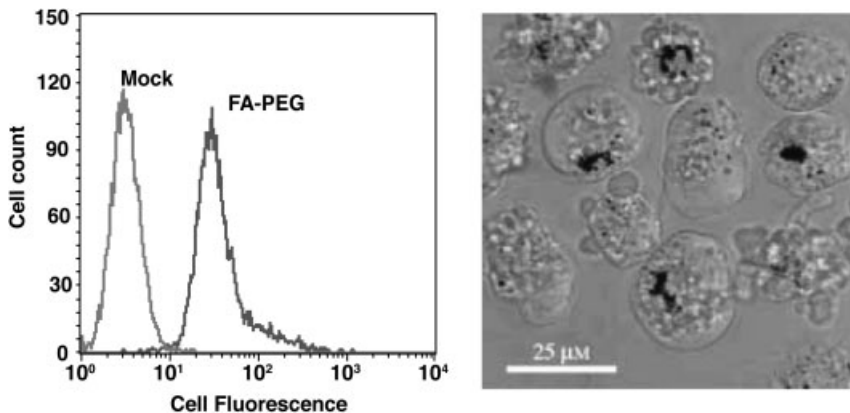


Fig. 2.20. $(C_{14}CO)_2$ -DNA-1 complexes specifically bind to folate receptor-presenting KB cells. Cells were incubated for 3 h with fluorescent DNA complexes. FACS analyses

indicated cellular binding. A Complementary experiment using confocal microscopy indicated that the complexes (darker spots) are further internalized into endosomes.

2.5.2

Biomedical Application: Cell Targeting and Internalization Properties of Folate-PEG-coated Nanoparticles

The abilities of folate-PEG-enveloped DNA particles to carry genes into carcinoma cells were examined using flow cytometry and confocal microscopy (Fig. 2.20). KB cells derived from a human nasopharyngeal cancer were chosen as targets because they conditionally express a large number of folic acid receptors upon folic acid starvation. The $(C_{14}CO)_2$ -DNA particles were labeled with the fluorescent DNA intercalating dye YOYO and incubated 3 h with the KB cells that expressed large quantity of folate receptors (about 10^6 receptors per cell). Flow cytometric analyses show an increased in fluorescence binding to cells with folate-PEG-coated nanoparticles in comparison to untreated cells. To examine whether cell anchorage was followed by endocytosis, the cellular fate of the DNA nanoparticles was observed by confocal fluorescence microscopy. As shown in Fig. 2.20, complexes were internalized in cell perinuclear compartments that very much resemble lysosomes.

2.6

Concluding Remarks

Following initial findings from over a decade ago that cationic lipids and polymers carry genes into eukaryotic cells, a lot of effort has been dedicated to improve transfection efficiency by structural modification of the carriers. Exploration of classical pharmacological methods (such as structure and function) has led to molecules capable of transfecting fast dividing cells in culture at a multiplicity of infection of about 10^6 gene copies per cell. Their ease of handling as well as their general efficiency for almost all adherent cell lines has made them common tools in cellular

biology. Today, these vectors remain far too simple for *in vivo* gene delivery; the prerequisite to gene therapy. Efforts are currently being made to stabilize these DNA–vector “nanoparticles” in the 100- to 1000-nm range with an inert coat and to equip them with targeting elements [33]. As discussed in this chapter, size restriction of the DNA delivery vehicles is crucial for diffusion *in vivo*. Chemical solutions were found to condense DNA into stable particles with the minimal size (single plasmid condensation). In turn, vehicles incorporating fewer copies of effectors need more activity and specificity. Strategies developed for tethering novel functions onto DNA–surfactant complexes had allowed the preparation of DNA particles having key viral properties such as stability and small size for diffusion and ligands for receptor-mediated endocytosis. However, at this stage, key parameters such as endosome escape or nuclear import are still missing. The pending challenge is in adding these extra functions to the DNA delivery vehicle without interfering with all the other ones. Development of supramolecular systems is still in its infancy and will definitely benefit from a better understanding of biochemistry of the cell and how macromolecules interact together to produce wanted events. Gene therapy relies on the development of effective multicomponent delivery vectors. Following initial findings from over a decade ago that cationic lipids and polymers can facilitate gene transportation into eukaryotic cells, a great deal of effort has been dedicated to improve transfection efficiency by structural modification of the carrier. Exploration of classical pharmacological methods (such as structure and function) has led to molecules capable of transfecting fast dividing cells in culture at a multiplicity of infection of about 10^6 gene copies per cell. Their ease of handling as well as their general efficiency for almost all adherent cells lines has made them common tools in cellular biology. The size of a DNA plasmid limits the number of gene copies in delivery vehicles for achieving cell contact in an organism. As discussed in this chapter, stable nanoparticles consisting of a single DNA plasmid can be prepared, and even coated with some functional elements for cell targeting and internalization. Today, DNA nanoparticles are still inefficient in escaping endosomes and require further sophistication. The next obstacle to overcome is the disruption of endosomal membranes, most likely facilitated by the attachment of endosomal disrupting agents such as DOPE or fusogenic peptides. Needless to say, DNA delivery systems with the smallest size incorporate fewer copies of effectors. The implication is that effectors should be more active and specific. The development of nanometric supramolecular systems capable of effective *in vivo* gene delivery is still in its infancy, and will benefit from a better understanding of cellular biochemistry and the interactions between constructed nanoparticles and cellular components.

References

- 1 WATSON, J. D., CRICK, F. H. C., A structure for deoxyribose nucleic acid, *Nature* 1953, 171, 737–739.
- 2 SAENGER, W., *Principles of Nucleic Acid Structure*, Springer, Berlin, 1983.
- 3 CAVAZZANA-CALVO, M., HACEIN-BEY,

- S., DE SAINT BASILE, G., GROSS, F., YVON, E., NUSBAUM, P., SELZ, F., HUE, C., CERTAIN, S., CASANOVA, J. L., BOUSSO, P., DEIST, F. L., FISCHER, A., Gene therapy of human severe combined immunodeficiency (SCID)-X1 disease, *Science* **2000**, *288*, 669–672.
- 4 HACEIN-BEY-ABINA, S., VON KALLE, C., SCHMIDT, M., LE DEIST, F., WULF-FRAAT, N., MCINTYRE, E., RADFORD, I., VILLEVAL, J. L., FRASER, C. C., CAVAZZANA-CALVO, M., FISCHER, A., A serious adverse event after successful gene therapy for X-linked severe combined immunodeficiency, *N. Engl. J. Med.* **2003**, *348*, 255–256.
- 5 MARSHALL, E., Gene therapy. Second child in French trial is found to have leukemia, *Science* **2003**, *299*, 320.
- 6 BALTER, M., Gene therapy on trial, *Science* **2000**, *288*, 951–957.
- 7 AGUILAR, L. K., AGUILAR-CORDOVA, E., Evolution of a gene therapy clinical trial. From bench to bedside and back, *J. Neurooncol.* **2003**, *65*, 307–315.
- 8 ZUBER, G., DAUTY, E., NOTHISEN, M., BELGUISE, P., BEHR, J. P., Towards synthetic viruses, *Adv. Drug Deliv. Rev.* **2001**, *52*, 245–253.
- 9 LEDLEY, F. D., Pharmaceutical approach to somatic gene therapy, *Pharm. Res.* **1996**, *13*, 1595–1614.
- 10 RENSEN, P. C., SLIEDREGT, L. A., FERNS, M., KIEVIET, E., VAN ROSSENBERG, S. M., VAN LEEUWEN, S. H., VAN BERKEL, T. J., BIESSEN, E. A., Determination of the upper size limit for uptake and processing of ligands by the asialoglycoprotein receptor on hepatocytes *in vitro* and *in vivo*, *J. Biol. Chem.* **2001**, *276*, 37577–37584.
- 11 KAWABATA, K., TAKAKURA, Y., HASHIDA, M., The fate of plasmid DNA after intravenous injection in mice: involvement of scavenger receptors in its hepatic uptake, *Pharm. Res.* **1995**, *12*, 825–830.
- 12 CANTOR, C. A., SCHIMMEL, P. R., *Biophysical Chemistry. Part III: The Behavior of Biological Macromolecules*, Freeman, San Francisco, CA, **1980**.
- 13 VERKMAN, A. S., Solute and macromolecule diffusion in cellular aqueous compartments, *Trends Biochem. Sci.* **2002**, *27*, 27–33.
- 14 COLLAS, I., COURVALIN, J. C., Sorting nuclear membrane proteins at mitosis, *Trends Cell Biol.* **2000**, *10*, 5–8.
- 15 PANTE, N., KANN, M., Nuclear pore complex is able to transport macromolecules with diameters of ~39 nm, *Mol. Biol. Cell* **2002**, *13*, 425–434.
- 16 BLOOMFIELD, V. A., DNA condensation, *Curr. Opin. Struct. Biol.* **1996**, *6*, 334–341.
- 17 BEHR, J., Gene transfer with synthetic cationic amphiphiles; prospects for gene therapy, *Bioconjug. Chem.* **1994**, *5*, 382–389.
- 18 VIJAYANATHAN, V., THOMAS, T., THOMAS, T. J., DNA nanoparticles and development of DNA delivery vehicles for gene therapy, *Biochemistry* **2002**, *41*, 14085–14094.
- 19 DUNLAP, D. D., MAGGI, A., SORIA, M. R., MONACO, L., Nanoscopic structure of DNA condensed for gene delivery, *Nucleic Acids Res.* **1997**, *25*, 3095–3101.
- 20 VIJAYANATHAN, V., THOMAS, T., ANTONY, T., SHIRAHATA, A., THOMAS, T. J., Formation of DNA nanoparticles in the presence of novel polyamine analogues: a laser light scattering and atomic force microscopy study, *Nucleic Acids Res.* **2004**, *32*, 127–134.
- 21 SARKAR, T., CONWELL, C. C., HARVEY, L. C., SANTAI, C. T., HUD, N. V., Condensation of oligonucleotides assembled into nicked and gapped duplexes: potential structures for oligonucleotide delivery, *Nucleic Acids Res.* **2005**, *33*, 143–151.
- 22 KOLTOVER, I., SALDIIT, T., RADLER, J. O., SAFINYA, C. R., An inverted hexagonal phase of cationic liposome–DNA complexes related to DNA release and delivery, *Science* **1998**, *281*, 78–81.
- 23 MATULIS, D., ROUZINA, I., BLOOMFIELD, V. A., Thermodynamics of cationic lipid binding to DNA and DNA condensation: roles of electrostatics and hydrophobicity, *J. Am. Chem. Soc.* **2002**, *124*, 7331–7342.
- 24 LUCAS, P., MILROY, D. A., THOMAS, B. J., MOSS, S. H., POUTON, C. W.,

- Pharmaceutical and biological properties of poly(amino acid)/DNA polyplexes, *J. Drug Target.* **1999**, *7*, 143–156.
- 25 KOPATZ, I., REMY, J. S., BEHR, J. P., A model for non-viral gene delivery: through syndecan adhesion molecules and powered by actin, *J. Gene Med.* **2004**, *6*, 769–776.
- 26 LISZIEWICZ, J., TROCIO, J., WHITMAN, L., VARGA, G., XU, J., BAKARE, N., ERBACHER, P., FOX, C., WOODWARD, R., MARKHAM, P., ARYA, S., BEHR, J. P., LORI, F., DermaVir: a novel topical vaccine for HIV/AIDS, *J. Invest. Dermatol.* **2005**, *124*, 160–169.
- 27 OHANA, P., SCHACHTER, P., AYESH, B., MIZRAHI, A., BIRMAN, T., SCHNEIDER, T., MATOUK, I., AYESH, S., KUPPEN, P. J., DE GROOT, N., CZERNIAK, A., HOCHBERG, A., Regulatory sequences of H19 and IGF2 genes in DNA-based therapy of colorectal rat liver metastases, *J. Gene Med.* **2005**, *7*, 366–374.
- 28 ZALIPSKY, S., Functionalized poly(ethylene glycol) for preparation of biologically relevant conjugates, *Bioconjug. Chem.* **1995**, *6*, 150–165.
- 29 KONSTAN, M. W., DAVIS, P. B., WAGENER, J. S., HILLIARD, K. A., STERN, R. C., MILGRAM, L. J., KOWALCZYK, T. H., HYATT, S. L., FINK, T. L., GEDEON, C. R., OETTE, S. M., PAYNE, J. M., MUHAMMAD, O., ZIADY, A. G., MOEN, R. C., COOPER, M. J., Compacted DNA nanoparticles administered to the nasal mucosa of cystic fibrosis subjects are safe and demonstrate partial to complete cystic fibrosis transmembrane regulator reconstitution, *Hum. Gene Ther.* **2004**, *15*, 1255–1269.
- 30 KIRCHEIS, R., BLESSING, T., BRUNNER, S., WIGHTMAN, L., WAGNER, E., Tumor targeting with surface-shielded ligand–polycation DNA complexes, *J. Control Release* **2001**, *72*, 165–170.
- 31 ZHANG, X. Q., WANG, X. L., ZHANG, P. C., LIU, Z. L., ZHUO, R. X., MAO, H. Q., LEONG, K. W., Galactosylated ternary DNA/polyphosphoramidate nanoparticles mediate high gene transfection efficiency in hepatocytes, *J. Controlled Rel.* **2005**, *102*, 749–763.
- 32 ERBACHER, P., BETTINGER, T., BRION, E., COLL, J. L., PLANK, C., BEHR, J. P., REMY, J. S., Genuine DNA/polyethylenimine (PEI) complexes improve transfection properties and cell survival, *J. Drug Target.* **2004**, *12*, 223–236.
- 33 DEMENEIX, B., HASSANI, Z., BEHR, J. P., Towards multifunctional synthetic vectors, *Curr. Gene Ther.* **2004**, *4*, 445–455.
- 34 MEL'NIKOV, S. M., SERGEYEV, V. G., YOSHIKAWA, Y., Transition of double-stranded DNA chains between random coil and compact globule states induced by cooperative binding of cationic surfactants, *J. Am. Chem. Soc.* **1995**, *117*, 9951–9956.
- 35 BLESSING, T., REMY, J.-S., BEHR, J.-P., Monomolecular collapse of plasmid DNA into stable virus-like particles, *Proc. Natl Acad. Sci. USA* **1998**, *95*, 1427–1431.
- 36 BLESSING, T., REMY, J.-S., BEHR, J.-P., Template oligomerization of DNA-bound cations produces calibrated nanometric particles, *J. Am. Chem. Soc.* **1998**, *120*, 8519–8520.
- 37 DAUTY, E., REMY, J. S., BLESSING, T., BEHR, J. P., Dimerizable cationic detergents with a low cmc condense plasmid DNA into nanometric particles and transfect cells in culture, *J. Am. Chem. Soc.* **2001**, *123*, 9227–9234.
- 38 LLERES, D., DAUTY, E., BEHR, J., MELY, Y., DUPORTAIL, G., DNA condensation by an oxidizable cationic detergent. Interactions with lipid vesicles, *Chem. Phys. Lipids* **2001**, *111*, 59–71.
- 39 LABAT-MOLEUR, F., STEFFAN, A. M., BRISSON, C., PERRON, H., FEUGEAS, O., FURSTENBERGER, P., OBERLING, F., BRAMBILLA, E., BEHR, J. P., An electron microscopy study into the mechanism of gene transfer with lipopolyamines, *Gene Ther.* **1996**, *3*, 1010–1017.
- 40 LLERES, D., CLAMME, J. P., DAUTY, E., BLESSING, T., KRISHNAMOORTHY, G., DUPORTAIL, G., MELY, Y., Investigation of the stability of dimeric cationic

- surfactant/DNA complexes and their interaction with model membrane systems, *Langmuir* **2002**, *18*, 10340–10347.
- 41 LOONTIENS, F. G., REGENFUSS, P., ZECHEL, A., DUMORTIER, L., CLEGG, R. M., Binding characteristics of Hoechst 33258 with calf thymus DNA, poly [d(A–T)], and d(CCGGAATCCGG): multiple stoichiometries and determination of tight binding with a wide spectrum of site affinities, *Biochemistry* **1990**, *29*, 9029–9039.
- 42 GLAZER, A. N., PECK, K., MATHIES, R. A., A stable double-stranded DNA–ethidium homodimer complex: application to picogram fluorescence detection of DNA in agarose gels, *Proc. Natl Acad. Sci. USA* **1990**, *87*, 3851–3855.
- 43 WAGNER, E., COTTEN, M., MECHTLER, K., KIRIAPPAS, H., BIRNSTIEL, M. L., DNA-binding transferrin conjugates as functional gene-delivery agents: synthesis by linkage of polylysine or ethidium homodimer to transferrin carbohydrate moiety, *Bioconj. Chem.* **1991**, *2*, 226–231.
- 44 LE DOAN, T., PERROUAULT, L., PRASEUTH, D., HABHOUB, N., DECOUT, J. L., THUONG, N. T., LHOMME, J., HELENE, C., Sequence-specific recognition, photocrosslinking and cleavage of the DNA double helix by an oligo-[alpha]-thymidylate covalently linked to an azidoproflavine derivative, *Nucleic Acids Res.* **1987**, *15*, 7749–7760.
- 45 MOSER, H. E., DERVAN, P. B., Sequence-specific cleavage of double helical DNA by triple helix formation, *Science* **1987**, *238*, 645–650.
- 46 FAUCON, B., MERGNY, J. L., HELENE, C., Effect of third strand composition on the triple helix formation: purine versus pyrimidine oligodeoxynucleotides, *Nucleic Acids Res.* **1996**, *24*, 3181–3188.
- 47 NEVES, C., BYK, G., SCHERMAN, D., WILS, P., Coupling of a targeting peptide to plasmid DNA by covalent triple helix formation, *FEBS Lett* **1999**, *453*, 41–45.
- 48 BRANDEN, L. J., MOHAMED, A. J., SMITH, C. I., A peptide nucleic acid–nuclear localization signal fusion that mediates nuclear transport of DNA, *Nat. Biotechnol.* **1999**, *17*, 784–787.
- 49 VAYSSE, L., HARBOTTLE, R., BIGGER, B., BERGAU, A., TOLMACHOV, O., COUTELLE, C., Development of a self-assembling nuclear targeting vector system based on the tetracycline repressor protein, *J. Biol. Chem.* **2004**, *279*, 5555–5564.
- 50 LIANG, K. W., HOFFMAN, E. P., HUANG, L., Targeted delivery of plasmid DNA to myogenic cells via transferrin-conjugated peptide nucleic acid, *Mol. Ther.* **2000**, *1*, 236–243.
- 51 UHEREK, C., WELS, W., DNA-carrier proteins for targeted gene delivery, *Adv. Drug Deliv. Rev.* **2000**, *44*, 153–166.
- 52 ZUBER, G., MCDERMOTT, J., KARANJIA, S., ZHAO, W., SCHMID, M. F., BARKLIS, E., Assembly of retrovirus capsid-nucleocapsid proteins in the presence of membranes or RNA, *J. Virol.* **2000**, *74*, 7431–7441.
- 53 YOUNGQUIST, R. S., DERVAN, P. B., Sequence-specific recognition of B-DNA by oligo(*N*-methylpyrrole-carboxamide)s, *Proc. Natl Acad. Sci. USA* **1985**, *82*, 2565–2569.
- 54 ZUBER, G., ZAMMUT-ITALIANO, L., DAUTY, E., BEHR, J. P., Targeted gene delivery to cancer cells: directed assembly of nanometric DNA particles coated with folic acid, *Angew. Chem. Int. Ed.* **2003**, *42*, 2666–2669.
- 55 WONG, J. Y., KUHLE, T. L., ISRAELACHVILI, J. N., MULLAH, N., ZALIPSKY, S., Direct measurement of a tethered ligand–receptor interaction potential, *Science* **1997**, *275*, 820–822.

3

Lipoplexes

Sarah Weisman

3.1

Introduction

The introduction of nucleic acids into cells, either plasmid DNA for gene expression or antisense oligodeoxynucleotides (ODN) or small interference RNA (siRNA) for gene silencing, is a valuable tool for biological research and a promising therapeutic treatment for genetic disease. The prevalent means of transport for gene therapy is the use of viral vectors [1]. A synthetic alternative, cationic lipid-mediated nucleic acid delivery (lipofection) [2], has been intensively studied over recent years [3–7]. Lipofection has low efficiency compared to viral vectors, but its advantages include negligible immunogenicity, ease of large-scale production and no limit on the size of the gene transported. Eighty-seven clinical trials of gene therapy via lipofection are currently in progress, aiming to treat cystic fibrosis, arterial disease and many types of cancer [8].

Mixing anionic nucleic acids with cationic lipids leads to spontaneous self-assembly of ordered aggregates known as lipoplexes. Lipoplexes have great potential, but our understanding of the mechanisms of lipoplex function is still incomplete. This chapter will give a brief overview of the current state of knowledge about lipoplexes, with special attention to their microscopic structure, and the relationships between structure and delivery efficiency. The chapter will first address the composition, structure and function of DNA lipoplexes, and then discuss ODN and siRNA lipoplexes in terms of their differences from DNA complexes.

3.2

DNA Lipoplexes

3.2.1

Composition

Cationic lipids do not usually occur in nature, but a wide variety of lipids have been synthesized for the purposes of gene therapy. Cationic lipids contain a cationic

head group, a linker and a hydrophobic moiety, most often two hydrocarbon chains. The effects of variations in lipid structure on the properties of lipoplexes have been recently reviewed elsewhere [7, 9]. The chemical structures of some popular cationic lipids from different families are presented in Table 3.1.

Cationic lipids are often combined with neutral (helper) lipids in order to improve lipofection efficiency. The presence of helper lipids can tune the surface charge density, the preferred microstructure and the stability of lipoplexes. The chemical structures of the three most common helper lipids are presented in Table 3.1. Mixed cationic–neutral lipid systems self-assemble in aqueous solution, usually forming liposomes, which are bilayer membranes closed in upon themselves (Fig. 3.1).

Mixture of anionic DNA with cationic liposomes in aqueous solution leads to spontaneous and nearly instantaneous complexation. The DNA–lipid interaction is endothermic [10, 11]; the driving force for lipoplex formation is the entropy gain from the release of bound counterions [12] and water molecules [13]. The process of lipoplex formation is shown schematically in Fig. 3.1.

DNA in lipoplexes is located in close contact with the lipids and can neutralize the cationic lipid head group charges [14]. In positively charged complexes (with an excess of lipid) the DNA is fully protected from degradation by nucleases or interaction with fluorescent dye [15, 16]. Hence, we infer that DNA is condensed and encapsulated within lipoplexes.

3.2.2

Nanostructure and Microstructure

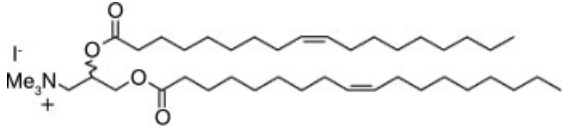
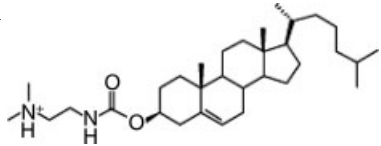
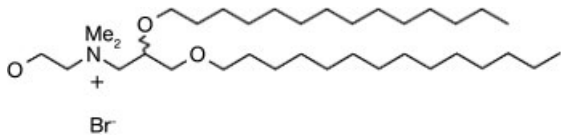
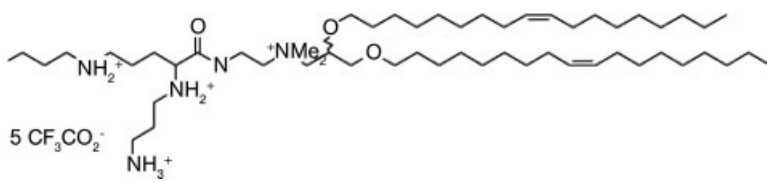
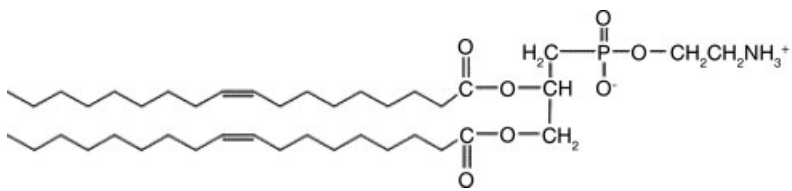
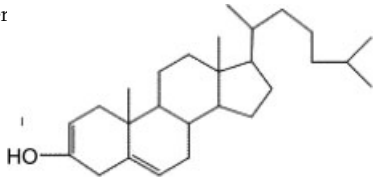
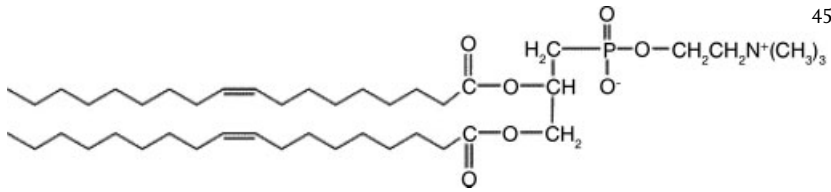
3.2.2.1 Equilibrium Morphology

There are two known supramolecular structures adopted by DNA lipoplexes at equilibrium. The lamellar phase consists of DNA molecules sandwiched between cationic membranes [18, 19]. The inverted hexagonal phase contains DNA molecules coated by monolayers of cationic lipid and arranged in a hexagonal matrix [20, 21]. The different morphologies are shown schematically in Fig. 3.2.

The condensed lamellar (L_{α}^C) or “sandwich” phase is characterized by a constant interlamellar water gap, $w \sim 2.6$ nm, corresponding to the diameter of a DNA helix surrounded by a thin hydration shell [18]. DNA organizes within the monolayer as a lattice of parallel helices. As DNA molecules are rigid, with a persistence length of around 50 nm, this is the only efficient packing regime. The interhelical DNA spacing, d , is variable, depending on both the membrane charge density and the DNA/lipid charge ratio. Under isoelectric conditions, with full neutralization of lipid and DNA charges, $d^* = e/(l_0\sigma_M)$, where e is the electron charge, l_0 is the distance between anionic charges on the DNA backbone and σ_M is the cationic membrane charge density (dependent on the cationic/neutral lipid ratio). If the cationic membrane includes helper lipids, DNA may induce lipid demixing. Cationic lipids concentrate close to the DNA helices to achieve local charge matching [19].

The inverse hexagonal (H_{II}^C) or “honeycomb” phase has a typical water tube diameter of about 2.8 nm, sufficient to contain a hydrated DNA helix [20]. The DNA

Tab. 3.1. Some popular cationic and helper lipids for lipofection

Name	Structure	Literature hits [17]
Cationic lipids [7]		
DOTAP		256
DC-Chol		113
DMRIE		59
DOSPA		16
Helper lipids [9]		
DOPE		389
Cholester		243
DOPC		45

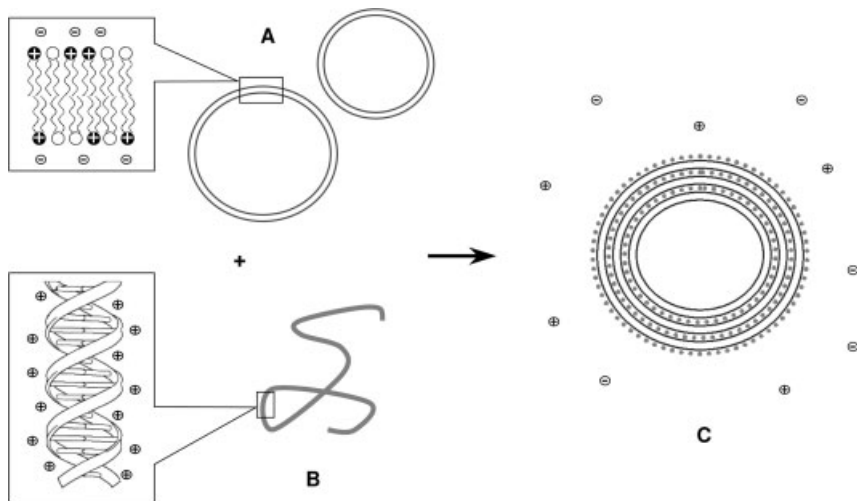


Fig. 3.1. Schematic representation of lipoplex formation. (A) Liposomes composed of cationic and neutral lipids. (B) DNA random coil. (C) Condensation of DNA with lipids forms lipoplexes. Complexation is driven by entropy gain due to counterion release.

is tightly and symmetrically enveloped, so this structure can provide very effective charge neutralization. Adding DNA to lamellar lipid bilayers sometimes induces the formation of an inverse hexagonal complex. This phenomenon occurs in soft membranes with low bending rigidity, e.g. systems where short-chain alcohols have been added as cosurfactants.

The preferred structure of lipoplexes consisting of two or more lipid species depends on the packing geometry of the lipid components. Most lipids with two hydrocarbon chains are roughly “cylindrical”, meaning that the cross-sectional areas of their head group and their tail group are comparable. These lipids favor the formation of planar bilayers. Thus, lipoplexes where all lipid molecules are cylindrical usually form only a lamellar complex. Some neutral lipids with small head groups, e.g. DOPE, have “inverse conical” shapes and can promote the formation of an inverse hexagonal phase.

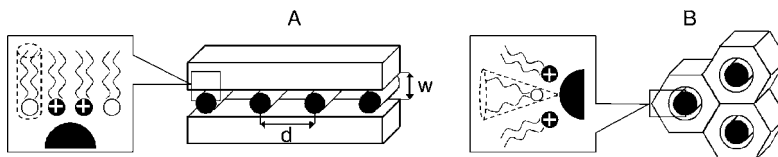


Fig. 3.2. Schematic representation of equilibrium structures of lipoplexes. (A) The L_x^C lamellar phase, promoted by cylindrically shaped helper lipids. (B) The H_{II}^C inverse hexagonal phase, promoted by inverse conical

helper lipid molecules. In (A), w is the constant interlamellar water gap, d is the variable interhelical DNA distance and lipids can locally demix to efficiently neutralize DNA charge. (Adapted from Ref. [5].)

Phase diagrams of DNA lipoplex systems have been constructed both experimentally and theoretically [22–24]. In a mixed lipid system, increasing the mole fraction of DOPE or a similar inverse conical helper lipid can drive a structural transition from lamellar to inverse hexagonal lipoplexes. At high DNA/lipid charge ratios lipoplexes coexist with free DNA and at low DNA/lipid charge ratios lipoplexes coexist with pure lipid phases. Lamellar lipoplexes can be negatively overcharged at excess DNA ($d < d^*$) or positively overcharged at excess lipid ($d > d^*$) and can accommodate different fractions of helper lipid, so there is a single-phase L_x^C region over a range of component ratios. Inverse hexagonal lipoplexes have no structural or compositional degrees of freedom, thus they only exist as isoelectric complexes in equilibrium with other phases.

Some DNA lipoplex systems that form the condensed lamellar phase have demonstrated three-dimensional interlayer correlations [25–27]. These occur if the cationic lipid membranes are flexible and can partially wrap around the DNA in order to improve charge matching. This produces periodic membrane undulations, as shown in Fig. 3.3. The orientation of DNA helices in different layers is correlated and there is some positional coupling between DNA helices in different layers. The range of the interactions depends on the membrane properties.

The size and sequence of DNA molecules apparently does not affect the lipoplex microstructures formed [28]. The structure of DNA helices within lipoplexes remains in a B-conformation, though in a variant form in which the base–base interactions are perturbed [29].

3.2.2.2 Nonequilibrium Morphology

Lipoplex systems under conditions relevant for gene therapy often have not reached thermodynamic equilibrium. Lipoplexes are usually prepared by adding DNA to cationic liposomes. Direct imaging by transmission electron microscopy (TEM) has demonstrated that this procedure can produce a variety of metastable morphologies [30–33]. Slight differences in preparation conditions can apparently cause large variations in the dynamics of complex formation.

Figure 3.4(b) shows a model mechanism for the formation of lamellar lipoplexes [33]. The mechanism suggests that in the first step of complexation anionic DNA coats the surface of cationic liposomes. Following this, liposomes adsorb, rupture and roll over a host liposome, adding layers one by one to form a multilamellar

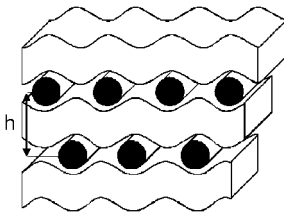


Fig. 3.3. Schematic representation of bilayer undulations and interlayer DNA correlations within lamellar lipoplexes. The lamellar repeat distance is denoted by h . (Adapted from Ref. [5].)

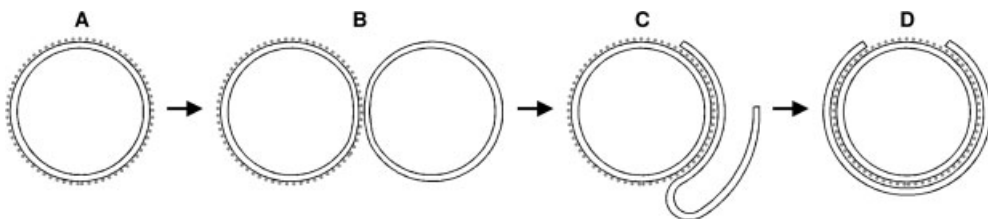
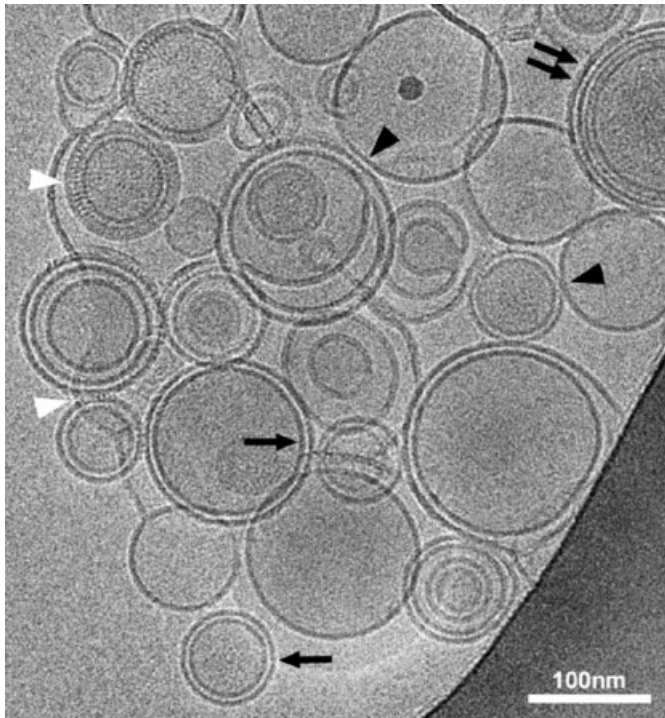


Fig. 3.4. (Above) Cryo-TEM image of a DOTAP/DOPC/DNA lipoplex with excess lipid. Black arrowheads indicate liposomes adsorbed to each other; black arrows mark pairs of concentric membranes adsorbed to each other; black double arrows indicate a stack of concentric membranes adsorbed to each other; white arrowheads mark parallel DNA helices clearly visible between adsorbed membranes. (Below) Model mechanism for interactions

between cationic liposomes and DNA. (A) DNA coats a liposome. (B) Two liposomes adsorb to each other. (C) One liposome ruptures after deformation and (D) rolls over the second liposome, yielding a pair of concentric membranes adsorbed to each other, possibly with an open membrane edge. Further layers adsorb similarly. (Adapted from Ref. [33].)

particle. This mechanism is in agreement with calorimetric measurements suggesting that lipoplex formation is a two-step process [34]. A fast exothermic interaction corresponds to DNA binding to liposome surfaces and a slower cooperative endothermic process is probably the reorganization of liposomes into lamellar complexes.

Figure 3.4(a) shows an example of a polymorphous lipoplex, imaged at our laboratory. The lipid composition of the system is expected to favor the lamellar phase at equilibrium. Several of the intermediate stages in the model mechanism of lipoplex formation are observed. The prevalence of metastable structures is a function of the time since preparation. It is also probably promoted by conditions of excess lipid, causing a shortage of free DNA to drive the complexation process forward. In systems with higher DNA charge ratios, multilamellar complexes form much more quickly.

Some DNA lipoplexes have been found to form “spaghetti” tubule structures, with individual DNA molecules coated by cationic lipid bilayers [30]. It has been demonstrated that these structures are metastable [21]; they may be intermediates in the formation of the inverse hexagonal phase.

3.2.2.3 Lipoplex Size

Lipoplex particles, with different compositions and under different preparation conditions, range in size from around 100 nm to several microns. At low or high DNA/lipid charge ratios the complexes are charged (with positive or negative ζ potential, respectively), and their size is stabilized by electrostatic repulsions. At charge ratios approaching the isoelectric point the ζ potential is near zero, and lipoplexes undergo extensive and irreversible aggregation [35]. Size growth is promoted by membrane defects that are believed to result from phase separations between DNA–lipid lamellar domains and uncomplexed bilayers [36].

Increasing mole fraction of helper lipids increases lipoplex size [35]. This is probably due to lower membrane charge density and thus weaker electrostatic repulsions. A medium of high ionic strength masks electrostatic repulsions and facilitates lipoplex growth [37].

Lipoplexes prepared from large cationic liposomes are larger than those prepared from small liposomes [35]. The extent of lipoplex aggregation increases with time.

3.2.3

Lipofection Efficiency

3.2.3.1 *In Vitro*

Lipoplexes must surmount many barriers to successfully deliver DNA to the cell nucleus. A diagram of the most likely mechanism of lipofection is shown in Fig. 3.5. The first stage is binding of a lipoplex to the cell due to nonspecific electrostatic interactions between cationic membranes and anionic proteoglycan residues on the cell surface [38]. Cell association is enhanced for positively charged lipoplexes and for large aggregates, the latter probably due to a faster rate of settling on the cultured cells [39]. The most efficient DNA/lipid mixing ratio for lipofection is a moderate excess of cationic charge [40].

The primary pathway for lipoplex entry into cells is endocytosis [41, 42]. Fusion of lipoplexes with the cell membrane also occurs, but there is no correlation between the degree of lipid mixing and the lipofection efficiency [43]. Possibly a fusion event releases DNA outside the cell, or inside the cell, but too distant from the cell nucleus.

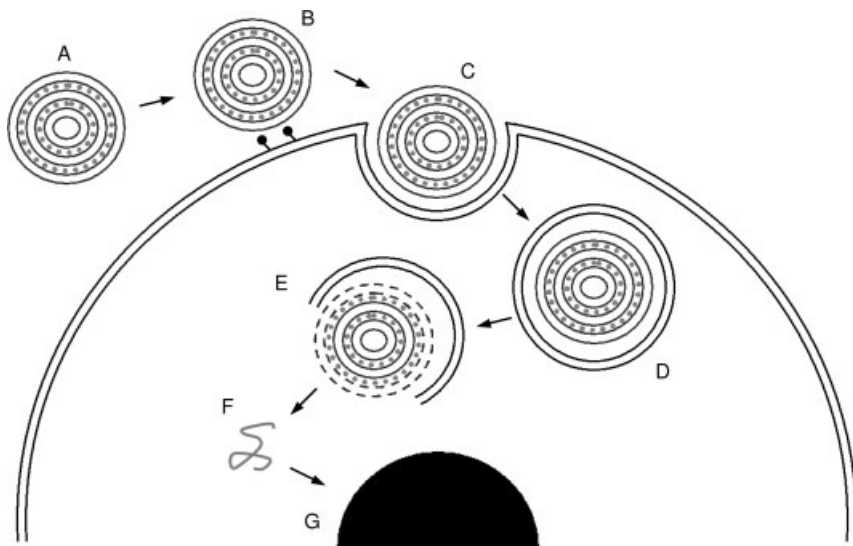


Fig. 3.5. Schematic representation of the most likely mechanism of lipofection. (A) A lipoplex approaches the cell. (B) Adsorption to the cell surface due to electrostatic interactions. (C) Entry to the cell by endocytosis. (D) Transport within an endosome. (E) Fusion or disruption of the endosome. (F) Release of DNA. (G) Entry to the nucleus by intracellular trafficking. (Adapted from Ref. [59].)

A recent report has demonstrated that small particles (200 nm or below) enter cells mainly by clathrin-mediated endocytosis and larger particles (around 500 nm) by caveolae-mediated endocytosis, while very large particles (1 μm or above) are not internalized at all [44]. Small particles are delivered to lysosomes for digestion within a few hours, but larger particles have an extended residence time within endosomal compartments, increasing their probability of escape into the cytosol [44]. These results may explain the common empirical finding that lipoplex size has a significant influence on transgene expression. There is an optimal lipoplex size for greatest lipofection efficiency [35, 37, 45].

Release of lipoplexes from endosomal compartments is widely considered a rate-determining step for lipofection. Efficient lipoplex formulations are able to escape from endosomes, while inefficient formulations remain trapped [46, 47]. The endosome membrane can be disrupted by lipid exchange or fusion with lipoplexes. Inverse hexagonal phase lipoplexes are reported to fuse rapidly with anionic membranes, disrupting the membrane and releasing DNA [20] and hexagonal lipoplex structure has been correlated with efficient lipofection [48, 49]. Lipid mixing between cationic lipids and anionic lipids found in the endosomal membrane can also induce local formation of a hexagonal phase, due to ion pair charge neutralization [50, 51]. This destabilization of bilayers is hindered by the presence of cylindrically shaped helper lipid, but is facilitated by inverse conical shaped helper lipid. Formation of a nonbilayer phase in lipoplex–membrane mixtures appears to be critical for efficient endosome escape [51].

A recent report has proposed that the barrier preventing lamellar lipoplex fusion with the anionic endosomal membrane is kinetic rather than thermodynamic [47]. The height of the activation barrier depends on lipoplex membrane bending rigidity and cationic charge density. Efficiency of lipofection increases exponentially with membrane charge density to a plateau, where delivery efficiency of the lamellar phase competes with that of the hexagonal phase [47]. Other studies have suggested that increased membrane fluidity (decreased bending rigidity) enhances lipofection efficiency [52, 53].

DNA may dissociate from lipoplexes during endosomal escape or intact lipoplexes may be released into the cytoplasm [54]. Direct microinjection of lipoplexes into either the cytoplasm or the nucleus results in efficient complex dissociation, so intracellular release of DNA is probably not a limiting step for lipofection [55]. Interestingly, microinjection of lipoplexes or naked DNA into the cytoplasm produces significantly less gene expression than endocytosis-mediated lipofection. Endosomes may play a role in lipofection by transporting the lipoplexes close to the cell nucleus [3].

Transfer of DNA into the nucleus is a very inefficient process. Particles with diameters of up to around 40 nm are able to enter the nucleus by active transport through the nuclear pores [56], but most genes delivered by lipoplexes are much larger than this. Shorter DNA molecules are correlated with increased lipofection efficiency [28]. Dividing cell lines have an alternative nuclear access pathway, as the nuclear envelope fragments during mitosis. Transgene expression is enhanced immediately following mitosis [57], but the duration of the mitosis phase is only around 1 h in a typical cell cycle of 24 h. DNA located in the cytoplasm is degraded by nucleases, with a half-life of approximately 90 min [58].

In general, increasing the lipoplex dose administered improves lipofection efficiency. However, this approach is limited by the toxicity thresholds of cationic lipids [59–61]. Efforts to develop less-toxic lipid formulations for both *in vitro* and *in vivo* applications are in progress.

In addition to the factors described here, lipofection efficiency also depends on the interrelations between cationic/helper lipid formulation, DNA sequence and target cell type. The reasons behind these effects are poorly understood.

3.2.3.2 *In Vivo*

The ultimate aim of research in the field of lipoplexes is to achieve effective systemic delivery of therapeutic genes to humans. Unfortunately, lipofection efficiency *in vivo* is much lower than *in vitro*, due to a number of extracellular barriers. Intravenous injection of lipoplexes is followed by unfavorable interactions with blood components and by highly restricted uptake to tissues.

Exposure of cationic lipoplexes to blood serum dramatically inhibits *in vitro* DNA delivery in some systems [62, 63], but not others [64]. Serum does not displace DNA from lipoplexes, but it reverses the ζ potential of the complexes due to anionic serum proteins binding to lipoplex surfaces [63]. Incubation with low concentrations of serum can promote bridging and extensive lipoplex aggregation, which is correlated with reduced *in vivo* lipofection efficiency. Incubation with

high concentrations of serum yields homogenous coating of serum proteins and sterically stabilizes lipoplex size [65].

Inclusion of inverse conical helper lipids in lipoplexes significantly reduces their *in vivo* lipofection efficiency [66]. It has been reported that lipoplex structures of this type disintegrate in serum, with penetration and binding of serum proteins to all cationic membranes, inside and out [65]. This both exposes DNA to nucleases in the blood and has detrimental implications for intracellular processing. Even in less extreme cases, serum can interfere with mixture between lipoplexes and anionic liposomes, an analog of endosomal membranes [63]. In agreement, lipoplexes incorporating serum have been shown to fail to escape from endosomes [64].

Long-term incubation (above 30 min) of lipoplexes in blood causes partial degradation of DNA, due to imperfect protection from nucleases [67]. However, this may not be a significant effect, as more than 97% of lipoplexes have been cleared from the blood within 5 min of intravenous injection into mice. At this time the majority of lipoplexes are associated with the lungs, probably partially due to entrapment in the extensive pulmonary microvasculature. Later a large fraction of lung lipoplexes relocates to the liver [67].

Lipoplex particles are, in general, too large to extravasate from the bloodstream. Uptake and expression of lipoplexes in the lungs and most other organs is predominantly by capillary endothelial cells [68]. Uptake of lipoplexes in the liver and spleen is primarily due to elimination of foreign particles by macrophages, which does not lead to significant transgene expression [68]. Some success has been reported in lipofection of tumor tissue, as tumors have a permeable endothelial barrier [69, 70]. An ability to extravasate under these conditions has been attributed to a specific lipoplex structure, bilamellar invaginated vesicles, which yields relatively small and very flexible particles.

Intravenous administration of lipoplexes is an excellent technique for gene delivery to endothelial cells [71]. Efficient targeting of other cell types requires modification of lipoplexes. One current direction of research is development of “stealth lipoplexes”, an analog of well-known stealth liposomes. Lipoplexes are coated with the biocompatible polymer polyethylene glycol (PEG), with the possible addition of a targeting ligand. PEGylation provides steric protection from interactions with serum proteins and reduces nonspecific uptake by the lung endothelial cells, so it greatly extends the residence time of lipoplexes in the circulation [72]. However, PEGylation has been shown to strongly inhibit lipofection in cell culture, due to stabilization of the lamellar phase and preclusion of endosomal escape, unless the PEG molecules desorb [73, 74]. This approach is promising, but needs further work.

3.3 ODN Lipoplexes

Antisense ODN, short single-strand DNA molecules, are designed to target and bind a specific messenger RNA, blocking gene expression. Antisense design is

not straightforward, but one ODN drug has been approved and many others are in clinical trials [75]. Cationic lipid-mediated delivery of ODN increases antisense activity by several orders of magnitude [76, 77].

The structure of ODN lipoplexes is similar to that of DNA lipoplexes; both lamellar [78] and inverse hexagonal [79] phases have been observed. In ODN lamellar lipoplexes, however, there is no evidence of ordering within the ODN monolayers. As ODN molecules are relatively short and flexible, they probably orient randomly between the cationic membranes [80].

The thickness of ODN monolayers in the lamellar phase has been measured as around 1.2 nm [80]. This suggests that there is insufficient room for a hydration layer between ODN molecules and cationic membranes as is seen in DNA lipoplexes. In agreement, ODN molecules neutralize cationic lipid charges more efficiently than DNA does, implying that ODN is located in closer contact with the membrane [81, 14]. We consider complete dehydration of ODN unlikely, so we speculate that ODN may adopt a different conformation between cationic mem-

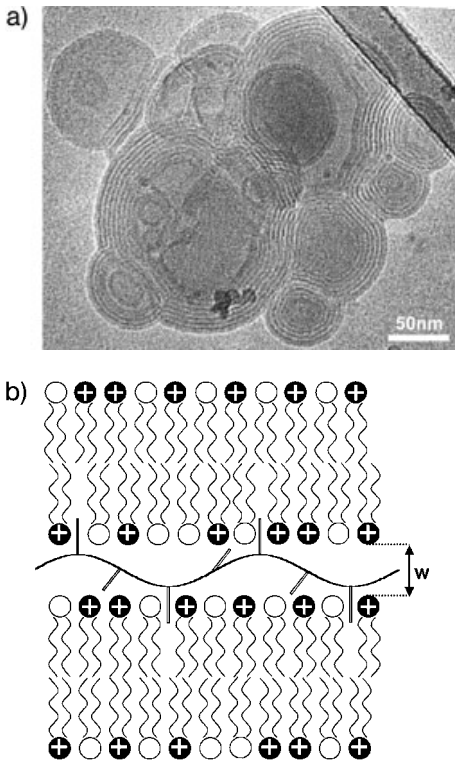


Fig. 3.6. (A) Cryo-TEM image of a DOTAP/ODN lipoplex with excess lipid. A condensed multilamellar phase is seen. (B) Schematic representation of the ODN-lipid lamellar phase. The interlamellar water gap is denoted by w . We speculate that ODN molecule side-groups may penetrate into the lipid bilayer.

branes than in aqueous solution. Instead of a helical backbone with side-groups facing inwards to maximize base-stacking interactions, side-groups may point outwards, leaving a central water tube. Bases would then penetrate into the head-group area of the cationic membranes. Figure 3.6(A) shows an example of a condensed lamellar lipoplex imaged at our laboratory. Figure 3.6(B) shows our suggested model of lamellar structure with ODN bases intercalated between lipid head groups. This hypothesis needs further investigation.

ODN lipoplexes enter cells by endocytosis [77, 82] as DNA lipoplexes do. However, the nuclear membrane is not a major barrier for ODN molecules. After microinjection into the cell, ODN is found to preferentially locate in the nucleus [83], with the rate of uptake inversely proportional to molecular size [84]. ODN is delivered to the nucleus by active transport through nuclear pores [85].

3.4

siRNA Lipoplexes

siRNA, short double-strand RNA molecules, has recently become a popular tool for gene silencing [86]. Successful cationic lipid-mediated delivery of siRNA has been reported [87], but as yet little research has focused on the properties of siRNA lipoplexes. siRNA lipoplexes would be expected to be similar to DNA lipoplexes, but an early report suggests that the effect of lipoplex size may be less critical for siRNA delivery than for DNA delivery [88].

Nuclear entry is probably not a significant barrier for siRNA lipofection, as RNA interference activity seems to be primarily located in the cytoplasm [86]. Further research into the structure and function of siRNA lipoplexes is needed in order to optimize siRNA delivery and to facilitate the development of this exciting field.

Acknowledgments

Cryo-TEM work was performed at the Hannah and George Krumholz Laboratory for Advanced Microscopy at the Technion, part of the Technion Project on Complex Fluids, in collaboration with Y. Talmon, Y. Barenholz and D. Hirsch-Lerner, funded by an Israel Science Foundation grant. Thanks to Y. Talmon for help in editing this manuscript.

References

- 1 M. A. KAY, J. C. GLORIOSO, L. NALDINI, Viral vectors for gene therapy: the art of turning infectious agents into vehicles of therapeutics, *Nat. Med.* **2001**, 7, 33–40.
- 2 P. L. FELGNER, T. R. GADEK, M. HOLM, R. ROMAN, H. W. CHAN, M. WENZ, J. P. NORTHROP, G. M. RINGOLD, M. DANIELSEN, Lipofection: a highly efficient, lipid-mediated DNA-transfection procedure, *Proc. Natl Acad. Sci. USA* **1987**, 84, 7413–7417.

- 3 A. ELOUAHABI, J.-M. RUYSSCHAERT, Formation and intracellular trafficking of lipoplexes and polyplexes, *Mol. Ther.* **2005**, *11*, 336–347.
- 4 K. EWERT, N. L. SLACK, A. AHMAD, H. M. EVANS, A. J. LIN, C. E. SAMUEL, C. R. SAFINYA, Cationic lipid–DNA complexes for gene therapy: understanding the relationship between complex structure and gene delivery pathways at the molecular level, *Curr. Med. Chem.* **2004**, *11*, 133–149.
- 5 S. MAY, A. BEN-SHAUL, Modeling of cationic lipid–DNA complexes, *Curr. Med. Chem.* **2004**, *11*, 151–167.
- 6 D. SIMBERG, S. WEISMAN, Y. TALMON, Y. BARENHOLZ, DOTAP (and other cationic lipids): chemistry, biophysics, and transfection, *Crit. Rev. Ther. Drug Carrier Syst.* **2004**, *21*, 257–317.
- 7 I. TRANCHANT, B. THOMPSON, C. NICOLAZZI, N. MIGNET, D. SCHERMAN, Physicochemical optimization of plasmid delivery by cationic lipids, *J. Gene Med.* **2004**, *6*, S24–S35.
- 8 Extensive and current information on clinical trials in the field of gene therapy can be found at <http://www.wiley.co.uk/genetherapy/clinical/>.
- 9 S. ZHANG, Y. XU, B. WANG, W. QIAO, D. LIU, Z. LI, Cationic compounds used in lipoplexes and polyplexes for gene delivery, *J. Controlled Rel.* **2004**, *165*–180.
- 10 M. T. KENNEDY, E. V. POZHARSKI, V. A. RAKHMANOVA, R. C. MACDONALD, Factors governing the assembly of cationic phospholipid–DNA complexes, *Biophys. J.* **2000**, *78*, 1620–1633.
- 11 D. MATULIS, I. ROUZINA, V. A. BLOOMFIELD, Thermodynamics of cationic lipid binding to DNA and DNA condensation: roles of electrostatics and hydrophobicity, *J. Am. Chem. Soc.* **2002**, *124*, 7331–7342.
- 12 K. WAGNER, D. HARRIES, S. MAY, V. KAHL, J. O. RÄDLER, A. BEN-SHAUL, Direct evidence for counterion release upon cationic lipid–DNA condensation, *Langmuir* **2000**, *16*, 303–306.
- 13 D. HIRSCH-LERNER, Y. BARENHOLZ, Hydration of lipoplexes commonly used in gene delivery: follow-up by laurdan fluorescence changes and quantification by differential scanning calorimetry, *Biochim. Biophys. Acta* **1999**, *1461*, 47–57.
- 14 N. J. ZUIDAM, Y. BARENHOLZ, Electrostatic and structural properties of complexes involving plasmid DNA and cationic lipids commonly used for gene delivery, *Biochim. Biophys. Acta* **1998**, *1368*, 115–128.
- 15 S. J. EASTMAN, C. SIEGEL, J. TOUSIGNANT, A. E. SMITH, S. H. CHENG, R. K. SCHEULE, Biophysical characterization of cationic lipid:DNA complexes, *Biochim. Biophys. Acta* **1997**, *1325*, 41–62.
- 16 Y. XU, S.-W. HUI, P. FREDERIK, F. C. SZOKA, Physicochemical characterization and purification of cationic lipoplexes, *Biophys. J.* **1999**, *77*, 341–353.
- 17 Journal papers referring to the applications of a given lipid for gene therapy were found by searching the CAPLUS database in Scifinder[®]: <http://www.cas.org/SCIFINDER/scicover2.html>.
- 18 J. O. RÄDLER, I. KOLTOVER, T. SALDITT, C. R. SAFINYA, Structure of DNA–cationic liposome complexes: DNA intercalation in multilamellar membranes in distinct interhelical packing regimes, *Science* **1997**, *275*, 810–814.
- 19 D. HARRIES, S. MAY, W. M. GELBART, A. BEN-SHAUL, Structure, stability, and thermodynamics of lamellar DNA–lipid complexes, *Biophys. J.* **1998**, *75*, 159–173.
- 20 I. KOLTOVER, T. SALDITT, J. O. RÄDLER, C. R. SAFINYA, An inverted hexagonal phase of cationic liposome–DNA complexes related to DNA release and delivery, *Science* **1998**, *281*, 78–81.
- 21 S. MAY, A. BEN-SHAUL, DNA–lipid complexes: stability of honeycomb-like and spaghetti-like structures, *Biophys. J.* **1997**, *73*, 2427–2440.
- 22 I. KOLTOVER, T. SALDITT, C. R. SAFINYA, Phase diagram, stability, and overcharging of lamellar cationic lipid–DNA self-assembled complexes, *Biophys. J.* **1999**, *77*, 915–924.

- 23 D. SIMBERG, D. DANINO, Y. TALMON, A. MINSKY, M. E. FERRARI, C. J. WHEELER, Y. BARENHOLZ, Phase behavior, DNA ordering, and size instability of cationic lipoplexes, *J. Biol. Chem.* **2001**, 276, 47453–47459.
- 24 S. MAY, D. HARRIES, A. BEN-SHAUL, The phase behavior of cationic lipid–DNA complexes, *Biophys. J.* **2000**, 78, 1681–1697.
- 25 F. ARTZNER, R. ZANTL, G. RAPP, J. O. RÄDLER, Observation of a rectangular columnar phase in condensed lamellar cationic lipid–DNA complexes, *Phys. Rev. Lett.* **1998**, 81, 5015–5018.
- 26 B. J. BATTERSBY, R. GRIMM, S. HUEBNER, G. CEVC, Evidence for three-dimensional interlayer correlations in cationic lipid–DNA complexes as observed by cryo-electron microscopy, *Biochim. Biophys. Acta* **1998**, 1372, 379–383.
- 27 D. HARRIES, S. MAY, A. BEN-SHAUL, Curvature and charge modulations in lamellar DNA–lipid complexes, *J. Phys. Chem. B* **2003**, 107, 3624–3630.
- 28 P. KREISS, B. CAMERON, R. RANGARA, P. MAILHE, O. AGUERRE-CHARRIOL, M. AIRIAU, D. SCHERMAN, J. CROUZET, B. PITARD, Plasmid DNA size does not affect the physicochemical properties of lipoplexes but modulates gene transfer efficiency, *Nucleic Acids Res.* **1999**, 27, 3792–3798.
- 29 C. S. BRAUN, G. S. JAS, S. CHOOSAKOON-KRIANG, G. S. KOE, J. G. SMITH, C. R. MIDDAGH, The structure of DNA within cationic lipid/DNA complexes, *Biophys. J.* **2003**, 84, 1114–1123.
- 30 B. STERNBERG, F. L. SORGI, L. HUANG, New structures in complex formation between DNA and cationic liposomes visualized by freeze-fracture electron microscopy, *FEBS Lett.* **1994**, 356, 361–366.
- 31 J. GUSTAFSSON, G. ARVIDSON, G. KARLSSON, M. ALMGREN, Complexes between cationic liposomes and DNA visualized by cryo-TEM, *Biochim. Biophys. Acta* **1995**, 1235, 305–312.
- 32 N. S. TEMPLETON, D. D. LASIC, P. M. FREDERIK, H. H. STREY, D. D. ROBERTS, G. N. PAVLAKIS, Improved DNA:liposome complexes for increased systemic delivery and gene expression, *Nat. Biotechnol.* **1997**, 15, 647–652.
- 33 S. HUEBNER, B. J. BATTERSBY, R. GRIMM, G. CEVC, Lipid–DNA complex formation: reorganization and rupture of lipid vesicles in the presence of DNA as observed by cryoelectron microscopy, *Biophys. J.* **1999**, 76, 3158–3166.
- 34 V. PECTOR, J. BACKMANN, D. MAES, M. VANDENBRANDEN, J.-M. RUYSSCHAERT, Biophysical and structural properties of DNA–diC₁₄–amidine complexes, *J. Biol. Chem.* **2000**, 275, 29533–29538.
- 35 N. J. ZUIDAM, D. HIRSCH-LERNER, S. MARGULIES, Y. BARENHOLZ, Lamellarity of cationic liposomes and mode of preparation of lipoplexes affect transfection efficiency, *Biochim. Biophys. Acta* **1999**, 1419, 207–220.
- 36 D. HIRSCH-LERNER, Y. BARENHOLZ, Probing DNA–cationic lipid interactions with the fluorophore trimethylammonium diphenylhexatriene (TMADPH), *Biochim. Biophys. Acta* **1998**, 1370, 17–30.
- 37 P. C. ROSS, S. W. HUI, Lipoplex size is a major determinant of *in vitro* lipofection efficiency, *Gene Ther.* **1999**, 6, 651–9.
- 38 K. A. MISLICK, J. D. BALDESCHWIELER, Evidence for the role of proteoglycans in cation-mediated gene transfer, *Proc. Natl Acad. Sci. USA* **1996**, 93, 12349–12354.
- 39 M. T. GIRÃO DA CRUZ, S. SIMÕES, P. P. C. PIRES, S. NIR, M. C. PEDROSA DE LIMA, Kinetic analysis of the initial steps involved in lipoplex–cell interactions: effect of various factors that influence transfection activity, *Biochim. Biophys. Acta* **2001**, 1510, 136–141.
- 40 F. SAKURAI, R. INOUE, Y. NISHINO, A. OKUDA, O. MATSUMOTO, T. TAGA, F. YAMASHITA, Y. TAKAKURA, M. HASHIDA, Effect of DNA/liposome mixing ratio on the physicochemical characteristics, cellular uptake and intracellular trafficking of plasmid DNA/cationic lipid complexes and subsequent gene expression, *J. Controlled Rel.* **2000**, 66, 255–269.

- 41 J. ZABNER, A. J. FASBENDER, T. MONINGER, K. A. POELLINGER, M. J. WELSH, Cellular and molecular barriers to gene transfer by a cationic lipid, *J. Biol. Chem.* **1995**, *270*, 18997–19007.
- 42 D. S. FRIEND, D. PAPAHAJIOPOULOS, R. J. DEBS, Endocytosis and intracellular processing accompanying transfection mediated by cationic liposomes, *Biochim. Biophys. Acta* **1996**, *1278*, 41–50.
- 43 T. STEGMANN, J.-Y. LEGENDRE, Gene transfer mediated by cationic lipids: lack of a correlation between lipid mixing and transfection, *Biochim. Biophys. Acta* **1997**, *1325*, 71–79.
- 44 J. REJMAN, V. OBERLE, I. S. ZUHORN, D. HOEKSTRA, Size-dependent internalization of particles via the pathways of clathrin- and caveolae-mediated endocytosis, *Biochem. J.* **2004**, *377*, 159–169.
- 45 C. KAWAURA, A. NOGUCHI, T. FURUNO, M. NAKANISHI, Atomic force microscopy for studying gene transfection mediated by cationic liposomes with a cationic cholesterol derivative, *FEBS Lett.* **1998**, *421*, 69–72.
- 46 B. MUI, Q. F. AHKONG, L. CHOW, M. J. HOPE, Membrane perturbation and the mechanism of lipid-mediated transfer of DNA into cells, *Biochim. Biophys. Acta* **2000**, *1467*, 281–292.
- 47 A. J. LIN, N. L. SLACK, A. AHMAD, C. X. GEORGE, C. E. SAMUEL, C. R. SAFINYA, Three-dimensional imaging of lipid gene-carriers: membrane charge density controls universal transfection behavior in lamellar cationic liposome–DNA complexes, *Biophys. J.* **2003**, *84*, 3307–3316.
- 48 A. J. LIN, N. L. SLACK, A. AHMAD, I. KOLTOVER, C. X. GEORGE, C. E. SAMUEL, C. R. SAFINYA, Structure and structure–function studies of lipid/plasmid DNA complexes, *J. Drug Target.* **2000**, *8*, 13–27.
- 49 J. SMISTEROVÁ, A. WAGENAAR, M. C. A. STUART, E. POLUSHKIN, G. TEN BRINKE, R. HULST, J. B. F. N. ENGBERTS, D. HOEKSTRA, Molecular shape of the cationic lipid controls the structure of cationic lipid/dioleoylphosphatidylethanolamine–DNA complexes and the efficiency of gene delivery, *J. Biol. Chem.* **2001**, *276*, 47615–47622.
- 50 I. M. HAFEZ, N. MAURER, P. R. CULLIS, On the mechanism whereby cationic lipids promote intracellular delivery of polynucleic acids, *Gene Ther.* **2001**, *8*, 1188–1196.
- 51 I. S. ZUHORN, U. BAKOWSKY, E. POLUSHKIN, W. H. VISSER, M. C. A. STUART, J. B. F. N. ENGBERTS, D. HOEKSTRA, Nonbilayer phase of lipoplex–membrane mixture determines endosomal escape of genetic cargo and transfection efficiency, *Mol. Ther.* **2005**, *11*, 801–810.
- 52 A. E. REGELIN, S. FANKHAENEL, L. GÜRTECH, C. PRINZ, G. VON KIEDROWSKI, U. MASSING, Biophysical and lipofection studies of DOTAP analogs, *Biochim. Biophys. Acta* **2000**, *1464*, 151–164.
- 53 M. E. FERRARI, D. RUSALOV, J. ENAS, C. J. WHEELER, Synergy between cationic lipid and co-lipid determines the macroscopic structure and transfection activity of lipoplexes, *Nucleic Acids Res.* **2002**, *30*, 1808–1816.
- 54 A. EL OUAHABI, M. THIRY, V. PECTOR, R. FUKS, J. M. RUYSSCHAERT, M. VANDENBRANDEN, The role of endosome destabilizing activity in the gene transfer process mediated by cationic lipids, *FEBS Lett.* **1997**, *414*, 187–192.
- 55 S. CORNELIS, M. VANDENBRANDEN, J.-M. RUYSSCHAERT, A. ELOUAHABI, Role of intracellular cationic liposome–DNA complex dissociation in transfection mediated by cationic lipids, *DNA Cell Biol.* **2002**, *21*, 91–97.
- 56 N. PANTÉ, M. KANN, Nuclear pore complex is able to transport macromolecules with diameters of ~39 nm, *Mol. Biol. Cell* **2002**, *13*, 425–434.
- 57 W.-C. TSENG, F. R. HASELTON, T. D. GIORGIO, Mitosis enhances transgene expression of plasmid delivered by cationic liposomes, *Biochim. Biophys. Acta* **1999**, *1445*, 53–64.
- 58 D. LECHARDEUR, K. J. SOHN, M. HAARDT, P. B. JOSHI, M. MONCK, R. W.

- GRAHAM, B. BEATTY, J. SQUIRE, H. O'BRODOVICH, G. L. LUKACS, Metabolic instability of plasmid DNA in the cytosol: a potential barrier to gene transfer, *Gene Ther.* **1999**, *6*, 482–497.
- 59 D. D. LASIC, N. S. TEMPLETON, Liposomes in gene therapy, *Adv. Drug Deliv. Rev.* **1996**, *20*, 221–266.
- 60 C. R. DASS, Lipoplex-mediated delivery of nucleic acids: factors affecting *in vivo* transfection, *J. Mol. Med.* **2004**, *82*, 579–591.
- 61 J.-S. ZHANG, F. LIU, L. HUANG, Implications of pharmacokinetic behavior of lipoplex for its inflammatory toxicity, *Adv. Drug Deliv. Rev.* **2005**, *57*, 689–698.
- 62 V. ESCRIOU, C. CIOLINA, F. LACROIX, G. BYK, D. SCHERMAN, P. WILS, Cationic lipid-mediated gene transfer: effect of serum on cellular uptake and intracellular fate of lipopolyamine/DNA complexes, *Biochim. Biophys. Acta* **1998**, *1368*, 276–288.
- 63 O. ZELPHATI, L. S. UYECHI, L. G. BARRON, F. C. SZOKA, Effect of serum components on the physico-chemical properties of cationic lipid/oligonucleotide complexes and on their interactions with cells, *Biochim. Biophys. Acta* **1998**, *1390*, 119–133.
- 64 I. S. ZUHORN, W. H. VISSER, U. BAKOWSKY, J. B. F. N. ENGBERTS, D. HOEKSTRA, Interference of serum with lipoplex–cell interaction: modulation of intracellular processing, *Biochim. Biophys. Acta* **2002**, *1560*, 25–36.
- 65 D. SIMBERG, S. WEISMAN, Y. TALMON, A. FAERMAN, T. SHOSHANI, Y. BARENHOLZ, The role of organ vascularization and lipoplex–serum initial contact in intravenous murine lipofection, *J. Biol. Chem.* **2003**, *278*, 39858–39865.
- 66 Y. K. SONG, F. LIU, S. CHU, D. LIU, Characterization of cationic liposome-mediated gene transfer *in vivo* by intravenous administration, *Hum. Gene Ther.* **1997**, *8*, 1585–1594.
- 67 R. NIVEN, R. PEARLMAN, T. WEDEKING, J. MACKEIGAN, P. NOKER, L. SIMPSON-HERREN, J. G. SMITH, Biodistribution of radiolabeled lipid–DNA complexes and DNA in mice, *J. Pharm. Sci.* **1998**, *87*, 1292–1299.
- 68 J. W. MCLEAN, E. A. FOX, P. BALUK, P. B. BOLTON, A. HASKELL, R. PEARLMAN, G. THURSTON, E. Y. UMEMOTO, D. M. McDONALD, Organ-specific endothelial cell uptake of cationic liposome–DNA complexes in mice, *Am. J. Physiol.* **1997**, *273*, H387–H404.
- 69 R. RAMESH, T. SAEKI, N. S. TEMPLETON, L. JI, L. C. STEPHENS, I. ITO, D. R. WILSON, Z. WU, C. D. BRANCH, J. D. MINNA, J. A. ROTH, Successful treatment of primary and disseminated human lung cancers by systemic delivery of tumor suppressor genes using an improved liposome vector, *Mol. Ther.* **2001**, *3*, 337–350.
- 70 H. Y. SHI, R. LIANG, N. S. TEMPLETON, M. ZHANG, Inhibition of breast tumor progression by systemic delivery of the maspin gene in a syngeneic tumor model, *Mol. Ther.* **2002**, *5*, 755–761.
- 71 J. D. HOOD, M. BEDNARSKI, R. FRAUSTO, S. GUCCIONE, R. A. REISFELD, R. XIANG, D. A. CHERESH, Tumor regression by targeted gene delivery to the neovasculature, *Science* **2002**, *296*, 2404–2407.
- 72 C. NICOLAZZI, N. MIGNET, N. DE LA FIGUERA, M. CADET, R. T. IBAD, J. SEGUIN, D. SCHERMAN, M. BESSODES, Anionic polyethylene glycol lipids added to cationic lipoplexes increase their plasmatic circulation time, *J. Controlled Rel.* **2003**, *88*, 429–443.
- 73 F. SHI, L. WASUNGU, A. NOMDEN, M. C. A. STUART, E. POLUSHKIN, J. B. F. N. ENGBERTS, D. HOEKSTRA, Interference of poly(ethylene glycol)–lipid analogs with cationic-lipid-mediated delivery of oligonucleotides; role of lipid exchangeability and non-lamellar transitions, *Biochem. J.* **2002**, *366*, 333–341.
- 74 L. Y. SONG, Q. F. AHKONG, Q. RONG, Z. WANG, S. ANSELL, M. J. HOPE, B. MUI, Characterization of the inhibitory effect of PEG–lipid conjugates on the intracellular delivery of plasmid and antisense DNA mediated by cationic lipid liposomes,

- Biochim. Biophys. Acta* **2002**, *1558*, 1–13.
- 75 F. SHI, D. HOEKSTRA, Effective intracellular delivery of oligonucleotides in order to make sense of antisense, *J. Controlled. Rel.* **2004**, *97*, 189–209.
- 76 C. F. BENNETT, M. Y. CHIANG, H. CHAN, J. E. SHOEMAKER, C. K. MIRABELLI, Cationic lipids enhance cellular uptake and activity of phosphorothioate antisense oligonucleotides, *Mol. Pharm.* **1992**, *41*, 1023–1033.
- 77 O. ZELPHATI, F. C. SZOKA, Intracellular distribution and mechanism of delivery of oligonucleotides mediated by cationic lipids, *Pharm. Res.* **1996**, *13*, 1367–1372.
- 78 S. C. SEMPLE, S. K. KLIMUK, T. O. HARASYM, N. D. SANTOS, S. M. ANSELL, K. F. WONG, N. MAURER, H. STARK, P. R. CULLIS, M. J. HOPE, P. SCHERRER, Efficient encapsulation of antisense oligonucleotides in lipid vesicles using ionizable aminolipids: formation of novel small multilamellar vesicle structures, *Biochim. Biophys. Acta* **2001**, *1510*, 152–166.
- 79 I. JÄÄSKELÄINEN, B. STERNBERG, J. MÖNKKÖNEN, A. URTTI, Physicochemical and morphological properties of complexes made of cationic liposomes and oligonucleotides, *Int. J. Pharm.* **1998**, *167*, 191–203.
- 80 S. WEISMAN, D. HIRSCH-LERNER, Y. BARENHOLZ, Y. TALMON, Nanostructure of cationic lipid–oligonucleotide complexes, *Biophys. J.* **2004**, *87*, 609–614.
- 81 V. M. MEIDAN, J. S. COHEN, N. AMARIGLIO, D. HIRSCH-LERNER, Y. BARENHOLZ, Interaction of oligonucleotides with cationic lipids: the relationship between electrostatics, hydration and state of aggregation, *Biochim. Biophys. Acta* **2000**, *1464*, 251–261.
- 82 K. LAPPALAINEN, R. MIETTINEN, J. KELLOKOSKI, I. JÄÄSKELÄINEN, S. SYRJÄNEN, Intracellular distribution of oligonucleotides delivered by cationic liposomes: light and electron microscopic study, *J. Histochem. Cytochem.* **1997**, *45*, 265–274.
- 83 J. P. LEONETTI, N. MECHTI, G. DEGOLS, C. GAGNOR, B. LEBLEU, Intracellular distribution of microinjected antisense oligonucleotides, *Proc. Natl Acad. Sci. USA* **1991**, *88*, 2702–2706.
- 84 G. L. LUKACS, P. HAGGIE, O. SEKSEK, D. LECHARDEUR, N. FREEDMAN, A. S. VERKMAN, Size-dependent DNA mobility in cytoplasm and nucleus, *J. Biol. Chem.* **2000**, *275*, 1625–1629.
- 85 R. HARTIG, R. L. SHOEMAN, A. JANETZKO, S. GRÜB, P. TRAUB, Active nuclear import of single-stranded oligonucleotides and their complexes with non-karyophilic macromolecules, *Biol. Cell* **1998**, *90*, 407–426.
- 86 C. D. NOVINA, P. A. SHARP, The RNAi revolution, *Nature* **2004**, *430*, 161–164.
- 87 J. Q. YIN, J. GAO, R. SHAO, W.-N. TIAN, J. WANG, Y. WAN, siRNA agents inhibit oncogene expression and attenuate human tumor cell growth, *J. Exp. Ther. Oncol.* **2003**, *3*, 194–204.
- 88 S. SPAGNOU, A. D. MILLER, M. KELLER, Lipidic carriers of siRNA: differences in the formulation, cellular uptake, and delivery with plasmid DNA, *Biochemistry* **2004**, *43*, 13348–13356.

4

DNA–Chitosan Nanoparticles for Gene Therapy: Current Knowledge and Future Trends

Julio C. Fernandes, Marcio José Tiera and Françoise M. Winnik

4.1

Introduction

Chitosan is a polysaccharide usually obtained from deacetylation of chitin, which after cellulose is the second most abundant natural biopolymer found in nature. It may be extracted from various sources, particularly from exoskeletons of arthropods such as crustaceans, fungi, insects, annelids, mollusks, coelenterates, etc. [1, 2].

Approximately 1000 clinical trials are listed on the *Journal of Gene Medicine's* online “Gene Therapy Clinical Trials Worldwide” and more than 25% of these use nonviral vectors. This broad category encompasses a variety of technologies, essentially all of which involve complexing and sometimes condensing DNA with an agent that allows it to nonspecifically enter a cell, either by membrane fusion, endocytosis or a membrane-disrupting event. Chitosan is positively charged [1, 2] and thus can be complexed with DNA. It does not need sonication or organic solvents for its preparation, therefore minimizing possible damage to DNA during complexation.

The goal of this chapter is to introduce the reader to chitosan as a DNA carrier, as well as different variables and strategies to improve cellular transfection. The first two sections present the fundamental properties of chitosan as well as how different parameters related to the nonmodified structure affect the transfection efficiency. The third section provides the reader with an understanding of the multiple barriers that must be solved prior to practical use, discussing all the approaches employed and their limitations. The following sections present different procedures to obtain nano- and microparticles for gene therapy, and the potential clinical applications of chitosan–DNA polyplexes.

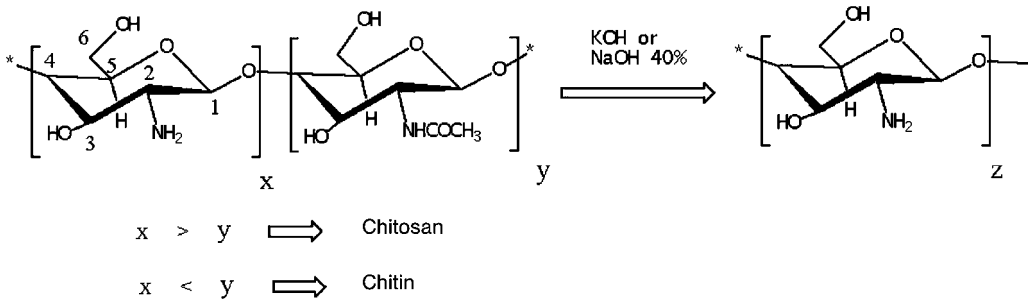


Fig. 4.1. Chemical structure of chitin and chitosan, and the deacetylation process to produce the highly deacetylated product. The commonly used numbering for the carbon atoms is shown in the 2-amino-2-deoxy-D-glucopyranose ring.

4.2

Chitosan as a Carrier for Gene Therapy

4.2.1

Chitosan Chemistry

The structures of chitin and chitosan correspond to those of poly[$\beta(1 \rightarrow 4)$ -2-acetamido-2-deoxy-D-glucopyranose] and poly[$\beta(1 \rightarrow 4)$ -2-amino-2-deoxy-D-glucopyranose], respectively (Fig. 4.1). Chitosan is mainly manufactured from crustaceans (crab, krill and crayfish), primarily because a large amount of the crustacean exoskeleton is available as a byproduct of food processing. In general, the isolation of chitin from crustacean shell waste consists of three basic steps: demineralization (calcium carbonate and calcium phosphate separation), deproteinization (protein separation) and decolorization (removal of pigments). These three steps are the standard procedure for chitin production [3]. Chitosan is obtained after hydrolysis of the acetamide groups of chitin. However, both units are commonly found in the commercialized samples, since chitosans having high degree of deacetylation (DA > 99%) are obtained only through successive hydrolysis with strong bases such as KOH and NaOH, and the degree of deacetylation is strongly dependent of the alkali concentration and temperature (Fig. 4.1) [4]. The source of chitin and the deacetylation process can dramatically change the properties of the final product and deacetylation in alkaline medium leads to depolymerization [5, 6]. However, it has been recently reported that chitin extracted from squid pens can be hydrolyzed under conditions that allow us to obtain chitosans of high molecular weight [7]. The homopolymer is a weak base with a pK_a value of the D-glucosamine residue of about 6.2–7.0, and is therefore insoluble at neutral and alkaline pH values. In acidic media the amine groups will be positively charged, conferring a high charge density to the polysaccharide. As in all polyelectrolytes, the dissociation constant of chitosan is not constant, but depends on the degree of dissociation at

which it is determined. The pK_a value can be calculated using Katchalsky's equation [2]:

$$pK_a = \text{pH} + \log\left[\frac{1 - \alpha}{\alpha}\right] = pK_0 - \varepsilon\Delta\psi(\alpha)/kT$$

where $\Delta\psi$ is the difference in electrostatic potential between the surface of the polyanion and the reference, α is the degree of dissociation, kT is Boltzmann's constant and ε is the electron charge. Extrapolation of the pK_a values to $\alpha = 1$, where the polymer is uncharged and hence the electrostatic potential becomes zero, makes it possible for the value of the intrinsic dissociation constant of the ionizable groups, pK_0 , to be determined. The value obtained does not depend of the degree of *N*-acetylation, whereas the pK_a value is highly dependent on this parameter, since the electrostatic potential will vary depending on the amount of the free amino groups. The pK_0 value is called the intrinsic pK_a of the chitosan. However, chitosans of low molecular weight having degrees of deacetylation higher than 0.4 are also easily soluble in weakly acidic solvents such as acetic acid and formic acid [8]. The physicochemical behavior in aqueous solution is highly dependent of the pH and degree of acetylation, and has received more attention only recently. Berth et al., working on chitosans from 95 to 175 kDa, have recently determined the radius of gyration of chitosan (R_G) [9, 10]. The R_G is an alternative measure of the size of the polymer chain and it can be measured by light scattering measurements. R_G expresses the square mean radius of each one of the elements of the chain measured from its center of gravity. The study established the relationship between the molecular weight and R_G of chitosan in aqueous solution, and the author indicated that chitosan behaved more like a Gaussian coil instead of the worm-like chain model found in common polyelectrolytes. At the same time the presence of *N*-acetyl groups on the chitosan backbone imparts hydrophobic properties. Schatz et al. [11] have studied a homogeneous series of chitosans with different degrees of acetylation and almost the same degree of polymerization in ammonium acetate buffer. Their results indicate that the aqueous solution behavior depends only on the degree of acetylation. Three distinct domains of degree of acetylation were defined and correlated to the different behaviors of chitosans: (a) a polyelectrolyte domain for DA < 20%, (b) a transition domain for DA = 20–50% where chitosan loses its hydrophilicity and (iii) a hydrophobic domain for DA > 50% where polymer associations can arise. Conformations of chitosan chains varying from 160 to 270 kDa were studied by the calculations of the persistence lengths (L_p). The average value was found to be close to 5 nm, in agreement with the wormlike chain model, but no significant variation of L_p with the degree of acetylation was noticed. Pa et al. [12] have also reported that the particle sizes of chitosan molecules in dilute acetic acid/water solutions increased with decreasing pH. Light scattering studies data also demonstrated that the second virial coefficient (A_2) increased with decreasing pH, suggesting that the solubility of chitosan in water increased with increasing acetic acid concentration. Signini et al. [13] have also shown that acid-free aqueous solutions of chitosan hydrochloride

of variable ionic strengths ($0.06 \leq \mu \leq 0.3$ M) are free of aggregation as evaluated by the values of the Huggins constants ($0.31 \leq k \leq 0.63$).

As with other polysaccharides, the biodegradation and biocompatibility are important properties of chitosan, making it an attractive polymer for a variety of biomedical and pharmaceutical applications. In addition to the degradation by chitinases [14], chitosanases [15], papain [16–19] and other proteases [20], partially acetylated chitosan may be also degraded by lysozymes of the human serum [21], by oxidative/reductive depolymerization [22] and by acid hydrolysis reactions [23]. In the acid hydrolysis the protonation of the glycosidic oxygen is recognized as the first step of the mechanism, which leads to formation of a cyclic carbonium–oxonium ion, yielding the reducing sugar end group after the addition of water [24, 25]. In addition to enzymatic and acid hydrolysis, alkaline treatment with ultrasonication can be used to obtain either chitosan of decreasing molecular weight [26] or oligomers having a few glucosamine units [27].

4.2.2

General Strategies for Chitosan Modification

In the chitosan structure, two groups are particularly susceptible to react through nucleophilic attack, i.e. the free amine and/or acetamide groups and the hydroxyl groups linked to the glucopyranose ring. The hydroxyl groups can be modified by substitution of the hydrogen atoms, but their reactivities are smaller than that of the amino group. Various procedures targeting the hydroxyl groups employ a sequence of protection/depotection reactions aimed at obtaining derivatives with a well-defined structure [28]. However, under appropriate conditions, a variety of other reactions can be easily conducted to selectively modify the free amine groups. The literature presents a wide range of procedures to target the amine group, aiming to improve the properties of chitosan for a particular purpose. The modifications include those aiming at the separation technologies of chiral molecules [29], recovery of metals [30, 31], antimicrobial activity [32], antitumoral carriers [33], biomedical applications [34, 35] and vectors for gene therapy [36–39] (Figs. 4.2 and 4.3). Kumar et al. [40] and Kurita [41] have recently reviewed the procedures for the modification of chitosan, and those of major importance are summarized in Tables 4.1 and 4.2.

4.2.3

Chitosan–DNA interactions: Transfection Efficacy of Unmodified Chitosan

The first report on chitosan as a possible carrier for gene therapy was made by Mumper et al. in 1995 [125]. Since then it has been reported that besides its immunogenicity, chitosan molecules condense efficiently with DNA to form tight polyplexes avoiding degradation by DNases [126]. However, before using chitosan–DNA nanoparticles *in vivo*, one must study their interaction and cell behavior. Since macrophages play an important role in inflammatory processes, Chellat et al. [127] have investigated the effects of chitosan–DNA nanoparticles on the hu-

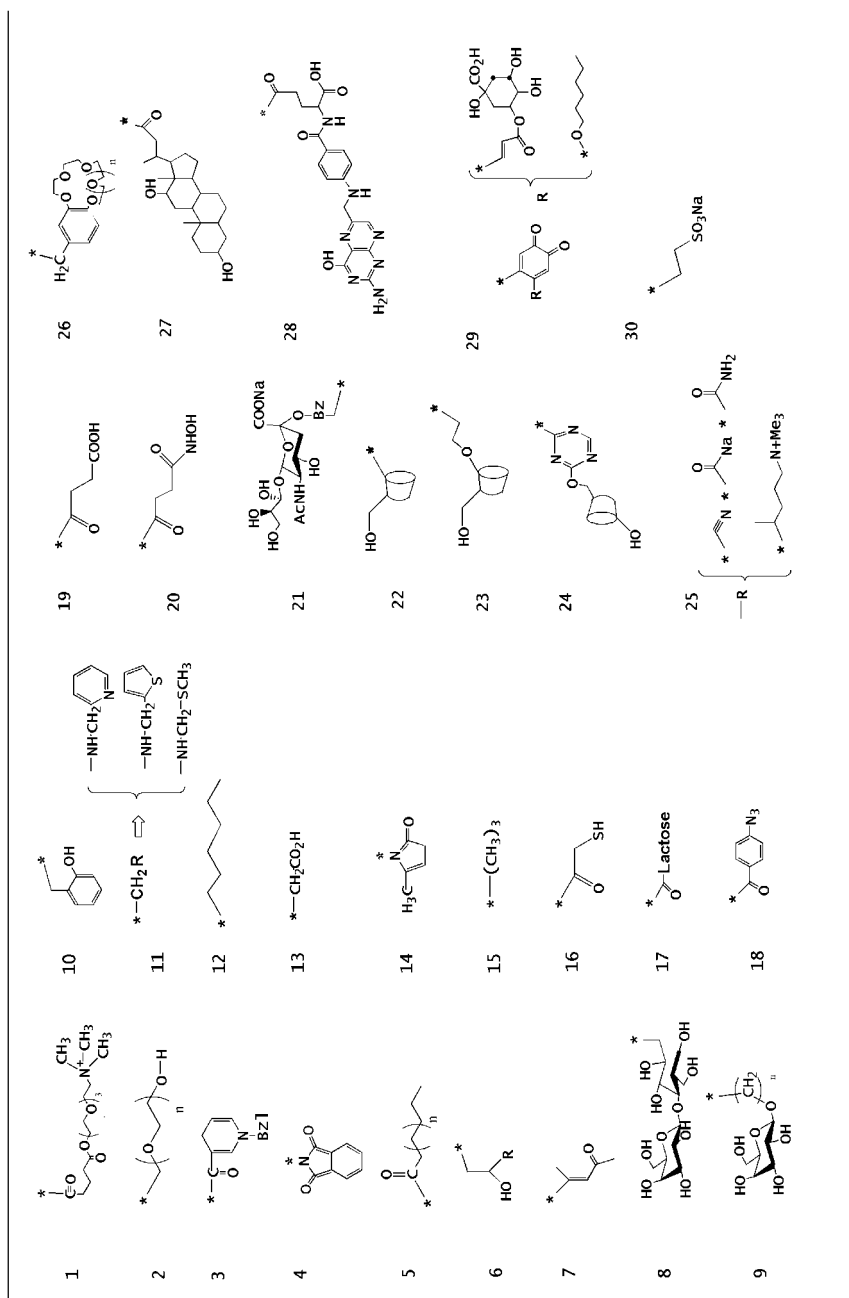


Fig. 4.2. Chemical structure of N-chitosan derivatives. The asterisk indicates the position at which the amino group of chitosan chain is attached. In the 4 and 14 derivatives the nitrogen atom belongs to the main chain of chitosan.

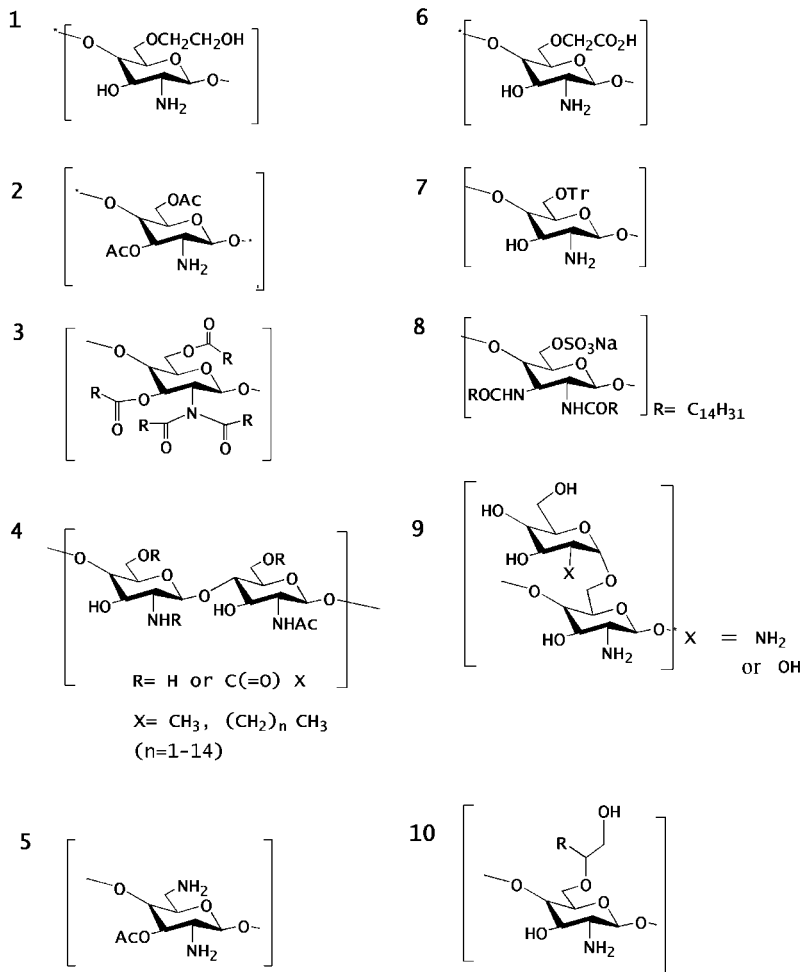


Fig. 4.3. Chemical structure of *O*-chitosan derivatives obtained either by regioselective substitution or by controlling the reaction conditions.

man THP-1 cell line. Cytokine [tumor necrosis factor- α , and interleukin (IL)-1b, IL-6 and IL-10] and metalloproteinase (MMP-2 and MMP-9) release as well as their inhibitors (TIMP-1 and TIMP-2) were assessed after incubation with different amounts of nanoparticles. Cytokine secretion was not detected even in the presence of high amounts of nanoparticles. On the contrary, the secretion of MMP-9 in cell supernatants increased significantly after 24 and 48 h in comparison to non-treated cells. MMP-2 secretion was augmented only after 48 h for the highest con-

Tab. 4.1. N-Chitosan derivatives and their proposed applications

No.	Derivative	Potential applications	References
1	cationic	protein carrier	42
2	pegylated	protein carrier and gene therapy	43–47
3	nicotinylated	separation technologies	48–50
4	phthaloylation	preparation of chitosan derivatives	51–54
5	acylation	separation technologies	55, 56
6	hydroxyalkylation	components for toiletries	57, 58
7	acylvinyl	metal adsorption	59
8	sugar-modified	drug carrier	60–63
9	sugar-modified	drug carrier	60, 64–65
10	salicylaldehyde	metal adsorption	66
11	phthalaldehyde	metal adsorption	67
12	alkylated	gene therapy	68–71
13	carboxymethylated	drug delivery/metal absorption	72–76
14	methylpyrrolidinone	biomedical applications	77, 78
15	trimethylated	gene therapy	79–85
16	thioglycolic acid	pharmaceutical	86
17	lactobionic acid	biomedical	87–89
18	<i>p</i> -azidebenzoic acid	biomedical	87–89
19	succinylated	drug delivery	90–92
20	hydroxylaminated	drug delivery	90
21	sialic acid	pharmaceutical	93, 94
22	cyclodextrin	drug delivery/cosmetics/analytical chemistry	95, 96
23	cyclodextrin	drug delivery/cosmetics/analytical chemistry	97, 98
24	cyclodextrin	drug delivery/cosmetics/analytical chemistry	99
25	acrylic	drug delivery	43
26	crown-ether bound	metal adsorption	100
27	deoxycholic acid	gene therapy	101–104
28	folic acid	gene therapy	105
29	<i>o</i> -quinones	medical applications	106
30	vinylsulfonate	antimicrobial	107

Tab. 4.2. O-Chitosan derivatives and their proposed applications

No.	Derivative	Potential applications	References
1	O-hydroxyethyl	protein carrier/gene therapy	108–110
2	acylation	metal absorption	111
3	acylation	metal absorption	112
4	acylation	electromagnetic shielding materials	113
5	amination	gene therapy	114
6	carboxymethylated	drug carrier/metal absorption	115–118
7	triphenylmethyl	drug carrier	119, 120
8	sulfated/acylated	anticoagulant/antiretroviral agents	121
9	mannoside	antimicrobial agents	122–124
10	acylated	enzyme immobilizers	57, 58

centrations of nanoparticles (10 and 20 mg mL⁻¹ DNA content). The authors have concluded that exposure of THP-1 macrophages to chitosan–DNA nanoparticles did not induce the release of proinflammatory cytokines.

The chitosan–DNA interaction is driven mainly by the electrostatic interaction between the amino groups of chitosan and the charged phosphate groups of DNA [35]. In a slightly acid medium this interaction is fully favored since almost all amine groups will be charged. MacLaughlin et al. [128] have studied the interaction of oligomeric chitosans (8–102 kDa) with plasmids containing a cytomegalovirus (CMV) promoter and a chloramphenicol acetyltransferase. On the basis of transmission electron microscopy they have observed that chitosan of 8 kDa condensed plasmids into toroids and rod-shaped particles. Using the microcalorimetry technique, the interaction could be followed and the exothermic heat output was indicated to provide a significant contribution to the free energy of the interaction. The authors have also observed a small endothermic peak at the ratio of neutrality, which was attributed to an entropic contribution to the free energy. The sizes of the particles were estimated to be 66 nm by light scattering measurements. The sizes of the particles were also shown to be dependent on the chitosan molecular weight and plasmid concentration. Complexes of a 1:6 (+/–) charge ratio showed a decrease in size as the molecular weight of the chitosan decreased and an increase in size was observed by increasing the plasmid concentration [38]. Recently, Danielsen et al. [129], employing atomic force microscopy (AFM), have confirmed that polyplexes made from mixing plasmid DNA (pDNA) with chitosan from 10 to 200 kDa yielded a blend of toroids and rods (Fig. 4.4). The ratios between the fractions of toroids and rods were observed to decrease with increasing degree of acetylation (DA) of the chitosan, indicating that the charge density of chitosan, proportional

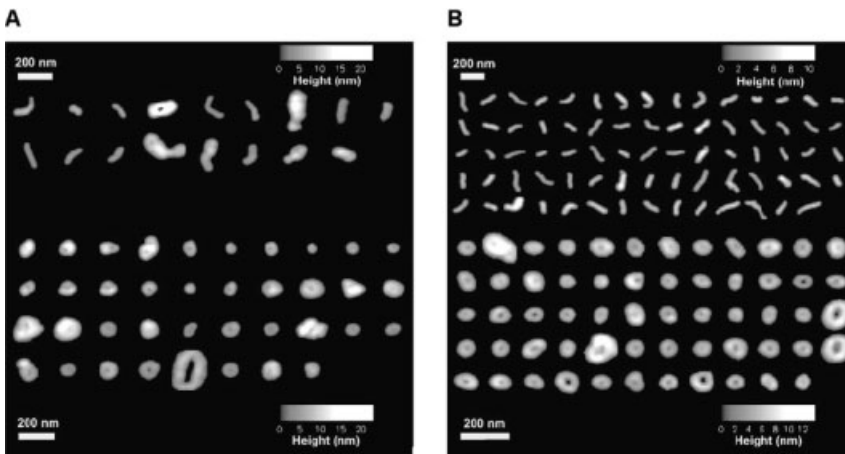


Fig. 4.4. Image galleries of toroidal and rod-like ensembles for complexes obtained using chitosan with various degrees of acetylation (DA). The chitosans ($^*DA = 0.01$, $M_n = 162$ kDa) (A) and ($^*DA = 0.15$, $M_n = 196$ kDa) (B)

were used to form complexes with pDNA pBR322. cDNA 4 μ g mL⁻¹ and average charge ratios was adjusted to 1. (Adapted from Ref. [129], with permission.)

to (1 – DA), is important in determining the shape of the compacted DNA. The amount of chitosan required to fully compact DNA into well-defined toroidal and rod-like structures was found to be strongly dependent on the chitosan molecular weight, and thus its total charge. A higher charge ratio (+/–) was needed for the shorter chitosans, showing that an increased concentration of the low degree of polymerization (DP) chitosan could compensate for the reduced interaction strength of the individual ligands with DNA. Liu et al. [130] have showed that the charge density is an important parameter by studying the formation of polyplexes at different pH values. Working with 99% deacetylated 5-kDa chitosan their results indicated that upon interacting with chitosan, the DNA molecules retained a B conformation and the binding affinity of chitosan to DNA was dependent on the pH of media. At pH 5.5, highly charged chitosan had a strong binding affinity with DNA; in pH 12.0 medium, only weak interactions existed. However, the authors have reported that no typical toroidal patterns were observed, which was attributed to the strong compaction of DNA caused by highly charged chitosan.

In a recent report, Kiang et al. have showed that in fact the electrostatic interaction with the chitosan chain is very important to efficiently bind DNA. They reported that the charge (+/–) ratio to achieve complete DNA complexation increases for chitosans having smaller degrees of deacetylation, which in turn affects the stabilization of the particles, affecting the transfection *in vitro* and *in vivo* [131]. However, other interactions such as hydrogen bonding and hydrophobic interactions cannot be neglected since hydrophobic interactions have also been detected in aqueous solutions of the polyelectrolyte itself, leading to formation of polymer chain aggregates [132, 133]. Therefore, it is reasonable consider that the formation of polyplexes may result from a combined electrostatic/hydrophobic driving force leading to the packing of chitosan–DNA polyplexes.

Various parameters such as molecular weight, charge (+/–) ratio, pH and particle size have been shown to affect the transfection efficiency. Koping Hoggard et al. [134, 135] prepared monodisperse oligomers of chitosan that were fully deacetylated (6, 8, 10, 12, 14 and 24mers) with very low polydispersity and ultrapure chitosan (UPC) of 154 kDa. Depending on the chain length of chitosan, charge ratio and buffer properties, chitosan–DNA complexes appeared as different physical shapes such as coils, soluble globules, soluble aggregates, precipitated globules and precipitated aggregates. It was shown that only UPC and 24mer chitosans could form stable complexes with DNA, and the 24mer was more efficient in mediating gene expression *in vitro* and *in vivo* than was UPC. Sato et al. [136] have also found that molecular mass of chitosan, pH of medium and serum concentration are very important to promote transfection efficiency. Working on chitosan samples whose average molecular weights were 15, 52 and 100 kDa, they found that transfection efficiency mediated by chitosan of 100 kDa was less than that by chitosan of 15 and 52 kDa, but clearly indicating that a dependence on cell lines was also observed. However, Bozkir et al. [137] have suggested that formulations with high-molecular-weight (HMW) chitosan can be an effective nonviral gene vector in animal studies. The authors have studied the influence of two different prep-

aration methods, i.e. solvent evaporation and complex coacervation method, on the encapsulation of a model plasmid with chitosan. Protection of encapsulated pDNA from nuclease attack offered by these nanoparticles was confirmed by assessing degradation in the presence of DNase I and the transformation of the plasmids with incubated nanoparticles was examined by the β -galactosidase assay. The results obtained showed that pDNA existed as a mixture of both supercoiled (84.2%) and open circular (15.8%) forms, and that the formulation prepared by the complex coacervation method effectively protected the supercoiled form of pDNA. There were no significant changes in nanoparticle size and ζ potential values at pH 5.5 for a period of 3 months, but differences in particle sizes were observed after lyophilization with a cryoprotective agent. The efficiency of nanoparticle-mediated transformation to *Escherichia coli* cells was significantly higher than naked DNA or poly-L-lysine (PLL)–DNA polycation complexes. The transfection studies were performed in COS-7 cells. A 3-fold increase in gene expression was produced by nanoparticles as compared to the same amount of naked pDNA.

The charge (+/–) ratio of the polyplexes has also been indicated as important to effectively proceed with the transfection process. Assuming that DNA wrapped in inter-polyelectrolyte complexes is well protected from DNase degradation, the following step is then to reach its target, i.e. the cell. Although the mechanism of internalization contact and crossing of the cell membrane is not fully understood, it is well accepted that the polyelectrolyte complex chitosan–DNA, exhibiting a net positive charge, binds to the negatively charged cell membrane [138]. Therefore, a net positive charge is fundamental in the process and the level of transfection is shown to increase with the charge (+/–) ratio, reaching a maximum and decreasing at higher stoichiometries. It has been reported by Ishi et al. that the level of transfection with plasmid–chitosan complexes was found to be highest when the charge (+/–) ratio was between 3 and 5, and transfection medium contained 10% serum at pH 7.0 [139]. Lee et al. using low-molecular weight (LMW) chitosan found the most efficient transfection was obtained at a charge (+/–) ratio 3:1 [140], while MacLaughlin et al. have reported that the highest level of expression was obtained at a ratio of 2:1 complex made with chitosan 102 kDa [128]. However, it must be considered that the transfection efficiency of chitosan–DNA nanoparticles is also cell-type dependent and the chitosan:plasmid ratio must be controlled to obtain the appropriate particle size when aiming to maximize the transfection [141]. The particle size is recognized as a key parameter since it may affect blood circulation time and cellular uptake. It has been reported that polycation–DNA gene delivery systems mostly enter the cell by endocytosis or pinocytosis, having a size requirement of less than 100 nm [141, 142]. However, the experimental results available are contradictory and reasonable transfection efficiencies were reported for particles having sizes varying from 100 nm [143] to 2.0 μ m [144]. Recently, on the basis of AFM images, Liu et al. have proposed that chitosan–DNA complexes in the range of several hundreds of nanometers are transferred into the cell mainly via endocytosis [145].

After internalization, the following crucial step in gene delivery with cationic

polymers is the escape of the polymer–DNA complexes from the endosome. The inefficient release of the DNA–polymer complex from endocytic vesicles into the cytoplasm is indicated as one of the primary causes of poor gene deliver. In this respect the approach is to enhance endosomal escape by using cationic polymers with a pK_a slightly below the physiological pH. The endosomal escape is believed take place through the mechanism named the “proton sponge”, and the importance of this step has been recognized and reviewed recently by Cho et al. [146]. This hypothesis has been proposed to explain the high transfection activity of polyethyleneimine (PEI) [147]. It has been demonstrated that PEI has a buffering capacity over a broad pH range; hence, once PEI-based polyplexes are present in the endosome, they can absorb protons that are pumped into this organelle. Due to repulsion between the protonated amine groups, swelling of the polymer occurs. Moreover, to prevent the build up of a charge gradient due to the influx of protons, an influx of Cl^- ions also occurs. The influx of both protons and Cl^- ions increases the osmolarity of the endosome and causes water absorption. The combination of swelling of the polymer and osmotic swelling of the endosome leads to a destabilization of the endosome and release of its contents into the cytoplasm [147]. Subsequently, transport to and uptake in the nucleus as well as dissociation of the polyplex has to occur before transcription of the DNA takes place. However, Funhoff et al., working with a series of synthetic polymers [148], indicated that endosomal escape is not always enhanced by polymer buffering at low pH. In this respect, research focusing on chitosan is scarce, but it is believed that protonation of the free amine groups of chitosan must contribute to the unpacking of the DNA, delivering it in the cytoplasm. Ishi et al. [139] have indicated that when the transfection is performed at pH 6.5 chitosan cannot release from the endosome due to the fact that chitosan is drastically protonated when the pH of medium is altered from pH 7 to 6. Recently, to enhance the transfection efficiency of chitosan, water-soluble chitosan (WSC) was coupled with urocanic acid (UA) and the transfection efficiency was investigated [149]. The authors reported that the transfection efficiency of chitosan into 293T cells was greatly enhanced after coupling with UA and increased with an increase of UA content in the urocanic acid-modified chitosan. Kiang et al. [150] have used poly(propyl acrylic acid) (PPAA) as an approach to enhance the release of endocytosed drugs into the cytoplasmic compartment of the cell. The release of pDNA from the endosomal compartment was enhanced by incorporating this polymer in chitosan nanoparticles. *In vitro* transfection studies confirmed that the incorporation of PPAA into the chitosan–DNA nanoparticles enhanced gene expression in both HEK 293 and HeLa cells compared to chitosan nanoparticles alone. The dose and time at which PPAA was incorporated during the complex formation affected the release of DNA and transfection efficiency. The authors have suggested that the PPAA triggered membrane disruption resulting in the release of DNA from the endosomal compartment.

Therefore neither high cellular uptake, membrane destabilizing activity, endosomal escape nor nuclear localization alone is adequate for high transfection. More studies aiming at a better understanding of these steps as well how the released DNA is expressed will be necessary to improve the transfection efficacy.

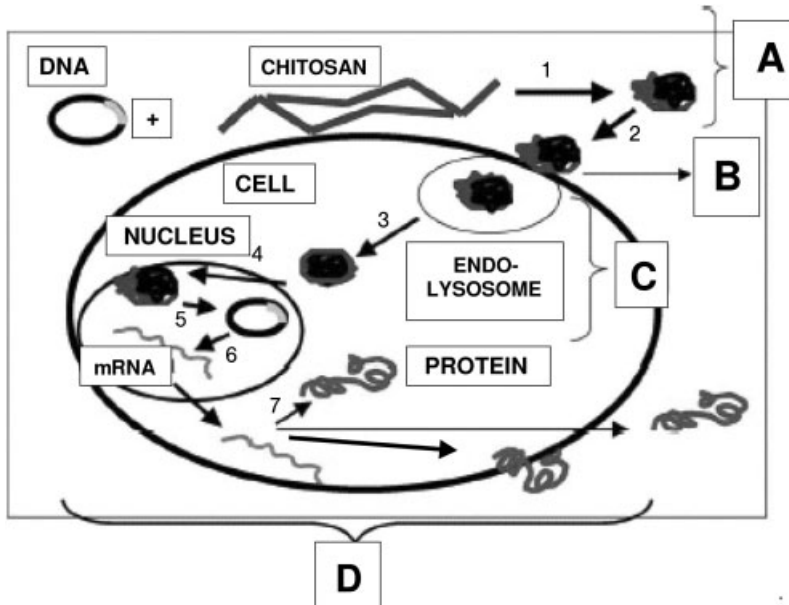


Fig. 4.5. Schematic gene therapy mechanism. (A) Bioavailability and extracellular trafficking, and gene-vector complexation (1); (B) internalization and endocytosis by the cell membrane (2); (C) intracellular trafficking and uptake of the vector complex into intracellular endolysosome: (3) DNA–chitosan release from the endosome into the cytoplasm and (4) internalization of the complex into the nucleus; (D) gene expression: (5) DNA dissociation from the vector, (6) mRNA transcription from the gene and (7) protein translation from mRNA. The protein can be secreted out of the cell, released into the cytoplasm or fixed onto the membrane. (Adapted from Ref. [251].)

4.3

Modified Chitosans: Strategies to Improve the Transfection Efficacy

4.3.1

The Effects of Charge Density/Solubility and Degree of Acetylation

Many strategies have been employed to improve the transfection efficiency taking into account the biological steps involved in gene delivery (Fig. 4.5). The literature on this subject shows that the main method is the modification of chitosan structure aiming at providing the necessary capabilities to overcome the barriers previously mentioned, i.e. decreasing the interaction with blood components, vascular endothelial cells and uptake by the reticuloendothelial system (RES), avoiding the degradation of therapeutic DNA by serum nucleases, improving the particle size, internalization, endosomal escape and nuclear import. The attachment of a group or a polymer chain may be either at the main-chain or at the preformed nanoparticles.

The simplest modification in the chitosan structure is to vary the degree of acetylation. This is expected to affect the chitosan–DNA interactions since the charge density is decreased, i.e. the number amino groups is decreased, giving the polymer chain an increased hydrophobic character. Kiang et al. have recently studied the effect of the degree of chitosan deacetylation on the efficiency of gene transfection [131]. They concluded that a decreased degree of deacetylation resulted in a decrease in overall luciferase expression levels in HEK 293, HeLa and SW756 cells due to particle destabilization in the presence of serum proteins. The degree of deacetylation was shown to affect DNA binding, release and gene transfection efficiency *in vitro* and *in vivo*. Various workers aiming to increase the transfection have also investigated trimethylation (quaternization) of the amino groups [81, 84, 151, 152]. The advantage of trimethylated chitosans arises from their higher solubility when compared with the nonmodified polymer. Trimethyl chitosan (TMO) derivatives of 40% (TMO-40) and 50% (TMO-50) degrees of quaternization were synthesized, and examined for their transfection efficiencies in two cell lines: COS-1 and Caco-2 [81, 84]. Results showed that quaternized chitosan oligomers were able to condense DNA and form complexes with a size ranging from 200 to 500 nm. Chitoplexes were shown to transfect COS-1 cells to a lesser extent than DOTAP (*N*-[1-(2,3-dioleoyloxy)propyl]-*N,N,N*-trimethylammonium sulfate)–DNA lipoplexes. Both DOTAP–DNA lipoplexes and chitoplexes resulted in lower transfection efficiency in Caco-2 cell cultures than in COS-1 cells; however, quaternized chitosan oligomers proved to be superior to DOTAP.

4.3.2

Improving the Physicochemical Characteristics of the Nanoparticulate Systems: Solubility, Aggregation and RES Uptake

After administration, the DNA must be capable of surviving in the bloodstream for a significant length of time so that it can reach the target tissue. Therefore, circulation time is a fundamental factor for reaching the target cells in successful gene delivery, especially in cases of intravenous injection [153]. Nanoparticles will usually be taken up by the liver, spleen and other parts of the RES depending on their surface characteristics. Particles with more hydrophobic surfaces will preferentially be taken up by the liver, followed by the spleen and lungs [154]. Cationic polymer–DNA complexes also show short plasma circulation times with rapid hepatic uptake and accumulation or deposition in organs such as the skin and intestine. Aggregation of cationic particles, such as cationic polymer–DNA complexes, can occur following interaction with blood components. Albumin is known to bind to cationic particles. The binding of albumin may be enough to cause aggregation of particles in the bloodstream, by reducing their ζ potential and, hence, reducing the charge repulsion between particles. Extensive aggregation could lead to physical deposition in the capillary bed. Therefore, it is necessary to prevent unwanted interactions between particles and the dynamic environment of the blood circulation by introducing hydrophilic surfaces to the cationic particles. In the absence of a hydrophilic surface, opsonization prepares the particles for uptake by fixed macro-

phages of the mononuclear phagocytic system (MPS). The MPS is a collection of phagocytic cells that are present in tissue of the RES and are collectively responsible for clearance of particles from the circulation. The activity of RES is not to clear charged particles. In practice, typically 80–90% of hydrophobic particles are opsonized and taken up by fixed macrophages of the liver and spleen, often within a few minutes of intravenous administration. Opsonization represents a major biological barrier to the delivery of DNA using condensed particles. Therefore, the modification of chitosan by introducing hydrophilic polymers may create a “cloud” of hydrophilic chains at the particle surface, which may avoid interactions with proteins and phagocytes, thus prolonging the circulation time in the bloodstream [154].

Many hydrophilic groups can be attached to the chitosan backbone or to preformed nanoparticles to improve solubility in water [43–47]. Sashiva et al. [43] have used the Michael reaction of chitosan in water containing acetic acid with various acryl reagents. The modification was controlled by varying the temperature, reaction time and amount of the acryl reagent, and has provided chitosan derivatives showing good biodegradation characteristics. Nanospheres synthesized by salt-induced complex coacervation of cDNA, and gelatin and chitosan were evaluated as gene delivery vehicles [155]. These nanospheres were subsequently modified by introducing PEG₅₀₀₀ chains. The attachment of these groups avoided the aggregation of particles during lyophilization and storage for 1 month did not alter the properties of the nanospheres. Chitosan–DNA nanospheres were effective in transfecting HEK 293 cells, but not HeLa cells, and the transfection efficiency was not affected by PEG derivatization. Poly(vinyl pyrrolidone) was also grafted on galactosylated chitosan (GCPVP) and showed improved physicochemical properties over the unmodified chitosan [156]. The binding strength of GCPVP 10K–DNA was superior to that of GCPVP 50K–DNA, which was attributable to its higher flexibility due to the smaller size. However, DNase I protection of GCPVP 10K–DNA was inferior to that of GCPVP 50K–DNA. The DNA-binding properties mainly depended on the molecular weight of chitosan and composition of PVP.

4.3.3

Targeting Mediated by Cell Surface Receptors

It is well known that some kinds of saccharides play important roles in biological recognition on cellular surfaces. Liver parenchymal cells exclusively express large numbers of asialoglycoprotein receptors that strongly bind with galactose [157, 158]. The asialoglycoprotein receptor (ASGP-R) is known to be present only on hepatocytes at a high density of 500 000 receptors per cell and retained on several human hepatoma cell lines [159, 160]. This characteristic may be explored in many ways to target the cells. In a recent study on the biodegradability it was demonstrated that chitosan modification with gluconic acid enhanced susceptibility to lysozyme [161]. D-Gluconic acid is a hydrophilic sugar derivative that may be covalently attached to the chitosan backbone, providing multifunctional properties. As a consequence, by simple modification with gluconic acid and acetic anhydride, it is possible to control the aqueous solubility. The ASGP-R system cannot only bind

galactose-containing ligands, but can also internalize them within membrane-bound vesicles or endosomes [162]. Once a ligand binds to the galactose receptor, the ligand–receptor complex is rapidly internalized and the receptor recycles back to the surface [163, 164], allowing high binding capacity and efficient uptake of galactosylated ligands by liver cells. Murata et al. have suggested that the utilization of a prequaternized and subsequently galactosylated chitosan could be used to transfect cells HepG2 cells [164]. Park et al. have used this specificity to synthesize galactosylated chitosan (GC) in an attempt to transfect HepG2 human hepatoblastoma cells and HeLa human cervix epithelial carcinoma cells [165–167]. The particle sizes for the DNA complexes using GC-13K and GC-18K show a tendency to decrease with increasing charge ratio of GC to DNA, and had minimum values around 240 and 100 nm, respectively, at the charge ratio of 5. The cytotoxicity study showed that GC prepared by water-soluble chitosan had no cytotoxic effects on cells. The results showed that the transfection efficiency into HepG2, which has ASGP-Rs, was higher than that into HeLa without ASGP-Rs. The attachment of PEG to GC (GPC) was also performed in other work by the same group with the aim to improve the stability in water and enhance the cell permeability [168]. In this case it was reported that GCP–DNA complexes were only transfected into HepG2 having ASGP-Rs, indicative of a specific interaction of ASGP-Rs on cells and galactose ligands on GCP. The transfection with GCP–DNA complexes was subsequently investigated by confocal laser scanning microscopy using primary hepatocytes and HepG2 human hepatocarcinoma cell line [169]. The more efficient transfection of the complex occurred in the human-derived HepG2 cells than in primary hepatocytes. Erbacher et al. [170] synthesized lactosylated-modified chitosan derivatives (having various degrees of substitution) and tested their transfection efficiencies in many cell lines. The *in vitro* transfection was found to be cell-type dependent. HeLa cells were efficiently transfected by this modified carrier even in the presence of 10% serum, but neither chitosan nor lactosylated chitosans have been able to transfect HepG2 and BNL CL2 cells. Gao et al. [171] have used highly purified LMW chitosan (LMWC) to attach lactobionic acid (LA) bearing a galactose group. A series of galactosylated LMWC (gal-LMWC) having different group contents was obtained. The transfection efficiency was evaluated in human hepatocellular carcinoma cells (HepG2), L-02, SMMC-7721 and human cervix adenocarcinoma (HeLa) cell lines *in vitro*. The transfection of the gal-LMWC–DNA complex showed a very selective transfection to hepatocytes and the efficiency was shown to increase with the improvement of the degree of galactosylation.

Transferrin is another interesting targeting ligand to attach to the chitosan backbone. Transferrin receptors are found on the surface of most proliferating cells, and, in elevated numbers, on erythroblasts and on many tumors where they have been linked to drug resistance [172]. Leong et al. have reported the conjugation of PEG to preformed nanoparticles of gelatin and chitosan using different procedures [141, 155]. Transferrin was bonded to nanospheres utilizing a sulfhydryl derivative obtained from the protein reaction with 2-iminothyalone, while PEG conjugation was performed utilizing PEG derivatives containing the succinimidyl attached to

the end of the backbone. For the chitosan carrier, the plain nanospheres were reported as effective as the pegylated chitosan-modified nanospheres. However, the conjugation of PEG to the surface of the nanospheres minimized any aggregation in solution [155]. In a subsequent work, Mao et al. attached transferrin to the nanospheres employing two different procedures – periodate oxidation and disulfide linkage [141]. The KNOB protein was also conjugated to the nanoparticles using a bis-succinimidyl PEG derivative. The conjugation of KNOB protein to chitosan–DNA nanoparticles was reported to increase the transfection efficiency 130-fold in HeLa cells and several fold in HEK 293 cells. Chitosan has also been investigated for its ability to form polymeric targeted vesicle drug carriers. Glycol chitosan modified by attachment of a strategic number of fatty acid pendant groups (11–16 mol%) assembles into unilamellar polymeric vesicles in the presence of cholesterol [173, 174]. These polymeric vesicles were found to be biocompatible and hemocompatible, and capable of entrapping water-soluble drugs aiming to target receptors overexpressed in some tumors. Recently, the *in vivo* biological evaluation of doxorubicin formulated in transferrin targeted polymeric vesicles made from palmitoylated glycol chitosan (GCP) was reported. The transferrin-conjugated vesicles showed a statistically significant uptake advantage when compared to the non-targeted vesicles [175].

Use of the folic acid receptor is another approach that can be used to target tumors since cancerous cells divide rapidly and need folic acid to DNA synthesis. This morphological phenomenon is best noted by upregulation of membrane folate binding protein expression for a subsequent increase in folate internalization. The conjugation of folic acid with PEI was done previously by Guo and Lee [176], and more recently by others authors [177, 178]. Guo et al. found that attaching folates to the distal termini of PEG-modified PEI greatly enhanced the transfection activity of the corresponding DNA complexes over polyplexes containing PEG-modified PEI. The enhancements were observed at all charge (+/–) ratios tested and could be blocked partially by coincubation with 200 μM of free folic acid, which suggested the involvement of the folate receptor (FR) in gene transfer. Folate conjugation, therefore, presents a potential strategy for tumor-selective targeted gene delivery. Recently, Mansouri et al. [105] have reported the first conjugation with chitosan. The nanoparticles obtained for folic acid-modified chitosan (FA-CH) showed a very low toxicity and the coacervation process utilized to obtain the FA-CH–DNA did not affect the integrity of the utilized plasmid. These new nanoparticles are currently being tested in transfection studies.

4.3.4

Hydrophobic Modification: Protecting the DNA and Improving the Internalization Process

Hydrophobic modification is expected to improve the interaction between the DNA and the chitosan since, apart from the electrostatic interactions, the hydrophobic interactions will be increased, which may provide better protection for DNA. *N*-dodecylated chitosan (CS-12) has been synthesized and assembled with DNA to

form a polyelectrolyte complex (PEC) [71]. Dissociation of CS-12–DNA complexes was investigated by the addition of LMW electrolytes and these small molecular salts dissociated the CS-12–DNA complex, inducing the release of DNA. The ability of Mg^{2+} to dissociate the CS-12–DNA complex was greater than compared to that of Na^+ and K^+ . The incorporation of CS-12 could enhance the thermal stability of DNA and AFM images showed a globule-like structure composed of 40–115 DNA molecules. Lee et al. synthesized deoxycholic acid-modified chitosan (DAMC) which contained 0.6–5.1 deoxycholic acid groups per 100 anhydroglucose units [102]. The mean diameter of DAMC in PBS solution was less than 180 nm with a unimodal size distribution [103, 104]. Complex formation between DAMC and pDNA was confirmed by electrophoresis on an agarose gel. In other work by the same authors the structure of DAMC was found to strongly depend on the molecular weight of chitosan ranging from 5 to 200 kDa [179]. The size of the chitosan aggregates was not precisely controlled by varying the degree of substitution, pH and ionic strength of the medium. Due to the chain rigidity of chitosan, the structure of self-aggregates was suggested to be a cylindrical bamboo-like structure when the molecular weight of chitosan was larger than 40 kDa, which might form a very poor spherical shape of a birdnest-like structure. Complex formation showed a strong dependency on the size and structure of chitosan self-aggregates, and significantly influenced the transfection efficiency of COS-1 cells (up to a factor of 10). Recently, Liu et al. proposed that hydrophobic modification increases internalization process, thus increasing the transfection efficiency [145]. A series of alkylated chitosans (ACSS) derivatives from alkyl bromides was synthesized employing a 99% deacetylated chitosan (CS). The CS and ACSSs were used as vectors for gene transfection, and the effects of hydrophobicity of the alkyl side-chain on the transfection activity were evaluated. It was reported that the complex formation between the ACSSs and DNA requires a relatively smaller amount of ACS compared to unmodified chitosan due to the hydrophobic interaction. The transfection was evaluated in C2C12 cell lines using pcDNA 3.1 plasmid encoding chloramphenicol acetyltransferase. The transfection level was reported to increase upon elongating the alkyl side-chain. The disadvantage of the hydrophobic modification is that the particles are more easily recognized by macrophages of the RES; hence, amphiphilic chitosan may in the future present more advantages than that exhibited by the hydrophobic modification alone [180–182].

4.4

Methods of Preparation of Chitosan Nanoparticles

4.4.1

Complex Coacervation

Numerous works using different methodologies have been published on the preparation of chitosan micro and nanoparticles; however, for gene therapy, complex coacervation has been the procedure most employed and most of the references

discussed in the previous sections of this chapter relate to this method. The process is a spontaneous phase separation that occurs when two oppositely charged polyelectrolytes are mixed in an aqueous solution. The electrostatic interaction between the two species of macromolecules results in the separation of a coacervate (polymer-rich phase) from the supernatant (polymer-poor phase). This phenomenon can be used to form microspheres and encapsulate a variety of compounds. The encapsulation process can be performed entirely in aqueous solution and at low temperatures, and has a good chance, therefore, of preserving the bioactivity of the encapsulant. In developing an injectable controlled release system, various authors have used the complex coacervation of chitosan and DNA as the main procedure to obtain nanoparticles. In general, chitosan is dissolved in acetic acid/sodium acetate buffer and vortexed rapidly with a pDNA solution at room temperature. Sato et al. [136] reported that complexes of luciferase plasmid (pGL3) with chitosan were prepared only by mixing 100 μL of pGL3 solution (1 mg mL^{-1}) with a given amount of chitosan solution (2.95 mg mL^{-1}). The mixtures were gently stirred at room temperature for a couple of hours. Koping-Hoggard et al. [134] reported the preparation chitosan–pDNA complexes were formulated by adding chitosan and then pDNA stock solutions to the solvent (deionized MilliQ water, $\text{pH } 6.2 \pm 0.1$ or 25 mM acetate buffer, $\text{pH } 5.0$) under intense stirring on a vortex mixer. The sizes of the aggregates (200–3400 nm) were determined by photon correlation spectroscopy, and found to be dependent of the DNA type, chitosan molecular weight and pH. Nanoparticles having sizes ranging from 170 to 180 nm were obtained by Kiang et al. [131] by heating chitosan and DNA solutions separately to 50–55 $^{\circ}\text{C}$, and then mixing equal volumes of both solutions under high vortexing for 30 s.

It has been reported that, depending of the molecular weight of chitosan, complexes of chitosan–DNA with mean sizes between 50 and 6000 nm can be obtained only by simple mixing followed by incubation [136, 139, 141]. In general, stable complexes are formed only when chitosan is added in molar excess relative to DNA, with ζ potential values between 10 and 20 mV, depending upon the degree of excess. Recently, Danielsen et al. [129] reported that the shape of the nanoparticles can vary depending on the degree of acetylation, molecular weight and concentration of chitosan. The DNA stock solution was diluted in NH_4Ac (150 mM, $\text{pH } 7.4$) and complexes were then prepared by adding the chitosan solution to the DNA solution. The average contour length $\langle L_c \rangle$ of the toroidal and rod-like DNA–chitosan polyplexes was found to be about 130 nm, independent of the linear or toroidal geometry of the complex and the chitosan employed (30–200 kDa). The complex sizes were found less than 1/10 of the contour length of the uncomplexed plasmid (pBR322, 4363 bp; Boehringer Mannheim) of 1.5 μm . Decreasing the charge density of the chitosan resulted in a decrease in the toroid-to-rod ratio, indicating that the strength of the intersegment interaction, mediated by the charge of the chitosan, is important in determining the shape of the DNA–chitosan complexes, with the toroid being the preferred structure for high intersegment attractions. The stability of these DNA–chitosan complexes was studied after exposure to heparin and hyaluronic acid (HA) using AFM and ethidium bromide (EtBr) fluo-

rescence assay. Studies of polyplex stability when challenged by HA showed that whereas HA was unable to dissociate the complexes, the degree of dissociation caused by heparin depended on both the chitosan chain length and the amount of chitosan used for complexation [183].

4.4.2

Crosslinking Methods

4.4.2.1 Chemical Crosslinking

The crosslinking procedures can be classified as (a) chemical crosslinking and (b) ionic crosslinking. The first involves the formation of covalent bonding between the chitosan chains and the chemical agents. The use of crosslinked nanospheres of chitosan for gene therapy has not been frequently found in the literature because after formation, chitosan–DNA nanoparticles obtained from the coacervation process are reported to be stable. At physiological pH, most of the positive charges would be neutralized and the hydrophobic chitosan becomes insoluble. This unique property ensured that nanoparticles formed at low pH could remain physically stable at physiological pH without chemical crosslinking; however, this was not observed, for example, for gelatin–DNA nanoparticles, which required a crosslinking agent to remain stable [141]. The process involves the precipitation of the polymer followed by chemical crosslinking [184, 185]. Precipitation can be done by sodium sulfate followed by chemical crosslinking using glutaraldehyde, formaldehyde or even using a natural crosslinking agent such as genepin [186, 187]. Recently, glutaraldehyde was used to obtain chitosan microparticles encapsulating an IL-2 expression plasmid [188]. Chitosan microspheres containing recombinant (r) IL-2 were prepared by using the precipitation technique. The rIL-2 encapsulation efficiency in the microspheres was high (75–98%) and the size was reported to vary from 1.45 to 2.00 μm . The authors noted that IL-2 was released from chitosan microspheres over a period of 3 months and remained biologically active, being completely recovered from the release medium. Akbuga et al. [189] have studied the effect of formulation variables (concentration and molecular weight of chitosan, plasmid amount, use of glutaraldehyde as a crosslinker) on microsphere properties. Plasmid-loaded chitosan microspheres were prepared by adding the pDNA to 50 mL of sodium sulfate solution (20% w/v) and this mixture was dropped into 50 mL of acidic solution of chitosan and stirred for 1 h at 500 rpm. The microspheres formed were washed with bidistilled water, separated by centrifugation, freeze-dried and then stored at 4 °C in a desiccator. A high level of IL-2 expression was reported with plasmid-loaded chitosan microspheres in MAT-LyLu, a rat prostate adenocarcinoma cell line, but the authors noted that addition of glutaraldehyde was not necessary for the formulation. Although no damage has been observed in the DNA structure after using glutaraldehyde as a co-crosslinker, it reduced pDNA release from microspheres.

4.4.2.2 Ionic Crosslinking or Ionic Gelation

In ionic crosslinking methods a variety of negatively charged compounds, from small ions to HMW polymers, can be used to produce micro- and nanoparticles

[37]. Ionic crosslinking in aqueous solution occurs due to the electrostatic interaction between the charged amino groups of chitosan and a salt or polyanion. The reactions with negatively charged components, either ions or molecules, can lead to the formation of a network between polymeric chains through ionic bridges. In ionic crosslinking, the entities reacting with chitosan are ions or ionic molecules with a well-defined molecular weight. In contrast, in polyelectrolyte complexation, the entities reacting with chitosan are polymers with a broad molecular weight distribution. In addition to its simplicity [190, 191], the method can be considered a safer alternative, since it avoids chemical crosslinking, and the possible toxicity of reagents and other undesirable effects [192]. There are two salts that have been frequently used in the preparation of chitosan particles by the ionic crosslinking mechanism: sodium tripolyphosphate (PSTP) [193, 194] and sodium sulfate [195]. Li et al. [196] prepared nanoparticles with a size range of 40–200 nm by an ionic gelation procedure using tripolyphosphate, sodium citrate and sodium hydroxide. Chitosan particles formed on the basis of ionic gelation with PSTP were demonstrated to be much more stable than those obtained with sodium citrate and sodium hydroxide. The ability of particles to complex DNA was investigated using gel retardation. Results showed that these chitosan particles have potential as vectors for the transfer of DNA into mammalian cells. Cellular transfection by the chitosan-pGL3-control particles showed a sustained expression of the luciferase gene for about 10 days. Jiang et al. [197] have also prepared chitosan microparticles with tripolyphosphate. The microparticles were tested for nasal vaccination loaded with *Bordetella bronchiseptica* dermonecrototoxin (BBD), a major virulence factor of a causative agent of atrophic rhinitis. The average particle size of the BBD-loaded chitosan microparticles was 4.39 μm . The results reported that released BBD from chitosan microparticles had immune-stimulating activity of the atrophic rhinitis vaccine *in vitro*. Numerous works have been published on ionic crosslinking (ionic gelation) [198–205]; however, these works mainly focused on the various pharmaceutical applications which have been recently reviewed by Kumar et al. [40], Agnoutri et al. [192] and Sinha et al. [37].

4.4.2.3 Emulsion Crosslinking

This method utilizes an acetic acid solution of chitosan, which is added to an organic solvent containing an emulsifier to form a water-in-oil emulsion (w/o). The chitosan solution is added dropwise under different conditions of stirring and temperature. The degree of stirring (i.e. time and speed of stirring during emulsification) determines the size of the dispersed droplets. By varying any one or both of these parameters, the size of droplets can be changed to obtain the product (i.e. chitosan microspheres) in the desired size range. Liquid paraffin is frequently used as the oil phase and, after the formation, the particles are crosslinked using chemical agents as glutaraldehyde or formaldehyde [206]. The literature abounds with reports wherein chitosan microspheres have been prepared for drug delivery. Akbgua and Durmaz [207] prepared chitosan microspheres containing furosemide from a w/o emulsion system using liquid paraffin as the external phase and a solution of chitosan in acetic acid as the disperse phase. Discrete spherical furosemide microspheres having a diameter range of 350–690 μm were produced. Micro-

sphere properties were affected by the preparation variables such as the type and concentration of chitosan, drug concentration, crosslinking process, viscosity of oil, and stirring rate during the preparation. An emulsification/solvent evaporation process was carried out under mild conditions for Genta et al. [208] to entrap the hydrophobic drug ketoprofen. Glutaraldehyde at different concentrations was used as the chemical crosslinking agent on microspheres constituted by different theoretical ketoprofen/chitosan ratios (1:2, 1:4 and 1:6 w/w). Chitosan microspheres were morphologically characterized for shape, surface characteristics and size distribution; chitosan/ketoprofen interactions inside microspheres were investigated by differential scanning calorimetry and powder X-ray diffraction. Recently, Kumbar et al. [209] have used the emulsion crosslinking method to prepare chitosan microspheres to encapsulate diclofenac sodium using three crosslinking agents: glutaraldehyde, sulfuric acid and heat treatment. Microspheres were spherical with smooth surfaces. The size of the microparticles ranged between 40 and 230 μm . Among the three crosslinking agents used, glutaraldehyde crosslinked microspheres showed the slowest release rates, whereas a quick release of diclofenac sodium was observed by the heat crosslinked microspheres. The influence of different parameters as well as the incorporation of different drugs has been extensively studied [210–217], including chitosan-coated systems (hybrid systems) [218, 219]. In these systems emulsions, nanocapsules and nanoparticles are coated by introducing chitosan into the external aqueous phase in which the formation of the colloidal structures take place. The chitosan coating is a result of the ionic interaction with nanoemulsions and nanocapsules, and no crosslinking is needed. In a recent work, Lee et al. [220] used chitosan as a condensing agent to enhance the transfection efficiency of a cationic emulsion-mediated gene delivery vehicle in human hepatoma cells (HepG2). The authors reported that the size of the complexes was reduced after condensation of DNA by chitosan. The results suggested that the use of chitosan enhanced the *in vitro* transfection efficiency and extended the *in vivo* gene transfer.

4.4.2.4 Spray Drying

Spray drying is a method based on drying atomized droplets in a stream of hot air. In this method, chitosan is first dissolved in aqueous acid solution containing a dissolved or dispersed drug, in which a suitable crosslinking agent is added. Particle size depends upon the size of nozzle, spray flow rate, atomization pressure, inlet air temperature and extent of crosslinking. He et al. [221] have prepared crosslinked and noncrosslinked chitosan microspheres. The authors reported that the particle size ranged from 2 to 10 μm , and that the size and ζ potential of the particles were influenced by the crosslinking level. The particles sizes as well as the ζ potential were observed to increase with decreasing amounts of the crosslinking agents (glutaraldehyde and formaldehyde). Mi et al. [222] have reported the preparation of microspheres with small size and good sphericity. A histological study of the genipin-crosslinked chitosan microspheres injected intramuscularly into the skeletal muscle of a rat model showed a less inflammatory reaction than its glutaraldehyde-crosslinked counterparts. The authors have suggested that the genipin-crosslinked chitosan microspheres may be a suitable polymeric carrier for

long-acting injectable drug delivery. Chitosan microspheres with hydrocortisone and hydrocortisone–hydroxypropyl- β -cyclodextrin inclusion complex were studied by Filipovi et al. [223]. Microspheres were studied with respect to particle size distribution, drug content and *in vitro* drug release. The results indicate that the hydrocortisone–hydroxypropyl- β -cyclodextrin inclusion complex is more water soluble than hydrocortisone alone. The hydrocortisone release rates from chitosan microspheres were influenced by the drug/polymer ratio in the manner that an increase in the release rate was observed when the drug loading was decreased. The influence of acid type on the release behavior of sodium diclofenac microspheres was studied by Orienti et al. [224]. Among the salts used, glutamic and aspartic salts provided the best control of release. Huang et al. [225] prepared chitosan microspheres by a spray-drying method using type A gelatin and ethylene oxide–propylene oxide block copolymer as modifiers. The microspheres were investigated using scanning electron microscopy (SEM) and microelectrophoresis. The particle shape, size and surface morphology of microspheres were affected by the concentration of gelatin. Betamethasone disodium phosphate (BTM)-loaded microspheres demonstrated good drug stability (less than 1% hydrolysis product), high entrapped efficiency (95%) and a positive surface charge (37.5 mV). The *in vitro* drug release from the microspheres was related to gelatin content. Microspheres containing gelatin/chitosan 0.4–0.6 (w/w) had a prolonged release pattern for 12 h. These formulation factors were correlated to particulate characteristics for optimizing BTM microspheres in pulmonary delivery. Recently, various systems have shown potential application for nasal [226, 227], pulmonary [228] and DNA [229] delivery.

4.4.2.5 Other Methods

Apart from those methods mentioned above, a number of other methods have been reported for the preparation of chitosan micro- and nanoparticles, such as the reverse micellar [231–233], emulsion droplet coalescence [234–238] and sieving [239] methods.

The reverse micellar method is similar to emulsion crosslinking in the sense that in both methods a w/o aggregate is formed; however, the reverse micelles are thermodynamically stable liquid mixtures of water, oil and surfactant. Macroscopically, they are homogeneous and isotropic, structured on a microscopic scale into aqueous and oil microdomains separated by surfactant-rich films. The main advantage of the reverse micellar method is a better control of particle sizes. In the phase diagram of a system in which reverse micelles exist, there is plenty of room to adjust the proportions of the organic solvent and water as well as the surfactant ratio. This allows the dimensions of the reverse micellar particles to be modulated by varying the degree of hydration (molar ratio of $[\text{H}_2\text{O}]/[\text{surfactant}]$) of the system. When the surfactant is kept at a constant concentration, increasing the water content will increase the volume of the reverse micelles. Alternatively, if the water content constant is kept constant, then increasing the surfactant concentration will cause the volume of reverse micellar particles to become smaller. Finally, if both the water and the surfactant concentrations are increased in a constant ratio, the volume of reverse micelles will not change, but the number of vesicles will

increase. Aghnoutri et al. have described this process in the following steps – preparation of the reverse micellar system, adding chitosan and drug, adding cross-linking agent, stirring overnight, evaporation of solvent, and purification [36]. Banerjee et al. [231] reported a procedure to prepare ultrafine crosslinked chitosan nanoparticles in an AOT–*n*-hexane reverse micellar system. They observed that the particle size is influenced by the degree of crosslinking and was found to be 30 nm when 10% of the amino groups in the polymeric chain had been crosslinked, whereas it was 110 nm when all the amino groups were crosslinked. These particles were thoroughly characterized, and electron micrographs reveal that the particles were spherical in shape and that lower crosslinking of the particles leads to smaller aggregates, while highly dense aggregates were formed at 100% crosslinking. The biodistribution of the particles after intravenous injection in mice showed that these particles remain in the blood for a considerable amount of time, and distribute in the heart, liver, kidneys, bladder and vertebral column. Other than these organs, the particles were distributed in the bone marrow, opening the possibility of using these particles for bone imaging and targeting purposes [231]. Andersson and Lofroth [232] investigated a new microemulsion based on heparin–chitosan complex suitable for oral administration. The microemulsion is based on ingredients that are acceptable to humans. These microemulsions were studied with or without biologically active ingredients by dynamic light scattering, turbidity, diffusion nuclear magnetic resonance and conductivity. Appropriate mixing and modifications of these microemulsions lead to nanometer-sized heparin–chitosan complexes [232].

In the emulsion droplet coalescence method, two w/o emulsions are prepared – one containing chitosan and the drug, and other a stable aqueous emulsion of NaOH. The solutions are mixed under high-speed stirring, which leads particle collision, forming solid microparticles that are centrifuged and washed. Gadopentetic acid-loaded chitosan nanoparticles have been prepared by this method for gadolinium neutron capture therapy – a cancer therapy that utilizes γ -rays emitted during the reaction $^{157}\text{Gd}(n, \gamma)^{158}\text{Gd}$ to kill tumor cells [234, 235]. The bioadhesive characteristics of chitosan and its capacity to recognize, to a certain extent, the tumor cells prompted research on the delivery of gadolinium with the aid of chitosan. Tokumitsu et al. [236] have reported that particles produced using 100% deacetylated chitosan had a mean particle size of 452 nm with 45% drug loading. Nanoparticles were obtained within the emulsion droplet. The size of the nanoparticle did not reflect the droplet size. Since gadopentetic acid is a bivalent anionic compound, it interacts electrostatically with the amino groups of chitosan, which would not have occurred if a crosslinking agent is used that blocks the free amino groups of chitosan. Thus, it was possible to achieve higher gadopentetic acid loading by using the emulsion droplet coalescence method compared to the simple emulsion crosslinking method.

Fully deacetylated chitosan was dissolved in 10% gadolinium diethylenetriamine-pentaacetic acid (GdDTPA) solution to obtain 2.5% chitosan concentration. Then, 1 mL of this solution was added to liquid paraffin (10 mL) with Arlacel 5% and stirred with a homogenizer to form a w/o emulsion. Separately, a similar emulsion

was prepared with NaOH and then the two emulsions were combined to solidify the chitosan droplets. Washing was done with toluene, ethanol and water. The mean particle diameter was around 400 nm and the gadolinium content was around 9%. The GdDTPA chelate was strongly retained by chitosan, so that gadolinium was not released to an isotonic phosphate buffer over 7 days. Actually, the gadolinium concentration in the tumor tissue was about 100 times higher compared to Magnevist controls at the time of the thermal neutron irradiation. Endocytic uptake of nanoparticles, strongly holding GdDTPA, was suggested by transmission electron microscopy studies that indicated that GdDTPA has a high affinity for the cells, contributing to the long retention of gadolinium in tumor tissue. The treatment led to suppression of tumor growth in the *in vivo* studies. In the controls, 14 days after irradiation, the increase of the tumor volume was 20–25%, while the tumor was suppressed in mice treated with the gadolinium preparation; also, the survival time was remarkably prolonged [237–240].

Agnihotri and Aminabhavi [241] have used a sieving method to obtain microparticles. The first step was the crosslinking of chitosan to obtain a nonsticky glassy hydrogel followed by passing through a sieve. A suitable quantity of chitosan was dissolved in 4% acetic acid solution to form a thick glassy hydrogel followed by passing through a sieve. A suitable quantity of chitosan was dissolved in 4% acetic acid solution to form a thick jelly mass that was crosslinked by adding glutaraldehyde. The nonsticky crosslinked mass was passed through a sieve with a suitable mesh size to obtain microparticles. The microparticles were washed with 0.1 N NaOH solution to remove the unreacted excess glutaraldehyde and dried overnight in an oven at around 40 °C. Clozapine was incorporated into chitosan before crosslinking with an entrapment efficiency up to 98.9%. Microparticles were irregular in shape, with average particle sizes in the range 543–698 μm . The *in vitro* release was extended up to 12 h, while the *in vivo* studies indicated a slow release of clozapine.

4.5

DNA Loading into Nano- and Microparticles of Chitosan

DNA loading into micro/nanoparticulates of chitosan is mainly done either during the preparation or by adsorption on the preformed particles. The process is very efficient since, as mentioned before, it is mainly driven by electrostatic interactions between the chitosan chain and the charged phosphate groups of DNA. However, the intrinsic characteristics of the carrier (chitosan and its derivatives) may affect the loading, such as the chitosan/DNA ratio and degree of acetylation, molecular weight, as well as experimental conditions like the pH and the presence of additives.

Leong et al. [44] have evaluated the encapsulation efficiency and loading level of DNA into nanospheres having a size range of 200–750 nm. The nanospheres were prepared by complex coacervation in the presence of sodium sulfate aqueous solution, using chitosan 390 kDa and two different pDNAs. The DNA loading level

was determined by the PicoGreen assay (Molecular Probes, Eugene, OR) after the nanospheres were digested with trypsin or chitosanase and lysozyme. The authors reported that over 95% of the DNA was captured by the phase separation, and also that the encapsulation efficiency and loading level were observed to increase with the molecular weight of the encapsulant.

In general, complete binding may be achieved by increasing the amount of chitosan in the formulation. Kiang et al. [131] have evaluated chitosans with various degrees of deacetylation for efficacy of nanoparticle formation, DNA binding efficiency, morphology, and *in vitro* and *in vivo* gene transfection efficiency. The nanoparticles obtained by complex coacervation had a particle size of approximately 150–200 nm. The authors reported that when comparing chitosans with similar degrees of deacetylation, HMW chitosan (390 kDa) with a degree of deacetylation of 90% binds DNA at a charge (+/–) ratio of approximately 3.3, medium-molecular-weight chitosan (209 kDa) with degree of deacetylation of 93% binds DNA at a charge (+/–) ratio of 4.0, while LMW chitosan (138 kDa) with a degree of deacetylation of 85% requires a charge (+/–) ratio of 5.0 to completely bind the DNA. Similarly, at constant molecular weight, when the degree of deacetylation is decreased, the DNA-binding capacity is decreased, i.e. more chitosan is required to completely bind the DNA. This result was observed by comparing gel electrophoresis assays. For HMW chitosan, the charge (+/–) ratio for complete DNA binding increased from 3.3 to 8.0 as the degree of deacetylation decreased from 90 to 62%.

Mao et al. [141] evaluated encapsulation efficiency and DNA loading level by measuring the difference between the total amount of DNA added in the nanoparticle preparation buffer and the amount of nontrapped DNA remaining in the aqueous suspension after the coacervation process. Under optimal conditions, almost all DNA (pRELuciferase, 11.9 kb) and chitosan were captured in the nanoparticles. Using the chitosan (390 kDa)–DNA system, nanoparticles were prepared in the presence of 25 mM Na₂SO₄ at a charge (+/–) ratio of 3.3, and the encapsulation efficiencies were 98.0 ± 2.0 and $92.7 \pm 3.7\%$, respectively, for DNA and chitosan. According to these results, the composition of the nanoparticles was calculated as 35.6 ± 0.9 and $64.4 \pm 0.9\%$ weight for DNA and chitosan, respectively. Recently, Bozkir and Saka [242] have formulated chitosan–pDNA nanoparticles using complex coacervation and solvent evaporation techniques. The important parameters for the encapsulation efficiency were investigated, including molecular weight and degree of deacetylation of chitosan. They found that the encapsulation efficiency of pDNA is directly proportional to the degree of deacetylation, but there is an inverse proportional relationship with the molecular weight of chitosan. The surface charge of the nanoparticles prepared by the complex coacervation method was slightly positive, with a ζ potential of +9 to +18 mV; nevertheless, nanoparticles prepared by the solvent evaporation method had a ζ potential around +30 mV. The pDNA–chitosan nanoparticles prepared by using highly deacetylated chitosan having 92.7, 98.0 and 90.4% encapsulation efficiency protected the encapsulated pDNA from nuclease degradation.

Recent studies on DNA-loaded microcapsules have also shown that higher amounts of DNA can be encapsulated into the chitosan particles. Akbuga et al.

[144] have studied pDNA-loaded chitosan microspheres for *in vitro* IL-2 expression. In order to study the effect of formulation variables (concentration and molecular weight of chitosan, plasmid amount, use of glutaraldehyde as a crosslinker, etc.) on microsphere properties, different microsphere formulations were prepared. For microparticle preparation, the pDNA was added to 50 mL of sodium sulfate solution (20% w/v) and this mixture was dropped into 50 mL of acidic solution of chitosan and stirred for 1 h at 500 rpm. Encapsulation efficiency was calculated by measuring the difference between the total amount of DNA added in the preparation medium and the amount of nontrapped DNA remaining in the aqueous supernatant suspension after the coacervation process. For this purpose, the supernatant was spectrophotometrically analyzed at 260 and 280 nm for DNA concentration. Microspheres prepared were about 1.45–2.00 mm in size and spherical in shape. The plasmid encapsulation efficiency of microspheres was about 85%. Plasmid encapsulation efficiency was affected by the initial plasmid amount – a higher encapsulation efficiency was obtained with a lower amount of plasmid. However, the authors reported that other factors (chitosan concentration, using LMW chitosan and the addition of glutaraldehyde) did not affect the encapsulation efficiency significantly.

Aral et al. [243] have prepared chitosan microspheres containing pDNA:PLL complexes. The pDNA:PLL complexes were added to a sodium sulfate solution (20% w/v) before dropping and this mixture was dropped into the chitosan solution (0.35% w/v in 1% Tween 80 and 2% acetic acid) and stirred for 1 h at 500 rpm. The encapsulation efficiency of chitosan microspheres was estimated by measuring the amount of drug in the supernatant after centrifugation. The encapsulation efficiency for pDNA:PLL complexes was about 90% (data not shown). The average sizes of chitosan microspheres were between 3.41 to 3.69 μm and independent of the pDNA:PLL ratio. Chitosan microspheres were evaluated for sustained-release of human rIL-2 and the effects of different formulation factors, such as chitosan and protein concentrations, the volume of sodium sulfate solution, technique of addition of rIL-2, and presence of glutaraldehyde during the encapsulation process, on the microsphere characteristics were investigated [244]. Protein loading of chitosan microspheres was achieved by using two different methods – rIL-2 was added to the sodium sulfate solution during the preparation or it was adsorbed onto the surface of empty microspheres. Spherical microspheres having diameters ranging from 1.11 to 1.59 μm were obtained. The microspheres had a narrow size distribution and the authors reported that higher amounts of rIL-2 could be encapsulated into the chitosan microspheres by both methods (more than 90%).

4.6 DNA Release and Release Kinetics

DNA release from chitosan nanoparticles can be understood as a mechanism occurring through a combination of release from the surface and/or inner of the

nanoparticles and release due to polymer erosion. The definition “kinetics of *in vitro* release” is more commonly used to describe DNA release in a buffer solution, in which salts and/or enzymes are added to test the stability of the particles. Another important subject is the “kinetics of *in vitro* gene expression”, which is a terminology to denote the release process in the presence of targeting cells. Limiting our discussion primarily to kinetics of *in vitro* release from nano- and microparticles, various parameters may affect the release, such as molecular weight of chitosan, charge (+/–) ratio, plasmid size, extent of crosslinking, method of preparation and the presence of additives. Studies on the kinetics of pDNA release from chitosan nanoparticles are not frequently found in the literature, and only recently has more quantitative work been performed on chitosan microparticles. Dastan and Turan [245] have studied the *in vitro* release of DNA microparticles (2.0 μm) suspended in phosphate buffer at pH 7.4. The suspension was shaken in a water bath at 37 °C, and at defined time intervals the supernatant was collected by centrifugation and microparticles were resuspended in fresh buffer. pDNA (pSV-Gal 6820 bp, pEGFP-N1 4733 bp and pBluescript SK⁺ 2961 bp) release into the supernatant was quantified by spectrophotometry. The authors reported that about 10–15% of total DNA loaded into the chitosan microparticles was initially released within the first hour followed by very slow release over 40–50 days. The results obtained showed that the release is dependent on both chitosan and pDNA concentration, as well as of pDNA molecular weight. It was shown that the DNA release rate from microparticles was higher for nanoparticles having a higher pDNA concentration and a lower chitosan concentration. The HMW plasmids were released slower than the smaller ones. Aral and Akubga [243, 246] have also studied the release of pDNA:PLL complexes (pUC18 2.69 kbp, that encoded galactosidase) from chitosan microspheres of about 3.5 μm . Release profiles of the chitosan microspheres were determined by incubating 10 mg samples of microspheres in phosphate-buffered saline (PBS, pH 7.4, BP) at 37 °C. Release studies were continued up to 40 days. All samples were measured spectrophotometrically and fluorometrically using Hoechst 33258 dye that specifically binds to DNA. The release of pDNA:PLL complexes from the microspheres showed no initial burst release. On the first day, 2.1–4.8% of the pDNA:PLL complexes was released from the studied formulations. This was attributed to the high positive charge of chitosan which could hinder the release of surface localized pDNA. At day 40, from 42–70% of the initial drug was released from chitosan microspheres.

Chitosan microspheres containing human rIL-2 were prepared by using the precipitation technique. The average diameter of microspheres was between 1.11 and 1.59 μm [244]. Protein release from chitosan microspheres was determined in PBS buffer in a water bath at 37 ± 0.5 °C. In general, the rIL-2 release profiles were biphasic, characterized by an initial protein burst followed by slow release. Among the different formulation parameters, for some of them the concentration of chitosan as well as the amount of glutaraldehyde affected the release. However, as the protein concentration increased, *in vitro* release significantly decreased. Moreover, the volume of sodium sulfate solution used in the microsphere preparations affected the release pattern of protein from chitosan microspheres. rIL-2 was re-

leased rapidly from chitosan microspheres when a larger volume of sodium sulfate solution was used during the preparation. In other work, Ozbas-Turan et al. [246] have encapsulated two plasmids (pGL2 6046 bp and pMK3 7213 bp) in the same microsphere structure and investigated *in vivo* release and transfection characteristics of chitosan microspheres (1.15–1.28 μm). They reported that very little burst effect was seen in the release profiles of two plasmid-loaded microspheres and that pDNAs were continuously released from chitosan microspheres. The *in vitro* release of pDNAs from microspheres was dependent on the plasmid amount and chitosan concentration. As the amount of plasmids increased, release decreased significantly. The same results were obtained with microspheres containing different concentrations of chitosan. The authors concluded that there was no significant difference between the release patterns of single- and double-plasmid loaded microspheres. In more a recent paper [144], the same group studied pDNA-loaded chitosan microspheres (1.5–2.0 μm) for *in vitro* IL-2 expression. They reported that all release profiles of the microspheres were similar and showed a small burst release of about 10–20% in the first 24 h and then slow release at a constant rate. DNA release was reported to change significantly with the chitosan concentration. Microspheres prepared with the highest concentration of chitosan exhibited the lowest DNA release. Microspheres prepared with HMW chitosan exhibit slow DNA release. As the molecular weight of chitosan increased, the release of pDNA from microspheres decreased. The molecular weight of chitosan was previously shown to be important in DNA release as reported by Xu and Du studying the release of bovine serum albumin from chitosan nanoparticles (20–200 nm) [200]. Moreover, DNA release was affected by the amount of plasmid entrapped. An increase in DNA content of microspheres resulted in a decrease in plasmid release.

The studies on the release of chitosan nanoparticles found in the literature mainly focus on the release of proteins and other drugs rather than on pDNAs. The importance of studying the release from nanoparticles is due to the advantages of nanoparticles over microspheres; it has been observed that nanoparticles can enter the cell by endocytosis or pinocytosis, having a size requirement less than 100 nm [141, 142]. Also the number of nanoparticles that cross the epithelium is greater than the number of microspheres [247]. Bozkir and Saka [242] have recently studied the effect of chitosan molecular structure and type of formulation on the release characteristics of chitosan nanoparticles. They found that the release of pDNA from the formulation prepared by complex coacervation was completed in 24 h, whereas the formulation prepared by evaporation technique released pDNA in 96 h; however, these release profiles were not statistically significant compared with formulations with similar structure.

4.7

Preclinical Evidence of Chitosan–DNA Complex Efficacy

We have previously demonstrated that chitosan–DNA complexes appear spherical with a mean size of less than 100 nm and a homogenous distribution of DNA

within the particle [249]. Our results are in agreement with previous studies [248]. The size of the complexes is of crucial importance to cellular uptake. Illum et al. have synthesized chitosan–DNA nanoparticles ranging from 20 to 500 nm and thus our complexes are smaller than other polymeric systems [248]. The smaller size complexes have the advantage of entering the cells through endocytosis and/or pinocytosis, and therefore increasing the transfection rate. The transfection efficacy seen *in vitro* is cell-type dependent and cell viability studies following incubation with nanoparticles confirmed the lack of toxicity of chitosan compared to cationic lipids such as lipofectamine [84, 136, 249].

In addition to condensing the pDNA, an efficient gene delivery system is required to transport the gene into the cell and see to its eventual release, leading to gene expression and subsequent protein synthesis (Fig. 4.5). It is thus necessary to test a gene carrier on different cells lines, especially cells that resemble those that will be targeted. We have incubated chitosan–DNA polyplexes with MG63 cells, which have characteristics resembling those of osteoblasts, and with mesenchymal stem cells (MSCs), which are implicated in the formation of tissues such as cartilage, bone, tendons and muscle [250]. Nanoparticles composed of chitosan of molecular weight 400 kDa and a DNA quantity equivalent to 10 mg resulted in a transfection that was statistically significant compared to cells received solely DNA. MG63 cells did not demonstrate the same level of transfection. This can be explained by a delayed internalization of the nanoparticles when compared to HEK 293 cells. In fact, fluorescent microscopy observations undertaken by our group on nanoparticles incubated with human osteoblasts indicate that the particles remain bound to the surface for as long as 1 week following incubation (Fernandes et al., personal observations). However, MSCs did demonstrate gene expression when transfected with chitosan–DNA nanoparticles. This was clearly seen by a number of cells turning blue following X-gal staining; however, their transfection efficacy is not statistically significant when compared to cells receiving solely naked DNA [249].

One major pitfall of *in vitro* studies is their lack of reproducibility *in vivo*. We addressed this question recently by injecting either 0.15 M NaCl (control) or 1 mg of naked or complexed VR1012 plasmid coding for the β -Gal gene (Vical, Anaheim, CA) with chitosan or lipofectamine in the anterior tibialis muscle of 6-week-old male BALB/c mice. One major finding of this pilot study was that chitosan–DNA nanoparticles administered in the anterior tibialis mice muscle revealed a high signal corresponding to β -Gal gene expression within 48 h [251]. In contrast, the administration of naked or DNA–lipofectamine in the anterior tibialis muscle did not reveal any β -Gal gene expression. From these preliminary data, we proposed that chitosan–DNA nanoparticles have the potential ability to transfect muscle cells *in vivo* and lead to protein synthesis.

To improve transfection efficiency, several derivatives of chitosan have been prepared based on reactions with the free amino groups. Mao et al. demonstrated that transferrin and KNOB protein conjugation improved transfection efficiency in HEK 293 and HeLa cells [141]. Trimethylated chitosan is prepared with different degrees of quaternization to increase the solubility of chitosan at neutral pH [84];

deoxycholic group-conjugated chitosan has been synthesized to develop a colloidal carrier for DNA [102]; both quaternarized chitosan and deoxylated modified chitosan have been shown to transfect COS-1 cells effectively *in vitro*. A lactosylated chitosan has also been shown to be able to complex with DNA and effectively transfect HeLa cells [143]. It has been noticed that transfection efficiency also depend on the cell type used and the chitosan derivatives.

Folic acid was chosen by our group as a ligand for targeting cell membrane and allowing nanoparticles endocytosis via the FR for a higher transfection yield. Importantly, the high affinity of folate to bind its receptor (1 nM) [252] and the small size of folate allows its use for specific cell targeting. Moreover, the ability of folic acid to bind the FR that enables endocytosis is not altered by covalent conjugation of small molecules [253–255]. FR is overexpressed on many human cancer cell surfaces [252] and the nonepithelial isoform of FR (FR β) is expressed on activated synovial macrophages present in large numbers in arthritis joints [256]. Folic acid has been used by many researchers like a ligand with cationic liposome and other polymers to target cells expressing FR. For example, Guo et al. showed that folic acid enhanced PEI-mediated transfection activity in the presence of serum into cultured mammalian cells [257]; Reddy et al. showed that folate-mediated endocytosis can be exploited to target transgenes to cancer cells expressing FR and that folate-derivatized DOPE have a high transfection activity [258].

4.8

Potential Clinical Applications of Chitosan–DNA in Gene Therapy

The chitosan–DNA system has been used in a novel gene transfer approach against respiratory syncytial virus infection, which at a single dose of about 1 mg/kg body weight is capable of decreasing viral titers by two orders of magnitude (100-fold) on primary infection. The immunologic mechanisms for the effectiveness of this prophylaxis include the induction of high levels of both serum IgG and mucosal IgA antibodies, the generation of an effective control response, and elevated lung-specific production of interferon (IFN)- γ with antiviral action. Although effective as a single-dose, it is possible that dose-escalation and prime-booster strategies of the intranasal gene transfer (IGT) vaccine might further enhance its effectiveness. In addition, IGT significantly decreases pulmonary inflammation and does not alter airway hyperresponsiveness, thus making it safe for *in vivo* use [259].

Coxsackievirus B3 (CVB3) infections are common causes of acute and chronic myocarditis for which no effective prophylactic treatment is available. Xu et al. [260] have described a prophylactic strategy using chitosan–DNA intranasal immunization to induce CVB3-specific immune responses. Intranasal administration of a chitosan–DNA complex prepared by votexing DNA with chitosan resulted in transgenic DNA expression in mouse nasopharynx. Mice immunized with chitosan–DNA (pcDNA3-VP1) encoding VP1, major structural protein of CVB3, produced much higher levels of serum IgG and mucosal secretory IgA compared

to mice treated with pcDNA3-VP1 or pcDNA3. Increased virus-specific cytotoxic activity of spleen cells derived from chitosan–DNA-vaccinated mice was also determined. Chitosan–pcDNA3-VP1 intranasal immunization resulted in 42.9% protection of mice against lethal CVB3 challenge and a significant reduction of viral load after acute CVB3 infection. The authors indicated that intranasal delivery of the chitosan–DNA vaccine successfully induced mucosal SIgA secretion and might be a promising vaccine candidate to protect against CVB3 infection.

The zona pellucida (ZP), the extracellular matrix surrounding oocytes, has received considerable attention as a potential target for contraception because of its key role in many reproductive processes, e.g. gamete interaction during fertilization, induction of acrosome reaction. Sun et al. [261] have constructed a eukaryotic expression vector pVAX1-pZP3a as an oral ZP DNA contraceptive vaccine and successfully encapsulated in nanoparticles with chitosan. After 5 days of feeding to mice, the transcription and expression of pZP3a was found in mouse alvine chorion. The authors suggested that the chitosan–pVAX1-pZP3 pDNA nanoparticles can successfully transfect the alvine chorion cells in mice *in vivo*.

In order to investigate the potential of chitosan in the form of an inhaled powder as a gene delivery system, Okamoto et al. prepared powders using pCMV-Luc as a reporter gene and a LM chitosan (3000–30 000) as a cationic vector with supercritical CO₂. The chitosan–DNA powders obtained were administered to the lungs of mice. The transfection efficiency of these powders was compared with that of DNA solutions and DNA powders without the cationic vector. The gene powder with the cationic polymer was found to be an excellent gene delivery system to the lungs, as evidenced by a high transfection rate and high expression of the luciferase protein. The benefits of the chitosan–DNA powders examined were summarized as follows: (a) the addition of chitosan suppressed the degradation of pCMV-Luc during the supercritical CO₂ process, (b) the addition of chitosan increased the yield of powders and (c) the chitosan–DNA powders increased the luciferase activity in the mouse lung compared with pCMV-Luc powders without chitosan or pCMV-Luc solutions with or without chitosan [262]. Bivas-Benita et al. [263] have proposed chitosan–DNA nanoparticles for pulmonary delivery of a DNA vaccine encoding HLA-A*0201-restricted T cell epitopes of *Mycobacterium tuberculosis*. The authors used an HLA-A2 transgenic mouse model to investigate the effects of pulmonary delivery of a new pDNA encoding eight HLA-A*0201-restricted T cell epitopes from *M. tuberculosis* formulated in chitosan nanoparticles. It was shown that the chitosan–DNA formulation was able to induce the maturation of dendritic cells, whereas chitosan solution alone could not, indicating the DNA was released from the particles and was able to stimulate dendritic cells. Pulmonary administration of the pDNA incorporated in chitosan nanoparticles was shown to induce increased levels of IFN- γ secretion compared to pulmonary delivery of plasmids in solution or the more frequently used intramuscular immunization route. The authors indicated that pulmonary delivery of DNA vaccines against tuberculosis may provide an advantageous delivery route compared to intramuscular immunization and that increased immunogenicity can be achieved by delivery of this DNA encapsulated in chitosan nanoparticles.

4.9

Conclusion

Gene therapy offers a promising approach for the treatment of genetic disorders, vaccine development and tissue engineering. However, such opportunities will only be attainable by the development of safe and efficient gene delivery systems. Such systems must protect the DNA, and allow it to enter the targeted cell and reach the nucleus where genetic expression will take place. Several nonviral approaches have been developed and improved for use in different clinical settings. Substantial progress has also been made in improving plasmid expression vectors. It is now possible to achieve gene expression in a controllable manner using gene switch systems. A number of *in vitro* and *in vivo* studies, including ours, showed that chitosan is a suitable material for efficient nonviral gene therapy. Several groups are conducting studies using different strategies that can be linked to chitosan–DNA nanoparticles (including targeting cell membrane receptors) for a higher transfection yield.

Chitosan–DNA nanoparticles, due to their reduced cytotoxicity and ability to transport and release genes intracellularly, where expression of the encoded protein occurs, are considered as a potential candidate for a nonviral gene carrier. Further improvements in nonviral gene therapy will rely on a better understanding of the cellular and *in vivo* barriers to gene transfer.

Acknowledgments

This study was supported by a research grant from The Arthritis Society of Canada. J. C. F. holds a clinician scientist scholarship of the Fonds de la recherche en sante du Quebec. M. J. T. holds a post-PhD scholarship from the CAPES program from Brazil.

References

- 1 K. KURITA, Controlled functionalization of the polysaccharide chitin, *Prog. Polym. Sci.* **2001**, *26*, 1921–1971.
- 2 G. A. F. ROBERTS, *Chitin Chemistry*, Macmillan, Basingstoke, **1992**.
- 3 H. K. No, S. P. MEYERS, Crawfish chitosan as a coagulant in recovery of organic compounds from seafood processing streams, *J. Agric. Food Chem.* **1989**, *37*, 580–583.
- 4 K. KURITA, T. SANNAN, Y. IWAKURA, Studies on chitin, 4: evidence for formation of block and random copolymers of *N*-acetyl-D-glucosamine and D-glucosamine by hetero- and homogeneous hydrolyses. *Makromol. Chem.* **1977**, *178*, 3197–3202.
- 5 A. DOMARD, M. RINAUDO, Preparation and characterization of fully deacetylated chitosan, *Int. J. Biol. Macromol.* **1983**, *5*, 49–53.
- 6 A. TOLAIMATE, J. DESBRIERES, M. RHAZI, A. ALAGUI, M. VINCENDON, P. VOTTERO, On the influence of deacetylation process on the physicochemical characteristics of chitosan from squid chitin, *Polymer* **2000**, *41*, 2463–2469.

- 7 A. TOLAIMATE, J. DESBRIERES, M. RHAZIA, A. ALAGUI, Contribution to the preparation of chitins and chitosans with controlled physico-chemical properties, *Polymer* **2003**, *44*, 7939–7952.
- 8 K. Y. LEE, W. S. HA, W. H. PARK, Blood compatibility and biodegradability of partially *N*-acylated chitosan derivatives, *Biomaterials* **1995**, *16*, 1211–1216.
- 9 G. BERTHA, H. DAUTZENBERG, M. G. PETER, Physico-chemical characterization of chitosans varying in degree of acetylation, *Carbohydr. Polym.* **1998**, *36*, 205–216.
- 10 G. BERTH, H. DAUTZENBERG, The degree of acetylation of chitosans and its effect on the chain conformation in aqueous solution, *Carbohydr. Polym.* **2002**, *47*, 39–51.
- 11 C. SCHATZ, C. VITON, T. DELAIR, C. PICHOT, A. DOMARD, Typical physicochemical behaviors of chitosan in aqueous solution, *Biomacromolecules* **2003**, *4*, 641–648.
- 12 J. H. PA, T. L. YU, Light scattering study of chitosan in acetic acid aqueous solutions, *Macromol. Chem. Phys.* **2001**, *202*, 985–991.
- 13 R. SIGNINI, J. DESBRIERES, S. P. CAMPANA FILHO, On the stiffness of chitosan hydrochloride in acid-free aqueous solutions, *Carbohydr. Polym.* **2000**, *43*, 351–357.
- 14 T. H. HUNG, Y. M. CHANG, H. Y. SUNG, C. T. CHANG, Purification and characterization of hydrolase with chitinase and chitosanase activity from commercial stem bromelain, *J. Agric. Food Chem.* **2002**, *50*, 4666–4673.
- 15 T. KUROIWA, S. ICHIKAWA, S. SATO, S. MUKATAKA, Improvement of the yield of physiologically active oligosaccharides in continuous hydrolysis of chitosan using immobilized chitosanases, *Biotechn. Bioeng.* **2003**, *84*, 121–127.
- 16 A. B. V. KUMAR, M. C. VARADARAJ, R. G. LALITHA, R. N. THARANATHAN, Low molecular weight chitosans: preparation with the aid of papain and characterization, *Biochim. Biophys. Acta Gen. Sub.* **2004**, *1670*, 137–146.
- 17 H. LIN, H. Y. WANG, C. H. XUE, M. Y. Preparation of chitosan oligomers by immobilized papain, *Enz. Microb. Technol.* **2002**, *31*, 588–592.
- 18 R. A. A. MUZZARELLI, M. TERBOJEVICH, C. MUZZARELLI, O. FRANCESCANGELI, Chitosans depolymerized with the aid of papain and stabilized as glycosylamines, *Carbohydr. Polym.* **2002**, *50*, 69–78.
- 19 M. TERBOJEVICH, A. COSANI, R. A. A. MUZZARELLI, Molecular parameters of chitosans depolymerized with the aid of papain, *Carbohydr. Polym.* **1996**, *29*, 63–68.
- 20 A. B. V. KUMAR, R. N. THARANATHAN, A comparative study on depolymerization of chitosan by proteolytic enzymes, *Carbohydr. Polym.* **2004**, *58*, 275–283.
- 21 K. M. VARURN, M. M. MYHR, R. J. N. HJERDE, O. SMIDSRØD, *In vitro* degradation rates of partially *N*-acetylated chitosans in human serum, *Carbohydr. Res.* **1997**, *299*, 99–101.
- 22 S. MAO, X. SHUAI, F. UNGER, M. SIMONA, D. BI, T. KISSEL, The depolymerization of chitosan: effects on physicochemical and biological properties, *Int. J. Pharm.* **2004**, *281*, 45–54.
- 23 M.-Y. LEE, F. VAR, Y. SHIN-YA, T. KAJIUCHI, J.-W. YANG, Optimum conditions for the precipitation of chitosan oligomers with DP 5–7 in concentrated hydrochloric acid at low temperature, *Proc. Biochem.* **1999**, *34*, 493–500.
- 24 M. L. SINNOTT, Catalytic mechanism of enzymic glycosyl transfer, *Chem. Rev.* **1990**, *90*, 1171–1202.
- 25 V. L. Y. YIP, S. G. WITHERS, Nature's many mechanisms for the degradation of oligosaccharides, *Org. Biol. Chem.* **2004**, *2*, 2707–2713.
- 26 E. S. K. TANG, M. HUANG, L. Y. LIM, Ultrasonication of chitosan and chitosan nanoparticles, *Int. J. Pharm.* **2003**, *265*, 103–114.
- 27 M. L. TSAIH, R. H. CHEN, Effect of degree of deacetylation of chitosan on the kinetics of ultrasonic degradation of chitosan, *J. Appl. Polym. Sci.* **2003**, *90*, 3526–3531.

- 28 K. KURITA, S. ISHII, K. TOMITA, S. NISHIMURA, K. SHIMODA, Reactivity characteristics of squid-chitin as compared with those of shrimp chitin: High potentials of squid chitin as a starting material for facile chemical modifications, *J. Polym. Sci. A Polym. Chem.* **1994**, *32*, 1027–1032.
- 29 P. FRANCO, A. SENSO, L. OLIVEROS, C. MINGUILLON, Covalently bonded polysaccharide derivatives as chiral stationary phases in high-performance liquid chromatography, *J. Chromatogr. A* **2001**, *906*, 155–170.
- 30 E. GUIBAL, Interactions of metal ions with chitosan-based sorbents: a review, *Separ. Purific. Technol.* **2004**, *38*, 43–74.
- 31 A. J. VARMA, S. V. DESHPANDE, J. F. KENNEDY, Metal complexation by chitosan and its derivatives: a review, *Carbohydr. Polym.* **2004**, *55*, 77–93.
- 32 E. I. RABEA, M. E.-T. BADAWY, C. V. STEVENS, G. SMAGGHE, W. STEURBAUT, Chitosan as antimicrobial agent: applications and mode of action, *Biomacromolecules* **2003**, *4*, 1457–1465.
- 33 Y. KATO, H. ONISHI, Y. MACHIDA, N-succinyl-chitosan as a drug carrier: water-insoluble and water-soluble conjugates, *Biomaterials* **2004**, *25*, 907–915.
- 34 J. BERGER, M. REIST, J. M. MAYER, O. FELT, N. A. PEPPAS, R. GURNY, Structure and interactions in covalently and ionically crosslinked chitosan hydrogels for biomedical applications, *Eur. J. Pharm. Biopharm.* **2004**, *57*, 19–34.
- 35 J. BERGER, M. REIST, J. M. MAYER, O. FELT, R. GURNY, Structure and interactions in chitosan hydrogels formed by complexation or aggregation for biomedical applications, *Eur. J. Pharm. Biopharm.* **2004**, *57*, 35–52.
- 36 K. A. JANES, P. CALVO, M. J. ALONSO, Polysaccharide colloidal particles as delivery systems for macromolecules, *Adv. Drug Deliv. Rev.* **2001**, *47*, 83–97.
- 37 V. R. SINHA, A. K. SINGLA, S. WADHAWAN, R. KAUSHIK, R. KUMRIA, K. BANSAL, S. DHAWAN, Chitosan microspheres as a potential carrier for drugs, *Int. J. Pharm.* **2004**, *274*, 1–33.
- 38 W. G. LIU, K. DE YAO, Chitosan and its derivatives – a promising non-viral vector for gene transfection, *J. Controlled Rel.* **2002**, *83*, 1–11.
- 39 G. BORCHARD, Chitosans for gene delivery, *Adv. Drug Deliv. Rev.* **2001**, *52*, 145–150.
- 40 M. N. V. R. KUMAR, R. A. A. MUZZARELLI, C. MUZZARELLI, H. SASHIWA, A. J. DOMB, Chitosan chemistry and pharmaceutical perspectives, *Chem. Rev.* **2004**, *104*, 6017–6084.
- 41 M. N. V. R. KUMAR, A review of chitin and chitosan applications, *React. Func. Polym.* **2000**, *46*, 1–27.
- 42 Y. M. XU, Y. M. DU, R. H. HUANG, L. P. GAO, Preparation and modification of N-(2-hydroxyl) propyl-3-trimethyl ammonium chitosan chloride nanoparticle as a protein carrier, *Biomaterials* **2003**, *24*, 5015–5022.
- 43 H. SASHIWA, N. YAMAMORI, Y. ICHINOSE, J. SUNAMOTO, S.-i. AIBA, Michael reaction of chitosan with various acryl reagents in water, *Biomacromolecules* **2003**, *4*, 1250–1254.
- 44 K. W. LEONG, H.-Q. MAO, V. L. TRUONG-LE, K. ROY, S. M. WALSH, J. T. AUGUST, DNA–polycation nanospheres as non-viral gene delivery vehicles, *J. Controlled Rel.* **1998**, *53*, 183–193.
- 45 M. SUGIMOTO, M. MORIMOTO, H. SASHIWA, H. SAIMOTO, Y. SHIGEMASA, Preparation and characterization of water-soluble chitin and chitosan derivatives, *Carbohydr. Polym.* **1998**, *36*, 49–59.
- 46 T. MUSLIM, M. MORIMOTO, H. SAIMOTO, Y. OKAMOTO, S. MINAMI, Y. SHIGEMASA, Synthesis and bioactivities of poly(ethylene glycol)–chitosan hybrids, *Carbohydr. Polym.* **2001**, *46*, 323–330.
- 47 M. MORIMOTO, H. SAIMOTO, Y. SHIGEMASA, Control of functions of chitin and chitosan by chemical modification, *Trends Glycosci. Glycotecnol.* **2002**, *14*, 205–222.
- 48 K. KURITA, S. IWAWAKI, S. ISHI, S. NISHIMURA, Introduction of poly(L-alanine) side chains into chitin as

- versatile spacer arms having a terminal free amino group and immobilization of NADH active sites, *J. Polym. Sci. A Polym. Chem.* **1992**, *30*, 685–688.
- 49 Y. NISHIYAMA, T. YOSHIDA, T. MORI, S. ISHII, K. KURITA, Asymmetric reduction with chitosan/dihydrionicotinamide conjugates: influence of L-alanine spacer arms on reducing performance, *React. Funct. Polym.* **1998**, *37*, 83–91.
- 50 K. INUI, K. TSUKARNOTO, T. MIYATA, T. URAGAMI, Permeation and separation of a benzene/cyclohexane mixture through benzoylchitosan membranes, *J. Membrane Sci.* **1998**, *138*, 67–75.
- 51 S. NISHIMURA, O. KOHGO, K. KURITA, C. VITAVATVONG, H. KUSUHARA, Syntheses of novel chitosan derivatives soluble in organic-solvents by regioselective chemical modifications, *Chem. Lett.* **1990**, *2*, 243–246.
- 52 S. NISHIMURA, O. KOHGO, K. KURITA, H. KUZUHARA, Chemospecific manipulations of a rigid polysaccharide: syntheses of novel chitosan derivatives with excellent solubility in common organic solvents by regioselective chemical modifications, *Macromolecules* **1991**, *24*, 4745–4748.
- 53 K. KURITA, K. TOMITA, T. TADA, S. NISHIMURA, S. ISHII, Reactivity characteristics of a new form of chitosan – facile *n*-phthaloylation of chitosan prepared from squid beta-chitin for effective solubilization, *Polym. Bull.* **1993**, *30*, 429–433.
- 54 K. KURITA, H. IKEDA, Y. YOSHIDA, M. SHIMOJOH, M. HARATA, Chemospecific protection of the amino groups of chitosan by controlled phthaloylation: facile preparation of a precursor useful for chemical modifications, *Biomacromolecules* **2002**, *3*, 1–4.
- 55 T. SEO, Y. I. GAN, T. KANBARA, T. IJIMA, The selective sorption of D,L-amino acids by chemically modified chitosan gels and its application to liquid chromatography, *J. Appl. Polym. Sci.* **1989**, *38*, 997.
- 56 T. SEO, H. OHTAKE, T. KANBARA, K. YONETAKE, T. IJIMA, Preparation and permeability of chitosan membranes having hydrophobic groups, *Makromol. Chem.* **1991**, *192*, 2447.
- 57 H. YAMADA, T. IMOTO, A convenient synthesis of glycolchitin, a substrate of lysozyme, *Carbohydr. Res.* **1981**, *92*, 160–162.
- 58 G. LANG, G. MARESCH, S. BIRKEL, Hydroxyalkyl chitosans, In R. A. A. MUZZARELLI, M. G. PETER (Eds.), *Chitin Handbook*. Atec Edizioni, Grottammare, **1997**, p. 61.
- 59 M. GOMEZ-GUILLEN, A. GOMEZ-SANCHEZ, M.-E. MARTIN-ZAMORA, A derivative of chitosan and 2,4-pentanedione with strong chelating properties, *Carbohydr. Res.* **1992**, *233*, 255–259.
- 60 L. D. HALL, M. YALPANI, Formation of branched-chain, soluble polysaccharides from chitosan, *J. Chem. Soc. Chem. Commun.* **1980**, 1153–1154.
- 61 M. YALPANI, L. D. HALL, Some chemical and analytical aspects of polysaccharide modifications. III. Formation of branched-chain, soluble chitosan derivatives, *Macromolecules* **1984**, *17*, 272–281.
- 62 M. MORIMOTO, H. SAIMOTO, H. USUI, Y. OKAMOTO, S. MINAMI, Y. SHIGEMASA, Biological activities of carbohydrate-branched chitosan derivatives, *Biomacromolecules* **2001**, *2*, 1133–1136.
- 63 X. LI, Y. TSUSHIMA, M. MORIMOTO, H. SAIMOTO, Y. OKAMOTO, S. MINAMI, Y. SHIGEMASA, Biological activity of chitosan–sugar hybrids: specific interaction with lectin, *Polym. Adv. Technol.* **2000**, *11*, 176–179.
- 64 Y. KATO, H. ONISHI, Y. MACHIDA, Biological characteristics of lactosaminated *N*-succinyl-chitosan as a liver-specific drug carrier in mice, *J. Controlled Rel.* **2001**, *70*, 295–307.
- 65 K. R. HOLME, L. D. HALL, Chitosan derivatives bearing C10-alkyl glycoside branches: a temperature-induced gelling polysaccharide, *Macromolecules* **1991**, *24*, 3828–3833.
- 66 L. D. HALL, M. YALPANI, Enhancement of the metal-chelating properties of chitin and chitosan, *Carbohydr. Res.* **1980**, *83*, C5–C7.

- 67 R. A. A. MUZZARELLI, F. TANFANI, S. MARIOTTI, M. EMANUELLI, *N*-(*o*-carboxybenzyl) chitosans: Novel chelating polyampholytes, *Carbohydr. Polym.* **1982**, *2*, 145–157.
- 68 S. HIRANO, A facile method for the preparation of novel membranes from *n*-acyl- and *n*-arylidene-chitosan gels, *Agric. Biol. Chem.* **1978**, *42*, 1939–1940.
- 69 R. A. A. MUZZARELLI, F. TANFANI, M. ENAMUELLI, S. MARIOTTI, The characterization of *N*-methyl, *N*-ethyl, *N*-propyl, *N*-butyl and *N*-hexyl chitosans, novel film-forming polymers, *J. Membrane Sci.* **1983**, *16*, 295–308.
- 70 K. KURITA, M. ISHIGURO, T. KATAJIMA, Studies on chitin: 17. Introduction of long alkylidene groups and the influence on the properties, *Int. J. Biol. Macromol.* **1988**, *10*, 124–125.
- 71 W. G. LIU, K. D. KAO, Q. G. LIU, Formation of a DNA/*N*-dodecylated chitosan complex and salt-induced gene delivery, *J. Appl. Polym. Sci.* **2001**, *82*, 3391–3395.
- 72 M. THANOU, M.-T. NIHOT, M. JANSEN, J. C. VERHOEF, H. E. JUNINGER, Mono-*N*-carboxymethyl chitosan (MCC), a polyampholytic chitosan derivative, enhances the intestinal absorption of low molecular weight heparin across intestinal epithelia *in vitro* and *in vivo*, *J. Pharm. Sci.* **2001**, *90*, 38–46.
- 73 Z. JIA, D. SHEN, W. XU, Synthesis and antibacterial activities of quaternary ammonium salt of chitosan, *Carbohydr. Res.* **2001**, *333*, 1–6.
- 74 R. A. A. MUZZARELLI, F. TANFANI, M. EMANUELLI, S. MARIOTTI, *N*-(carboxymethylidene)chitosans and *N*-(carboxymethyl)chitosans: novel chelating polyampholytes obtained from chitosan glyoxylate, *Carbohydr. Res.* **1982**, *107*, 199–214.
- 75 F. DELBEN, R. LAPASIN, S. PRICL, Flow properties of *N*-(carboxymethyl) chitosan aqueous systems in the sol and gel domains, *Int. J. Biol. Macromol.* **1990**, *12*, 9–13.
- 76 R. A. A. MUZZARELLI, M. WECKX, O. FILIPPINI, F. SIGON, Removal of trace metal ions from industrial waters, nuclear effluents and drinking water, with the aid of cross-linked *N*-carboxymethyl chitosan, *Carbohydr. Polym.* **1989**, *11*, 293–306.
- 77 R. A. A. MUZZARELLI, P. ILARI, M. TOMASETTI, Preparation and characteristic properties of 5-methyl pyrrolidinone chitosan, *Carbohydr. Polym.* **1993**, *20*, 99–105.
- 78 R. A. A. MUZZARELLI, G. GIAGINI, M. BELLARDINI, L. SIMONELLI, C. CASTALDINI, G. GRATTO, Osteoconduction exerted by methylpyrrolidinone chitosan used in dental surgery, *Biomaterials* **1993**, *14*, 39–43.
- 79 E. CURTI, D. DEBRITTO, S. P. CAMPANA, Methylation of chitosan with iodomethane: effect of reaction conditions on chemoselectivity and degree of substitution, *Macromol. Biosci.* **2003**, *3*, 571–576.
- 80 J.-I. MURATA, Y. OHYA, T. OUCHI, Design of quaternary chitosan conjugate having antennary galactose residues as a gene delivery tool, *Carbohydr. Polym.* **1997**, *32*, 105–109.
- 81 M. M. THANOU, A. F. KOTZE, T. SCHARRINGHAUSEN, H. L. LUESEN, A. G. DE BOER, J. C. VERHOEF, H. E. JUNGINGER, Effect of degree of quaternization of *N*-trimethyl chitosan chloride for enhanced transport of hydrophilic compounds across intestinal Caco-2 cell monolayers, *J. Controlled Rel.* **2000**, *64*, 15–25.
- 82 A. B. SIEVAL, M. THANOU, A. F. KOTZE, J. C. VERHOEF, J. BRUSSEE, H. F. JUNGINGER, Preparation and NMR characterization of highly substituted *N*-trimethyl chitosan chloride, *Carbohydr. Polym.* **1998**, *36*, 157–165.
- 83 M. THANOU, J. C. VERHOEF, S. G. ROMEIJIN, J. F. NAGELKERKE, F. W. H. M. MERKUS, H. E. JUNGINGER, Effects of *N*-trimethyl chitosan chloride, a novel absorption enhancer, on Caco-2 intestinal epithelia and the ciliary beat frequency of chicken embryo trachea, *Int. J. Pharm.* **1999**, *185*, 73–82.
- 84 M. THANOU, B. I. FLOREA, M. GELDOLF, H. E. JUNGINGER, G. BORCHARD,

- Quaternized chitosan oligomers as novel gene delivery vectors in epithelial cell lines, *Biomaterials* **2002**, *23*, 153–159.
- 85 I. M. LUBBEN, J. C. VERHOEF, G. BORCHARD, H. E. JUNGINGER, Chitosan and its derivatives in mucosal drug and vaccine delivery, *Eur. J. Pharm. Sci.* **2001**, *14*, 201–207.
- 86 C. E. KAST, A. BERNKOP-SCHNURCH, Thiolated polymers – thiomers: development and *in vitro* evaluation of chitosan–thioglycolic acid conjugates, *Biomaterials* **2001**, *22*, 2345–2352.
- 87 M. ISHIHARA, Photocrosslinkable chitosan hydrogel as a wound dressing and a biological adhesive, *Trends Glycosci. Glycotechnol.* **2002**, *14*, 331.
- 88 K. ONO, Y. SAITO, H. YURA, K. ISHIKAWA, A. KURITA, T. AKAIKE, M. ISHIHARA, Photocrosslinkable chitosan as a biological adhesive, *J. Biomed. Mater. Res.* **2000**, *49*, 289–295.
- 89 M. ISHIHARA, K. NAKANISHI, K. ONO, M. SATO, M. KIKUCHI, Y. SAITO, H. YURA, T. MATSUI, H. HATTORI, M. UENOYAMA, A. KURITA, Photocrosslinkable chitosan as a dressing for wound occlusion and accelerator in healing process, *Biomaterials* **2002**, *23*, 833–840.
- 90 K. AIEDEH, M. O. TAHA, Synthesis of iron-crosslinked chitosan succinate and iron-crosslinked hydroxamated chitosan succinate and their *in vitro* evaluation as potential matrix materials for oral theophylline sustained-release beads, *Eur. J. Pharm. Sci.* **2001**, *13*, 159–168.
- 91 Y. KATO, H. ONISHI, Y. MACHIDA, *N*-succinyl-chitosan as a drug carrier: water-insoluble and water-soluble conjugates, *Biomaterials* **2004**, *25*, 907–915.
- 92 Y. KATO, H. ONISHI, Y. MACHIDA, Evaluation of *N*-succinyl-chitosan as a systemic long-circulating polymer, *Biomaterials* **2000**, *21*, 1579–1585.
- 93 R. ROY, D. F. TROPPER, A. ROMANOWSKA, M. LETELLIER, L. COUSINEAU, S. J. MEUNIER, J. BORATYNSKI, Expedient syntheses of neoglycoproteins using phase-transfer catalysis and reductive amination as key reactions, *Glycoconj. J.* **1991**, *8*, 75–81.
- 94 H. SASHIWA, Y. MAKIMURA, Y. SHIGEMASA, R. ROY, Chemical modification of chitosan: preparation of chitosan–sialic acid branched polysaccharide hybrids, *Chem. Commun.* **2000**, 909–910.
- 95 S. CHEN, Y. WANG, Study on β -cyclodextrin grafting with chitosan and slow release of its inclusion complex with radioactive iodine, *J. Appl. Polym. Sci.* **2001**, *82*, 2414–2421.
- 96 S. VETTER, S. KOCH, A. D. SCHLUTER, Synthesis and polymerization of functionalized dendritic macromonomers, *J. Polym. Sci. A Polym. Chem.* **2001**, *39*, 1940–1954.
- 97 E. FURUSAKI, Y. UENO, N. SAKAIRI, N. NISHI, S. TOKURA, Facile preparation and inclusion ability of a chitosan derivative bearing carboxymethyl- β -cyclodextrin, *Carbohydr. Polym.* **1996**, *29*, 29–34.
- 98 T. TOJIMA, H. KATSURA, S. HAN, F. TANIDA, N. NISHI, S. TOKURA, N. SAKAIRI, Preparation of an β -cyclodextrin-linked chitosan derivative via reductive amination strategy, *J. Polym. Sci. A Polym. Chem.* **1998**, *36*, 1965–1968.
- 99 B. MARTLET, M. DEVASSIN, G. CRINI, M. WELTROWSKI, M. BOURDONNEAU, M. MORCELLET, Preparation and sorption properties of a β -cyclodextrin-linked chitosan derivative, *J. Polym. Sci. A Polym. Chem.* **2001**, *39*, 169–176.
- 100 X. H. TANG, S. Y. TAN, Y. T. WANG, Study of the synthesis of chitosan derivatives containing benzo-21-crown-7 and their adsorption properties for metal ions, *J. Appl. Polym. Sci.* **2002**, *83*, 1886–1891.
- 101 Y. H. KIM, S. H. GIHM, C. R. PARK, Structural characteristics of size-controlled self-aggregates of deoxycholic acid-modified chitosan and their application as a DNA delivery carrier, *Bioconj. Chem.* **2001**, *12*, 932–938.
- 102 K. Y. LEE, I. C. KWON, Y.-H. KIM, W. H. JO, S. Y. JEONG, Preparation of chitosan self-aggregates as a gene

- delivery system, *J. Controlled Rel.* **1998**, *51*, 213–220.
- 103 K. Y. LEE, W. H. JO, I. C. KWON, Y.-H. KIM, S. Y. JEONG, Physicochemical characteristics of self-aggregates of hydrophobically modified chitosans, *Langmuir* **1998**, *14*, 2329–2332.
- 104 K. Y. LEE, W. H. JO, I. C. KWON, Y. H. KIM, S. Y. JEONG, Structural determination and interior polarity of self-aggregates prepared from deoxycholic acid-modified chitosan in water, *Macromolecules* **1998**, *31*, 378–383.
- 105 S. MANSOURI, Synthèse et Caractérisation de nanoparticules folate–chitosan–ADN pour la thérapie génique. *Memorie de Maitrise*, Université de Montreal, **2004**.
- 106 G. KUMAR, P. J. SMITH, G. F. PAYNE, Enzymatic grafting of a natural product onto chitosan to confer water solubility under basic conditions, *Biotechnol. Bioeng.* **1999**, *63*, 154–165.
- 107 B. O. JUNG, C. H. KIM, K. S. CHOI, Y. M. LEE, J. J. KIM, Preparation of amphiphilic chitosan and their antimicrobial activities, *J. Appl. Polym. Sci.* **1999**, *72*, 1713–1719.
- 108 H. YAMADA, T. IMOTO, A convenient synthesis of glycolchitin, a substrate of lysozyme, *Carbohydr. Res.* **1981**, *92*, 160–162.
- 109 L. MARTIN, C. G. WILSON, F. KOOSHA, L. TETLEY, A. I. GRAY, S. SENEL, I. F. UCHEGBU, The release of model macromolecules may be controlled by the hydrophobicity of palmitoyl glycol chitosan hydrogels, *J. Controlled Rel.* **2002**, *80*, 87–100.
- 110 S. KWON, J. H. PARK, H. CHUNG, I. C. KWON, S. Y. JEONG, Physicochemical characteristics of self-assembled nanoparticles based on glycol chitosan bearing 5-cholanic acid, *Langmuir* **2003**, *19*, 10188–10193.
- 111 G. K. MOORE, G. A. F. ROBERTS, Reactions of chitosan: 4. Preparation of organosoluble derivatives of chitosan, *Int. J. Biol. Macromol.* **1982**, *4*, 246–249.
- 112 S. FUJII, H. KUMAGAI, M. NODA, Preparation of poly(acyl)chitosans, *Carbohydr. Res.* **1980**, *83*, 389–393.
- 113 H. SASHIWA, N. KAWASAKI, A. NAKAYAMA, E. MURAKI, N. YAMAMOTO, H. ZHU, H. NAGANO, Y. OMURA, H. SAIMOTO, Y. SHIGEMASA, S. ATBA, Chemical modification of chitosan. 13. Synthesis of organosoluble, palladium adsorbable, and biodegradable chitosan derivatives toward the chemical plating on plastics, *Biomacromolecules* **2002**, *3*, 1120–1125.
- 114 T. SATO, T. NAGASAKI, N. SAKAIRI, S. SHINKAI, 6-Amino-6-deoxychitosan. Preparation and application as plasmid vector in COS-1 cells, *Chem. Lett.* **2004**, *33*, 340–341.
- 115 R. TRUJILLO, Preparation of carboxymethylchitin, *Carbohydr. Res.* **1968**, *7*, 483–485.
- 116 Z. i. LI, X. P. ZHUANG, X. F. LIU, Y. L. GUAN, K. DE YAO, Study on antibacterial O-carboxymethylated chitosan/cellulose blend film from LiCl/N,N-dimethylacetamide solution, *Polymer* **2002**, *43*, 1541–1547.
- 117 M. RINAUDO, P. L. DUNG, C. GEY, M. MILAS, Substituent distributions on O,N-carboxymethylchitosans by ¹H and ¹³C NMR, *Int. J. Biol. Macromol.* **1992**, *14*, 122–128.
- 118 Xi-G. CHEN, H.-J. PARK, Chemical characteristics of O-carboxymethyl chitosans related to the preparation conditions, *Carbohydr. Polym.* **2003**, *53*, 355–359.
- 119 Y. NISHIYAMA, T. YOSHIKAWA, K. KURITA, K. HOJO, H. KAMADA, Y. TSUTSUMI, T. MAYUMI, K. KAWASAKI, Regioselective conjugation of chitosan with a laminin-related peptide, Tyr-Ile-Gly-Ser-Arg, and evaluation of its inhibitory effect on experimental cancer metastasis, *Chem. Pharm. Bull.* **1999**, *47*, 451.
- 120 Y. NISHIYAMA, T. YOSHIKAWA, K. KURITA, K. HOJO, H. KAMADA, Y. TSUTSUMI, T. MAYUMI, K. KAWASAKI, A conjugate from a laminin-related peptide, Tyr-Ile-Gly-Ser-Arg, and chitosan: efficient and regioselective conjugation and significant inhibitory activity against experimental cancer metastasis, *J. Chem. Soc. Perkin Trans.* **2000**, 1161–1165.

- 121 S. NISHIMURA, Y. MIURA, L. REN, M. SATO, A. YAMAGISHI, N. NISHI, S. TOKURA, K. KURITA, S. ISHII, An efficient method for the syntheses of novel amphiphilic polysaccharides by regioselective and thermoselective modifications of chitosan, *Chem. Lett.* **1993**, 1623–1626.
- 122 K. KURITA, M. KOBAYASHI, T. MUNAKATA, S. ISHII, S. NISHIMURA, Synthesis of nonnatural branched polysaccharides – regioselective introduction of alpha-mannoside branches into chitin, *Chem. Lett.* **1994**, 2063–2066.
- 123 K. KURITA, K. SHIMADA, Y. NISHIYAMA, M. SHIMOJOH, S. NISHIMURA, Nonnatural branched polysaccharides: synthesis and properties of chitin and chitosan having α -mannoside branches, *Macromolecules* **1998**, *31*, 4764–4769.
- 124 K. KURITA, T. KOJIMA, T. MUNAKATA, H. AKAO, T. MORI, Y. NISHIYAMA, M. SHIMOJOH, Preparation of non-natural branched chitin and chitosan, *Chem. Lett.* **1998**, 317–318.
- 125 R. J. MUMPER, J. WANG, J. M. CLASPELL, A. P. ROLLAND, Novel polymeric condensing carriers for gene delivery, *Proc. Int. Symp. Controlled Rel. Bioact. Mater.* **1995**, *22*, 178–179.
- 126 S. C. W. RICHARDSON, H. V. J. KOLBE, R. DUNCAN, Potential of low molecular mass chitosan as a DNA delivery system: biocompatibility, body distribution and ability to complex and protect DNA, *Int. J. Pharm.* **1999**, *178*, 231–243.
- 127 F. CHELLAT, A. GRANDJEAN-LAQUERRIERE, R. LE NAOUR, J. FERNANDES, L'H. YAHIA, M. GUENOUNOU, D. LAURENT-MAQUIN, Metalloproteinase and cytokine production by THP-1 macrophages following exposure to chitosan–DNA nanoparticles, *Biomaterials* **2005**, *26*, 961–970.
- 128 F. R. MACLAUGHLIN, J. MUMPER, J. WANG, J. M. TAGLIAFERRI, I. GILL, M. HINCHCLIFFE, A. P. ROLLAND, Chitosan and depolymerized chitosan oligomers as condensing carriers for *in vivo* plasmid delivery, *J. Controlled Rel.* **1998**, *56*, 259–272.
- 129 S. DANIELSEN, K. M. VARUM, B. T. STOKKE, Structural analysis of chitosan mediated DNA condensation by AFM: influence of chitosan molecular parameters, *Biomacromolecules* **2004**, *5*, 928–936.
- 130 W. LIU, S. SUN, Z. CAO, X. ZHANG, K. YAO, W. W. LU, K. D. K. LUK, An investigation on the physicochemical properties of chitosan/DNA polyelectrolyte complexes, *Biomaterials* **2005**, *26*, 2705–2711.
- 131 T. KIANG, J. WEN, H. W. LIM, K. W. LEONG, The effect of the degree of chitosan deacetylation on the efficiency of gene transfection, *Biomaterials* **2004**, *25*, 5293–5301.
- 132 C. SCHATZ, C. PICHOT, T. DELAIR, C. VITON, A. DOMARD, Static light scattering studies on chitosan solutions: from macromolecular chains to colloidal dispersions, *Langmuir* **2003**, *19*, 9896–9903.
- 133 O. E. PHILIPPOVA, E. V. VOLKOV, N. L. SITNIKOVA, A. R. KHOKHLOV, Two types of hydrophobic aggregates in aqueous solutions of chitosan and its hydrophobic derivative, *Biomacromolecules* **2001**, *2*, 483–490.
- 134 M. KOPING HOGGARD, Y. S. MELNIKOVA, K. M. VARUM, B. LINDMAN, P. ARTURSSON, Relationship between the physical shape and the efficiency of oligomeric chitosan as a gene delivery system *in vitro* and *in vivo*, *J. Gene Med.* **2003**, *5*, 130–141.
- 135 M. KOPING-HOGGARD, K. M. VARUM, M. ISSA, S. DANIELSEN, B. E. CHRISTENSEN, B. T. STROKE, P. ARTURSSON, Improved chitosan-mediated gene delivery based on easily dissociated chitosan polyplexes of highly defined chitosan oligomers, *Gene Therapy* **2004**, *11*, 1441–1452.
- 136 T. SATO, T. ISHII, Y. OKAHATA, *In vitro* gene delivery mediated by chitosan. Effect of pH, serum, and molecular mass of chitosan on the transfection efficiency, *Biomaterials* **2001**, *22*, 2075–2080.
- 137 A. BOZKIR, O. M. SAKA, Chitosan–DNA nanoparticles: Effect on DNA

- integrity, bacterial transformation and transfection efficiency, *J. Drug Target.* **2004**, *12*, 281–288.
- 138 V. CHAN, H. Q. MAO, K. W. LEONG, Chitosan-induced perturbation of dipalmitoyl-*sn*-glycero-3-phosphocholine membrane bilayer, *Langmuir* **2001**, *17*, 3749–3756.
- 139 T. ISHII, Y. OKAHATA, T. SATO, Mechanism of cell transfection with plasmid/chitosan complexes, *Biochim. Biophys. Acta* **2001**, *1514*, 51–64.
- 140 M. LEE, J. W. NAH, Y. KWON, J. J. KOH, K. S. KO, S. W. KIM, Water-soluble and low molecular weight chitosan-based plasmid DNA delivery, *Pharm. Res.* **2001**, *18*, 427–431.
- 141 H.-Q. MAO, K. ROY, V. L. TROUNG-LE, K. A. JANES, K. Y. LIN, Y. W., J. T. AUGUST, K. W. LEONG, Chitosan–DNA nanoparticles as gene carriers: synthesis, characterization and transfection efficiency, *J. Controlled Rel.* **2001**, *70*, 399–421.
- 142 M. A. WOLFERT, L. W. SEYMOUR, Characterization of vectors for gene therapy formed by self-assembly of DNA with synthetic block copolymers, *Human Gene Ther.* **1996**, *3*, 269–73.
- 143 P. ERBACHER, S. ZOU, T. BETTINGER, A.-M. STEFFAN, J.-S. REMY, Chitosan-based vector/DNA complexes for gene delivery: biophysical characteristics and transfection ability, *Pharm. Res.* **1998**, *15*, 1332–1339.
- 144 J. AKBUGA, E. OZBAS-TURAN, N. ERDOGAN, Plasmid-DNA loaded chitosan microspheres for *in vitro* IL-2 expression, *Eur. J. Pharm. Biopharm.* **2004**, *58*, 501–507.
- 145 W. G. LIU, X. ZHANG, S. J. SUN, G. J. SUN, K. DE YAO, *N*-alkylated chitosan as a potential nonviral vector for gene transfection, *Bioconjug. Chem.* **2003**, *14*, 782–789.
- 146 Y. W. CHO, J. D. KIM, K. PARK, Polycation gene delivery systems: escape from endosomes to cytosol, *J. Pharm. Pharmacol.* **2003**, *55*, 721–734.
- 147 O. BOUSSIF, F. LEZOUALCH, M. A. ZANTA, M. D. MERGNY, D. SCHERMAN, B. DEMENEIX, J.-P. BEHR, A versatile vector for gene and oligonucleotide transfer into cells in culture and *in vivo*: polyethylenimine, *Proc. Natl Acad. Sci. USA* **1995**, *92*, 7297–7301.
- 148 A. M. FUNHOFF, C. F. VAN NOSTRUM, G. A. KONING, Endosomal escape of polymeric gene delivery complexes is not always enhanced by polymers buffering at low pH, *Biomacromolecules* **2004**, *5*, 32–39.
- 149 T. H. KIM, J. E. IHM, Y. J. CHOI, J. W. NAH, C. S. CHO, Efficient gene delivery by urocanic acid-modified chitosan, *J. Controlled Rel.* **2003**, *93*, 389–402.
- 150 T. KIANG, C. BRIGHT, C. Y. CHEUNG, P. S. STAYTON, A. S. HOFFMAN, K. W. LEONG, Formulation of chitosan–DNA nanoparticles with poly(propyl acrylic acid) enhances gene expression, *J. Biomater. Sci. Polym. Ed.* **2004**, *15*, 1405–1421.
- 151 M. THANOU, B. I. FLOREA, H. E. JUNGINGER, G. BORCHARD, Quaternized chitosan oligomers as gene delivery vectors *in vitro*, *J. Controlled Rel.* **2003**, *87*, 294–295.
- 152 C. A. JANSMA, M. THANOU, H. E. JUNGINGER, G. BORCHARD, Preparation and characterization of 6-O-carboxymethyl-*N*-trimethyl chitosan derivative as a potential carrier for targeted polymeric gene and drug delivery, *STP Pharm. Sci.* **2003**, *13*, 63–67.
- 153 I. K. PARK, T. H. KIM, S. I. KIM, T. AKAIKE, C. S. CHO, Chemical modification of chitosan for gene delivery, *J. Dispersion Sci. Technol.* **2003**, *24*, 489–498.
- 154 L. B. PEPPAS, J. O. BLANCHETT, Nanoparticle and targeted systems for cancer therapy, *Adv. Drug Deliv. Rev.* **2004**, *56*, 1649–1659.
- 155 K. W. LEONG, H.-Q. MAO, V. L. TROUNG-LE, K. ROY, S. M. WALSH, J. T. AUGUST, DNA-polycation nanospheres as non-viral gene delivery vehicles, *J. Controlled Rel.* **1998**, *53*, 183–193.
- 156 I. K. PARK, J. E. IHM, Y. H. PARK, Y. J. CHOI, S. I. KIM, W. J. KIM, T. AKAIKE, C. S. CHO, Galactosylated chitosan (GC)-graft-poly(vinyl pyrrolidone) (PVP) as hepatocyte-targeting DNA carrier Preparation and

- physicochemical characterization of GC-graft-PVP/DNA complex (1), *J. Controlled Rel.* **2003**, *86*, 349–359.
- 157 G. Y. WU, C. H. WU, Receptor-mediated delivery of foreign genes to hepatocytes, *Adv. Drug Deliv. Rev.* **1998**, *29*, 243–248.
- 158 G. ASHWELL, J. HARFORD, Carbohydrate-specific receptors of the liver, *Ann. Rev. Biochem.* **1982**, *51*, 531–554.
- 159 R. J. FALLON, A. L. SCHWARTZ, Asialoglycoprotein receptor phosphorylation and receptor-mediated endocytosis in hepatoma cells. Effect of phorbol esters, *J. Biol. Chem.* **1988**, *63*, 13159–13166.
- 160 B. B. KNOWLES, C. C. HOWE, D. P. ADEN, Human hepatocellular carcinoma cell lines secrete the major plasma proteins and hepatitis B surface antigen, *Science* **1980**, *209*, 497–499.
- 161 J. H. PARK, Y. W. CHO, H. CHUNG, I. C. KWON, S. Y. JEONG, Synthesis and characterization of sugar-bearing chitosan derivatives: aqueous solubility and biodegradability, *Biomacromolecules* **2003**, *4*, 1087–1091.
- 162 G. ASHWELL, A. MORELL, The role of surface carbohydrates in the hepatic recognition and transport of circulating glycoproteins, *Adv. Enzymol.* **1974**, *41*, 99–128.
- 163 A. CIECHANOVER, A. L. SCHWARTZ, H. F. LODISH, Sorting and recycling of cell surface receptors and endocytosed ligands: the asialoglycoprotein and transferrin receptors, *J. Cell Biochem.* **1983**, *23*, 107–130.
- 164 J.-I. MURATA, Y. OHYA, T. OUCHI, Possibility of application of quaternary chitosan having pendant galactose residues as gene delivery tool, *Carbohydr. Polym.* **1996**, *29*, 69–74.
- 165 Y. K. PARK, Y. H. PARK, B. A. SHIN, E. S. CHOI, Y. R. PARK, T. AKAIKE, C. S. CHO, Galactosylated chitosan-graft-dextran as hepatocyte-targeting DNA carrier, *J. Controlled Rel.* **2000**, *69*, 97–108.
- 166 I. K. PARK, Y. H. PARK, B. A. SHIN, E. S. CHOI, Y. R. KIM, T. AKAIKE, C. S. CHO, Galactosylated chitosan-graft-dextran as hepatocyte-targeting DNA carrier, *J. Controlled Rel.* **2001**, *75*, 433.
- 167 T. H. KIM, I. K. PARK, J. W. NAH, Y. J. CHOI, C. S. CHO, Galactosylated chitosan/DNA nanoparticles prepared using water-soluble chitosan as a gene carrier, *Biomaterials* **2004**, *25*, 3783–3792.
- 168 I. K. PARK, T. H. KIM, Y. H. PARK, B. A. SHIN, E. S. CHOI, E. H. CHOWDHURY, T. AKAIKE, C. S. CHO, Galactosylated chitosan-graft-poly(ethylene glycol) as hepatocyte-targeting DNA carrier, *J. Controlled Rel.* **2001**, *76*, 349–362.
- 169 I. K. PARK, T. H. KIM, S. I. KIM, Y. H. PARK, W. J. KIM, T. AKAIKE, C. S. CHO, *Int. J. Pharm.* **2003**, *257*, 103–110.
- 170 P. ERBACHER, S. M. ZOU, T. BETTINGER, A. M. STEFFAN, J. S. REMY, Chitosan-based vector/DNA complexes for gene delivery: biophysical characteristics and transfection ability, *Pharm. Res.* **1998**, *15*, 1332–1339.
- 171 S. Y. GAO, J. N. CHEN, X. R. XU, Z. DING, Y. H. YANG, Z. C. HUA, J. F. ZHANG, Galactosylated low molecular weight chitosan as DNA carrier for hepatocyte-targeting, *Int. J. Pharm.* **2003**, *255*, 57–68.
- 172 K. BARABAS, W. P. FAULK, transferrin receptors associate with drug-resistance in cancer cells, *Biochem. Biophys. Res. Commun.* **1993**, *197*, 702–708.
- 173 I. F. UCHEGBU, A. G. SCHATZLEIN, L. TETLEY, A. I. GRAY, J. SLUDDEN, S. SIDDIQUE, E. MOSHA, Polymeric chitosan-based vesicles for drug delivery, *J. Pharm. Pharmacol.* **1998**, *50*, 453–458.
- 174 C. DUFES, A. G. SCHATZLEIN, L. TETLEY, A. I. GRAY, D. G. WATSON, J.-C. OLIVIER, W. COUET, I. F. UCHEGBU, Niosomes and polymeric chitosan based vesicles bearing transferrin and glucose ligands for drug targeting, *Pharm. Res.* **2000**, *17*, 1251–1258.
- 175 C. DUFES, J.-M. MULLER, W. COUET, J.-C. OLIVIER, I. F. UCHEGBU, A. G. SCHATZLEIN, Anticancer drug delivery

- with transferrin targeted polymeric chitosan vesicles, *Pharm. Res.* **2004**, *21*, 101–107.
- 176 W. GUO, R. L. LEE, Receptor-targeted gene delivery via folate-conjugated polyethylenimine, *AAPS Pharm. Sci.* **1999**, *1*, E19.
- 177 J. M. BENNS, A. MAHESHWARI, D. Y. FURGESON, R. I. MAHATO, S. W. KIM, Folate-PEG-folate-graft-polyethylenimine-based gene delivery, *J. Drug Target.* **2001**, *9*, 123–139.
- 178 J. M. BENNS, R. I. MAHATO, S. W. KIM, Optimization of factors influencing the transfection efficiency of folate-PEG-folate-graft-polyethylenimine, *J. Controlled Rel.* **2002**, *79*, 255–269.
- 179 Y. H. KIM, S. H. GIHM, C. R. PARK, K. Y. LEE, T. W. KIM, I. C. KWON, H. CHUNG, S. Y. JEONG, Structural characteristics of size-controlled self-aggregates of deoxycholic acid-modified chitosan and their application as a DNA delivery carrier, *Bioconjugate Chem.* **2001**, *12*, 932–938.
- 180 H. S. YOO, J. E. LEE, H. CHUNG, I. C. KWON, S. Y. JEONG, Self-assembled nanoparticles containing hydrophobically modified glycol chitosan for gene delivery, *J. Controlled Rel.* **2005**, *103*, 235–243.
- 181 S. KWON, J. H. PARK, H. CHUNG, I. C. KWON, S. Y. JEONG, Physicochemical characteristics of self-assembled nanoparticles based on glycol chitosan bearing 5-cholanic acid, *Langmuir* **2003**, *19*, 10188–10193.
- 182 W. SUI, G. SONG, G. CHEN, G. XU, Aggregate formation and surface activity property of an amphiphilic derivative of chitosan, *Colloids Surfaces A Physicochem. Eng. Aspects* **2005**, *256*, 29–33.
- 183 S. DANIELSEN, S. STRAND, C. L. DAVIES, B. T. STOKK, Glycosaminoglycan destabilization of DNA–chitosan polyplexes for gene delivery depends on chitosan chain length and GAG properties, *Biochim. Biophys. Acta Gen. Subj.* **2005**, *1721*, 44–54.
- 184 A. BERTHOLD, K. CREMER, J. KREUTER, Preparation and characterization of chitosan microspheres as drug carrier for prednisolone sodium phosphate as model for antiinflammatory drugs, *J. Controlled Rel.* **1996**, *39*, 17–25.
- 185 C. ARAL, S.-TURAN OZBAS, L. KABASAKAL, M. K.-UYSAL, J. AKBUGA, Studies of effective factors of plasmid DNA-loaded chitosan microspheres I. Plasmid size, chitosan concentration and plasmid addition techniques, *STP Pharm. Sci.* **2000**, *10*, 83–88.
- 186 F. L. MI, H. W. SUNG, S. S. SHYU, Drug release from chitosan–alginate complex beads reinforced by a naturally occurring cross-linking agent, *Carbohydr. Polym.* **2002**, *48*, 61–72.
- 187 F. L. MI, H. W. SUNG, S. S. SHYU, C. C. SU, C. K. PENG, Synthesis and characterization of biodegradable TPP/genipin co-crosslinked chitosan gel beads, *Polymer* **2003**, *44*, 6521–6530.
- 188 S. OZBAS-TURAN, J. AKBUGA, C. ARAL, Controlled release of interleukin-2 from chitosan microspheres, *J. Pharm. Sci.* **2002**, *91*, 1245–1251.
- 189 J. AKBUGA, S. OZBAS-TURAN, N. ERDOGAN, Plasmid-DNA loaded chitosan microspheres for *in vitro* IL-2 expression, *Eur. J. Pharm. Biopharm.* **2004**, *58*, 501–507.
- 190 A. POLK, B. AMSDEN, K. D. YAO, T. PENG, M. F. A. GOOSEN, Controlled-release of albumin from chitosan–alginate microcapsules, *J. Pharm. Sci.* **1994**, *83*, 178–185.
- 191 L. S. LIU, S. Q. LIU, S. Y. NG, M. FROIX, T. OHNO, J. HELLER, Controlled release of interleukin-2 for tumour immunotherapy using alginate/chitosan porous microspheres, *J. Controlled Rel.* **1997**, *43*, 65–74.
- 192 S. A. AGNIHOTRI, N. N. MALLIKARJUNA, T. M. AMINABHAVI, Recent advances on chitosan-based micro- and nanoparticles in drug delivery, *J. Controlled Rel.* **2004**, *100*, 5–28.
- 193 H. ZHANG, M. OH, C. ALLEN, E. KUMACHEVA, Monodisperse chitosan nanoparticles for mucosal drug delivery, *Biomacromolecules* **2004**, *5*, 2461–2468.
- 194 P. CALVO, C. REMUNAN-LOPEZ, J. L. VILA-JATO, M. J. ALONSO, Novel

- hydrophilic chitosan–polyethylene oxide nanoparticles as protein carriers, *J. Appl. Polym. Sci.* **1997**, *63*, 125–132.
- 195** H. Q. MAO, K. ROY, S. M. WALSH, J. T. AUGUST, K. W. LEONG, DNA chitosan nanospheres for gene delivery, *Proc. Int. Symp. Controlled Rel. Bioact. Mater.* **1996**, *23*, 401–402.
- 196** X. W. LI, D. K. L. LEE, A. S. C. CHAN, H. O. ALPAR, Sustained expression in mammalian cells with DNA complexed with chitosan nanoparticles, *Biochim. Biophys. Acta* **2003**, *1630*, 7–18.
- 197** H.-L. JIANG, I.-K. PARK, N.-R. SHIN, SANG. G. KANG, H.-S. YOO, S.-I. KIM, S.-B. S., T. AKAIKE, C.-S. CHO, *In vitro* study of the immune stimulating activity of an atrophic rhinitis vaccine associated to chitosan microspheres, *Eur. J. Pharm. Biopharm.* **2004**, *58*, 471–476.
- 198** A. M. DE CAMPOS, A. SANCHEZ, M. J. ALONSO, Chitosan nanoparticles: a new vehicle for the improvement of the delivery of drugs to the ocular surface. Application to cyclosporin A, *Int. J. Pharm.* **2001**, *224*, 159–168.
- 199** L. F. QI, Z. R. XU, Lead sorption from aqueous solutions on chitosan nanoparticles. *Colloids Surfaces A Physicochem. Eng. Aspects* **2004**, *251*, 183–190.
- 200** Y. XU, Y. DU, Effect of molecular structure of chitosan on protein delivery properties of chitosan nanoparticles, *Int. J. Pharm.* **2003**, *250*, 215–226.
- 201** A. VILA, A. SANCHEZA, K. JANES, I. BEHRENSB, T. KISSEL, J. L. V. JATO, M. J. ALONSO, Low molecular weight chitosan nanoparticles as new carriers for nasal vaccine delivery in mice, *Eur. J. Pharm. Biopharm.* **2004**, *57*, 123–131.
- 202** L. QI, Z. XU, X. JIANG, C. HU, X. ZOU, Preparation and antibacterial activity of chitosan nanoparticles, *Carbohydr. Res.* **2004**, *339*, 2693–2700.
- 203** T. LÓPEZ-LEÓN, E. L. S. CARVALHO, B. SEIJO, J. L. ORTEGA-VINUESA, D. BASTOS-GONZÁLEZ, Physicochemical characterization of chitosan nanoparticles: electrokinetic and stability behavior, *J. Colloid Interface Sci.* **2005**, *283*, 344–351.
- 204** K. A. JANES, M. P. FRESNEAU, A. MARAZUELA, A. FABRA, M. J. ALONSO, Chitosan nanoparticles as delivery systems for doxorubicin, *J. Controlled Rel.* **2001**, *73*, 255–267.
- 205** L.-S. LIU, S.-Q. LIU, S. Y. NG, M. FROIX, T. OHNO, J. HELLER, Controlled release of interleukin-2 for tumour immunotherapy using alginate/chitosan porous microspheres, *J. Controlled Rel.* **1997**, *43*, 65–74.
- 206** K. KOFUJI, C.-J. QIAN, Y. MURATA, S. KAWASHIMA, Preparation of chitosan microparticles by water-in-vegetable oil emulsion coalescence technique, *React. Func Polym.* **2005**, *62*, 77–83.
- 207** J. AKBUGA, G. DURMAZ, Preparation and evaluation of cross-linked chitosan microspheres containing furosemide, *Int. J. Pharm.* **1994**, *111*, 217–222.
- 208** I. GENTA, P. PERUGINI, B. CONTI, F. PAVANETTO, A multiple emulsion method to entrap a lipophilic compound into chitosan microspheres, *Int. J. Pharm.* **1997**, *152*, 237–246.
- 209** S. G. KUMBAR, A. R. KULKARNI, T. M. AMINABHAVI, Crosslinked chitosan microspheres for encapsulation of diclofenac sodium: effect of cross-linking agent, *J. Microencapsul.* **2002**, *19*, 173–180.
- 210** S. G. KUMBAR, T. M. AMINABHAVI, Synthesis and characterization of modified chitosan microspheres: Effect of the grafting ratio on the controlled release of nifedipine through microspheres, *J. Appl. Polym. Sci.* **2003**, *89*, 2940–2949.
- 211** A. A. AL-HELW, A. A. AL-ANGARY, G. M. MAHROUS, M. M. AL-DARDARI, Preparation and evaluation of sustained release cross-linked chitosan microspheres containing phenobarbitone, *J. Microencapsul.* **1998**, *15*, 373–82.
- 212** E. B. DENKBAS, M. SEYYAL, E. PISKIN, 5-fluorouracil loaded chitosan microspheres for chemoembolization, *J. Microencapsul.* **1998**, *16*, 741–749.
- 213** B. C. THANOO, M. C. SUNNY, A.

- JAYAKRISHNAN, Cross-linked chitosan microspheres – preparation and evaluation as a matrix for the controlled release of pharmaceuticals, *J. Pharm. Pharmacol.* **1992**, *44*, 283–286.
- 214 C. SANKAR, M. RANI, A. K. SRIVASTAVA, B. MISHRA, Chitosan based pentazocine microspheres for intranasal systemic delivery: development and biopharmaceutical evaluation, *Pharmazie* **2001**, *56*, 223–226.
- 215 S. R. JAMEELA, T. V. KUMARY, A. V. LAL, A. JAYAKRISHNAN, Progesterone-loaded chitosan microspheres: a long acting biodegradable controlled delivery system, *J. Controlled Rel.* **1998**, *52*, 17–24.
- 216 F. BUGAMELLI, M. A. RAGGI, I. ORIENTI, V. ZECCHI, Controlled insulin release from chitosan microparticles, *Arch. Pharm.* **1998**, *331*, 133–138.
- 217 X. PENG, L. ZHANG, Surface fabrication of hollow microspheres from *n*-methylated chitosan cross-linked with glutaraldehyde, *Langmuir* **2005**, *21*, 1091–1095.
- 218 P. CALVO, C. REMUNAN, J. L. VILA JATO, M. J. ALONSO, Development of positively charged colloidal drug carriers: chitosan coated polyester nanocapsules and submicron-emulsions, *Colloid Polym. Sci.* **1997**, *275*, 46–53.
- 219 C. PREGO, M. GARCIA, D. TORRES, M. J. ALONSO, Transmucosal macromolecular drug delivery, *J. Controlled Rel.* **2005**, *101*, 151–162.
- 220 M.-K. LEE, S.-K. CHUN, W.-J. CHOI, J.-K. KIM, S.-H. CHOI, A. KIM, K. t OUNGBHO, J.-S. PARK, W. S. AHN, C.-K. KIM, The use of chitosan as a condensing agent to enhance emulsion-mediated gene transfer, *Biomaterials* **2005**, *26*, 2147–2156.
- 221 P. HE, S. S. DAVIS, L. ILLUM, Chitosan microspheres prepared by spray drying, *Int. J. Pharm.* **1999**, *187*, 53–65.
- 222 F.-L. MI, Y.-C. TAN, H.-F. LIANG, H.-W. SUNG, *In vivo* biocompatibility and degradability of a novel injectable-chitosan-based implant, *Biomaterials* **2002**, *23*, 181–191.
- 223 J. FILIPOVIC-GRICIC, B. PERISSUTTI, M. MONEGHINI, D. VOINOVICH, A. MARTINAC, I. JALSENJAK, Spray-dried carbamazepine-loaded chitosan and HPMC microspheres: preparation and characterisation, *J. Pharm. Pharmacol.* **2003**, *55*, 921–931.
- 224 I. ORIENTI, T. CERCHIARA, B. LUPPI, F. BIGUCCI, G. ZUCCARI, V. ZECCHI, Influence of different chitosan salts on the release of sodium diclofenac in colon-specific delivery, *Int. J. Pharm.* **2002**, *238*, 51–59.
- 225 Y. C. HUANG, M. K. YEH, C. H. CHIANG, Formulation factors in preparing BTM-chitosan microspheres by spray drying method, *Int. J. Pharm.* **2002**, *242*, 239–242.
- 226 T. CERCHIARA, B. LUPPI, F. BIGUCCI, V. ZECCHI, Chitosan salts as nasal sustained delivery systems for peptidic drugs, *J. Pharm. Pharmacol.* **2003**, *55*, 1623–1627.
- 227 C. WITSCHI, R. J. MRSNY, *In vitro* evaluation of microparticles and polymer gels for use as nasal platforms for protein delivery, *Pharm. Res.* **1999**, *16*, 382–390.
- 228 Y. C. HUANG, M. K. YEH, S. N. CHENG, C. H. CHIANG, The characteristics of betamethasone-loaded chitosan microparticles by spray-drying method, *J. Microencapsulation* **2003**, *20*, 459–472.
- 229 H. O. ALPAP, S. SOMAVARAPU, K. N. ATUAH, V. W. BRAMWELL, Biodegradable mucoadhesive particulates for nasal and pulmonary antigen and DNA delivery, *Adv. Drug Deliv. Rev.* **2005**, *57*, 411–430.
- 230 E. S. K. TANG, M. HUANG, L. Y. LIM, Ultrasonication of chitosan and chitosan nanoparticles, *Int. J. Pharm.* **2003**, *265*, 103–114.
- 231 T. BANERJEE, S. MITRA, A. KINGH, R. KHARMA, A. MAITRA, Preparation, characterization and biodistribution of ultrafine chitosan nanoparticles, *Int. J. Pharm.* **2002**, *243*, 93–105.
- 232 M. ANDERSSON, J. E. LOFROTH, Small particles of a heparin/chitosan complex prepared from a pharmaceutically acceptable microemulsion, *Int. J. Pharm.* **2003**, *257*, 305.

- 233 S. MITRA, U. GAUR, P. C. GHOSH, A. N. MAITRA, Tumour targeted delivery of encapsulated dextran–doxorubicin conjugate using chitosan nanoparticles as carrier, *J. Controlled Rel.* **2001**, *74*, 317–23.
- 234 K. KOFUJI, C.-J. QIAN, Y. MURATA, S. KAWASHIMA, Preparation of chitosan microparticles by water-in-vegetable oil emulsion coalescence technique, *Reac. Func. Polym.* **2005**, *62*, 77–83.
- 235 H. SASHIWA, Y. SHIGEMASA, R. ROY, Chemical modification of chitosan part 2 – Novel N-alkylation of chitosan via Michael type reaction, *Chem. Lett.* **2000**, 862–863.
- 236 H. TOKUMITSU, H. ICHIKAWA, Y. FUKUMORI, Chitosan-gadopenetic acid complex nanoparticles for gadolinium neutron-capture therapy of cancer: preparation by novel emulsion-droplet coalescence technique and characterization, *Pharm. Res.* **1999**, *16*, 1830–1835.
- 237 F. SHIKATA, H. TOKUMITSU, H. ICHIKAWA, Y. FUKUMORI, *In vitro* cellular accumulation of gadolinium incorporated into chitosan nanoparticles designed for neutron-capture therapy of cancer, *Eur. J. Pharm. Biopharm* **2002**, *53*, 57–63.
- 238 H. TOKUMITSU, H. HIRATSUKA, Y. SAKURAI, T. KOBAYASHI, H. ICHIKAWA, Y. FUKUMORI, Gadolinium neutron-capture therapy using novel gadopenetic acid-chitosan complex nanoparticles: *in vivo* growth suppression of experimental melanoma solid tumor, *Cancer Lett.* **2000**, *150*, 177–182.
- 239 H. TOKUMITSU, H. ICHIKAWA, Y. FUKUMORI, Preparation of gadopenetic acid-loaded chitosan microparticles for gadolinium neutron-capture therapy of cancer by a novel emulsion-droplet coalescence technique, *Chem. Pharm. Bull.* **1999**, *47*, 838.
- 240 H. TOKUMITSU, H. ICHIKAWA, T. K. SAHA, Y. FUKUMORI, L. H. BLOCK, Design and preparation of gadolinium-loaded chitosan particles for cancer neutron capture therapy, *STP Pharm. Sci.* **2000**, *10*, 39.
- 241 S. A. AGNIHOTRI, T. M. AMINABHAVI, Controlled release of clozapine through chitosan microparticles prepared by a novel method, *J. Controlled Rel.* **2004**, *96*, 245–259.
- 242 A. BOZKIR, O. M. SAKA, Chitosan nanoparticles for plasmid DNA delivery: effect of chitosan molecular structure on formulation and release characteristics, *Drug Deliv.* **2004**, *11*, 107–112.
- 243 C. ARAL, J. AKBUGA, Preparation and *in vitro* transfection efficiency of chitosan microspheres containing plasmid DNA:poly(L-lysine) complexes, *J. Pharm. Pharm. Sci.* **2003**, *6*, 321–326.
- 244 S. OZBAS-TURAN, J. AKBUGA, C. ARAL, Controlled release of interleukin-2 from chitosan microspheres, *J. Pharm. Sci.* **2002**, *91*, 1245–1251.
- 245 T. DASTAN, K. TURAN, *In vitro* characterization and delivery of chitosan–DNA microparticles into mammalian cells, *J. Pharm. Pharm. Sci.* **2004**, *7*, 205–214.
- 246 S. OZBAS TURAN, C. ARAL, L. KABASAKAL, M. KEYER-UYSAI, J. AKBUGA, Co-encapsulation of two plasmids in chitosan microspheres as a non-viral gene delivery vehicle, *J. Pharm. Pharm. Sci.*, **2003**, *6*, 27–32.
- 247 S. MECLEAN, E. PROCESSER, D. O'MALLEY, N. CLARK, Z. RAMTOOLA, D. BRAYDEN, Binding and uptake of biodegradable poly-DL-lactide micro- and nanoparticles in intestinal epithelia, *Eur. J. Pharm. Sci.* **1998**, *6*, 153–163.
- 248 L. ILLUM, I. JABBAL-GILL, M. HINCHCLIFFE, A. N. FISHER, S. S. DAVIS, Chitosan as a novel nasal delivery system for vaccines, *Adv. Drug Deliv. Rev.* **2001**, *51*, 81–96.
- 249 K. CORSI, F. CHELLAT, L. YAHIA, J. C. FERNANDES, Mesenchymal stem cells, MG63 and HEK 293 transfection using chitosan–DNA nanoparticles, *Biomaterials* **2003**, *24*, 1255–1264.
- 250 A. I. CAPLAN, Mesenchymal stem cells and gene therapy, *Clin. Orthop. Rel. Res.* **2000**, *379* (Suppl.), 67–70.
- 251 S. MANSOURI, P. LAVIGNE, K. CORSI, M. BENDERDOUR, E. BEAUMONT, J. C. FERNANDES, Chitosan–DNA nanoparticles as non-viral vectors in gene therapy: strategies to improve

- transfection efficacy, *Eur. J. Pharm. Biophys.* **2004**, *57*, 1–8.
- 252 A. C. ANTONY, Folate receptors, *Annu. Rev. Nutr.* **1996**, *16*, 501–521.
- 253 S. WANG, J. LUO, D. A. LANTRIP, D. J. WATERS, C. J. MATHIAS, M. A. GREEN, P. L. FUCHS, P. S. LOW, Design and synthesis of [In-111]DTPA-folate for use as a tumor-targeted radiopharmaceutical, *Bioconjug. Chem.* **1997**, *8*, 673–679.
- 254 C. P. LEAMON, P. S. LOW, Delivery of macromolecules into living cells: a method that exploits folate receptor endocytosis, *Proc. Natl Acad. Sci. USA* **1991**, *88*, 5572–5576.
- 255 R. J. LEE, P. S. LOW, Delivery of liposomes into cultured kb cells via folate receptor-mediated endocytosis, *J. Biol. Chem.* **1994**, *269*, 3198–3204.
- 256 M. J. TURK, G. J. BREUR, W. R. WIDMER, C. M. PAULOS, L. C. XU, L. A. GROTE, P. S. LOW, Folate-targeted imaging of activated macrophages in rats with adjuvant-induced arthritis, *Arthritis Rheum.* **2002**, *46*, 1947–1955.
- 257 W. GUO, R. J. LEE, Efficient gene delivery via non-covalent complexes of folic acid and polyethylenimine, *J. Controlled Rel.* **2001**, *77*, 131–138.
- 258 J. A. REDDY, C. ABBURI, H. HOFLAND, S. J. HOWARD, I. VLAHOV, P. WILS, C. P. LEAMON, Folate-targeted, cationic liposome-mediated gene transfer into disseminated peritoneal tumors, *Gene Ther.* **2002**, *9*, 1542–1550.
- 259 M. KUMAR, A. K. BEHERA, R. F. LOCKEY, J. ZHANG, G. BHULLAR, C. PEREZ DE LA CRUZ, L.-C. CHEN, K. W. LEONG, S.-K. HUANG, S. S. MOHAPATRA, Intranasal gene transfer by chitosan–DNA nanospheres protects BALB/c mice against acute respiratory syncytial virus infection, *Hum. Gene Ther.* **2002**, *13*, 1415–1425.
- 260 W. XU, Y. SHEN, Z. JIANG, Y. WANG, Y. CHU, S. XIONG, Intranasal delivery of chitosan–DNA vaccine generates mucosal SIgA and anti-CVB3 protection, *Vaccine* **2004**, *22*, 3603–3612.
- 261 C.-J. SUN, S.-P. PAN, Q.-X. XIE, L.-J. XIAO, Preparation of chitosan-plasmid DNA nanoparticles encoding zona pellucida glycoprotein-3x and its expression in mouse, *Mol. Reprod. Dev.* **2004**, *68*, 182–188.
- 262 H. OKAMOTO, S. NISHIDA, H. TODO, Y. SAKABURA, K. IIDA, K. DANJO, Pulmonary gene delivery by chitosan-pDNA complex powder prepared by a supercritical carbon dioxide process, *J. Pharm. Sci.* **2003**, *92*, 371–380.
- 263 M. BIVAS-BENITA, K. E. VAN MEIJGAARDEN, K. L. M. C. FRANKEN, H. E. JUNGINGER, G. BORCHARD, T. H. M. OTTENHOFF, A. GELUK, Pulmonary delivery of chitosan–DNA nanoparticles enhances the immunogenicity of a DNA vaccine encoding HLA-A*0201-restricted T-cell epitopes of *Mycobacterium tuberculosis*, *Vaccine* **2004**, *22*, 1609–1615.

II

Protein & Peptide-based Nanomaterials

5

Plant Protein-based Nanoparticles

Anne-Marie Orecchioni, Cécile Duclairoir, Juan Manuel Irache and Evelyne Nakache

5.1

Introduction

Biopolymers, such as proteins, lipids or polysaccharides, are commonly used to encapsulate drugs in order to protect them from rapid degradation by environmental stress (e.g. light, heat, oxygen or pH sensitivity). Drug loading of carriers seems to be an attractive opportunity, especially if they are made from bioacceptable macromolecules, e.g. plant proteins. Colloidal carriers, in the form of nanoparticles with a diameter of 50–500 nm and up to a few micrometers, have the potential to deliver drugs to specific target sites and to achieve sustained drug release. Moreover encapsulation can modify the drug biodistribution and increase its bioavailability [1–4]. Nanoparticles can be formed from a variety of materials including synthetic polymers and biopolymers (i.e. natural compounds), such as proteins, lipids and carbohydrates [5]. Natural macromolecules from vegetable sources appear to be a very promising alternative to synthetic polymers due to their proven safety, especially those that are used as food sources. The selection of a suitable structural material has an important influence on its potential medical use. Comparing plant and animal proteins, it appears that vegetal proteins may be more disposable and cheaper than animal proteins. Moreover, for plant proteins, the purification process might be also simplified.

In general, protein nanoparticles display a number of interesting advantages. Among them, these carriers are biodegradable and metabolizable. Moreover, they can be prepared under “soft” conditions, without the use of toxic organic solvents or materials, and they can incorporate a wide variety of drugs in a relatively non-specific fashion [6]. Moreover, due to their defined primary structure, protein-based nanoparticles may offer various possibilities for surface modification and covalent attachment of drugs and ligands [7, 8].

Taking into account all of these advantages of plant proteins, this chapter will focus solely on the use of storage proteins from pea (legumin and vicilin) and wheat (gliadins) when used as a structural material to prepare nanoparticles, and their possible applications in pharmacy and medicine. These proteins are not the

only ones able to produce nano/microparticles for use as drug carriers – studies have also been performed on other plant proteins like soy glycinin from soybean seeds [9] and zein from corn [10]. However, the numbers of studies with these two proteins are very low. This chapter also includes an overview of the fabrication and applications of both conventional and “decorated” (i.e. conjugated) storage protein nanoparticles.

5.2

Description of Plant Proteins

Plant proteins are characterized by their three-dimensional organization. Two classes can be distinguished:

- Fibrous proteins composed of polypeptide chains joined together along a linear axis. They are involved in the structural material of living organisms.
- Globular proteins composed of one or, more frequently, several polypeptide chains rolled up to give a three-dimensional structure. Most of them are storage proteins.

Most vegetal proteins play an active role in biological processes, e.g. enzymes, and they can be classified by their physicochemical and extraction properties [11]. Four classes are listed:

- Vegetable albumins are hydrosoluble and rich in ionic residues (arginine, glutamic acid, lysine, tryptophan, etc.).
- Globulins are complex molecules and their amino acids composition is similar to that of albumins. However, their solubility needs an electrolyte medium.
- Prolamins are soluble in hydroalcoholic mixtures due to their high content of amino acids with hydrophilic residues.
- Glutelins cannot be dissolved in any of the aforementioned solvents, due to their high molecular mass and the presence of disulfide bonds; they are rich in lipophilic amino acids.

Storage proteins comprise proteins generated mainly during seed production and stored in the seed that serve as nitrogen sources for the developing embryo during germination [12, 13]. It is obviously more effective for the plant to use proteins instead of secondary plant products for this purpose. The average protein content of cereal grains is 10–15% of their dry weight [14], whereas for leguminose seeds it is about 20–25% [15, 16]. In addition to seeds, storage proteins can also be found in root and shoot tubers, e.g. potatoes.

No clear definition exists of what a storage protein is. The term is operational and was coined for all those proteins whose ratio in the total protein amount of the cell is greater than 5%. All of these proteins are characterized by the absence of enzymatic activity, act as a nitrogen source during seed germination and, usually, occur in an aggregated state confined in a membrane [17, 18].

Storage proteins are important for human nutrition (plant proteins), and numerous studies concerning their structure and biosynthesis have been published. For leguminoses, a simplifying rule says that they contain two types of storage proteins – legumin and vicilin. The legumins (as well as the vicilins) are very similar in different leguminose species. However, Gramineae contain a third type of storage proteins – prolamin – and, depending on the origin, it is distinguished between zein (from *Zea mays*) [19], hordein (from *Hordeum vulgare*) [20] and gliadin (from *Triticum aestivum* L.). In contrast to legumins and vicilins that are mainly located in the cotyledons of seeds, prolamines are found in the endosperm [21].

5.2.1

Pea Seed Proteins

Globulins are the main storage proteins in pea seeds [22]. These globulins were characterized by Osborne [23] according to their insolubility in distilled water and, on the contrary, by their solubility in buffered aqueous neutral salt solutions. When they are fractionated by centrifugation techniques, three different fractions have been described (with sedimentation coefficients of 2, 7 and 11S). The so-called 7 and 11S globulins represent the major pea seeds storage proteins – vicilin and legumin, respectively. These proteins display a number of similarities, including the adopted shape when solved in an aqueous solution and the similar size of the domains of the subunits forming these proteins [24, 25]. However, they can be differentiated by their molecular weight [22, 26] and different behavior at high temperature. In fact, vicilin has a size of about 200 kDa, whereas legumin is about 360 kDa [22, 26]. Furthermore, legumin does not coagulate at high temperature [27].

- Vicilin belongs to the group of so-called 7S globulins. It has a complex globular structure composed of two different types of subunits with molecular weights of about 50 and 60–70 kDa. These subunits form trimeric holoproteins in different combinations [22, 28]. Vicilin is rich in acidic amino acids (aspartic and glutamic acids), leucine and lysine [29, 30].
- Legumin belongs to the group of so-called 11S globulins [26]. This protein has a complex globular structure made of six pairs of subunits. Each of the subunits is composed of disulfide-linked acidic α -chains (molecular weight 40 kDa) and basic β -chains (molecular weight 20 kDa) [31]. Although the three-dimensional structure of legumin has not been yet determined, the sequence alignment of this protein appears to show some similarities with that of vicilin [24, 32].

5.2.2

Wheat Proteins

Storage proteins from the wheat seed are able to form a unique viscoelastic network called gluten. The properties of gluten make it useful in the production of food products such as bread, pasta and semolina, and more recently in biopackag-

ing materials [33]. The rheological properties of gluten are dependent on the protein interactions that are formed in the network, and these properties were found to be mainly influenced by physical parameters such as temperature and pressure [34–36].

Two main fractions are present in gluten – gliadin, which is soluble in 70% ethanol, made of single-chain polypeptides with an average molecular weight of 25–100 kDa linked by intramolecular disulfide bonds, and glutenin, an alcohol-insoluble fraction consisting of gliadin-like subunits stabilized by intermolecular disulfide bonds in large aggregates with a molecular weight greater than 106 kDa [37]. Because they account for about half of the total wheat gluten proteins, gliadin constitutes an important class of proteins that are involved in the various properties of the gluten [38, 39]. These proteins are polymorphic, and can be separated and classified on the basis of their electrophoretic mobility at acid pH values [40] in the following four fractions: α (molecular mass about 25–35 kDa), β (30–35 kDa), γ (35–40 kDa) and ω (55–70 kDa) groups [41–44]. All fractions have remarkably low solubility in aqueous solution except at extreme pH. This low water solubility has been attributed to the presence of interpolypeptide disulfide bonds and to the cooperative hydrophobic interactions which cause the protein chains to assume a folded shape. The amino acid composition shows that gliadin has equal amounts of apolar and neutral amino acids, mainly glutamine (about 40%). Furthermore, gliadin also has a high proline content (14%) and a very low proportion of charged amino acids [41, 45].

ω -Gliadin presents an isoelectric point (pI) ranging from 5.5 to 7 and has a few charged molecules with six to 11 basic amino acids per molecule. In contrast, α -, β - and γ -gliadins, with a pI range of 6.5–8, are still less charged than ω -gliadin [46].

5.3

Preparation of Protein Nanoparticles

Several methods have been reported in the literature for the preparation of nanoparticles from protein raw materials. Coacervation or controlled desolvation methods have been developed using solvent or electrolyte as the coacervation agent [47, 48] or by adjusting the pH or ionic strength [49, 50]. In the coacervation methods promoted by solvents, the first step consists of dispersing the macromolecules in an adequate solvent, then adding the mixture to a second solvent which is a nonsolvent of the macromolecules. A required condition is that the solvent and the nonsolvent phases are miscible.

The coacervation process is applied to a macromolecular solution to reduce the solubility in the system to such a degree that appropriate phase separation of the macromolecule takes place, i.e. the formation of a macromolecule-rich phase. The desolvation leads to macromolecule precipitation or to coacervate formation. It is assumed that, before phase separation is observed, a conformational change in the macromolecule occurs. The addition of a desolvating agent shrinks the macromolecule coil which becomes smaller and smaller until the phase separation from

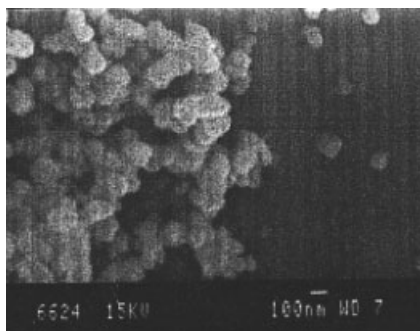


Fig. 5.1. Scanning electron micrograph of legumin nanoparticles. (From Ref. [52], permission pending).

the solvent occurs. It is possible to monitor the phenomenon by turbidity measurement. A desolvation agent decreases the turbidity because of the decrease in macromolecular size. To prepare small particles, it is important to maintain the system just outside the coacervation region. The addition of the coacervation agent should stop as soon as the Tyndall effect bounded to aggregation of macromolecules turns the system turbid [7]

5.3.1

Preparation of Legumin and Vicilin Nanoparticles

Legumin and vicilin have an aqueous solubility that is strongly pH and ionic strength dependent [30]. Nanoparticles from these pea proteins (Figs. 5.1 and 5.2) can be obtained by a simple coacervation or controlled desolvation method [50–52]. It was observed that extreme pH values enable their solubilization in aqueous medium. The coacervating or desolvating agent induces a progressive modification of the tertiary structure of the proteins, giving an increasing hydrophobic material which leads to submicronic aggregates or coacervates [53]. These coacervates are generally unstable and must be hardened for stabilization by physical or chemical

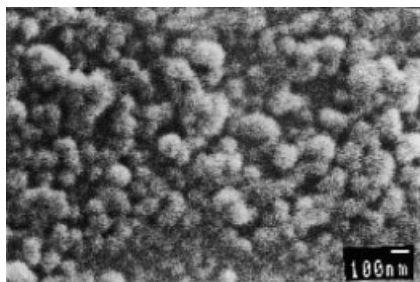


Fig. 5.2. Scanning electron micrograph of vicilin nanoparticles. (From Ref. [50]).

crosslinkage. In the case of these pea proteins, a three-step procedure can be employed to obtain nanoparticles.

In a first step, an unstable coacervate is obtained by mixing a solution of the chosen protein (pH 9) with a phosphate buffer solution. In a second step, the coacervates have to be hardened with a crosslinking agent in order to stabilize the just-forming coacervates. The most popular crosslinking agent is glutaraldehyde. This reagent reacts with the amino groups of the proteins, predominantly with the amino group of lysines, to form a Schiff base [54]. Finally, after the crosslinking, for pharmaceutical purposes, the obtained nanoparticles have to be purified. For this purpose, unreacted aldehyde can be neutralized with a sulfite and nanoparticles centrifuged in order to eliminate the nontransformed protein fraction onto particles.

Some comprehensive explanations of nanoparticles formation can be given. It is observed that, at a pH value close to 7, the coacervates show a submicronic size, but the percentages of coacervates yields are under 40% of the added protein. Similarly, the ionic strength of the buffer greatly influences the coacervate size and yield. The best experimental conditions to obtain small-sized particles (average diameter 500 nm) were found to be pH 6.8 and ionic strength 0.15 M for legumin, and pH 6.4 and ionic strength 0.10 M for vicilin [50, 52].

The isoelectric points of the two proteins are about 4.5. Thus, the balance between negative carboxyl groups (from glutamic and aspartic acids) and positive groups (from lysine and arginine) changes when the pH of the protein solution is less or greater than 4.5. Consequently, under environmental conditions close to the isoelectric point, these globulins would present a reduced interfacial charge which may enhance coacervate precipitation and phase separation. In other respects, for neutral pH values, legumin and vicilin would have a charge which may probably act against coacervate formation.

Concerning vicilin, in particular, a hypothesis for protein coacervate formation has been proposed. Under defined conditions, solubilized vicilin (7S form) may associate to yield an 11S insoluble form. This 11S form (probably a dimer of vicilin) may be responsible for the initial precipitation of vicilin which aggregates up to a critical size depending on environmental conditions (pH and ionic strength). The coacervate must be quickly hardened by crosslinkage in order to prevent the aggregates coalescing to a separate phase.

5.3.2

Preparation of Gliadin Nanoparticles

Gliadin nanoparticles (Fig. 5.3) can be prepared by a desolvation method in which a dissolution of gliadin in an organic solvent/water mixture is desolvated by the addition of a nonsolvent aqueous phase [50, 55]. Note that gliadin nanoparticles prepared in this way are stable and further treatment by heat or chemical crosslinking is not necessary to stabilize them. This fact can be explained by the extremely low solubility of gliadin in an aqueous medium and represents an advantage when compared with other protein nanoparticles (i.e. albumin, gelatin).

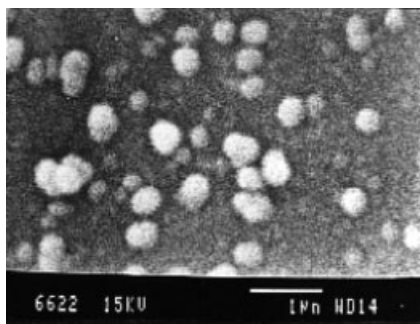


Fig. 5.3. Scanning electron micrograph of a gliadin nanoparticle. (From Ref. [8]).

In any case, gliadin nanoparticles can be hardened by chemical stabilization in order to modulate the drug release characteristics of nanoparticles or their *in vivo* distribution and interaction with the body.

Once produced (and eventually hardened by chemical crosslinkage), they have to be purified. The organic solvents are eliminated by evaporation under reduced pressure, whereas the amounts of protein not transformed onto nanoparticles and other impurities (i.e. the chemical crosslinker) are eliminated by dialysis, gel-permeation chromatography or, more frequently, subsequent centrifugations. Finally, nanoparticles can be also lyophilized to preserve their physicochemical properties for a long period of time. For lyophilization of gliadin nanoparticles, a solution of glucose 5% w/v has been proposed as a cryoprotector [56, 57].

In summary, this simple method allows the preparation of reproducible particle sizes with a narrow distribution. The main advantages are the production of nanoparticles in the absence of toxic organic solvents and the possibility of avoiding the chemical stabilization step to obtain stable nanoparticles. The selection of the solvent phase of gliadin has a significant influence on the size of the resulting nanoparticles. In this context, mixtures between either ethanol and water or acetone and water enable production of both smaller particle sizes and reproducible results. Another key factor concerns the nonsolvent of gliadin. In this case, an aqueous solution of NaCl (0.9% w/v) has been proposed [50]. When a mixture of ethanol and water is used, the size of the resulting nanoparticles is close to 450 nm and the yield of the process, determined by gravimetry and reverse-phase high-performance liquid chromatography (RP-HPLC), is about 90% [50, 56].

More recently, in order to understand the influence of environmental parameters governing gliadin nanoparticles size, a thermodynamic approach was investigated, i.e. the determination of the solubility parameter of the protein [58]. According to Hildebrand theory [59], the solubility parameter of gliadin was determined using a panel of solvents or mixtures of them. It is assumed that the solvent which best solubilizes gliadin has the same solubility parameter as the protein [60]. Different mixtures were prepared with bioacceptable solvents such as ethanol, ethylene glycol, propylene glycol and ultra-pure water. These solvents are usually considered

as references for the determination of the solubility parameters of biological compounds.

When a mixture of ethanol and water is used, the size of the resulting nanoparticles is close to 450 nm and the yield of the process, determined by gravimetry and RP-HPLC, is about 90% [50, 56]. However, a mixture of propylene glycol and water (73/27%) appears to be the best selection to obtain small gliadin nanoparticles of about 150 nm [58].

5.4

Drug Encapsulation in Plant Protein Nanoparticles

In order to evaluate the encapsulation ability of gliadin nanoparticles, different drugs were tested, chosen for their medical and/or pharmaceutical interest. The objective of this research was to determine the feasibility of nanoparticles loaded with hydrophilic or lipophilic drugs and furthermore in order to obtain as small-sized particles as possible. Attention was focused on the drug release mechanism. Four drugs were chosen – two lipophilic vitamins, i.e. all-*trans* retinoic acid [vitamin A (RA)] and α -tocopherol [vitamin E (VE)], and two hydrophilic drugs, i.e. a slightly polar mixture of linalool–linalyl acetate (LLA), components of the essential lavender oil, and the cationic amphiphilic benzalkonium chloride (BZC). For all these particulate systems, nanoparticles sizes were determined by scanning electron microscopy or photon correlation spectroscopy.

5.4.1

RA Encapsulation in Gliadin Nanoparticles

RA is involved in the proliferation and differentiation of epithelial tissues. This vitamin in acidic form reduces the size of sebaceous glands and sebum secretion, making it an attractive agent for the treatment of skin disorders such as acne, psoriasis, hyperkeratosis, ichthyosis and epithelial tumors [61, 62]. In the treatment of acne, it was demonstrated that RA prevents inflammatory lesions by loosening follicular impactions (microcomedones) and clearing the follicular canal of retained keratin [63]. Furthermore, RA has been proven effective against a range of malignancies in human clinical trials, although many patients relapsed after a remission [64]. *In vivo* studies have shown that RA is active against acute promyelocytic leukemia [65, 66]. Unfortunately, the limited duration of RA activity in this leukemia is a pharmacological adaptation resulting in reduced serum concentration after prolonged treatment [67]. Nevertheless, in spite of a real therapeutic interest, several drawbacks (e.g. teratogenicity) have been reported for the currently available dosage forms [62]. To overcome these inconveniences, and in an attempt to increase the therapeutic efficacy of RA, alternative dosage forms have been suggested – microemulsions [68] and liposomes for intravenous [69] and topical administration [70]. Another system suitable for controlled drug release could be nanoparticles from biopolymers. For this purpose, we have chosen nanoparticles from gliadin

din. They were prepared by the aforementioned desolvation method [50, 58]. These particles can be obtained by using only bioacceptable solvents such as ethanol and water. Their size, which is one of the determinant characteristics for medical purposes, can be optimized. These nanoparticles, showing good stability in phosphate-buffered saline (PBS), were assayed as carriers for RA. They have shown a quite good entrapment efficiency – about 75% of added drug at $60 \mu\text{g} (\text{mg gliadin})^{-1}$ and a payload of $74 \mu\text{g} (\text{mg gliadin})^{-1}$ nanoparticles [58]. In order to quantify more precisely the solvent effect, the size diameter was optimized through a solubility parameter study. The smallest size was reached for protein solubility solvent equal to that of gliadin. The average diameter of the particles was about 150 nm [58]. RA was released from these nanoparticles, in a two-step mechanism, characterized by an initial rapid release followed by a continuous diffusion process. The first release was found to be about 20% of the loaded drug and can be related either to the release of the drug entrapped in the peripheral domains of the nanoparticle matrix or to a simple desorption of superficial RA, whilst the second slower period was linear with respect to time and appeared to be a diffusion phenomenon. Furthermore, in this second step, about 20% of the drug was released by diffusion in 3 h.

These observations offer interesting prospects for the preparation of drug-loaded carriers for medical applications.

5.4.2

VE Encapsulation in Gliadin Nanoparticles

Drug carriers are interesting systems to prevent drawbacks related to the drug itself by decreasing its degradation rate. In order to test the protective power of nanoparticles against environmental stresses, a second lipophilic vitamin, VE, was encapsulated into gliadin nanoparticles. VE is known to act as a strong antioxidant or nitrosamine blocker to prevent the build-up of cellular peroxide [71]. The exposure to free oxygen species induces a rise in lipid peroxidation, which may cause injury at different sites of the body. For instance, the action of free radicals produced by a variety of environmental stresses (among them sun exposure) may promote skin damage, such as premature skin ageing [72], skin fragility and even skin cancers (melanoma or others) [73] related to a decrease in cellular immunity of the skin. VE appears to be one of the strongest free radical scavengers through its action as a chain-breaking antioxidant in membranes [74], preventing acute or chronic damage [75]. In addition to these biological activities, VE also exerts cosmetic functions; notably, it helps delay the progression of aging [76] and possesses a skin moisturizing power [77]. However, VE is degraded by oxygen, and dosage forms must be protected from light, heat and prolonged contact with air. Previous work has shown that the preparation of gliadin nanoparticles could be easily performed by a simple coacervation method. It is for this reason that gliadin has been chosen. Moreover, gliadin possesses the ability to interact with epidermal keratin due to its richness in proline [78]. VE-loaded gliadin nanoparticles have been characterized by their size, ζ potential, VE payload and entrapment efficiency.

When loaded, the gliadin particle size is about 900 nm and their charge is close to zero. They are suitable drug carriers with an optimum encapsulation rate of about $100 \text{ VE } \mu\text{g (mg gliadin)}^{-1}$ with an efficiency of more than 77%. The release behavior of VE-loaded nanoparticles may be interpreted as a “burst” effect, followed by a diffusion process through a homogeneous sphere [3].

5.4.3

Lipophilic, Hydrophilic or Amphiphilic Drug Encapsulation

In order to study the influence of drug polarity on nanoparticle characteristics such as particles size, drug loading and drug release, three different drugs with different polarities were chosen [79]. VE, studied in a previous paper [3], was employed as a model of a lipophilic drug, and the slightly polar LLA and the amphiphilic cationic benzalkonium chloride (BZC) as hydrophilic models. Their dielectric constants are, respectively, 4, 8 and 45 [80]. The choice of these drugs was governed by their utilization in pharmaceutical dosage forms:

- VE, widely used as strong antioxidant in many medical and cosmetic applications, is rapidly degraded because of its light, heat and oxygen sensitivity [3].
- Linalool and linalyl acetate are the major components of essential lavender oil used in aromatherapy. They possess antibacterial and antifungal properties [81]. They are used in topical formulations. They may cause skin irritation by reason of a potential caustic power. Gliadin encapsulation could be a fruitful method for LLA formulations. Furthermore, the interaction of gliadin proline with skin keratin associated with the controlled release of LLA may avoid some drawbacks of this drug.
- BZC is a quaternary ammonium used as an antiseptic and bactericide, spermicide [82], and virucide [83]. However, BZC can promote some allergies followed by mucous lesions. It is assumed that encapsulation into gliadin nanoparticles could minimize or avoid lesions promoted by this irritant quaternary ammonium and could improve the dosage form by delaying drug release.

Drug entrapment and efficiency were tested after encapsulation. The results showed that the amount of entrapped VE and LLA is higher than that of the cationic BZC, confirming a strong interaction between gliadins and apolar compounds, due to the apolarity of the proteins. When comparing drug entrapment, results show that the optimal VE concentration is obtained for $972.0 \text{ VE } \mu\text{g (mg gliadin)}^{-1}$, with an efficiency of 79.2%, the optimal LLA concentration corresponds to $980.0 \text{ LLA } \mu\text{g (mg gliadin)}^{-1}$, with an efficiency of 82.4%, and the optimal BZC concentration corresponds to $550.3 \text{ BZC } \mu\text{g (mg gliadin)}^{-1}$, with an efficiency of 52.3% (Table 5.1).

For drug release quantification, only VE and BZC were studied. The reason being that LLA should be studied under a controlled atmosphere and not in a liquid medium. Such differences between media used did not allow an easy comparison to other drugs. For VE and BZC, drug releases were, respectively, 13 and 11% after

Tab. 5.1. Drug encapsulation characteristics in gliadin nanoparticles.

Drug	Polarity (dielectric constant)	Payload (%)	Encapsulation efficacy (%)
VE	Apolar (4)	97.2	79.2
LLA	slightly polar (8)	82.4	98.0
BZC	polar (amphiphilic cationic) (45)	66.0	52.3

1 h, and 30.6 and 11.7% after 30 h. The phenomenon observed can be interpreted as a burst effect completed by a drug diffusion process through a homogeneous sphere. Both release diffusion parts of the profiles have been modeled with a diffusion process in a homogenous sphere. However, the diffusion coefficients are different according to VE or BZC, i.e. 1.12×10^{-20} and $6.36 \times 10^{-21} \text{ m}^2 \text{ s}^{-1}$, respectively. This could be related to the different affinity of the gliadin for the two drugs. In organic phases, diffusion coefficients are usually about $10^{-9} \text{ m}^2 \text{ s}^{-1}$. Here, the coefficients are clearly much lower, which confirm that the drug is retained by the nanoparticle matrix.

In conclusion, it can be observed that whatever the polar drug character, this gliadin nanoparticulate system is able to entrap the drug with an acceptable payload and encapsulation efficiency [79].

5.5

Preparation of Ligand–Gliadin Nanoparticle Conjugates

In general, proteins produce biodegradable particles whose physicochemical properties can be modulated by the crosslinking process employed for their stabilization. Furthermore, due to the presence of numerous functional groups (i.e. amino and carboxylic residues), proteins are excellent candidates for the preparation of conjugates, formed by the attachment of molecules capable of providing specificity to the surface of nanoparticles. In this context, different ligands have been proposed, including antibodies [84, 85], lectins [86, 87], carbohydrates [88] and other biological ligands, in order to recognize or bind particular molecules [89, 90].

However, the association of ligands with nanoparticles can be achieved by different procedures, including covalent linkage and adsorption processes [91]. Ideally, the ligand should be conjugated to particles through a covalent linkage, which is more stable than adsorption procedures, without affecting its specificity. Noncovalent attachment relies on a fortuitous process. Further, it is difficult to control the amount of ligand which is associated and this process is useful only for those proteins that will associate nonspecifically [92]. Different techniques for covalent attachment may be envisaged, depending on the principal functional groups located on the carrier surface. The most widely used methods of ligand coupling are the use of cyanogen bromide [84, 93] and periodate [94, 95] for hydroxyl

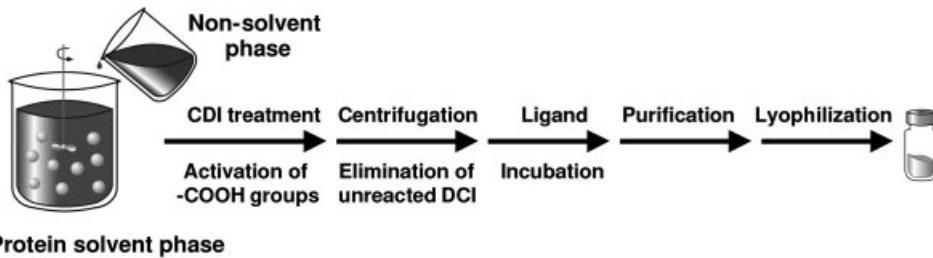


Fig. 5.4. Route for the preparation of ligand–gliadin nanoparticle conjugates by desolvation of gliadin followed by CDI activation and further incubation with the ligand.

groups, glutaraldehyde [96, 97] and ethylene glycol diglycidyl ether [98] for amino groups, and carbodiimide (CDI) for carboxylic groups [99, 100].

This last technique is the one preferred in order to obtain conjugates between a ligand and protein nanoparticles [87, 101–103]. CDI involves the activation of carboxylic acid groups to give NH-activated carboxylic acid groups which can react with free amino groups of the ligand polypeptide chains [104]. In proteins, these carboxylic groups can be found on aspartic and glutamic acid residues. For vicilin, these amino acids represent about 19 groups per 1000 amino acid residues [101]. For gliadin, these amino acids only represent 21 and 71 groups per 1000 amino acid residues, respectively [45, 105]. In spite of gliadin having a very low proportion of these two amino acids, it appears that the coupling reaction is efficient enough to provide acceptable lectin binding.

Figure 5.4 summarizes the preparation of lectin–nanoparticle conjugates. In brief, the first step of the manufacturing protocol involves the activation of the carboxylic groups on the gliadin nanoparticles by addition of a CDI derivative [i.e. 1-(3-dimethylaminopropyl)-3-ethyl-carbodiimide hydrochloride]. After incubation, the suspension of “activated” nanoparticles has to be centrifuged in order to remove the unreacted reagent. Then, the nanoparticles are dispersed in an aqueous medium and incubated with the desired ligand for the coupling reaction by overnight incubation at room temperature [101, 102]. Finally, the resulting conjugates are purified and lyophilized using glucose as a cryoprotector [103].

Different parameters can influence the yield of the process. In spite of the fact that the CDI reaction can effectively occur up to at least pH 7.5 without any significant loss of yield, it has been reported that the optimal pH ranges between 4.7 and 6 [106]. This fact was also observed by Arango et al. who showed evidence of superior binding of a *Dolichus biflorus* lectin (DBA) to the surface of gliadin nanoparticles with 2-(*N*-morpholino)ethanesulfonic acid (MES) buffer (1 mM, pH 5.5) rather than with PBS (1 mM, pH 7.4) [103]. This may be explained as being due to the proton of the carboxylic group facilitating the rupture of one double link of the CDI molecule [107], forming the *O*-acylisourea intermediate. This active residue is then able to react directly with primary amines forming amide bonds and

releasing the CDI derivative. Moreover, at neutral pH, the overall charge of both the nanoparticles and the ligand would be negative. Therefore, ligand approaches to a nanoparticle surface and subsequent binding would not be favored by the phenomenon of charge repulsion [108].

Another critical factor affecting ligand binding to the surface of protein nanoparticles is the reaction time between the CDI and the gliadin. Therefore, an increase in the reaction time induced a dramatic decrease in the amount of the ligand binding to the nanoparticle surface. This could be due to the degradation of the reactive *O*-acylisourea complex. In fact, this complex is rapidly hydrolyzed in aqueous solution, having a constant rate measured in seconds [109]. If the target amine does not interact with the *O*-acylisourea intermediate before its hydrolysis, the desired binding cannot occur. This is especially problematic when the target molecule is in low concentration [106], as usually occurs in the binding of active ligands to the surface of nanoparticles. Another possible explanation for the DBA binding decrease could be the formation of the stable *N*-acylurea derivative [110].

However, the amount of CDI used to activate functional groups on the surface of nanoparticles is also important. A low amount of CDI may require longer reaction periods. However, the use of high amounts of CDI may induce irreversible aggregation of nanoparticles. This may be explained by the presence of both carboxylic and amine groups on the surface of the nanoparticles. Therefore, at high CDI concentrations, self-polymerization may take place [106]. In any case, in order to obtain a good binding efficiency, it is necessary to find a balance between the reaction time and the amount of CDI used to activate the nanoparticles.

Finally, another important factor concerns the amount of ligand used in the incubation with the activated nanoparticles. For gliadin nanoparticles, a maximum of ligand binding occurs when the amount of ligand incubated with activated nanoparticles is about $50 \mu\text{g} (\text{mg gliadin})^{-1}$ nanoparticles [103].

5.6

Bioadhesive Properties of Gliadin Nanoparticles

Bioadhesion is classically defined as the ability of a material to adhere to a biological substrate with the objective of improving the therapeutic efficiency of drugs by increasing the residence time at the site of activity or absorption [111, 112]. It is interesting to note that a number of drugs remain poorly available when administered by the oral route. Among other reasons, this fact can be related either to a low mucosal permeability for the drug or to its low solubility in the mucosal fluids. In both cases, an important fraction of the given dose is eliminated from the alimentary canal prior to being absorbed. The use of bioadhesive nanoparticles can be an adequate strategy to improve drug bioavailability. In fact, these carriers may enhance the drug absorption rate by reducing the diffusion barrier between the dosage form and the site of action or absorption. Similarly, they may prolong the residence time of the drug in the gut and, therefore, increase the time during which absorption can occur.

For bioadhesion studies, gliadin nanoparticles were labeled with carbazole, which is a hydrophobic fluorescent molecule.

5.6.1

Ex Vivo Studies with Gastrointestinal Mucosal Segments

In order to evaluate the bioadhesive capacity of these carriers, nanoparticles were incubated with fresh portions of rat gastrointestinal mucosa using a plate of aluminum with a slit in the center [113]. The mucosa in the slit of the plate was covered with 1 mL of suspensions (containing 4 mg mL^{-1} nanoparticles) and the incubation time was fixed for 30 min. After incubation, the suspensions were sucked off and the samples were rinsed with 5 mL 0.9% NaCl solution to eliminate the non-attached particles. Then, the mucus layer including the adsorbed particles was drawn from the membrane and digested with NaOH for 24 h. After total dissolution of mucus, carbazole extraction was performed with 1.5 mL methanol, vortexed for 1 min and centrifuged at $20\,000 \text{ g}$ for 10 min. Finally, the amounts of adhered nanoparticles or conjugates were estimated by fluorometry [103].

Gliadin nanoparticles were able to develop rapid interaction with the gut mucosa. In fact, the adsorption equilibrium for nanoparticles and conjugates was reached in less than 30 min [103]. Similarly, under the experimental conditions used [4 mg (particles or conjugates) mL^{-1}], no saturation was observed on the apparent surface of mucosa delimited by the device.

Figure 5.5 shows the interactions of gliadin nanoparticles with intestinal mucosa samples. Comparing the different anatomical regions, gliadin nanoparticles

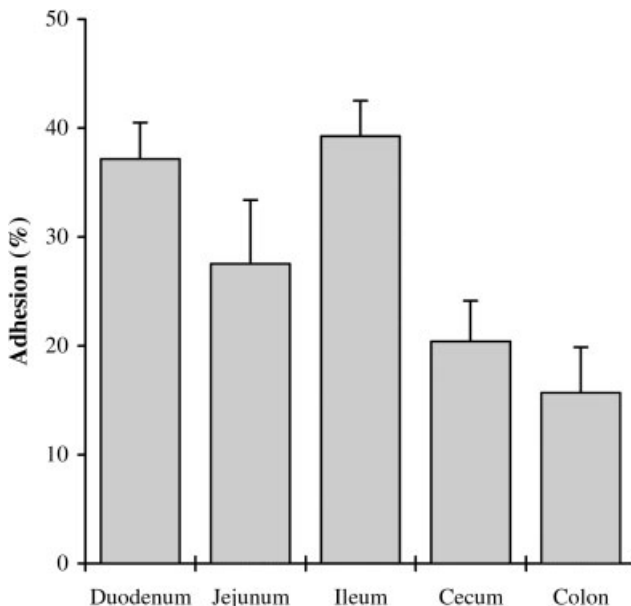


Fig. 5.5. Adhesive interactions of gliadin nanoparticles in isolated intestinal segments ($n = 4$).

showed a high affinity for the small intestine segments. However, no significant differences in the extent of interaction were found between the duodenum, jejunum and ileum ($P < 0.05$). Therefore, for ileum or duodenum portions, the amount of nanoparticles interacting with the mucosa was calculated to be close to 8 g m^{-2} , which represents about 40% of the nanoparticles placed in contact with the gastrointestinal tract. In this context, the interaction of poly(styrene) nanoparticles with intestinal segments (under similar experimental conditions) was size dependent and the largest amount of latex able to interact with the mucosa was about 1 g m^{-2} [113, 114]. Similarly, gliadin nanoparticles interacted about 8-fold more with the intestinal mucosa than poly(isobutyl cyanoacrylate) nanoparticles [115]. For large intestine portions, the interaction of gliadin nanoparticles strongly decreased. This may be explained by a reduction of both the mucosa surface and the mucin concentration along the gastrointestinal tract. According to these results, it appears that gliadin nanoparticles would be useful for improving the bioavailability of drugs. These powerfully adhesive carriers may prolong the residence time and enhance drug absorption, thus reducing the diffusion pathway.

However, DBA–gliadin nanoparticle conjugates displayed a different ability to develop adhesive interactions with the gut mucosa. In the small intestine, these conjugates showed an adhesive interaction similar to the controls ($P < 0.05$) and, for all segments, this interaction was close to 10% of the initial concentration placed in contact with the mucosa. However, in the large intestine a significant increase of about 100% was found for DBA conjugates. This fact can be explained by the reported capability of DBA to strongly react with the colonic epithelial surface [116, 117] due to the presence of *N*-acetyl-D-galactosamine (specific sugar for DBA) residues, which provide the substrate for their site-specific interaction.

Finally, concerning the interaction of gliadin nanoparticles with Peyer's patches, it was found that gliadin nanoparticles showed 3.5 times more capacity of interaction with these lymphoid tissues than DBA conjugates [103].

All of these results confirmed that gliadin nanoparticles displayed a high interactive potential with biological surfaces. However, the possible interaction between the biological substrate and these nanoparticles is of a nonspecific nature. This fact means that these colloidal systems interact in the same way with a number of components of the biological substrate, without showing target properties for a particular region or cell structure [118].

5.6.2

***In Vivo* Studies with Laboratory Animals**

In order to evaluate the *in vivo* bioadhesive capacity of gliadin nanoparticles and their influence on the pharmacokinetics of the loaded drug, animals were gavaged with a single dose of nanoparticle formulations dispersed in 0.5 mL water. For the bioadhesion study, the gastrointestinal tract of animals was cut in different portions, rinsed with saline and digested with sodium hydroxide. The fluorescent marker was extracted with methanol and determined by spectrofluorimetry. The amount of carbazole, determined in the mucosa segments, was used for the

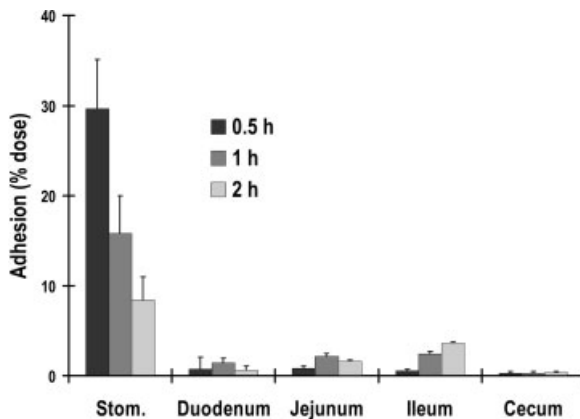


Fig. 5.6. Gastrointestinal transit profile of gliadin nanoparticles. Single administration of a single oral dose of 30 mg. Data expressed as the mean \pm SD ($n = 4$). (Adapted from Ref. [102]).

estimation of the interacted nanoparticulate fractions. For the pharmacokinetics studies, blood samples were taken from the ophthalmic venous plexus, centrifuged and assayed for carbazole content by an HPLC method with fluorescent detection [57]. *In vivo* studies demonstrated that gliadin nanoparticles displayed a high adhesive potential with a clear tropism for the stomach mucosa (Fig. 5.6). Thus, thirty minutes post-administration, about 30% of the initial dose remained adhered within the gut. However, around 90% of the adhered nanoparticles were localized in the stomach. Similarly, 1 h after administration, only 18% of the initial dose could be found in the stomach and their presence in other intestinal regions was also negligible. Finally, at 2 h post-administration, only about 8% of the given dose was found adhered to the mucosa [119]. This profile of bioadhesion (tropism for the stomach mucosa and rapid decline of the adhered fraction over the time) was not significantly affected when nanoparticles were coated with DBA [103].

Nevertheless, in order to study the influence of the degree of crosslinking on the bioadhesive profile of nanoparticles and carbazole absorption, two different formulations were prepared. The first one resulted from the crosslinking of gliadin nanoparticles with glutaraldehyde with 2 h prior purification (CL-NP). The second one (DCL-NP) was obtained after treatment of gliadin nanoparticles with a CDI derivative for 1 h and subsequent treatment with glutaraldehyde for 2 h [57] (Tab. 5.2).

Within the stomach, the bioadhesive profile of gliadin nanoparticles was found to be influenced by the crosslinkage. Thus, noncrosslinked nanoparticles displayed a higher initial ability to develop adhesive interactions than crosslinked nanoparticles. However, the elimination rate of the adhered fraction was higher for noncrosslinked than for stabilized nanoparticles [57, 119]. On the contrary, the crosslinking process allowed a similar amount of carriers adhered to the mucosa to be

Tab. 5.2. Physicochemical characteristics of the different formulations based on gliadin nanoparticles ($n = 6$).

	Size (nm)	ζ potential (mV)	Fixed ligand ($\mu\text{g mg}^{-1}$)	Loaded carbazol ($\mu\text{g mg}^{-1}$)
NP	460 \pm 19	27.5 \pm 0.8	–	12.6 \pm 1.2
CL-NP	453 \pm 24	24.5 \pm 0.5	–	12.2 \pm 0.8
DCL-NP	478 \pm 31	21.2 \pm 1.3	–	12.1 \pm 1.6
BSA-NP	514 \pm 18	34.7 \pm 1.7	20.8 \pm 1.7	12.5 \pm 0.6
DBA-NP	521 \pm 13	32.4 \pm 0.9	23.5 \pm 2.6	12.6 \pm 0.9

CL-NP: nanoparticles crosslinked with glutaraldehyde; DCL-NP: nanoparticles crosslinked with CDI and glutaraldehyde; BSA-NP: bovine serum albumin–gliadin nanoparticle conjugates (control); DBA-NP: *D. biflorus* lectin–gliadin nanoparticle conjugates.

maintained for at least 1 h, which was calculated to be around 15% of the given dose (Fig. 5.7).

Another interesting point is that, within the stomach, the adhered nanoparticles appear to accumulate in the nonglandular region [119]. In this last region, cross-linked nanoparticles have a 1.5 times higher adhesive intensity than nonhardened nanoparticles. Similarly, the mean residence time of the adhered fraction to the stomach mucosa was about 95 min higher for crosslinked than for conventional gliadin nanoparticles [119].

This high adhesive capacity of gliadin nanoparticles may be explained by the protein composition with a high content of neutral and lipophilic residues. Neutral amino acids may promote hydrogen-bonding interactions with the mucosa, while

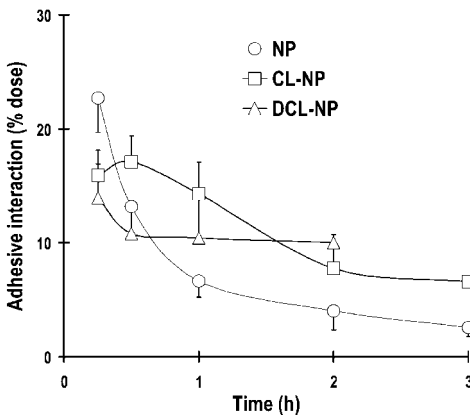


Fig. 5.7. Evolution of nonhardened gliadin nanoparticles (NP), nanoparticles crosslinked with glutaraldehyde (CL-NP), and nanoparticles crosslinked with CDI and glutaraldehyde (DCL-NP) in the stomach mucosa, as a function of

time, after single oral administration 20 mg particles ($1.14 \text{ mg carbazole kg}^{-1}$). The results are expressed as the percentage of the given dose ($n = 6$).

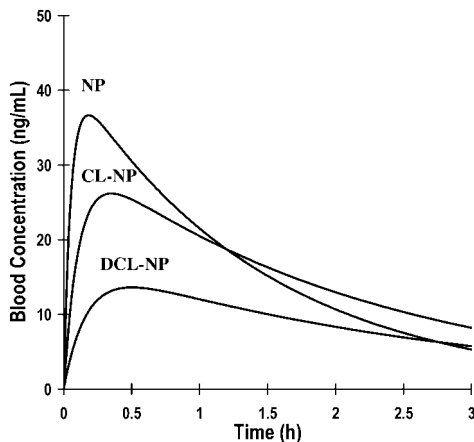


Fig. 5.8. Carbazole plasma levels after the oral administration of a single dose of $1.14 \text{ mg carbazole kg}^{-1}$ loaded in NP, CL-NP or DCL-NP ($n = 12$).

the lipophilic components may develop hydrophobic interactions with the biological support [115, 118, 120]. On the other hand, a more energetic crosslinking process reduces the ability of nanoparticles to develop adhesive interactions within the mucosa; however, this process would decrease the degradation rate of gliadin nanoparticle and, thus, provide a prolonged residence in the mucosa. For crosslinkage with glutaraldehyde, the adhered fraction of nanoparticles is constant for at least 1 h, whereas for nanoparticles crosslinked with CDI and glutaraldehyde, the adhered fraction (around 10% given dose) remained constant for at least 2 h.

Concerning the pharmacokinetic study, Fig. 5.8 shows the carbazole plasma concentration provided by nonhardened and crosslinked nanoparticles when administered by the oral route. It is interesting to note that when carbazole was formulated as an aqueous suspension it was not possible to determine the T_{\max} , C_{\max} and the elimination rate. Similarly, the area under of curve (AUC) was around zero since their absorption was negligible. This fact is typical for hydrophobic drugs with very poor aqueous solubility [121–124].

However, when formulated in nonhardened nanoparticles, the bioavailability of carbazole was calculated to be about 40% of the dose. For crosslinked nanoparticles, the bioavailability was close to the 50%. Moreover, the crosslinkage enables us to increase the T_{\max} , and to decrease the C_{\max} and the elimination rate. Similarly, the mean residence time was significantly increased in comparison with nonhardened nanoparticles and an aqueous solution of carbazole [57].

These pharmacokinetic results can be explained by the ability of gliadin nanoparticles to develop bioadhesive interactions within the stomach mucosa. Once gliadin nanoparticles are adhered to the mucosa, they would release the loaded molecules to the absorbing cell layer, minimizing losses to the luminal environment and increasing the local drug concentration. In this context, the active molecule (carbazole in this study) would be able to show a first-order absorption process. However,

the digestion of nanoparticles either in luminal fluids or adhered in the mucus may provide an instantaneous release component which may be related to a first-order absorption. In fact, the interactions developed by gliadin nanoparticles within the stomach mucosa are the key phenomena influencing carbazole absorption. This hypothesis was confirmed by a deconvolution model [57].

5.7

Future Perspectives

For pharmaceutical dosage forms it is well known that, whatever the administration mode, the principal objectives to be reached are the enhancement of the efficiency associated with a reduced toxicity and controlled drug release. Furthermore, if administered by a parenteral route, it is hoped that a major amount of the drug reaches the target site avoiding undesirable side-effects, i.e. a modification of drug distribution is required [125, 126].

Colloidal carriers in the form of nanoparticles have this potential to deliver drugs to specific target sites and to achieve sustained drug release. The bioacceptability of such nanoparticulate systems is strongly size dependent and, for intravessel administration, the diameter must be smaller than that of the smallest blood capillary. Consequently, size optimization is a very important parameter.

Furthermore, for medical applications, it is of interest to test their potential for parenteral administration, and particularly the humoral and cellular responses of protein particles after injection in animals. The first reports have been published describing these responses for native legumin and legumin nanoparticles after intradermal injection in rats [127]

5.7.1

Size Optimization

Bearing in mind this important condition, all the parameters involved in the preparation of gliadin nanoparticles have been optimized (some results have been published [55]; other are in progress). The studied parameters were:

- Choice of the protein solvent
- Protein concentration
- Temperature during the experimental procedure
- Solvent/nonsolvent ratio
- Shear rate imposed during mixing
- Nanoparticle size evolution with time

Concerning the choice of the protein solvent, it was demonstrated that the closer the solubility parameter of the protein is to that of the solvent, the smaller the particle size (and correspondingly higher the amount of protein solubilized), under the experimental conditions chosen.

Other important experimental conditions were the solvent/nonsolvent ratio, the

temperature and the shear rate during the procedure. The data available showed that the best ratio must be less than unity and that an elevated temperature (compatible with protein thermolability, about 35 °C) decreases the particle size. Moreover, an optimum shear rate was observed for each protein concentration in the medium.

Concerning the size evolution of the nanoparticles with time, the first results showed that this parameter is a determinant for high protein concentrations. For instance, for a supersaturated solution of protein, the size increases 10 times in 100 min, ranging from 70 nm after 1 min to about 700 nm after 100 min. This is in favor of a spontaneous nucleation which occurs as soon as the non-solvent is added to the medium. In order to obtain a large range of nanoparticle sizes, it now remains to resolve the stabilization of the particles whatever their size.

In all of these abovementioned works the particle sizes of nanoparticles were greater than 100 nm. There are currently limitations on achieving nanoparticles with a size less than 100 nm and new developments are anticipated in the future.

5.7.2

Immunization in Animals

Preliminary experiments were performed on legumine nanoparticles in order to evaluate the capacities of biodegradable plant protein nanoparticles as drug delivery systems. More particularly, as it is possible to think that these nanoparticulate carriers could be considered as safe for oral or topical administrations, it was of interest to test their potential after injection [127]. In this context, humoral and cell-mediated responses were analyzed in rats. They were immunized with an intradermal injection of legumin or legumin nanoparticles of about 250 nm. Legumin and legumin nanoparticles were suspended in a sterile saline solution mixed with complete Freund's adjuvant (CFA). A control group of rats was inoculated only with saline solution and CFA.

Humoral responses. These responses against legumin and legumin nanoparticles were examined by usually appropriate techniques, i.e. Western blot and ELISA [127]. Both techniques showed that sera from rats immunized with legumin strongly expressed antibodies against this protein. On the contrary, serum samples from rats inoculated with legumin nanoparticles did not contain detectable amount of antibodies. Hence, legumin appears to be a potent inductor of the humoral immune response, while the use of legumin nanoparticles seems able to avoid the production of antibodies against them. However, the mechanism implicated in the absence of any humoral response to the legumin nanoparticles is far from clear. Mirshahi et al. [127] suggested some explanations: the chemical cross-linkage with glutaraldehyde [52] may produce some irreversible conformational changes in the protein tertiary structure making it less antigenic than the native protein [128], glutaraldehyde release could modify the surrounding cells and thus the lymphocyte response to antigens [129] or legumin nanoparticles were not sufficiently degraded to allow antigen formation during the period over which

experiment was carried out (1 month). Work is in progress to better understand this behavior.

Cell-mediated response. This was evaluated by *in vitro* lymphocyte proliferation assay 10 and 30 days after intradermal injection. Neither legumin nor legumin nanoparticles stimulated an immunogenic response [127]. This absence of response may be explained by a cytostatic effect of legumin. In a previous work (unpublished observations) it was noticed that legumin and legumin nanoparticles have a suppressive effect on *in vitro* fibroblast proliferation. These observations have to be confirmed.

Taking into consideration this cytostatic effect of legumin nanoparticles, it should be interesting to use them as pharmaceutical devices for the delivery of antitumor drugs in local cancer treatment.

Similar experimental work has to be carried out with the other plant proteins, gliadin and vicilin, in order to explore their medical and pharmaceutical potential as drug delivery systems.

From these *in vivo* and *in vitro* results, it can be assumed that plant proteins possess a role exceeding that of inert excipients. They have an influence on the entrapment efficiency of the drug and compatibility with tissues (essentially gliadin). In the future, it will be of interest to test these natural materials as encapsulating agents for the protection of sensitive drug from degradation (peptides, insulin, genes, etc.) and their ability to control drug release.

5.8

Conclusion

The method used to prepare all plant proteins nanoparticles was a controlled desolvation method using only bioacceptable solvents. This procedure, avoiding toxic solvents, allowed the preparation of submicronic nanoparticulate systems with a narrow size distribution, and quite good yields and entrapment efficiency, making them susceptible to scale-up and industrial use. For gliadin, either hydrophilic or lipophilic drugs could be entrapped satisfactorily. Furthermore, gliadin nanoparticles possess a high interactive potential with biological surfaces, as demonstrated by *ex vivo* and *in vivo* animal experimentations. It appears that gliadin nanoparticles are interesting oral carriers to improve bioavailability of drugs. Nevertheless, in the future, efforts should be made to obtain a complete understanding of all the mechanisms implicated in the metabolism of these colloidal systems at the biomolecular level, in order to use them for medical applications.

References

- 1 F. PUISIEUX, G. BARRATT, G. COURRAZE, P. COUVREUR, J. P. DEVISSAGUET, C. P. DUBERNET, E. FATTAL, H. FESSI, C. VAUTHIER, S. BENITA, Polymeric micro and nanoparticles as drug carriers. In

- Polymeric Biomaterials*, S. DIMITRIU (Ed.), Marcel Dekker, New York, 1994, pp. 747–795.
- 2 M. J. ALONSO, Nanoparticulate drug carrier technology. *Drug Pharm. Sci.* 1996, 77, 203–242.
 - 3 C. DUCLAIROIR, A. M. ORECCHIONI, P. DEPRAETERE, E. NAKACHE, Alpha-tocopherol encapsulation and *in-vitro* release from wheat gliadin nanoparticles. *J. Microencapsul.* 2002, 19, 53–60.
 - 4 S. GOIN, Microencapsulation: industrial appraisal of industrial technologies and trends. *Trends Food Sci. Technol.* 2004, 15, 330–347.
 - 5 E. NAKACHE, N. POULAIN, F. CANDAU, A. M. ORECCHIONI, J. M. IRACHE, Biopolymer and polymer nanoparticles and their biomedical applications. In *Handbook of Nanostructured Materials and Nanotechnology*, H. S. NALWA (Ed.), Vol. 5: *Organics, Polymers and Biological Materials*, Academic Press, New York, 2000, pp. 577–638.
 - 6 P. A. KRAMER, Albumin microspheres as vehicles for achieving specificity in drug delivery. *J. Pharm. Sci.* 1974, 63, 1646–1647.
 - 7 W. LIN, A. G. A. COOMBES, M. C. DAVIES, S. S. DAVIS, L. ILLUM, Preparation of sub 100 nm human serum albumin nanospheres using a pH-coacervation method. *J. Drug Target.* 1993, 1, 237–243.
 - 8 I. EZPELETA, J. M. IRACHE, S. STAINMESSE, C. CHABENAT, J. GUEGUEN, Y. POPINEAU, A. M. ORECCHIONI, Gliadin nanoparticles for the controlled release of all *trans*-retinoic acid. *Int. J. Pharm.* 1996, 131, 191–200.
 - 9 J. LAZKO, Y. POPINEAU, J. LEGRAND, Soy glycinin microcapsules by simple coacervation method. *Colloids Surfaces B.* 2004, 37, 1–8.
 - 10 X. LIU, Q. SUN, H. WANG, L. ZHANG, J. Y. WANG, Microspheres of corn protein, Zein, for an ivermectin drug delivery. *Biomaterials* 2005, 26, 109–115.
 - 11 M. N. MIÈGE, Protein tips and distribution. In *Encyclopedia of Plant Physiology*, D. BOULTER and B. PARTHIER (Eds.), Springer, Berlin, 1982, pp. 291–345.
 - 12 C. DOMONEY, R. CASEY, Measurement of gene number for seed storage proteins in *Pisum*. *Nucleic Acids Res.* 1985, 13, 687–699.
 - 13 M. A. CHOWDHURY, A. E. SLINKARD, Genetic diversity in grass pea (*Lathyrus sativus* L.). *Genet. Resources Crop Evol.* 2000, 47, 163–169.
 - 14 K. S. G. WONG, J. WANG, L. TAO, J. TAN, J. G. ZHANG, D. A. PASSEY, J. YU, compositional gradients in Gramineae genes. *Genome Res.* 2002, 12, 851–856.
 - 15 G. H. MCINTOSH, D. L. TOPPING, Food legumes in human nutrition. In *Proceedings of the Third International Food Legumes Research Conference*, Adelaide, Australia, R. KNIGHT (Ed.), 2000, pp. 655–660.
 - 16 D. W. GRIFFITHS, D. A. LAWES, Variation in the crude protein content of field beans (*Vicia faba* L.) in relation to the possible improvement of the protein content of the crop. *Euphytica* 1978, 27, 487–495.
 - 17 H. LEVANONY, R. RUBIN, Y. ALTSCHULER, G. GALILI, Evidence for a novel route of wheat storage proteins to vacuoles. *J. Cell Biol.* 1992, 119, 1117–1128.
 - 18 I. HOHL, D. G. ROBINSON, M. J. CRISPEELS, G. HINZ, Transport of storage proteins to the vacuole is mediated by vesicles without a clathrin coat. *J. Cell Sci.* 1996, 109, 2539–2550.
 - 19 M. I. GELI, M. TORRENT, D. LUDEVID, Two structural domains mediate two sequential events in γ -zein targeting: protein endoplasmic reticulum retention and protein body formation. *Plant Cell* 1994, 6, 1911–1922.
 - 20 B. G. FORDE, A. HEYWORTH, J. PYWELL, M. KREIS, Nucleotide sequence of a B1 hordein gene and the identification of possible upstream regulatory elements in endosperm storage protein genes from barley, wheat and maize. *Nucleic Acids Res.* 1985, 13, 7327–7339.
 - 21 N. ROSENBERG, Y. SHIMONI, Y. ALTSCHULER, H. LEVANONY, M. VOLOKITA, and G. GALILI, Wheat (*Triticum aestivum* L.) γ -gliadin

- accumulates in dense protein bodies within the endoplasmic reticulum of yeast. *Plant Physiol.* **1993**, *102*, 61–69.
- 22 K. MÜNTZ, Globulins from legume seeds: structure and function during storage and reactivation. In *Plant Proteins from European Crops*, J. GUEGUEN, Y. POPINEAU (Eds.), Springer, Berlin, **1998**, pp. 3–12.
 - 23 T. B. OSBORNE, *The Vegetable Proteins*, 2nd edn., Longmans Green, New York, **1924**.
 - 24 P. ARGOS, S. V. L. NARAYANA, N. C. NIELSEN, Structural similarity between legumin and vicilin storage proteins from legumes. *EMBO J.* **1985**, *4*, 1111–1118.
 - 25 P. E. M. GIBBS, K. B. STRONGIN, A. MCPHERSON, Evolution of legume seed storage protein: a domain common to legumins and vicilins is duplicated in vicilins. *Mol. Biol. Evol.* **1989**, *6*, 614–623.
 - 26 I. A. POPELLO, V. V. SUCHKOV, V. Y. GRINBERG, V. B. TOLTOGUZOV, Liquid/liquid phase equilibrium in globulin/salt/water systems: legumin. *J. Sci. Food Agric.* **1990**, *51*, 345–353.
 - 27 K. D. SCHWENKE, D. ZIRWER, K. GAST, E. GÖRNITZ, K. J. LINOW, J. GUEGUEN, Changes of the oligomeric structure of legumin from pea (*Pisum sativum* L.) after succinylation. *Eur. J. Biochem.* **1990**, *194*, 621–627.
 - 28 J. A. GATEHOUSE, G. W. LYCETT, A. J. DELAUNY, R. R. R. CROY, D. BOULTER, Sequence specificity of the post-translational proteolytic cleavage of vicilin, a seed storage protein of pea (*Pisum sativum* L.). *Biochem. J.* **1983**, *212*, 427–432.
 - 29 E. DERBYSHIRE, D. J. WRIGHT, D. BOULTER, Legumin and vicilin, storage proteins of legume seeds. *Phytochemistry* **1976**, *13*, 3–24.
 - 30 J. GUEGUEN, A. T. VU, F. SCHAEFFER, Large scale purification and characterization of pea globulins. *J. Sci. Food Agric.* **1984**, *35*, 1024–1033.
 - 31 D. CAER, B. COLAS, Protease susceptibility and amino group accessibility to trinitrobenzenesulfonic acid of legumin during its glycosylation. *J. Agric. Food Chem.* **1993**, *41*, 544–546.
 - 32 M. C. LAWRENCE, T. IZARD, M. BEUCHAT, R. J. BLAGROVE, P. M. COLEMAN, Structure of phaseolin at 2.2 Å resolution. Implications for a common vicilin/legumin structure and the genetic engineering of seed storage proteins. *J. Mol. Evol.* **1994**, *238*, 748–776.
 - 33 S. GUILBERT, N. GONTARD, Edible and biodegradable food packaging, in *Foods and Packaging Materials – Chemical Interactions*, P. ACKERMANN, M. JÄGERSTAD, T. OHLSSON (Eds.), Royal Society of Chemistry, Cambridge, **1995**, pp. 159–168.
 - 34 J. HARGREAVES, Y. POPINEAU, M. LE MESTE, M. HEMMINGGA, Molecular flexibility in wheat gluten proteins submitted to heating. *FEBS Lett.* **1995**, *373*, 103–107.
 - 35 A. APICHTSRANGKON, A. E. BELL, D. A. LEDWARD, J. D. SCOFIELD, Dynamic viscoelastic behavior of high-pressure-treated wheat gluten. *Cereal Chem.* **1999**, *76*, 777–782.
 - 36 J. LEFEBVRE, Y. POPINEAU, G. DESHAYES, L. LAVENANT, Temperature-induced changes in the dynamic rheological behavior and size distribution of polymeric proteins for gluteins from wheat near-isogenic lines differing in HMW-glutenin subunit composition. *Cereal Chem.* **2000**, *77*, 193–201.
 - 37 J. A. BIETZ, J. A. ROTHFUS, Comparison of peptides from wheat gliadin and glutenin. *Cereal Chem.* **1970**, *47*, 381–392.
 - 38 P. R. SHEWRY, Cereal seed storage proteins. In *Seed Development and Germination*, J. KIGEL, G. GALLI (Eds.), NY Bale, Hong Kong, **1995**, pp. 45–72.
 - 39 D. D. KASARDA, Structure and properties of α -gliadins. *Ann. Technol. Agric.* **1980**, *29*, 151–173.
 - 40 J. H. WOYCHIK, R. A. BOUNDY, R. A. DIMLER, Starch gel electrophoresis of wheat gluten proteins with concentrated urea. *Arch. Biochem. Biophys.* **1961**, *84*, 477–482.
 - 41 M. BYERS, J. MIFFLIN, S. J. SMITH, A quantitative comparison of the extraction of protein fractions from

- wheat grain by different solvents, and of the polypeptide and amino acid composition of the alcohol-soluble proteins. *J. Sci. Food Agric.* **1983**, *34*, 447–462.
- 42 D. L. DU CROS, C. W. WRIGLEY, Improved electrophoretic methods for identifying cereal varieties. *J. Sci. Food Agric.* **1979**, *30*, 785–794.
- 43 C. LARRÉ, Y. POPINEAU, W. LOISEL, Fractionation of gliadins from common wheat by cation exchange FPLC. *J. Cereal Chem.* **1991**, *14*, 231–241.
- 44 H. WIESER, W. SEILMER, H. D. BELITZ, Quantitative determination of gliadin subgroups from different wheat cultivars. *J. Cereal Sci.* **1994**, *19*, 149–155.
- 45 H. HE, R. R. ROACH, R. C. HOSENEY, Effect of nonchaotropic salts on flour bread-making properties. *Cereal Chem.* **1992**, *69*, 366–371.
- 46 Y. POPINEAU, S. DENERY-PAPINI, *Protéines Végétales*, Lavoisier, Paris, **1996**.
- 47 R. BODMEIER, H. CHEN, E. PAERATAKUL, A novel approach to the oral delivery of micro- or nanoparticles. *Pharm. Res.* **1989**, *6*, 413–417.
- 48 M. S. EL-SAMALIGY, P. ROHDEWALD, Reconstituted collagen nanoparticles, a novel drug carrier delivery system. *J. Pharm. Pharmacol.* **1983**, *35*, 537–539.
- 49 D. J. BURGESS, O. N. SINGH, Spontaneous formation of small sized albumin/acacia coacervate particles. *J. Pharm. Pharmacol.* **1993**, *45*, 586–591.
- 50 I. EZPELETA, J. M. IRACHE, S. STAINMESSE, J. GUEGUEN, A. M. ORECCHIONI, Preparation of small-sized particles from vicilin (vegetal protein from *Pisum sativum* L.) by coacervation. *Eur. J. Pharm. Biopharm.* **1996**, *42*, 36–41.
- 51 J. M. IRACHE, L. BERGOUNOUX, I. EZPELETA, J. GUEGUEN, A. M. ORECCHIONI, Optimization and *in vitro* stability of legumin nanoparticles obtained by a coacervation method. *Int. J. Pharm.* **1995**, *126*, 103–109.
- 52 T. MIRSHAHI, J. M. IRACHE, J. GUEGUEN, A. M. ORECCHIONI, Development of drug delivery systems from vegetal proteins: legumin nanoparticles. *Drug Dev. Ind. Pharm.* **1996**, *22*, 841–846.
- 53 J. J. MARTY, R. C. OPPENHEIM, P. SPEISER, Nanoparticles: a new colloidal drug delivery system. *Pharm. Acta Helv.* **1978**, *53*, 17–23.
- 54 I. EZPELETA, J. M. IRACHE, J. GUEGUEN, A. M. ORECCHIONI, Properties of glutaraldehyde cross-linked vicilin nano- and micro-particles. *J. Microencapsul.* **1997**, *14*, 557–565.
- 55 C. DUCLAIROIR, E. NAKACHE, H. MARCHAIS, A. M. ORECCHIONI, Formation of gliadin nanoparticles: influence of the solubility parameter of the protein solvent. *Colloid Polym. Sci.* **1998**, *276*, 321–327.
- 56 M. A. ARANGO, M. A. CAMPANERO, Y. POPINEAU, J. M. IRACHE, Evaluation and characterization of gliadin nanoparticles and isolates by reversed-phase HPLC. *J. Cereal Sci.* **2000**, *31*, 223–228.
- 57 M. A. ARANGO, M. A. CAMPANERO, M. J. RENEDE, G. PONCHEL, J. M. IRACHE, Gliadin nanoparticles as carriers for the oral administration of lipophilic drugs. Relationship between bioadhesion and pharmacokinetics. *Pharm. Res.* **2001**, *18*, 1521–1527.
- 58 C. DUCLAIROIR, J. M. IRACHE, E. NAKACHE, A. M. ORECCHIONI, C. CHABENAT, Y. POPINEAU, Gliadin nanoparticles: formation, all-*trans*-retinoic acid entrapment and release, size optimization. *Polym. Int.* **1999**, *79*, 327–333.
- 59 J. HILDEBRAND, R. SCOTT, *Regular Solutions*, Prentice-Hall, Englewood Cliffs, NJ, **1962**.
- 60 A. F. M. BARTON, *Handbook of Solubility Parameters and Other Cohesion Parameters*, 2nd edn., CRC Press, Boca Raton, FL, **1991**.
- 61 J. T. ELDER, A. ASTROM, U. PETTERSON, A. TAVAKKOL, C. E. GRIFFITHS, A. KRUST, P. KASTNER, P. CHAMSON, J. J. VOORHES, Differential regulation of retinoic acid receptors and binding proteins in human skin. *J. Invest. Dermatol.* **1992**, *98*, 673–679.
- 62 A. H. LEWIN, M. E. BOS, F. C. ZUSI, X.

- NAIR, G. WHITING, P. BOURQUIN, G. TETRAULT, F. I. CAROL, Evaluation of retinoids as therapeutic agents in dermatology. *Pharm. Res.* **1994**, *11*, 192–200.
- 63 R. M. LAVKER, J. J. LEYDEN, E. G. THORNE, An ultrastructural study of the effects of topical tretinoin on microcomedones. *Clin. Ther.* **1992**, *14*, 773–780.
- 64 J. DRACH, G. LOPEZ-BERESTEIN, T. MCQUEEN, M. ANDREEFF, K. METHA, Induction of differentiation in myeloid leukemia cells lines and acute promyelocytic leukemia cells by liposomal all-*trans* retinoic acid. *Cancer Res.* **1993**, *53*, 2100–2104.
- 65 S. CASTAIGNE, C. CHOMIENNE, M. T. DANIEL, P. FENAUX, R. BERGER, L. DEGOS, All-*trans* retinoic acid as a differentiation therapy in acute promyelocytic leukemias. I. Clinical results. *Blood*, **1990**, *76*, 1704–1710.
- 66 K. SEITER, W. H. MILLER, E. J. FELDMAN, T. AHMED, Z. ARLIN, Pilot study of all-*trans* retinoic acid as post-remission therapy in patients with acute promyelocytic leukemia. *Leukemia*, **1995**, *9*, 15–18.
- 67 L. DELVA, M. CORNIC, N. BALITRAND, C. CHOMIENNE, Application thérapeutique de l'acide rétinoïque dans la leucémie aiguë promyélocytaire. *Immunoanal. Biol. Spec.* **1991**, *25*, 17–21.
- 68 T. TAKINO, K. KOISHI, Y. TAKAKURA, M. HASHIDA, Long circulating emulsion carrier systems for highly lipophilic drugs. *Biol. Pharm. Bull.* **1994**, *17*, 121–125.
- 69 K. METHA, T. SADEGHI, T. MCQUEEN, G. LOPEZ-BERESTEIN, Liposome encapsulation circumvents the hepatic clearance mechanisms of all-*trans* retinoic acid. *Leuk. Res.* **1994**, *18*, 587–596.
- 70 V. MASINI, F. BONTE, A. MEYBECK, J. WEPIERRE, Cutaneous bioavailability in hairless rats of tretinoin in liposomes or gel. *J. Pharm. Sci.* **1993**, *82*, 17–21.
- 71 B. IDSON, Dry skin moisturizing and emolliency. *Cosm. Toil.* **1992**, *107*, 69–78.
- 72 J. H. EPSTEIN, Photocarcinogenesis, skin cancer and aging. *J. Am. Acad. Dermatol.* **1983**, *9*, 487–502.
- 73 A. J. SOBER, Solar exposure in the etiology of cutaneous melanoma. *Photodermatol.* **1987**, *4*, 23–31.
- 74 A. L. TAPPEL, Vitamin E as the biological lipid antioxidant. *Vitamins Hormones* **1962**, *20*, 493–510.
- 75 L. H. KLIGMAN, A. M. KLIGMAN, Photoaging in dermatology. *Photodermatology* **1986**, *3*, 215–227.
- 76 R. C. WESTER, H. I. MAIBACH, Absorption of tocopherol into and through human skin. *Cosm. Toil.* **1997**, *112*, 53–57.
- 77 P. M. MAYER, W. PITTERMANN, S. WALLAT, The effects of Vitamin E on the skin. *Cosm. Toil.* **1993**, *108*, 99–109.
- 78 A. TEGLIA, G. SECCHI, New protein ingredients for skin detergency: relative wheat protein–surfactant complexes. *Int. J. Cosm. Sci.* **1994**, *16*, 235–246.
- 79 C. DUCLAIROIR, A. M. ORECCHIONI, P. DEPRAETERE, F. OSTERSTOCK, E. NAKACHE, Evaluation of gliadins nanoparticles as drug delivery systems: a study of three different drugs. *Int. J. Pharm.* **2003**, *353*, 133–144.
- 80 A. A. MARYOTT, E. R. SMITH, Table of dielectric constants of pure liquids. In *Circular 514*, National Bureau of Standards, New York, **1951**.
- 81 M. LIS-BALCHIN, S. HART, Studies on the mode of action of the essential oil of lavender (*Lavandula angustifolia* P. MILLER). *Phytother. Res.* **1999**, *13*, 540–542.
- 82 E. AUBENY, J. C. COLAU, A. NANDEUIL, Local spermicidal contraception: a comparative study of the acceptability and safety of a new pharmaceutical formulation of benzalkonium chloride, the vaginal capsule, with a reference formulation, the pessary. *Eur. J. Contracept. Health Care* **2000**, *5*, 61–67.
- 83 M. A. WAINBERG, B. SPIRA, G. BLEAU, R. THOMAS, Inactivation of human immunodeficiency virus type 1 in tissue culture fluid and in genital secretion by the spermicide

- benzalkonium chloride. *J. Clin. Microbiol.* **1990**, *28*, 156–158.
- 84 I. H. AL-ABDULLA, G. W. MELLOR, M. S. CHILDSTONE, A. M. SIDKI, D. S. SMITH, Comparison of three different activation methods for coupling antibodies to magnetisable cellulose particles. *J. Immunol. Methods* **1989**, *122*, 253–258.
- 85 C. WEBER, S. REISS, K. LANGER, Preparation of surface modified protein nanoparticles by introduction of sulfhydryl groups. *Int. J. Pharm.* **2000**, *211*, 67–78.
- 86 C. M. LEHR, J. A. BOUWSTRA, W. KOK, A. B. J. NAACH, A. G. DE BOER, H. E. JUNGINGER, Bioadhesion by means of specific binding of tomato lectin. *Pharm. Res.* **1992**, *9*, 547–553.
- 87 J. M. IRACHE, C. DURRER, D. DUCHÊNE, G. PONCHEL, Preparation and characterization of lectin–latex conjugates for specific bioadhesion. *Biomaterials* **1994**, *15*, 899–904.
- 88 A. MARUYAMA, T. ISHIHARA, N. ADACHI, T. AKAIKE, Preparation of nanoparticles bearing high density carbohydrate chains using carbohydrate-carrying polymers as emulsifier. *Biomaterials* **1994**, *15*, 1035–1042.
- 89 M. ROSER, D. FISCHER, T. KISSEL, Surface-modified biodegradable albumin nano- and microspheres. II: effect of surface charges on *in vitro* phagocytosis and biodistribution in rats. *Eur. J. Pharm. Biopharm.* **1998**, *46*, 255–263.
- 90 K. LANGER, C. COESTER, C. WEBER, H. VON BRIESEN, J. KREUTER, Preparation of avidin-labeled protein nanoparticles as carriers for biotinylated peptide nucleic acid. *Eur. J. Pharm. Biopharm.* **2000**, *49*, 303–307.
- 91 W. LIN, M. C. GARNETT, M. C. DAVIES, F. BIGNOTTI, P. FERRUTI, S. S. DAVIS, L. ILLUM, Preparation of surface-modified albumin nanospheres. *Biomaterials* **1997**, *18*, 559–565.
- 92 G. V. BETAGERI, C. D. V. BLACK, J. Szebani, L. M. WAHL, J. N. WEINSTEIN, Fc-receptor-mediated targeting of antibody-bearing liposomes containing dideoxycytidine triphosphate to human monocyte/macrophages. *J. Pharm. Pharmacol.* **1993**, *45*, 48–53.
- 93 N. G. DOLINNAYA, N. I. SOKOLOVA, D. T. ASHIRBEKOVA, Z. A. SHABAROVA, The use of BrCN for assembling modified DNA duplexes and DNA–RNA hybrids; comparison with water soluble carbodiimide. *Nucleic Acids Res.* **1991**, *19*, 3067–3072.
- 94 D. M. BOORSMA, J. G. STREEFKERK, Periodate or glutaraldehyde for preparing peroxidase conjugates? *J. Immunol. Methods* **1979**, *30*, 245–255.
- 95 P. TIJSSEN, E. KURSTACK, Highly efficient and simple methods for the preparation of peroxidase and active peroxidase–antibody conjugates for enzyme immunoassays. *Anal. Biochem.* **1984**, *136*, 451–457.
- 96 S. AVRAMEAS, B. GUILBERT, Enzyme-immunoassay for measurement of antigens using peroxidase conjugates. *Biochimie* **1972**, *54*, 837–842.
- 97 H. OTTO, H. TAKAMIYA, A. VOGT, A two-stage method for cross-linking antibody globulin to ferritin by glutaraldehyde. Comparison between the one-stage and the two-stage method. *J. Immunol. Methods* **1973**, *3*, 137–146.
- 98 S. SANO, K. KATO, Y. IKADA, Introduction of functional groups onto the surface of polyethylene for protein immobilization. *Biomaterials* **1993**, *14*, 817–822.
- 99 R. S. MOLDAY, W. J. DREYER, A. REMBAUM, S. P. S. YEN, New immunolabelled spheres: visual markers of antigens on lymphocytes for scanning electron microscopy. *J. Cell Biol.* **1975**, *64*, 75–88.
- 100 N. R. SHENOY, J. M. BAILEY, J. E. SHIVELY, Carboxylic acid-modified polyethylene: a novel support for the covalent immobilization of polypeptides for C-terminal sequencing. *Protein Sci.* **1992**, *1*, 58–67.
- 101 I. EZPELETA, J. M. IRACHE, S. STAINMESSE, C. CHABENAT, J. GUEGUEN, A. M. ORECCHIONI, Preparation of lectin–vicilin nanoparticle conjugates using the

- carbodiimide coupling technique. *Int. J. Pharm.* **1996**, *142*, 227–233.
- 102 I. EZPELETA, M. A. ARANGO, J. M. IRACHE, S. STAINMESSE, C. CHABENAT, Y. POPINEAU, A. M. ORECCHIONI, Preparation of *Ulex europaeus* lectin–gliadin nanoparticle conjugates and their interaction with gastrointestinal mucus. *Int. J. Pharm.* **1999**, *191*, 25–32.
- 103 M. A. ARANGO, G. PONCHEL, A. M. ORECCHIONI, M. J. RENEDE, D. DUCHENE, J. M. IRACHE, Bioadhesive potential of gliadin nanoparticulate systems. *Eur. J. Pharm. Sci.* **2000**, *11*, 333–341.
- 104 L. H. OLDE DAMINK, P. J. DIJKSTRA, M. J. VAN LUYN, P. B. VAN WACHEM, P. NIEUWENHUIS, J. FEIJEN, *In vitro* degradation of dermal sheep collagen cross-linked using a water-soluble carbodiimide. *Biomaterials* **1996**, *17*, 679–684.
- 105 J. A. EWART, Slow triplet β -gliadin from Capelle-Desprez. *J. Sci. Food Agric.* **1983**, *34*, 653–656.
- 106 G. T. HERMANSON (Ed.), *Zero-length Cross-linkers. Bioconjugate Techniques*, Academic Press, Orlando, FL, **1996**.
- 107 D. BASTOS, J. L. ORTEGA, F. J. DE LAS NIEVES, R. HIDALGO, Carboxylated latexes for covalent coupling antibodies I. *J. Colloid Interface Sci.* **1995**, *176*, 232–239.
- 108 J. L. ORTEGA, D. BASTOS, R. HIDALGO, Comparative studies on physically adsorbed and chemically IgG to carboxylated latexes II. *J. Colloid Interface Sci.* **1995**, *176*, 240–247.
- 109 D. HOARE, D. KOSHLAND, A method for the quantitative modifications and estimation of carboxylic acid groups in proteins. *J. Biol. Chem.* **1967**, *242*, 2447–2453.
- 110 J. V. STAROS, R. W. WRIGHT, D. M. SWINGLE, Enhancement by *N*-hydroxysulfosuccinimide of water soluble carbodiimide-mediated coupling reactions. *Anal. Biochem.* **1986**, *156*, 220–222.
- 111 J. K. VASIR, K. TAMBWEKAR, S. GARG, Bioadhesive microspheres as a controlled drug delivery system. *Int. J. Pharm.* **2003**, *255*, 13–32.
- 112 R. GURNY, J. M. MEYER, N. A. PEPPAS, Bioadhesive intraoral release systems: design, testing and analysis. *Biomaterials* **1984**, *5*, 336–340.
- 113 C. DURRER, J. M. IRACHE, F. PUISIEUX, D. DUCHENE, G. PONCHEL, Mucoadhesion of latexes I. Analytical methods and kinetics studies. *Pharm. Res.* **1994**, *11*, 674–679.
- 114 J. M. IRACHE, C. DURRER, D. DUCHÈNE, G. PONCHEL, Bioadhesion of lectin–latex conjugates to rat intestinal mucosa. *Pharm. Res.* **1996**, *13*, 1714–1717.
- 115 G. PONCHEL, M. J. MONTISCI, A. DEMBRI, C. DURRER, D. DUCHENE, Mucoadhesion of colloidal particulate systems in the gastrointestinal tract. *Eur. J. Pharm. Biopharm.* **1997**, *44*, 25–31.
- 116 P. LANCE, R. LEV, Colonic oligosaccharide structures deduced from lectin-binding studies before and after desialylation. *Hum. Pathol.* **1991**, *22*, 307–312.
- 117 R. SHARMA, U. SCHUMACHER, The influence of diets and gut microflora on lectin binding patterns of intestinal mucin in rats. *Lab. Invest.* **1995**, *73*, 558–564.
- 118 G. PONCHEL, J. M. IRACHE, Specific and non-specific bioadhesive particulate systems for oral delivery to the gastrointestinal tract, *Adv. Drug Del. Rev.* **1998**, *34*, 191.
- 119 M. A. ARANGO, M. A. CAMPANERO, J. M. IRACHE, Potencial bioadhesivo de las nanoparticulas de gliadina en el estómago. *Rev. Colomb. Cien. Quim. Farm.* **2004**, *33*, 38–47.
- 120 J. M. GU, J. R. ROBINSON, H. S. LEUNG, Binding of acrylic polymers to mucin-epithelial surfaces. Structure/property relationship. *Crit. Rev. Ther. Drug Carrier Syst.* **1998**, *5*, 21.
- 121 N. SUBRAMANIAN, S. RAY, S. K. GHOSAL, R. BHADRA, S. P. MOULIK, Formulation design of self-micro-emulsifying drug delivery systems for improved oral bioavailability of celecoxib. *Biol. Pharm. Bull.* **2004**, *27*, 1993–1999.
- 122 A. T. M. SERAJUDDIN, P. C. SHEE, D.

- MUFSON, D. F. BERNSTEIN, M. A. AUGUSTINE, Effect of vehicle amphiphilicity on the dissolution and bioavailability of a poorly water-soluble drug from solid dispersion. *J. Pharm. Sci.* **1988**, *77*, 414–417.
- 123** B. J. AUNGST, N. NGUYEN, N. J. ROGERS, S. ROWE, M. HUSSAIN, L. SHUM, S. WHITE, Improved oral bioavailability of an HIV protease inhibitor using Gelucire 44/14 and Labrasol vehicles. *Bull Tech. Gattefosse* **1994**, *87*, 49–54.
- 124** R. N. GURSOY, S. BENITA, Self-emulsifying drug delivery systems (SEDDS) for improved oral delivery of lipophilic drugs. *Biomed. Pharmacother.* **2004**, *58*, 173–182.
- 125** S. J. DOUGLAS, S. S. DAVIS, L. ILLUM, Nanoparticles in drug delivery. *Crit. Rev. Ther. Drug Carrier System*, **1987**, *3*, 233–261.
- 126** P. ERLICH, *Collected Studies on Immunity*, Wiley, New York, **1906**.
- 127** T. MIRSHAHI, J. M. IRACHE, C. NICOLAS, M. MIRSHAHI, J. P. FAURE, J. GUEGUEN, C. HEQUET, A. M. ORECCHIONI, Adaptive immune responses of legumin nanoparticles. *J. Drug Target.* **2002**, *10*, 625–631.
- 128** O. SCHUSSLER, M. SHEN, L. SHEN, S. M. CARPENTIER, S. KAVERI, A. CARPENTIER, Effect of human immunoglobulins on the immunogenicity of porcine bioprostheses. *Ann. Thorac. Surg.* **2001**, *71*, S396–S400.
- 129** D. WIEBE, J. MEGERMAN, G. J. L'ITALIEN, W. M. ABBOT, Glutaraldehyde release from vascular prosthesis of biologic origin. *Surgery* **1988**, *104*, 26–33.

6 Peptide Nanoparticles

Klaus Langer

6.1 Introduction

The primary objective of a therapy with pharmacological active compounds is the controlled delivery of the compound to its site of action. After administration most drugs show a certain distribution throughout the body which depends mainly on their physicochemical characteristics. Only a certain fraction of the drug reaches its site of action; the other fraction may be responsible for unwanted or toxic side-effects. Therefore, a lot of concepts and drug delivery systems for the targeting of drugs to their specific site of action have been developed. A promising method is drug loading to colloidal drug carrier systems such as microemulsions, liposomes and nanoparticles. Liposomes, mainly consisting of phospholipids and cholesterol, are characterized by good biocompatibility; however, they suffer from the disadvantage of a short shelf-life and drug leakage. In comparison to liposomes, nanoparticles are solid colloidal particles in the size range between 10 and 1000 nm. They consist of macromolecular material and can be prepared by a polymerization reaction starting with the corresponding monomers or by the dispersion of preformed polymers [1]. In principle, a drug compound can be bound to the surface of such a nanoparticulate system after particle preparation, or can be entrapped or dissolved into the particle matrix (Fig. 6.1).

The ideal colloidal delivery system should be nontoxic and able to be degraded *in vivo* after reaching its site of action. Among the different materials used for the preparation of drug carrier systems, proteins would appear promising, since they can lead to biodegradable and nonantigenic drug carrier systems [2]. Protein-based nanoparticles are relatively easy to prepare and their size distribution can be monitored easily [3]. As a result of the defined primary structure of proteins, the protein-based nanoparticles may offer various possibilities for surface modification as well as the attachment of drugs and compounds for drug-targeting purposes such as antibodies or ligands for cell-specific receptor complexes.

This chapter gives an overview of nanoparticulate, and in some cases microparticulate, systems based on proteins. Only nanoparticles intended to be used as drug carrier systems and in some rare cases for diagnostic purposes will be described.

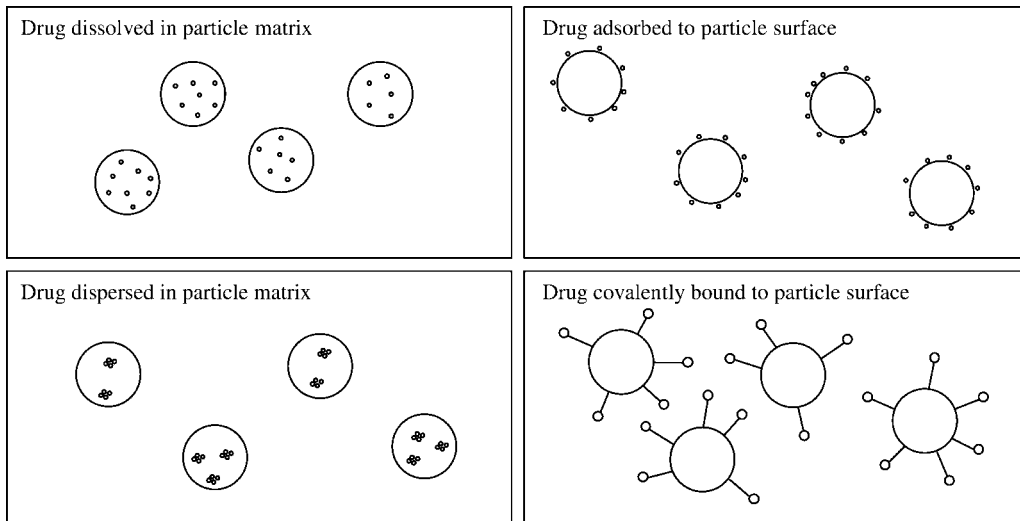


Fig. 6.1. Schematic representation of drug binding (small circles) to particulate drug carrier systems (large circles).

The chapter provides an overview of the preparation techniques for protein-based particle systems starting with the first attempts during the 1960s. Based on this earlier work, the attempts to optimize the preparation techniques in order to achieve nanoparticles instead of microparticles are outlined. Different emulsion techniques are compared to the desolvation or coacervation techniques. After the description of the preparation techniques the idea of particle surface modification in order to modify the particle properties under *in vivo* and *in vitro* conditions will be outlined. Nanoparticle systems which focus on cell-specific drug targeting are illustrated. After the preparation and surface modification review, up-to-date applications of protein-based particle systems for clinical studies, therapy and diagnostics are presented.

6.2

Starting Materials for the Preparation of Nanoparticles

Many preparation techniques for nanoparticles were established in the 1970s and 1980s, and these methods were developed further during the following years. The starting materials for particle preparation can be subdivided depending on the preparation technique used [4]:

- I. Preparation by polymerization reactions
 1. Polyacrylamide [5, 6]
 2. Poly(alkyl methacrylates) [7–9]

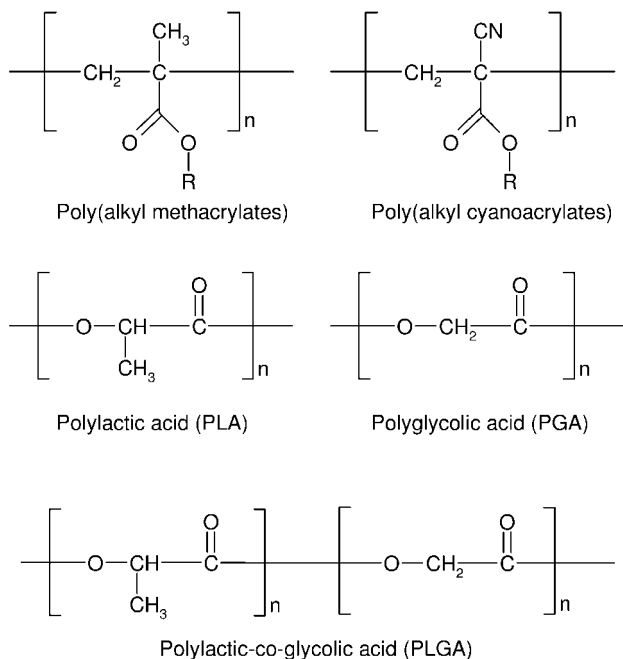


Fig. 6.2. Schematic representation of the most important synthetic polymers used for the preparation of nanoparticles as drug delivery systems.

3. Poly(alkyl cyanoacrylates) [10]
 4. Polyglutaraldehyde [11]
- II. Preparation by dispersion of preformed polymers
1. Natural macromolecules: serum albumin, gelatin, alginate [12–14]
 2. Synthetic macromolecules: poly(lactic acid) (PLA), poly(lactic-co-glycolic acid) (PLGA), polyacrylate, poly- ϵ -caprolactone [15–17]
- III. Preparation by dispersion of solid lipids [18, 19]

The structures of the most important synthetic polymers for the preparation of nanoparticles are outlined in Fig. 6.2. For the preparation of nanoparticles as drug delivery systems, artificial polymers such as poly(alkyl methacrylates) and poly(alkyl cyanoacrylates) were most often used, and nanoparticles were formed by polymerization reactions of the respective monomers. These polymers mainly differ in their biodegradation behavior. Whereas poly(alkyl methacrylates) are poorly biodegradable, the biodegradability of poly(alkyl cyanoacrylates) depends mainly on the length of the ester side-chain [20]. In addition to poor biodegradability, a further disadvantage of nanoparticle preparation by polymerization reactions can be seen in the fact that the resulting drug carrier system may contain unreacted toxic monomers. To avoid this problem and to achieve particle systems of high biocompatibility, preparation techniques involving the use of purified natural

macromolecules or preformed synthetic polymers have been developed. Due to their enhanced biocompatibility, nanoparticles based on PLA, PLGA, solid lipids as well as particle systems based on proteins as starting materials are of growing interest.

6.3

Preparation Methods

As previously outlined, nanoparticles based on artificial polymers such as poly(alkyl methacrylates) and poly(alkyl cyanoacrylates) are prepared by polymerization reactions starting with the corresponding monomers. Whereas poly(alkyl methacrylate)-based nanoparticles are usually prepared by polymerization in a continuous phase in the presence of a polymerization initiator [7, 21], poly(alkyl cyanoacrylate) nanoparticles are prepared by an emulsion polymerization technique initiated by bases present in the polymerization medium [10]. In comparison to these preparation conditions, nanoparticles based on proteins such as serum albumin, casein or gelatin are prepared by dispersion techniques of the preformed polymer. Different methods for their preparation have been described, based on emulsion formation, desolvation or coacervation. In addition to drug carrier systems consisting of either natural or artificial polymers, recently mixed compositions consisting of bovine serum albumin (BSA) loaded gelatin nanoparticles incorporated in hydrophobic PLGA microspheres have been described [22].

6.3.1

Nanoparticle Preparation by Emulsion Techniques

Emulsification of an aqueous drug-containing protein solution in an oily phase was most often used as an established method for the preparation of microspheres (Fig. 6.3). The resulting droplets of the water-in-oil emulsion were stabilized by a crosslinking procedure in the presence of bifunctional aldehydes such as glutaraldehyde or by thermal denaturation. The resulting particle size depends on the droplet size of the protein-containing aqueous phase dispersed within the oily phase. Most of the emulsion techniques described in the literature result in the formation of particles in the size range of several micrometers (i.e. microparticles/microspheres). In some cases the emulsion techniques can be optimized for the preparation of nanoparticles [23]. Most often serum albumin of different origin as well as gelatin have been used as starting materials for the preparations. In the following sections the preparation techniques are divided with regard to the nature of the protein; preparation techniques leading to the formation of microparticles are described as well as methods resulting in the formation of nanoparticles.

6.3.1.1 Emulsion Technique for the Preparation of Albumin-based Microspheres and Nanoparticles

Human serum albumin (HSA) is widely used as a microsphere material since it is considered nonantigenic for human use, biodegradable and readily available. Fur-

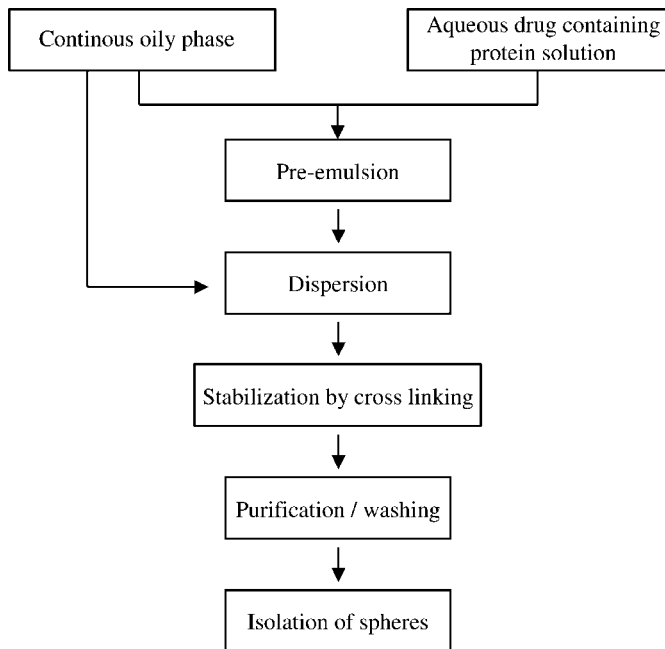


Fig. 6.3. Flow chart of nanoparticle preparation by emulsion techniques.

thermore, HSA is a well-defined starting material with a well-known primary structure (Table 6.1) enabling modifications by protein chemistry under stoichiometric conditions. In addition to the use of HSA, other albumin derivatives such as BSA [3] and rabbit serum albumin [24] have been described for the preparation of colloidal drug carrier systems. Although microaggregates and microspheres based on albumin derivatives were reported as early as the 1940s and 1950s, the first descriptions of albumin-based microspheres with a uniform size and predictable physicochemical characteristics were at the end of the 1960s by Rhodes et al. [25] and Zolle et al. [26] who used the system in a radioactive-labeled form for diagnostic purposes. Several further diagnostic applications for such kinds of serum albumin-based microspheres were published in the following years [27–29]. The emulsification methods for the preparation of microspheres had to be modified in order to produce nanoparticulate drug carrier systems instead of microparticles. The group of Scheffel et al. was the first to produce HSA-based particles in the nanometer size range between 300 and 1000 nm, so-called nanospheres, by a modified emulsion technique, and used the system after radioactive labeling to investigate the toxicity and body distribution of such a carrier system [30]. The first description of albumin nanoparticles prepared by a modified method of Scheffel et al. for drug delivery purposes was published by Kramer [31]. In the manuscript the incorporation of the anticancer agent mercaptopurine was outlined, and it was shown that over 85% of the drug present in the original emulsion was associated

Tab. 6.1. Quantitative amino acid composition of HSA divided into different properties of amino acid side-chains (the one letter code is given in brackets; amino acids usually used for covalent modification by protein chemistry are outlined in italics)

Amino acid	Number/HSA
Amino acids with hydrocarbon side-chains	
Gly [G]	12
Ala [A]	62
Val [V]	41
Leu [L]	61
Ile [I]	8
Phe [F]	31
Pro [P]	24
Amino acids with nonionic but polar side-chains	
Ser [S]	24
Thr [T]	28
<i>Cys [C]</i>	35
Met [M]	6
Trp [W]	1
Tyr [Y]	18
Asn [N]	17
Gln [Q]	20
Basic amino acids	
<i>Lys [K]</i>	59
Arg [R]	24
His [H]	16
Acidic amino acids	
<i>Asp [D]</i>	36
<i>Glu [E]</i>	62

with the microspheres in the size range between 200 and 1200 nm. Further experiments with the more hydrophilic drug daunorubicin were performed and it was observed that the amount of incorporated drug could be increased with the hydrophilicity of the drug compound. Kramer outlined that such carrier systems are of growing need for drugs with pronounced systemic toxicities and enable drug delivery to target tissues in precise dosages and with minimal interaction with normal tissues.

The main problems with the preparation in an oil-in-water emulsion are the purification of the resulting nanoparticles and the thermal stress for the incorporated drug in the case of particle stabilization by heat denaturation. In most cases the nanospheres have to be washed several times with organic solvents such as diethyl ether and these solvents have to be eliminated prior to the application of the carrier system. To circumvent the problem of the thermal stress during particle stabilization Widder et al. described the chemical crosslinking of HSA microspheres in the size range of about 1 μm by the use of 2,3-butanedione [13]. The group incorpo-

rated doxorubicin into different particle preparations and compared the heat-denatured microspheres with their proposed chemical crosslinked systems, and showed that the stability of both preparations was identical, but that the drug release behavior was mainly influenced by the stabilization procedure. In the following years the group mainly focused on the incorporation of magnetite particles as well as the drug compound into the microsphere matrix in order to achieve drug targeting by magnetic guidance. The applications of such magnetic microspheres were described in the field of diagnostics [32–34] and tumor therapy [35–40].

A complete and systematic study regarding the influence of HSA concentration, emulsification time and power, stirring rate, heat stabilization temperature, and the type of the nonaqueous phase was carried out by Gallo et al. [14]. As an initial procedure for particle preparation they used an aqueous solution of BSA and dispersed this solution in cottonseed oil by ultrasonication. The resultant emulsion was added dropwise to a larger amount of cottonseed oil at 125 °C under stirring in order to stabilize the resulting microspheres by heat denaturation. The influences of different preparation parameters such as albumin concentration, emulsification time, emulsification power and aqueous-to-oil phase volume ratio on the final particle size were evaluated. They found that the procedure for preparing albumin microspheres can withstand a large range of variability until significant changes in the particle characteristics can be observed. Optimal conditions for the preparation of smaller and more uniform microspheres were found by increasing the protein concentration as well as the temperature of heat stabilization. The group of Gupta et al. described in detail the preparation of albumin microspheres loaded with adriamycin [41, 42] as well as adriamycin and magnetite [43]. They focused on the *in vitro* drug release characteristics of these kinds of microspheres and found that the drug release was dependent on the presence of magnetite as well as on the stabilization temperature during the preparation process.

In a systematic study based on a central composite design, Müller et al. proposed a new emulsion method for the preparation of albumin nanoparticles [23]. They established an emulsion method using ultrasound and static mixing for the preparation of sub-200 nm particles. The statistical method used for the evaluation of the different process parameters revealed that only albumin concentration and aqueous phase volume showed a significant influence on the parameters of particle size, polydispersity and yield.

A comprehensive review of the preparation of albumin microspheres by emulsion techniques was given by Gupta and Hung [44–46]. In a methodological review Arshady et al. discussed the main basic features of the preparation procedure such as the crosslinking technique, droplet formation and stabilization, particle size, and size distribution [47].

6.3.1.2 Emulsion Technique for the Preparation of Gelatin-based Microspheres and Nanoparticles

In principle, the emulsion method for the preparation of serum albumin microspheres can be adapted for gelatin microsphere preparation. Gelatin offers some advantages as a matrix material: it is a natural, inexpensive, low-immunogenic,

Tab. 6.2. Quantitative amino acid composition of gelatin A divided into different properties of amino acid side chains (the one letter code is given in brackets; amino acids usually used for covalent modification by protein chemistry are outlined in italics)

Amino acid	Amount (%)
Amino acids with hydrocarbon side-chains	
Gly [G]	33.0
Ala [A]	11.2
Val [V]	2.6
Leu [L]	2.4
Ile [I]	1.0
Phe [F]	1.4
Pro [P]	13.2
Amino acids with nonionic but polar side chains	
Ser [S]	3.5
Thr [T]	–
<i>Cys [C]</i>	–
Met [M]	3.6
Trp [W]	–
Tyr [Y]	0.3
Asn [N]	1.6
Gln [Q]	2.5
Basic amino acids	
<i>Lys [K]</i>	2.7
Arg [R]	4.9
His [H]	0.4
Acidic amino acids	
<i>Asp [D]</i>	2.9
<i>Glu [E]</i>	4.8

nontoxic and good biodegradable macromolecule which is registered as an excipient for pharmaceutical formulations. As a protein-based product, gelatin possesses several functional groups which are available for covalent modifications. Due to the preparation of gelatin by hydrolysis of collagen, no defined primary structure can be given and, therefore, the composition of gelatin is most often described by the percentage amount of the respective amino acids (Table 6.2).

The influence of the preparation parameters on the physicochemical characteristics of drug-loaded gelatin microspheres was investigated by Esposito et al. [48]. As model drugs clonidine hydrochloride, TAPP-Br and bromocriptine mesylate were chosen in order to evaluate their encapsulation efficiency and release characteristics. As previously observed for drug incorporation in albumin-based particles [31], the drug loading was mainly dependent on the hydrophilic–hydrophobic balance of the drug molecule, with hydrophobic drugs showing a reduced trapping efficiency. This was due to an increased drug concentration in the oily phase of the emulsion system with increasing hydrophobicity of the drug. The release profile of

the hydrophilic drug TAPP-Br was characterized by a biphasic behavior, whereas the more hydrophobic drugs were released by a fast first-order release mechanism.

The nanoencapsulation of BSA in the matrix of gelatin-based nanoparticles was described by Li et al. [49]. BSA-containing gelatin nanoparticles of a spherical shape and a diameter of 840 nm were achieved. *In vitro* studies revealed BSA release by a diffusion-controlled mechanism. The release kinetic was mainly influenced by the water content of the particles as well as by the temperature of particle stabilization.

6.3.1.3 Emulsion Technique for the Preparation of Casein-based Microspheres and Nanoparticles

As well as the application of albumin and gelatin for the preparation of particulate drug carrier systems, the emulsion techniques described so far can also be applied to other proteins. In order to achieve microspheres with an enhanced hydrophilicity, casein was used as a further starting material for microsphere preparation. Chen et al. compared casein and albumin for the preparation of microspheres and their efficiency as a drug carrier system for doxorubicin [50]. They prepared the microspheres based on a water-in-oil emulsion technique in combination with glutaraldehyde stabilization. Compared with albumin, the surface charge of the casein system was more negative and the microspheres exhibited a slower release of drug *in vitro*. Under *in vivo* conditions in a tumor model in rats the casein system showed greater antitumoral potency than did the albumin system at equal amounts of the drug. Due to this observation it was considered that the carrier matrix can influence the potency of the incorporated drug.

The disadvantage of the casein-based microspheres was their poor spherical geometry. Therefore, the preparation of casein microspheres was further optimized by a new emulsion technique using aliphatic polyurethane in a mixture of hexane and dichloromethane as the dispersion medium, which achieved spherical, glutaraldehyde crosslinked microspheres [51, 52]. In comparison to established emulsion techniques, the avoidance of surfactants during particle preparation with this new method was advantageous. The proposed emulsion technique was used for the preparation of microspheres loaded with the cytotoxic drug methotrexate [53]. The versatility of the method was demonstrated by the synthesis of albumin as well as casein microspheres, leading to mean particle sizes of 54 and 172 μm , respectively. They compared both preparations and observed a comparable drug loading as well as a comparable drug release of about 35% in 24 h for both the casein and albumin systems. The applicability of the preparation method of casein microspheres in the presence of the stabilizer polyurethane was demonstrated in combination with different drugs such as methotrexate [53], theophylline [54], 5-fluorouracil [55] and progesterone [56]. Under *in vivo* conditions it was shown that progesterone-loaded casein microspheres hold promise for sustained drug release up to 5 months. After intramuscular injection into rabbits over this time period constant plasma concentrations of 1–2 ng mL^{-1} were observed without any significant burst release of the drug.

With regard to surface modification, Latha et al. reported that the hydrophilicity

of the casein spheres can be imparted by an end-capping process of the residual aldehyde groups present from the glutaraldehyde crosslinking with glycine or 2-aminoethanol. Comparable end-capping procedures were described earlier by Longo et al. for the preparation of HSA microspheres which were sterically stabilized by the incorporation of artificial polymers such as poly(methyl methacrylate) [57, 58].

6.3.2

Nanoparticle Preparation by Coacervation

As previously described, the disadvantages of the emulsion methods for particle preparation are (a) use of organic solvents for the removal of the oily residues of the preparation process, and (b) removal of surfactants that are used for emulsion stabilization during the preparation and remain on the particle surface. Even in the case of optimized emulsion techniques using aliphatic polyurethane in a mixture of hexane and dichloromethane [51, 52] the resulting nanoparticles have to be purified from the organic compounds of the dispersion medium. In addition to the disadvantage of extensive purification steps, the emulsion techniques preferentially lead to microparticles instead of particles in the nanometer size range, which mostly impedes an intravenous route of administration. Therefore, as alternative methods, the coacervation techniques and desolvation methods, derived from the coacervation method of microencapsulation, have been described for the preparation of nanoparticles. Compared to the emulsion techniques, coacervation methods are simpler and the resulting particles can more easily be cleaned. Beyond these advantages, the resulting particles are mostly in the nanometer size range.

Coacervation is defined as the separation of a colloidal dispersion into a colloid-rich and a colloid-poor phase by careful control of temperature, pH, electrolyte addition or other factors. The coacervate or colloid-rich phase forms as droplets, which makes the system opaque. In principle, coacervation techniques can be subdivided in simple and complex coacervation. Simple coacervation is characterized by the use of only one colloid and involves removal of the associated water from around the dispersed colloid by agents with greater affinity for water, such as various alcohols and salts. The dehydrated molecules of the colloidal dispersion tend to aggregate with surrounding molecules to form the coacervate. Simple coacervation techniques for the preparation of nanoparticles are often described by the term “desolvation”. In contrast, complex coacervation involves the use of more than one colloid. The coacervation is accomplished mainly by charge neutralization of the colloids carrying opposite charges rather than by dehydration.

6.3.2.1 Complex Coacervation Techniques for the Preparation of Nanoparticles

An example of complex coacervation is the preparation of nanoparticles based on albumin and heparin described by Liu and Leong [59]. The group described a coacervate from complexation of HSA and heparin as the clinically used components for the entrapment, and controlled release of drugs in the molecular weight range between 262 and 67 000 Da. Particle preparation was performed by simply mixing

an acidic HSA solution, which contained the respective drug, with a heparin solution. Due to the opposite charges of both polymers, phase separation under the preparation conditions occurs leading to the formation of nanoparticles. The resulting particles were stabilized by a crosslinking procedure with a carbodiimide derivative. Drug-loading studies were performed with a multitude of compounds showing that a high loading efficiency was observed especially with positively charged drugs. Due to a proteolytic degradation of the carrier system, the *in vitro* release of the drugs was faster in cell culture medium than in phosphate-buffered saline. In addition to the use of albumin, complex coacervation techniques can be carried out with different proteins such as casein [60] and gelatin [61]. In combination with gelatin, complex coacervation was most often used for the incorporation of plasmid DNA in particulate systems. For example, a method for the incorporation of plasmid DNA into a gelatin-based nanoparticle system by salt-induced complex coacervation followed by a crosslinking step with 1-ethyl-3-(3-dimethylamino-propyl)carbodiimide (EDC) was reported [61–64]. Comparable coacervation procedures for the preparation of plasmid DNA-containing nanoparticles based on the polysaccharide chitosan were described by Mao et al. and Roy et al., with the exception that the chitosan–DNA coacervate was stable without any further crosslinking step [65, 66].

6.3.2.2 Simple Coacervation (Desolvation) Techniques for the Preparation of Nanoparticles

As previously outlined, nanoparticle preparation by simple coacervation techniques is often described by the term “desolvation”. Using desolvation techniques, the phase separation of the colloidal solution is carried out by salting out, temperature change, pH variation or addition of water-miscible organic solvents such as alcohols. In the field of nanoparticle preparation, the addition of salts such as sodium sulfate or ammonium sulfate as well as the addition of organic solvents such as alcohols or acetone is most often used. In a second preparation step the nanoparticles have to be stabilized either by chemical crosslinking using bifunctional aldehydes or by thermal denaturation (Fig. 6.4).

The first paper describing desolvation procedures for the preparation of nanoparticles as drug carrier systems was at the end of the 1970s by Marty et al. [12]. The group established a general method for the preparation of nanoparticles based on HSA, BSA, ethylcellulose and casein. In principle, an aqueous macromolecule solution was prepared and the desolvation was performed under the control of turbidimetric measurements by the addition of either a sodium sulfate solution or ethanol. After the addition of a small amount of a resolating agent the resulting nanoparticles were stabilized by chemical crosslinking with glutaraldehyde. The resulting nanoparticles could be purified by a gel-filtration procedure and stored in a solid form after freeze-drying. For the drug loading of the nanoparticles Marty et al. described the incorporation method in which the drug is either added to the aqueous macromolecule solution or to the solution of the desolvating agent. A comparable desolvation procedure was used by El-Samaligy and Rohdewald in order to incorporate triamcinolone diacetate in gelatin-based nanoparticles [67, 68].

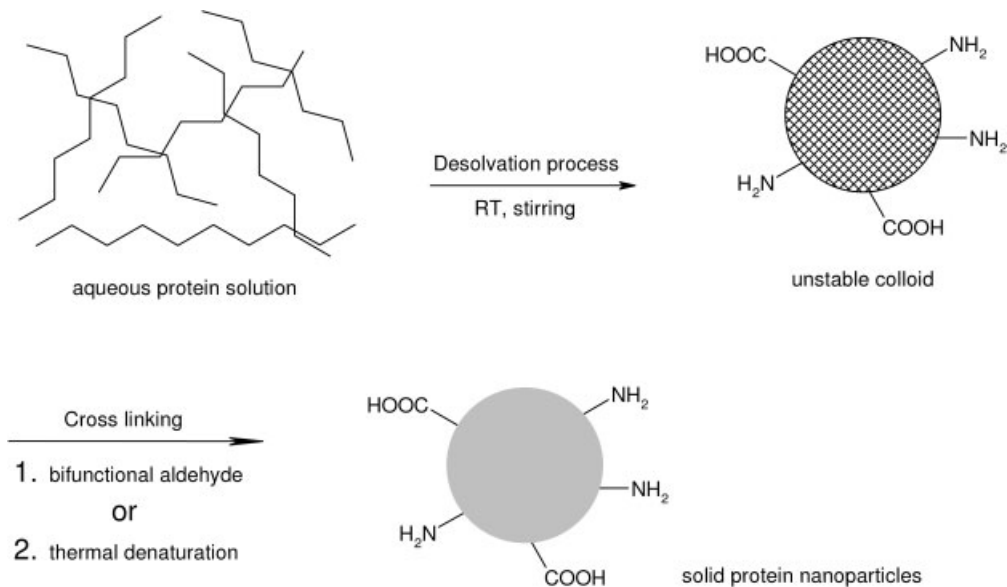


Fig. 6.4. Nanoparticle preparation by desolvation (simple coacervation) of an aqueous protein solution followed by particle stabilization by crosslinking.

They prepared nanospheres in the size range of about 200 nm by addition of isopropanol to an ammonium sulfate coacervated HSA system.

The binding and *in vitro* release of the nucleoside analogue ganciclovir (GCV) in combination with BSA prepared by desolvation techniques was studied in several publications [69–72]. The binding of the drug to preformed nanoparticles was compared to the entrapment of GCV during nanoparticle formation. The highest drug-loading capacity was observed for nanoparticles prepared by the addition of the drug to a solution of albumin leading to adsorptive drug binding prior to the formation of the carrier by desolvation. The release profile of the nanoparticle preparations was characterized by a biphasic pattern with an initial and rapid release followed by a slower step for up to 5 days [70]. The amount of rapidly released GCV was highest for nanoparticles with drug bound by adsorption to the preformed carrier. Under cell culture conditions the latter preparation was the most active formulation in the antiviral test assays, whereas the formulation with incorporated drug produced the highest decrease on cytotoxicity of the free drug [72]. The nanoparticles were intended to be used after intravitreal injection as a drug delivery system for therapy of cytomegalovirus infection. Therefore, the ocular disposition after intravitreal injection as well as the toxicity induced by the prolonged presence of BSA nanoparticles was studied [71]. It was observed that a significant amount of the nanoparticles remained in the vitreous cavity for a prolonged period of time in combination with no signs of autoimmune phenomena or alterations in the behavior of ophthalmic cells. The same group investigated nanoparticles pre-

pared by the same techniques for suitability as a drug carrier system for antiviral phosphodiester and phosphorothioate oligonucleotides [73] as well as for their ability to reach the central nervous system in an experimental allergic encephalomyelitis animal model [74].

The suitability of HSA-based nanoparticles to target drugs into cells of the reticuloendothelial system (RES) and to establish a potential therapy of the HIV infection was investigated in a number of studies. The nanoparticles were prepared by desolvation techniques and desolvation was performed by the addition of ethanol. After purification, the nanoparticles were incubated with primary human monocytes/macrophages in order to evaluate cell accumulation. Nanoparticles with a diameter of 200 nm were found to be most useful for targeting antiviral substances such as azidothymidine to macrophages [75]. It was observed that cells infected with a monocytotropic HIV isolate possessed an even higher particle uptake than noninfected cells and thus HSA nanoparticles were recommended as promising carrier systems for targeting drugs into HIV-infected cells of the RES. In an electron microscopy study, the process of cellular particle uptake was demonstrated to be phagocytosis [76]. In this study the intracellular degradation of the nanoparticles was followed and it was observed that particle degradation started within some hours after particle uptake. Within 3 days after particle incubation the process was almost terminated. Based on these observations HSA nanoparticles loaded with the drugs azidothymidine (AZT) and dideoxycytidine (ddC) were tested for their ability to prevent HIV infection in monocytes/macrophages [77]. According to the proposed methods of Marty et al. [12], drug loading was performed by the incorporation method in which the drug is added to the aqueous macromolecule solution prior to protein desolvation. Under cell culture conditions the nanoparticles loaded with the nucleoside analogs were effective against HIV infection, but they showed no superiority in relation to free drug. This was attributed to a fast and easy cellular uptake of the tested substances in free form which does not require drug delivery by nanoparticles.

The suitability of albumin nanoparticles as drug carrier systems for antisense oligonucleotides was studied by Arnedo et al. [78]. Nanoparticles were prepared based on BSA by a simple coacervation process and a phosphodiester oligonucleotide was either incorporated into the particle matrix by incubation with the albumin prior the coacervation process or adsorbed to preformed nanoparticles. Due to the electrostatic interactions that were responsible for drug adsorption to preformed nanoparticles, the adsorbed amount was susceptible to changes in pH and ionic strength of the medium. In comparison to drug loading by adsorption, the incorporation of the drug during nanoparticle formation resulted in a stable entrapment of the antisense oligonucleotide, which complies with earlier results achieved with the nucleoside analog GCV [70]. Only the incorporative method of drug binding was suitable for protection of the antisense compound against enzymatic degradation.

In most of the studies described so far the effective drug loading to the nanoparticles was of major importance, but preparation parameters influencing the physicochemical characteristics of the particles were virtually ignored. The first sys-

tematic investigations for selective control of particle size and size distribution during the desolvation procedure were described in 1993 by Lin et al. [79]. They proposed the preparation of HSA nanoparticles of diameter around 100 nm using a surfactant-free pH-coacervation method. The particles were prepared by the dropwise addition of acetone to an aqueous HSA solution at pH values between 7 and 9, followed by glutaraldehyde crosslinking and purification by gel-permeation chromatography. It was found that particle size was reduced with increasing pH of the HSA solution, apparently due to increased ionization of the HSA (isoelectric point $pI = 5.3$) which leads to repulsion of the HSA molecules and aggregates during particle formation. HSA nanoparticles were obtained in a size range between 90 and 250 nm by adjusting the pH and by controlling the amount of added acetone. The described nanoparticles were of spherical shape, but transmission electron microscopy (TEM) revealed a broad size distribution. No further data concerning the polydispersity of the nanoparticles prepared under different conditions was given. A major shortcoming of the paper is that the pH was adjusted in the absence of salt, whereas it is well known that, under these conditions, pH measurements applying glass electrodes are of limited reliability, in particular in the presence of high concentrations of protein [80].

The process of protein desolvation for the preparation of nanoparticles was adopted and studied in more detail by the group of Langer et al. with the objective to establish particle preparation under well-defined conditions [81–85]. In an earlier study a desolvation method for the preparation of nanoparticles based on HSA and gelatin was described, and the resulting particles were characterized with respect to size, ζ potential and number of available amino groups on their surface [81]. In this study the amount of the desolvating agent ethanol in the desolvation process was found to control particle size, but the variability in size at a given ethanol amount was high. The high size variability was confirmed by sedimentation velocity analysis in an analytical ultracentrifuge and electron microscopy [84]. In part, this variability has to be attributed to the manual performance of the desolvation process, characterized by a drop-by-drop addition of the desolvating agent. The conditions of particle stabilization by chemical crosslinking in the presence of the bifunctional compound glutaraldehyde or by heat denaturation showed no influence on the resulting particle size, but the degree of chemical crosslinking mainly influenced the number of amino groups on the surface of HSA nanoparticles as well as the ζ potential of the colloid. With regard to a controllable particle size in combination with a reproducible desolvation method, a pump-controlled preparation method was established in a following study which enabled particle preparation under defined conditions (Fig. 6.5) [85]. Based on this new preparation procedure several factors of the preparation process such as rate of ethanol addition, pH value and ionic composition of the HSA solution, protein concentration, and conditions of particle purification were evaluated. Most of the parameters studied showed only a minor influence on the particle characteristics. Only the pH value of the HSA solution prior to the desolvation procedure was identified as the major factor determining particle size. These observations were in good agreement with the earlier work of Lin et al. [79] which was described above. By

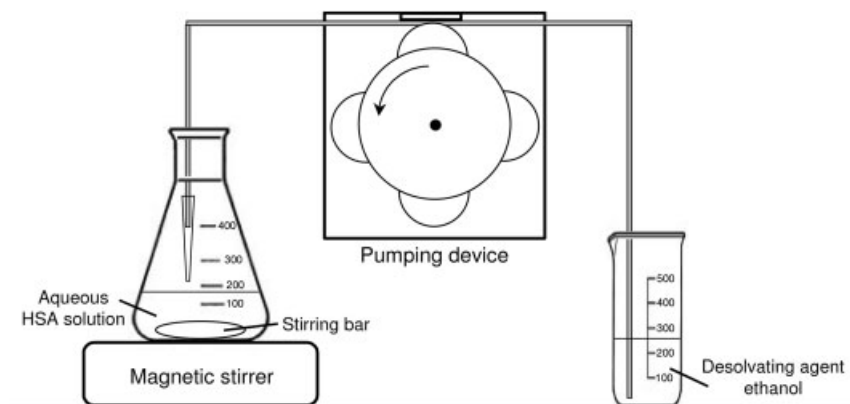


Fig. 6.5. Simple pump-controlled system for reproducible protein desolvation.

sedimentation velocity analysis it was demonstrated that application of a pump-controlled system in combination with a defined pH adjustment leads to well-defined mean particle sizes as well as narrow size distributions.

6.4

Basic Characterization Techniques for Peptide Nanoparticles

A rational development of a protein-based colloidal carrier system requires a systematic characterization of the resulting nanoparticles. In particular, physicochemical parameters such as particle size, size distribution, ζ potential and surface morphology are of major importance.

Photon correlation spectroscopy (PCS) was used in most of the pharmaceutical studies as the standard method for determination of particle size and size distribution. In principle, PCS uses Brownian motion to measure the size of particles. In brief a diffusion coefficient D of the particles in suspension is determined by laser light scattering. Based on this coefficient D and the well-known Stokes–Einstein equation, a “Stokes’ diameter” or hydrodynamic diameter is calculated, which is not equivalent to a weight or number diameter. The advantage of PCS can be seen in a rapid determination of particle size within several seconds or minutes. However, the user has to be aware of the limitations of PCS, such as low resolving power and well-known problems of mathematically ill-conditioned analysis of the autocorrelation function. The resulting particle size distributions can be strongly biased, being critically dependent on the model used for raw data analysis.

As well as PCS, sedimentation velocity analysis in an analytical ultracentrifuge, a standard technique for characterizing particle size distributions in macromolecular chemistry, can also be used in the field of pharmaceuticals as an appropriate technique for particle sizing. In principle, during the centrifugation process the apparent absorbance (turbidity) of the nanoparticle sample versus radius is measured followed by data modeling as a distribution of nondiffusing spherical particles. As

the migration of particles in a gravitational field of an ultracentrifuge shows a stronger size dependence than the diffusion coefficient D measured by PCS, this method has the potential for significantly higher resolution [86, 87] and therefore is much less mode dependent. Therefore, due to the superior resolving power of this technique more detailed information about the particle size distribution can be obtained. The suitability of ultracentrifugation for characterization of HSA nanoparticles was confirmed by Vogel et al. [84]. The study revealed that HSA nanoparticles prepared by a manual performed desolvation process, characterized by a drop-by-drop addition of the desolvating agent, showed a high variability in particle size. The same technique can also be applied to confirm the reproducibility of particle preparation under optimized preparation conditions [85].

Different microscopic techniques such as electron microscopy (reflection and transmission) and atomic force microscopy (AFM) are useful for determination of particle shape and surface morphology. For example, knowledge of particle shape is a basic requirement for reasonable application of analytical techniques such as PCS and analytical ultracentrifugation – spherical particle shape is an imperative prerequisite for particle size analysis by PCS. In the field of analytical ultracentrifugation, information about particle shape is necessary to apply the proper mathematical model to the apparent absorbance versus radius raw data. For instance, using TEM, it was confirmed that the process of protein desolvation described above for the preparation of HSA nanoparticles led to a spherical particle shape [84]. Therefore, the particle system was well suited for size analysis using PCS or sedimentation velocity analysis. Directly after manual particle preparation and purification, the samples showed a slightly broader size distribution which could be fractionated into narrow distributions by preparative density gradient centrifugation (Fig. 6.6).

In addition to TEM, AFM is another useful technique to obtain more detailed information about surface morphology. AFM is a widely used experimental technique for the characterization of nanostructures. In particular, due to its ability to map variations in material properties with nanometer resolution, AFM is well suited to probe potential subcomponents or substructures of nanoparticles. An AFM picture of HSA nanoparticles prepared by protein desolvation under the same conditions described for the sample in Fig. 6.6 is depicted in Fig. 6.7. The height image of the sample confirms the spherical nature of the nanoparticles, whereas the phase image reveals a substructure in the size range of about 15 nm, showing the crosslinked nature of these particles.

The stability and electrical behavior of nanoparticles can be assessed by determination of the ζ potential of the particle colloid under varying pH and buffer conditions. Titration experiments are useful to find the optimal handling and storage conditions for the particle system as well as to determine the isoelectric point of the nanoparticles. For example, the group of Langer et al. used titration experiments for the determination of the ζ potential in order to take a more detailed look at the effect of pH and buffer variation on the stability of HSA nanoparticles [85]. They observed positively charged nanoparticles at a pH of 3. With increasing pH value the ζ potential was reduced to about -50 mV at pH values between 7 and 10. The salt dependency of the ζ potential was determined by titration experiments

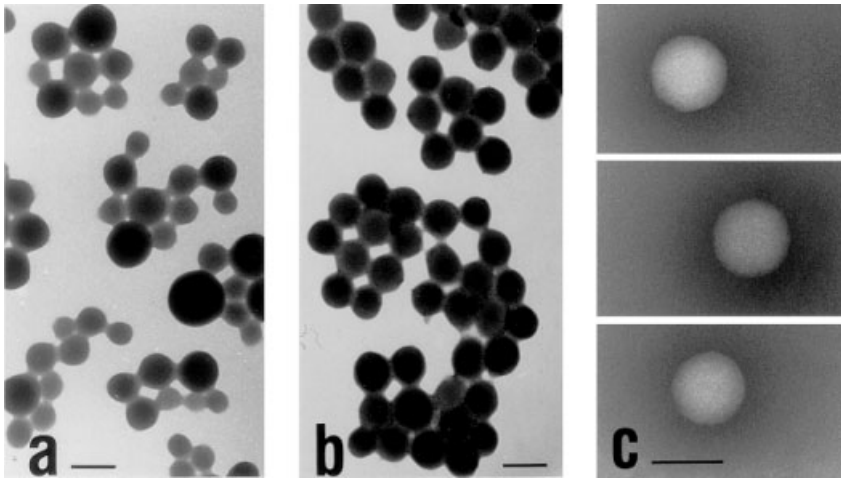


Fig. 6.6. Morphology of HSA nanoparticles by means of TEM of negatively stained samples: (a) unfractionated particles, (b) particles in the fraction of highest turbidity from a sucrose gradient and (c) three arbitrary selected particles of sample (b) on films glow discharged for 30 s. Bar length = 200 nm. (From Ref. [84].)

with concentrated buffer systems. As could be expected, due to a shielding of the surface charge with increasing buffer concentration the ζ potential of the colloid was reduced. However, it became obvious that a phosphate buffer can be used at least up to concentrations of 150 mM without reducing particle surface charge to a degree that leads to isoelectric aggregation of the particles. Furthermore, the effect of crosslinking on the isoelectric point (pI) of HSA nanoparticles was determined. Glutaraldehyde crosslinking of the particle matrix was found to decrease the pI value of the particles significantly. Such a reduction could be expected for a covalent reaction of glutaraldehyde with lysine side-chains of the protein HSA.

In addition to the basic characterization techniques outlined within this chapter, drug-loading efficiency as well as characterization of the chemical surface structure is of major importance. The influence of drug properties and particle preparation techniques on the drug-loading efficiency was described above within the overview of preparation methods. The analysis of the chemical surface structure depends mainly on the nature of the functional groups on the particle surface or the surface modification strategy used. Different ways of surface modification and the methods suitable for characterization of the resulting particle surface structures are outlined below.

6.5

Drug Targeting with Nanoparticles

Most often nanoparticulate drug carrier systems were prepared in order to modify the body distribution of the entrapped drug and to transport the drug to its site of

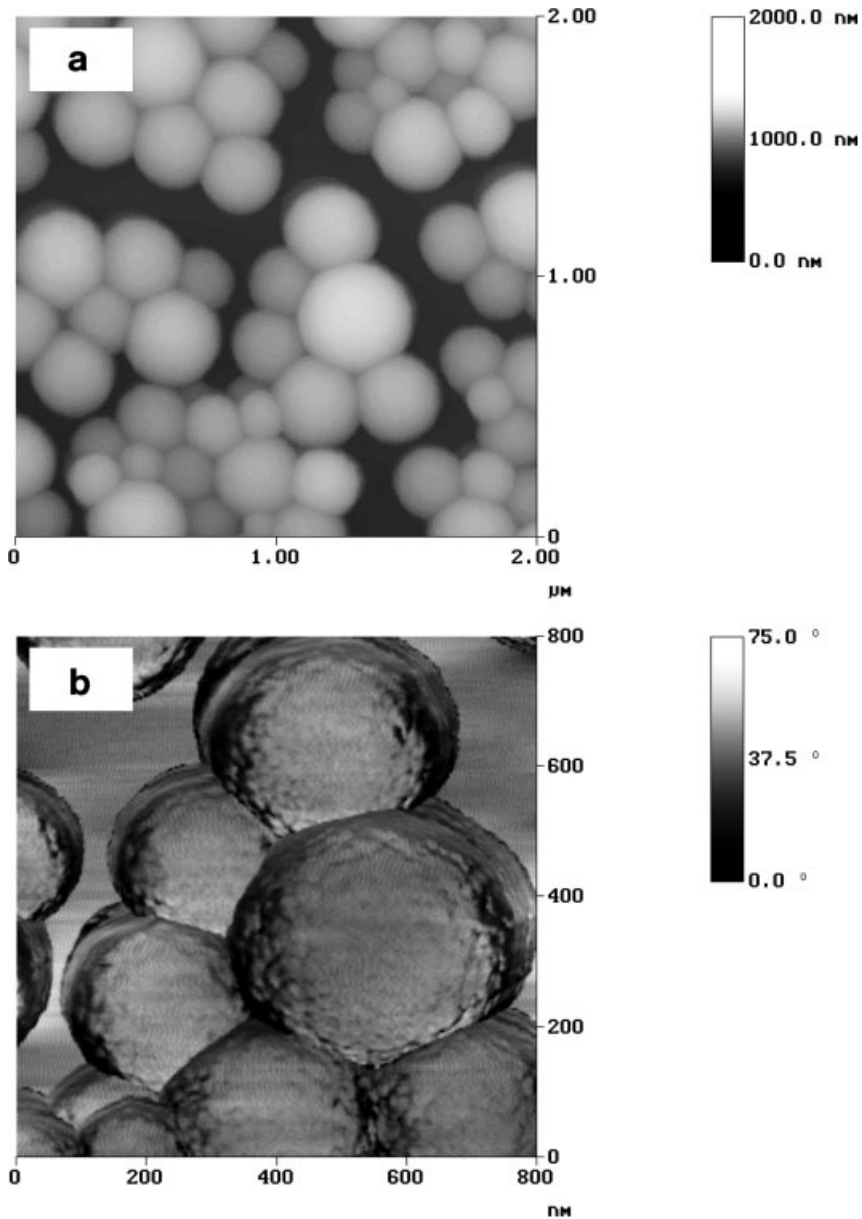


Fig. 6.7. Morphology of HSA nanoparticles by means of AFM in tapping mode on a Nanoscope IIIa (Digital Instruments, Santa Barbara, CA) with rotated tapping mode etched silicon probe (RTESP) tips. (a) Height image of nanoparticles on mica. (b) Phase image of the

central part of (a) with crosslinked substructure visible. (From Professor U. S. Schubert, Eindhoven University of Technology, Laboratory of Macromolecular Chemistry and Nanoscience, Eindhoven, The Netherlands.)

action (i.e. drug targeting). When nanoparticles are administered intravenously they are quickly recognized by the mononuclear phagocyte system (MPS) and cleared from the circulation. The size of the nanoparticles as well as the hydrophobicity of their surface determine the *in vivo* fate of the system, with larger particle size and higher hydrophobicity leading to a more pronounced adsorption of blood components (i.e. opsonization) followed by a more rapid clearance from circulation. Therefore, hydrophilic surface structures in combination with small particle sizes (100–200 nm) are crucial parameters for developing nanoparticulate drug carriers with extended half-lives in blood.

6.5.1

Passive Drug Targeting with Particle Systems

After intravenous injection, unmodified nanoparticles enable passive drug targeting, which is characterized by particle uptake in cells of the MPS. Particle accumulation in macrophages of the liver, spleen and bone marrow as well as in circulating monocytes is observed. The resulting body distribution of the particulate carrier systems is mainly influenced by two physicochemical properties – particle size and surface characteristics [88]. Concerning particle size, the particles should be small enough not to be removed by simple filtration mechanisms in a capillary bed after intravenous injection. On the other hand, surface characteristics such as hydrophilicity/lipophilicity represent the major determinants for protein adsorption in biological fluids and may modify particle interaction with specific plasma membrane receptors, thus leading to elimination of the particles from the systemic circulation. The mechanism of protein adsorption on particle surfaces in conjunction with the recognition of such coated particles by monocytes and macrophages is named opsonization. After intravenous administration of nanoparticle suspensions the particles are normally rapidly coated by adsorption of specific blood components known as opsonins. After this coating the particles are recognized by the MPS and are rapidly eliminated from the central blood circulation. As well as the surface characteristics, the opsonization process seems to be influenced by the surface curvature of the carrier system, with smaller carriers leading to a reduced adsorption of proteins and opsonins, and in turn to a reduced uptake of such systems by phagocytic cells [89].

Therefore, a reduction of the opsonization process leading to a prolongation of the plasma half-life is of major importance in order to achieve a modified body distribution. Coating of the particles with opsonins can be reduced by the introduction of a more hydrophilic surface structure in combination with a reduced particle size. Different techniques to achieve a hydrophilic particle surface are outlined below.

6.5.2

Active Drug Targeting with Particle Systems

In contrast to passive drug-targeting strategies, active drug targeting enables the transport of the particle system to body compartments not accessible to the un-

modified system. Therefore, in a first step of particle preparation it is required to achieve a more hydrophilic surface structure which leads to a prolongation of the plasma half-life. In a second step, the particle system has to be equipped with ligands, so-called drug-targeting ligands, which enable cell-specific accumulation of the particle system.

6.5.3

Surface Modifications of Protein-based Nanoparticles

In order to achieve a prolonged circulation half-life and to enable active drug targeting the opsonin adsorption has to be reduced by (a) the choice of a suitable particle size and (b) surface modification of the drug carrier system. An appropriate approach in this direction is the modification of the particle surface by different hydrophilic compounds.

As well as modification of the particle surface with hydrophilic compounds in order to modify the pharmacokinetic behavior, surface modification techniques with the aim of enhanced drug loading have also been described. For example, in a paper by Hnatowich and Schlegel, albumin microspheres were synthesized and the particle surface was modified by the covalent attachment of the chelating agents EDTA and DTPA [90]. The resulting particles were used for the attachment of the radionuclide ^{67}Gd by transcomplexation from a gadolinium acetate solution.

6.5.4

Surface Modification by Different Hydrophilic Compounds

In the field of protein-based nanoparticles the first attempts to achieve a more hydrophilic particle surface were made on the basis of albumin nanoparticles [91, 92]. Based on the method of Longo et al. [57], microspheres were prepared and stabilized by glutaraldehyde crosslinking. Hydrophilic surface modifications were achieved by quenching free aldehyde groups of glutaraldehyde with different amino-functional compounds such as ethanolamine and glycine. The stability of the chemical surface modification was confirmed in fresh human serum and in aqueous solutions of different pH values. Under cell culture conditions the phagocytic uptake of the surface-modified nanoparticles was mainly dependent on the resulting ζ potential, with a higher particle charge leading to a more pronounced cellular uptake. Contrary to the results of the cellular uptake study, no differences in blood circulation times and organ accumulation between different nanoparticle preparations were observed after intravenous injection in rats [93]. Therefore, the effect of surface modification by hydrophilic low-molecular-weight compounds remained questionable.

With regard to active drug targeting with nanoparticles (see below), hydrophilic systems with functional groups at their surface are necessary to which ligands such as antibodies can be attached. The emulsion methods for particle preparations employ a lipophilic external phase and therefore produce microspheres with a hydrophobic surface due to the preferential orientation of lipophilic amino acids

of the albumin molecules to the outer lipophilic phase of the water-in-oil emulsion. MacAdam et al. developed a method for the preparation of albumin microspheres which had chemically reactive groups such as carboxylic and amino groups on the surface to which ligands could be attached [3]. Carboxylic groups were introduced by the reaction of amino groups with iodoacetic acid under alkaline conditions. The group described methods for the quantitative determination of these groups at the particle surface using the radioactive probes [^{14}C]glycine ethyl ester and [^{14}C]sodium acetate.

6.5.5

Surface Modification by Polyethylene Glycol (PEG) Derivatives

In addition to the modifications with low-molecular-weight compounds described above, several approaches were taken to introduce a hydrophilic steric barrier at the particle surface, i.e. by modification of the particle surface with PEG derivatives. Lin et al. performed several approaches for the introduction of PEG chains onto the surface of HSA nanoparticles. Based on their established preparation method for HSA nanoparticles [79] outlined above, Lin et al. compared HSA nanoparticles either stabilized by the glutaraldehyde method or a novel Dextranox-MPEG crosslinking procedure [94]. Dextranox-MPEG is a methyl PEG-substituted oxidized dextran which created a sterically stabilizing polyethylene oxide surface layer surrounding the nanospheres. They tested the electrolyte- and pH-dependent flocculation of both preparations, and concluded that the higher stability of the proposed nanospheres depended mainly on a hydrated steric barrier surrounding the Dextranox-MPEG crosslinked nanospheres, whereas the glutaraldehyde crosslinked system was mainly stabilized by electrostatic repulsive forces. As an alternative method for steric stabilization of HSA nanoparticles, Lin et al. established a nanoparticle preparation based on two different PEG–HSA conjugates, namely a poly(amidoamine)–poly(ethylene glycol) copolymer grafted HSA (HSA–PAA–PEG) and a poly(thioetheramido acid)–poly(ethylene glycol) copolymer grafted HSA (HSA–PTAAC–PEG) [95]. As with the Dextranox-MPEG crosslinked nanoparticles, they confirmed the existence of a hydrated steric barrier surrounding the nanospheres by electrolyte- and pH-dependent flocculation tests, and showed a reduced plasma protein adsorption on the particle surface compared with unmodified nanoparticles. More recently, Lin et al. developed a third method for surface modification of HSA nanoparticles with PEO chains on the basis of methoxy-PEG modified HSA (HSA–mPEG) and evaluated the resulting nanoparticles as outlined for copolymer grafted HSA [96]. The ζ potential of the resulting nanoparticles was significantly lower than that of unmodified nanoparticles and the existence of a hydrated steric barrier was confirmed. The two PEG-modified albumin nanoparticle systems prepared on either HSA–PTAAC–PEG or HSA–mPEG were compared to HSA-based nanoparticles with regard to drug loading and *in vitro* drug release using the model compound rose Bengal [97]. The drug-loading efficiency of HSA–mPEG-based nanoparticles was much lower than that of nanoparticles prepared with unmodified HSA, indicating that less drug–protein binding

sites were available in the HSA–mPEG molecule as compared to the HSA molecule. The *in vitro* drug release of the different particle preparations in the presence of trypsin was mainly dependent on the PEG modification, with a slower drug release in the case of PEG-modified nanoparticles. This observation suggests that not only the behavior in biological systems will be modified by surface modification, but that the existence of a steric barrier on the surface of the nanoparticles mainly influences the enzymatic degradation and consequently the drug release properties of the particles.

6.5.6

Surface Modification by Drug-targeting Ligands

In order to achieve a system which enables active drug targeting, in addition to a hydrophilic steric barrier at the particle surface which prevents opsonization, the particle system has to be equipped with drug-targeting ligands. In combination with nanoparticulate systems, in most cases antibodies were described as drug-targeting ligands. The first conjugation reactions between particle surfaces and cell-specific antibodies were described in the 1970s for latex particle systems based on synthetic polyacrylates [98, 99]. The first reports of antigen-specific binding were achieved with these particles. In a further step, the nanoparticles were loaded with magnetite, and were used as magnetic microspheres for labeling and separation of lymphocytes and erythrocytes [100]. In the following years antibody-modified synthetic nanoparticles intended for active drug targeting have been synthesized and characterized in detail [101–104]. Apart from polyacrylate-based nanoparticles, other starting materials such as silica [105], PLA [106] and proteins [107–109] were used for the preparation of ligand-modified nanoparticles in later studies.

A first study with protein-based nanoparticles surface modified with cell-specific antibodies was described by Akasaka et al. [107]. An antitumoral antibody was covalently attached to primary amino groups of BSA nanoparticles prepared with glutaraldehyde crosslinking by covalent linkage (Schiff's base formation) of aldehyde groups at the surface of the nanospheres with amino groups of the antibody. Although in this first study with antibody-modified albumin nanoparticles the specificity of the free antibody for tumor cells was clearly demonstrated, tumor cell binding after conjugation of the respective antibody to the nanoparticles remained unclear. After intravenous administration of the antibody-modified nanoparticles in tumor-bearing mice the carrier system was found to be localized mainly in the liver, lungs and kidneys of the animals.

In a further study, antimucus polyclonal antibodies were covalently linked to the surface of albumin microspheres in order to achieve an oral drug delivery system with delayed gastrointestinal transit [110]. Three different particle systems with either a hydrophobic, a hydrophilic or a carboxymethylated surface were used [3] and the linkage was performed by the carbodiimide reaction using 1-ethyl-3-(3-dimethylaminopropyl)carbodiimide. The group observed that only hydrophilic and carboxymethylated microspheres with surface-attached antibody bound significantly more mucin from suspension. The same particle preparations also showed stronger

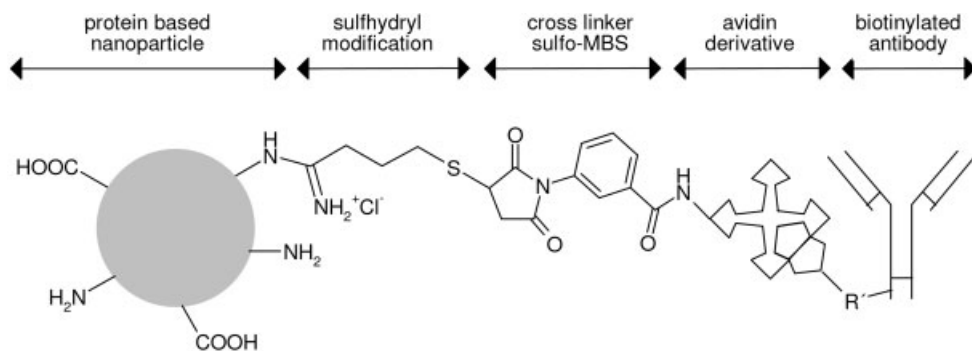


Fig. 6.8. Schematic representation of antibody-loaded avidin-modified nanoparticles for cell-type-specific targeting.

binding to isolated gut segments than the other control preparations. The results supported the finding that the combination of a hydrophilic particle surface with a drug-targeting ligand is a precondition for a site-specific carrier system.

In a recent study by Wartlick et al., gelatin as well as HSA nanoparticles were described for cell-type-specific targeting of different breast cancer cells with varying HER2 expression levels [108]. Both particle preparations were prepared by established desolvation techniques and were surface modified in a first step by the covalent attachment of the avidin derivative NeutrAvidinTM. The avidin binding was performed with the heterobifunctional PEG-based crosslinker NHS-PEG3400-Mal. The humanized monoclonal antibody trastuzumab (HerceptinTM) was used as drug targeting ligand. For the attachment of the antibody to the nanoparticle surface trastuzumab was biotinylated and bound to the particle surface by avidin–biotin complex formation (Fig. 6.8). Under cell culture conditions the resulting antibody-modified nanoparticles showed a highly specific targeting to HER2-overexpressing breast cancer cells. The attachment to the surface of the cells was time and dose dependent, and effective intracellular uptake by receptor-mediated endocytosis was demonstrated. The results indicated that the proposed preparations hold promise for selective drug targeting of tumors expressing a specific tumor antigen.

The same group described a comparable nanoparticulate system based on gelatin for specific drug targeting to T lymphocytes [109]. Using avidin–biotin complex formation a biotinylated anti-CD3 antibody was bound to the surface of NeutrAvidin-modified nanoparticles. The objective of the work was the comprehensive quantification of every chemical reaction step during the preparation procedure of the nanoparticles, including determination of the molecular weight distribution of the starting material gelatin, characterization of the particle surface and determination of the integrity of the covalently attached proteins after conjugation reaction. High compatibility of the nanoparticles with tumor cells was demonstrated under cell culture conditions. The suitability of the proposed particles for receptor-mediated cellular uptake in lymphocytic cells was demonstrated in a separate paper [111].

6.5.7

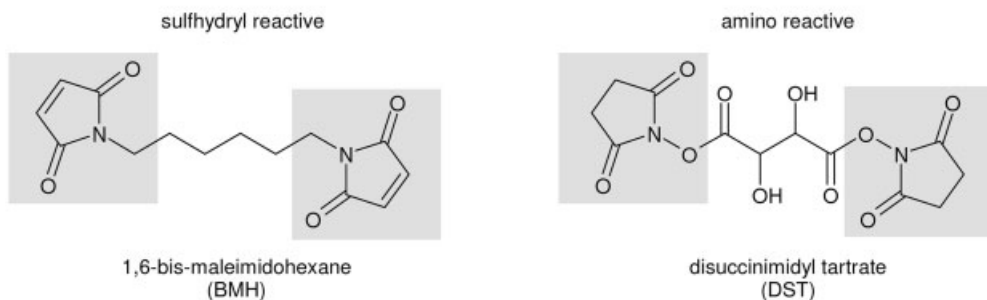
Different Surface Modification Strategies

In the case of protein-based nanoparticles the covalent attachment needs a well-defined particle system with functional groups on its surface, which can be used for the respective coupling reaction with the drug-targeting ligand. Therefore, in a number of papers the characterization of the particle surface with regard to functional groups as well as techniques for the introduction of functional groups was described. In the field of protein chemistry, it is mainly amino groups and carboxylic groups that can be used for covalent coupling reactions. In example, proteins such as HSA offer several target sites for covalent modification such as the ϵ -amino groups of lysine and the carboxylic groups of asparaginic and glutaminic acid. For glutaraldehyde-stabilized nanoparticles the remaining carbonyl residues of the crosslinker can be used as a further target site.

In a first study by Weber et al., as well as the optimization of the desolvation process for the preparation of HSA and gelatin nanoparticles, the number of available amino groups on the surface of the nanoparticles was determined spectrophotometrically using the reagent 2,4,6-trinitrobenzenesulfonic acid (TNBS) [81]. It was observed that the number of amino groups was mainly dependent on the amount of the crosslinking agent glutaraldehyde used for particle stabilization. As could be expected, increasing amounts of glutaraldehyde led to a decreasing number of available amino groups on the particle surface.

Protein conjugation most often is achieved by the use of established bifunctional crosslinkers, which can be subdivided into homobifunctional and heterobifunctional crosslinkers (Fig. 6.9). Most often heterobifunctional crosslinkers were used which combine two different specific binding sites – one for primary amino groups and one for sulfhydryl groups – in one molecule. Examples for such bifunctional crosslinkers are the homobifunctional substances 1,6-bis-maleinimido-hexane (BMH) [112], disuccinimidyl tartrate (DST) [113] and the heterobifunctional compounds *m*-maleimidobenzoyl-*N*-hydroxysulfosuccinimide ester (sulfo-MBS) [108, 109, 114] or sulfosuccinimidyl-4-*N*-maleimidomethylcyclohexane-1-carboxylate (sulfo-SMCC) [115]. In order to attach an amino group-containing compound to protein-based nanoparticles by the use of such crosslinkers, it is imperative that the nanoparticles expose reactive sulfhydryl groups on their surface. However, as the primary structure of most proteins reveal, there is only a negligibly small number of reactive sulfhydryl groups available in the genuine protein. Therefore, different methods for the introduction of reactive sulfhydryl groups onto the particle surface were described. The objective of a study by Weber et al. was to establish several methods for the introduction of thiol groups onto the surface of HSA nanoparticles [116]. In addition to the ϵ -amino groups of lysine, the carboxyl groups of asparaginic and glutaminic acid, and the carbonyl groups of the crosslinker glutaraldehyde were used for the introduction of reactive sulfhydryl groups. In principle, the thiol groups were introduced by the reaction with dithiothreitol or 2-iminothiolane, by quenching reactive aldehyde residues with cystaminiumdichloride, or by coupling L-cysteine and cystaminiumdichloride by the aqueous car-

1. homobifunctional cross linkers



2. heterobifunctional cross linkers

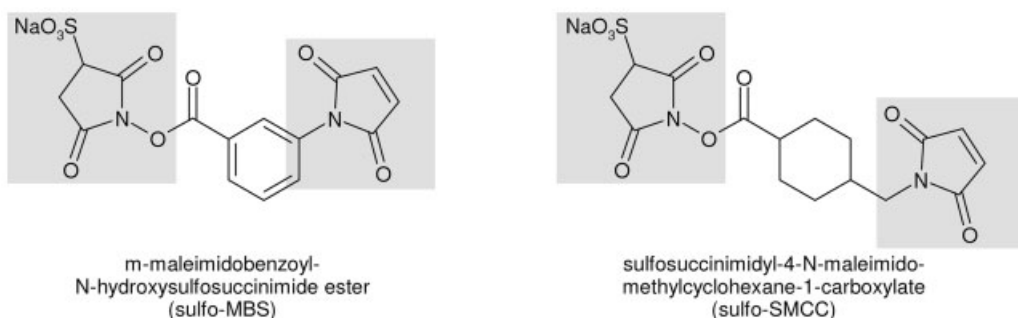


Fig. 6.9. Examples of different bifunctional crosslinkers in use for protein chemistry. The reactive groups of the respective crosslinker are outlined in grey.

bodiimide reaction. The resulting nanoparticulate systems were characterized with regard to the number of available sulfhydryl groups and it was shown that the proposed reaction conditions enabled surface modification under well-defined conditions.

In a further step, the sulfhydryl-modified nanoparticles were used for the covalent attachment of functional proteins via bifunctional crosslinkers which reacted in a first step with amino groups of the protein and in a second step with the sulfhydryl groups introduced onto the particle surface [109, 114].

6.6

Applications as Drug Carriers and for Diagnostic Purposes

Protein-based nanoparticles as well as microspheres have been described as drug carrier systems and for diagnostic purposes under *in vitro* and *in vivo* conditions in many studies. A brief overview over the different fields of application will be given below. The main focus is on particle preparations tested under *in vivo* condi-

tions in animals or under clinical conditions in humans; the overview of the *in vivo* studies is divided by the route of application. As well as the often used parenteral application route, topical or peroral administration of the nanoparticles and microspheres was described in some studies.

6.6.1

Protein-based Nanoparticles in Gene Therapy

The main goal in gene therapy is the formulation of optimal gene delivery vehicles that can achieve efficient gene transfer without immunogenic, cytotoxic and inflammatory effects. In a multitude of previous studies different vectors of viral origin were described, based on either recombinant forms of viruses such as retrovirus, adenovirus or adeno-associated virus (AAV) [117, 118]; however, these systems often suffered from the above-mentioned disadvantages. Nonviral approaches, including lipoplexes, polyplexes and nanoparticles, have advantages over viral systems such as safety, low cost, stability, ease of manufacturing and high flexibility concerning the size of the delivered transgene. However, their lack of specificity and their inability to deliver prolonged gene expression have proved to be drawbacks. Although the current synthetic systems are less efficient than viral vectors, rapid advances have achieved efficient levels of gene transfer. One promising approach is the development of nanoparticles which contain a gene construct inside a protective matrix, which protects them from immune recognition and destruction after systemic application.

In the field of protein-based nanoparticles there are many papers describing the preparation of plasmid DNA-loaded nanoparticles by different coacervation methods, and the subsequent quantification of the transfection efficiency under *in vitro* and *in vivo* conditions. For example, Truong-Le et al. reported a method for the incorporation of plasmid DNA coding for firefly luciferase into gelatin-based nanoparticle system. The nanoparticles were prepared by a salt-induced complex coacervation and were stabilized by crosslinking with EDC [61]. The authors described the incorporation of chloroquine in the particle matrix as well as the binding of transferrin and calcium ions to the resulting system. The transfection efficacy was tested in human kidney epithelial (HEK) 293 cells, and it was shown that the highest gene transfer efficiency was seen when transferrin, CaCl_2 and chloroquine were simultaneously built into the microspheres.

In 1997, the same group described a crosslinked DNA–gelatin nanosphere preparation containing a β -galactosidase plasmid construct driven by an AAV promoter [62]. The nanospheres showed improved stability of the incorporated DNA in comparison to free DNA in the presence of serum. The *in vivo* application of the plasmid-loaded nanospheres in mice resulted in a 10–30 times higher β -galactosidase expression than that observed for naked DNA whereas the injection of a AAV preparation showed a 50–100 times higher expression. The application of the nanoparticle preparation was characterized by a modest anti- β -galactosidase antibody response and a potent cytotoxic T lymphocyte response.

Comparable nanoparticle preparations containing either a cystic fibrosis [cystic

fibrosis transport regulator (CFTR)] or a green fluorescent protein (GFP) gene construct were described by the same group as gene delivery systems for the treatment of cystic fibrosis [119, 120]. The preparations were administered to the lung of rabbits by the use of a bronchoscope. Gene expression of the GFP reporter gene was observed in 43% of the brushed airway epithelial cells from the nanosphere-treated animals. The coencapsulation of sodium 4-phenylbutyrate into DNA–gelatin nanoparticles led to a correction of the cAMP-stimulated chloride conductance in cystic fibrosis epithelial cells. In 1998, Truong-Le et al. described the application of their DNA–gelatin nanospheres for the transfection of HEK 293 cells [63]. The nanospheres were characterized with regard to their DNA encapsulation efficiency, particle size, particle matrix structure as well as their stability in different media. The DNA release was mainly influenced by the nature of the incubation medium as well as by the amount of EDC used for particle stabilization. The highest DNA release was observed in trypsin solution and with low amounts of crosslinking reagent EDC, indicating the possibility to prepare a controlled release nanosphere preparation by variation of the crosslinking conditions. The results of the *in vitro* transfection showed that the most effective nanosphere preparation consisted of a DNA–gelatin coacervate, which was surface modified by the attachment of transferrin, and exhibited incorporated chloroquine and calcium chloride. The cell incubation with the optimal nanosphere preparation achieved a transfection level comparable to Lipofectamine™, Lipofectin™ and Ca–DNA coprecipitate techniques. The quantification of *in vivo* β -galactosidase expression subsequent to an intramuscular injection in mice revealed that the nanosphere preparation was much more effective than naked DNA or DNA in Lipofectamine complexes, but that the expression rate was significantly lower than that after DNA delivery with an AAV vector system.

Leong et al. compared the gelatin–DNA nanospheres with chitosan–DNA nanospheres surface modified by the covalent introduction of PEG and transferrin [121]. In comparison to the gelatin–DNA nanospheres the chitosan–DNA nanospheres showed enhanced *in vitro* transfection efficiency in HEK 293 cells, but without further enhancement effects of transferrin or by coencapsulated chloroquine. The authors showed that the optimal DNA delivery preparation mainly depended on the respective cell line and marker gene under evaluation: gelatin–DNA nanospheres were effective in transfecting HeLa cells; however, as mentioned above, when compared to chitosan, nanospheres showed only a reduced effect in HEK 293 cells. The group showed that the transfection efficiency of chitosan–DNA nanospheres was neither influenced by the storage time in suspension nor by a lyophilization step after particle preparation.

In 1999, Truong-Le et al. further characterized the coacervation conditions for the preparation of gelatin–DNA nanospheres of defined physicochemical characteristics [64]. The biological integrity of the proposed nanosphere preparations was demonstrated by a more than 50% transfection of human tracheal epithelial cells with DNA encoding CFTR. The DNA-loaded nanospheres were able to complement human bronchial epithelial cells defective in CFTR-mediated chloride transport activity with a functional CFTR.

Apart from the application of gelatin as the starting material for the preparation of plasmid DNA-loaded systems, nanoparticles based on albumin were described as well. In a study by Rhaese et al., the preparation and characterization of nanoparticles consisting of DNA, HSA and polyethyleneimine was described, and their transfection efficiency was tested in HEK 293 cells [122]. A high transfection efficiency that was nearly in the range of commercially available transfection reagents such as Superfect™ and DOTAP™ was observed when the particles were prepared at a N/P ratio of 6.0. The efficiency was comparable to that exerted by the classical calcium phosphate-mediated transfection.

6.6.2

Parenteral Application Route

The body distribution of particulate systems after parenteral administration and the modification of the distribution by variation of the particle characteristics have been determined in many studies. Some of these studies that used magnetite-loaded particles under external magnetic guidance have been addressed previously [35–40]. These studies used albumin-based particles as drug carrier systems for cytostatic agents such as doxorubicin for tumor therapy. However, such particles systems are also well suited as superparamagnetic resonance contrast material for the diagnosis of organs of the MPS and tumor diagnosis [34].

6.6.2.1 Preclinical Studies with Protein-based Particles

The influence of covalent surface modification on the body distribution of albumin nanoparticles after intravenous application was studied by Roser et al. [93]. An accumulation of the particles in the central nervous system of rats was observed in an experimental animal model of allergic encephalomyelitis. A later immunohistochemical study of Merodio et al. revealed that circulating macrophages, which migrated to the damaged sites, and resident activated microglial cells were involved in the distribution of the nanoparticles [74].

Albumin-based particles have been used for varying applications. For example, Martodam et al. studied albumin microspheres as drug carriers for an inhibitor of the leukocyte elastase (EC 3.4.21.11) leading to drug accumulation in the lung of rats [123]. Kinsey et al. used albumin particles for transfection under *in vivo* conditions [124]. They described a covalent conjugation between HSA and polyethyleneimine using a reductive cleavable spacer structure. Under elevated temperature and acidic reaction conditions the resulting conjugate was transferred to macroaggregates which were drug loaded with plasmid DNA encoding for GFP. The intravenous application of the preparation in mice resulted in a local transfection in the lung, whereas other tissues were not affected.

6.6.2.2 Clinical Studies with Protein-based Particles

The clinical application of particle systems based on HSA has also been described. In all of these studies the administration of the particle systems was by the parenteral route.

In an early study cisplatin-loaded albumin microparticles were used for clinical chemotherapy. An infusion of the particle system through the lingual artery was performed in seven patients with advanced carcinoma of the tongue [125]. Due to a particle size of about 56 μm an arterial embolism in the tumor area was achieved. Specimens were taken at different time intervals after administration, and it was observed that by the fourth week almost all carcinoma cells were killed and that microspheres were hydrolyzed and vanished within 6 weeks. A combined effect of cytotoxicity and ischemic necrosis of the tumor after microembolism was discussed.

The ability of albumin nanoparticles to act as a carrier system for paclitaxel was investigated in many clinical studies. The albumin-stabilized nanoparticle formulation ABI-007 (American Bioscience, Santa Monica, CA) was designed to overcome insolubility problems encountered with paclitaxel and eliminates the need for toxic solvents such as Cremophor EL, which is part of the commercially available paclitaxel formulation TaxolTM. Toxicities and antitumor activity of intra-arterial administration of paclitaxel-loaded albumin nanoparticles were determined in patients with advanced head and neck carcinoma [126]. The intra-arterial administration of the particles to 43 patients was well tolerated by most of the patients and required no premedication. In total, 120 treatment cycles were completed and the cytostatic activity of the particulate preparation was compared with Taxol. The maximum tolerated dose of the particle formulation in a single administration was 270 mg m^{-2} and most dose levels showed considerable antitumor activity. Complete and partial response was observed in 80.9% of the patients. In a later study, the antitumor activity of the same preparation ABI-007 was studied in patients with advanced squamous cell carcinoma of the tongue [127]. Twenty-three previously untreated patients received intra-arterial therapy with paclitaxel-loaded albumin nanoparticles. Within this study about 78% of the patients had a clinical and radiologic objective response, 13% showed a stable disease, and 9% showed disease progression. The pharmacokinetic behavior and toxicity profile of ABI-007 was studied by Ibrahim et al. [128]. In comparison to the commercially available preparation Taxol, no acute hypersensitivity reactions were observed during the infusion of the nanoparticle formulation. Compared to Taxol, the nanoparticle formulation offered several features of clinical interest such as rapid infusion rate, no requirement for premedication and a high maximum tolerated dose. Further clinical trials in metastatic breast cancer patients were completed, and the evaluation for the treatment of other tumors such as nonsmall lung cancer, ovarian cancer, melanoma and cervical cancers was reported [129, 130]. Based on the promising results of the clinical trials, the FDA recently approved ABI-007 under the trade mark AbraxaneTM as a new protein-bound breast cancer drug.

In the field of diagnostic applications, protein-based nanoparticles are mainly used as ultrasound contrast agents. The concept of contrast enhancement using gas-filled microspheres was developed during the past two decades. A multitude of clinical trials were performed and different commercially preparations are available. In the field of protein-based systems, AlbutexTM was described as air-filled albumin microspheres prepared from sonicated 5% HSA. After intravenous or in-

tracoronary injection the microspheres are ideal agents for myocardial contrast echocardiography. Animal studies showed that although the microspheres are mainly in the size range of several micrometers, Albunex did not alter coronary blood flow, left ventricular function or systemic hemodynamics [131]. Comparable results were achieved under clinical conditions, and it was demonstrated that intravenous injection of Albunex appears to be safe without any adverse hemodynamic and respiratory effects [132]. After intravenous injection the albumin microspheres were found to cross the pulmonary circulation. A further clinical study in 71 patients with three intravenous doses of Albunex showed that all injections were well tolerated and no serious side-effects were noted in any of the patients [133]. An extensive physical and biochemical characterization of Albunex microspheres was described by Christiansen et al. [134]. They found out that the preparation contains mainly air-filled microspheres in a size range from 1 to 15 μm with less than 5% being larger than 10 μm . In particular, the microsphere fraction between 4 and 10 μm was assumed to give the main contribution to the ultrasound signal in the left ventricle of the heart after intravenous injection. Only 1.5% of the total protein in suspension represents the microsphere protein, whereas the remaining protein was soluble albumin molecules. In addition to Albunex, a second preparation based on heat-denatured HSA was licensed as an echocardiographic contrast agent: Optison™ consist of gas-filled albumin microspheres, but contains octafluoropropane instead of air entrapped in the particle system. Due to incorporation of the less soluble octafluoropropane the microspheres persist much longer *in vivo* as compared to microspheres filled with air [135].

As well as the diagnostic applications, several attempts have been made at therapeutic applications of gas-filled microspheres such as Albunex, including ultrasound-intensified thrombolysis, tissue targeting and drug delivery [136, 137]. For example, albumin-coated microbubbles were used as a drug carrier system for plasmid DNA [138]. The preparation was injected intramuscularly in mice and even in the absence of ultrasound significantly improved transfection efficiency was observed. In the presence of ultrasound the transfection efficiency was significantly increased in older animals. Therefore, protein-based microbubbles are considered as a promising approach for gene delivery in muscle.

6.6.3

Topical Application of Protein-based Particles

Apart from parenteral application, other routes such as topical or peroral applications have been described for protein-based particle systems. With regard to topical application, albumin particles were used as drug carrier systems for the ophthalmic administration of pilocarpine [139–141]. After drug binding to the particulate systems a significant prolongation in reduction of the intraocular pressure (IOP) was observed. Based on the kinetic data of IOP reduction and miosis, an increase in pilocarpine bioavailability of 50–70 and 50–90% was calculated, respectively.

6.6.4

Peroral Application of Protein-based Particles

At first sight, due to enzymatic degradation in the gastrointestinal tract, peroral administration of protein-based particles seems to be a difficult approach. However, the peroral application was investigated in a number of studies. Widder et al. described a suspension of magnetite-loaded albumin microspheres as a paramagnetic oral magnetic resonance contrast agent [34]. Under *in vitro* conditions the proposed microspheres were stable over a broad range of pH and tolerated proteolytic enzyme exposure over 24 h. The peroral administration of the microspheres was studied under *in vivo* conditions in rabbits and dogs, and the system appeared effective as a small bowel contrast material.

In a further study, protein microspheres were described as adjuvants for oral vaccination [142]. The model antigen ovalbumin was entrapped into gelatin microspheres which were stabilized with different amounts of the bifunctional aldehyde glutaraldehyde. In comparison to ovalbumin in solution, the oral administration of the particulate system in mice led to a significantly increased secretion of anti-ovalbumin IgA antibodies at the intestinal mucosa as well as by urinary excretion. This effect was attributed to an effective accumulation of the particles in immunocompetent regions of the gastrointestinal tract, the so-called Peyer's patches.

The body distribution after peroral administration of radioactively labeled alginate BSA nanoparticles to rats was investigated by Yi et al. [143]. Nanoparticles about 166 nm and drug loaded with 5-fluorouracil were used for the pharmacokinetic study. After oral administration the nanoparticles were mainly distributed in the liver, spleen, lungs and kidneys of the rats. Using micro-autoradiographic experiments, particle accumulation in Kupffer cells of the liver, liver parenchymal cells and phagocytes of the spleen was observed. Therefore, the group proposed protein-based nanoparticles suitable to enter the body circulation after gastrointestinal passage.

6.7

Immunological Reactions with Protein-based Microspheres

As was outlined previously, the formulation of a device for the controlled release of biologically active substances has been a goal for many researchers. For injectable preparations it is advantageous to use a matrix material that is well tolerated and produces no adverse immunological reactions. Since protein-based particle systems undergo structural alterations induced during the preparation process of the colloid, the formation of new epitopes that may provoke an immunological response in recipients may occur. Different animal and clinical studies have been described in order to assess the possible immunogenicity of particulate systems.

In 1981, Lee et al. reported the preparation of hormone-containing albumin microspheres as a sustained release drug delivery system for progesterone [24]. For their immunological studies they prepared a particle matrix based on rabbit serum albumin in the size range of about 100 μm , and injected the resulting spheres in-

tramuscularly and subcutaneously in male rabbits. They described a good tolerance of the carrier system after application. No significant fluctuations of body temperature or weight were observed during the experiment. Rabbits that had received injections for several months did not show any adverse immunological symptoms.

The immune response of Alburnex microspheres was studied by Christiansen et al. [144]. Within this study 34 healthy volunteers received four injections of either Alburnex or 5% HSA at 4-week intervals. Analysis of blood samples did not reveal any formation of IgE or IgG antibodies directed against the microsphere protein or albumin in any of the recipient. Likewise, no adverse reaction was observed when Alburnex was administered to allergic individuals having cat albumin as one of their allergens. The authors concluded from their data that there is no evidence that heat-aggregated albumin of the Alburnex microspheres may provoke an immunological reaction upon repeated injection of the preparation. In a following study, the safety of Alburnex administration was confirmed [145]. Within this study the albumin microspheres were repeatedly administered to 12 healthy volunteers over a period of time long enough to allow development of immune reactions. No formation of microsphere-specific IgE and IgG antibodies was observed after multiple Alburnex exposure.

Clinical evaluations of adverse reactions were performed in the preliminary stages of ABI-007 (Abraxane) approval as a new protein-bound breast cancer drug. Within these studies adverse reactions against the particulate formulation were compared to events after administration of the commercial paclitaxel formulation Taxol. The particulate formulation was characterized by a reduced number of total and severe hypersensitivity reactions.

6.8

Concluding Remarks

Many studies have described nanoparticles and microparticles promising drug carrier systems. Among the different materials used for particle preparation, proteins are especially promising, since they can lead to biodegradable carrier systems for a multitude of application routes. This chapter has summarized the preparation techniques of protein-based particle systems as well as the potentials of surface modifications and drug targeting. The promising results of the particle systems under preclinical and clinical evaluation have been outlined. Recently, the first protein-based particle system was approved by the FDA for tumor therapy. Therefore, there is hope that in future years protein-based particle systems will improve the treatments of several disease and will give patients a better quality of life.

References

- 1 KREUTER, J., Evaluation of nanoparticles as drug-delivery systems I: preparation methods, *Pharm. Acta Helv.* **1983**, *58*, 196–209.

- 2 RUBINO, O. P., KOWALSKY, R., SWARBRICK, J., Albumin microspheres as a drug delivery system: relation among turbidity ratio, degree of cross-linking, and drug release, *Pharm. Res.* **1993**, *10*, 1059–1065.
- 3 MACADAM, A. B., SHAFI, Z. B., JAMES, S. L., MARRIOTT, C., MARTIN, C. P., Preparation of hydrophobic and hydrophilic albumin microspheres and determination of surface carboxylic acid and amino residues, *Int. J. Pharm.* **1997**, *151*, 47–55.
- 4 ALLÉMANN, E., GURNY, R., DOELKER, E., Drug-loaded nanoparticles – preparation methods and drug targeting issues, *Eur. J. Pharm. Biopharm.* **1993**, *39*, 173–191.
- 5 BIRRENBACH, G., SPEISER, P. P., Polymerized micelles and their use as adjuvants in immunology, *J. Pharm. Sci.* **1976**, *65*, 1763–1766.
- 6 COUVREUR, P., TULKENS, P., ROLAND, M., TROUET, A., SPEISER, P., Nanocapsules: a new type of lysosomotropic carrier, *FEBS Lett.* **1977**, *84*, 323–326.
- 7 KREUTER, J., SPEISER, P. P., *In vitro* studies of poly(methyl methacrylate) adjuvants, *J. Pharm. Sci.* **1976**, *65*, 1624–1627.
- 8 BERG, U. E., Immunstimulation durch hochdisperse Polymer suspensionen, *Dissertation*, ETH Zürich, **1979**.
- 9 HARMIA, T., SPEISER, P., KREUTER, J., Nanoparticles as drug carriers in ophthalmology, *Pharm. Acta Helv.* **1987**, *62*, 322–331.
- 10 COUVREUR, P., ROLAND, M., SPEISER, P., Biodegradable submicroscopic particles containing a biologically active substance and compositions containing them, *US patent 4,329,332*, **1982**.
- 11 McLEOD, A. D., LAM, F. C., HUNG, C. T., Optimized synthesis of polyglutaraldehyde nanoparticles using central composite design, *J. Pharm. Sci.* **1988**, *77*, 704–710.
- 12 MARTY, J. J., OPPENHEIM, R. C., SPEISER, P., Nanoparticles – a new colloidal drug delivery system, *Pharm. Acta Helv.* **1978**, *53*, 17–23.
- 13 WIDDER, K., FLOURET, G., SENYEI, A., Magnetic microspheres: synthesis of a novel parenteral drug carrier, *J. Pharm. Sci.* **1979**, *68*, 79–82.
- 14 GALLO, J. M., HUNG, C. T., PERRIER, D. G., Analysis of albumin microsphere preparation, *Int. J. Pharm.* **1984**, *22*, 63–74.
- 15 KRAUSE, H. J., SCHWARTZ, A., ROHDEWALD, P., Polylactic acid nanoparticles, a colloidal drug delivery system for lipophilic drugs, *Int. J. Pharm.* **1985**, *27*, 145–155.
- 16 BODMEIER, R., CHEN, H., Indomethacin polymeric nanosuspensions prepared by microfluidization, *J. Controlled Rel.* **1990**, *12*, 223–233.
- 17 ALLÉMANN, E., GURNY, R., DOELKER, E., Preparation of aqueous polymeric nanodispersions by reversible salting-out process, influence of process parameters on particle size, *Int. J. Pharm.* **1992**, *87*, 247–253.
- 18 SPEISER, P., Lipidnanopellets als Trägersystem für Arzneimittel zur peroralen Anwendung, *European patent 0167825*, **1990**.
- 19 MÜLLER, R. H., LUCKS, J. S., Arzneistoffträger aus festen Lipidteilchen (Feste Lipidnanosphären (SLN)), *European patent 0605497 B1*, **1996**.
- 20 VEZIN, W. R., FLORENCE, A. T., *In vitro* heterogeneous degradation of poly(*n*-alkyl alpha-cyanoacrylates), *J. Biomed. Mater. Res.* **1980**, *14*, 93–106.
- 21 BERG, U. E., KREUTER, J., SPEISER, P. P., SOLIVA, M., Herstellung und *In-vitro*-Prüfung von polymeren Adjuvantien für Impfstoffe, *Pharm. Ind.* **1986**, *48*, 75–79.
- 22 LI, J. K., WANG, N., WU, X. S., A novel biodegradable system based on gelatin nanoparticles and poly(lactic-co-glycolic acid) microspheres for protein and peptide drug delivery, *J. Pharm. Sci.* **1997**, *86*, 891–895.
- 23 MÜLLER, G. M., LEUENBERGER, H., KISSEL, T., Albumin nanospheres as carriers for passive drug targeting: An optimized manufacturing technique, *Pharm. Res.* **1996**, *13*, 32–37.
- 24 LEE, T. K., SOKOLOSKI, T. D., ROYER, G. P., Serum albumin beads: an injectable, biodegradable system for the sustained release of drugs, *Science* **1981**, *213*, 233–235.

- 25 RHODES, B. A., ZOLLE, I., BUCHANAN, J. W., WAGNER, H. N., Radioactive albumin microspheres for studies of the pulmonary circulation, *Radiology* **1969**, *92*, 1453–1460.
- 26 ZOLLE, I., RHODES, B. A., WAGNER, H. N., Preparation of metabolizable radioactive human serum albumin microspheres for studies of the circulation, *Int. J. Appl. Radiat. Isot.* **1970**, *21*, 155–167.
- 27 BURDINE, J. A., SONNEMAKER, R. E., RYDER, L. A., SPJUT, H. J., Perfusion studies with technetium-99m human albumin microspheres (HAM), *Radiology* **1970**, *95*, 101–107.
- 28 MASERI, A., MANCINI, P., CONTINI, C., PESOLA, A., DONATO, L., Method for the estimate of total coronary flow by ⁹⁹Tc tagged albumin microspheres, *J. Nucl. Biol. Med.* **1971**, *15*, 58–60.
- 29 RHODES, B. A., STERN, H. S., BUCHANAN, J. A., ZOLLE, I., WAGNER, H. N., Lung scanning with ^{99m}Tc-microspheres, *Radiology* **1971**, *99*, 613–621.
- 30 SCHEFFEL, U., RHODES, B. A., NATARAJAN, T. K., WAGNER, H. N., Albumin microspheres for study of the reticuloendothelial system, *J. Nucl. Med.* **1972**, *13*, 498–503.
- 31 KRAMER, P. A., Albumin microspheres as vehicles for achieving specificity in drug delivery, *J. Pharm. Sci.* **1974**, *63*, 1646–1647.
- 32 WIDDER, K. J., SENYEI, A. E., OVADIA, H., PATERSON, P. Y., Magnetic protein A microspheres: a rapid method for cell separation, *Clin. Immunol. Immunopathol.* **1979**, *14*, 395–400.
- 33 WIDDER, D. J., GREIF, W. L., WIDDER, K. J., EDELMAN, R. R., BRADY, T. J., Magnetite albumin microspheres: a new MR contrast material, *Am. J. Roentgenol.* **1987**, *148*, 399–404.
- 34 WIDDER, D. J., EDELMAN, R. R., GRIEF, W. L., MONDA, L., Magnetite albumin suspension: a superparamagnetic oral MR contrast agent, *Am. J. Roentgenol.* **1987**, *149*, 839–843.
- 35 WIDDER, K. J., SENYEI, A. E., RANNEY, D. F., Magnetically responsive microspheres and other carriers for the biophysical targeting of antitumor agents, *Adv. Pharmacol. Chemother.* **1979**, *16*, 213–271.
- 36 SENYEI, A. E., REICH, S. D., GONCZY, C., WIDDER, K. J., *In vivo* kinetics of magnetically targeted low-dose doxorubicin, *J. Pharm. Sci.* **1981**, *70*, 389–391.
- 37 WIDDER, K. J., MORRIS, R. M., POORE, G., HOWARD, D. P., SENYEI, A. E., Tumor remission in Yoshida sarcoma-bearing rats by selective targeting of magnetic albumin microspheres containing doxorubicin, *Proc. Natl. Acad. Sci. USA* **1981**, *78*, 579–581.
- 38 WIDDER, K. J., MORRIS, R. M., POORE, G. A., HOWARD, D. P., SENYEI, A. E., Selective targeting of magnetic albumin microspheres containing low-dose doxorubicin: total remission in Yoshida sarcoma-bearing rats, *Eur. J. Cancer Clin. Oncol.* **1983**, *19*, 135–139.
- 39 WIDDER, K. J., MARINO, P. A., MORRIS, R. M., HOWARD, D. P., POORE, G. A., SENYEI, A. E., Selective targeting of magnetic albumin microspheres to the Yoshida sarcoma: ultrastructural evaluation of microsphere disposition, *Eur. J. Cancer Clin. Oncol.* **1983**, *19*, 141–147.
- 40 RETTENMAIER, M. A., STRATTON, J. A., BERMAN, M. L., SENYEI, A., WIDDER, K., WHITE, D. B., DISAIA, P. J., Treatment of a syngeneic rat tumor with magnetically responsive albumin microspheres labeled with doxorubicin or protein A, *Gynecol. Oncol.* **1987**, *27*, 34–43.
- 41 GUPTA, P. K., HUNG, C. T., PERRIER, D. G., Albumin microspheres I. release characteristics of adriamycin, *Int. J. Pharm.* **1986**, *33*, 137–146.
- 42 GUPTA, P. K., HUNG, C. T., PERRIER, D. G., Albumin microspheres II. Effect of stabilization temperature on the release of adriamycin, *Int. J. Pharm.* **1986**, *33*, 147–153.
- 43 GUPTA, P. K., HUNG, C. T., LAM, F. C., PERRIER, D. G., Albumin microspheres III. Synthesis and characterization of microspheres containing adriamycin and magnetite, *Int. J. Pharm.* **1988**, *43*, 167–177.
- 44 GUPTA, P. K., HUNG, C. T., Albumin

- microspheres I: physico-chemical characteristics, *J. Microencapsul.* **1989**, *6*, 427–462.
- 45 GUPTA, P. K., HUNG, C. T., Albumin microspheres II: applications in drug delivery, *J. Microencapsul.* **1989**, *6*, 463–472.
- 46 GUPTA, P. K., HUNG, C. T., Magnetically controlled targeted micro-carrier systems, *Life Sci.* **1989**, *44*, 175–186.
- 47 ARSHADY, R., Albumin microspheres and microcapsules: methodology of manufacturing techniques, *J. Controlled Rel.* **1990**, *14*, 111–131.
- 48 ESPOSITO, E., CORTESI, R., NASTRUZZI, C., Gelatin microspheres: influence of preparation parameters and thermal treatment on chemico-physical and biopharmaceutical properties, *Biomaterials* **1996**, *17*, 2009–2020.
- 49 LI, J. K., WANG, N., WU, X. S., Gelatin nanoencapsulation of protein/peptide drugs using an emulsifier-free emulsion method, *J. Microencapsul.* **1998**, *15*, 163–172.
- 50 CHEN, Y., WILLMOT, N., ANDERSON, J., FLORENCE, A. T., Comparison of albumin and casein microspheres as a carrier of doxorubicin, *J. Pharm. Pharmacol.* **1987**, *39*, 978–985.
- 51 KNEPP, W. A., JAYAKRISHNAN, A., QUIGG, J. M., SITREN, H. S., BAGNALL, J. J., GOLDBERG, E. P., Synthesis, properties, and intratumoral evaluation of mitoxantrone-loaded casein microspheres in Lewis lung carcinoma, *J. Pharm. Pharmacol.* **1993**, *45*, 887–891.
- 52 LATHA, M. S., JAYAKRISHNAN, A., A new method for the synthesis of smooth, round, hydrophilic protein microspheres using low concentrations of polymeric dispersing agents, *J. Microencapsul.* **1995**, *12*, 7–12.
- 53 JAYAKRISHNAN, A., KNEPP, W. A., GOLDBERG, E. P., Casein microspheres: preparation and evaluation as a carrier for controlled release, *Int. J. Pharm.* **1994**, *106*, 221–228.
- 54 LATHA, M. S., JAYAKRISHNAN, A., Glutaraldehyde cross-linked bovine casein microspheres as a matrix for the controlled release of theophylline: *in-vitro* studies, *J. Pharm. Pharmacol.* **1994**, *46*, 8–13.
- 55 LATHA, M. S., JAYAKRISHNAN, A., RATHINAM, K., MOHANTY, M., Casein as a carrier matrix for 5-fluorouracil: drug release from microspheres, drug–protein conjugates and *in-vivo* degradation of microspheres in rat muscle, *J. Pharm. Pharmacol.* **1994**, *46*, 858–862.
- 56 LATHA, M. S., LAL, A. V., KUMARY, T. V., SREEKUMAR, R., JAYAKRISHNAN, A., Progesterone release from glutaraldehyde cross-linked casein microspheres: *in vitro* studies and *in vivo* response in rabbits, *Contraception* **2000**, *61*, 329–334.
- 57 LONGO, W. E., IWATA, H., LINDHEIMER, T. A., GOLDBERG, E. P., Preparation of hydrophilic albumin microspheres using polymeric dispersing agents, *J. Pharm. Sci.* **1982**, *71*, 1323–1328.
- 58 LONGO, W. E., GOLDBERG, E. P., Hydrophilic albumin microspheres, *Methods Enzymol.* **1985**, *112*, 18–26.
- 59 LIU, S. Q., LEONG, K. W., Delivery of protein and low-molecular weight drug by coacervate human serum albumin and heparin, *Proc. Int. Symp. Controlled Rel. Bioact. Mater.* **1997**, *24*, 911–912.
- 60 SANTINHO, A. J., PEREIRA, N. L., DE FREITAS, O., COLLETT, J. H., Influence of formulation on the physicochemical properties of casein microparticles, *Int. J. Pharm.* **1999**, *186*, 191–198.
- 61 TRUONG-LE, V. L., WALSH, S. M., AUGUST, J. T., LEONG, K. W., Gene transfer by gelatin–DNA coacervate, *Proc. Int. Symp. Controlled Rel. Bioact. Mater.* **1995**, *22*, 466–467.
- 62 TRUONG-LE, V. L., HAI-QUAN, M., WALSH, S., LEONG, K. W., AUGUST, J. T., Delivery of DNA vaccine using gelatin–DNA nanospheres, *Proc. Int. Symp. Controlled Rel. Bioact. Mater.* **1997**, *24*, 39–40.
- 63 TRUONG-LE, V. L., AUGUST, J. T., LEONG, K. W., Controlled gene delivery by DNA–gelatin nanospheres, *Hum. Gene Ther.* **1998**, *9*, 1709–1717.
- 64 TRUONG-LE, V. L., WALSH, S. M., SCHWEIBERT, E., MAO, H.-Q., GUGGINO, W. B., AUGUST, J. T.,

- LEONG, K. W., Gene transfer by DNA gelatin nanospheres, *Arch. Biochem. Biophys.* **1999**, *361*, 47–56.
- 65 MAO, H.-Q., ROY, K., TRUONG-LE, V., AUGUST, J. T., LEONG, K. W., DNA-chitosan nanospheres: derivatization and storage stability, *Proc. Int. Symp. Controlled Rel. Bioact. Mater.* **1997**, *24*, 671–672.
- 66 ROY, K., MAO, H.-Q., LEONG, K. W., DNA-chitosan nanospheres: transfection efficiency and cellular uptake, *Proc. Int. Symp. Controlled Rel. Bioact. Mater.* **1997**, *24*, 673–674.
- 67 EL-SAMALIGY, M., ROHDEWALD, P., Triamcinolone diacetate nanoparticles, a sustained release drug delivery system suitable for parenteral administration, *Pharm. Acta Helv.* **1982**, *57*, 201–204.
- 68 EL-SAMALIGY, M. S., ROHDEWALD, P., Reconstituted collagen nanoparticles, a novel drug carrier delivery system, *J. Pharm. Pharmacol.* **1983**, *35*, 537–539.
- 69 MERODIO, M., CAMPANERO, M. A., MIRSHAHI, T., MIRSHAHI, M., IRACHE, J. M., Development of a sensitive method for the determination of ganciclovir by reversed-phase high-performance liquid chromatography, *J. Chromatogr. A* **2000**, *870*, 159–167.
- 70 MERODIO, M., ARNEDE, A., RENEDE, M. J., IRACHE, J. M., Ganciclovir-loaded albumin nanoparticles: characterization and *in vitro* release properties, *Eur. J. Pharm. Sci.* **2001**, *12*, 251–259.
- 71 MERODIO, M., IRACHE, J. M., VALAMANESH, F., MIRSHAHI, M., Ocular disposition and tolerance of ganciclovir-loaded albumin nanoparticles after intravitreal injection in rats, *Biomaterials* **2002**, *23*, 1587–1594.
- 72 MERODIO, M., ESPUELAS, M. S., MIRSHAHI, M., ARNEDE, A., IRACHE, J. M., Efficacy of ganciclovir-loaded nanoparticles in human cytomegalovirus (HCMV)-infected cells, *J. Drug Target.* **2002**, *10*, 231–238.
- 73 ARNEDE, A., IRACHE, J. M., MERODIO, M., ESPUELAS MILLAN, M. S., Albumin nanoparticles improved the stability, nuclear accumulation and anticytomegaloviral activity of a phosphodiester oligonucleotide, *J. Controlled Rel.* **2004**, *94*, 217–227.
- 74 MERODIO, M., IRACHE, J. M., ECLANCHER, F., MIRSHAHI, M., VILLARROYA, H., Distribution of albumin nanoparticles in animals induced with the experimental allergic encephalomyelitis, *J. Drug Target.* **2000**, *8*, 289–303.
- 75 SCHÄFER, V., VON BRIESEN, H., ANDRESEN, R., STEFFAN, A. M., ROYER, C., TRÖSTER, S., KREUTER, J., RÜBSAMEN-WAIGMANN, H., Phagocytosis of nanoparticles by human immunodeficiency virus (HIV)-infected macrophages: a possibility for antiviral drug targeting, *Pharm. Res.* **1992**, *9*, 541–546.
- 76 SCHÄFER, V., VON BRIESEN, H., RÜBSAMEN-WAIGMANN, H., STEFFAN, A. M., ROYER, C., KREUTER, J., Phagocytosis and degradation of human serum albumin microspheres and nanoparticles in human macrophages, *J. Microencapsul.* **1994**, *11*, 261–269.
- 77 BENDER, A., SCHÄFER, V., STEFFAN, A. M., ROYER, C., KREUTER, J., RÜBSAMEN-WAIGMANN, H., VON BRIESEN, H., Inhibition of HIV *in vitro* by antiviral drug-targeting using nanoparticles, *Res. Virol.* **1994**, *145*, 215–220.
- 78 ARNEDE, A., ESPUELAS, S., IRACHE, J. M., Albumin nanoparticles as carriers for a phosphodiester oligonucleotide, *Int. J. Pharm.* **2002**, *244*, 59–72.
- 79 LIN, W., COOMBES, A. G. A., DAVIES, M. C., DAVIS, S. S., ILLUM, L., Preparation of sub-100 nm human serum albumin nanospheres using a pH-coacervation method, *J. Drug Target.* **1993**, *1*, 237–243.
- 80 WESTCOTT, C. C., *pH Measurements*, Academic Press, New York, **1978**, pp. 123–130.
- 81 WEBER, C., COESTER, C., KREUTER, J., LANGER, K., Desolvation process and surface characterisation of protein nanoparticles, *Int. J. Pharm.* **2000**, *194*, 91–102.
- 82 WEBER, C., KREUTER, J., LANGER, K., Desolvation process and surface

- characteristics of HSA-nanoparticles, *Int. J. Pharm.* **2000**, *196*, 197–200.
- 83 COESTER, C. J., LANGER, K., VON BRIESEN, H., KREUTER, J., Gelatin nanoparticles by two step desolvation – a new preparation method, surface modifications and cell uptake, *J. Microencapsul.* **2000**, *17*, 187–193.
- 84 VOGEL, V., LANGER, K., BALTHASAR, S., SCHUCK, P., MÄCHTLE, W., HAASE, W., VAN DEN BROEK, J. A., TZIATZIOS, C., SCHUBERT, D., Characterization of serum albumin nanoparticles by sedimentation velocity analysis and electron microscopy, *Progr. Colloid Polym. Sci.* **2002**, *119*, 31–36.
- 85 LANGER, K., BALTHASAR, S., VOGEL, V., DINAUER, N., VON BRIESEN, H., SCHUBERT, D., Optimization of the preparation process for human serum albumin (HSA) nanoparticles, *Int. J. Pharm.* **2003**, *257*, 169–180.
- 86 MÄCHTLE, W., High-resolution, submicron particle size distribution analysis using gravitational-sweep sedimentation, *Biophys. J.* **1999**, *76*, 1080–1091.
- 87 SCHUCK, P., ROSSMANITH, P., Determination of the sedimentation coefficient distribution by least-squares boundary modeling, *Biopolymers* **2000**, *54*, 328–341.
- 88 MOGHIMI, S. M., HUNTER, A. C., MURRAY, J. C., Long-circulating and target-specific nanoparticles: theory and practice, *Pharm. Rev.* **2001**, *53*, 283–318.
- 89 HARASHIMA, H., SAKATA, K., FUNATO, K., KIWADA, H., Enhanced hepatic uptake of liposomes through complement activation depending on the size of liposomes, *Pharm. Res.* **1994**, *11*, 402–406.
- 90 HNATOWICH, D. J., SCHLEGEL, P., Albumin microspheres labeled with Ga-67 by chelation: concise communication, *J. Nucl. Med.* **1981**, *22*, 623–626.
- 91 KISSEL, T., ROSER, M., Influence of chemical surface-modifications on the phagocytic properties of albumin nanoparticles, *Proc. Int. Symp. Controlled Rel. Bioact. Mater.* **1991**, *18*, 275–276.
- 92 ROSER, M., KISSEL, T., Surface-modified biodegradable nano- and microspheres. I. Preparation and characterization, *Eur. J. Pharm. Biopharm.* **1993**, *39*, 8–12.
- 93 ROSER, M., FISCHER, D., KISSEL, T., Surface-modified biodegradable albumin nano- and microspheres. II: effect of surface charges on *in vitro* phagocytosis and biodistribution in rats, *Eur. J. Pharm. Biopharm.* **1998**, *46*, 255–263.
- 94 LIN, W., COOMBES, A. G. A., GARNETT, M. C., DAVIES, M. C., SCHACHT, E., DAVIS, S. S., ILLUM, L., Preparation of sterically stabilized human serum albumin nanospheres using a novel dextranox-MPEG crosslinking agent, *Pharm. Res.* **1994**, *11*, 1588–1592.
- 95 LIN, W., GARNETT, M. C., DAVIES, M. C., BIGNOTTI, F., FERRUTI, P., DAVIS, S. S., ILLUM, L., Preparation of surface-modified albumin nanospheres, *Biomaterials* **1997**, *18*, 559–565.
- 96 LIN, W., GARNETT, M. C., SCHACHT, E., DAVID, S. S., ILLUM, L., Preparation and *in vitro* characterization of HSA-mPEG nanoparticles, *Int. J. Pharm.* **1999**, *189*, 161–170.
- 97 LIN, W., GARNETT, M. C., DAVIS, S. S., SCHACHT, E., FERRUTI, P., ILLUM, L., Preparation and characterisation of rose Bengal-loaded surface-modified albumin nanoparticles, *J. Controlled Rel.* **2001**, *71*, 117–126.
- 98 MOLDAY, R. S., DREYER, W. J., REMBAUM, A., YEN, S. P. S., Latex spheres as markers for studies of cell surface receptors by scanning electron microscopy, *Nature* **1974**, *249*, 81–83.
- 99 MOLDAY, R. S., DREYER, W. J., REMBAUM, A., YEN, S. P. S., New immunolabelled spheres: visual markers of antigens on lymphocytes for scanning electron microscopy, *J. Cell Biol.* **1975**, *64*, 75–88.
- 100 MOLDAY, R. S., YEN, S. P., REMBAUM, A., Application of magnetic microspheres in labelling and separation of cells, *Nature* **1977**, *268*, 437–438.
- 101 ROLLAND, A., BOUREL, D., GENETET, B., LE VERGE, R., Monoclonal antibodies covalently coupled to

- polymethacrylic nanoparticles: *in vitro* specific targeting to human T lymphocytes, *Int. J. Pharm.* **1987**, *39*, 173–180.
- 102** BOUREL, D., ROLLAND, A., LE VERGE, R., GENETET, B., A new immunoreagent for cell labeling – CD3 monoclonal antibody covalently coupled to fluorescent polymethacrylic nanoparticles, *J. Immunol. Methods* **1988**, *106*, 161–167.
- 103** ILLUM, L., JONES, P. D. E., KREUTER, J., BALDWIN, R. W., DAVIS, S. S., Adsorption of monoclonal antibodies to polyhexylcyanoacrylate nanoparticles and subsequent immunospecific binding to tumour cells *in vitro*, *Int. J. Pharm.* **1983**, *17*, 65–76.
- 104** VELGE-ROUSSEL, F., BRETON, P., GUILLON, X., LESCURE, F., BRU, N., BOUT, D., HOEBEKE, J., Immunochemical characterization of antibody-coated nanoparticles, *Experientia* **1996**, *52*, 803–806.
- 105** SANTRA, S., ZHANG, P., WANG, K., TAPEC, R., TAN, W., Conjugation of biomolecules with luminophore-doped silica nanoparticles for photostable biomarkers, *Anal. Chem.* **2001**, *73*, 4988–4993.
- 106** OLIVIER, J. C., HUERTAS, R., LEE, H. J., CALON, F., PARDRIDGE, W. M., Synthesis of pegylated immunonanoparticles, *Pharm. Res.* **2002**, *19*, 1137–1143.
- 107** AKASAKA, Y., UEDA, H., TAKAYAMA, K., MACHIDA, Y., NAGAI, T., Preparation and evaluation of bovine serum albumin nanospheres coated with monoclonal antibodies, *Drug Des. Deliv.* **1988**, *3*, 85–97.
- 108** WARTLICK, H., MICHAELIS, K., BALTHASAR, S., STREBHARDT, K., KREUTER, J., LANGER, K., Highly specific HER2-mediated cellular uptake of antibody-modified nanoparticles in tumour cells, *J. Drug Target.* **2004**, *12*, 461–471.
- 109** BALTHASAR, S., MICHAELIS, K., DINAUER, N., VON BRIESEN, H., KREUTER, J., LANGER, K., Preparation and characterisation of antibody modified gelatin nanoparticles as drug carrier system for uptake in lymphocytes, *Biomaterials* **2005**, *26*, 2723–2732.
- 110** MACADAM, A. B., SHAFI, Z. B., MARRIOTT, C., MARTIN, G. P., JAMES, S. L., Anti-mucus polyclonal antibody production, purification and linkage to the surface of albumin microspheres, *Int. J. Pharm.* **2000**, *195*, 147–158.
- 111** DINAUER, N., BALTHASAR, S., WEBER, C., KREUTER, J., LANGER, K., VON BRIESEN, H., Selecting targeting of antibody-conjugated nanoparticles to leukemic cells and primary T-lymphocytes, *Biomaterials*, **2005**, *26*, 5898–5960.
- 112** STALTERI, M. A., MATHER, S. J., A cross-linked monoclonal antibody fragment for improved tumor targeting, *Bioconjug. Chem.* **1995**, *6*, 179–186.
- 113** NOVAK, P., YOUNG, M. M., SCHOENIGER, J. S., KRUPPA, G. H., A top-down approach to protein structure studies using chemical cross-linking and Fourier transform mass spectrometry, *Eur. J. Mass Spectrom.* **2003**, *9*, 623–631.
- 114** LANGER, K., COESTER, C., WEBER, C., VON BRIESEN, H., KREUTER, J., Preparation of avidin-labeled protein nanoparticles as carriers for biotinylated peptide nucleic acid, *Eur. J. Pharm. Biopharm.* **2000**, *49*, 303–307.
- 115** HYLARIDES, M. D., MALLETT, R. W., MEYER, D. L., A robust method for the preparation and purification of antibody/streptavidin conjugates, *Bioconjug. Chem.* **2001**, *12*, 421–427.
- 116** WEBER, C., REISS, S., LANGER, K., Preparation of surface modified protein nanoparticles by introduction of sulfhydryl groups, *Int. J. Pharm.* **2000**, *211*, 67–78.
- 117** VERMA, I. M., SOMIA, N., Gene therapy – promises, problems and prospects, *Nature* **1997**, *389*, 239–242.
- 118** FELGNER, P. L., Nonviral strategies for gene therapy, *Sci. Am.* **1997**, *276*, 102–106.
- 119** WALSH, S. M., FLOTTE, T. R., BECK, S., ALLEN, S., GUGGINO, W. B., AUGUST, T., LEONG, K. W., Delivery of CFTR gene to rabbit airways by gelatin–DNA microspheres, *Proc. Int. Symp.*

- Controlled Rel. Bioact. Mater.* **1996**, *23*, 73–74.
- 120** WALSH, S. M., FLOTTE, T. R., TRUONG-LE, V. L., RUBENSTIEN, R., BECK, S., AUGUST, T., ZEITLIN, P., LEONG, K. W., Combination of drug and gene delivery by gelatin nanospheres for the treatment of cystic fibrosis, *Proc. Int. Symp. Controlled Rel. Bioact. Mater.* **1997**, *24*, 75–76.
- 121** LEONG, K. W., MAO, H.-Q., TRUONG-LE, V. L., ROY, K., WALSH, S. M., AUGUST, J. T., DNA-polycation nanospheres as non-viral gene delivery vehicles, *J. Controlled Rel.* **1998**, *53*, 183–193.
- 122** RHAESE, S., VON BRIESEN, H., RÜBSAMEN-WAIGMANN, H., KREUTER, J., LANGER, K., Human serum albumin–polyethylenimine nanoparticles for gene delivery, *J. Controlled Rel.* **2003**, *92*, 199–208.
- 123** MARTODAM, R. R., TWUMASI, D. Y., LIENER, I. E., POWERS, J. C., NISHINO, N., KREJCAREK, G., Albumin microspheres as carrier of an inhibitor of leukocyte elastase: potential therapeutic agent for emphysema, *Proc. Natl Acad. Sci. USA* **1979**, *76*, 2128–2132.
- 124** KINSEY, B., HUA, P., BARRY, M., ORSON, F., Polyethylenimine conjugated to macroaggregated albumin mediates high level transfection *in vitro* and *in vivo*, *Proc. Int. Symp. Controlled Rel. Bioact. Mater.* **1999**, *26*, 5027.
- 125** LI, H., WANG, C., WEN, Y., WU, H., Treatment of squamous cell carcinoma of the tongue using arterial embolism with cisplatin-loaded albumin microspheres: a microstructural and ultrastructural investigation, *Chin. J. Dent. Res.* **1999**, *2*, 61–66.
- 126** DAMASCELLI, B., CANTU, G., MATTAVELLI, F., TAMPLENIZZA, P., BIDOLI, P., LEO, E., DOSIO, F., CERROTTA, A. M., DI TOLLA, G., FRIGERIO, L. F., GARBAGNATI, F., LANOCITA, R., MARCHIANO, A., PATELLI, G., SPREAFICO, C., TICHA, V., VESPRO, V., ZUNINO, F., Intraarterial chemotherapy with polyoxyethylated castor oil free paclitaxel, incorporated in albumin nanoparticles (ABI-007): phase II study of patients with squamous cell carcinoma of the head and neck and anal canal: preliminary evidence of clinical activity, *Cancer* **2001**, *92*, 2592–2602.
- 127** DAMASCELLI, B., PATELLI, G. L., LANOCITA, R., TOLLA, G. D., FRIGERIO, L. F., MARCHIANO, A., GARBAGNATI, F., SPREAFICO, C., TICHA, V. V., GLADIN, C. R., PALAZZI, M., CRIPPA, F., OLDINI, C., CALO, S., BONACCORSI, A., MATTAVELLI, F., COSTA, L., MARIANI, L., CANTU, G., A novel intraarterial chemotherapy using paclitaxel in albumin nanoparticles to treat advanced squamous cell carcinoma of the tongue: preliminary findings, *Am. J. Roentgenol.* **2003**, *181*, 253–260.
- 128** IBRAHIM, N. K., DESAI, N., LEGHA, S., SOON-SHIONG, P., THERIAULT, R. L., RIVERA, E., ESMALI, B., RING, S. E., BEDIKIAN, A., HORTOBAGYI, G. N., ELLERHORST, J. A., Phase I and pharmacokinetic study of ABI-007, a Cremophor-free, protein-stabilized, nanoparticle formulation of paclitaxel, *Clin. Cancer Res.* **2002**, *8*, 1038–1044.
- 129** ABI 007, *Drugs R&D* **2003**, *4*, 303–305.
- 130** ABI 007, *Drugs R&D* **2004**, *5*, 155–159.
- 131** KELLER, M. W., GLASHEEN, W., KAUL, S., Alunex: a safe and effective commercially produced agent for myocardial contrast echocardiography, *J. Am. Soc. Echocardiogr.* **1989**, *2*, 48–52.
- 132** GENY, B., METTAUER, B., MUAN, B., BISCHOFF, P., EPAILLY, E., PIQUARD, F., EISENMANN, B., HABEREY, P., Safety and efficacy of a new transpulmonary echo contrast agent in echocardiographic studies in patients, *J. Am. Coll. Cardiol.* **1993**, *22*, 1193–1198.
- 133** FEINSTEIN, S. B., CHEIRIF, J., TEN CATE, F. J., SILVERMAN, P. R., HEIDENREICH, P. A., DICK, C., DESIR, R. M., ARMSTRONG, W. F., QUINONES, M. A., SHAH, P. M., Safety and efficacy of a new transpulmonary ultrasound contrast agent: initial multicenter clinical results, *J. Am. Coll. Cardiol.* **1990**, *16*, 316–324.
- 134** CHRISTIANSEN, C., KRYVI, H.,

- SONTUM, P. C., SKOTLAND, T., Physical and biochemical characterization of Albunex, a new ultrasound contrast agent consisting of air-filled albumin microspheres suspended in a solution of human albumin, *Biotechnol. Appl. Biochem.* **1994**, *19*, 307–320.
- 135** PODELL, S., BURRASCANO, C., GAAL, M., GOLEC, B., MANIQUIS, J., MEHLHAFF, P., Physical and biochemical stability of Optison, an injectable ultrasound contrast agent, *Biotechnol. Appl. Biochem.* **1999**, *30*, 213–223.
- 136** KASPRZAK, J. D., TEN CATE, F. J., New ultrasound contrast agents for left ventricular and myocardial opacification, *Herz* **1998**, *23*, 474–482.
- 137** CORREAS, J. M., BRIDAL, L., LESAVRE, A., MEJEAN, A., CLAUDON, M., HELENON, O., Ultrasound contrast agents: properties, principles of action, tolerance, and artifacts, *Eur. Radiol.* **2001**, *11*, 1316–1328.
- 138** LU, Q. L., LIANG, H. D., PARTRIDGE, T., BLOMLEY, M. J., Microbubble ultrasound improves the efficiency of gene transduction in skeletal muscle *in vivo* with reduced tissue damage, *Gene Ther.* **2003**, *10*, 396–405.
- 139** ZIMMER, A. K., KREUTER, J., SAETTONI, M. F., ZERBE, H., Size dependency of albumin carrier systems on *in vivo* effects of pilocarpine in the rabbit eye, *Proc. Int. Symp. Controlled Rel. Bioact. Mater.* **1991**, *18*, 493–494.
- 140** ZIMMER, A. K., KREUTER, J., SAETTONI, M. F., ZERBE, H., Evaluation of pilocarpine-loaded albumin particles as controlled drug delivery systems for the eye. I. *In vitro* and *in vivo* characterisation, *J. Controlled Rel.* **1994**, *32*, 57–70.
- 141** ZIMMER, A. K., CHETONI, P., SAETTONI, M. F., ZERBE, H., KREUTER, J., Evaluation of pilocarpine-loaded albumin particles as controlled drug delivery systems for the eye. II. Co-administration with bioadhesive and viscous polymers, *J. Controlled Rel.* **1995**, *33*, 31–46.
- 142** NAKAMURA, N., YAMASHITA, S., TSUME, Y., NADAI, T., SEZAKI, H., KOHNO, T., TABATA, Y., IKADA, Y., Potential efficacy of gelatin microspheres as a new adjuvant for oral vaccination, *STP Pharma Sci.* **1998**, *8*, 64–73.
- 143** YI, Y. M., YANG, T. Y., PAN, W. M., Preparation and distribution of 5-fluorouracil ¹²⁵I sodium alginate-bovine serum albumin nanoparticles, *World J. Gastroenterol.* **1999**, *5*, 57–60.
- 144** CHRISTIANSEN, C., VEBNER, A. J., MUAN, B., VIK, H., HAIDER, T., NICOLAYSEN, H., SKOTLAND, T., Lack of an immune response to Albunex, a new ultrasound contrast agent based on air-filled albumin microspheres, *Int. Arch. Allergy Immunol.* **1994**, *104*, 372–378.
- 145** GENY, B., BISCHOFF, P., MUAN, B., PIQUARD, F., THIRANOS, J. C., EPAILLY, E., LAMBRECHS, M., JUELS RUD-VEBNER, A., EISENMANN, B., HABEREY, P., Safety of a new transpulmonary echo-contrast agent (Albunex) in repeated echocardiographic studies in patients, *Clin. Cardiol.* **1997**, *20*, 111–115.

7

Albumin Nanoparticles

Juan Manuel Irache and Socorro Espuelas

7.1

Introduction

Albumin is generally regarded to mean serum albumin or plasma albumin; however, the word albumin is also used to describe a protein or a group of proteins defined by its solubility in water [1, 2]. The albumin literature, already vast, is well served by a number of comprehensive reviews [3–7]. This particular contribution will focus solely on the use of serum albumin as a structural material to prepare nanoparticles, and their possible applications in pharmacy and medicine.

Albumin has substantial value in physicochemical and immunochemical applications. Since serum albumin is so common in the blood and so easy to purify, it was one of the first proteins to be studied by scientists. Its stabilizing and growth supplement properties make albumin ideal for use in cell culture and other commercial applications in which expensive reagents, such as hormones, enzymes and antibodies, require stabilization and/or dilution to maintain their functional integrity for long periods of time [3]. Clinically, albumin is indicated for use as a volume expander for hypovolemia, for treatment of hypoalbuminemia, thermal injuries and certain edematous states, and as an adjunct to cardiopulmonary surgery [8–11]. In North America alone, where it is estimated that the amount of albumin required for a 70-kg patient is approximately 175 g, around 100 000 kg year⁻¹ are consumed in surgery and shock trauma [12].

Another important field of application is the use of this material in the development of drug delivery systems. In the last 30 years, both bovine serum albumin (BSA) and human serum albumin (HSA) have been widely employed to prepare microparticles and nanoparticles. More than 100 different drugs or diagnostic molecules have been incorporated in albumin particles to be administered by different routes, including intravenous, intramuscular, ophthalmic and nasal routes. A great deal of research has already been conducted in the field of microparticles to determine and evaluate the different possibilities of their use as drug delivery systems and diagnosis tools. Some of these successful efforts have enabled the development of new products as contrast agents for diagnostic purposes (i.e. OptisonTM). However, albumin nanoparticles, whose development was later than that for mi-

roparticles, are currently being studied by a number of research groups. These carriers appear to offer promising applications, including new therapeutic strategies for both the treatment of cancer and neurological diseases.

This chapter presents an overview of the fabrication and applications of both conventional and “decorated” albumin nanoparticles. After a description of the different preparative processes, representative applications of the albumin nanoparticles are also presented.

7.2

Serum Albumin

Serum albumin or plasma albumin is an abundant, multifunctional protein. It is the major protein component of blood plasma, occurring there at a concentration of around 0.6 mM (range 35–50 g L⁻¹), but this represents only approximately 40% of the albumin present in the body. The remainder is found in the extravascular space of tissues.

Serum albumin is a single-chain protein, soluble in water, without any prosthetic groups or covalently bound carbohydrate and lipid [7]. HSA has 585 amino acid residues, whereas BSA is built from 583 amino acid residues [7, 13]. The molecular mass of both molecules is 66.5 kDa. In contrast, the secondary and tertiary structures are not completely known. Based on hydrodynamic experiments [14, 15] and low-angle X-ray scattering [16], serum albumin was postulated to adopt an oblate ellipsoid with dimensions of 140 × 40 Å [17, 18]. However, studies using ¹H nuclear magnetic resonance indicated that this structure was unlikely; rather, a heart-shaped structure has been proposed [19]. This last structure of serum albumin was also confirmed from X-ray crystallographic data [20].

On the basis of the amino acid sequence, Brown proposed a three-domain model for the protein [21]. Each domain is believed to consist of six helices forming a hydrophobic channel with basic and hydrophobic amino acid residues placed at the ends. According to Fourier transform IR (FT-IR) spectra, X-ray crystallographic and differential scanning calorimetry analyses, albumin has about 67% α -helix, 10% turn and 23% extended chain, but no β -sheet [22, 23]. The analyses have also shown that the three homologous domains (I, II and III) are comprised of two subdomains (A and B) with distinct helical folding patterns that are connected by flexible loops [6, 24]. In addition, albumin domains appear to be stabilized by an internal network of disulfide bonds, bearing a number of ionizable groups with opposite signs [7, 23].

Modifications in the secondary as well as tertiary structures of BSA and HSA occur in dependence of pH, temperature and various kinds of denaturants. A number of studies have been carried out by use of various spectroscopic techniques to explore heat-induced denaturation of albumin [25–29]. The major conclusions reached from them were that conformational changes of the albumin molecule are reversible in the temperature range of 42–50 °C, but unfolding of alpha-helices

are irreversible in the temperature range of 52–60 °C. Above 70 °C, the gel formation by unfolding of albumin advances further [23, 30].

Albumin is synthesized by the liver and released into the circulation, where it possesses a half-life of 19 days [31, 32]. In the blood, serum albumin slowly diffuses across the endothelial linings of the capillaries. The bulk flow of water in the interstitial fluids and lymphatic vessels provides a means of removing albumin from the tissues. Albumin also diffuses into the cerebrospinal fluid, but the rate is so slow compared to the rate of production of the fluid that the concentration is virtually immeasurable [32]. When there is a breakdown in the blood–cerebrospinal fluid barrier, e.g. as occurs in meningitis [33] or multiple sclerosis [34], albumin is found in the fluid as a result of an increased rate of entry.

In mammals, the principal function of albumin is to provide colloid osmotic pressure, preventing plasma loss from the capillaries [6]. Other important functions of serum albumin are to maintain the pH between physiological limits and act as a source for rapid replacement of tissue proteins [35, 36]. Perhaps the most outstanding property of albumin is its ability to bind reversibly to an incredible variety of ligands. Albumin is the principal carrier of fatty acids that are otherwise insoluble in circulating plasma [37]. In fact, each albumin molecule can carry seven fatty acid molecules in deep crevices of the protein, burying their carbon-rich tails safely away from the surrounding water. More recently, serum albumin has been shown to be an important reservoir of the biological regulator and neuro-modulator, nitric oxide [38].

Serum albumin is also a versatile carrier protein, active against a variety of substances with widely differing properties (hydrophobic or hydrophilic, anionic or cationic, etc.). Thus, albumin assists in the distribution, metabolism or regulation of many marginally soluble substances such as calcium ions, tryptophan, various steroid hormones and many drugs [39]. In fact, serum albumin possesses a unique capability to bind, covalently or reversibly, a great number of various endogenous and exogenous compounds. Binding to serum albumin controls the free, active concentration of a drug, provides a reservoir for a long duration of action, and ultimately affects drug absorption, metabolism, distribution and excretion.

7.3

Preparation of Albumin Nanoparticles

Albumin nanoparticles (Fig. 7.1) have been studied as suitable carriers for drug delivery. The major reported advantages are their biodegradability [40, 41], absence of toxicity [42] and easy preparation by relatively simple methods [43]. Because of their defined primary structure, albumin-based nanoparticles may offer various possibilities for surface modification and covalent attachment of drugs and ligands. Furthermore, the albumin-based nanoparticles could allow the electrostatic adsorption of positively or negatively charged molecules without the requirements of other compounds. In addition, protein nanoparticles can be easily prepared under

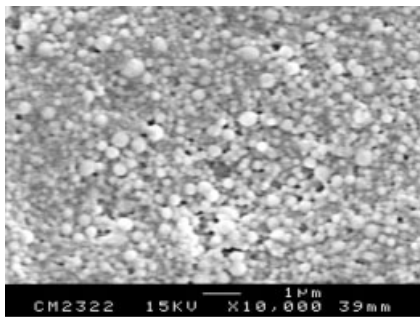


Fig. 7.1. Scanning electron microscope image of albumin nanoparticles with an average diameter of about 250 nm. (From Ref. [48].)

soft conditions and incorporate several types of molecules [44, 45]. All of these advantages make albumin one of the most versatile materials to prepare nanoparticles.

7.3.1

“Conventional” Albumin Nanoparticles

Several different methods for the preparation of albumin nanoparticles have been described in the literature; however, many of them are modifications of the two basic techniques – emulsification and coacervation or controlled desolvation.

Emulsification is a relatively simple method to prepare albumin particles; however, control of the particle size is difficult. In fact, albumin particles below 500 nm are difficult to obtain by this procedure [46]. On the other hand, coacervation is more versatile and permits a certain control of the particle size, although careful selection of encapsulation conditions and materials is needed to yield high encapsulation efficiencies.

Once albumin particles have been prepared, the carriers have to be stabilized. Two main methods are used in the stabilization of albumin nanoparticles – thermal treatment at elevated temperatures (95–170 °C) or via the use of chemical reagents. This stabilization or “hardening” process affects the biodegradability and stability of nanoparticles and, thus, their drug release properties [40, 47, 48]. In fact, this step is necessary to prolong the *in vitro* and *in vivo* half-life of the resulting albumin nanoparticles [49].

In heat stabilization, albumin particles are hardened by thermal means, rendering the albumin insoluble by formation of interchain amide links between neighboring amino and carboxylic groups of the protein. [50–52]. This method of stabilization is usually associated with the preparation of nanoparticles by emulsification [40, 43, 47, 53]. The major drawback of the heat-stabilization method relates to the fact that during the formation of the particles and the drug-entrapment

Tab. 7.1. Studies describing the preparation of conventional albumin nanoparticles

Type of albumin	Method of preparation	Desolvating agent	Crosslinking agent	Size (nm)	Yield (%)	Reference
BSA	emulsification with ultrasound and chemical stabilization	–	glutaraldehyde	160–2000	7–99	62
BSA	pH coacervation method (pH 5.5) and chemical stabilization	ethanol	glutaraldehyde	225–300	60–80	48, 63, 64
HSA	pH coacervation method (pH 9) and chemical stabilization	acetone	glutaraldehyde	120–135	ND	44
HSA	pH-coacervation method (pH 7–9) and chemical stabilization	ethanol	glutaraldehyde	150–280	66–95	65
HSA	desolvation and chemical stabilization	ethanol	glutaraldehyde	236	ND	66
HSA	pH control and heat treatment	–	–	240	90	67

ND: not determined.

process, the temperature is sometimes very high. Although a higher temperature may be of little consequence for highly stable drugs, it can potentially lead to degradation and loss of drug efficiency.

To alleviate this problem, room-temperature chemical stabilization methodologies have been developed involving the use of formaldehyde [54, 55], glutaraldehyde [46–48, 50, 51, 56–58], 2,3-butadione [54] and, more recently, methyl polyethylene glycol (PEG)-modified oxidized Dextran (Dextranox-MPEG) [59]. Among all these chemicals, glutaraldehyde is the most popular agent for chemical crosslinkage. The reaction between albumin (proteins in general) and glutaraldehyde leads to the coupling of two amino groups located in the same protein molecule or to form bridges between albumin chains [51]. Glutaraldehyde predominantly reacts with the ϵ -amino group on lysine and the N-amino terminal groups of the albumin [47, 60, 61].

Table 7.1 summarizes some of the studies concerning the optimization and preparation of unmodified or conventional albumin nanoparticles.

7.3.1.1 Preparation of Albumin Nanoparticles by Desolvation or Coacervation

The desolvation of albumin with organic solvents followed by chemical crosslinkage is a commonly used method for the preparation of protein nanoparticles. In general, the coacervating agent induces some progressive modifications of the protein's tertiary structure to give an increasingly hydrophobic material, which tends to form submicronic aggregates of desolvated protein (coacervates) [68]. These co-

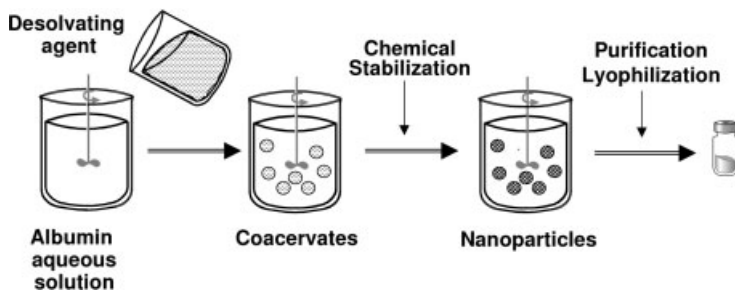


Fig. 7.2. Route for the preparation of albumin nanoparticles by a coacervation method followed by chemical stabilization with glutaraldehyde.

acervates are usually unstable and have to be hardened by physical or chemical crosslinkage. Stabilized coacervates are known as nano- or microparticles depending on their size.

The preparation of albumin nanoparticles by desolvation involves a three-step procedure. In the first step, an unstable dispersed system (coacervates) is obtained by addition of a desolvating agent of albumin (usually, acetone or ethanol) to an aqueous solution of the protein. Then, the coacervates are hardened by thermal stabilization or, more frequently, chemical crosslinkage and, finally, the resulting nanoparticles are purified and lyophilized. Figure 7.2 summarizes this process.

(a) *First step: preparation of albumin coacervates.* Albumin coacervates are obtained from an aqueous solution of the protein and after the addition of a desolvating agent of albumin. Among the different desolvating agents of proteins, acetone and ethanol have been widely employed. The reasons for this selection are their acceptability by pharmaceutical regulations and their easy elimination from the aqueous medium containing the albumin coacervates.

In 1993, Lin et al. described the preparation of HSA nanoparticles using a surfactant-free pH coacervation method [44]. These particles, in a size range between 90 and 250 nm, were prepared by the dropwise addition of acetone to an aqueous albumin solution at pH values between 7 and 9. The size of the resulting nanoparticles appeared to be dependent on the pH and the protein concentration [44].

Another interesting desolvating agent is ethanol. In this case, the addition of ethanol to an aqueous solution of albumin induces the formation of coacervates, whose size increased by increasing the volume of ethanol added up to a ethanol:water ratio of 1.5. Above this ratio, the particle size of albumin coacervates remains constant, but the particle concentration (yield of the process) continues to increase [48, 52]. Similarly, the rate of ethanol addition may influence the width of the particle size distribution – a higher rate of ethanol addition leads to a decrease of the heterogeneity of the albumin coacervates [65].

As a function of the pH and ionic strength of the albumin solution, the appear-

ance of the coacervate changed markedly and it is possible to prepare coacervates with different sizes. Thus, higher pH values lead to smaller nanoparticles; however, the yield of the process decreases [44, 48, 65]. Using acetone as a desolvating agent, the key parameter controlling the size of the resulting nanoparticles appears to be the pH of the medium. It was found that with increasing pH value of the albumin solution, particle size was reduced. This fact can be explained to an increased ionization of the HSA, by increasing the pH of the medium (the isoelectric point of albumin is 5.3) which leads to a repulsion of the albumin molecules and aggregates during particle formation. However, increasing salt concentration of the aqueous solution of the protein induces the formation of large particles. The presence of salts or the use of buffers interferes with the desolvation process. With phosphate buffers (pH 7–8), salt precipitation occurs during desolvation with ethanol. On the contrary, alkaline borate buffers (pH 8–9) or HEPES (pH 7.5) induce the precipitation of albumin in large aggregates [65].

Another important factor affecting the size and yield of nanoparticles produced by desolvation is temperature. Thus, preparation at 4 or 40 °C produces significantly smaller particles than at 20 and 30 °C. In addition, at 30 and 40 °C, clearly more particles are produced than at lower temperatures due to the lower solubility of albumin at higher temperatures under these conditions [52].

(b) *Second step: stabilization of albumin coacervates.* Once albumin coacervates are generated they have to be stabilized to reduce the rate of dissolution of albumin in water. The most popular technique is chemical stabilization with glutaraldehyde. In principle, two factors are important to consider – reagent concentration and duration of the crosslinking process. For the production of stable nanoparticles, the lowest required concentration appears to be at least up to 40% of the theoretical amount of glutaraldehyde that is necessary for the quantitative reaction with the amino groups in the albumin molecule [6, 46, 52]. The crosslinker reacts during variable periods of time ranging from 1 to 24 h. In any case, a large amount of glutaraldehyde or a long reaction time may result in a significant increase in both the size and polydispersion of the resulting nanoparticles [48]. Recently, the chemical stabilization process of albumin nanoparticles was optimized with 1.56 µg glutaraldehyde (mg protein)⁻¹ for 2 h. Under these conditions, no significant differences in the size, polydispersity and yield of albumin coacervates and nanoparticles were observed [63].

Again, the presence of buffers may negatively affect the stabilization process. Thus, the use of a Tris buffer (pH 8–9), characterized by the presence of amino groups, may negatively affect the efficacy of the crosslinking process with glutaraldehyde [65].

Another possibility is thermal stabilization. Chen et al. described the stabilization of HSA microspheres prepared by desolvation in acetone/water mixtures at 75 °C for 15–30 min [69]. Similar results were obtained by Weber et al. preparing albumin nanoparticles by desolvation with ethanol [52].

(c) *Third step: purification.* Purification of nanoparticles for pharmaceutical purposes is mandatory. The addition of sodium metabisulfite can be a good strategy to block unreacted aldehyde groups [70]. Other possibilities are dialysis, gel-

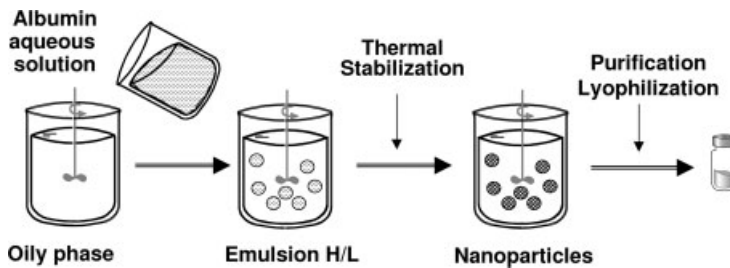


Fig. 7.3. Route for the preparation of albumin nanoparticles by an emulsification method followed by thermal stabilization.

permeation chromatography or, more frequently, subsequent centrifugations to eliminate any remaining protein molecules not transformed onto nanoparticles.

Finally, nanoparticles can be also lyophilized to preserve their physicochemical properties for a long period of time. For lyophilization of albumin nanoparticles, glucose [71], mannose [72] and mannitol [48, 73] have been proposed as cryoprotectors.

In summary, the main advantage of the desolvation process is the absence of toxic organic solvents and its application to the encapsulation of hydrophilic molecules. However, one of the main drawbacks appears to be that there is a close relationship between the size and yield of nanoparticles obtained by this manufacturing method. Therefore, a smaller particle size corresponds to a smaller amount of protein transformed into the nanoparticles.

7.3.1.2 Preparation of Albumin Nanoparticles by Emulsification

Figure 7.3 summarizes a flow diagram of the preparation of albumin nanoparticles by an emulsification technique. For this purpose, an aqueous solution containing the protein is first emulsified in a lipophilic phase (i.e. cotton seed oil or an organic solvent). The two nonmiscible phases are dispersed with the help of high surfactant concentrations and/or energetic stirring procedures (i.e. ultrasounds). Thus, the albumin droplets are thermally stabilized by heating at a temperature higher than 110 °C for a variable period of time (10–30 min) [74, 75]. Then, nanoparticles are centrifuged, washed several times with organic solvents (i.e. diethyl ether or alcohol) and resuspended by sonication to remove residual oil [74, 76, 77].

With respect to emulsion techniques applying serum albumin, a complete and systematic study concerning the influence of protein concentration, emulsification time and power, stirring rate, heat stabilization temperature, and the type of non-aqueous phase was carried out by Gallo et al. [54]. More recently, a method for the preparation of BSA nanoparticles in the sub-200 nm range was described by Müller et al. [62]. In this case the aqueous solution of albumin was injected with a syringe in a solution of organic solvents containing a thickening agent (hydroxypropylcellulose). This emulsion was sonicated and forced to circulate during homogenization through a static mixing device. Finally, nanoparticles were cross-

linked with glutaraldehyde, isolated by centrifugation and washed with *n*-hexane. The emulsification process was carried out in a home-made apparatus, allowing transfer to larger scales [62].

The preparation of nanoparticles by this technique is not easy and involves a number of important drawbacks, including the use of surfactants for emulsion stabilization and the use of organic solvents to eliminate oil residues. In addition, the complete removal of the dispersion agents or oil residues remaining on the particle surface is difficult and time consuming.

7.3.1.3 Other Techniques to Prepare Albumin Nanoparticles

Recently, a new procedure to produce albumin nanoparticles of about 250 nm has been proposed by pH control and heat treatment [67]. In this new procedure, an aqueous solution of albumin at pH 10.65 is heated at 80 °C for a set period. Then, the solution is rapidly cooled to room temperature, the pH of the solution adjusted to 6.04 and the resulting solution stirred for 90 min. Under these conditions, the solution becomes turbid and the albumin nanoparticles are formed.

Another possibility to obtain albumin nanoparticles is by using the sonochemical method. This method was developed by Suslick et al. for the synthesis of non-aqueous liquid-filled microcapsules and air-filled microbubbles [78, 79]. According to this process, the particles are formed by chemically crosslinking cysteine residues of the protein with an HO₂ radical formed around a micrometer-sized gas bubble or a nonaqueous droplet. The chemical crosslinking is responsible for the formation of the albumin particles and is a direct result of the ultrasound radiation on an aqueous medium [80]. However, this technique yields heterogeneous batches with wide size distributions, i.e. between 400 and 2800 nm [81].

7.3.2

Surface-modified Albumin Nanoparticles

The surface of albumin nanoparticles possesses several amino and carboxylic groups which are available for covalent modification and drug or protein attachment [82]. These functional groups can be employed to couple targeting ligands such as primary amines [83], avidin [84] and PEG derivatives [59] as well as to covalently bind a variety of drugs.

An interesting approach to modify the surface of albumin nanoparticles is their association with PEG derivatives (or pegylation). PEGs are one of the most popular polymers for surface modification of colloidal drug carriers. In fact, PEGs were found to reduce interactions of the nanoparticles with the cells of mononuclear phagocyte system (MPS), thereby prolonging nanoparticle circulation in the blood stream after parenteral administration [85–87]. The steric repulsion resulting from a loss of conformational entropy of the bound PEG chains upon the approach of a foreign substance and the low interfacial free energy of PEG in water contribute to the extraordinary physiological properties of nanoparticles covered with PEG [85, 88]. Similarly, PEG grafted to surfaces of biomedical devices showed an increase of their biocompatibility [89, 90].

Concerning the preparation of pegylated albumin nanoparticles, little differences with respect of the preparative methods of conventional nanoparticles are observed. The mode of PEG attachment to these nanoparticles is carried out mainly by covalent grafting [91, 92], which is preferable than simple adsorption because of the higher stability of the resulting PEG layer around particle surface. This covalent attachment can be obtained by either synthesis of the PEG–albumin complex before manufacture of nanoparticles or by direct pegylation during the process of nanoparticle formation. The first attempt to prepare pegylated nanoparticles was developed by Lin et al. [59]. In this case HSA nanoparticles with a size of about 170 nm were prepared by a pH coacervation method, using acetone as desolvating agent and crosslinking with Dextranox-MPEG, which created a sterically stabilizing polyethylene oxide surface layer surrounding the nanoparticles.

Later, this same research group proposed the preparation of surface-modified albumin nanoparticles with PEG–albumin conjugates previously synthesized. Thus, pegylated albumin nanoparticles of around 100–140 nm were prepared from either poly(amidoamine)–PEG copolymer-grafted HSA (HSA–PAA–PEG) or poly(thioetheramido acid)–PEG copolymer-grafted HSA (HSA–PTAAC–PEG). These nanoparticles were produced using a pH coacervation method and cross-linked with glutaraldehyde [93].

In all cases, the existence of a hydrated steric barrier surrounding the nanoparticles was confirmed and these pegylated nanoparticles showed reduced plasma protein adsorption on their surface compared with unmodified particles. However, the use of PEG–albumin conjugates, rather than crosslinkage with Dextranox-MPEG, was more useful to obtain nanoparticles with a sole polyoxyethylene barrier on albumin nanoparticles [94]. More recently, pegylated nanoparticles prepared from mPEG–albumin conjugates have been reported [94]. However, when albumin is modified with mPEG, the amphipatic nature of the PEG molecule confers a higher solubility of albumin–PEG conjugates in organic solvents. This fact makes it difficult to induce coacervation of albumin, and thereby form nanoparticles, by using water miscible solvents. To solve this problem, ethyl acetate was introduced in the coacervation method [94]. Table 7.2 summarizes some of the reported methods to prepare pegylated albumin nanoparticles.

7.3.3

Drug Encapsulation in Albumin Nanoparticles

Albumin particles can load a high variety of drugs; however, the best results are obtained with hydrophilic molecules having high albumin-binding abilities. The association of a given drug or active molecule with albumin nanoparticles can be carried out by simple adsorption to the surface of the freshly prepared nanoparticles or during the process of fabrication of these carriers. In any case, the drug-loading efficiency is significantly influenced by the degree of binding between the drug and the albumin molecule [95, 96]. The higher the degree of binding between drug and the albumin molecules, the greater the loading capacity.

Tab. 7.2. Studies describing the preparation of pegylated albumin nanoparticles

Type of albumin	Method of preparation	Desolvating agent	Crosslinking agent	Size (nm)	Reference
HSA	pH coacervation (pH 9) and chemical stabilization	acetone	Dextranox-mPEG	170	59
HSA-PTAAC-PEG	pH coacervation (NaOH 0.5 M, 10 μ L) and chemical stabilization	acetone	glutaraldehyde	128–130	93
HSA-PAA-PEG	pH coacervation (NaOH 0.5 M, 10 μ L) and chemical stabilization	acetone	glutaraldehyde	106–138	93
HSA-mPEG	coacervation and chemical stabilization	acetone/ ethylacetate	glutaraldehyde	155	94

The incorporation of a drug (or active molecule) into the albumin nanoparticles by adsorption postparticle preparation can be carried out by simple dispersion of nanoparticles in an aqueous solution of the drug. This process is quite simple and has been used to load pilocarpine nitrate [71, 97] or hydrocortisone [70]. The adsorption capacity of molecules on the surface of albumin nanoparticles appears to be dependent on both their polarizability and hydrophobic properties [98]. For diluted solutions of model dyes (as generally used in drug delivery), the adsorption isotherms of these molecules on unloaded albumin particles exhibited Langmuir behavior suggesting monolayer formation in the initial stages of the sorption process. In addition, the amount of dye adsorbed to the surface of albumin particles increased with increasing hydrophobicity [98].

Adsorption and chemical stabilization can also be performed at the same time. Furthermore, in some cases, chemical crosslinkage can be also used to bind the given drug to the surface of albumin nanoparticles. This fact can be of interest to increase the loading capacity of albumin nanoparticles and to obtain more sustained drug release profiles. This strategy was applied for the loading of urokinase [99], ganciclovir (GCV) [48] and interferon- γ [64]. Finally, albumin nanoparticles can be also used as a substrate to covalently bind active molecules by means of other chemical reactions involving different functional groups than that used by glutaraldehyde. This is case for the binding of the chelating agent diethylenetriaminepentaacetic acid [100] and cytochrome *c* [67] to the surface of albumin nanoparticles.

The second possibility consist of simultaneous incubation between the drug and protein before emulsification or desolvation. This strategy was followed for the loading of a number of drugs, including rose Bengal [72], GCV [48], 5-fluorouracil (5-FU) [101], methotrexate [102] and antisense oligonucleotides [63, 103]. An interesting modification of this “incubation step” consist of the use of a complex coacer-

vation method to load DNA. In this case, albumin nanoparticles can be formed by interaction of DNA with albumin in the presence of polyethylenimine (PEI) with the aid of sodium sulfate as a desolvating agent. It is assumed that during complex formation DNA and PEI get entangled into the forming matrix of albumin, thus building up nanoparticles of a spherical shape. The particles were stabilized by using a carbodiimide derivative as crosslinking agent [104]. A more simple method to load oligonucleotides in nanoparticles containing albumin was developed by Vogel et al. [105]. In this case, nanoparticles or proticles (as they were called by the authors) were obtained by simple incubation of protamine, oligonucleotide and albumin in an aqueous solution buffered at pH 7.0.

In general, the incubation method is preferred because it is simpler and gives higher encapsulation efficiencies than the adsorption procedure. Furthermore, this incubation previous to the protein coacervation or emulsification permits the dispersion of drugs or materials with low aqueous solubility and, thus, their incorporation to albumin nanoparticles.

However, the presence of modified albumins or surface “decorated” nanoparticles can also negatively affect the encapsulation or adsorption of the given drug. Thus, Lin et al. reported the lower incorporation of rose Bengal in pegylated nanoparticles when compared with undecorated nanoparticles. This fact appears to be a consequence of the blockage of active binding sites in the albumin molecule by the PEG derivative [72].

7.4

Biodistribution of Albumin Nanoparticles

Few biodistribution or pharmacokinetic studies of albumin nanoparticles have been conducted. In healthy animals, no significant differences in the targeting properties of nanoparticles from albumin or from other materials have been reported. Thus, 15 min after the intravenous injection of a single dose of albumin nanoparticles, around 80% of the given dose was localized in the liver [83]. Figure 7.4 shows the capture of fluorescently labeled albumin nanoparticles for phagocyte cells in the liver. Similarly, no significant differences were found in the distribution of albumin nanoparticles when these carriers were coated to render them with positive, neutral or negative surface charges [83].

Nevertheless, the coating of polymer nanoparticles with albumin has been used as strategy to prevent their rapid clearance by mononuclear phagocyte system *in vitro* [106] and *in vivo* [107, 108]. It appears that albumin coating of nanoparticles may impair the adsorption of other serum proteins, such as opsonins C3b or IgG, that promote the receptor-mediated uptake by phagocyte cells. However, some evidence suggests that albumin, during nanoparticles formation, undergoes conformational changes (unpublished data) and the behavior of albumin nanoparticles would not be comparable with albumin-coated particles.

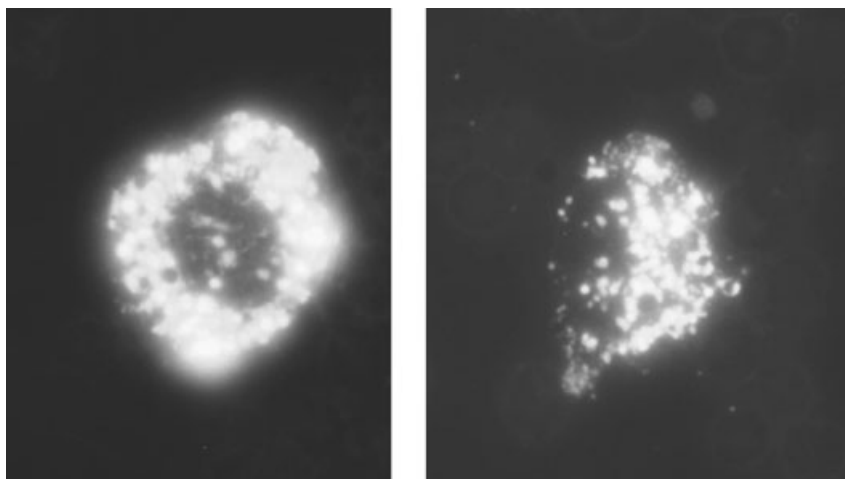


Fig. 7.4. Capture of fluorescently labeled albumin nanoparticles by cells of the MPS in the liver.

Merodio et al. studied the distribution of albumin nanoparticles in a model of multiple sclerosis in order to evaluate the potential of these carriers to cross the blood–brain barrier (BBB) [109]. The BBB is a unique membranous barrier that tightly separates the brain from the circulating blood. The capillaries of the brain and spinal cord lack the small pores and fenestrations of general capillaries, and are sealed with tight junctions [110]. The endothelial cells together with glial cells (i.e. astrocytes and pericytes) and the basal membrane constitute this barrier [111]. The result is a complex obstacle for many drugs. Many neurological disorders are characterized by significant alterations in the BBB, such as Alzheimer’s disease, multiple sclerosis, tumors, cytomegalovirus (CMV) or HIV infections [112].

The pathogenesis of multiple sclerosis includes white and grey mater lesions, myelin breakdown, and active inflammation [113]. The study of this disease was extensively performed with the induction in mice of experimental allergic encephalomyelitis (EAE), which displays similar neurological disorders to those observed in the multiple sclerosis disease [114]. Different strategies have been proposed to target pathological tissues within the central nervous system (CNS), including liposomes [115] and recombinant adeno-associated virus [116]. Similarly, Kumagai et al. proposed that cationized albumin is able to traverse the capillary walls of isolated brain capillaries and can be used for brain delivery [117].

More recently, the distribution of albumin nanoparticles (of about 300 nm) in the EAE animal model was carried out [109]. These nanoparticles were administered intraperitoneally, and 4 h after their administration were localized in the damaged and inflamed areas of the CNS, mainly in the lumbar portion of the spinal cord, the optic chiasma or the cerebellar lobules [109]. Immunohistochemical

studies revealed that circulating macrophages, which migrate to the damaged areas within the CNS, and resident activated microglial cells were involved in the distribution of albumin nanoparticles.

7.5

Pharmaceutical Applications

Albumin micro- and nanoparticles have a wide range of biomedical applications, including their use as diagnostic agents, oligonucleotide and DNA delivery, cancer treatment, and ocular drug delivery.

7.5.1

Albumin Nanoparticles for Diagnostic Purposes

Albumin nanoparticles have been proposed for imaging purposes because of a number of advantages, including their increased stability, prolonged *in vivo* half-life, reduction of possible adverse effects, concentration of the agent resulting in lower doses and ease of administration [118]. Their main uses are as radiopharmaceuticals and echo-contrast agents.

7.5.1.1 Radiopharmaceuticals

One of the first attempts to use albumin nanoparticles as diagnostic tools was carried out by Scheffel et al. in 1972 [76]. In this case, ^{99m}Tc -labeled albumin nanoparticles (of about 0.3–1 μm size) were successfully used to visualize the liver and spleen by measuring gamma-rays coming from the isotope with a gamma camera [76]. Later, albumin nanoparticles were proposed for the study of the lymphatic system and identify sentinel nodes in breast cancer [119]. The sentinel node procedure for breast cancer allows for accurate staging of the axilla, while axillary node dissection can be avoided in patients with no sentinel node metastasis [120]. For this purpose, the radioactive tracers most commonly used are ^{99m}Tc sulfur colloid (US) and ^{99m}Tc -labeled albumin nanoparticles (Europe) [121]. They are distinctly different in size, and the smaller albumin nanoparticles show earlier retention and higher uptake into the sentinel nodes [122]. Nevertheless, both have been shown to be more effective in the identification of these nodes than microparticles, which show a tendency to remain in the injection site and a lower ability to enter into the lymphatic system [123, 124]. In addition, with albumin nanoparticles the subdermal/intradermal injection appears to be a reliable alternative [125, 126]. These albumin nanoparticles appear also to be effective in the diagnosis of melanoma [127], head and neck squamous cell carcinoma [128], and cervical cancer [129]. Finally, it is interesting to note that these radiopharmaceutical agents have also been proposed for the treatment of solid cancers [130, 131].

7.5.1.2 Echo-contrast Agents

Albumin nanoparticles, containing very small amounts of gas, are adequate echo-contrast agents [80, 132, 133]. These particles are prepared by sonication and can be used as an ultrasound contrast agent in echocardiography for the diagnosis of cardiac disease [134] and monitoring of myocardial perfusion [132, 135]. Two-dimensional contrast echocardiography uses the reflection of ultrasound to image heart tissue *in vivo*. To enhance image quality, a solution containing micro- or nanobubbles of albumin (size lower than 10 μm) may be injected intravenously to perfuse the cardiovascular system; these bubbles change the acoustic impedance of the blood flow, resulting in dramatically improved echo contrast with the surrounding tissues [136].

7.5.2

Albumin Nanoparticles as Carriers for Oligonucleotides and DNA

Antisense oligonucleotides are very potent drugs for the treatment of important diseases such as oncogene-related cancers or viral infections. Although antisense therapy provides a level of selectivity not available with traditional drugs, their therapeutic potential is currently hampered by their poor biological stability, limited cellular uptake and the poor cytoplasm delivery, where they have to reach their complementary targets. The use of colloidal carriers is a possible strategy to circumvent both stability and permeability problems. Cationic lipids and liposomes have been the most widely exploited, as long as polyanionic oligonucleotides interact spontaneously with positive molecules. However, they are toxic and show instability in presence of serum. Biodegradable nanoparticles made of several types of polymers have been also studied, i.e. polylactic acid (PLA)–PEG, poly(alkylacrylates), chitosan or alginates. Several groups have reported the advantages of using albumin nanoparticles as carriers for oligonucleotides, as compared with other types of polymers [63, 103, 137, 138]. Apart from protecting unmodified oligonucleotides from degradation [63, 138] and improving the cellular uptake [103] protein nanoparticles were able to load appreciable amounts of oligonucleotides without additional positive components [63]. What is more, albumin nanoparticles not only improved the cellular uptake of the oligonucleotides, but led to a significant accumulation of the oligonucleotide in the cytosol compartment of cells, in the absence of endosomolytic agents [103, 138].

The rationale for using albumin nanoparticles for cytoplasmic delivery of oligonucleotides is supported by the spontaneous interaction between these molecules and the protein as well as the fusogenic activity of albumin at low pH. Plasma albumin is their endogenous carrier that governs their transport and tissue distribution. Srinivanan et al. [139] (for HSA) and Arnedo et al. [137] determined values of binding constants that confirmed the high affinity between the protein and the oligonucleotides. It seems that the oligonucleotides bind to site I within the albumin [139]. The affinity was affected by the presence of other molecules associated to the protein (e.g. fatty acids). Also, the length and nature of the backbone in the

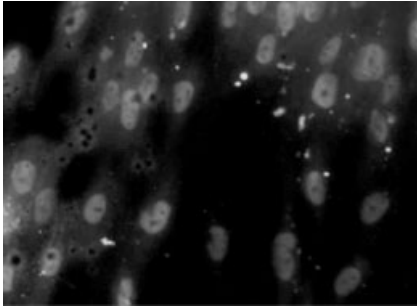


Fig. 7.5. Effect of albumin nanoparticles on the subcellular distribution pattern of a fluorescent phosphodiester oligonucleotide loaded in albumin nanoparticles after 24 h incubation time at 37 °C with MRC-5 fibroblasts.

oligonucleotides and the drug/albumin ratio had an influence in the stoichiometry of the interaction [103, 137, 139]. The consequence was that albumin nanoparticles were able to load oligonucleotides by simple incubation between the protein and the polyanions before desolvation, and further crosslinking of the protein coacervates with glutaraldehyde [63, 103]. Also, the adsorption of the oligonucleotides onto preformed nanoparticles was possible [63] and mainly addressed by electrostatic interactions. In addition, albumin nanoparticles encapsulated modified oligonucleotides with more efficiency than unmodified ones in accordance with a higher binding affinity of the native protein with a phosphorotioate backbone [103, 138].

The influence of albumin nanoparticles in cellular uptake and further intracellular distribution has also been evaluated. With an unmodified oligonucleotide Arnedo et al. [138] observed that albumin nanoparticles delayed and decreased the uptake of the oligonucleotide in MRC-5 cells. More important was the effect of albumin nanoparticles in the pattern of intracellular distribution of the oligonucleotide, from a punctate pattern for being concentrated in vesicular compartments to a more diffused cytoplasmic distribution [66, 103, 138]. Figure 7.5 shows this distribution of albumin nanoparticles within the cytoplasm of fibroblasts. This modification in the pattern of intracellular distribution was attributed to fusogenic properties of albumin at low pH, as previously tested in artificial systems with liposomes [140]. Figure 7.6 summarizes the proposed mechanism for the cell internalization and transport of antisense oligonucleotides by albumin nanoparticles.

The oligonucleotides are small molecules that bind to site I in the molecule of native albumin, DNA forms a complex much better with cationized albumin [141]. The system was less toxic than other positive molecules [142], but also it was unable to transfect cells. More frequently, the native protein has been co-associated to DNA-PEI complexes [104] or DNA-protamine lipoplexes [143, 144]. The presence of albumin stabilized the complexes through a decrease in their positive charge that prevented their aggregation in the presence of serum. With similar stabilization role, albumin was also incorporated into oligonucleotide-protamine particles [105].

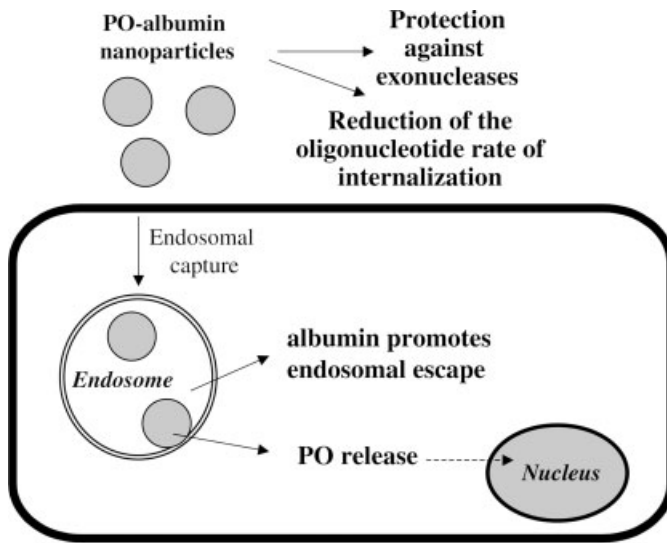


Fig. 7.6. Proposed mechanism of the protective effect of albumin nanoparticles on the cell internalization and transport of antisense oligonucleotides (PO).

7.5.3

Albumin Nanoparticles in the Treatment of Cancer

Albumin nanoparticles have been proposed as carriers for different antitumor drugs, including 5-FU, methotrexate and paclitaxel.

7.5.3.1 Fluorouracil and Methotrexate Delivery

The use of albumin nanoparticles of about 660 nm containing 5-FU for cancer chemotherapy was investigated several years ago [145–147]. Upon intravenous injection into healthy mice, the nanoparticles were found accumulated in the liver and other elements of the MPS. However, when nanoparticles were injected intraperitoneally in Ehrlich ascites carcinoma-bearing mice, phagocytosis of the albumin carriers by tumoral cells was observed and suppression of tumor growth was noted [146]. Furthermore, following injection of multiple doses of 5-FU-loaded albumin nanoparticles, the lifespan of the mice increased by about 30% compared to a control treatment with the free drug [146]. More recently, a similar formulation of 5-FU-loaded albumin nanoparticles (size about 640 nm) was found effective in mice with a 2-fold increase in the antitumor activity of this drug compared with a free 5-FU solution [101]. Another interesting work concerns the ability of sodium alginate–BSA nanoparticles to increase the oral bioavailability of 5-FU. These carriers (about 170 nm) were able, after oral administration, to enter into the circulation and target the tissues rich in phagocytes, such as the liver and spleen [148].

However, albumin nanoparticles induced a markedly different biodistribution of

methotrexate when administered in animals by an intravenous route [102]. In fact, the incorporation of this drug in albumin nanoparticles increased its accumulation in the lungs of animals [102].

7.5.3.2 Paclitaxel Delivery

The more interesting and complete studies of the potential of albumin nanoparticles to deliver antitumor drugs have been carried out with paclitaxel. Paclitaxel (Taxol[®]) is used extensively in the treatment of breast cancer [149], and, due to its low aqueous solubility, is currently formulated with ethanol and the nonionic surfactant Cremophor EL (polyoxyethylated castor oil) to enhance drug delivery [150]. However, these excipients may contribute to the side-effects associated with the use of paclitaxel, ultimately reducing the quality of life in patients undergoing treatment. Cremophor may contribute to side-effects induced by paclitaxel, as well as the hypersensitivity reactions that occur in 25–50% of patients during infusion that require premedication with histamine blockers and glucocorticoids [151]. Furthermore, the formulation including Cremophor and ethanol leaches plasticizers from PVC bags and infusion sets, resulting in the need for preparation and administration of paclitaxel in glass bottles or non-PVC infusion systems [152].

In order to overcome these drawbacks and to increase its antitumor efficacy, paclitaxel was covalently bound to albumin nanoparticles. This new formulation of about 150 nm allows for a higher concentration of paclitaxel, resulting in a decreased infusion volume and time, and does not require nonstandard infusion sets [149, 153]. In animal models, paclitaxel–albumin nanoparticles resulted in increased delivery of chemotherapeutic drugs to the tumor compared with solvent-based drugs. The mechanism for this advantage is being actively studied and may be related to albumin-activated transport of molecules into tissues by binding to the gp60 albumin receptor on blood vessels with subsequent accumulation of albumin nanoparticles in tumors [154].

In metastatic breast cancer, a pivotal randomized controlled phase III clinical trial was recently completed comparing the safety and efficacy of 260 mg m⁻² of paclitaxel–albumin nanoparticles versus paclitaxel injection (Taxol) at a dose of 175 mg m⁻². Despite a 50% higher dose of chemotherapy infused over 30 min without premedication for hypersensitivity, paclitaxel–albumin nanoparticles were well tolerated and provided better results than the conventional formulation [154, 155]. In January 2005, the FDA approved this new albumin nanoparticle formulation (Abraxane[™]) for metastatic breast cancer [156].

Paclitaxel-loaded albumin nanoparticles have also been proved to be effective in the treatment of squamous carcinomas of the head and neck, uterus, and anal canal. In phase I/II studies, complete pathological responses occurred in 1.16, 20 and 18.8% of patients, respectively [157, 158]. In another study, the intra-arterial infusion of paclitaxel incorporated into human albumin nanoparticles for use as induction chemotherapy before definitive treatment of advanced squamous cell carcinoma of the tongue proved to be reproducible and effective to preserve this organ [159]. In fact, 78% of the treated patients had a clinical and radiological objective response (complete, 26%; partial, 52%) and only 9% showed disease progression.

Another interesting attempt concerning the delivery of paclitaxel is its association with pegylated albumin nanoparticles. Due to their low interaction and recognition by the MPS, these pegylated carriers appear to be of interest to passively target inflamed regions within the body, including the CNS and the colon [160].

7.5.3.3 Albumin Nanoparticles in Suicide Gene Therapy

In recent years, suicide gene therapy has been proposed for the treatment of a number of cancers. This therapy implies the use of suicide genes that code for enzymes which can transform a prodrug into a cytotoxic product [161]. Thus, the tumoral cell is rendered sensitive to a type of chemotherapy which is relatively nontoxic for the rest of the body [162]. In this context, the therapeutic combination of the herpes virus thymidine kinase (HSV-tk) and GCV has shown great clinical promise as gene therapy for the treatment of a number of cancers including hepatocarcinoma [163], neuroblastoma [164], ovarian [165], pancreatic [166] and prostate cancers [167]. The viral transfection can be carried out by adenoviruses [162, 163, 165, 166] and the expression of this gene in the cell yields the enzyme that converts the nontoxic prodrug GCV into a highly toxic metabolite [168].

In a recent work, the ability of albumin nanoparticles to concentrate GCV in the hepatocytes evidenced by the increase in the antitumoral efficacy of the HSV-tk/GCV combination [169]. In this work, mice were previously treated with 4×10^{10} pfu kg^{-1} adenovirus (AdCMV-tk) by intravenous administration and 48 h later received the GCV treatment. The use of albumin nanoparticles demonstrated a higher ability to concentrate this drug in the liver of animals as compared with the conventional formulation. In addition, the histologic analysis of the liver also revealed great cellular damage in terms of necrotizing area and perivascular inflammatory reactions (Fig. 7.7). It seems that the greater and more prolonged hepatic concentration of GCV released from the nanoparticles led to the accumulation of the toxic metabolite of GCV in the liver. These nanoparticulate carriers offered the additional advantage of increasing the plasma half-life of the drug and its tissue distribution, as determined by the pharmacokinetic analysis [169]. There-

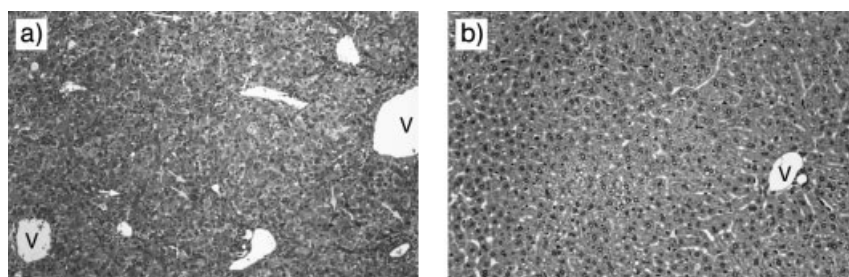


Fig. 7.7. (a) Liver section from mice that were treated with 4×10^{10} pfu kg^{-1} AdCMV-tk and, 48 h later, received GCV-loaded albumin nanoparticles. (b) Liver section of a nontreated mouse. Hematoxylin & eosin dye; magnification: $\times 100$. Green arrows: ballooning and acidophilic bodies; yellow arrow: apoptotic bodies; V: vessel. (From Ref. [169].)

fore, the use of these nanoparticles permits a higher distribution to the liver, which can be of interest to decrease the drug dose and frequency of administration.

7.5.4

Magnetic Albumin Nanoparticles

Magnetic drug delivery by particulate carriers is a very efficient method of delivering a drug to a localized disease site. Very high concentrations of chemotherapeutic or radiological agents can be achieved near the target site, such as a tumor, without any toxic effects to normal surrounding tissue or to the whole body [170]. It is thus possible to replace large amounts of freely circulating drug with much lower amounts of drug targeted magnetically to localized disease sites, reaching effective and up to several-fold increased localized drug levels [55, 74, 171, 172].

In magnetically targeted therapy, a cytotoxic drug is attached to a biocompatible magnetic nanoparticle carrier (size in the range of 10–500 nm), such as albumin-coated magnetite [170]. When the particles are administered intravenously, external, high-gradient magnetic fields are used to concentrate the complex at a specific target site within the body. The process of drug localization is based on the competition between forces exerted on the particles by the blood compartment and magnetic forces generated from the magnet, i.e. the applied field. When the magnetic forces exceed the linear blood flow rates in arteries (10 cm s^{-1}) or capillaries (0.05 cm s^{-1}), the magnetic particles are retained at the target site and may be internalized by the endothelial cells of the target tissue [173, 174]. The drug can be released from drug/carrier either via enzymatic activity or changes in physiological conditions such as pH, osmolality or temperature [175] and be taken up by the tumor cells. This system, in theory, has major advantages over the normal, non-targeted methods of cytotoxic drug therapy.

The use of magnetic particles for the treatment of liver cancer was proposed for the first time at the end of the 1970s by Widder et al. The intra-arterial injection of these particles containing ultrafine ferroferric oxide and a prototype drug, doxorubicin hydrochloride, in the same target site resulted in 100-fold higher dose compared to free doxorubicin administered intravenously [78, 176–178]. Since those studies, success in cytotoxic drug delivery and tumor remission has been reported by several groups using animals models including pigs [179, 180], rabbits [175] and rats [181]. This technique has also been employed to target cytotoxic drugs to brain tumors [182]. More recently, magnetic albumin nanoparticles containing adriamycin have shown their ability to target a malignant liver tumor in rats [183]. In the presence of the magnetic field, these albumin nanoparticles accumulate in the liver tumor rather than in the normal tissue. Even if the magnetic field is not applied, magnetic albumin nanoparticles in tumor tissues still increase to 2.8 times that of normal liver tissues. In addition, the authors report that, in the presence of magnetic fields, these albumin nanoparticles may drive the drug to the tumoral tissues, preserving normal organs against exposure to chemotherapeutic drugs [183].

7.5.5

Albumin Nanoparticles for Ocular Drug Delivery

7.5.5.1 Topical Drug Delivery

Ocular administration is associated with rapid elimination of drug formulations from the precorneal area due to drainage through the naso-lacrimal duct and dilution by tear turnover. These processes result in a very low percentage of the drug administered (less than 5%) that could penetrate through the cornea and reach the intraocular tissues. Many studies have demonstrated an enhanced accumulation of nanoparticles in the conjunctival cul-de-sac and better drug bioavailability compared to conventional ophthalmic dosage forms, such as solutions and ointments [184, 185]. The colloidal systems can be administered as simple eye drops and, due to their low viscosity, minimize the temporary hindrance of the patient sight. The frequency of application could be reduced due to sustained drug delivery from the nanoparticle matrix.

Albumin nanoparticles have proved effective for the administration of pilocarpine and hydrocortisone in the interior of the eye [70, 72, 186]. In inflamed conjunctiva, the application of hydrocortisone-coated albumin nanoparticles (size between 100 and 300 nm) led to a higher drug bioavailability than the reference solution, which was rapidly eliminated by lacrimation. In addition, the albumin particles were more efficiently retained at the inflamed area than the normal conjunctiva. Consequently, in the inflamed eye, hydrocortisone-loaded nanoparticles enabled targeting to the precorneal area away from the inner segments of the eye [70].

Similarly, pilocarpine-coated albumin nanoparticles dramatically increased the ocular bioavailability of the drug compared with a reference solution [71]. The association of albumin nanoparticles with bioadhesive polymers was proved effective to increase the residence time of nanoparticles in contact with the eye and, thus, increase drug bioavailability [97]. In the presence of bioadhesives, the nanoparticles induced a significant improved pharmacological response in rabbits (i.e. miotic activity and reduction in the intraocular pressure) when compared with particle dispersions in buffer or free solutions. The best results were obtained with the association of albumin nanoparticles with either bovine submaxillary mucin or carbopol. This fact was due to the higher interaction of these bioadhesive polymers with both nanoparticles and precorneal mucus than other viscosity-enhanced polymers [97].

7.5.5.2 Intravitreal Drug Delivery

Another problem associated with the treatment of ocular pathologies is the difficulty for a given drug, topically administered, to absorb and reach therapeutic concentrations in the inner tissues of the eye for prolonged periods of time. Sometimes, when chronic treatment is necessary, local intravitreal administration becomes necessary. However, due to the short half-life of the given drugs, frequent injections are necessary to maintain the therapeutic levels. These continuous ad-

ministrations increase the risk of cataracts, retinal detachments, hemorrhages or endophthalmitis [187, 188].

Human CMV (HCMV) is a member of the Herpesviridae family of viruses, which are large DNA viruses that share biological properties of latency and reactivation [189]. In patients with AIDS and those immunocompromised due to hematopoietic stem cell transplantation or solid organ transplantation, HCMV is a major cause of morbidity and mortality [189, 190]. HCMV infections are the major cause of visual loss in these patients. Thus about 20–25% of patients with AIDS develop CMV retinitis during the course of their illness [191]. Without treatment this necrotizing retinitis progresses, resulting in irreversible blindness [192]. In cardiac and liver transplant patients, HCMV infection doubles the 5- and 3-year rates of graft failure, respectively [193]. In the absence of antiviral prophylaxis, symptomatic infections occur in approximately 39% of heart/lung recipients, 25% of heart transplants, 29% of liver transplants and 8% of patients receiving renal transplants [194].

For the treatment of HCMV retinitis, local intravitreal therapy with different antivirals is currently used. In this context, albumin nanoparticles have been proposed as carriers for intravitreal controlled delivery of diethylenetriaminepentaacetic acid (DTPA) [100], GCV [48, 73, 195] and the antisense oligonucleotide fomivirsen [138]. In all cases, these carriers allowed significant increases of the anti-HCMV activity of the loaded drug *in vitro*. These results of antiviral activities seemed to be directly correlated to drug internalization by infected cells [73, 100, 138]. For DTPA-loaded nanoparticles, it appears that these particles were internalized by UKF-NB-3 cells and HFF. This cellular uptake mediated by the drug carrier systems may explain the increased anti-HCMV and cytotoxic effects of DTPA coupled to protein-based drug carrier systems. Another interesting key point is that the improvement of the antiviral activity of GCV when loaded in albumin nanoparticles was not related to any cytotoxic effect on fibroblasts or corneal cells [73].

In order to study the distribution and toxicity of albumin nanoparticles within the eye, these carriers were dispersed in saline and administered to laboratory animals by the intravitreal route [196]. Two weeks after the single injection, a large portion of the administered dose appeared to be localized, quite broadly distributed, overlying the inferior portion of this cavity (see Fig. 7.8). However, some minor fractions were also located in the iris and ciliary body, which can be explained by the higher porosity of these ocular organs and, probably also, by an elimination mechanism of the particles via the ophthalmic anterior chamber. This route of elimination has been described for macromolecules and takes several days to be completed [197]. However, the histological evaluation of the different ocular tissues suggested that albumin nanoparticles are well tolerated after their intravitreal injection. These analyses were confirmed by the absence of cellular infiltrations following the association of the nanoparticles to ocular cells. In addition, no sign of degeneration of the eye receptors was observed [196]. In all cases, the retina kept its cytoarchitecture, with no signs of alteration in the photoreceptor and neuronal

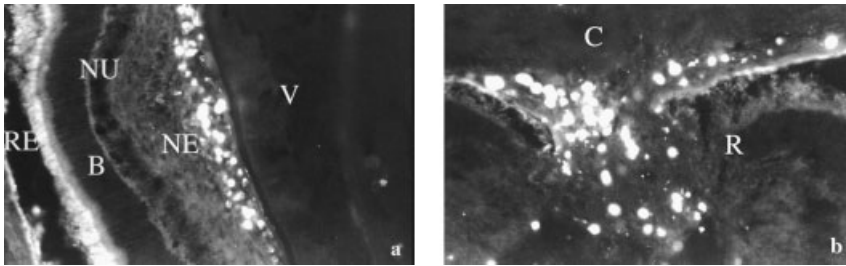


Fig. 7.8. Immunofluorescence detection of albumin nanoparticles by streptavidin–FITC staining 2 weeks after their injection in the vitreous cavity (a) and in the blood–aqueous barrier adjacent area and ciliary muscle (b).

Total magnification: $\times 200$. B: Bacillary layer; C: ciliary muscle; NE: neuronal interplay area; NU: outer and inner nuclear layers; R: retina; RE: retinal epithelium; V: vitreous cavity. (From Ref. [196].)

layers of the retina. Finally, immunohistochemistry studies also confirmed the lack of ability of albumin nanoparticles to generate autoimmune phenomena, which can stimulate the generation of pathogenic immune responses such as “retinitis pigmentosa” [198] and autoimmune uveoretinitis [199]. In summary, albumin nanoparticles appear to be safe carriers for the intravitreal delivery of drugs.

7.6

Concluding Remarks

This chapter summarizes the preparation and main applications of albumin nanoparticles for pharmaceutical purposes. The use of albumin nanoparticles can offer a number of advantages, including their biodegradability, and the simplicity of preparation in an aqueous environment without the need for harmful solvents and chemicals. Furthermore, the inherent ability of albumin to spontaneously bind a high variety of molecules facilitates their loading in the resulting nanoparticles. In addition, drugs or ligands can also be easily bound to the protein and, thus, modify the surface properties of the resulting nanoparticles. All of these possibilities make albumin nanoparticles versatile carriers for pharmaceutical purposes.

Albumin nanoparticles are currently used as diagnostic tools and as adjuvants to improve the efficacy of the treatment with paclitaxel. However, in the future, the possibility exists that albumin nanoparticles may offer adequate solutions to some pharmaceutical problems such as the delivery of antisense oligonucleotides (and DNA) and the targeting of the CNS for the adequate treatment of neurological disorders.

References

- 1 OSBORNE, T. B., *The Proteins of the Wheat Kernel*. Publication 84, Carnegie Institute, Washington, DC, 1907.
- 2 SHEWRY, P. R., TATHAM, A. S., FORDE, J., KREIS, M., MIFLIN, B. J., The classification and nomenclature of wheat gluten proteins: a reassessment. *J. Cereal Sci.* **1986**, *4*, 97–106.
- 3 CHUANG, V. T., KRAGH-HANSEN, U., OTAGIRI, M., Pharmaceutical strategies utilizing recombinant human serum albumin, *Pharm. Res.* **2002**, *19*, 569–577.
- 4 PETERS, T., Serum albumin, *Adv. Protein Chem.* **1985**, *37*, 161–245.
- 5 KRAGH-HANSEN, U., Structure and ligand binding properties of human serum albumin, *Dan. Med. Bull.* **1990**, *37*, 57–84.
- 6 CARTER, D. C., HO, J. X., Structure of serum albumin, *Adv. Protein Chem.* **1994**, *45*, 152–203.
- 7 PETERS, T. JR., *All about Albumin: Biochemistry, Genetics and Medical Applications*, Academic Press, San Diego, CA, 1996.
- 8 ERSTAD, B. L., CAMPBELL, D. J., ROLLINS, C. J., RAPPAPORT, W. D., Albumin and prealbumin concentrations in patients receiving post-operative parenteral nutrition, *Pharmacotherapy* **1994**, *14*, 458–462.
- 9 COLGAN, K., Responsible use of blood products in response to supply and demand, *Pharmacotherapy* **2000**, *57*, 2094–2098.
- 10 FLECK, A., SMITH, G., Albumin in intensive care, *Br. J. Intensive Care* **1998**, *8*, 93–95.
- 11 WILKES, M. M., NAVICK, R. J., Albumin verses hydroxyethyl starch in cardiopulmonary bypass surgery: a meta-analysis of postoperative bleeding, *Ann. Thorac. Surg.* **2001**, *72*, 527–534.
- 12 KESHAVJEE, S., Medicine and money: the ethical transformation of medical practice, *Med. Educ.* **2004**, *38*, 271–275.
- 13 WEIJERS, R. N. M., Amino acid sequence in bovine serum albumin, *Clin. Chem.* **1977**, *23*, 1361–1362.
- 14 SQUIRE, P. G., MOSER, P., O'KONSKI, C. T., The hydrodynamic properties of bovine serum albumin monomer and dimer, *Biochemistry* **1968**, *7*, 4261–4272.
- 15 WRIGHT, A. K., THOMPSON, M. R., Hydrodynamic structure of bovine serum albumin determined by transient electric birefringence. *Biophys. J.* **1975**, *15*, 137–141.
- 16 BLOOMFIELD, V., The structure of bovine serum albumin at low pH, *Biochemistry* **1966**, *5*, 684–689.
- 17 BENDEDOUCH, D., CHEN, S. H., Structure and interparticle interactions of bovine serum albumin in solution studied by small-angle neutron scattering. *J. Phys. Chem.* **1983**, *87*, 1473–1477.
- 18 FENG, L., HU, C. Z., ANDRADE, J. D., Scanning tunneling microscopic images of adsorbed serum albumin on highly oriented pyrolytic graphite, *J. Colloid Interface Sci.* **1988**, *126*, 650–653.
- 19 BOS, O. J. M., LABRO, J. F. A., FISCHER, M. J. E., WITLING, J., JANSSEN, L. H. M., The molecular mechanism of the neutral-to-base transition of human serum albumin, *J. Biol. Chem.* **1989**, *264*, 953–959.
- 20 CARTER, D. C., HE, X. M., MUNSON, S. H., TWIGG, P. D., GERNERT, K. M., BROOM, M. B., MILLER, T. Y., Three-dimensional structure of human serum albumin, *Science* **1989**, *244*, 1195–1198.
- 21 BROWN, J. R., Serum albumin, amino acid sequence. In *Albumin: Structure, Function and Uses*, ROSENOER, V. M., ORAZ, M., ROTSHILD, M. A. (Eds.), Pergamon Press, Oxford, 1977, pp. 27–51.
- 22 YAMAZAKI, M., YANO, H., AOKI, K., Differential scanning calorimetric studies on bovine serum albumin: I. Effects of pH and ionic strength, *Int. J. Biol. Macromol.* **1990**, *12*, 263–268.
- 23 MURAYAMA, K., TOMIDA, M., Heat-induced secondary structure and

- conformation change of bovine serum albumin investigated by Fourier transform infrared spectroscopy, *Biochemistry* **2004**, *43*, 11526–11532.
- 24 SUGIO, S., KASHIMA, A., MOCHIZUKI, S., NODA, M., KOBAYASHI, K., Crystal structure of human serum albumin at 2.5 Å resolution, *Protein Eng.* **1999**, *12*, 439–446.
 - 25 WETZEL, R., BECLER, M., BEHLKE, J., BILLWITZ, H., BOHM, S., EBERT, B., HAMAN, H., KRUMBIEGEL, J., LASSMANN, G., Temperature behavior of human serum albumin, *Eur. J. Biochem.* **1980**, *104*, 469–478.
 - 26 GALLER, J., RIVET, P., DE CERTAINES, J., ¹H- and ²H-NMR study of bovine serum albumin solutions, *Biochim. Biophys. Acta* **1987**, *915*, 1–18.
 - 27 SHIMADA, K., CHEFTEL, J. C., Sulfhydryl group/disulphide bond interchange reactions during heat induced gelation of whey protein isolate, *J. Agric. Food Chem.* **1988**, *37*, 161–168.
 - 28 TAKEDA, K., WADA, A., YAMAMOTO, K., MORIYAMA, Y., AOKI, K., Conformational change of bovine serum albumin by heat treatment, *J. Protein Chem.* **1989**, *8*, 653–659.
 - 29 ZIEGLER, G. R., FOEGEDING, E. A., The gelation of proteins, *Adv. Food Nutr. Res.* **1990**, *34*, 203–298.
 - 30 ROEFS, S. P. F. M., DE KRUIF, K. G., A model for the determination and aggregation of beta-lactoglobulin, *Eur. J. Biochem.* **1994**, *226*, 883–889.
 - 31 PRINSEN, B. H., DE SAIN-VAN DER VELDEN, M. G., Albumin turnover: experimental approach and its application in health and renal diseases. *Clin. Chim. Acta* **2004**, *347*, 1–14.
 - 32 DOWEIKO, J. P., NOMPLEGGI, D. J., Role of albumin in human physiology and pathophysiology, *J. Parenteral Enteral Nutr.* **1991**, *15*, 207–211.
 - 33 QUAGLIARELLO, V. J., MA, A., STUKENBROK, H., PALADE, G. E., Ultrastructural localization of albumin transport across the cerebral microvasculature during experimental meningitis in the rat, *J. Exp. Med.* **1991**, *174*, 657–672.
 - 34 MINAGAR, A., ALEXANDER, J. S., Blood–brain barrier disruption in multiple sclerosis, *Multiple Sclerosis* **2003**, *9*, 540–549.
 - 35 FIGGE, J., ROSSING, T. H., FENCL, V., The role of serum proteins in acid–base equilibria. *J. Lab. Clin. Med.* **1991**, *117*, 453–467.
 - 36 LAIHO, K., Albumin as a marker of plasma transudation in experimental skin lesions. *Int. J. Legal Med.* **2004**, *118*, 282–288.
 - 37 STAMLER, J. S., JARAKI, O., OSBORNE, J., SIMON, D. I., KEANEY, J., VITA, J., SINGEL, D., VALERI, C. R., LOSCALZO, J., Nitric oxide circulates in mammalian plasma primarily as a S-nitroso adduct of serum albumin, *Proc. Natl Acad. Sci. USA* **1992**, *89*, 7674–7677.
 - 38 MURAVSKAYA, E. V., LAFKO, A. G., MURAVSKII, V. A., Modification of transport function of plasma albumin during atherosclerosis and *diabetes mellitus*, *Bull. Exp. Biol. Med.* **2003**, *135*, 433–435.
 - 39 CLARK, A. H., JUDGE, F. J., RICHARDS, J. B., STUBBS, J. M., SUGGETT, A., Electron microscopy of network structures in thermally-induced globular protein gels, *Int. J. Peptide Protein Res.* **1981**, *17*, 380–392.
 - 40 MORIMOTO, Y., FUJIMOTO, S., Albumin microspheres as drug carriers, *Crit. Rev. Ther. Drug Carrier Syst.* **1985**, *2*, 19–63.
 - 41 RUBINO, O. P., KOWALSKY, R., SWARBRICK, J., Albumin microspheres as a drug delivery system: relation among turbidity ratio, degree of cross-linking, and drug release, *Pharm. Res.* **1993**, *10*, 1059–1065.
 - 42 RHODES, B. A., ZOLLE, I., BUCHANAN, J. W., WAGNER, H. N. JR., Radioactive albumin microspheres for studies of the pulmonary circulation, *Radiology* **1969**, *92*, 1453–1460.
 - 43 MACADAM, A. B., SHAFI, Z. B., JAMES, S. L., MARRIOTT, C., MARTIN, G. P., Preparation of hydrophobic and hydrophilic albumin microspheres and determination of surface carboxylic acid and amino residues, *Int. J. Pharm.* **1997**, *151*, 47–55.
 - 44 LIN, W., COOMBES, A. G. A., DAVIES,

- M. C., DAVIS, S. S., ILLUM, L., Preparation of sub 100 nm human serum albumin nanospheres using a pH-coacervation method, *J. Drug Target.* **1993**, *1*, 237–243.
- 45 GESELOWITZ, D. A., NECKERS, L. M., Bovine serum albumin is a major oligonucleotide-binding protein found on the surface of cultured cells, *Antisense Res Dev.* **1995**, *5*, 213–217.
- 46 ROSER, M., KISSEL, T., Surface-modified biodegradable nano- and microspheres. I. Preparation and characterization, *Eur. J. Pharm. Biopharm.* **1993**, *39*, 8–12.
- 47 LEE, T. K., SOKOLOSKI, T. D., ROYER, G. P., Serum albumin beads: an injectable, biodegradable system for the sustained release of drugs, *Science* **1981**, *213*, 233–235.
- 48 MERODIO, M., ARNEO, A., RENEDE, M. J., IRACHE, J. M., Ganciclovir-loaded albumin nanoparticles: characterization and *in vitro* release properties. *Eur. J. Pharm. Sci.* **2001**, *12*, 251–259.
- 49 ARSHADI, R., Albumin microspheres and microcapsules: methodology of manufacturing techniques, *J. Controlled Rel.* **1990**, *14*, 111–131.
- 50 WEITZEL, R., BECKER, M., BEHLKE, J., BILLWITZ, H., BOHM, S., EBERT, B., HAMANN, H., KRUMBIEGEL, J., LASSMANN, G., Temperature behavior of human serum albumin, *Eur. J. Biochem.* **1980**, *104*, 469–478.
- 51 BURGESS, D. J., DAVIS, S. S., TOMLINSON, E., Potential use of albumin microspheres as a drug delivery system. I. Preparation and *in vitro* release of steroids, *Int. J. Pharm.* **1988**, *46*, 69–76.
- 52 WEBER, C., COESTER, C., KREUTER, J., LANGER, K., Desolvation process and surface characterisation of protein nanoparticles, *Int. J. Pharm.* **2000**, *194*, 91–102.
- 53 GALLO, J. M., HUNG, C. T., PERRIER, D. G., Analysis of albumin microsphere preparation, *Int. J. Pharm.* **1984**, *22*, 63–74.
- 54 KATTI, D., KRISHNAMURTI, N., Preparation of albumin microspheres by an improved process, *J. Microencapsul.* **1999**, *16*, 231–242.
- 55 WIDDER, K., FLUORET, G., SENYEI, A. E., Magnetic microspheres: synthesis of a novel parenteral drug carrier, *J. Pharm. Sci.* **1979**, *68*, 79–82.
- 56 BURGER, J. J., TOMLINSON, E., DE ROO, J. E., PALMER, J., Technetium-99m labeling of albumin microspheres intended for drug targeting, *Methods Enzymol.* **1985**, *112*, 43–56.
- 57 RATCLIFFE, J. H., HUNNEYBALL, I. M., SMITH, A., WILSON, C. G., DAVIS, S. S., Preparation and evaluation of biodegradable polymeric systems for the intra-articular delivery of drugs, *J. Pharm. Pharmacol.* **1984**, *36*, 431–436.
- 58 EZPELETA, I., IRACHE, J. M., GUEGUEN, J., ORECCHIONI, A. M., Properties of glutaraldehyde cross-linked vicilin nano- and microparticles, *J. Microencapsul.* **1997**, *14*, 557–565.
- 59 LIN, W., COOMBES, A. G., GARNETT, M. C., DAVIES, M. C., SCHACHT, E., DAVIS, S. S., ILLUM, L., Preparation of sterically stabilized human serum albumin nanospheres using a novel Dextranox-MPEG crosslinking agent, *Pharm Res.* **1994**, *11*, 1588–1592.
- 60 HABEEB, A. F. S. A., HIRAMOTO, R., Reaction of proteins with glutaraldehyde, *Arch. Biochem. Biophys.* **1968**, *126*, 16–26.
- 61 PETERS, K., RICHARDS, F. M., Chemical cross-linking: reagent and problems in studies of membrane structure, *Annu. Rev. Biochem.* **1977**, *46*, 523–551.
- 62 MÜLLER, G. M., LEUENBERGER, H., KISSEL, T., Albumin nanospheres as carriers for passive drug targeting: an optimized manufacturing technique, *Pharm. Res.* **1996**, *13*, 32–37.
- 63 ARNEO, A., ESPUELAS, S., IRACHE, J. M., Albumin nanoparticles as carriers for a phosphodiester oligonucleotide, *Int. J. Pharm.* **2002**, *244*, 59–72.
- 64 SEGURA, S., ESPUELAS, S., RENEDE, M. J., IRACHE, J. M., Potential of albumin nanoparticles as carriers for interferon-gamma, *Drug Dev. Ind. Pharm.* **2005**, *31*, 271–283.
- 65 LANGER, K., BALTHASAR, S., VOGEL, V.,

- DINAUER, N., VON BRIESEN, H., SCHUBERT, D., Optimization of the preparation process for human serum albumin (HSA) nanoparticles, *Int. J. Pharm.* **2003**, *257*, 169–180.
- 66 BRZOSKA, M., LANGER, K., COESTER, C., LOITSCH, S., WAGNER, T. O., MALLINCKRODT, C., Incorporation of biodegradable nanoparticles into human airway epithelium cells – *in vitro* study of the suitability as a vehicle for drug or gene delivery in pulmonary diseases, *Biochem. Biophys. Res. Commun.* **2004**, *318*, 562–570.
- 67 TAKEOKA, S., TERAMURA, Y., OHKAWA, H., IKEDA, Y., TSUCHIDA, E., Conjugation of Von Willebrand factor-binding domain of platelet glycoprotein Ib α to size-controlled albumin microspheres, *Biomacromolecules* **2000**, *1*, 290–295.
- 68 MARTY, J. J., OPPENHEIMER, R. C., SPEISER, P., Nanoparticles – a new colloidal drug delivery system, *Pharm. Acta Helv.* **1978**, *53*, 17–23.
- 69 CHEN, C. Q., LIN, W., COOMBES, A. G., DAVIS, S. S., ILLUM, L., Preparation of human serum albumin microspheres by a novel acetone-heat denaturation method, *J. Microencapsul.* **1994**, *11*, 395–407.
- 70 ZIMMER, A. K., MAINCENT, P., THOUVENOT, P., KREUTER, J., Hydrocortisone delivery to healthy and inflamed eyes using micellar polysorbate 80 solution or albumin nanoparticles, *Int. J. Pharm.* **1994**, *110*, 211–222.
- 71 ZIMMER, A. K., CHETONI, P., SAETTONI, M. F., ZERBE, H., KREUTER, J., Evaluation of pilocarpine-loaded albumin particles as drug delivery systems for controlled delivery in the eye. I. *In vitro* and *in vivo* characteristics, *J. Controlled Rel.* **1994**, *32*, 57–70.
- 72 LIN, W., GARNETT, M. C., DAVIS, S. S., SCHACHT, E., FERRUTI, P., ILLUM, L., Preparation and characterisation of rose Bengal-loaded surface-modified albumin nanoparticles, *J. Controlled Rel.* **2001**, *71*, 117–126.
- 73 MERODIO, M., ESPUELAS, M. S., MIRSHAHI, M., ARNEDO, A., TRACHE, J. M., Efficacy of ganciclovir-loaded nanoparticles in human cytomegalovirus (HCMV) infected cells, *J. Drug Target.* **2002**, *10*, 231–238.
- 74 WIDDER, K. J., MORRIS, R. M., POORE, G. A., HOWARD, D. P., SENYEI, A. E., Selective targeting of magnetic albumin microspheres containing low-dose doxorubicin – total remission in Yoshida sarcoma-bearing rats, *Eur. J. Cancer Clin. Oncol.* **1983**, *19*, 135–139.
- 75 CHANG, B. S., MAHONEY, R. R., Enzyme thermostabilization by bovine serum albumin and other proteins: evidence for hydrophobic interactions, *Biotechnol. Appl. Biochem.* **1995**, *22*, 203–214.
- 76 SCHEFFEL, U., RHODES, B. A., NATARAJAN, T. K., WAGNER, H. N. JR., Albumin microspheres for studies of reticuloendothelial system, *J. Nucl. Med.* **1972**, *13*, 498–503.
- 77 KRAMER, P. A., Albumin microspheres as vehicles for achieving specificity in drug delivery, *J. Pharm. Sci.* **1974**, *63*, 1646–1647.
- 78 SUSLICK, K. S., GRINSTAFF, M. W., Protein microencapsulation of nonaqueous liquids, *J. Am. Chem. Soc.* **1999**, *112*, 7807–7809.
- 79 SUSLICK, K. S., GRINSTAFF, M. W., Proteinaceous microbubbles: synthesis of an echo contrast agent, *Proc. Natl Acad. Sci. USA* **1991**, *88*, 7708–7710.
- 80 SUSLICK, K. S., GRINSTAFF, M. W., KOLBECK, K. J., WONG, M., Characterization of sonochemically prepared proteinaceous microcapsules, *Ultrason. Sonochem.* **1994**, *1*, S65–S68.
- 81 AVIVI (LEVI), S., NITZAN, Y., DROR, R., GEDANKEN, A., An easy sonochemical route for the encapsulation of tetracycline in bovine serum albumin microspheres, *J. Am. Chem. Soc.* **2003**, *125*, 15712–15713.
- 82 WEBER, C., REISS, S., LANGER, K., Preparation of surface modified protein nanoparticles by introduction of sulfhydryl groups, *Int. J. Pharm.* **2000**, *211*, 67–78.
- 83 ROSER, M., FISCHER, D., KISSEL, T., Surface-modified biodegradable albumin nano- and microspheres. II: effect of surface charges on *in vitro* phagocytosis and biodistribution in

- rats, *Eur. J. Pharm. Biopharm.* **1998**, *46*, 255–263.
- 84 LANGER, K., COESTER, C., WEBER, C., VON BRIESEN, H., KREUTER, J., Preparation of avidin-labeled protein nanoparticles as carriers for biotinylated peptide nucleic acid, *Eur. J. Pharm. Biopharm.* **2000**, *49*, 303–307.
- 85 GREF, R., MINAMITAKE, Y., PERACCHIA, M. T., TRUBETSKOY, V., TORCHILIN, V., LANGER, R., Biodegradable long-circulating polymeric nanospheres, *Science* **1994**, *263*, 1600–1603.
- 86 GREF, R., DOMB, A., QUELLEC, P., BLUNK, T., MULLER, R. H., VERVATZ, J. M., LANGER, R., The controlled intravenous delivery of drugs using PEG-coated sterically stabilized nanospheres, *Adv. Drug Deliv. Rev.* **1995**, *16*, 215–233.
- 87 PERACCHIA, M. T., FATTAL, E., DESMAELE, D., BESNARD, M., NOEL, J. P., GOMIS, J. M., APPEL, M., D'ANGELO, J., COUVREUR, P., Stealth PEGylated polycyanoacrylate nanoparticles for intravenous administration and splenic targeting, *J. Controlled Rel.* **1999**, *60*, 121–128.
- 88 OTSUKA, H., NAGASAKI, Y., KATAOKA, K., PEGylated nanoparticles for biological and pharmaceutical applications, *Adv. Drug Deliv. Rev.* **2003**, *55*, 403–419.
- 89 DEIBLE, C. R., BECKMAN, E. J., RUSSELL, A. J., WAGNER, W. R., Creating molecular barriers to acute platelet deposition on damaged arteries with reactive polyethylene glycol, *J. Biomed. Mater. Res.* **1998**, *41*, 251–256.
- 90 JO, S., PARK, K., Surface modification using silanated poly(ethylene glycol)s, *Biomaterials* **2000**, *21*, 605–616.
- 91 STOLNIK, S., ILLUM, L., DAVIS, S. S., Long circulating microparticulate drug carriers, *Adv. Drug Deliv. Rev.* **1995**, *16*, 195–214.
- 92 YONCHEVA, K., CAMPANERO, M. A., GÓMEZ, S., GAMAZO, C., IRACHE, J. M., Bioadhesive properties of pegylated nanoparticles, *Expert Opin. Drug Del.* **2005**, *2*, 205–218.
- 93 LIN, W., GARNETT, M. C., DAVIES, M. C., BIGNOTTI, F., FERRUTI, P., DAVIS, S. S., ILLUM, L., Preparation of surface-modified albumin nanospheres, *Biomaterials* **1997**, *18*, 559–565.
- 94 LIN, W., GARNETT, M. C., SCHACHT, E., DAVIS, S. S., ILLUM, L., Preparation and *in vitro* characterization of HSA-mPEG nanoparticles, *Int. J. Pharm.* **1999**, *189*, 161–170.
- 95 OPPENHEIM, R. C., Solid colloidal drug delivery systems: nanoparticles, *Int. J. Pharm.* **1981**, *8*, 217–234.
- 96 OPPENHEIM, R. C., GIPPS, E. M., FORBES, J. F., WHITEHEAD, R. H., Development and testing of proteinaceous nanoparticles containing cytotoxics, In *Microspheres and Drug Therapy: Pharmaceutical, Immunological and Medical Aspects*, DAVIS, S. S., ILLUM, L., MCVIE, J. G., TOMLINSON, E. (Eds.), Elsevier, New York, **1984**, pp. 117–128.
- 97 ZIMMER, A. K., ZERBE, H., KREUTER, J., Evaluation of pilocarpine-loaded albumin particles as drug delivery systems for controlled delivery in the eye. II. Co-administration with bioadhesive and viscous polymers, *J. Controlled Rel.* **1995**, *33*, 31–46.
- 98 EGBARIA, K., FRIEDMAN, M., Adsorption of fluorescein dyes on albumin microspheres, *Pharm Res.* **1992**, *9*, 629–635.
- 99 BHARGAVA, K., ANDO, H. Y., Immobilization of active urokinase on albumin microspheres: use of a chemical dehydrant and process monitoring, *Pharm Res.* **1992**, *9*, 776–781.
- 100 MICHAELIS, M., LANGER, K., ARNOLD, S., DOERR, H. W., KREUTER, J., CINATL, J. JR., Pharmacological activity of DTPA linked to protein-based drug carrier systems, *Biochem. Biophys. Res. Commun.* **2004**, *323*, 1236–1240.
- 101 SANTHI, K., DHANARAJ, S. A., JOSEPH, V., PONNUSANKAR, S., SURESH, B., A study on the preparation and anti-tumor efficacy of bovine serum albumin nanospheres containing 5-fluorouracil, *Drug Dev. Ind. Pharm.* **2002**, *28*, 1171–1179.
- 102 SANTHI, K., DHANARAJ, S. A., KOSHY, M., PONNUSANKAR, S., SURESH, B., Study of biodistribution of

- methotrexate-loaded bovine serum albumin nanospheres in mice, *Drug Dev. Ind. Pharm.* **2000**, *26*, 1293–1296.
- 103 WARTLICK, H., SPÄNKUCH-SCHMITT, B., STREBHARDT, K., KREUTER, J., LANGER, K., Tumour cell delivery of antisense oligonucleotides by human serum albumin nanoparticles, *J. Controlled Rel.* **2004**, *96*, 483–495.
- 104 RHAESE, S., VON BRIESEN, H., RUBSAMEN-WAIGMANN, H., KREUTER, J., LANGER, K., Human serum albumin–polyethylenimine nanoparticles for gene delivery, *J. Controlled Rel.* **2003**, *92*, 199–208.
- 105 VOGEL, V., LOCHMANN, D., WEYERMANN, J., MAYER, G., TZIATZIOS, C., VAN DER BROEK, J. A., HAASE, W., WOUTERS, D., SCHUBERT, U. S., KREUTER, J., ZIMMER, A., SCHUBERT, D., Oligonucleotide–protamine–albumin nanoparticles: preparation, physical properties, and intracellular distribution. *J. Controlled Rel.* **2005**, *103*, 99–111.
- 106 THIELE, L., MERKLE, H. P., WALTER, E., Phagocytosis and phagosomal fate of surface-modified microparticles in dendritic cells and macrophages, *Pharm. Res.* **2003**, *20*, 221–228.
- 107 BORCHARD, G., KREUTER, J., The role of serum complement on the organ distribution of intravenously administered poly (methyl methacrylate) nanoparticles: effects of pre-coating with plasma and with serum complement. *Pharm. Res.* **1996**, *13*, 1055–1058.
- 108 OGAWARA, K., FURUMOTO, K., NAGAYAMA, S., MINATO, K., HIGAKI, K., KAI, T., KIMURA, T., Pre-coating with serum albumin reduces receptor-mediated hepatic disposition of polystyrene nanosphere: implications for rational design of nanoparticles, *J. Controlled Rel.* **2004**, *100*, 451–455.
- 109 MERODIO, M., IRACHE, J. M., ECLANCHER, F., MIRSHAHI, M., VILLARROYA, H., Distribution of albumin nanoparticles in animals induced with the experimental allergic encephalomyelitis, *J. Drug Target.* **2000**, *8*, 289–303.
- 110 BODOR, N., BUCHWALD, P., Recent advances in the brain targeting of neuropharmaceuticals by chemical delivery systems, *Adv. Drug Deliv. Rev.* **1999**, *36*, 229–254.
- 111 CORNFORD, E. M., HYMAN, S., Blood–brain barrier permeability to small and large molecules, *Adv. Drug. Deliv. Rev.* **1999**, *36*, 145–163.
- 112 ROUSSEAU, V., DENIZOT, B., LE JEUNE, J. J., JALLET, P., Early detection of liposome brain localization in rat experimental allergic encephalomyelitis, *Exp. Brain Res.* **1999**, *125*, 255–264.
- 113 FILIPPI, M., TORTORELLA, C., ROVARIS, M., BOZZALI, M., POSSA, F., SORMANI, M. P., IANNUCCI, G., COMI, G., Changes in the normal appearing brain tissue and cognitive impairment in multiple sclerosis, *J. Neurol. Neurosurg. Psychiatry* **2000**, *68*, 157–161.
- 114 VILLARROYA, H., MARIE, Y., OUALLET, J. C., LE SAUX, F., TCHELINGERIAN, J. L., BAUMANN, N., Expression of TNF alpha in central neurons of Lewis rat spinal cord after EAE induction, *J. Neurosci. Res.* **1997**, *49*, 592–599.
- 115 STEIN, C. S., ST LOUIS, J., GILBERT, J. J., STREJAN, G. H., Treatment of spinal cord-induced experimental allergic encephalomyelitis in the Lewis rat with liposomes presenting central nervous system antigens, *J. Neuroimmunol.* **1990**, *28*, 119–130.
- 116 GUY, J., QI, X., HAUSWIRTH, W. W., Adeno-associated viral-mediated catalase expression suppresses optic neuritis in experimental allergic encephalomyelitis, *Proc. Natl Acad. Sci. USA* **1998**, *95*, 13847–13852.
- 117 KUMAGAI, A. K., EISENBERG, J. B., PARDRIDGE, W. M., Absorptive mediated endocytosis of cationized albumin and a beta-endorphin-cationized albumin chimeric peptide by isolated brain capillaries. Model system of blood–brain carrier transport, *J. Biol. Chem.* **1987**, *262*, 15214–15219.
- 118 WHEATLEY, M. A., NARAYANA, P., Diagnostic use of microspheres. In *Encyclopedia of Controlled Drug*

- Delivery*, MATHIOWITZ, E., KREITZ, M. R., PEPPAS, L. B. (Eds.), Wiley, New York, 1999, vol. I, p. 340.
- 119 NIEWEG, O. E., JANSSEN, L., VALDES OLMOS, R. A., RUTGERS, E. J., PETERSE, J. L., HOEFNAGEL, K. A., KROON, B. B., Lymphatic mapping and sentinel lymph node biopsy in breast cancer, *Eur. J. Nucl. Med.* **1999**, *4*, S11–S16.
- 120 RAHUSEN, F., PIJPPERS, R., VAN DIEST, P., BLEICHRODT, R. P., TORRENGA, H., MEIJER, S., The implementation of the sentinel node biopsy as a routine procedure for patients with breast cancer, *Surgery* **2000**, *128*, 6–12.
- 121 VALDES OLMOS, R. A., TANIS, P. J., HOEFNAGEL, C. A., NIEWEG, O. E., MULLER, S. H., RUTGERS, E. J. Th., KOOI, M. L. K., KROON, B. B. R., Improved sentinel node visualization in breast cancer by optimizing the colloid particle concentration and tracer dosage, *Nucl. Med. Commun.* **2001**, *22*, 579–586.
- 122 VAN DER ENT, F. W., KENGEN, R. A., VAN DER POL, H. A., POVEL, J. A., STROEKEN, H. J., HOOFWIJK, A. G., Halsted revisited: internal mammary sentinel lymph node biopsy in breast cancer, *Ann. Surg.* **2001**, *234*, 79–84.
- 123 WILHELM, A., MIJNHOUT, G., FRANSSSEN, E., Radiopharmaceuticals in sentinel lymph-node detection – an overview, *Eur. J. Nucl. Med.* **1999**, *26*, S36–S42.
- 124 LEIDENIUS, M. H., LEPPANEN, E. A., KROGERUS, L. A., SMITTEN, K. A., The impact of radiopharmaceutical particle size on the visualization and identification of sentinel nodes in breast cancer, *Nucl. Med. Commun.* **2004**, *25*, 233–238.
- 125 HILL, A. D., TRAN, K. N., AKHURST, T., YEUNG, H., YEH, S. D., ROSEN, P. P., BORGES, P. I., CODY, H. S. 3rd., Lessons learned from 500 cases of lymphatic mapping for breast cancer, *Ann. Surg.* **1999**, *229*, 528–535.
- 126 ROUMEN, R. M., GEUSKENS, L. M., VALKENBURG, J. G., In search of the true sentinel node by different injection techniques in breast cancer patients, *Eur. J. Surg. Oncol.* **1999**, *25*, 347–351.
- 127 PIJPPERS, R., BORGSTEIN, P. J., MEIJER, S., KRAG, D. N., HOEKSTRA, O. S., GREUTER, H. N., TEULE, G. J., Transport and retention of colloidal tracers in regional lymphoscintigraphy in melanoma: influence on lymphatic mapping and sentinel node biopsy, *Melanoma Res.* **1998**, *8*, 413–418.
- 128 NIEUWENHUIS, E. J., VAN DER WAAL, I., LEEMANS, C. R., KUMMER, A., PIJPPERS, R., CASTELIJNS, J. A., BRAKENHOFF, R. H., SNOW, G. B., Histopathologic validation of the sentinel node concept in oral and oropharyngeal squamous cell carcinoma, *Head Neck* **2005**, *27*, 150–158.
- 129 PIJPPERS, R., BUIST, M. R., VAN LINGEN, A., DIJKSTRA, J., VAN DIEST, P. J., TEULE, G. J., KENEMANS, P., VERHEIJEN, R. H., The sentinel node in cervical cancer: scintigraphy and laparoscopic gamma probe-guided biopsy, *Eur. J. Nucl. Med. Mol. Imaging* **2004**, *31*, 1479–1486.
- 130 ORDER, S. E., SIEGEL, J. A., LUSTIG, R. A., PRINCIPATO, R., ZEIGER, L. S., JOHNSON, E., ZHANG, H., LANG, P., PILCHIK, N. B., METZ, J., DENITTIS, A., BOERNER, P., BEUERLEIN, G., WALLNER, P. E., A new method for delivering radioactive cytotoxic agents in solid cancers, *Int. J. Radiat. Oncol. Biol. Phys.* **1994**, *30*, 715–720.
- 131 WILDER, R. B., DENARDO, G. L., DENARDO, S. J., Treatment of cancer with intratumoral infusion of radioisotopes, *Int. J. Radiat. Oncol. Biol. Phys.* **1994**, *30*, 737–739.
- 132 TEI, C., KONDO, S., MEERBAUM, S., ONG, K., MAURER, G., WOOD, F., SAKAMAKI, T., SHIMOURA, K., CORDAY, E., SHAH, P. M., Correlation of myocardial echo contrast disappearance rate (“washout”) and severity of experimental coronary stenosis, *J. Am. Coll. Cardiol.* **1984**, *3*, 39–46.
- 133 CHUANG, V. T., KRAGH-HANSEN, U., OTAGIRI, M., Pharmaceutical strategies utilizing recombinant human serum albumin, *Pharm. Res.* **2002**, *19*, 569–577.
- 134 KERBER, R. E., *Echocardiography in Coronary Artery Diseases*, Future, New York, **1988**.

- 135 KAUL, S., GLASHEEN, W. P., OLINER, J. D., KELLY, P., GASCHO, J. A., Relation between anterograde blood flow through a coronary artery and the size of the perfusion bed it supplies: experimental and clinical implications, *J. Am. Coll. Cardiol.* **1991**, *17*, 1403–1413.
- 136 POWSNER, S. M., KELLER, M. W., SANIIE, J., FEINSTEIN, S. B., Quantitation of echo-contrast effects, *Am. J. Physiol. Imaging* **1986**, *1*, 124–128.
- 137 ARNEDO, A., IRACHE, J. M., GONZÁLEZ GAITANO, G., VALGAÑÓN, M., ESPUELAS, S., Bovine serum albumin modified the intracellular distribution and improved the antiviral activity of an oligonucleotide, *J. Drug Target.* **2003**, *11*, 197–204.
- 138 ARNEDO, A., IRACHE, J. M., MERODIO, M., ESPUELAS, S., Albumin nanoparticles: fusogenic carriers that improved the stability, nuclear accumulation and anticytomegaloviral activity of an oligonucleotide, *J. Controlled Rel.* **2004**, *94*, 217–227.
- 139 SRINIVASAN, S. K., TEWARY, H. K., IVERSEN, P. L., Characterization of binding sites, extent of binding, and drug interactions of oligonucleotides with albumin, *Antisense Res. Dev.* **1995**, *5*, 131–139.
- 140 SATO, Y., KANEKO, K., MIKAMI, K., MIZUGAKI, M., SUZUKI, Y., Isolation of bovine serum albumin fragment P-9 and P-9-mediated fusion of small unilamellar vesicles, *Biol. Pharm. Bull.* **1999**, *22*, 1360–1365.
- 141 FISCHER, D., BIEBER, T., BRUSSELBACH, S., ELSASSER, H., KISSEL, T., Cationized human serum albumin as a non-viral vector system for gene delivery? Characterization of complex formation with plasmid DNA and transfection efficiency, *Int. J. Pharm.* **2001**, *225*, 97–111.
- 142 FISCHER, D., LI, Y., AHLEMEYER, B., KRIEGLSTEIN, J., KISSEL, T., *In vitro* cytotoxicity testing of polycations: influence of polymer structure on cell viability and hemolysis, *Biomaterials* **2003**, *24*, 1121–1131.
- 143 FANCA, H., SIMOES, S., PEDROSO DE LIMA, M. C., Association of albumin or protamine to lipoplexes: enhancement of transfection and resistance to serum, *J. Gene Med.* **2004**, *6*, 681–692.
- 144 ZELPHATI, O., UYECI, L. S., BARRON, L. G., SZOKA, F. C. JR., Effect of serum components on the physicochemical properties of cationic lipid/oligonucleotide complexes and on their interactions with cells, *Biochim. Biophys. Acta* **1998**, *1390*, 119–133.
- 145 MORIMOTO, Y., AKIMOTO, M., SUGIBAYASHI, K., NADAI, T., KATO, Y., Drug-carrier property of albumin microspheres in chemotherapy. IV. Antitumor effect of single-shot or multiple shot administration of microsphere-entrapped 5-fluorouracil on Ehrlich ascites or solid tumor in mice, *Chem. Pharm. Bull.* **1980**, *28*, 3087–3092.
- 146 SUGIBAYASHI, K., AKIMOTO, M., MORIMOTO, Y., NADAI, T., KATO, Y., Drug-carrier property of albumin microspheres in chemotherapy. III. Effect of microsphere-entrapped 5-fluorouracil on Ehrlich ascites carcinoma in mice, *J. Pharm. Dyn.* **1979**, *2*, 350–355.
- 147 SUGIBAYASHI, K., MORIMOTO, Y., NADAI, T., KATO, Y., HASEGAWA, A., ARITA, T., Drug-carrier property of albumin microspheres in chemotherapy. II. Preparation and tissue distribution in mice of microsphere-entrapped 5-fluorouracil, *Chem. Pharm. Bull.* **1979**, *27*, 204–209.
- 148 YI, Y. M., YANG, T. Y., PAN, W. M., Preparation and distribution of 5-fluorouracil ¹²⁵I sodium alginate-bovine serum albumin nanoparticles, *World. J. Gastroenterol.* **1999**, *5*, 57–60.
- 149 IBRAHIM, N. K., DESAI, N., LEGHA, S., SOON-SHIONG, P., THERIAULT, R. L., RIVERA, E., ESMAELI, B., RING, S., BEDIKIAN, A., HORTOBAGYI, G. N., ELLERHOST, J. A., Phase I and pharmacokinetic study of ABI-007, a cremophor-free, protein-stabilized, nanoparticle formulation of paclitaxel, *Clin. Cancer Res.* **2002**, *8*, 1038–1044.
- 150 DORR, R., Pharmacology and toxicology of Cremophor EL diluent, *Ann. Pharmacother.* **1994**, *28*, S11–S14.
- 151 WEISS, R., DONEHOWER, R., WIERNIK,

- P. H., OHNUMA, T., GRALLA, R. J., TRUMP, D. L., BAKER, J. R. JR., VAN ECHO, D. A., VON HOFF, D. D., LEYLAND-JONES, B., Hypersensitivity reactions from Taxol, *J. Clin. Oncol.* **1990**, *8*, 1263–1268.
- 152 WAUGH, W., TRISSEL, L., STELLA, V., Stability, compatibility, and plasticizer extraction of Taxol (NSC-125973) injection diluted in infusion solutions and stored in various containers, *Am. J. Hosp. Pharm.* **1991**, *48*, 1520–1524.
- 153 KOLODZIE, F. D., JOHN, M., KHURANA, C., FARB, A., WILSON, P. S., ACAMPADO, E., DESAI, N., SOON-SHIONG, P., VIRMANI, R., Sustained reduction of in-stent neointimal growth with the use of a novel systemic nanoparticle paclitaxel, *Circulation* **2002**, *106*, 1195–1198.
- 154 GARBER, K., Paclitaxel formulation hints at new chemotherapy approach, *J. Natl. Cancer Inst.* **2004**, *96*, 90–91.
- 155 BAYES, M., RABASEDA, X., PROUS, J. R., Gateways to clinical trials. *Methods Find. Exp. Clin. Pharmacol.* **2004**, *26*, 211–244.
- 156 NCI Cancer Bull. **2005**, January 18, 2(3), http://www.cancer.gov/ncicancerbulletin/NCI_Cancer_Bulletin_011805/page5.
- 157 DAMASCELLI, B., CANTÙ, G., MATTAVELLI, F., TAMPLINIZZA, P., BIDOLI, P., LEO, E., DOSIO, F., CERROTTA, A. M., DI TOLLA, G., FRIGERIO, L. F., GARBAGNATI, F., LANOCITA, R., MARCHIANÒ, A., PATELLI, G., SPREAFICO, C., TICHÀ, V., VESPRO, V., ZUNINO, F., Intraarterial chemotherapy with polyoxyethylated castor oil free paclitaxel, incorporated in albumin nanoparticles (ABI-007): phase II study of patients with squamous cell carcinoma of the head and neck and anal canal: preliminary evidence of clinical activity, *Cancer* **2001**, *92*, 2592–2602.
- 158 DAMASCELLI, B., PATELLI, G., LANOCITA, R., DI TOLLA, G., MARCHIANO, A., SPREAFICO, C., FRIGERIO, L. F., GARBAGNATI, F., TICHÀ, V., SOON-SHIONG, P., Intra-arterial paclitaxel in albumin nanoparticles controls squamous carcinoma at various sites, *Proc. Am. Soc. Clin. Oncol.* **2003**, *22*, 509 (abstr 2050).
- 159 DAMASCELLI, B., PATELLI, G. L., LANOCITA, R., DI TOLLA, G., FRIGERIO, L. F., MARCHIANO, A., GARBAGNATI, F., SPREAFICO, C., TICHÀ, V., GLADIN, C. R., PALAZZI, M., CRIPPA, F., OLDINI, C., CALÒ, S., BONACCORSI, A., MATTAVELLI, F., COSTA, L., MARIANI, L., CANTÙ, G., A novel intraarterial chemotherapy using paclitaxel in albumin nanoparticles to treat advanced squamous cell carcinoma of the tongue: preliminary findings, *Am. J. Roentgenol.* **2003**, *181*, 253–260.
- 160 DOSIO, F., ARPICCO, S., BRUSA, P., STELLA, B., CATTTEL, L., Poly(ethylene glycol)–human serum albumin–paclitaxel conjugates: preparation, characterization and pharmacokinetics, *J. Controlled Rel.* **2001**, *75*, 107–117.
- 161 BAILEY, S. M., HART, I., LOHMEYER, L., Ganciclovir and the HSV-tk enzyme prodrug system in cancer therapy, *Drugs of the Future* **1998**, *23*, 401–413.
- 162 QIAN, C., BILBAO, R., BRUÑA, O., PRIETO, J., Induction of sensitivity to ganciclovir in human hepatocellular carcinoma cells by adenovirus-mediated gene transfer of herpes simplex virus thymidine kinase, *Hepatology* **1995**, *22*, 118–123.
- 163 SANGRO, B., QIAN, C., SCHMITZ, V., PRIETO, J., Gene therapy of hepatocellular carcinoma and gastrointestinal tumors, *Ann. NY Acad. Sci.* **2002**, *963*, 6–12.
- 164 BELTINGER, C., FULDA, S., WALCZAK, H., DEBATIN, K. M., Trail enhances thymidine kinase/ganciclovir gene therapy of neuroblastoma cells, *Cancer Gene Ther.* **2002**, *9*, 372–381.
- 165 ALVAREZ, R. D., GÓMEZ NAVARRO, J., WANG, M., BARNES, M. N., STRONG, T. V., ARANI, R. B., ARAFAT, W., HUGHES, J. V., SIEGAL, G. P., CURIEL, D. T., Adenoviral-mediated suicide gene therapy for ovarian cancer, *Mol. Ther.* **2000**, *2*, 524–530.
- 166 CARRIO, M., ROMAGOSA, A., MERCADE, E., MAZO, A., NADAL, M., GOMEZ-FOIX, A. M., FILLAT, C., Enhanced pancreatic

- tumor regression by a combination of adenovirus and etrovirus mediated delivery of the HSV/tk gene, *Gene Ther.* **1999**, *6*, 547–553.
- 167 HASSAN, W., SANDFORD, M. A., WOO, S. L., CHEN, S. H., HALL, S. J., Prospects for herpes-simplex-virus thymidine-kinase and cytokine prostate cancer, *World J. Urol.* **2000**, *18*, 130–135.
- 168 LINK, C. J., SEREGINA, T., TRAYNOR, A., BURT, R. K., Cellular suicide therapy of malignant disease, *Oncologist* **2000**, *5*, 68–74.
- 169 MERODIO, M., RUIZ, J., BUSTOS, M., MARTÍNEZ-GALAN, F., CAMPANERO, M. A., IRACHE, J. M., Encapsulation of ganciclovir in albumin nanoparticles enhances the thymidine kinase suicide gene therapy, *J. Drug Deliv. Sci. Technol.* **2005**, *14*, 121–127.
- 170 HÄFELI, U. O., Magnetically modulated therapeutic systems, *Int. J. Pharm.* **2004**, *277*, 19–24.
- 171 WIDDER, K. J., SENYEI, A. E., SCARPELLI, D. G., Magnetic microspheres: a model system specific drug delivery *in vivo*, *Proc. Soc. Exp. Biol. Med.* **1978**, *158*, 141–146.
- 172 WIDDER, D. J., EDELMAN, R. R., GRIEF, W. L., MONDA, L., Magnetite albumin suspension: a superparamagnetic oral MR contrast agent, *Am. J. Roentgenol.* **1987**, *149*, 839–843.
- 173 TIEFENAUER, L. X., TSCHIRKY, A., KUHNE, G., ANDRES, R. Y., *In vivo* evaluation of magnetite nanoparticles for use as a tumor contrast agent in MRI, *Magn. Reson. Imaging* **1996**, *14*, 391–402.
- 174 CHUNFU, Z., JINQUAN, C., DUANZHI, Y., YONGXIAN, W., YANLIN, F., JIAJU, T., Preparation and radiolabeling of human serum albumin (HSA)-coated magnetite nanoparticles for magnetically targeted therapy, *Appl. Radiat. Isot.* **2004**, *61*, 1255–1259.
- 175 ALEXIOU, C., ARNOLD, W., KLEIN, R. J., PARAK, F. G., HULIN, P., BERGEMANN, C., ERHARDT, W., WAGENPFEL, S., LUBBE, A. S., Locoregional cancer treatment with magnetic drug targeting, *Cancer Res.* **2000**, *60*, 6641–6648.
- 176 WIDDER, K. J., SENYEI, A. E., RANNEY, D. F., Magnetically responsive microspheres and other carriers for the biophysical targeting of antitumor agents, *Adv. Pharmacol. Chemother.* **1979**, *16*, 213–271.
- 177 WIDDER, K. J., MORRIS, R. M., POORE, G. A., HODWARD, D. P., SENYEI, A. E., Tumor remission in Yoshida sarcoma-bearing rats by selective targeting of magnetic albumin microspheres containing doxorubicin, *Proc. Natl. Acad. Sci. USA* **1981**, *78*, 579–581.
- 178 WIDDER, K. J., MORINO, P. A., MORRIS, R. M., HODWARD, D. P., POORE, G. A., SENYEI, A. E., Selective targeting of magnetic albumin microspheres to the Yoshida sarcoma: ultrastructural evaluation of microsphere disposition, *Eur. J. Cancer Clin. Oncol.* **1983**, *19*, 141–147.
- 179 GOODWIN, S., PETERSON, C., HOB, C., BITTNER, C., Targeting and retention of magnetic targeted carriers (MTCS) enhancing intra-arterial chemotherapy, *J. Magn. Magn. Mater.* **1999**, *194*, 132–139.
- 180 GOODWIN, S. C., BITTNER, C. A., PETERSON, C. L., WONG, G., Single-dose toxicity study of hepatic intra-arterial infusion of doxorubicin coupled to a novel magnetically targeted drug carrier, *Toxicol. Sci.* **2001**, *60*, 177–183.
- 181 PULLER, S. K., GALLO, J. M., Enhanced brain tumor selectivity of cationic magnetic polysaccharide microspheres, *J. Drug Target.* **1999**, *6*, 215–228.
- 182 PULLER, S. K., CICCOTTO, S. L., GALLO, J. M., Distribution of small magnetic particles in brain tumor-bearing rats, *J. Neurooncol.* **1999**, *41*, 99–105.
- 183 GONG, L. S., ZHANG, Y. D., LIU, S., Target distribution of magnetic albumin nanoparticles containing adriamycin in transplanted rat liver cancer model, *Hepatobiliary Pancreat. Dis. Int.* **2004**, *3*, 365–368.
- 184 GURNY, R., IBRAHIM, H., AEBI, A., BURI, P., WILSON, C. G., WASHINGTON, N., Design and evaluation of controlled release system for the eye, *J. Controlled Rel.* **1987**, *6*, 367–373.

- 185 DESHPANDE, A. A., HELLER, J., GURNY, R., Biodegradable polymers for ocular drug delivery, *Crit. Rev. Ther. Drug Carrier Syst.* **1998**, *15*, 381–420.
- 186 ZIMMER, A., KREUTER, J., Microspheres and nanoparticles used in ocular delivery systems, *Adv. Drug Deliv. Rev.* **1995**, *16*, 61–73.
- 187 HEINEMANN, M. H., *Staphylococcus epidermis* endophthalmitis complicating intravitreal antiviral therapy of cytomegalovirus retinitis, *Am. J. Ophthalmol.* **1989**, *107*, 643–644.
- 188 COCHEREAU-MASSIN, I., LEHOANG, P., LAUTIER-FRAU, M., ZAZOUN, L., MARCEL, P., ROBINET, M., MATHERON, S., KATLAMA, C., GHARAKHANIAN, S., ROZENBAUM, W., Cytomegalovirus retinitis in AIDS: treatment with intravitreal injections of ganciclovir, *Ophthalmology* **1991**, *98*, 1348–1355.
- 189 NICHOLS, W. G., BOECKH, M., Recent advances in the therapy and prevention of CMV infections, *J. Clin. Virol.* **2000**, *16*, 25–40.
- 190 NOBLE, S., FAULDS, D., Ganciclovir. An update of its use in the prevention of cytomegalovirus infection and disease in transplant recipients, *Drugs* **1998**, *56*, 115–146.
- 191 KEMPEN, J. H., MARTIN, B. K., WU, A. W., BARRON, B., THORNE, J. E., JABS, D. A., The effect of cytomegalovirus retinitis on the quality of life of patients with AIDS in the era of highly active anti-retroviral therapy, *Ophthalmology* **2003**, *110*, 987–995.
- 192 CANTRILL, H. L., HENRY, K., MELROE, N. H., KNOBLOCH, W. H., RAMSAY, R. C., BALFOUR, H. H. JR., Treatment of cytomegalovirus retinitis with intravitreal ganciclovir, *Ophthalmology* **1989**, *96*, 367–374.
- 193 STREBLOW, D. N., KREKLYWICH, C., YIN, Q., DE LA MELENA, V. T., CORLESS, C. L., SMITH, P. A., BRAKEBILL, C., COOK, J. W., VINK, C., BRUGGEMAN, C. A., NELSON, J. A., ORLOFF, S. L., Cytomegalovirus-mediated upregulation of chemokine expression correlates with the acceleration of chronic rejection in rat heart transplants. *J. Virol.* **2003**, *77*, 2182–2194.
- 194 SAGEDA, S., NORDAL, K. P., HARTMANN, A., SUND, S., SCOTT, H., DEGRE, M., FOSS, A., LEIVSTAD, T., OSNES, K., FAUCHALD, P., ROLLAG, H., The impact of cytomegalovirus infection and disease on rejection episodes in renal allograft recipients, *Am. J. Transplant.* **2002**, *2*, 850–856.
- 195 IRACHE, J. M., MERODIO, M., ARNEDO, A., CAMAPANERO, M. A., MIRSHAHI, M., ESPUELAS, S., Albumin nanoparticles for the intravitreal delivery of anticytomegaloviral drugs, *Mini Rev. Med. Chem.* **2005**, *5*, 293–305.
- 196 MERODIO, M., IRACHE, J. M., VALAMANESH, F., MIRSHAHI, M., Ocular disposition and tolerance of ganciclovir-loaded albumin nanoparticles after intravitreal injection in rats, *Biomaterials* **2002**, *23*, 1587–1594.
- 197 MAURICE, D. M., MISHIMA, S., Pharmacology of the eye. In *Handbook of Experimental Pharmacology*, SEARS, M. L. (Ed.), Springer-Verlag, Berlin, 1984, vol. 69, pp. 19–116.
- 198 CASPI, R. R., CHAN, C. C., LEAKE, W. C., HIGUCHI, M., WIGGERT, B., CHADER, G. J., Experimental autoimmune uveoretinitis in mice. Induction by a single eliciting event and dependence on quantitative parameters of immunization, *J. Autoimmun.* **1990**, *3*, 237–246.
- 199 DE KOZAK, Y., MIRSHAHI, M., BOUCHEIX, C., FAURE, J. P., Modulation of experimental autoimmune uveoretinitis by active immunization with autoantigen specific monoclonal antibodies, *Eur. J. Immunol.* **1989**, *17*, 541–547.

8

Nanoscale Patterning of S-Layer Proteins as a Natural Self-assembly System

Margit Sára, D. Pum, C. Huber, N. Ilk, M. Pleschberger and U. B. Sleytr

8.1

Introduction

Nanobiotechnology uses concepts from molecular biology, biochemistry and chemistry to identify components, processes and principles for the construction of self-assembling materials and devices. In particular, biological systems provide an enormous diversity of higher-order functional structures and patterns arising from molecular self-assembly. Most frequently, the initial step of molecular organization into functional units and complex supramolecular structures requires arrangement of molecules into ordered arrays. Recently, considerable efforts have been devoted to exploit natural self-assembly systems and to introduce variations into natural molecules (e.g. proteins and DNA) to achieve basic building blocks for specific structures and applications [1–8].

This chapter is intended to provide a survey of the unique general principles of crystalline bacterial cell surface layer (S-layer) proteins and fusion proteins thereof. In general, S-layer proteins form the outermost cell surface structure of many bacteria and archaea. Monomolecular S-layer protein lattices are composed of single species of protein or glycoprotein subunits with the inherent ability to self-assemble into two-dimensional arrays on the bacterial cell surface, or after isolation, on artificial supports, such as silicon wafers, noble metals, plastics, Langmuir lipid films or liposomes [4–8]. Thus, genetically and/or chemically modified S-layer proteins are exploited as building blocks and templates for generating functional nanostructures at the meso- and macroscopic scale for both life and nonlife science applications. In addition, S-layer-specific heteropolysaccharides are used as biomimetic linkers to solid supports and lipid layers to achieve binding and recrystallization in uniform orientation.

8.2

General Properties of S-Layers

8.2.1

Structure, Isolation, Self-Assembly and Recrystallization

Transmission electron microscopic (TEM) studies on the mass distribution of S-layers and subsequent two- and three-dimensional analysis including computer image enhancement led to structural information down to a range of 0.35–1.5 nm [4, 9]. Bacterial S-layer lattices are generally 5–20 nm thick, whereas S-layer lattices of archaea reveal a thickness up to 70 nm. High-resolution images of the surface topography of S-layers under biological conditions were obtained by applying scanning force microscopy (SFM) [4, 9, 10–12]. A common feature of S-layers is, with respect to the orientation on the cell, their smooth outer surface and more corrugated inner surface. The proteinaceous subunits of S-layers are aligned either in lattices with oblique (p1, p2), square (p4) or hexagonal (p3, p6) symmetry with a center-to-center spacing of the morphological units of approximately 3.5–35 nm. Hexagonal lattice symmetry is predominant among archaea [13, 14]. S-layers are highly porous protein lattices with a surface porosity of 30–70%. As S-layers are mostly composed of a single species of subunits, they exhibit pores of identical size and morphology [4]. However, in many S-layer proteins, two or even more distinct classes of pores with diameters in the range of 2–8 nm were identified.

Most techniques for isolation and purification of S-layer proteins involve mechanical disruption of bacterial cells and subsequent differential centrifugation to separate cell wall fragments [4, 15]. Complete solubilization of S-layers into their constituent subunits and release from the bacterial envelope can be achieved by treatment with high concentrations of hydrogen bond breaking agents (e.g. guanidine hydrochloride) or by dramatic changes in the pH value of the environment. Bacterial S-layer proteins are not covalently linked to each other or to the supporting cell wall component. While different combinations of weak bonds (hydrophobic, ionic and hydrogen bonds) are responsible for the structural integrity of S-layers, bonds holding the S-layer subunits together are stronger than those binding S-layer proteins to the underlying cell envelope layer [15, 16]. S-layer proteins reassemble into two-dimensional arrays during removal of the disrupting agent used in the dissolution procedure. Self-assembly products may have the form of flat sheets, open-ended cylinders or closed vesicles [4–8, 15].

Recrystallization of S-layer proteins on technologically relevant substrates, such as silicon wafers, noble metals, plastics, flat lipid layers or liposomes, revealed a broad application potential for these crystalline arrays in micro- and nanotechnology [4–8]. The formation of coherent crystalline arrays strongly depended on the S-layer protein species, the environmental conditions of the bulk phase (e.g. temperature, pH, ion composition and ionic strength) and, in particular, on the surface properties of the substrate [17, 18]. Crystal growth was simultaneously initiated at many randomly distributed nucleation points and proceeded in-plane

until the crystalline domains met, thus leading to a closed, coherent mosaic of individual, several micrometer large S-layer patches [17, 18].

Reassembly of isolated S-layer subunits at the air/water interface and on Langmuir films proved to be an easy and reproducible way for generating coherent S-layer lattices at a large scale [19, 20]. In accordance with S-layer proteins recrystallized on solid surfaces, the orientation of the protein arrays at liquid interfaces was determined by the anisotropy in the physicochemical surface properties of the protein lattice. Electron microscopic examination revealed that recrystallized S-layer proteins were oriented with their outer charge neutral, more hydrophobic surface against the air/water interface and with their negatively charged, more hydrophilic inner surface against the positively charged or zwitterionic head groups of phospholipid or tetraether lipid films [19, 20]. According to the recrystallization on solid supports, a closed mosaic of individual monocrystalline domains was formed.

Furthermore, isolated S-layer proteins were capable to recrystallize on liposomes and on nanocapsules [21–25], thereby forming closed S-layer cages. However, electron microscopic investigations showed that numerous lattice faults were introduced into the crystalline array as necessary for bending the two-dimensional protein lattice.

8.2.2

Chemistry and Molecular Biology

Chemical analyses and genetic studies revealed that the monomolecular S-layer is the result of the secretion and subsequent crystallization of a single homogeneous protein or glycoprotein species with a molecular mass ranging from 40 to 200 kDa [4, 26]. Most S-layer proteins are weakly acidic with isoelectric points (pI s) in the range of 4–6 [26]. Exceptions were reported for the S-layer proteins of lactobacilli [27] and that of *Methanothermobacter feravidus* [28] which possess pI s of 9–11 and 8.4, respectively. Typically, S-layer proteins have a large portion of hydrophobic amino acids (40–60 mol%), possess little or no sulfur-containing amino acids and consist of about 25 mol% charged amino acids. The most frequent posttranslational modification of S-layer proteins is glycosylation [29–31]. The glycan chains of S-layer proteins from Gram-positive bacteria closely resemble the architecture of lipopolysaccharides (LPS) occurring in the outer membrane of Gram-negative bacteria than that of eukaryotic glycan structures.

Information regarding the secondary structure of S-layer proteins is either derived from the amino acid sequence or from circular dichroism (CD) measurements indicating that approximately 20% of the amino acids are organized as α -helices and about 40% occur as β -sheets. Aperiodic foldings and β -turn content may vary between 5 and 45%. Secondary structure predictions based on protein sequence data revealed that most α -helical segments are arranged in the N-terminal part.

During the last two decades, numerous S-layer genes from bacteria and archaea of quite different taxonomical position were sequenced and cloned [26]. At least for S-layer proteins of Bacillaceae, common structural organization principles were

identified, as they typically contain three S-layer homology (SLH) motifs [32] on the N-terminal part. Each SLH motif consists of 50–55 amino acids, from which 10–15 are conserved. In most S-layer proteins, three SLH motifs form the SLH domain which specifically recognizes a distinct type of pyruvylated cell wall heteropolysaccharide, termed secondary cell wall polymer (SCWP), as the proper anchoring structure to the rigid cell wall layer [33–41]. This binding mechanism between SLH domains and pyruvylated SCWPs is widespread amongst prokaryotes, and is considered as having been conserved during evolution [40]. The construction of knockout mutants in *Bacillus anthracis* and *Thermus thermophilus* in which the gene encoding a putative pyruvyl transferase was deleted demonstrated that the pyruvic acid residues play an essential role for the binding process [34, 40]. This observation was supported by surface plasmon resonance (SPR) spectroscopy measurements in which native and chemically modified SCWPs devoid of pyruvic acid residues were used for interaction studies [38]. By applying the dissection approach [41], it became apparent that at least in the case of the S-layer protein SbsB of *Geobacillus stearothermophilus* PV72/p2, the SLH domain (rSbsB_{32–208}) corresponded to the SCWP-binding domain, whereas the larger C-terminal part (rSbsB_{209–920}) represented the self-assembly domain [38, 41].

Although the S-layer proteins SbsA, SbsC and SgsE from *G. stearothermophilus* wild-type strains do not possess an SLH domain on the N-terminal part [42–45], they reveal a highly conserved N-terminal region which specifically recognizes a cell wall heteropolysaccharide containing 2,3-dideoxy-diacetamido mannosamine uronic acid [46] as negatively charged component [42–44]. In these S-layer proteins, arginine and tyrosine typically occurring in carbohydrate binding proteins such as lectins [47] are accumulated on the N-terminal part. In S-layer proteins of *Lactobacillus helveticus*, *L. crispatus* and *L. acidophilus* strains, the conserved C-terminal part was found to be responsible for cell wall anchoring [48], which is most probably mediated by a neutral cell wall polysaccharide [49]. According to the suggestion that S-layer proteins represent cell surface located, carbohydrate-binding, lectin-like proteins [50], the N-terminal region of the S-layer protein from the Gram-negative bacterium *Caulobacter crescentus* recognizes a distinct type of LPS as a binding site to the outer membrane [51, 52]. In *Campylobacter fetus*, a pathogenic organism, two serotypes are distinguished that depend on the type of LPS in the outer membrane. In type A cells, the S-layer protein SapA and its homologs are bound via a conserved N-terminal region to type A LPS, while in type B cells, specific binding was observed between the N-terminal part of SapB and its homologs and type B LPS [53].

For S-layer-carrying bacteria with a generation time of 20 min, about 500 subunits must be synthesized per second, translocated through the plasma membrane and incorporated into the existing protein lattice [15, 16]. Thus, promoters preceding S-layer genes must be very strong [26]. For some S-layer genes, two or even more promoters were identified which are most probably used in different growth stages [26, 27, 37, 43]. With the exception of the S-layer proteins from the Gram-negative bacteria *C. crescentus* and *C. fetus*, all others sequenced so far are produced with an N-terminal secretion signal peptide. For *C. crescentus* and *C. fetus*, type I

secretion signals were detected on the C-terminal part [54]. In contrast, a conserved gene (*abcA*) was identified in the downstream region of the genes encoding the S-layer proteins of the Gram-negative bacteria *Aeromonas salmonicida* and *Aeromonas hydrophila*. This gene encodes a protein that has ATP-binding activity and belongs to the ABC family of transporter proteins, regulates the synthesis of S-layer-specific O-polysaccharide chains in LPS and activates transcription of the S-layer genes [55, 56]. The existence of a translational autoregulation system was reported for *T. thermophilus* [57]. Three genes specifically repressing the expression of the S-layer gene promoter were identified. One of these genes corresponds to the C-terminal fragment of the S-layer protein SlpA which binds to the 5'-untranslated region of the *slpA* mRNA [57].

S-layer variation leads to the expression of alternate S-layer proteins, and was described for pathogens and non-pathogens. In non-pathogens, S-layer variation is frequently induced in response to altered environmental conditions, such as increased oxygen supply [58–60], whereas in pathogens, altered cell surface properties most probably protect the cells from the lytic activity of the immune system [53]. In general terms, two different types of S-layer variation can be distinguished. In the first type, which was observed for *C. fetus* [53, 61] and *G. stearothermophilus* ATCC 12980 [62], only the C-terminal part of the S-layer protein was exchanged, but both the N-terminal region and the S-layer-specific LPS or SCWP remained conserved. In the second type of S-layer variation, which was described for various *G. stearothermophilus* strains, a completely new type of S-layer protein and SCWP was synthesized, and S-layer variation also led to a change in the lattice type [59, 60]. At the molecular level, S-layer variation was either caused by intrachromosomal DNA rearrangement, as observed for *C. fetus* [53, 63], or variant formation depended on recombinational events between a naturally occurring plasmid and the chromosome [64]. In contrast, in *Lactobacillus brevis*, S-layer variation involved activation of transcription by a soluble factor rather than by DNA rearrangement [58]. Regarding the development of S-layer-deficient strain variants, the importance of insertion sequence (IS) elements was demonstrated for various organisms [65–67].

8.2.3

S-Layers as Carbohydrate-binding Proteins

As described above, the interaction between the N-terminal part of the S-layer proteins SbsB and SbpA and the corresponding SCWP was found to be highly specific [35, 38, 41]. The most detailed interaction studies were carried out with the SLH domain of SbsB (rSbsB_{32–208}) and the corresponding SCWP of *G. stearothermophilus* PV72/p2 [38]. Data evaluation from SPR measurements and the setup where the SLH domain was immobilized to the sensor chip indicated the existence of at least two binding sites on a single SCWP molecule with an overall $K_d = 7.7 \times 10^{-7}$ M. In order to distinguish between the different binding sites, the inverted setup where the SCWP was immobilized to the sensor chip and the SLH domain represented the soluble analyte was investigated. Data analysis was performed according to an extension of the heterogeneous ligand model which allowed us to

Tab. 8.1. K_d values for rSbpA_{31–1268}, rSbpA_{31–318} and rSbsB_{32–209}

S-layer protein	K_{d1}	K_{d2}	K_{d3}
rSbpA _{31–1268}	8.4×10^{-12}	7.0×10^{-9}	2.1×10^{-4}
rSbpA _{31–318}	1.2×10^{-11}	3.0×10^{-8}	2.4×10^{-2}
rSbsB _{32–209}	6.7×10^{-11}	6.1×10^{-8}	2.6×10^{-5}

discriminate between three different kinds of binding sites with low ($K_d = 2.6 \times 10^{-5}$ M), medium ($K_d = 6.1 \times 10^{-8}$ M) and high ($K_d = 6.7 \times 10^{-11}$ M) affinity. Although the existence of three different kinds of binding sites can be explained by structural heterogeneities frequently associated with naturally occurring polysaccharides, it cannot be excluded that the high-affinity binding site resulted from avidity effects caused by binding of at least SLH dimers (Table 8.1) [38]. The existence of three potential binding sites and similar affinity constants were demonstrated for the S-layer protein SbpA and the SCWP of *Bacillus sphaericus* CCM 2177 [35]. However, in the case of SbpA, the three SLH motifs and an SLH-like motif were required for reconstituting the functional SCWP-binding domain (Table 8.1).

For the exploitation of SCWPs as biomimetic linkers to solid supports to guarantee an oriented binding and recrystallization of S-layer proteins, these heteropolysaccharides were extracted from peptidoglycan-containing sacculi with hydrofluoric acid and precipitated with ethanol [68, 69]. After purification by size-exclusion chromatography, the latent aldehyde group of the reducing end of the polymer chain was modified with carbodihydrazide and the Schiff base was reduced with sodium borohydride [38]. Sulfhydryl groups were introduced by reaction of the free amine group with 2-methyl mercaptobutyrimidate (2-iminothiolane). Such modified SCWPs carrying a free terminal sulfhydryl group were used for direct adsorption to gold substrates, as required for SPR [70–72] or surface plasmon field enhanced spectroscopy [73]. For covalent binding to supports carrying free amine groups, the sulfhydryl group of the polymer chain (termed thiolated SCWP) was activated with *m*-maleimidobenzoyl-*N*-hydroxysuccinimide ester (MBS) which, as a heterobifunctional crosslinker, could react with amine groups, e.g. of amine-modified cellulose microbeads [72]. Another possibility to activate thiolated SCWP can be seen in the use of the heterobifunctional crosslinker sulfosuccinimidyl 6-[3'-2-(pyridyldithio)-propionamido]hexanoate (Sulfo-LC-SPDP) [38].

8.3

Nanoscale Patterning of S-Layer Proteins

8.3.1

Properties of S-Layer Proteins Relevant for Nanoscale Patterning

S-layers represent a first order self-assembly system that has been optimized in the course of evolution. As S-layers are composed of single protein or glycoprotein species, they have repetitive (physicochemical) properties down to the subnanometer scale [4–8, 74]. Furthermore, functional groups such as amine and carboxylic acid

groups have identical positions and orientation on each subunit in the protein lattice. In the case of S-layer glycoproteins, the carbohydrate chains are attached to the same amino acid positions in the primary sequence [45]. Isolated S-layer subunits frequently maintain the ability to self-assemble in suspension and to recrystallize into a monomolecular protein lattice on various types of solid supports, such as gold chips, silicon wafers, plastics or glass, as well as on flat lipid layers or liposomes [4–8, 74]. The N-terminal region of S-layer proteins specifically recognizes a distinct type of SCWP as the proper anchoring structure in the rigid cell wall layer. These heteropolysaccharides can be exploited as biomimetic linkers to solid supports [38, 70–72], so that the S-layer subunits attach with their inner surface carrying the N-terminal region. S-layer proteins are ideal candidates for genetic engineering. So far, a single cysteine residue has been inserted at various amino acid positions, leading to numerous mutated S-layer protein forms [75]. As S-layer proteins usually do not possess sulfur-containing amino acids, this modification is particularly attractive, since the whole spectrum of sulfur chemistry can be applied to covalently link functional entities via the cysteine residue to the S-layer subunits. Studies on the structure–function relationship of selected S-layer proteins by producing N- or C-terminally truncated forms revealed that the N-terminal region functions as cell wall anchoring domain, whereas the middle and C-terminal part are responsible for lattice and pore formation [35]. However, in some S-layer proteins even more than 200 amino acids in the C-terminal part could be deleted without any influence on the self-assembly and recrystallization properties [37, 44].

To sum up, S-layer lattices are composed of identical protein or glycoprotein species. This implies that functional sequences introduced by genetic engineering and/or chemical modification are repetitively aligned in exact positions down to the subnanometer scale. This cannot be achieved with amorphous polymers which are three-dimensional networks where only random immobilization can occur [4]. In contrast, functional sequences fused to S-layer proteins or inserted into their primary sequence have identical positions and orientation on each S-layer subunit. Moreover, two or even more sequences with different functionalities can be fused to or inserted into a single S-layer protein, leading to multifunctional S-layer fusion proteins. Another possibility can be seen in the co-recrystallization of different types of engineered S-layer proteins which would also lead to multifunctional protein lattices. Apart from this variability, it is possible that the functional sequences or domains are exposed on the outermost surface of the monomolecular protein lattice and are therefore easily accessible to further binding and reaction partners or they may be inserted inside the pores, which could be advantageous for nanoparticle binding. Thus, S-layer proteins can be considered as an extremely versatile and flexible self-assembly system with considerable application potential in nanobiotechnology.

8.3.2

Immobilization of Functionalities by Chemical Methods

Chemical modification and labeling experiments revealed that S-layer lattices possess a high density of functional groups on the outermost surface. For covalent at-

tachment of foreign (macro)molecules, the carboxylic acid groups originating from either aspartic acid or glutamic acid were activated with carbodiimide and subsequently reacted with free amine groups of functional macromolecules, such as Protein A [76–78], monoclonal antibodies [70, 79–82] or various enzymes [4]. In order to prevent inter- and intramolecular crosslinking reactions, the ϵ -amine groups from lysine residues were first modified with monofunctional imidoesters or the S-layer lattice was crosslinked with amine group-specific bifunctional reagents, such as imidoesters or glutaraldehyde. For immobilization of macromolecules, S-layers were either used as self-assembly products which were mostly double layers or as S-layer-carrying cell wall fragments which consisted of the peptidoglycan-containing layer and two mirror-symmetrically arranged S-layer lattices [76]. The amount of monoclonal antibodies, enzymes and streptavidin that could be immobilized to S-layer lattices corresponded approximately to a monolayer of randomly oriented molecules [4]. Quantification of immobilized Protein A, which is extremely elongated, revealed that the molecules were bound in preference with their long axis perpendicularly to the plane of the S-layer lattice [76, 78, 79]. Thus, binding capacities of 290 ng Protein A cm^{-2} S-layer lattice were obtained, which was more than 3 times above the theoretical saturation capacity of a planar surface of 90 ng cm^{-2} when calculated with the Stoke's radius. S-layer-carrying cell wall fragments deposited on microporous supports and carrying a monolayer of monoclonal antibodies were exploited for the development of novel types of dipstick-style solid-phase immunoassays, which due to the low nonspecific adsorption of S-layer proteins for serum components showed excellent signal-to-noise ratios [80, 81]. In the case of Protein A, affinity microparticles with a size of approximately 1 μm were prepared, which represented cup-shaped structures with a complete outer and inner S-layer arranged in mirror symmetric fashion [76]. Such affinity microparticles were used as IgG-specific adsorbents in affinity crossflow filtration systems for the removal of human IgG from serum [77], as required for blood purification of patients suffering from autoimmune disease [78]. Due to their high surface to volume ratio and the high density of immobilized Protein A, affinity microparticles revealed an excellent binding capacity for IgG which was in the range of 40 $\mu\text{g mg}^{-1}$ wet pellet [76–78].

8.3.3

Patterning by Genetic Approaches

8.3.3.1 The S-Layer Proteins SbsA, SbsB and SbsC

The S-layer protein SbpA of *B. sphaericus* CCM 2177 consists (including a 30-amino-acid long signal peptide) in total of 1268 amino acids [37]. SbpA self-assembles into a square (p4) lattice structure with a center-to-center spacing of the morphological units of 13.1 nm. The self-assembly process is strongly dependent on the presence of bivalent cations, such as calcium ions [36]. In the absence of bivalent cations, this S-layer protein stays in the water-soluble state. The N-terminal part of SbpA comprises three typical SLH motifs, but for reconstituting the functional SCWP-binding domain, an additional 58-amino-acid long SLH-like

motif located behind the third SLH motif was required [35]. The SCWP of *B. sphaericus* CCM 2177 consists of disaccharide repeating units that are composed of N-acetyl glucosamine (GlcNAc) and N-acetyl mannosamine (ManNAc). The ManNAc residues carry a pyruvate ketal which endows the polymer chains with a negative net charge [36]. Studies on the structure–function relationship revealed that up to 237 C-terminal amino acids could be deleted without influencing the formation of the p4 lattice structure [35, 36]. However, the deletion of 350 C-terminal acids was linked to a change from square (p4) to oblique (p1) lattice symmetry. By producing various C-terminally truncated forms and performing surface accessibility screens, it became apparent that amino acid position 1068 is located on the outer surface of the square lattice [37]. This was the reason why the C-terminally truncated form rSbpA_{31–1068} was exploited as base form for the construction of several S-layer fusion proteins [70–72, 83]. An N- and C-terminally truncated form (rSbpA_{203–1031}) was capable of self-assembly into the square (p4) lattice structure with a center-to-center spacing of the morphological units and a protein mass distribution similar to that formed by full-length rSbpA [35]. These findings indicated that the segment between amino acids 203 and 1031 is responsible for the self-assembly process and for pore formation.

The S-layer protein SbsB of *G. stearothersophilus* PV72/p2 consists (including a 31-amino-acid long signal peptide) in total of 920 amino acids [84]. By applying the dissection approach, it could be demonstrated that SbsB is composed of the N-terminal SCWP-binding domain which corresponds to the SLH domain and the C-terminal self-assembly domain [38, 41]. As the removal of fewer than 10 C-terminal amino acids led to water-soluble rSbsB forms, the C-terminal part can be considered extremely sensitive against deletions [75, 85]. When the C-terminal end of full-length SbsB was exploited for linking foreign functional sequences, water-soluble S-layer fusion proteins were obtained [85], which recrystallized into the oblique (p1) lattice only on solid supports precoated with SCWP of *G. stearothersophilus* PV72/p2. As demonstrated by SPR spectroscopy, the SLH domain comprising the three SLH motifs specifically recognizes the SCWP of *G. stearothersophilus* PV72/p2 as a binding site [35]. The polymer chains are composed of GlcNAc and ManNAc in the molar ratio of approximately 2:1 [69], and contain pyruvate ketals which provide a net negative charge. The use of chemically modified SCWP in SPR interaction studies clearly showed that it is not the N-acetyl groups of the amino sugars, but the pyruvic acid residues that play a crucial role in the recognition and binding process [38]. Furthermore, thermal as well as guanidine hydrochloride-induced equilibrium unfolding profiles monitored by intrinsic fluorescence and CD spectroscopy allowed us to characterize the SLH domain (rSbsB_{32–208}) as an α -helical protein with a single cooperative unfolding transition. The C-terminal self-assembly domain (rSbsB_{209–920}) could be characterized as a β -sheet protein with typical multidomain unfolding and a lower stability as stand-alone protein [41].

Recently, chimeric S-layer proteins either comprising the N-terminal part of SbpA and the C-terminal part of SbsB (rSbpA–SbsB), or vice versa, the N-terminal part of SbsB and the C-terminal part of SbpA (rSbsB–SbpA), have been con-

structed [35]. The aim was to create a spectrum of S-layer proteins that bind to the same type of SCWP, but assemble into different lattice types. Accordingly, rSbsB and rSbsb–SbpA specifically recognized the SCWP of *G. stearothersophilus* PV72/p2 as a binding site, but in contrast to rSbsB which assembled into an oblique (p1) lattice, the chimeric protein rSbsb–SbpA formed a square (p4) lattice structure. In addition, in rSbsB–SbpA the surface-located amino acid position 1068 of the SbpA primary sequence was exploited as a fusion site for foreign functional sequences [37, 74]. However, rSbpA and the chimeric protein rSbpA–SbsB recognized the SCWP from *B. sphaericus* CCM 2177 as a binding site, but they self-assembled into different lattice types, i.e. square (p4) for rSbpA and oblique (p1) for rSbpA–SbsB [35].

SbsC is the S-layer protein of *G. stearothersophilus* ATCC 12980 and consists (including a 30-amino-acid long signal peptide) in total of 1099 amino acids [43]. Isolated SbsC self-assembles into an oblique lattice. SbsC does not possess an SLH domain on the N-terminal part, but reveals a conserved N-terminus region which was also found in S-layer proteins of other *G. stearothersophilus* wild-type strains, such as PV72/p6, DSM 2358 [42] and NRS 2004/3a [45], as well as in a temperature-derived strain variant of strain ATCC 12980 [62]. This type of N-terminal part which comprises amino acids 31–257 specifically recognizes the SCWP that contains 2,3-dideoxy-diacetamido mannosamine uronic acid as a negatively charged component [42, 46]. Studies on the structure–function relationship of SbsC revealed that the N-terminal part is responsible for cell wall anchoring via the specific SCWP. In the C-terminal part, up to 179 amino acids leading to rSbsC_{31–920} could be deleted without interfering with the formation of the oblique lattice structure [44]. Further deletion of C-terminal amino acids led to SbsC forms that were still able of self-assembling, but such self-assembly products did not show a regular lattice structure (rSbsC_{31–880}), whereas rSbsC_{31–844} even represented a completely water-soluble form which was used for three-dimensional crystallization experiments [86].

8.3.3.2 S-Layer Fusion Proteins

In general, a broad spectrum of chimeric S-layer fusion proteins was constructed and heterologously expressed in *Escherichia coli*. S-layer fusion proteins were based on the S-layer proteins SbsB, SbpA and SbsC. For generating a universal affinity matrix for binding any kind of biotinylated molecules, S-layer–streptavidin fusion proteins were constructed [73, 85]. The strong interaction between streptavidin and biotin as a biomolecular coupling system is commonly used in biotechnology [86]. Minimum-sized core streptavidin (118 amino acids) was either fused to N- or C-terminal positions of SbsB, the S-layer protein of *G. stearothersophilus* PV72/p2, or to the C-terminal end of rSbpA_{31–1068} [37]. The S-layer proteins SbsB and SbpA show different lattice characteristics. SbsB forms an oblique S-layer lattice with p1 symmetry and lattice parameters of $a = 10.4$ nm, $b = 7.9$ nm and a base angle of $\gamma = 81^\circ$, while SbpA forms a square S-layer lattice with a center-to-center spacing of 13.1 nm.

The genes encoding the fusion proteins and core streptavidin were expressed in-

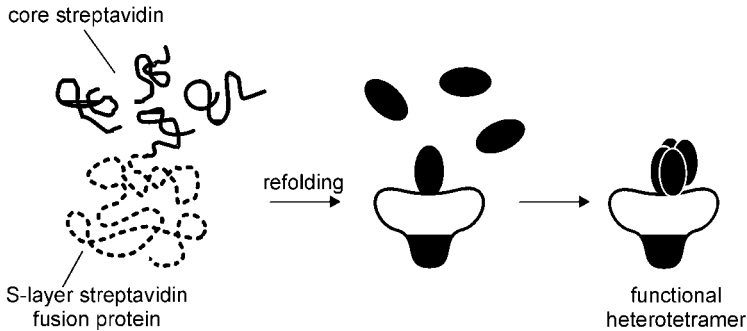


Fig. 8.1. Schematic drawing illustrating the disintegration and rapid dilution step leading to functional heterotetramers of a C-terminal S-layer-streptavidin fusion protein.

independently in *E. coli* and isolated from the host cells [73, 85]. To obtain functional heterotetramers, a refolding procedure was developed by subjecting a mixture of fusion protein with excess core streptavidin to denaturing and renaturing (Fig. 8.1). Two dominant tetramer species, one consisting of one molecule of fusion protein and three molecules of streptavidin (heterotetramers), and the other one consisting of four molecules of streptavidin (homotetramers) were formed during rapid dilution. Heterotetramers were separated from homotetramers and from the S-layer-streptavidin fusion protein by gel-permeation and affinity chromatography. In the latter, the pH-dependent affinity of iminobiotin to streptavidin was exploited. The exceptional stability of streptavidin in 5% SDS at room temperature and denaturation upon boiling allowed the application of the gel-shift assay to control rapid dilution and purification (Fig. 8.2). The desired properties of heterotetramers consisting of one chain of S-layer-streptavidin fusion protein and three chains of streptavidin were the maintenance of the recrystallization properties of the S-layer protein moiety, as well as biotin binding.

Recrystallization experiments were either performed in suspension, on peptidoglycan-containing sacculi, on liposomes or on various solid supports, such as silicon or gold chips which were optionally precoated with thiolated SCWP of *B. sphaericus* CCM 2177 or *G. stearothermophilus* PV72/p2. Heterotetramers comprising the N-terminal rSbsB-streptavidin fusion protein formed self-assembly products in suspension, and recrystallized on liposomes and silicon wafers [85], whereas heterotetramers based on the C-terminal rSbpA₃₁₋₁₀₆₈-streptavidin fusion protein showed dirigible self-assembly formation due to the calcium ion dependency of lattice formation of SbpA. Such heterotetramers recrystallized on gold surfaces which were optionally precoated with SCWP [73] (Fig. 8.3). Analysis of negatively stained preparations of self-assembly products formed by heterotetramers revealed that neither the oblique S-layer lattice of SbsB nor the square lattice of SbpA was changed due to the presence of the fusion partner. Due to unhindered lattice formation and unchanged lattice parameters, the streptavidin moiety was considered as being located above the plane on the outer surface of

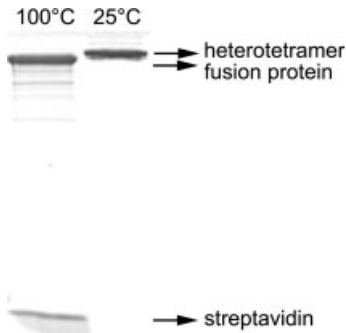


Fig. 8.2. Gel-shift assay of SDS extracts from heterotetramers purified by gel-permeation and affinity chromatography. The heterotetramers show the specific property of remaining in the

native state in 5% SDS at 25 °C, but dissociate into the S-layer–streptavidin fusion protein and streptavidin in 5% SDS at 100 °C.

the protein lattice. Digital image reconstructions of self-assembly products of heterotetramers containing the N-terminal rSbsB–streptavidin fusion protein in comparison to the SbsB lattice showed an additional protein mass on the SLH domain which resulted from the fused streptavidin [85] (Fig. 8.4). All self-assembly experiments confirmed that the first of the desired properties was present, i.e. unhindered recrystallization of the fusion protein into a two-dimensional crystalline array.

Since the fusion proteins were constructed from the wild-type streptavidin sequence, the biotin-binding sites were assumed to show the typical high affinity to

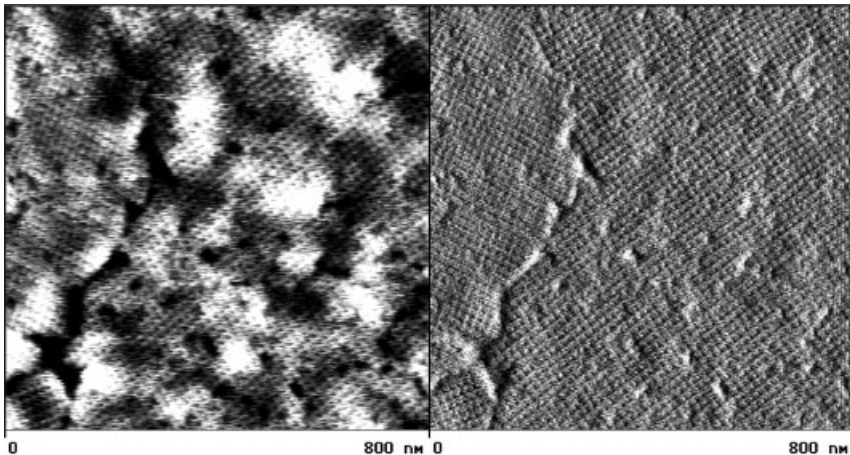


Fig. 8.3. SFM image of heterotetramers consisting of one chain of rSbpA_{31–1068}–streptavidin fusion protein and three chains of streptavidin. The heterotetramers recrystallized

into the square lattice structure on gold chips precoated with thiolated SCWP of *B. sphaericus* CCM 2177. Right: deflection mode. Left: height mode.

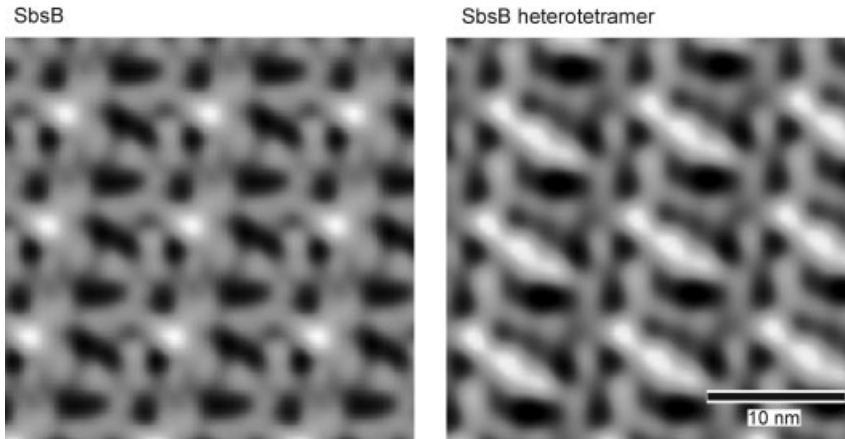


Fig. 8.4. Digital image reconstructions of electron micrographs taken of negatively stained preparations of self-assembly products formed by SbsB (left) and heterotetramers consisting of one chain of the N-terminal

rSbsB–streptavidin fusion protein and three chains of streptavidin (right). The streptavidin moiety of the heterotetramers can be seen as the additional protein mass above the plane of the oblique ($p1$) lattice structure.

biotin. However, it remained to be investigated if biotin-binding sites were sterically blocked by the large fusion partner SbsB or SbpA. The biotin-binding ability of soluble heterotetramers was determined by fluorescence quenching of tryptophan residues in the binding pockets of streptavidin upon biotin binding [73, 85, 87, 88]. Biotin, as well as biotinylated insulin (M_r 6 kDa), biotinylated horseradish peroxidase (M_r 44 kDa) and biotinylated serum albumin (M_r 66 kDa) were used for the fluorescence titration experiments. In comparison to free streptavidin which was used as reference protein, heterotetramers showed an even higher binding capacity for D-biotin, biotinylated insulin and biotinylated horseradish peroxidase. For biotinylated serum albumin, a similar binding capacity was determined.

In general, heterotetramers based on S-layer streptavidin fusion proteins are considered a universal affinity matrix for binding biotinylated molecules. As proof-of-principle, heterotetramers comprising C-terminal S-layer streptavidin fusion proteins were recrystallized on peptidoglycan-containing sacculi which were subsequently incubated with biotinylated ferritin as a marker that can be visualized by TEM. As shown in Fig. 8.5, heterotetramers based on the rSbpA_{31–1068}–streptavidin fusion protein showed excellent recrystallization properties, as well as high affinity to biotinylated ferritin.

As a first application approach, monolayers of heterotetramers based on the rSbpA_{31–1068}–streptavidin fusion protein were recrystallized on gold surfaces which were optionally precoated with thiolated SCWP. The obtained affinity matrix was used to perform hybridization experiments. In a first step, biotinylated oligonucleotides (30mers) were bound to the streptavidin moiety of the heterotetramers. Subsequently, complementary oligonucleotides were hybridized carrying one or two mismatches or they were without any mismatch (Fig. 8.6). Evaluation of the

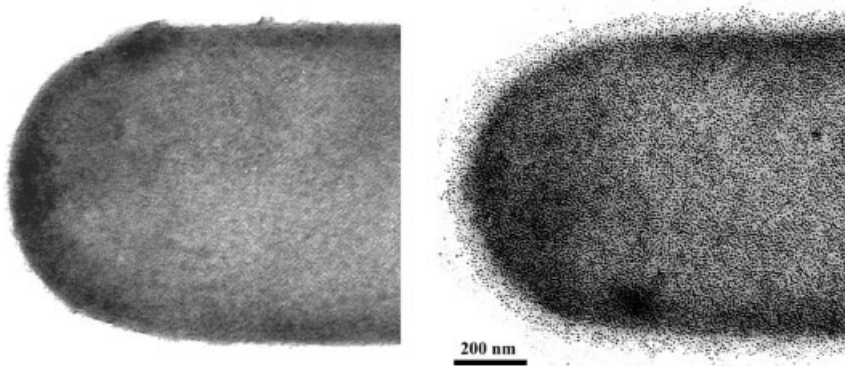


Fig. 8.5. Electron micrographs of negatively-stained preparations of heterotetramers consisting of one chain of rSbpA₃₁₋₁₀₆₈-streptavidin fusion protein and three chains of streptavidin. The heterotetramers were recrystallized on peptidoglycan-containing sacculi of *B. sphaericus* CCM 2177 (left) and subsequently incubated with biotinylated ferritin (right).

hybridization experiments were performed by applying surface-plasmon-field-enhanced fluorescence spectroscopy which combines the advantages of the high optical field intensities of surface plasmon waves with the sensitive detection of fluorescence light emission [89, 90]. For generating functional monomolecular protein lattices, two strategies were pursued – direct recrystallization of heterotetramers on plain gold chips or recrystallization on SCWP-coated gold chips. In both cases, the amount of recrystallized heterotetramers corresponded well to the theoretically calculated value for a monolayer [85]. The advantage of recrystallization on plain gold chips was seen in the strong interaction between the inner surface of the S-layer subunits and gold. This fact could be exploited to regenerate the

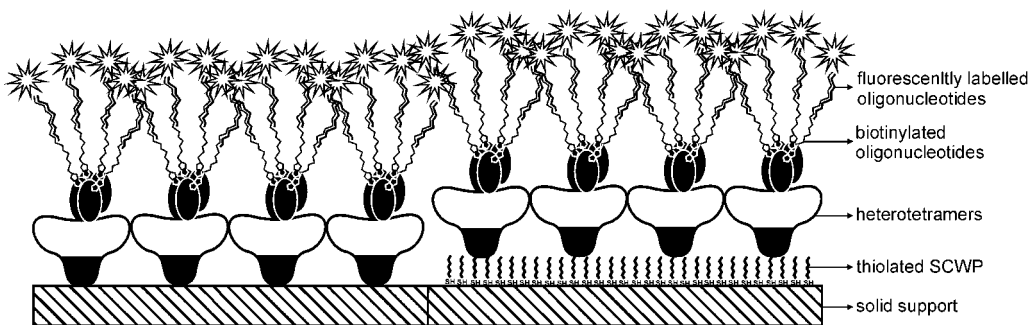


Fig. 8.6. Schematic drawing of heterotetramers consisting of one chain of rSbpA₃₁₋₁₀₆₈-streptavidin fusion protein and three chains of streptavidin, either recrystallized on plain gold chips or on gold

chips precoated with thiolated SCWP. After recrystallization into a monomolecular protein lattice, biotinylated oligonucleotides were bound to which fluorescently labeled oligonucleotides could hybridize.

sensor surface without any loss of heterotetramers, which could not be removed from the gold chip even with ethanol or chaotropic agents such as urea or guanidine hydrochloride. However, the advantage of using SCWP-coated gold chips lies in the unambiguously oriented recrystallization of the heterotetramers via their SCWP-binding domain located on the inner surface, as well in the lower detection limit for fluorescently labeled oligonucleotides. The latter can be explained by the fact that a higher distance between the gold surface and the fluorescently labeled oligonucleotides reduces quenching of fluorescence signals caused by the gold layer. However, monolayers generated on SCWP-coated gold chips were less stable, which was attributed to the rather labile gold-thiol linkage acting between the thiolated SCWP and the gold support. Nonspecific adsorption of DNA did not play a role which could be demonstrated by incubation of the sensor surface with oligonucleotides carrying two mismatches. For hybridization experiments on monolayers generated by recrystallization of heterotetramers on gold chips precoated with thiolated SCWP, fluorescently labeled oligonucleotides carrying one mismatch were used. The fluorescence intensity increased linearly at the beginning of the hybridization reaction, so that the linear slope of the increase in fluorescence intensity plotted versus the concentration of the hybridizing oligonucleotides showed a linear correlation [73]. In a different set of hybridization experiments which were performed on monolayers generated by direct recrystallization of heterotetramers on plain gold chips, the concentration of oligonucleotides carrying one mismatch was stepwise increased. The Langmuir isotherm which indicated that oligonucleotides in solution were in equilibrium with those bound to the monolayer carrying the biotinylated oligonucleotides could be established from the obtained fluorescence intensities (Fig. 8.7) [73]. The detection limit was found to be 1.57 pM on monolayers generated by recrystallization of heterotetramers on gold chips precoated with thiolated SCWP, whereas on plain gold chips the detection limit was determined to be at least 8.2 pM.

To conclude, the results obtained with heterotetramers consisting of one chain of S-layer streptavidin fusion protein and three chains of core streptavidin showed that the self-assembly properties of the S-layer protein moiety could be combined with the biotin-binding properties of streptavidin. First hybridization experiments indicated that a functional sensor surface could be generated by recrystallization of heterotetramers on gold chips, which could find numerous applications in (nano)biotechnology.

In a first approach, an S-layer fusion protein comprising the C-terminally truncated form rSbpA₃₁₋₁₀₆₈ and the variable region of a heavy chain camel antibody directed against lysozyme was constructed. The *Camelidae* is the only taxonomic family known to possess functional heavy chain antibodies lacking light chains and the first constant region. These unique antibody isotypes interact with the antigen by virtue of a single variable domain, termed VHH. A single VHH domain has a molecular mass of only 15 000 and is the smallest known complete antigen-binding fragment from a functional immunoglobulin (Fig. 8.8). The single-domain nature of VHHs gives rise to several unique features as compared to antigen-binding derivatives of conventional antibodies. As well as the advantage of

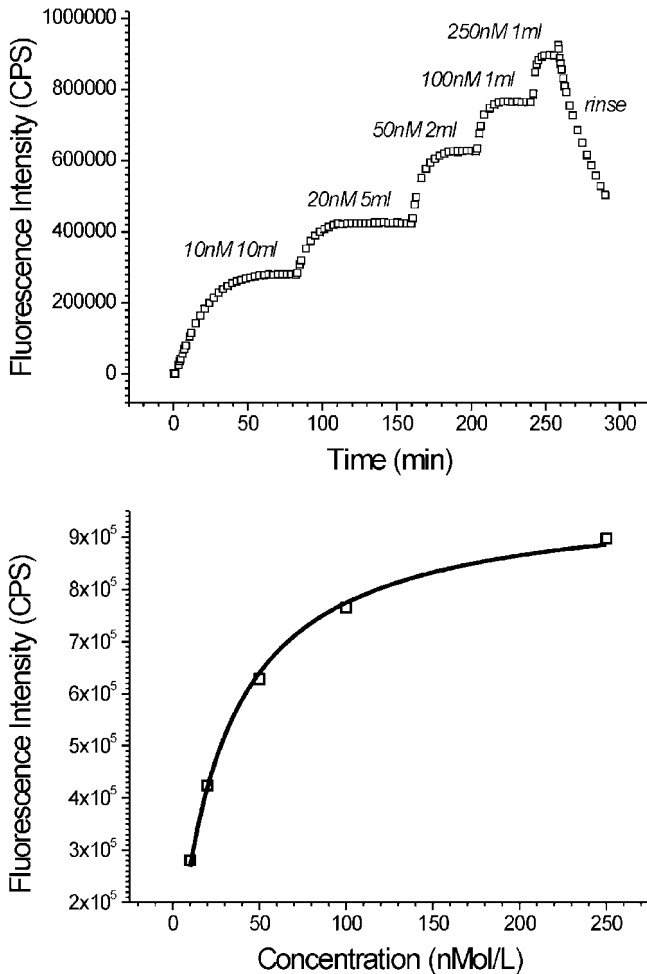


Fig. 8.7. Langmuir adsorption isotherm experiment of fluorescently labeled oligonucleotides carrying one mismatch hybridizing to complementary, biotinylated oligonucleotides bound to heterotetramers consisting of one chain of rSbpA₃₁₋₁₀₆₈-streptavidin fusion protein and three chains of streptavidin. By increasing the concentration of the fluorescently labeled oligonucleotides, higher equilibrium levels were reached (left side). The fluorescence intensities at the equilibrium are plotted against the concentrations of the solutions giving the Langmuir adsorption isotherm (right side).

single-gene cloning and selection from an *in vivo* matured library, recombinant VHs have other technological, functional and physicochemical advantages, such as (a) high expression yields and ease of purification, (b) a highly soluble and stable single domain immunoglobulin fold, (c) the generation of antigen-specific, high-affinity binders, (d) the recognition of unique conformational epitopes with the dominant involvement of its enlarged complementary determining regions, and

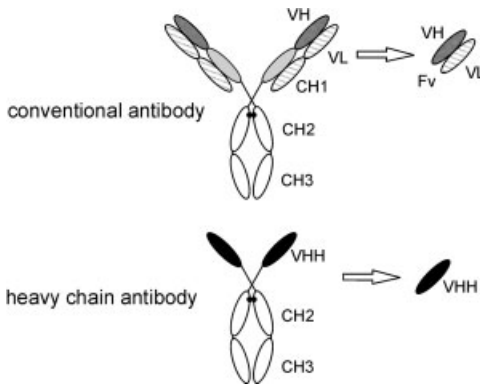


Fig. 8.8. Schematic drawing showing conventional (top) and heavy chain IgG antibodies (bottom) present in the serum of *Camelidae*. The complete light chains (dotted areas) and CH1 domains (black areas) are absent in heavy chain camel antibodies. The antigen-binding domains (Fv) of conventional antibodies as obtained after proteolysis or after

expression of the gene encoding VH or VL fragments are shown. The recombinant VHH (curved areas), the variable domain of a heavy chain camel antibody, can be obtained after cloning and expression. The VHH is the minimal intact antigen-binding fragment that can be generated.

(d) the close homology to human VHs (variable domain of the heavy chain) fragments [91, 92]. These features can be expected to lead to a number of applications in which VHHs perform better than conventional antibody fragments, e.g. as enzyme inhibitors, as modular building units for multivalent or multifunctional constructs, or as immunoadsorbents and detection units in biosensors. Due to these properties, VHHs clearly offer an improvement over conventional, more complex, antibody fragments, e.g. in diagnostic applications, for which the stability of the biomolecular probes is critical. Moreover, VHHs constitute ideal modular building blocks for manifold molecular constructs [91, 92]. To explore the potential advantages of camel single-domain antibodies and to gain insight into how they recognize their target, the crystal structure of a camel VHH complexed with hen's egg lysozyme was solved [93].

For construction of an S-layer fusion protein comprising the sequence of a single variable region of a camel heavy chain antibody directed against lysozyme (cAb-Lys3), the C-terminal truncation rSbpA₃₁₋₁₀₆₈ was selected as the base form. The obtained S-layer fusion protein, termed rSbpA₃₁₋₁₀₆₈/cAb-Lys3 was considered as a model system for the construction of further chimeric proteins, which comprised rSbpA₃₁₋₁₀₆₈ and cAbs directed against various antigens. Independent of the use of soluble or self-assembled rSbpA₃₁₋₁₀₆₈/cAb-Lys3, the camel antibody sequence remained accessible to lysozyme binding [70]. This was also observed for monolayers which were generated by recrystallization of the S-layer fusion protein on polystyrene substrates or on gold chips precoated with thiolated SCWP. In both cases, cAb-Lys3 was located on the outer S-layer surface and remained functional. As proof-of-principle could be provided with this model system, an S-layer fusion

protein incorporating the sequence of a variable domain of a heavy chain camel antibody (cAb-PSA-N7) directed against the prostate-specific antigen (PSA) was constructed [71]. PSA is a useful marker to screen potential prostate cancer patients. The current diagnostic test systems determine the concentration of total PSA with monoclonal antibodies that recognize free as well as PSA complexed with α_1 -antichymotrypsin (ACT). For their application in a PSA biosensor, VHHs recognizing free and complexed PSA are desired. Moreover, the kinetic requirements in the biosensor impose a high probe density that can probably only be achieved with single domain VHHs.

To generate a PSA-specific sensing layer for SPR measurements, the S-layer fusion protein rSbpA₃₁₋₁₀₆₈/cAb-PSA-N7 was recrystallized on gold chips precoated with thiolated SCWP [71]. The formation of the monomolecular protein lattice was confirmed by SFM, as well as by the level of the measured SPR signal. As derived from response levels measured for binding of PSA to a monolayer consisting of rSbpA₃₁₋₁₀₆₈/cAb-PSA-N7, the molar ratio between bound PSA and the S-layer fusion protein was 0.78, which means that at least three PSA molecules were bound per morphological unit of the square S-layer lattice [71]. To summarize, by using thiolated SCWP as a biomimetic linker to gold chips, a sensing layer for SPR could be generated by recrystallization of this S-layer fusion protein (Fig. 8.9). Due to the crystalline structure of the S-layer lattice, the fused ligand sequence showed a well-defined distance in the protein lattice and, according to the selected fusion site in the S-layer protein, they were located on the outermost surface, which reduced diffusion-limited reactions. A further advantage can be seen in the constant and low distance of the ligands from the optically active gold layer, which is exclusively determined by the thickness of the S-layer and lies in the range of only 10–15 nm. Thus, S-layer fusion proteins incorporating camel antibody sequences can be considered as key elements for the development of label-free detection systems such as SPR, surface acoustic wave (SAW) or quartz crystal microbalance (QCM-D), in which the binding event can be measured directly by the mass increase without the need of any labeled molecule.

The sequence encoding rSbpA₃₁₋₁₀₆₈ was also used as a base form for the construction of an IgG-binding fusion protein [72]. As fusion partner, the sequence

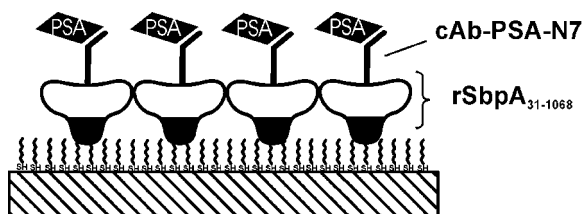


Fig. 8.9. Schematic drawing of the S-layer fusion protein rSbpA₃₁₋₁₀₆₈/cAb-PSA-N7 which was recrystallized on gold chips precoated with the thiolated SCWP. The monomolecular protein lattice was able to specifically bind PSA on the outermost surface.

encoding the Z domain, a synthetic analog of the IgG-binding domain of Protein A from *Staphylococcus aureus* was used. Protein A consists of a cell-wall-targeting domain and five other domains, termed C, B, A, D and E, with C next to the cell wall. X-ray analysis revealed that the B domain of Protein A consists of two contact sites that interact with the Fc part of IgG [94], leaving the Fab regions free for binding the antigen. Based on this knowledge, the synthetic Z domain which is 58 amino acids long and binds to the Fc part of IgG was constructed [95]. To generate the S-layer fusion protein, the 5'-end of the sequence encoding two copies of the Z domain was fused via a short linker to the gene encoding rSbpA₃₁₋₁₀₆₈ [72]. After heterologous expression in *E. coli*, the S-layer fusion protein was isolated from the host cells, purified by size-exclusion chromatography under denaturing conditions in guanidine hydrochloride, dialyzed and recrystallized on SPR gold chips which were precoated with thiolated SCWP of *B. sphaericus* CCM 2177. As shown by SFM, a monomolecular protein lattice with square symmetry was formed. The resonance units indicating the amount of bound protein corresponded to 4.3×10^{-5} nM mm⁻², which was in good accord with the theoretical value for a monolayer of 3.9×10^{-5} nM mm⁻². Native monolayers or monolayers crosslinked with the bifunctional imidoester dimethylpimelinimidate (DMP) were finally exploited for binding of human IgG. The amount that could be bound by the native monolayer was 2.9×10^{-5} nM or 4.35 ng IgG mm⁻², whereas in the case of the DMP-crosslinked monolayer 2.8×10^{-5} nM or 4.20 ng IgG mm⁻² could attach. These values corresponded to 65 and 67% of the theoretical saturation capacity of a planar surface for IgG (6.5 ng mm⁻²) with the Fab regions in the condensed state. As derived from these binding capacities, on average 2.7 and 2.6 IgG molecules were bound per morphological unit of the square S-layer lattice consisting of four identical subunits of the S-layer fusion protein.

For preparing biocompatible microparticles for the microsphere-based detoxification system (MDS) [78] to remove autoantibodies from sera from patients suffering from autoimmune disease, the S-layer fusion protein was recrystallized on SCWP-coated, 3- μ m cellulose-based microbeads. The MDS is an alternative approach to conventional immunoadsorption systems, in which the plasma does not perfuse on an adsorption column, but is recirculated into a filtrate compartment of a membrane module (Fig. 8.10). The addition of microbeads to the plasma circuit allows the rapid removal of the pathogenic substrates. In the case of microbeads that were covered with a native monolayer, the binding capacity was 1065 μ g human IgG mg⁻¹ S-layer fusion protein. For DMP-treated microbeads, a binding capacity of 870 μ g IgG mg⁻¹ S-layer fusion protein was determined. These values corresponded to 78 or 65% of the theoretical saturation capacity of a planar surface for IgG having the Fab regions in the condensed state. Bound IgG could be eluted with glycine-HCl buffer at a pH value of 2.2 and the microbeads were used for further IgG-binding experiments [72].

The major birch pollen allergen Bet v1 shares IgE epitopes with all tree pollen allergens from closely related species (e.g. alder hazel, hornbeam, beech). Because of high sequence identities among these allergens and well-studied cross-reactions with B cell epitopes, Bet v1 represents a model allergen [96]. The gene encoding

Microspheres Based Detoxification-System

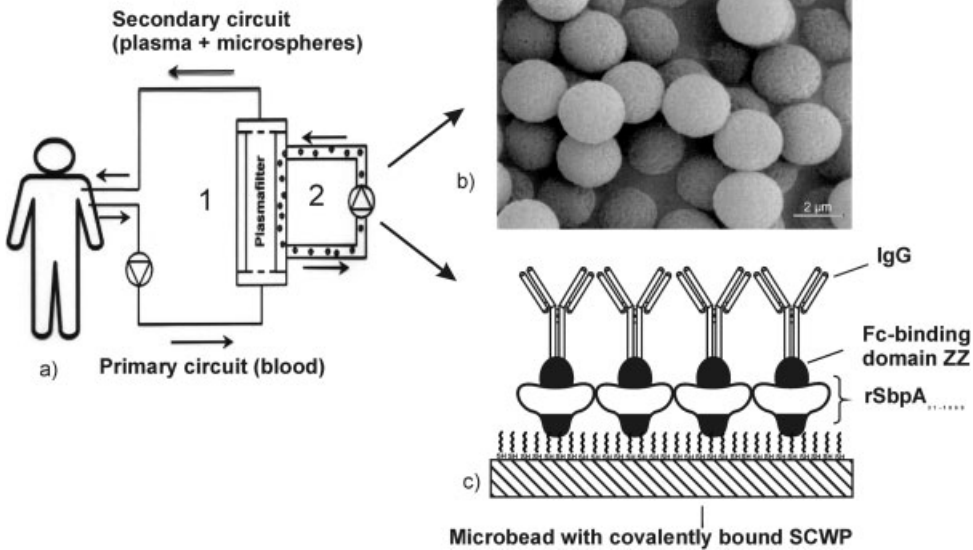


Fig. 8.10. (a) Schematic drawing demonstrating the working principle of the MDS. (b) Amine-modified cellulose microspheres. (c) Schematic drawing of microbeads covered with a monolayer consisting of rSbpA₃₁₋₁₀₆₈/ZZ. The S-layer

fusion protein was recrystallized on amine-modified cellulose microbeads to which thiolated SCWP had been covalently bound before. The fused ZZ domains could bind human IgG via the Fc part.

the chimeric S-layer proteins rSbsC₃₁₋₉₂₀/Bet v1 and rSbpA₃₁₋₁₀₆₈/Bet v1 carrying Bet v1 at the C-terminal end were cloned and expressed in *E. coli*. Ultrathin sections of whole *E. coli* cells induced to express the gene encoding rSbsC₃₁₋₉₂₀/Bet v1 revealed the presence of intracellular sheet-like or cylindrical structures [97], whereas rSbpA₃₁₋₁₀₆₈/Bet v1 accumulated in the form of inclusion bodies in the cytoplasm of the host cells [37]. The fusion proteins maintained the ability to self-assemble, as well as the functionality of the fused allergen to bind a Bet v1-specific monoclonal mouse antibody BIP1 (Fig. 8.11). The location and accessibility of the allergen moiety on the outer surface of the S-layer lattice were demonstrated by immunogold labeling of rSbsC₃₁₋₉₂₀/Bet v1 or rSbpA₃₁₋₁₀₆₈/Bet v1 recrystallized on native peptidoglycan-containing sacculi of *G. stearothermophilus* ATCC 12980 or *B. sphaericus* CCM 2177 [37, 97]. Thereby, the specific interaction between the N-terminal part of the S-layer proteins and the corresponding SCWP was exploited. The aim for the production of these S-layer fusion proteins was to use them for the development of diagnostic test systems to determine the concentration of Bet v1-specific IgE in patients' whole blood, plasma or serum. For that purpose, rSbpA₃₁₋₁₀₆₈/Bet v1 recrystallized as a monolayer on SCWP-coated plastic foils

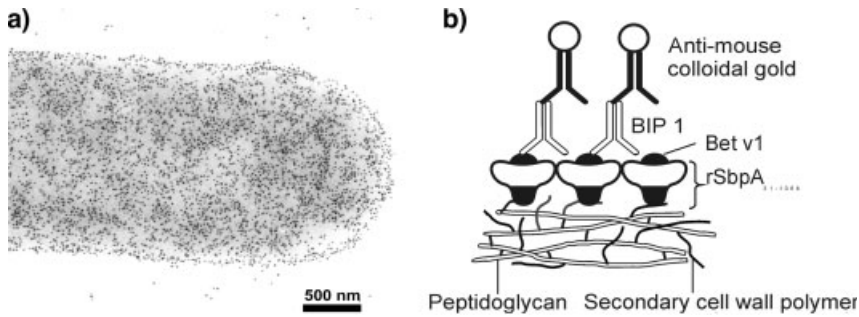


Fig. 8.11. (a) Electron micrograph of a negatively stained preparation demonstrating immunogold-labeling of rSbpA₃₁₋₁₀₆₈/Bet v1 recrystallized on peptidoglycan-containing

sacculi of *B. sphaericus* CCM 2177 using the Bet v1-specific monoclonal mouse antibody BIP1. (b) Schematic drawing of (a).

was used as reaction zone in dipstick-style solid-phase immunoassays for determination of Bet v1-specific IgE in serum samples of patients suffering from atopic allergy. In a recent study, the applicability of rSbsC₃₁₋₉₂₀/Bet v1 as a novel approach to design vaccines with reduced allergenicity in combination with strong immunomodulating capacity for immunotherapy of type I allergy was demonstrated [98]. This fusion protein exhibited all relevant Bet v1-specific B and T cell epitopes, but was significantly less efficient in releasing histamine than free Bet v1. In cells of birch pollen-allergic individuals, the fusion protein was capable of modulating the allergen-specific T_H2-dominated response into a more balanced T_H1/T_H0-like phenotype accompanied by enhanced production of interferon- γ and interleukin-10 [98]. To conclude, rSbsC₃₁₋₉₂₀/Bet v1 could find applications as carrier/adjuvants to design vaccines for specific immunotherapy of type 1 allergy with improved efficacy and safety.

Artificial lipid vesicles termed liposomes are widely used as delivery systems for enhancing the efficiency of various biologically active molecules [99]. S-layer-coated liposomes (S-liposomes) revealed an enhanced stability towards thermal and mechanical stress factors [24], and they represent simple model systems resembling features of virus envelopes. Thus, S-liposomes could find application in drug delivery or in gene therapy. In a recent study, the nucleotide sequence encoding enhanced green fluorescent protein (EGFP), a red-shifted green fluorescent protein (GFP)-derivative possessing a 30 times brighter fluorescence intensity at 488 nm than wild-type GFP [100], was fused to the 3'-end of the sequence encoding the C-terminally truncated form rSbpA₃₁₋₁₀₆₈ [83]. The chimeric gene encoding rSbpA₃₁₋₁₀₆₈/EGFP was cloned and expressed in *E. coli* host cells. As confirmed by fluorescence microscopy, 1 h after induction of expression an intense EGFP fluorescence was detected in the cytoplasm of the host cells. Expression at 28 °C instead of 37 °C, as usual for *E. coli* expression strains, resulted in clearly increased fluorescence intensity, indicating that the folding process of the EGFP moiety was

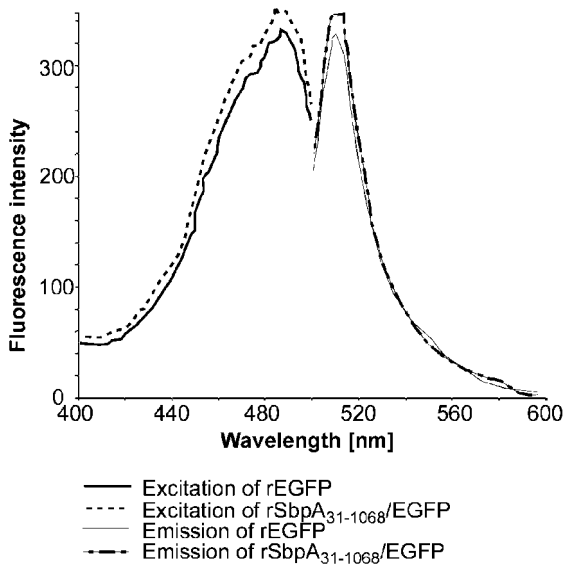


Fig. 8.12. Fluorescence excitation and emission spectra of rEGFP and of the fusion protein rSbpA₃₁₋₁₀₆₈/EGFP. Both proteins were applied in the same molar ratio and exhibited identical excitation peaks at 488 nm and emission peaks at 507 nm.

temperature sensitive. Electron microscopic investigation of ultrathin-sectioned preparations revealed that the S-layer fusion protein was located in inclusion bodies within the cytoplasm of the *E. coli* cells. To protect the EGFP portion against oxidation and to maintain the *in vitro* EGFP fluorescence capability, isolation of rSbpA₃₁₋₁₀₆₈/EGFP and purification by gel-permeation chromatography was performed in the presence of reducing agents. Comparison of excitation and emission spectra of rEGFP and rSbpA₃₁₋₁₀₆₈/EGFP indicated identical maxima at 488 and 507 nm, respectively (Fig. 8.12). Because of its intrinsic fluorescence, the fusion protein was recrystallized on positively charged liposomes and their uptake by eukaryotic cells was investigated by confocal laser scanning microscopy. The major part of the liposomes was internalized within 2 h of incubation and entered the HeLa cells by endocytosis [83]. In further studies, the uptake of liposomes coated with rSbpA₃₁₋₁₀₆₈/EGFP in combination with other S-layer fusion proteins, such as heterotetramers, by target cells and the functionality of transported drugs could be investigated simultaneously without any additional labeling.

Furthermore, this fusion protein was used for recrystallization on silicon wafers covered with polyelectrolytes, as well as for coating of hollow polyelectrolyte capsules. Fluorescence spectroscopy proved that the adsorption of rSbpA₃₁₋₁₀₆₈/EGFP on hollow capsules did not shift the fluorescence emission of the chromophore [25].

8.4

Spatial Control over S-Layer Reassembly

For many technical applications of S-layers, spatial control over reassembly is mandatory. For example, when S-layers are used as affinity matrix for the development of biochips or as templates in the fabrication of nanoelectronic devices, it is not necessary that the monolayer covers the entire area. Micromolding in capillaries is a well known soft-lithographical technique. In this technique, a poly(dimethylsiloxane) (PDMS) mold is first brought in conformal contact with a flat substrate, such as a silicon wafer. Subsequently, the S-layer protein solution is dropped onto the substrate in front of the channel openings of the attached mold and then the solution is sucked in so that the S-layer protein can recrystallize at all surfaces including the silicon. After removal of the mold, a patterned S-layer remains on the support. SFM is best suited to control the crystallinity of the S-layer monolayer and the border line to the blank areas. As micromolding in capillaries restricts the reassembly of the S-layer proteins to certain areas on a solid support, it offers the advantage that all preparation steps can be performed under ambient conditions. Proof-of-principle was shown for patterning the S-layer protein SbpA from *B. sphaericus* CCM 2177 on a silicon wafer with several different line-and-space ratios [101]. The S-layer protein showed perfect long-range order, and no visible leakage of the proteins into the tight interface between substrate and mold.

An alternative to micromolding in capillaries is patterning by conventional optical lithography using deep ultraviolet light (DUV) for exposure. In this approach, the S-layer protein was recrystallized on a silicon wafer covering the entire surface area. In the following step, the S-layer monolayer was dried in a stream of dry nitrogen prior to exposure in order to remove any water layer between the sample and the mask [102]. This is a critical step as denaturation of the S-layer protein and consequently loss of its structural integrity and functionality may occur. Then, a microlithographic mask was brought in conformal contact with the S-layer. The mask is usually made of a patterned chromium layer on quartz glass. Two different wavelengths of DUV were tested: argon fluoride excimer laser radiation (ArF; wavelength 193 nm) and krypton fluoride excimer laser radiation (KrF; wavelength 248 nm). SFM demonstrated that the S-layer protein was completely removed by ArF radiation with two pulses of $100\text{--}200\text{ mJ cm}^{-2}$ each and retained its structural integrity in the unexposed regions. Section analysis revealed a height difference between exposed and unexposed areas of about 8 nm, clearly demonstrating that the S-layer was completely removed in the exposed areas. According to the well-known paradigm of optics stating that the resolution is determined by the wavelength of the irradiating light, the highest achievable resolution was in the range of 100 nm. In contrast, the S-layer was not ablated by KrF irradiation. Instead, investigation of the irradiated S-layer lattice showed that increasing the electron dose from 10 pulses of about 100 mJ cm^{-2} to 10 pulses of about 35 mJ cm^{-2} only led to carbonization, but not to ablation, of the protein lattice.

8.5

S-Layers as Templates for the Formation of Regularly Arranged Nanoparticles

An important key to the fabrication of highly ordered functional arrays of nanoparticles is to provide suitable templates for spatially controlled particle deposition. The application of self-assembly systems for achieving perfect positional control at the molecular level appears feasible, both theoretically and experimentally, and offers striking advantages in the manufacturing process. S-layer proteins seem to be perfectly suited for this purpose as they have the intrinsic property to reassemble into two-dimensional arrays at various interfaces including silicon surfaces. Moreover, functional groups are repeated with the periodicity of the S-layer lattice at a distance of approximately 10 nm, thereby leading to regular arrays (superlattices) of bound foreign molecules and particles.

8.5.1

Binding of Molecules and Nanoparticles to Functional Domains

Geometrically confined binding of molecules on S-layer lattices may be induced by noncovalent and covalent forces. The pattern of bound molecules frequently reflects the lattice symmetry, the size of the morphological units and the surface properties of the underlying S-layer. For example, polycationic ferritin (PCF) is a 12 nm large, topographical marker for labeling negatively charged groups for TEM analysis. In several studies, PCF was used to determine the net charge of the outer and inner S-layer surface. In the case of the strictly anaerobic, hyperthermophilic archaeon *Thermoproteus tenax*, PCF was bound to the outer S-layer surface in an absolutely regular manner and reflected the hexagonal symmetry of the underlying S-layer [103]. The distance between the PCF molecules was about 30 nm and corresponded exactly to the center-to-center spacing of the morphological units (Fig. 8.13). The hexagonal super-lattice generated by the bound PCF exhibited the same orientation as the unlabeled S-layer with one axis perpendicularly to the longitudinal axis of the cells. *Methanospirillum hungatei* is a methanogenic archaeon which possesses a hollow tubular sheath that surrounds chains of cells. The sheaths show oblique (p2) lattice symmetry and they are composed of individual hoops [104]. The sheaths could be densely labeled with PCF molecules, which fitted to the widths of the hoops and were thus bound in exact rows. A superlattice of PCF was also observed on the hexagonal S-layer of *Thermoanaerobacter thermohydrosulfuricus* L111-69 after converting the hydroxyl groups from the carbohydrate chain of this S-layer glycoprotein into carboxylic acid groups which was achieved by succinylation [105]. The size of the PCF molecules corresponded well to the center-to-center spacing of the morphological units of the hexagonal lattice of 14.2 nm. Ultrathin-sections of such modified S-layers revealed that due to the length of the carbohydrate chains, the PCF molecules formed even two superimposed layers. In contrast, covalent attachment of ferritin to the carbodiimide-activated carboxylic acid groups of the acidic amino acids led only to small patches of hexago-

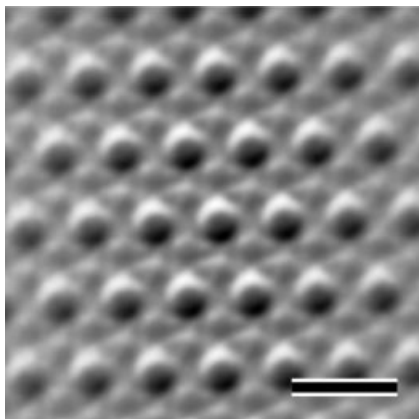


Fig. 8.13. TEM image of a freeze-dried preparation of PCF regularly bound to the hexagonally ordered S-layer of *Thermoproteus tenax*. The signal-to-noise ratio was enhanced by crosscorrelation averaging. Bar: 50 nm.

nally ordered ferritin molecules. On the glutaraldehyde-treated, crosslinked outer S-layer surface of the square lattice from *B. sphaericus* CCM 2177 with a lattice constant of 13.1 nm, PCF molecules were bound to the net negatively charged carboxylic acid groups of the acidic amino acids and clearly reflected the square symmetry of the underlying S-layer lattice.

In another approach the S-layer protein SbpA from *B. sphaericus* CCM 2177 was recrystallized on SiO₂-coated grids [106]. These grids were mimicking the surface properties of silicon wafers, but allowed investigation of the preparations by TEM. In particular, when rendered hydrophilic by oxygen plasma treatment, the S-layer protein formed a monolayer with the outer surface exposed to the environment. It could be demonstrated that after crosslinking the free amine groups in the S-layer lattice with glutaraldehyde and activation of the free carboxylic acid groups with carbodiimide, a close-packed monolayer of 4 nm amino-functionalized CdSe nanoparticles was covalently bound to the protein lattice. However, the amine-functionalized nanoparticles did not resemble the lattice parameters of the S-layer very well as approximately 1.6×10^6 carboxylic acid groups μm^{-2} offered too many equivalent binding sites. Furthermore, for studying the noncovalent binding of nanoparticles, anionic citrate-stabilized gold nanoparticles (5 nm diameter) were used [106, 107]. The negatively charged gold nanoparticles were bound at the inner surface of S-layer self-assembly products. The amount of bound gold nanoparticles per unit area depended on the size of the nanoparticles. Gold nanoparticles with a size of about 10 nm were only randomly bound, whereas 2 nm nanoparticles were densely packed on the S-layer surface. Nevertheless, 5 nm gold nanoparticles were regularly bound, resembling the underlying square S-layer lattice.

8.5.2

In Situ Synthesis of Nanoparticles on S-Layers

As an alternative to the regular binding of preformed nanoparticles, S-layers can be also used as periodic nanometric templates in the nucleation of inorganic nanoparticles. The very first experiments were performed almost two decades ago and used S-layer fragments deposited onto a solid substrate as a porous mask [108]. In this and the following works [109–111], various metals were evaporated onto the S-layer fragments forming nanoparticles arrays on the substrate due to the periodic arrangement of the pores in the protein lattice. After removal of the S-layer and excess material by ion milling, the regular pattern of metallic nanoparticles became available for further use. It was also demonstrated that S-layer proteins recrystallized on solid supports or S-layer self-assembly products which were deposited on such supports could be used to induce the formation of CdS particles [112] or gold nanoparticles [113]. Inorganic superlattices of CdS with either oblique or square lattice symmetries were fabricated by exposing the S-layer lattices to cadmium ion solutions followed by slow reduction with hydrogen sulfide. Precipitation of the inorganic phase was confined to the pores of the S-layers with the result that CdS superlattices with prescribed symmetries were obtained. In a similar procedure a square superlattice of uniform 4–5 nm gold particles with a 13.1 nm repeat distance was fabricated by exposing a square S-layer lattice which carried thiol groups that had been introduced by chemical modification before to a tetrachloroauric(III) acid solution [113]. TEM analysis showed that the gold nanoparticles were formed in the pore region during electron irradiation of an initially grainy gold coating covering the whole S-layer lattice. The shape of the gold particles resembled the morphology of the pore region of the square S-layer lattice. Electron diffraction patterns revealed that the gold nanoparticles were crystalline, but in the long-range order not crystallographically aligned. Furthermore, this technique was also used for the precipitation of metal nanoparticles from solutions, such as palladium from PdCl₂, nickel from NiSO₄, platinum from K₂PtCl₆, lead from Pb(NO₃)₂ and ferrum from KFe [Fe(CN)₆]. Wet chemistry was also applied for producing platinum nanoparticles on the S-layer of *Sporosarcina ureae* [114–117]. One morphological unit of the S-layer lattice of *S. ureae* revealed seven platinum cluster sites with a diameter of around 1.9 nm. These experiments clearly demonstrated that nanocrystal superlattices can be induced by S-layers as templates with a broad range of particle sizes (5–15 nm diameter), interparticle spacings (up to 30 nm) and lattice symmetries (oblique, square or hexagonal).

8.6

Conclusions and Outlook

Basic research on the structure, genetics, chemistry, assembly and function of S-layers has led to a broad spectrum of applications in nanobiotechnology and biomimetics. The remarkable intrinsic feature of S-layer proteins and the possibilities for

genetic modifications and combining S-layer lattices with other functional molecules in a spatial predictable way turns them into unique patterning elements for bottom-up strategies. Although, up to now the development of S-layer technologies has primarily focused on life science applications, an important field of future applications concerns nonlife sciences and bioinspired nanomaterials.

Acknowledgments

This work was supported by the Austrian Science Fonds (FWF; project P17170-MOB) and by the Erwin Schrödinger-Society for Nanosciences.

References

- 1 CLARK, J., SINGER, E. M., KORNS, D. R., SMITH, S. S., Design and analysis of nanoscale bioassemblies, *BioTechniques* **2004**, *36*, 992–1001.
- 2 NIEMEYER, C. M., MIRKIN, C. A. (Eds.), *Nanobiotechnology: Concepts, Applications and Perspectives*, Wiley-VCH, Weinheim, **2004**.
- 3 SEEMAN, N. C., BELCHER, A. M., Emulating biology: building nanostructures from the bottom up, *Proc. Natl Acad. Sci. USA* **2002**, *99*, 6451–6455.
- 4 SLEYTR, U. B., MESSNER, P., PUM, D., SÁRA, M., Crystalline bacterial cell surface layers (S-layers): from supramolecular cell structure to biomimetics and nanotechnology, *Angew. Chem. Int. Ed.* **1999**, *38*, 1034–1054.
- 5 SLEYTR, U. B., SÁRA, M., PUM, D., Crystalline bacterial cell surface layers (S-layers): a versatile self-assembly system, In *Supramolecular Polymerization*, CIFERRI, A. (Ed.), Marcel Dekker, New York, **2000**, pp. 177–213.
- 6 SLEYTR, U. B., SÁRA, M., PUM, D., SCHUSTER, B., MESSNER, P., SCHÄFFER, C., Self Assembly protein systems: microbial S-layers, In *Biopolymers 7*, STEINBÜCHEL, A., FAHNSTOCK, S. (Eds.), Wiley-VCH, Weinheim, **2003**, pp. 285–338.
- 7 SLEYTR, U. B., PUM, D., SÁRA, M., SCHUSTER, B., Molecular nanotechnology with 2-D protein crystals, In *Encyclopedia of Nanoscience and Nanotechnology 5*, NALWA, H. S. (Ed.), Academic Press, San Diego, CA, **2004**, pp. 693–702.
- 8 SLEYTR, U. B., PUM, D., SCHUSTER, B., SÁRA, M., Molecular nanotechnology and nanobiotechnology with two-dimensional protein crystals (S-layers), In *Nano-Surface Chemistry*, ROSOFF, M. (Ed.), Marcel Dekker, New York, **2001**, pp. 333–389.
- 9 SCHUSTER, B., GYÖRVARY, E., PUM, D., SLEYTR, U. B., Nanotechnology with S-layer proteins, In *Protein Nanotechnology: Protocols, Instrumentation and Applications*, VO-DINH, T. (Ed.), Humana Press, Totowa, NJ, **2005**, pp. 101–124.
- 10 KARRASCH, S., HEGERL, R., HOCH, J., BAUMEISTER, W., ENGEL, A., Atomic force microscopy produces faithful high-resolution images of protein surfaces in an aqueous environment, *Proc. Natl Acad. Sci. USA* **1994**, *91*, 836–838.
- 11 MÜLLER, D. J., BAUMEISTER, W., ENGEL, A., Conformational change of the hexagonally packed intermediate layer of *Deinococcus radiodurans* monitored by atomic force microscopy, *J. Bacteriol.* **1996**, *178*, 3025–3030.
- 12 SCHEURING, S., STAHLBERG, H., CHAMI, M., HOUSSIN, C., RIGAUD,

- J. L., ENGEL, A., Charting and unzipping the surface layer of *Corynebacterium glutamicum* with the atomic force microscope, *Mol. Microbiol.* **2002**, *44*, 675–684.
- 13 KÖNIG, H., Archaeobacterial cell envelopes, *Can. J. Microbiol.* **1988**, *34*, 395–406.
- 14 STETTER, K. O., Hyperthermophilic prokaryotes, *FEMS Microbiol. Rev.* **1996**, *18*, 149–158.
- 15 MESSNER, P., SLEYTR, U. B., Crystalline bacterial cell-surface layers, *Adv. Microbiol. Physiol.* **1992**, *33*, 213–275.
- 16 SLEYTR, U. B., BEVERIDGE, T. J., Bacterial S-layers, *Trends Microbiol.* **1999**, *7*, 253–260.
- 17 PUM, D., SLEYTR, U. B., Monomolecular reassembly of a crystalline bacterial cell surface layer (S-layer) on untreated and modified silicon surfaces, *Supramol. Sci.* **1995**, *2*, 193–197.
- 18 GYÖRVÁRY, E. S., STEIN, O., PUM, D., SLEYTR, U. B., Self-assembly and recrystallization of bacterial S-layer proteins at silicon supports imaged in real time by atomic force, *J. Microsc.* **2003**, *212*, 300–306.
- 19 PUM, D., WEINHANDL, M., HÖDL, C., SLEYTR, U. B., Large-scale recrystallization of the S-layer of *Bacillus coagulans* E38-66 at the air/water interface and on lipid films, *J. Bacteriol.* **1993**, *175*, 2762–2766.
- 20 PUM, D., SLEYTR, U. B., Large scale reconstitution of crystalline bacterial surface layer (S-layer) proteins at the air/water interface and on lipid films, *Thin Solid Films* **1994**, *244*, 882–886.
- 21 KÜPCÜ, S., SÁRA, M., SLEYTR, U. B., Liposomes coated with crystalline bacterial cell surface protein (S-layer) as immobilization structures for macromolecules, *Biochim. Biophys. Acta* **1995**, *1235*, 263–269.
- 22 KÜPCÜ, S., LOHNER, K., MADER, C., SLEYTR, U. B., Microcalorimetric study on the phase behaviour of S-layer coated liposomes, *Mol. Membr. Biol.* **1998**, *15*, 69–74.
- 23 MADER, C., KÜPCÜ, S., SÁRA, M., SLEYTR, U. B., Stabilizing effect of an S-layer on liposomes towards thermal or mechanical stress, *Biochim. Biophys. Acta* **1999**, *1418*, 106–116.
- 24 MADER, C., KÜPCÜ, S., SLEYTR, U. B., SÁRA, M., S-layer-coated liposomes as a versatile system for entrapping and binding target molecules, *Biochim. Biophys. Acta* **2000**, *1463*, 142–150.
- 25 TOCA-HERRERA, J. L., KRASTEV, R., BOSIO, V., KÜPCÜ, S., PUM, D., FERY, A., SÁRA, M., SLEYTR, U. B., Recrystallization of bacterial S-layers on flat polyelectrolyte surfaces and hollow polyelectrolytes capsules, *Small* **2005**, *1*, 339–348.
- 26 SÁRA, M., SLEYTR, U. B., S-Layer proteins, *J. Bacteriol.* **2000**, *182*, 859–868.
- 27 BOOT, H. J., KOLEN, C. P., POWELS, P. H., Identification, cloning, and nucleotide sequence of a silent S-layer protein gene of *Lactobacillus acidophilus* ATCC 4356 which has extensive similarity with the S-layer protein gene of this species, *J. Bacteriol.* **1995**, *177*, 7222–7230.
- 28 BRÖCKL, G., BEHR, M., FABRY, S., HENSEL, R., KAUEWITZ, H., BIENDL, E., KÖNIG, H., Analysis and nucleotide sequence of the genes encoding the surface-layer glycoproteins of the hyperthermophilic methanogens *Methanothermus fervidus* and *Methanothermus sociabilis*, *Eur. J. Biochem.* **1991**, *199*, 147–152.
- 29 MESSNER, P., SCHÄFFER, C., Surface layer glycoproteins of bacteria and archaea, In *Glycomicrobiology*, DOYLE, R. J. (Ed.), Kluwer, New York, **2000**, pp. 93–125.
- 30 SCHÄFFER, C., MESSNER, P., Glycobiology of surface layer proteins, *Biochimie* **2001**, *83*, 591–599.
- 31 NOVOTNY, R., PFÖSTL, A., MESSNER, P., SCHÄFFER, C., Genetic organization of chromosomal S-layer glycan biosynthesis loci of Bacillaceae, *Glycoconj. J.* **2004**, *20*, 435–447.
- 32 ENGELHARDT, H., PETERS, J., Structural research on surface layers: a focus on stability, surface layer homology domains, and surface layer-cell wall interactions, *J. Struct. Biol.* **1998**, *124*, 276–302.
- 33 BRECHTEL, E., BAHL, H., In *Thermo-*

- anaerobacterium thermosulfurigenes* EM1 S-layer homology domains do not attach to peptidoglycan, *J. Bacteriol.* **1999**, *181*, 5017–5023.
- 34 CAVA, F., DE PEDRO, M. A., SCHWARZ, H., HENNE, A., BERENQUER, J., Binding to pyruvylated compounds as an ancestral mechanism to anchor the outer envelope in primitive bacteria, *Mol. Microbiol.* **2004**, *52*, 677–690.
- 35 HUBER, C., ILK, N., RÜNZLER, D., EGELSEER, E. M., WEIGERT, S., SLEYTR, U. B., SÁRA, M., The three S-layer-like homology motifs of the S-layer protein SbpA of *Bacillus sphaericus* CCM 2177 are not sufficient for binding to the pyruvylated secondary cell wall polymer, *Mol. Microbiol.* **2005**, *55*, 197–205.
- 36 ILK, N., KOSMA, P., PUCHBERGER, M., EGELSEER, E. M., MAYER, H. F., SLEYTR, U. B., SÁRA, M., Structural and functional analyses of the secondary cell wall polymer of *Bacillus sphaericus* CCM 2177 that serves as an S-layer-specific anchor, *J. Bacteriol.* **1999**, *181*, 7643–7646.
- 37 ILK, N., VÖLLENKLE, C., EGELSEER, E. M., BREITWIESER, A., SLEYTR, U. B., SÁRA, M., Molecular characterization of the S-layer gene, *sbpA*, of *Bacillus sphaericus* CCM 2177 and production of a functional S-layer fusion protein with the ability to recrystallize in a defined orientation while presenting the fused allergen, *Appl. Environ. Microbiol.* **2002**, *68*, 3251–3260.
- 38 MADER, C., HUBER, C., MOLL, D., SLEYTR, U. B., SÁRA, M., Interaction of the crystalline bacterial cell surface layer protein SbsB and the secondary cell wall polymer of *Geobacillus stearothermophilus* PV72 assessed by real-time surface plasmon resonance biosensor technology, *J. Bacteriol.* **2004**, *186*, 1758–1768.
- 39 MESNAGE, S., TOSI-COUTURE, E., FOUET, A., Production and cell surface anchoring of functional fusions between the SLH motifs of the *Bacillus anthracis* S-layer proteins and the *Bacillus subtilis* levansucrase, *Mol. Microbiol.* **1999**, *31*, 927–936.
- 40 MESNAGE, S., FONTAINE, T., MIGNOT, T., DELEPIERRE, M., MOCK, M., FOUET, A., Bacterial SLH domain proteins are non-covalently anchored to the cell surface via a conserved mechanism involving wall polysaccharide pyruvylation, *EMBO J.* **2000**, *19*, 4473–4484.
- 41 RÜNZLER, D., HUBER, C., MOLL, D., KÖHLER, G., SÁRA, M., Biophysical characterization of the entire bacterial surface layer protein SbsB and its two distinct functional domains, *J. Biol. Chem.* **2004**, *279*, 5207–5215.
- 42 EGELSEER, E. M., LEITNER, K., JAROSCH, M., HOTZY, C., ZAYNI, S., SLEYTR, U. B., SÁRA, M., The S-layer proteins of two *Bacillus stearothermophilus* wild-type strains are bound via their N-terminal region to a secondary cell wall polymer of identical chemical composition, *J. Bacteriol.* **1998**, *180*, 1488–1495.
- 43 JAROSCH, M., EGELSEER, E. M., MATTANOVICH, D., SLEYTR, U. B., SÁRA, M., S-layer gene *sbsC* of *Bacillus stearothermophilus* ATCC 12980: molecular characterization and heterologous expression in *Escherichia coli*, *Microbiology* **2000**, *146*, 273–281.
- 44 JAROSCH, M., EGELSEER, E. M., HUBER, C., MOLL, D., MATTANOVICH, D., SLEYTR, U. B., SÁRA, M., Analysis of the structure-function relationship of the S-layer protein SbsC of *Bacillus stearothermophilus* ATCC 12980 by producing truncated forms, *Microbiology* **2001**, *147*, 1353–1363.
- 45 SCHÄFFER, C., WUGEDITSCH, T., KÄHLIG, H., SCHEBERL, A., ZAYNI, S., MESSNER, P., The surface layer (S-layer) glycoprotein of *Geobacillus stearothermophilus* NRS 2004/3a. Analysis of its glycosylation, *J. Biol. Chem.* **2002**, *277*, 6230–6239.
- 46 SCHÄFFER, C., KÄHLIG, H., CHRISTIAN, R., SCHULZ, G., ZAYNI, S., MESSNER, P., The diacetamidodideoxyuronic-acid-containing glycan chain of *Bacillus stearothermophilus* NRS 2004/3a represents the secondary cell-wall polymer of wild-type *B. stearothermophilus* strains, *Microbiology* **1999**, *145*, 1575–1583.

- 47 WEIS, W. I., Cell-surface carbohydrate recognition by animal and viral lectins, *Curr. Opin. Struct. Biol.* **1997**, *7*, 624–630.
- 48 SMIT, E., OLING, F., DEMEL, R., MARTINEZ, B., POWWELS, P. H., The S-layer protein of *Lactobacillus acidophilus* ATCC 4356: identification and characterisation of domains responsible for S-protein assembly and cell wall binding, *J. Mol. Biol.* **2001**, *305*, 245–257.
- 49 MASUDA, K., KAWATA, T., Reassembly of a regularly arranged protein in the cell wall of *Lactobacillus buchneri* and its reattachment to cell walls: chemical modification studies, *Microbiol. Immunol.* **1985**, *29*, 927–938.
- 50 SÁRA, M., Conserved anchoring mechanisms between crystalline cell surface S-layer proteins and secondary cell wall polymers in Gram-positive bacteria?, *Trends Microbiol.* **2001**, *9*, 47–49.
- 51 AWRAM, P., SMIT, J., Identification of lipopolysaccharide O-antigen synthesis genes required for attachment of the S-layer of *Caulobacter crescentus*, *Microbiology* **2001**, *147*, 1451–1460.
- 52 BINGLE, W. H., NOMELLINI, J. F., SMIT, J., Linker mutagenesis of the *Caulobacter crescentus* S-layer protein: toward a definition of an N-terminal anchoring region and a C-terminal secretion signal and the potential for heterologous protein secretion, *J. Bacteriol.* **1997**, *179*, 601–611.
- 53 DWORKIN, J., BLASER, M. J., Molecular mechanisms of *Campylobacter fetus* surface layer protein expression, *Mol. Microbiol.* **1997**, *26*, 433–440.
- 54 BINGLE, W. H., NOMELLINI, J. F., SMIT, J., Cell-surface display of a *Pseudomonas aeruginosa* strain K pilin peptide within the paracrystalline S-layer of *Caulobacter crescentus*, *Mol. Microbiol.* **1997**, *26*, 277–288.
- 55 NOONAN, B., TRUST, T. J., The leucine zipper of *Aeromonas salmonicida* AbcA is required for the transcriptional activation of the P2 promoter of the surface-layer structural gene, vapA, in *Escherichia coli*, *Mol. Microbiol.* **1995**, *17*, 379–386.
- 56 NOONAN, B., TRUST, T. J., Molecular analysis of an A-protein secretion mutant of *Aeromonas salmonicida* reveals a surface layer-specific protein secretion pathway, *J. Mol. Biol.* **1995**, *248*, 316–327.
- 57 CASTAN, P., DE PEDRO, M. A., RISCO, C., VALLES, C., FERNANDEZ, L. A., SCHWARZ, H., BERENQUER, J., Multiple regulatory mechanisms act on the 5' untranslated region of the S-layer gene from *Thermus thermophilus* HB8, *J. Bacteriol.* **2001**, *183*, 1491–1494.
- 58 JAKAVA-VILJANEN, M., AVALL-JAASKELAINEN, S., MESSNER, P., SLEYTR, U. B., PALVA, A., Isolation of three new surface layer protein genes (*slp*) from *Lactobacillus brevis* ATCC 14869 and characterization of the change in their expression under aerated and anaerobic conditions, *J. Bacteriol.* **2002**, *184*, 6786–6795.
- 59 SÁRA, M., PUM, D., KÜPCÜ, S., MESSNER, P., SLEYTR, U. B., Isolation of two physiologically induced variant strains of *Bacillus stearothermophilus* NRS 2004/3a and characterization of their S-layer lattices, *J. Bacteriol.* **1994**, *176*, 848–860.
- 60 SÁRA, M., KUEN, B., MAYER, H. F., MANDL, F., SCHUSTER, K. C., SLEYTR, U. B., Dynamics in oxygen-induced changes in S-layer protein synthesis from *Bacillus stearothermophilus* PV72 and the S-layer-deficient variant T5 in continuous culture and studies of the cell wall composition, *J. Bacteriol.* **1996**, *178*, 2108–2117.
- 61 DWORKIN, J., TUMMURU, M. K., BLASER, M. J., A lipopolysaccharide-binding domain of the *Campylobacter fetus* S-layer protein resides within the conserved N terminus of a family of silent and divergent homologs, *J. Bacteriol.* **1995**, *177*, 1734–1741.
- 62 EGELSEER, E. M., DANHORN, T., PLESCHBERGER, M., HOTZY, C., SLEYTR, U. B., SÁRA, M., Characterization of an S-layer glycoprotein produced in the course of S-layer variation of *Bacillus stearothermophilus* ATCC 12980 and sequencing and cloning of the *sbsD* gene encoding the protein moiety, *Arch. Microbiol.* **2001**, *177*, 70–80.

- 63 GROGONO-THOMAS, R., BLASER, M. J., AHMADI, M., NEWELL, D. G., Role of S-layer protein antigenic diversity in the immune responses of sheep experimentally challenged with *Campylobacter fetus* subsp. *fetus*, *Infect. Immun.* **2003**, *71*, 147–154.
- 64 SCHOLZ, H. C., RIEDMANN, E., WITTE, A., LUBITZ, W., KUEN, B., S-layer variation in *Bacillus stearothermophilus* PV72 is based on DNA rearrangements between the chromosome and the naturally occurring megaplasmids, *J. Bacteriol.* **2001**, *183*, 1672–1679.
- 65 GUSTAFSON, C. E., CHU, S., TRUST, T. J., Mutagenesis of the paracrystalline surface protein array of *Aeromonas salmonicida* by endogenous insertion elements, *J. Mol. Biol.* **1994**, *237*, 452–463.
- 66 EGELSEER, E. M., IDRIS, R., JAROSCH, M., DANHORN, T., SLEYTR, U. B., SÁRA, M., ISBst12, a novel type of insertion-sequence element causing loss of S-layer-gene expression in *Bacillus stearothermophilus* ATCC 12980, *Microbiology* **2000**, *146*, 2175–2183.
- 67 SCHOLZ, H., HUMMEL, S., WITTE, A., LUBITZ, W., KUEN, B., The transposable element IS4712 prevents S-layer gene (*sbsA*) expression in *Bacillus stearothermophilus* and also affects the synthesis of altered surface layer proteins, *Arch. Microbiol.* **2000**, *174*, 97–103.
- 68 RIES, W., HOTZY, C., SCHOCHER, I., SLEYTR, U. B., SÁRA, M., Evidence that the N-terminal part of the S-layer protein from *Bacillus stearothermophilus* PV72/p2 recognizes a secondary cell wall polymer, *J. Bacteriol.* **1997**, *179*, 3892–3898.
- 69 SÁRA, M., DEKITSCH, C., MAYER, H. F., EGELSEER, E. M., and SLEYTR, U. B., Influence of the secondary cell wall polymer on the reassembly, recrystallization and stability properties of the S-layer protein from *Bacillus stearothermophilus* PV72/p2., *J. Bacteriol.* **1998**, *180*, 4146–4153.
- 70 PLESCHBERGER, M., NEUBAUER, A., EGELSEER, E. M., WEIGERT, S., LINDNER, B., SLEYTR, U. B., MUYLDERMANS, S., SÁRA, M., Generation of a functional monomolecular protein lattice consisting of an S-layer fusion protein comprising the variable domain of a camel heavy chain antibody, *Bioconjug. Chem.* **2003**, *14*, 440–448.
- 71 PLESCHBERGER, M., SAERENS, D., WEIGERT, S., SLEYTR, U. B., MUYLDERMANS, S., SÁRA, M., EGELSEER, E. M., An S-layer heavy chain camel antibody fusion protein for generation of a nanopatterned sensing layer to detect the prostate-specific antigen by surface plasmon resonance technology, *Bioconjug. Chem.* **2004**, *15*, 664–671.
- 72 VÖLLENKLE, C., WEIGERT, S., ILK, N., EGELSEER, E. M., WEBER, V., LOTH, F., FALKENHAGEN, D., SLEYTR, U. B., SÁRA, M., Construction of a functional S-layer fusion protein comprising an immunoglobulin G-binding domain for development of specific adsorbents for extracorporeal blood purification, *Appl. Environ. Microbiol.* **2004**, *70*, 1514–1521.
- 73 HUBER, C., LIU, J., EGELSEER, E. M., MOLL, D., KNOLL, W., SLEYTR, U. B., SÁRA, M., Heterotetramers formed by an S-layer-streptavidin fusion protein and core-streptavidin as nanoarrayed template for biochip development, *SMALL* (accepted).
- 74 SÁRA, M., PUM, D., SCHUSTER, B., SLEYTR, U. B., S-layers as patterning element for nanobiotechnological applications, *J. Nanosci. Nanotechnol.* **2005**, in press.
- 75 HOWORKA, S., SÁRA, M., WANG, Y., KUEN, B., SLEYTR, U. B., LUBITZ, W., BAYLEY, H., Surface-accessible residues in the monomeric and assembled forms of a bacterial surface layer protein, *J. Biol. Chem.* **2000**, *275*, 37876–37886.
- 76 WEINER, C., SÁRA, M., SLEYTR, U. B., Novel protein A affinity matrix prepared from two-dimensional protein crystals, *Biotechnol. Bioeng.* **1994**, *43*, 321–330.
- 77 WEINER, C., SÁRA, M., DASGUPTA, G., SLEYTR, U. B., Affinity cross-flow filtration: purification of IgG with a

- novel protein A affinity matrix prepared from two-dimensional protein crystals, *Biotechnol. Bioeng.* **1994**, *44*, 55–65.
- 78 WEBER, V., WEIGERT, S., SÁRA, M., SLEYTR, U. B., FALKENHAGEN, D., Development of affinity microparticles for extracorporeal blood purification based on crystalline bacterial cell surface proteins, *Ther. Apher.* **2001**, *5*, 433–438.
- 79 BREITWIESER, A., KÜPCÜ, S., HOWORKA, S., WEIGERT, S., LANGER, C., HOFFMANN-SOMMERGRUBER, K., SCHEINER, O., SLEYTR, U. B., SÁRA, M., 2-D protein crystals as an immobilization matrix for producing reaction zones in dipstick-style immunoassays, *Biotechniques* **1996**, *21*, 918–925.
- 80 BREITWIESER, A., MADER, C., SCHOCHER, I., HOFFMANN-SOMMERGRUBER, K., SCHEINER, O., ABERER, W., SLEYTR, U. B., SÁRA, M., A novel dipstick developed for rapid Bet v 1-specific IgE detection: recombinant allergen immobilized via a monoclonal antibody to crystalline bacterial cell-surface layers, *Allergy* **1998**, *53*, 786–793.
- 81 VÖLKELE, D., ZIMMERMANN, K., BREITWIESER, A., SCHEIFLINGER, F., SCHWARZ, H. P., SÁRA, M., SLEYTR, U. B., DORNER, F., Immunochemical detection of prion protein on dipsticks prepared with crystalline bacterial cell-surface layers, *Transfusion* **2003**, *43*, 1677–1682.
- 82 SÁRA, M., SLEYTR, U. B., Crystalline bacterial cell surface layers (S-layers): from cell structure to biomimetics, *Progr. Biophys. Mol. Biol.* **1996**, *65*, 83–111.
- 83 ILK, N., KÜPCÜ, S., MONCAYO, G., KLIMT, S., ECKER, R. C., HOFER-WARBINEK, R., EGELSEER, E. M., SLEYTR, U. B., SÁRA, M., A functional chimeric S-layer-enhanced green fluorescent protein to follow the uptake of S-layer-coated liposomes into eukaryotic cells, *Biochem. J.* **2004**, *379*, 441–448.
- 84 KUEN, B., KOCH, A., ASENBAUER, E., SÁRA, M., LUBITZ, W., Molecular characterization of the *Bacillus stearothermophilus* PV72 S-layer gene *sbsB* induced by oxidative stress, *J. Bacteriol.* **1997**, *179*, 1664–1670.
- 85 MOLL, D., HUBER, C., SCHLEGEL, B., PUM, D., SLEYTR, U. B., SÁRA, M., S-layer-streptavidin fusion proteins as template for nanopatterned molecular arrays, *Proc. Natl Acad. Sci. USA* **2002**, *99*, 14646–14651.
- 86 PAVKOV, T., OBERER, M., EGELSEER, E. M., SÁRA, M., SLEYTR, U. B., KELLER, W., Crystallization and preliminary structure determination of the C-terminal truncated domain of the S-layer protein SbsC, *Acta Crystallogr. D* **2003**, *59*, 1466–1468.
- 87 WILCHEK, M., BAYER, E. A., Foreword and introduction to the book (strept)avidin–biotin system, *Biomol. Eng.* **1999**, *16*, 1–4.
- 88 KURZBAN, G. P., GITLIN, G., BAYER, E. A., WILCHEK, M., HOROWITZ, P. M., Biotin binding changes the conformation and decreases tryptophan accessibility of streptavidin, *J. Protein Chem.* **1990**, *9*, 673–82.
- 89 LIEBERMANN, T., KNOLL, W., Surface-plasmon field-enhanced fluorescence spectroscopy, *Colloids Surfaces A* **2000**, *171*, 115–130.
- 90 LIEBERMANN, T., KNOLL, W., SLUKA, P., HERRMANN, R., Complement hybridization from solution to surface-attached probe-oligonucleotides observed by surface-plasmon-field fluorescence spectroscopy, *Colloids Surfaces A* **2000**, *169*, 337–350.
- 91 MUYLDERMANS, S., Single domain camel antibodies: current status, *Mol. Biotechnol.* **2001**, *74*, 277–302.
- 92 NGUYEN, V. K., DESMYTER, A., MUYLDERMANS, S., Functional heavy-chain antibodies in *Camelidae*, *Adv. Immunol.* **2001**, *79*, 261–269.
- 93 DESMYTER, A., TRANSUE, T. R., GHAHROUDI, M. A., THI, M., POORTMANS, F., HAMERS, R., MUYLDERMANS, S., WYNES, L., Crystal structure of a camel single-domain VH antibody fragment in complex with lysozyme, *Nat. Struct. Biol.* **1996**, *3*, 803–811.
- 94 ELIASSON, M., OLSSON, A.,

- PALMCRANTZ, E., WIBERG, K., INGANAS, M., LINDBERG, M., UHLEN, M., Chimeric IgG-binding receptors engineered from *staphylococcal* protein A and *streptococcal* protein G, *J. Biol. Chem.* **1988**, *263*, 4323–4327.
- 95 NILSSON, B., MOKS, T., JANSSON, B., ABRAHAMSEN, L., ELMBLAD, A., HOLMGREN, E., HEINRICHSON, C., JONES, T. A., UHLEN, M., A synthetic IgG-binding domain based on staphylococcal protein A, *Protein Eng.* **1987**, *1*, 107–113.
- 96 BREITENEDER, H., PETTENBURGER, K., BITO, A., VALENTA, R., KRAFT, D., RUMPOLD, H., SCHEINER, O., BREITENBACH, M., The gene coding for the major birch pollen allergen Betv1, is highly homologous to a pea disease resistance response gene, *EMBO J.* **1989**, *8*, 1935–1938.
- 97 BREITWIESER, A., EGELSEER, E. M., ILK, N., MOLL, D., HOTZY, C., BOHLE, B., EBNER, C., SLEYTR, U. B., SÁRA, M., A recombinant bacterial cell surface (S-layer)-major birch pollen allergen-fusion protein (rSbsC/Bet v1) maintains the ability to self-assemble into regularly structured monomolecular lattices and the functionality of the allergen, *Protein Eng.* **2002**, *15*, 243–249.
- 98 BOHLE, B., BREITWIESER, A., ZWÖLFER, B., JAHN-SCHMID, B., SÁRA, M., SLEYTR, U. B., EBNER, C., A novel approach to specific allergy treatment: the recombinant fusion protein of a bacterial cell surface (S-layer) protein and the major birch pollen allergen Bet v 1 (rSbsC-Bet v 1) combines reduced allergenicity with immunomodulating capacity, *J. Immunol.* **2004**, *172*, 6642–6648.
- 99 LASIC, D. D., PAPAHDJOPOULOS, D., Liposomes revisited, *Science* **1995**, *267*, 1275–1276.
- 100 CORMACK, B. P., VALDIVIA, R. H., FALKOW, S., FACS-optimized mutants of the green fluorescent protein (GFP), *Gene* **1996**, *173*, 33–38.
- 101 GYÖRVARY, E. S., O'RIORDAN, A., QUINN, A., REDMOND, G., PUM, D., SLEYTR, U. B., Biomimetic nanostructure fabrication: non-lithographic lateral patterning and self-assembly of functional bacterial S-layers at silicon supports, *Nano Lett.* **2003**, *3*, 315–319.
- 102 PUM, D., STANGL, G., SPONER, C., FALLMANN, W., SLEYTR, U. B., Deep UV patterning of monolayers of crystalline S-layer protein on silicon surfaces, *Colloids Surfaces B* **1997**, *8*, 157–162.
- 103 MESSNER, P., PUM, D., SÁRA, M., STETTER, K. O., SLEYTR, U. B., Ultrastructure of the cell envelope of the archaeobacteria *Thermoproteus tenax* and *Thermoproteus neutrophilus*, *J. Bacteriol.* **1986**, *166*, 1046–1054.
- 104 STEWART, M., BEVERIDGE, T. J., SPROTT, G. D., Crystalline order to high resolution in the sheath of *Methanospirillum hungatei*: a cross-beta structure, *Mol. Biol.* **1985**, *183*, 509–515.
- 105 SÁRA, M., KÜPCÜ, S., SLEYTR, U. B., Localization of the carbohydrate residue of the S-layer glycoprotein from *Clostridium thermohydrosulfuricum* L111-69, *Arch. Microbiol.* **1989**, *151*, 416–420.
- 106 GYÖRVARY, E. S., SCHRÖDTER, A., TALAPIN, D. V., WELLER, H., PUM, D., SLEYTR, U. B., Formation of nanoparticle arrays on S-layer protein lattices, *J. Nanosci. Nanotechnol.* **2004**, *4*, 115–120.
- 107 HALL, S. R., SHENTON, W., ENGELHARDT, H., MANN, S., Site-specific organization of gold nanoparticles by biomolecular templating, *Chem. Phys. Chem.* **2001**, *3*, 184–186.
- 108 DOUGLAS, K., CLARK, N. A., ROTHSCHILD, K. J., Nanometer molecular lithography, *Appl. Phys. Lett.* **1986**, *48*, 676–678.
- 109 DOUGLAS, K., DEVAUD, G., CLARK, N. A., Transfer of biological derived nanometer-scale patterns to smooth substrates, *Science* **1992**, *257*, 642–644.
- 110 WINNINGHAM, T. A., GILLIS, H. P., CHOUTOV, D. A., MARTIN, K. P., MOORE, J. T., DOUGLAS, K., Formation of ordered nanocluster arrays by self-assembly on nanopatterned Si(100) surfaces, *Surface Sci.* **1998**, *406*, 221–228.

- 111 MALKINSKI, L., CAMLEY, R. E., CELINSKI, Z., WINNINGHAM, T. A., WHIPPLE, S. G., DOUGLAS, K., Hexagonal lattice of 10 nm magnetic dots, *J. Appl. Phys.* **2003**, *93*, 7325–7327.
- 112 SHENTON, W., PUM, D., SLEYTR, U. B., MANN, S., Synthesis of cadmium sulphide superlattices using self-assembled bacterial S-layers, *Nature* **1997**, *389*, 585–587.
- 113 DIELUWEIT, S., PUM, D., SLEYTR, U. B., Formation of a gold superlattice on an S-layer with square lattice symmetry, *Supramol. Sci.* **1998**, *5*, 15–19.
- 114 POMPE, W., MERTIG, M., KIRSCH, R., WAHL, R., CIACHI, L. C., RICHTER, J., SEIDEL, R., VINZELBERG, H., Formation of metallic nanostructures on biomolecular templates, *Z. Metallkunde* **1999**, *90*, 1085–1091.
- 115 MERTIG, M., KIRSCH, R., POMPE, W., ENGELHARDT, H., Fabrication of highly oriented nanocluster arrays by biomolecular templating, *Eur. Phys. J. D* **1999**, *9*, 45–48.
- 116 WAHL, R., MERTIG, M., RAFF, J., SELENSKA-POBELL, S., POMPE, W., Electron-beam induced formation of highly ordered palladium and platinum nanoparticle arrays on the S-layer of *Bacillus sphaericus* NCTC 9602, *Adv. Mater. Sci. Technol.* **2001**, *13*, 736–741.
- 117 MERTIG, M., WAHL, R., LEHMANN, M., SIMON, P., POMPE, W., Formation and manipulation of regular metallic nanoparticle arrays on bacterial surface layers: an advanced TEM study, *Eur. Phys. J. D* **2001**, *16*, 317–320.

III

Pharmaceutically Important Nanomaterials

9

Methods of Preparation of Drug Nanoparticles

Jonghwi Lee, Gio-Bin Lim and Hesson Chung

9.1

Introduction

The recent rapid progress in techniques supporting drug discovery such as genomics, proteomics, high-throughput methods, etc., has exponentially increased the number of newly introduced potential drug candidates [1]. A new drug candidate undergoes a series of time-consuming investigations. Currently, only about five to 10 drugs among 3000–10 000 candidates go into phase I clinical studies and only one of them finally reaches the market [1]. Among the numerous research steps to launch a new drug, the formulation study is becoming one of the most critical bottlenecks, mainly because of the relatively slow advance of formulation-related technologies. What is worse is that the physical and chemical properties of drugs are being diversified, and so more intelligent and functional drug delivery systems are required. As a consequence, the development of novel drug delivery systems and formulation techniques are critical issues in the pharmaceutical research.

Nanoformulation, i.e. formulation using nanoparticles, is at the center of the recent pharmaceutical research and development. The industrial application of nanoparticles of active pharmaceutical ingredients (API) ranges from traditional simple emulsion [2–5] to solid dispersion systems developed a few years ago mainly with the help of the rapid progress of wet comminution techniques [6–19].

Various benefits have been achieved by using nanoparticles [6–22]. First of all, distinct increases in dissolution rate, bioavailability and rate of absorption have helped the formulation of relatively insoluble API (Figs. 9.1 and 9.2). It is known that, in general, as the size of API particles decreases, their processability decreases and bioavailability increases (Fig. 9.1). The burden of processing difficulty can be released by using advanced nanotechnologies. The increase of surface area as a function of particle size is schematically illustrated in Fig. 9.2, which triggers the increase of dissolution rate and bioavailability. Furthermore, the increases have made the early phase of drug discovery more effective. They also enable higher dose loading into a smaller dosage volume. Nanoparticles can be incorporated into various drug delivery systems for more effective and intelligent delivery [23,

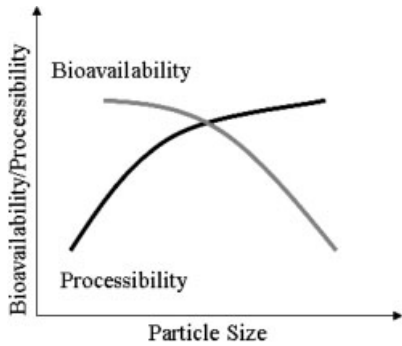


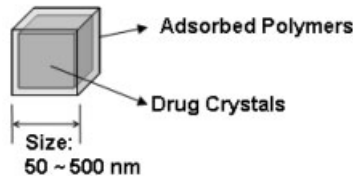
Fig. 9.1. Dependence of bioavailability and processability of a formulation on the particle size of the drug.

24]. Reformulation using nanoparticles often removes harsh excipients, extreme pH and organic solvents currently used. Longer retention in blood and tumors, improvement in the stability of drugs, taste masking, and reduction in fed/fasted variability are often also obtained [24].

As particle size decreases, the extra Gibbs free energy resulting mainly from the surface energy of nanoparticles significantly increases [25]. Therefore, how to deal with the extra Gibbs free energy is the major issue in the preparation and subsequent treatment of nanoparticles. If a nanoparticulate system is considered to be a system having N smaller noninteracting systems (ensembles), the total Gibbs equation will be:

$$E_t = TS_t - pV_t + \sum \mu_i N_{it} + EN \tag{1}$$

Structure of Drug Nanocrystals



Effect of Size Reduction

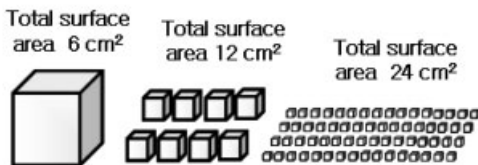


Fig. 9.2. Schematic illustration of the structure of drug nanocrystals, and the relationship between particle size and surface area.

where t indicates total, μ_i is the chemical potential of component i , N_i is the number of molecules of component i and E is the “subdivision potential” [25]. The fourth term on the right-hand side is an extra one for the nanosize effects (e.g. surface tension), which increases as API particle size decreases.

Nanoparticle preparation techniques under active development can be categorized into two major routes – kinetic and thermodynamic approaches. The kinetic approach relies on external energies to compensate for the elevated Gibbs free energy of nanoparticles, such as high energy flow, sonication and electrostatic fields. The thermodynamic approach makes use of interfacial energy. For example, the stabilization ability of polymers and surfactants or supercritical fluids (SCFs) can be successfully employed for reducing the fourth term. The stabilizers can cover the surface of nanocrystals, and pay the thermodynamic penalty of the fresh interface between drug and liquid medium. Proteins and lipids can be stable in nanoparticulate forms in water if their conformation makes the fourth term negligible.

In the kinetic approach, the utilization of various energies has been tried to achieve the maximum efficiency. Without the external energies, the resulting particles cannot maintain their stability and so a poststabilization mechanism which remains active after processing is often employed. As a result, the actual processing of nanoparticles often combines both approaches. The combination usually offers better efficiency.

9.2

Structures of Drug Nanoparticles

Pharmaceutical nanoparticles can take various physical forms depending on their final delivery routes and API properties. They can be classified on the basis of their physical states and internal structures. Solid or liquid monolithic nanoparticles are the simplest cases. They require a proper medium to minimize their interfacial energy. Emulsions and lipids have their unique structures to adjust themselves to the surrounding environments. A solid dispersion has a different structure from emulsions and lipids, but the structure is determined by the same thermodynamic origin. By controlling surface/interface energy and kinetic obstacles, various internal structures of nanoparticles from a simple core/shell to more complicated structures can be engineered.

9.3

Thermodynamic Approaches

The interfacial energy related to the preparation of nanoparticles can be minimized by using proper materials in proper regions. Thermodynamic approaches mainly rely on the chemical identity and self-assembly behavior of materials. The micelle structures of traditional surfactants provide good examples, although their pharma-

ceutical applications are often limited due to their poor biocompatibility. Water soluble polymers can form nanoparticles in water by adding a crosslinking agent such as chitosan nanoparticles crosslinked by tripolyphosphate [26, 27], or by simple emulsion or dispersion preparation methods using oil and water mixtures [2–5]. Protein nanoparticles are also available by crosslinking or desolvation [28]. Precipitation by salting-out or solvent evaporation, or other phase separation phenomena, has been intensively investigated to conveniently prepare nanoparticles [29]. Surface active agents such as surfactants or block copolymers can adapt unique structures at the interface, resulting in a reduction in interfacial energy and successful preparation of nanoparticles [30–34]. Lipid systems, which have been intensively examined and widely adapted in the pharmaceutical area, provide typical examples of the thermodynamic approaches. Before moving on to a deeper discussion on lipid systems, it might be helpful to mention that the terminology “thermodynamic approaches” does not necessarily imply that the methods use only thermodynamically stable states.

9.3.1

Lipid-based Pharmaceutical Nanoparticles

Lipid-based drug delivery systems have been used to improve pharmacokinetic profiles, to reduce side-effects and to improve patient compliance. These lipid-based drug delivery systems can utilize various macro- and microstructures that lipids form in a variety of settings. Most popular lipid-based pharmaceutical particles include liposomes and oil-in-water-type lipid emulsions. Parenteral lipid emulsion has been around for more than 40 years to provide nutrition to patients who cannot consume food orally. Parenteral emulsion consists of vegetable oil particles dispersed in an aqueous environment by the use of the natural lipid emulsifier, lecithins. While the oil and lipid themselves or the emulsions as a whole are used to improve the health of the patients, they are used as tools to carry API to the destinations in the body when they are used as drug carriers. The drugs marketed in the form of lipid emulsion-based drug delivery systems include diazepam (Pharmacia) and propofol (Baxter and Astra Zeneca).

It took longer time for liposomes to appear on the market as drug carriers due to the instabilities of the formulation. Commercialization of the liposomal doxorubicin formulation Doxil[®] has been realized by designing a very stable liposome both *in vitro* and *in vivo* [35, 36]. The success has boosted the morale of the scientists working in the field, and has initiated a flurry of research and discovery of novel and innovated lipid-based pharmaceutical particles. Nowadays, new lipid-based drug delivery systems based on original designs appear frequently in the literature. Even though not all of them can be successful drug carriers, they can serve as stepping stones to understand lipid phase behavior and to improve current formulations. In this chapter, the physical characteristics of lipids will be introduced as a background to understand how and why lipids behave as they do, together with frequently encountered lipid-based particulate systems.

9.3.2

What is a Lipid?

Lipids can be defined as fatty acids, their derivatives and related molecules that are soluble in organic solvents and sparingly soluble in water. The major role of lipids in the living organism is to build the cell membrane. The majority of lipids encountered in nature are amphiphilic in that they embody both polar and apolar elements in one molecule. Dietary lipids are mostly neutral lipids or triglycerides with very low aqueous solubility. There are also classes of lipids that can self-assemble and form a variety of lyotropic liquid crystalline phases having crystalline periodicity and liquid-like molecular diffusibility. This nature of hydrated lipids can help us to design lipid-based nanoparticles.

Lipid phase behavior can be understood by realizing that there exists a lateral pressure function across a lipid monolayer [37–40]. A force profile can be drawn along the direction normal to the lipid monolayer since different forces are dominant in different regions along the lipid molecules (Fig. 9.3). A lipid molecule can be divided roughly into the head group, polar/nonpolar interface and hydrocarbon chain regions. Head groups repel each other due to steric, hydration and electrostatic effects. There is an attractive force in the polar/nonpolar interfacial region in order to minimize the exposure of the interfacial area to the surroundings. Hydrocarbon chains repel each other due to thermally induced rotational motion around the carbon atoms. A lipid monolayer compensates for the imbalance in the lateral stress and can become a planar or curved surface as a result if there exist no other energy terms. In reality, the contributions from other energy terms could easily override the spontaneous tendency of bending the lipid monolayers. These other energy terms include electrostatic interactions, van der Waals interactions and others.

Since the energy of bending is an important energy term to understand in lipid self-assembly, it will be discussed in more detail. The curvature elastic energy describes the energy associated with bending the surface as follows [41]:

$$\Delta G = k_c/2 \langle H - H_0 \rangle^2 - k_g \langle K \rangle \quad (2)$$

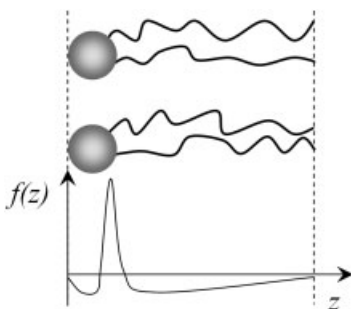


Fig. 9.3. The lateral stress profile along a lipid monolayer. A positive value along the $f(z)$ -axis represents the attractive force.

where k_c and k_g are the rigidity or bending modulus and the Gaussian curvature constant, respectively, and $\langle \rangle$ denotes the average obtained by integrating over a unit surface. Curvature is defined as a reciprocal of the radius of a circle that can be drawn to the tangent of the surface. The principal curvatures C_1 and C_2 are the minimum and maximum of the normal curvatures at a point. Two orthogonal principal curvatures or their average and product values, the mean [$H = (C_1 + C_2)/2$] and the Gaussian ($K = C_1 C_2$) curvatures, can define the curvature of the surface at a given point.

9.3.3

Liquid Crystalline Phases of Hydrated Lipids with Planar and Curved Interfaces

The vast variety of naturally occurring lipids adopt one or more of the liquid crystalline phases at, or close to, physiological conditions either with planar or curved interfaces. In this section, the lamellar, hexagonal and cubic phases of hydrated lipids will be described although they are bulk phases since they can be micronized into useful pharmaceutical nanoparticles such as liposomes, hexosomes and cubosomes, respectively.

Biomembranes usually incorporate a lipid bilayer structure that has been successfully modeled by the lamellar liquid crystalline (L_x) phase at physiological conditions. In the L_x phase, lipid molecules arrange into stacked sheets (Fig. 9.4). The apolar hydrocarbons are located inside and the head groups line up at the surface of the sheets. Water molecules are located between the layers formed by the head groups. The lamella is a planar structure with zero curvature. The lamellar phase is often described as a frustrated structure since the bilayers cannot overcome an

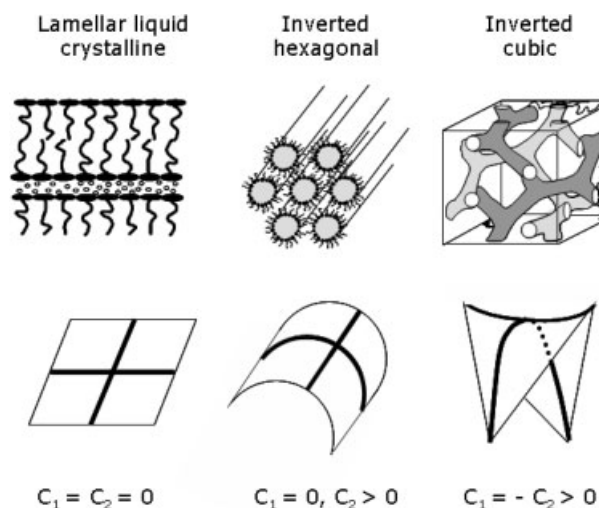


Fig. 9.4. Liquid crystalline phases of hydrated lipids and the principal curvatures at the interface between hydrocarbon chain termini.

energy barrier to curl up (called the “packing energy”) even when a curved surface is preferred and, thus, remain flat [42].

The so-called inverted hexagonal (H_{II}) phase composed of long cylinders with hexagonally packed aqueous cores is found in hydrated lipids (Fig. 9.4). The lipid head groups coat the surface of the central water-filled cylinders and the hydrocarbon chains constitute the continuous medium. One of the principal curvatures along the cylinder is zero, but the other is around 0.02 \AA^{-1} . Another curved liquid crystalline phase encountered in hydrated lipids is the bicontinuous cubic phase [43]. In the bicontinuous cubic phase, each component, lipid or water, forms separate and continuous channels, and the interface between the lipid and water forms the networks of tubes that have three-dimensional cubic symmetry. The interface between the termini of hydrocarbon chains in the cubic phase can be described as the infinite periodic minimal surface whose mean curvature is zero everywhere since the two principal curvatures are identical in quantities with different signs [44, 45].

The appearance and the texture of the hexagonal and the cubic phase are similar to white toothpaste and waxy gel, respectively. They both are very viscous and do not dilute in water. Drugs can be encapsulated in the water channels, hydrocarbon regions as well as interfacial regions.

9.3.4

Oil-in-water-type Lipid Emulsion

Neutral lipids such as triglycerides phase-separate and form thermodynamically stable bulk oil phases (L_2 phase) in the aqueous system. Fractionizing them into micronized particles would create a large interface between the particles and water. However, this process is entropically favorable – the increased interfacial area between oil and water increases the Gibbs free energy [46]. Emulsification occurs when external energy is provided in the form of stirring, sonicating or microfluidizing. Spontaneous emulsification can also occur when the interfacial energy between oil particles and water is close to zero.

Lipid emulsions have been widely used in pharmaceutical and medical fields as drug carriers. To be applied as parenteral, oral or topical formulations, emulsions must be physically stable and nontoxic [47]. The diameter of oil droplets in stable lipid emulsions is typically less than 500 nm. Many emulsion products are currently on the market, including propofol injectable emulsion (Baxter and Astra Zeneca).

To formulate stable emulsions, suitable emulsifiers should be added to the formulation [48]. It is also important to choose an appropriate oil to increase the stability and biocompatibility of the emulsion [49].

9.3.5

Liposomes

A liposome is a vesicle made of lipid shells and filled with a portion of an aqueous phase. Liposomes used as drug delivery systems are mostly small unilamellar vesicles (SUV) and smaller-sized multilamellar vesicles (MLV) between 50 and 100

nm in diameter. For pharmaceutical use, a hydrophobic drug can be incorporated in the shell or in the inner aqueous phase. Since a liposome is not a thermodynamically stable system, it can be produced by applying sufficient mechanical force to break up the lamellae and overcome the curvature energy cost to form a closed constrained vesicle from the bulk lamellar liquid crystalline phase [50].

Even though liposomes have been used widely as drug delivery systems, there have been many problems in using conventional liposomes. Phospholipid liposomes are very unstable and form aggregates upon storage. In the blood stream, they are cleared out by the reticuloendothelial system (RES) as they can be recognized as foreign bodies [51, 52]. The breakthrough occurred when long-circulating liposomes were designed by incorporating lipids with covalently attached polyethylene glycol (PEG) [53]. These, so-called, “stealth” liposomes have a relatively long half-life (approximately 1 day) in blood circulation and can be targeted to a desired tissue *in vivo*. The repulsive barrier properties of lipid-grafted PEG polymer chains originate mainly from a steric pressure and this simple polymer steric stabilization is the basis for the extended *in vivo* circulation times observed for polymer-grafted liposomes [53].

Along with “stealth” technology, another novel technique has been put into the development of successful liposome formulations. Conventionally, drug encapsulation efficiency into the liposome has been very low since a liposome is prepared by dispersing the bulk L_v phase in the aqueous system containing drugs. Considering a liposome with a radius of 50 nm and a shell with a single bilayer whose thickness is 5 nm. If the total lipid concentration was 3% (w/w) in the aqueous system at the beginning, a rough calculation gives around 8% (v/v) of the trapped aqueous phase inside the liposome. In reality, the bilayer has one to three layers and therefore the drug trapping efficiency is almost always lower than 8%. A revolutionary technique called remote loading technology was devised to increase the trapping efficiency of drugs [54]. A relatively hydrophobic drug, e.g. doxorubicin, can penetrate the lipid bilayer freely. The inner aqueous phase is rendered acidic with the bulk aqueous phase at a higher pH, then the protonated doxorubicin forms precipitates out inside and cannot escape from the liposome droplet.

When a single lipid species is used to form liposome, different mean curvatures of the outer and inner bilayers could destabilize the liposome. Adding a small amount of lipids with different spontaneous curvature could release the tension by being preferentially distributed in one of the leaflets.

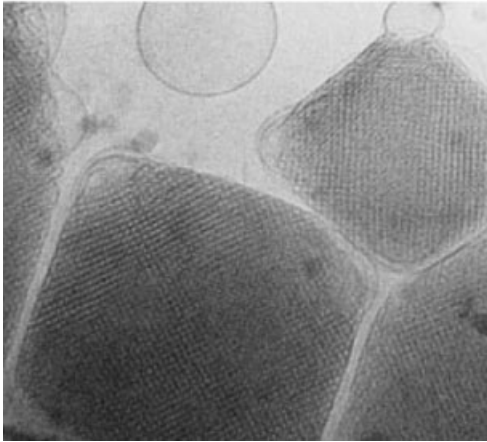
Many attempts have been made to prepare stable liposomes as drug delivery systems and probes to identify proteins by adding the polymerizable lipids with conjugated double or triple bonds that can be polymerized by applying heat or UV light [55] or metal-chelating lipids [56].

9.3.6

Cubosomes and Hexosomes

In the early 1990s, Swedish scientists succeeded in dispersing the lipid cubic phase in water by adding emulsifiers [57, 58]. They have termed the dispersed cubic

Cubosome



Hexosome

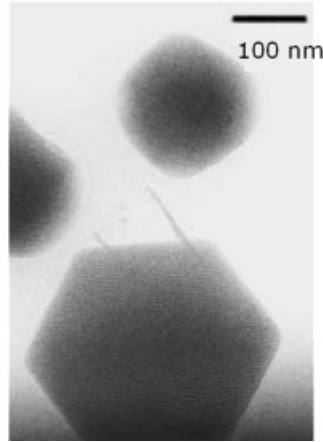


Fig. 9.5. Cryo-transmission electron microscopy photograph of cubosomes and hexosomes formed in the monoolein–water system. (Reproduced with permission from Ref. [58].)

phase as a “cubosome”. A cubosome is prepared by micronizing the hydrated lipid cubic phase in water. The interior of a cubosome comprises a thermodynamically stable cubic phase wherein lipid and water components constitute continuous, but separate, three-dimensional channels, and there exists a curved interface between the lipid head group and water (Fig. 9.5). Therefore, cubosome formulations could be advantageous over the conventional emulsion- or liposome-type formulations as they can solubilize amphiphilic as well as hydrophobic and hydrophilic drugs. To increase the stability of cubosome preparation, different preparation procedures have been devised. Precursor type formulation that forms a cubosome spontaneously in the presence of water has been developed [59, 60]. A dry-powder-type formulation was also prepared [61]. Cubosomes have been elegantly described in mathematical terms [62] and have been developed as drug carriers by the scientists in Camurus AB (www.camurus.se). Like liposomes, cubosomes have also been polymerized successfully by utilizing reactive monoglyceride [63]. The term “hexosome” refers to a dispersed hexagonal phase and can also be produced by mechanically micronizing the hydrated hexagonal phase in water (Fig. 9.5).

9.3.7

Other Lipid-based Pharmaceutical Nanoparticles

A hollow lipid microcylinder has been produced by cooling a liposome solution composed of chiral diacetylenic lipids [64, 65]. Diacetylenic lipids are those with conjugated triple bonds in the middle of hydrocarbon chains. Due to the chirality of the diacetylenic lipid, the bilayer twists to form a tubular structure. Microtubules have a diameter of approximately 0.5 μm and a length ranging up to a few centi-

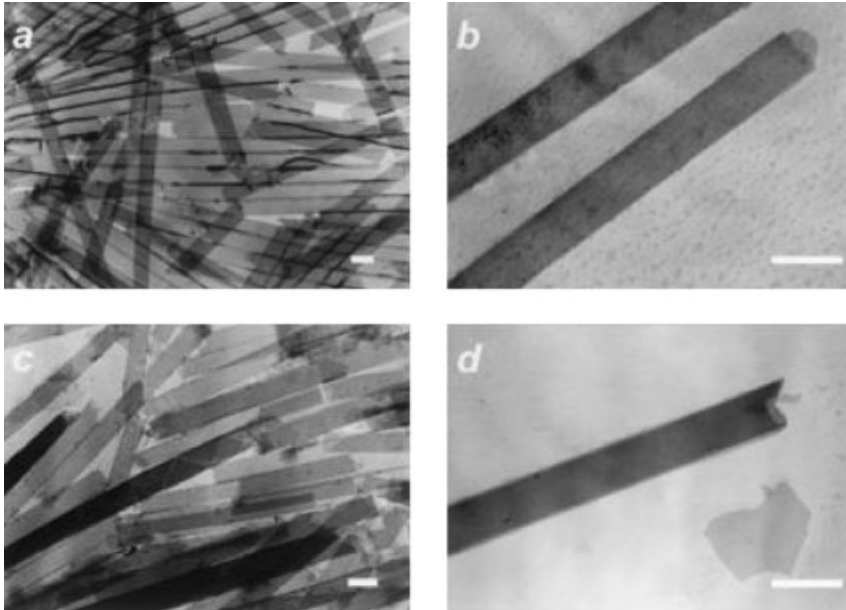


Fig. 9.6. Electron micrographs of lipid tubules in methanol/water (7:3) at lipid concentrations of 1 (a and b) and 5 mg ml⁻¹ (c and d). The scale bar represents 1 μm. (Reproduced with permission from *Proc. Natl Acad. Sci. USA* **1996**, 93, 12943–12946.)

meters. The bilayer forms a band arranged like a wrapping paper of a cigar, separated by layers of water (Fig. 9.6). The inside (in the place of the cigar itself) is hollow and filled with water in an excess water environment. Antifouling agents have been encapsulated into the interior of the microtubules and released in a sustained fashion [66].

Lipid cochleates are stable precipitates made from phosphatidylserine and calcium ions [67]. The structure of cochleates consists of a continuous, solid lipid bilayer sheet rolled up in a spiral (Fig. 9.7). Unlike lipid tubules, there is no hollow space for water in the cochleate system. The amphotericin B/cochleate system has been shown to treat *Candida* infection when administered orally [68]. Cochleates have also been used to deliver proteins and peptides for vaccine applications [69].

9.4

Mechanical Approaches

9.4.1

Types of Processing

The subdivisional potential penalty in Eq. (1) can be paid by mechanical energy input to produce and maintain nanoparticles. Comminution to prepare pharmaceu-

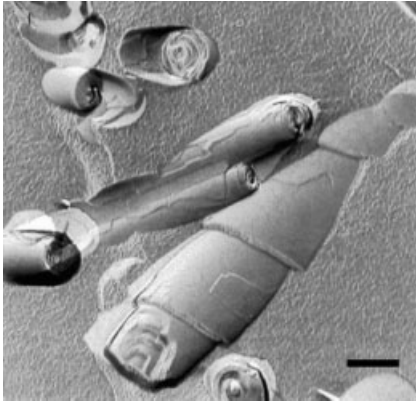


Fig. 9.7. Scanning electron micrographs after freeze-fracturing cochleate cylinders. Scale bar: 200 nm. (Reproduced with permission from *J. Controlled Rel.* **2002**, *81*, 7–23.)

tical nanoparticles uses mechanical energy. As the size of particles decreases, the required mechanical energy dramatically increases. To relieve the burden of energy input, additional support by surface active agents is generally used (Fig. 9.2) [9–10]. A series of recent successful commercializations of nanoformulations using this technique proves its efficiency.

Based on the type of mechanical energy employed, two typical types of processing exist – shearing and fracturing [70]. For shear force generation, high-speed stirrers and high-shear mills are commonly used in the processing of low-viscosity systems [71]. When a high-viscosity system is involved, shear force generation requires different types of equipment such as extruders, roll mills, heavy-duty mixers, etc. Fracturing is conveniently triggered by impact mills such as ball and jar mills.

Comminution processes using media such as ceramic balls have commonly been used to reduce the size of API. Both the wet and dry conditions can be used, but individual nanoparticles in the dry state are relatively unstable. When a liquid medium is used, heat dissipation is much more effective, and, more importantly, the surface of nanoparticles can properly be wetted and stabilized by surface active agents. Therefore, wet comminution is more common in pharmaceutical nanoparticle processing. Ball and jar mills, vibratory mills, various attritors, etc., are of this type [18, 19, 70].

In ball milling, grinding media is put into a cylindrical vessel with the drug. The vessel is designed to rotate along an axis and the grinding media undergo a cascading action that provides mechanical energy to reduce the particle size [8]. The critical speed is a speed where cascading stops due to high centrifugal force. Ball milling should use a speed lower than the critical speed to maintain its cascading action. Attrition contributes more to particle size reduction below the critical speed. The shape, size and density of grinding media affect comminution process.

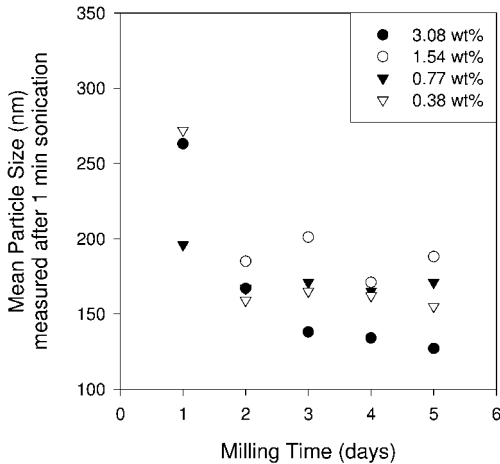


Fig. 9.8. Particle size reduction as a function of time during wet milling. The concentration of hydroxypropyl cellulose in the mother liquid is shown. (a) Nanoparticles on a glass slide ($2 \times 2 \mu\text{m}$). (b) Nanoparticulate compact ($1 \times 1 \mu\text{m}$) (compaction pressure = 136 MPa). (Reproduced with permission from Ref. [6].)

An increase in the density and hardness of grinding media usually increases the speed and amount of particle size reduction. A decrease in the size of media produces the same results. Nonetheless, in wet comminution using surface active ingredients, the surface properties of materials appear to be more important than the properties of the grinding media [6]. Figure 9.8 shows a typical result of particle size reduction as a function of milling time in the presence of a polymeric stabilizer.

High-speed stirrers such as blade stirrers and rotor-stator dispersers produce the same high-shear flow to obtain nanoparticles as high-shear mills such as colloid mills, homogenizers, ultrasonic dispersers, etc. [8, 70, 71]. In a typical design of high-pressure homogenization, the initial mainstream of a liquid (a dispersion system) is separated into two liquid streams, and then they collide with each other producing severe deformation and cavitation in the dispersion system [72]. Particle size reduction mainly results from the deformation and cavitation action of high-pressure liquid streams. The final particle size and its distribution significantly depend on the various processing parameters.

9.4.2

Characteristics of Wet Comminution

In the wet comminution processes of nanoparticles, comminution continually fractures organic crystals while polymer chains adsorb onto fresh surfaces and stabilize each broken particle. The “primary” particle size produced by wet milling is not necessarily the same as the particle size actually measured in water by a light scattering method (Fig. 9.8). It is possible that some primary particles form aggre-

gates. Ideally, the smallest size of primary particles that can be achieved by mechanical breaking is related to the size of the damage zone ahead of the crack tip. According to the Irwin's equation of linear elastic fracture mechanics, the size of the damage zone (r_d) (lower particle size limit) is related to the stress intensity factor (K_{IC}) and yield stress (σ_y) as follows [6, 73]:

$$r_d = 1/6\pi(K_{IC}/\sigma_y)^2 \quad (3)$$

If a set of typical values of K_{IC} (0.05 MPam^{1/2}) and σ_y (50 MPa) for organic crystals is used [6, 74], r_d is around 50 nm. Accurate calculation is rarely possible due to the anisotropy of crystals and uncertainty in σ_y values, as well as the difficulty in measuring the stress state, loading rate and temperature in wet milling. However, the size of the damage zone (r_d) will put a lower limit on the particle size that can be attained by wet comminution [75, 76].

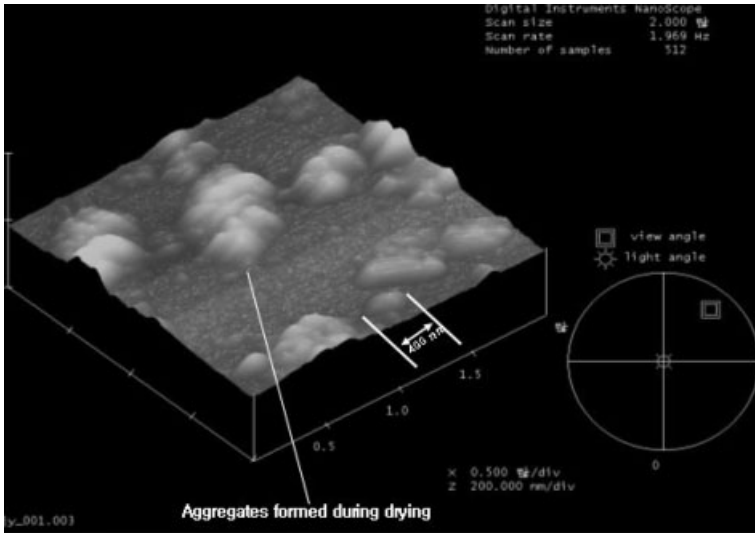
In the actual successful processing as shown in Fig. 9.8, the mean size of drug particles depends more on polymeric stabilizers than on mechanical energies. In semidilute polymer solutions, the adsorption of polymer chains will occur if the free energy reduction associated with adsorption can compensate for the accompanying entropy loss [77]. Since steric stabilization involves adsorption/desorption processes and masking of dispersion forces, it naturally depends on the concentration of polymer in bulk solution (concentration in mother liquid), the size of particles, type of solvent, etc. The amount of adsorbed polymers was found to initially increase with an increase in the concentration of polymer in bulk solution and eventually reach a saturation point [6].

For polymers to provide effective steric stabilization, strong adsorption at full coverage and a long time scale for desorption are necessary [77]. The common minimum layer thickness requirement for stabilization is around $(0.05\text{--}0.2) \times$ particle size [77] and previous reports showed enough surface coverage based on a simple approximation [6]. When naproxen and hydroxypropyl cellulose were used as a drug and a stabilizer, the surface coverage of hydroxypropyl cellulose in 150-nm particles was estimated to be around $1.5 \mu\text{g cm}^{-2}$, which corresponds to an average polymer layer thickness of around 15 nm. It is uncertain whether this result can be generalized for other polymer-stabilized nanocrystal systems. More precise calculation requires an understanding of the polymer morphology on the surface of drugs. Unfortunately, direct measurement of the thickness of polymeric stabilizers has remained unsatisfactory. The atomic force micrographs in Fig. 9.9 clearly show nanoparticles, but no detailed information on polymeric stabilizers.

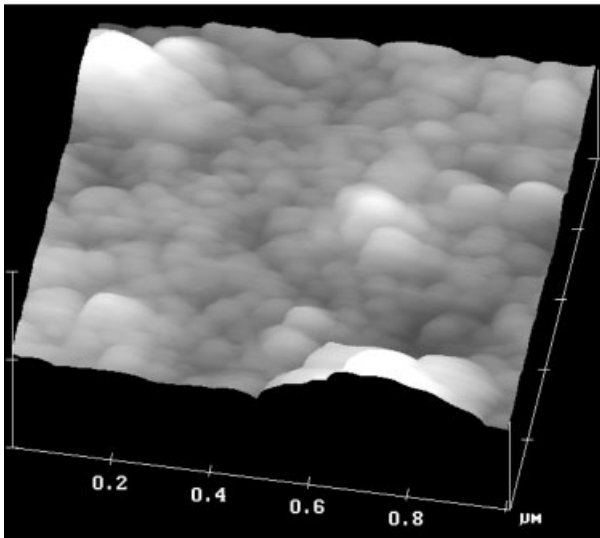
9.4.3

Drying of Liquid Nanodispersions

In the wet comminution processes, the steric stabilization of polymers is effective only in a liquid medium. While the use of a liquid medium is convenient for nanoparticle preparation, solid dosage forms are generally more important than liquid forms in the pharmaceutical industry. Therefore, a drying process should be em-



a) Nanoparticles on glass slide (2x2 μm)



b) Nanoparticulate compacte (1x1 μm) (compaction pressure = 136 MPa)

Fig. 9.9. Tapping mode atomic force microscopy images of nanoparticles dried on a glass side from an aqueous dispersion (a) and the surface of a nanoparticulate compacte (b). (Reproduced with permission from Ref. [6].)

ployed to connect the wet process and the conventional unit operations of solid dosage formulation. Various drying processes such as spray drying, fluidized bed drying, freeze drying, etc., can be used to prepare dried nanoparticles.

Since the initial thermodynamic and kinetic compensations of the wet comminution process become inactive as drying progresses, nanoparticles easily form aggregates too strong to be dispersed in a liquid medium later. Nanoparticles slowly dried under ambient conditions show their aggregation tendency as can be seen in Fig. 9.9(a). Special care needs to be taken to keep each nanoparticle apart from each other (“re-dispersible”). Otherwise, the advantages of nanof ormulation cannot be fully utilized in solid dosage forms. The drying process of nanoparticle dispersions has become a critical issue in the pharmaceutical industry.

Drying nanoparticle dispersions using conventional processes such as spray drying, freeze drying, etc., is not a trivial process development [16–20]. Solid dosage formulation needs well-dispersed API nanocrystals (Figs. 9.8 and 9.9). For that reason, the key property of dried nanoparticles is their “re-dispersibility”, i.e. whether they can restore their initial nanometer sizes when they are re-dispersed into an aqueous medium. The re-dispersibility can be defined as D_0/D (%), where D_0 is the initial mean particle size after preparation of the nanoparticle dispersion and D is the particle size of re-dispersed powder in water. Then, 100% re-dispersibility indicates that dried powders can fully revert to the original nanoparticles upon re-dispersion into water.

Drying certainly increases the chances of aggregation of nanocrystals and polymers. Steric stabilization requires active polymer chain movement in water, which will be restricted as water is frozen or removed. Thus, it is a natural consequence for nanocrystal dispersion to become less stable during drying or freezing (freeze drying). Furthermore, the crystallization (crystal growth) of water in freeze drying tends to exclude foreign particles from crystal regions and lead them to aggregate. Therefore, for better re-dispersibility, fast drying or freezing is necessary and a soluble compound such as a cryoprotectant is frequently added to serve as a medium where solid nanoparticles are dispersed after drying. It was reported that there is a critical freezing rate for a solid dispersion below which its re-dispersibility decreases from 70–100 to 2–3% [78].

Since drug nanoparticles are covered by adsorbed polymer chains, the breaking strength of aggregates into primary nanoparticles would depend on how strongly the polymer chains become entangled during drying [79]. Therefore, to prevent strong entanglement, the frequency and duration time of contacts between nanoparticles need to be minimized by increasing drying speed. In an extreme case of aggregation, API nanoparticles may fuse together. The re-dispersion of fused aggregates can hardly be expected.

For a dispersion system, re-dispersibility might be treated as a result of competition between drying speed and particle collision frequency. The motion of an “ideal” spherical particle could be characterized by using its hydrodynamic diameter, d . The average apparent velocity of the particle, v_{app} , is:

$$v_{app} = x/t = (2D/t)^2 \quad (4)$$

where diffusion coefficient, $D = kT/3\pi\eta d$, x is the average distance traveled by a particle, t is the time, k is the Boltzmann constant, T is the temperature and η is the viscosity [70, 77]. If a set of typical values is employed, v_{app} can be obtained for a certain time interval, t . The apparent velocity v_{app} is only an approximation and often fails to describe actual particle motion. However, it seems to hold true that as the concentration increases, the collision frequency increases, resulting in an increase in aggregation tendency. It requires the detailed analysis of interparticle force fields, polymer chain mobility, local heat and mass transfer, etc., to determine how fast a nanoparticle dispersion should be dried.

9.5

SCF Approaches

The use of near critical or SCFs for micro/nanoparticle formation has recently been shown to be good in improving particle characteristics such as size, size distribution, shape and morphology. SCF technology can be an attractive recrystallization method for some difficult-to-comminute materials such as certain explosives, “waxy” or “soft” dyes, polymers and pharmaceutical compounds, etc., that require very small particles and narrow size distribution. Once used, the SCFs can be recycled from dissolved solutes by just depressurizing. Thus, the SCF processes are environmentally benign. The stainless construction, small number of moving part and totally enclosed system are also favorable for the pharmaceutical current good manufacturing practice (cGMP) requirements.

9.5.1

SCF Characteristics

More than 100 years ago it was found that SCFs could dissolve nonvolatile compounds [80]. In the pressure–temperature diagram for a pure substance (Fig. 9.10), two nearby phases coexist at the solid curves and three phases (liquid, vapor and solid) exist together at the triple point (TP). “Supercritical” means the state of matter where the temperature and pressure of a single fluid are above the critical point (CP) where the liquid–vapor phase boundaries (equilibrium curve) diminish. The temperature and pressure at the CP are referred to as the critical temperature (T_c) and critical pressure (P_c), respectively. By literal definition, the SCF is a fluid that is at temperature and pressure higher than those at CP, and the area is called a SCF region. In that region the substance can be brought into the vapor and liquid without an abrupt phase change by lowering the pressure and temperature, respectively. However, due to economic considerations, SCF processing is generally carried out in the vicinity of the CP with reduced temperature (T/T_c) in the range of 1.01–1.1 and reduced pressure (P/P_c) in the range of 1.0–4.0.

SCFs have advantageous properties of gases and liquids such as a liquid-like density (high solvation power), and gas-like diffusivity and viscosities (high mass transfer rates, i.e. good mixing properties). In addition, near zero surface tension

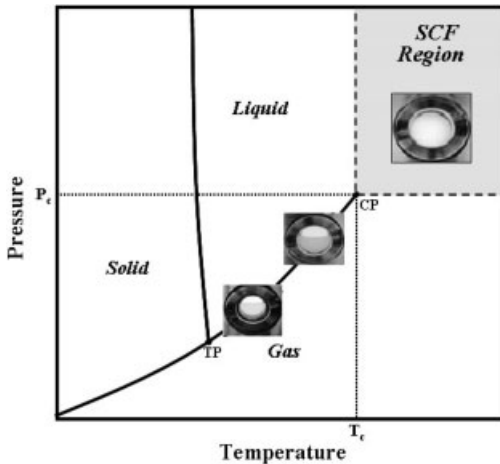


Fig. 9.10. P - T diagram of a pure substance.

enables SCFs to easily migrate into various microstructures. For particle formation, SCFs are very compressible near the CP, and their density and solvent power can be changed dramatically by a small change of either pressure or temperature. Consequently, their density and solvent power are continuously controlled for selective operation in the SCF region a little distant from the CP. The solvent power can be explained by a high enhancement factor of 10^4 – 10^6 (a dimensionless measure of solvent power defined as the measured solubility of a substance in the solvent divided by the solubility in an ideal gas) [81].

Carbon dioxide is one of the most extensively used SCFs (SCCO_2) due to its relatively low T_c (31.1 °C) which makes it attractive for processing heat-labile substances such as pharmaceutical ingredients (Fig. 9.11). Additionally, it has a moderate P_c (73.8 bar) and a good solvation power compared to other SCFs. It is nontoxic, nonflammable and relatively inexpensive (US\$0.11–0.15 kg^{-1}) with high purity.

9.5.2

Classification of SCF Particle Formation Processes

There have been a number of review articles for micro- and nanoparticle formation using SCFs recently [82–88]. In the past 20 years various types of SCF particle formation processes have been developed using different nucleating and growth mechanisms, such as rapid expansion of supercritical solution (RESS), gas antisolvent (GAS) process, supercritical antisolvent (SAS) process, solution-enhanced dispersion by SCFs (SEDS), particles from gas-saturated system (PGSS), etc. Among these techniques, RESS, SAS and SEDS are generally known to achieve nanoparticle formation.

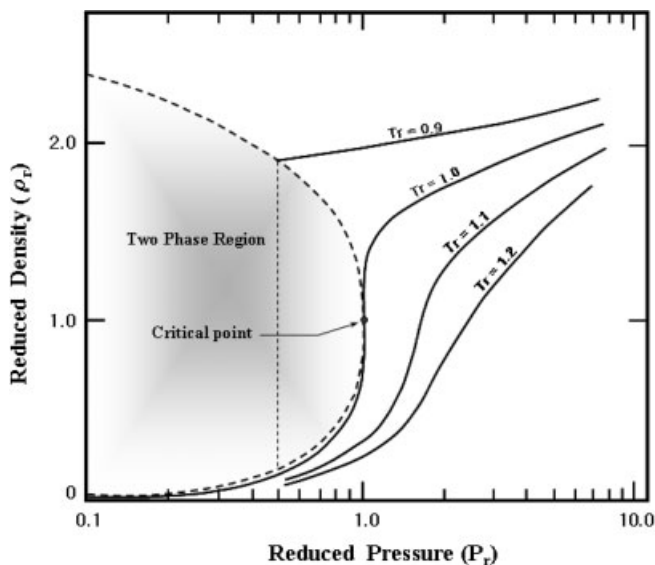


Fig. 9.11. Reduced density–reduced pressure diagram for CO₂ at various reduced temperatures (T_r) in the vicinity of the CP.

9.5.3

RESS

This process is used for materials soluble in a SCF. As shown in Fig. 9.12, the RESS process simply uses a pump, extractor, nozzle and precipitator. Using the compressed SCF, the solutes located in the extractor are dissolved and the supercritical solution is introduced into the precipitator at low pressure (normally atmospheric pressure) through capillary or laser-drilled disk-type nozzles. The resulting rapid pressure drop in solution causes fast evaporation of SCFs and a dramatic decrease in the solvation power of the solution, which leads to a high degree of homogeneous supersaturation and simultaneous formation of very small particles. This high supersaturation ratio, rapidly propagating mechanical perturbation and thermal cooling enable the production of nanoparticles with a narrow size distribution.

This technique can be used without any toxic organic solvent and, thus, is considered a contamination-free process. The general limitation of this process comes from the low solubility of hydrophilic or high-molecular-weight pharmaceuticals, resulting in poor throughput capacity even though a cosolvent is added to improve the solvent power of SCF.

Many works have focused on atomization of pharmaceuticals, either to obtain very fine particles with a narrow size distribution [89–93] or microcapsules which include an API in the carrier [94–96].

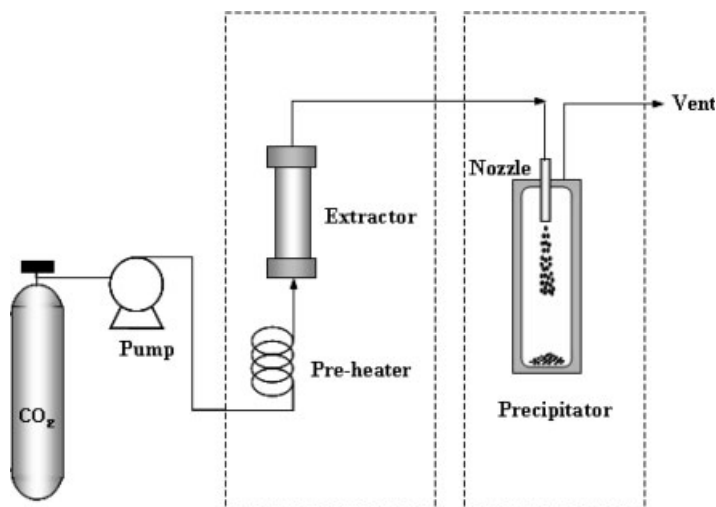


Fig. 9.12. RESS process.

9.5.4

SAS

This process can be used for the crystallization of substances insoluble in SCF (Fig. 9.13). Some similar techniques are called the aerosol solvent extraction system (ASES) or precipitation with a compressed antisolvent (PCA) process. Drug and/or carrier are first dissolved into a liquid solvent, and the solution is sprayed from the top of and into a precipitator through a nozzle, where the SCF flows concurrently downward acting as an antisolvent for particle formation (Fig. 9.13). Two particle precipitation mechanisms proceed simultaneously at a high speed, i.e. the diffusion of a SCF into a liquid solution droplet (volumetric expansion of the organic solvent) and the evaporation of the liquid solvent into a SCF (depletion of the solvent from the liquid solution droplet). These phenomena generate a high degree of supersaturation of the solution, resulting in fast nucleation and growth, and consequently produce solute nanoparticles. After collection of a sufficient amount of particles, liquid solution pumping is stopped and pure SCF continues to flow through the vessel to remove residual solvent from particles.

The operation pressure, temperature, jet breakup, droplet size and mass transfer rates between droplets and the antisolvent phase control the particle size and morphology. In this process, the rate of SCF mass transfer into droplets influences particle formation, whereas the rate of solvent mass transfer into the SCF from droplets has an effect on particle agglomeration. This process can also be operated in a continuous mode that facilitates scaleup for the mass production of particles.

Many investigations have been carried out on atomization of pure pharmaceutical components such as insulin [97–100], ascorbic acid [101], pure biopolymer microspheres (dextran [102] and polylactic acid (PLA) [103]), and microcapsules

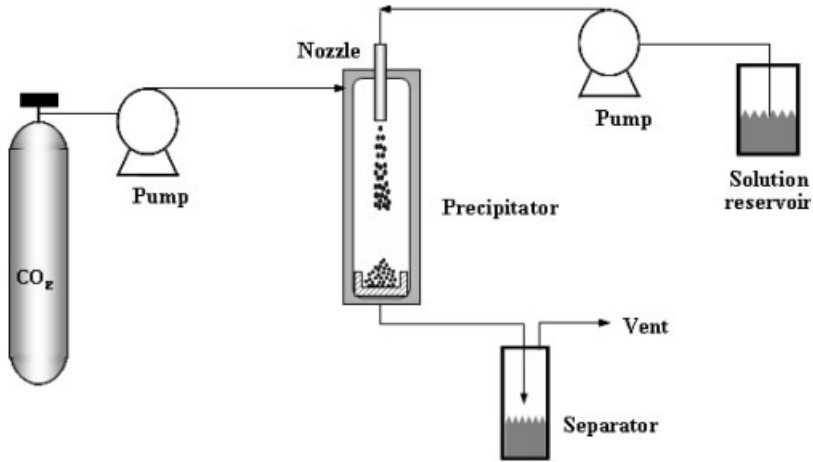
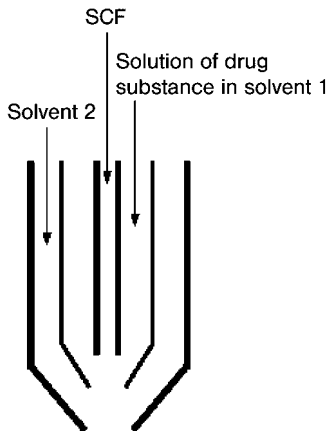


Fig. 9.13. SAS process.

which include an API in the carrier (chemotrypsin in PLA [104], lysozyme in PLA [104] and naproxen in PLA [105]).

9.5.5
SEDS

The SEDS process is a modified version of the SAS. It enhances mixing efficiency by adopting a two- or three-coaxial-channel nozzle (Fig. 9.14) to facilitate smaller particle production. In this process, SCF is used both as an antisolvent and as a



Coaxial nozzle system

Fig. 9.14. Three-coaxial-channel nozzle system for SEDS process.

solution dispersion enhancer. Due to the high velocity of a SCF stream, faster breakup of solution and high mass transfer rates are achieved between the SCF and the solution, and so very fine particles are attained. With a three-coaxial-channel nozzle, one SCF stream and two organic solutions or two SCF streams and one organic solution can be combined. An aqueous solution can also be treated to form particles of water-soluble compounds such as proteins (lysozyme and trypsin [106]) and sugars (lactose, maltose, threhalose and sucrose [107]) using an aqueous solution of API/ethanol or methanol/SCCO₂ system.

9.6

Electrostatic Approaches

The recent advance of spraying techniques under a high electrical field has opened unique possibilities for nanoformulation [108–113]. Electro spraying to prepare monodisperse pharmaceutical nanoparticles is currently being under active investigation and many intriguing successes have been reported. Herein, electro spraying will be briefly introduced as an emerging technology.

9.6.1

Electrical Potential and Interfaces

The effect of electrical charges on the surface energy of a solid or liquid has been an interesting subject under thorough investigation. Common electrical charges are generated by the preferential adsorption of ions. In the electro spraying processes, an intentionally applied electrical field can effectively facilitate nanoparticle preparation [70]. When the interface between a solid and water is charged, the interfacial tension is reduced because of the greater interaction with water. This effect is much smaller with an oil drop. The contact angle actually follows the decrease of interfacial tension.

When an electrical field is applied between a nozzle and a collection part in spraying, the size of drop generated from a nozzle is reduced depending on the amount of applied charge (Fig. 9.15). Without an electrical field, the final size of a drop from a nozzle depends on the surface energy and the gravitational force of the drop (dripping mode in Fig. 9.16). With the aid of an electrical field, drops of smaller size overcome their surface energy and detach themselves from the tip of the nozzle (microdripping mode in Fig. 9.16) [114, 115]. As the electrical field increases further, the decrease of drop size reaches a different stage. The charged surface of the drop can no longer sustain its integrity and induces total breakup into droplets of much smaller size (Fig. 9.16). Usually, the droplets are of invisible nanometer size. Transition into this stage is easily confirmed by checking the formation of a Taylor cone (cone-jet in Fig. 9.16) structure at a nozzle tip [114].

The cone-jet mode was successfully explained by Talyor in 1964 [114]. The size of droplets is determined by the hydrostatic balance between electrical and surface tension forces. Further elaboration of the phenomena was later performed by Fer-

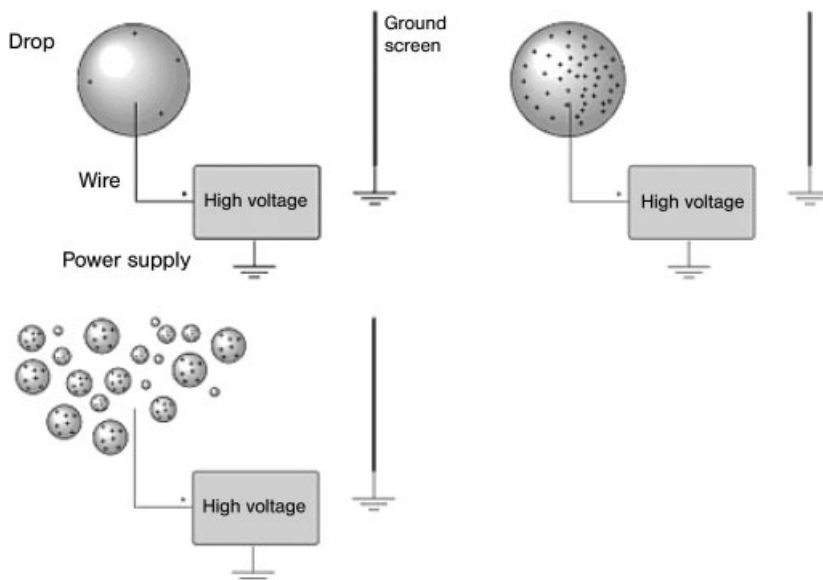


Fig. 9.15. Electrospinning induces the breakup of charged drops by a surface electrostatic force.

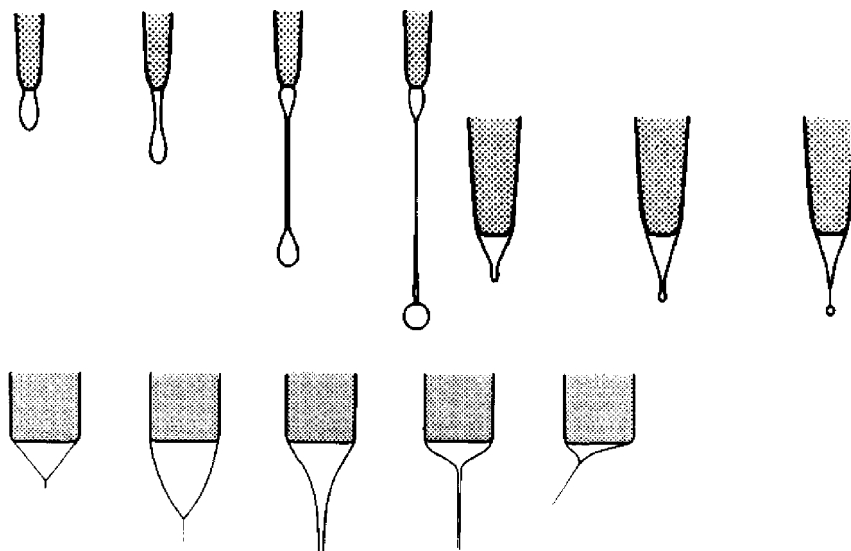


Fig. 9.16. Different stages of electrospinning drops (cyclohexanol): dripping mode (top left), microdripping mode (top right) and cone-jet mode (bottom). (Reproduced with permission from Ref. [115].)

nández de la Mora and Loscertales [116, 117] and Gañán-Calvo *et al.* [118–120]. The detailed relationship between current and flow rate was established depending on the properties of liquids employed. Particle size can be predicted in an ideal case from various parameters such as current, flow rate, permittivity and conductivity, etc. For example, when conductivity and viscosity are relatively low, particle diameter, d , is:

$$d \sim [(b - 1)^{1/2} Q \epsilon_0 / K]^{1/3} \quad (5)$$

and when both the viscosity and conductivity is high, d is:

$$d^{3/2} \sim Q/I \quad (6)$$

where I is the current, Q is the flow rate, b is the liquid to vacuum permittivity ratio, K is the electrical conductivity and ϵ_0 is the vacuum permittivity [116–120].

When the flow rate is relatively high, a ramified jet results instead of the cone-jet mode (Fig. 9.17). With relatively high conductivity and viscosity, electro spraying works in the spindle mode, which is often used to prepare nanofibers (Fig. 9.17) [114, 115]. Various factors such as flow rate, current, electrical conductivity, permittivity, liquid/gas surface tension, viscosity and density need to be considered to obtain a specific spraying mode, [117, 119–121].

9.6.2

Electrospraying

In a simple electro spraying case, an electrically conductive liquid is slowly injected into a capillary having a potential difference of at least several thousand volts between a plate and itself. Liquids turn into charged droplets out of the “Taylor cone” at the capillary tip (Figs. 15 and 16). Proper posttreatments lead the droplets to form stable pharmaceutical nanoparticles. When a coaxial capillary is used, core/shell-type nanoparticles can be obtained (Fig. 9.18); recently, nanoparticles with more complicated internal structures have been reported [116, 119, 122].

Conventional spraying gives unique advantages for pharmaceutical applications when combined with an electrical field. First, relatively monodisperse pharmaceutical nanoparticles can be conveniently prepared (Fig. 9.19). Since the size of droplets is determined by electrical surface charge, monodispersity can readily be accomplished, and size control is relatively easy. It is also an important bonus that organic solvents are not necessary for this technique. Compared to other preparation methods, electro spraying can be applied to pharmaceutical materials of various physical properties since this method does not significantly rely on the hydrophilicity of solvents and pharmaceutical materials. Proteins can be processed regardless of their surface hydrophilicities. Moreover, protein is known to be stable in high electrical fields. While other methods using organic solvents or mechanical energies often destroy the viability of proteins, electro spraying does not cause such

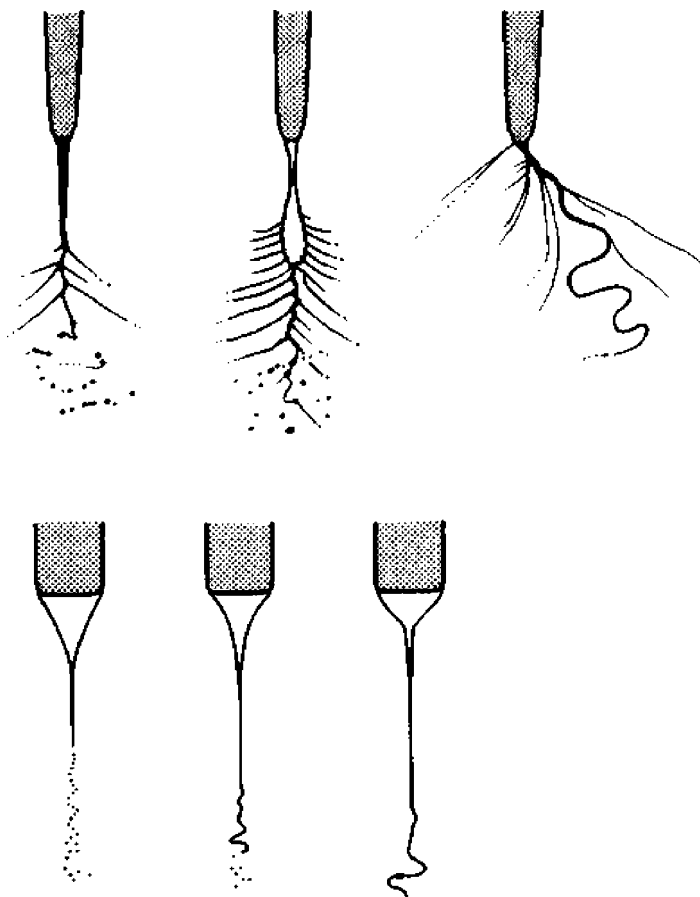


Fig. 9.17. Different stages of electro spraying: ramified jet and random spraying (top), and spindle mode (bottom). (Reproduced with permission from Ref. [115].)

problems [123]. As a result, nanoformulation of many different types of drugs, including proteins, can be developed using electro spraying technique.

Core/shell nanoparticles are especially useful for drug delivery systems (Fig. 9.18) [116]. Two liquids are injected into two coaxial capillaries under an electrical field and form nanoparticles as a result of the electrohydrodynamic force. The sizes of two capillaries can range from a few micrometers to several millimeters and the electrical field is applied to the outer capillary. The electrical potential of the inner capillary depends on the electrical conductivity of the liquid in the outer capillary. By changing flow rates and the electrical field, nano-encapsulated particles can be prepared. The size of core/shell particles and the thickness of coating shells depend on the various physical properties of materials, but they are easily controlled by adjusting flow rates of two liquids.

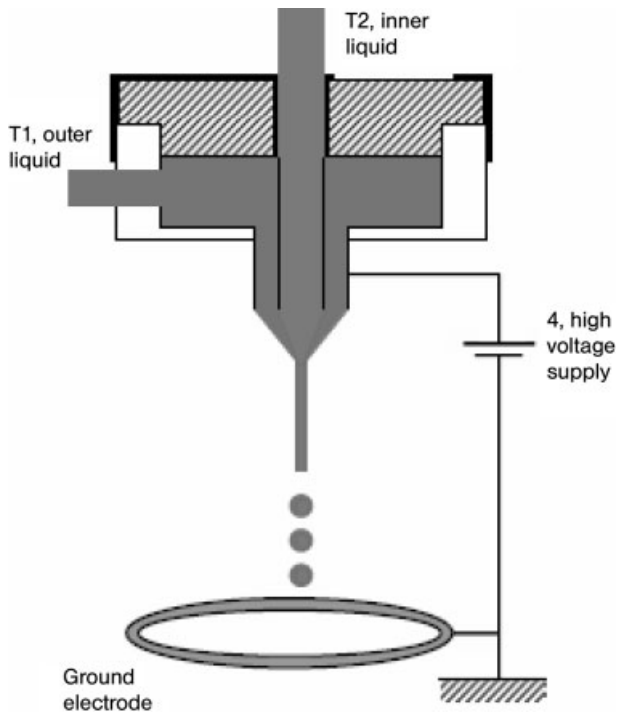


Fig. 9.18. Schematic illustration of coaxial electrospaying equipment to prepare core/shell drug particles. (Reproduced with permission from Ref. [116].)

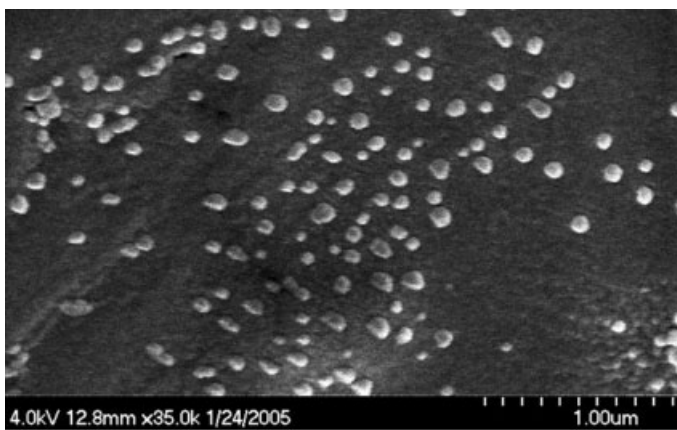


Fig. 9.19. Nanoparticles prepared from electrospaying.

The current during coaxial electrospraying mainly relies on the flow rate of more conductive liquid (driving liquid) between the two liquids employed. Whether the driving liquid is injected into the outer or inner capillary affects the core/shell particle formation mechanism. Once it is decided, the flow rate of driving liquid needs to be carefully controlled to obtain a proper current, and resulting particle size and internal structure.

References

- 1 PhRMA Analysis Reports, *Why Do Medicines Cost So Much?* and *Pharmaceutical Industry Profile*, 2005, <http://www.phrma.org/publications>.
- 2 LI, J. K., WANG, N., WU, X. S., A novel biodegradable system based on gelatin nanoparticles and poly(lactic-co-glycolic acid) microspheres for protein and peptide drug delivery, *J. Pharm. Sci.* **1997**, *86*, 891–895.
- 3 ZAMBAUX, M. F., BONNEAUX, F., GREF, R., DELLACHERIE, E., VIGNERON, C., MPEO–PLA nanoparticles: effect of MPEO content on some of their surface properties, *J. Biomed. Mater. Res.* **1999**, *44*, 109–115.
- 4 MURAKAMI, H., KOBAYASHI, M., TAKEUCHI, H., KAWASHIMA, Y., Evaluation of poly(DL-lactide-co-glycolide) nanoparticles as matrix material for direct compression, *Adv. Powder Technol.* **2000**, *11*, 311–322.
- 5 FOURNIER, E., DUFRESNE, M.-H., SMITH, D. C., RANGER, M., LEROUX, J.-C., A novel one-step drug-loading procedure for water-soluble amphiphilic nanocarriers, *Pharm. Res.* **2004**, *21*, 962–968.
- 6 LEE, J., Drug nano- and microparticles processed into solid dosage forms: physical properties, *J. Pharm. Sci.* **2003**, *92*, 2057–2068.
- 7 GRAU, M. J., KAYSER, O., MÜLLER, R. H., Nanosuspensions of poorly soluble drugs – reproducibility of small scale production, *Int. J. Pharm.* **2000**, *196*, 155–157.
- 8 LIU, R. (Ed.), *Particle Size Reduction in Water-insoluble Drug Formulation*, Interpharm Press, Buffalo Grove, IL, 2000.
- 9 LIVERSIDGE, G. G., CONZENTINO, P., Drug particle size reduction for decreasing gastric irritancy and enhancing absorption of naproxen in rats, *Int. J. Pharm.* **1995**, *125*, 309–313.
- 10 LIVERSIDGE, G. G., CUNDY, K., Particle size reduction for improvement of oral bioavailability of hydrophobic drugs: I. Absolute oral bioavailability of nanocrystalline danazol in beagle dogs, *Int. J. Pharm.* **1995**, *125*, 91–97.
- 11 MERISKO-LIVERSIDGE, E., SARPOTDAR, P., BRUNO, J., HAJJ, S., WEI, L., PELTIER, N., RAKE, J., SHAW, J. M., PUGH, S., POLLIN, L., JONES, J., CORBETT, T., COOPER, E., LIVERSIDGE, G. G., Formulation and antitumor activity evaluation of nanocrystalline suspensions of poorly soluble anticancer drugs, *Pharm. Res.* **1996**, *13*, 272–278.
- 12 SERAJUDDIN, A. T. M., Solid dispersion of poorly water-soluble drugs: early promises, subsequent problems, and recent breakthroughs, *J. Pharm. Sci.* **1999**, *88*, 1058–1066.
- 13 YAMADA, T., SAITO, N., IMAI, T., Effect of grinding with hydroxypropyl cellulose on the dissolution and particle size of a poorly water-soluble drug, *Chem. Pharm. Bull.* **1999**, *47*, 1311–1313.
- 14 ZHENG, J. Y., BOSCH, H. W., Sterile filtration of nanocrystal drug formulation, *Drug Dev. Ind. Pharm.* **1997**, *23*, 1087–1093.
- 15 MERISKO-LIVERSIDGE, E., MCGURK, S. L., LIVERSIDGE, G. G., Insulin nanoparticles: a novel formulation approach for poorly water soluble Zn-

- insulin, *Pharm. Res.* **2004**, *21*, 1545–1553.
- 16 BOSCH, H. W., OSTRANDER, K. D., HOVEY, D. C., Nanoparticulate compositions comprising amorphous cyclosporine and methods of making and using such compositions, *US patent 6,656,504*, **2003**.
 - 17 PACE, G. W., MISHRA, A. K., Water-insoluble drug particle process, *US patent 6,682,761*, **2004**.
 - 18 RYDE, N. P., RUDDY, S. B., Solid dose nanoparticulate compositions comprising a synergistic combination of a polymeric surface stabilizer and dioctyl sodium sulfosuccinate, *US patent 6,375,986*, **2002**.
 - 19 RYDE, N. P., RUDDY, S. B., Nanoparticulate dispersions comprising a synergistic combination of a polymeric surface stabilizer and dioctyl sodium sulfosuccinate, *US patent 6,592,903*, **2002**.
 - 20 CHAMBERS, E., MITRAGOTRI, S., Prolonged circulation of large polymeric nanoparticles by non-covalent adsorption on erythrocytes, *J. Controlled Rel.* **2004**, *100*, 111–119.
 - 21 SCHMIDT, C., BODMEIER, R., Incorporation of polymeric nanoparticles into solid dosage forms, *J. Controlled Rel.* **1999**, *57*, 115–125.
 - 22 AMIDON, G. L., LENNERNÄS, H., SHAH, V. P., CRISON, J. R., A theoretical basis for a biopharmaceutical drug classification: the correlation of *in vitro* drug product dissolution and *in vivo* bioavailability, *Pharm. Res.* **1995**, *12*, 413–420.
 - 23 THANOS, C. G., LIU, Z., GODDARD, M., REINEKE, J., BAILEY, N., CROSS, M., BURRILL, R., MATHIOWITZ, E., Enhancing the oral bioavailability of the poorly soluble drug dicumarol with a bioadhesive polymer, *J. Pharm. Sci.* **2003**, *92*, 1677–1689.
 - 24 GRET, R., MINAMITAKE, Y., PERACCHIA, M. T., TRUBETSKOY, V., TORCHILIN, V., LANGER, R., Biodegradable long-circulating polymeric nanospheres, *Science* **1994**, *263*, 1600–1603.
 - 25 HILL, T. L., A different approach to nanothermodynamics, *Nano Lett.* **2001**, *1*, 273–275.
 - 26 AGNIHOTRI, S. A., MALLIKARJUNA, N. N., AMINABHAVI, T. M., Recent advances on chitosan-based micro- and nanoparticles in drug delivery, *J. Controlled Rel.* **2004**, *100*, 5–28.
 - 27 XU, Y., DU, Y., HUANG, R., GAO, L., Preparation and modification of *N*-(2-hydroxyl) propyl-3-trimethyl ammonium chitosan chloride nanoparticle as a protein carrier, *Biomaterials* **2003**, *24*, 5015–5022.
 - 28 WEBER, C., COESTER, C., KREUTER, J., LANGER, K., Desolvation process and surface characterization of protein nanoparticles, *Int. J. Pharm.* **2000**, *194*, 91–102.
 - 29 GOVENDER, T., RILEY, T., EHTEZAZI, T., GARNETT, M. C., STOLNIK, S., ILLUM, L., DAVIS, S. S., Defining the drug incorporation properties of PLA-PEG nanoparticles, *Int. J. Pharm.* **2000**, *199*, 95–110.
 - 30 KATAOKA, K., HARADA, A., NAGASAKI, Y., Block copolymer micelles for drug delivery: design, characterization and biological significance, *Adv. Drug Deliv. Rev.*, **2001**, *47*, 113–131.
 - 31 TORCHILIN, V. P., Structure and design of polymeric surfactant-based drug delivery systems, *J. Controlled Rel.* **2001**, *73*, 137–172.
 - 32 RAO, V. M., STELLA, V. J., When can cyclodextrins be considered for solubilization purposes?, *J. Pharm. Sci.* **2003**, *92*, 927–932.
 - 33 ADAMS, M. L., LAVASANIFAR, A., KWON, G. S., Amphiphilic block copolymers for drug delivery, *J. Pharm. Sci.* **2003**, *92*, 1343–1355.
 - 34 SOPPIMATH, K. S., TAN, D. C.-W., YANG, Y.-Y., pH-Triggered thermally responsive polymer core-shell nanoparticles for drug delivery, *Adv. Mater.* **2005**, *17*, 318–323.
 - 35 LASIC, D. D., Doxorubicin in sterically stabilized liposomes, *Nature* **1996**, *380*, 561–562.
 - 36 PAPAHDJOPOULOS, D., ALLEN, T. M., GABIZON, A., MAYHEW, E., MATTHAY, K., HUANG, S. K., LEE, K., WOODLE, M. C., LASIC, D. D., REDEMANN, C., MARTIN, F. J., Sterically stabilized liposomes: improvements in pharmacokinetics and antitumor

- therapeutic efficacy, *Proc. Natl Acad. Sci. USA* **1991**, *88*, 11460–11464.
- 37 SEDDON, J. M., Structure of the inverted hexagonal (H_{II}) phase, and non-lamellar phase transitions of lipids, *Biochim. Biophys Acta* **1990**, *1031*, 1–69.
- 38 CANTOR, R. S., Lipid composition and the lateral pressure profile in bilayers, *Biophys. J.* **1999**, *76*, 2625–2639.
- 39 NIELSEN, C., ANDERSEN, O. S., Inclusion-induced bilayer deformations: effects of monolayer equilibrium curvature, *Biophys. J.* **2000**, *79*, 2583–2604.
- 40 SHILLCOCK, J. C., LIPOWSKY, R., Equilibrium structure and lateral stress distribution of amphiphilic bilayers from dissipative particle dynamics simulations, *J. Chem. Phys.* **2002**, *117*, 5048–5061.
- 41 HELFRICH, W., Elastic properties of lipid bilayers: theory and possible experiments, *Z. Naturforsch. C* **1973**, *28*, 693–703.
- 42 ANDERSON, D. M., GRUNER, S. M., LEIBLER, S., Geometrical aspects of the frustration in the cubic phases of lyotropic liquid crystals, *Proc. Natl Acad. Sci. USA* **1988**, *85*, 5364–5368.
- 43 BRIGGS, J., CHUNG, H., CAFFREY, M., The temperature–composition phase diagram and mesophase structure characterization of the monoolein/water system, *J. Phys. II* **1996**, *6*, 723–751.
- 44 SCRIVEN, L. E., Equilibrium bicontinuous structure, *Nature* **1976**, *263*, 123–125.
- 45 HYDE, S. T., ANDERSSON, S., ERICSSON, B., LARSSON, K., A cubic structure consisting of a lipid bilayer forming an infinite periodic minimal surface of the gyroid type in the glycerolmonooleate water system, *Z. Kristallogr.* **1984**, *168*, 213–219.
- 46 BECHER, P., *Encyclopedia of Emulsion Technology: Basic Theory*, Marcel Dekker, New York, **1983**.
- 47 FLOYD, G., Top ten considerations in the development of parenteral emulsions, *Pharm. Sci. Technol. Today* **1999**, *2*, 134–143.
- 48 WHEELER, J. J., WONG, K. F., ANSELL, S. M., MASIN, D., BALLY, M. B., Polyethylene glycol modified phospholipids stabilize emulsions prepared from triacylglycerol, *J. Pharm. Sci.* **1994**, *83*, 1558–64.
- 49 CHUNG, H., KIM, T. W., KWON, M., KWON, I. C., JEONG, S. Y., Oil components modulate physical characteristics and function of the natural oil emulsions as drug or gene delivery, *J. Controlled Rel.* **2001**, *71*, 339–350.
- 50 SZLEIFER, O. V., GERASIMOV, D., THOMPSON, H., Spontaneous liposome formation induced by grafted poly(ethylene oxide) layers: Theoretical prediction and experimental verification, *Proc. Natl Acad. Sci. USA* **1998**, *95*, 1032–1037.
- 51 LIU, Q., HU, Y., SONG, K., Liposome clearance from blood: different animal species have different mechanisms, *Biochim. Biophys. Acta* **1995**, *1240*, 277–284.
- 52 CULLIS, P. R., CHONN, A., SEMPLE, S. C., Interactions of liposomes and lipid-based carrier systems with blood proteins: relation to clearance behaviour *in vivo*, *Adv. Drug Deliv. Rev.* **1998**, *32*, 3–17.
- 53 NEEDHAM, T. J., MCINTOSH, D., LASIC, D., Hydration of polyethylene glycol-grafted liposomes, *Biochim. Biophys. Acta* **1992**, *1108*, 40–48.
- 54 CEH, B., LASIC, D. D., A rigorous theory of remote loading of drugs into liposomes, *Langmuir* **1995**, *11*, 3356–3368.
- 55 RHODES, G., XU, Z., BITTMAN, R., Structure of polymerizable bilayers VII: lateral organization of diacetylenic phosphatidylcholines with short proximal acyl chains, *Biochim. Biophys. Acta* **1992**, *1128*, 93–104.
- 56 ROY, B. C., SANTOS, M., MALLIK, S., CAMPIGLIA, A. D., Synthesis of metal chelating lipids to sensitize lanthanide ions, *J. Org. Chem.* **2003**, *68*, 3999–4007.
- 57 GUSTAFSSON, J., LJUSBERG-WAHREN, H., ALMGREN, M., LARSSON, K., Cubic lipid–water phase dispersed into submicron particles, *Langmuir* **1996**, *12*, 4611–4613.

- 58 GUSTAFSSON, J., LJUSBERG-WAHREN, H., ALMGREN, M., LARSSON, K., Submicron particles of reversed lipid phases in water stabilized by a nonionic amphiphilic polymer, *Langmuir* **1997**, *13*, 6964–6971.
- 59 CHUNG, H., KIM, J., UM, J. Y., KWON, I. C., JEONG, S. Y., Self-assembled nanocubicle as a carrier for peroral insulin delivery, *Diabetologia* **2002**, *45*, 448–451.
- 60 SPICER, P., HAYDEN, K., LYNCH, M., OFORI-BOATENG, A., BURNS, J., Novel process for producing cubic liquid crystalline nanoparticles (cubosomes), *Langmuir* **2001**, *17*, 5748–5756.
- 61 SPICER, P. T., SMALL, W. B., LYNCH, M. L., BURNS, J. L., Dry powder precursors of cubic liquid crystalline nanoparticles (cubosomes), *J. Nanoparticle Res.* **2002**, *4*, 297–311.
- 62 LARSSON, K., On periodic curvature and standing wave motions in cell membranes, *Chem. Phys. Lipids* **1997**, *88*, 15–20.
- 63 YANG, D., O'BRIEN, D. F., MARDER, S. R., Polymerized bicontinuous cubic nanoparticles (cubosomes) from a reactive monoacylglycerol, *J. Am. Chem. Soc.* **2002**, *124*, 13388–13389.
- 64 SCHNUR, J. M., Lipid tubules: a paradigm for molecularly engineered structures, *Science* **1993**, *262*, 1669–1675.
- 65 SPECTOR, M. S., PRICE, R. R., SCHNUR, J. M., Chiral lipid tubules, *Adv. Mater.* **1999**, *11*, 337–340.
- 66 SCHNUR, J. M., PRICE, R., RUDOLPH, A. S., Biologically engineered microstructures: controlled release applications, *J. Controlled Rel.* **1994**, *28*, 3–13.
- 67 PAPAHDJOPPOULOS, D., VAIL, W. J., JACOBSON, K., POSTE, G., Cochleate lipid cylinders: formation by fusion of unilamellar lipid vesicles, *Biochim. Biophys. Acta* **1975**, *394*, 483–491.
- 68 SANTANGELO, R., PADERU, P., DELMAS, G., CHEN, Z.-W., MANNINO, R., ZARIF, L., PERLIN, D., Oral efficacy of cochleate–amphotericin B (CAMB) in a mouse model with systemic candidiasis, *Antimicrob. Ag. Chemother.* **2000**, *44*, 2356–2360.
- 69 MANNINO, R. J., GOULD-FOGERITE, S., Antigen cochleate formulations for oral and systemic vaccination, In *New Generation Vaccines*, LEVINE, M. M. (Ed.), Marcel Dekker, New York, **1997**, pp. 000–000.
- 70 MORRISON, I. D., ROSS, S., *Colloidal Dispersions*, Wiley, New York, **2002**.
- 71 McDONALD, D. P., Micronization, *Mfg Chem. Aero. News* **1971**, 39.
- 72 YOSHII, H., SOOITTANTAWAT, A., LIU, X.-D., ATARASHI, T., FURUTA, T., AISHIMA, S., OHGAWARA, M., Flavor release from spray-dried maltodextrin/gum arabic or soy matrices as a function of storage relative humidity, *Inn. Food Sci. Em. Technol.* **2001**, *2*, 55.
- 73 KINLOCH, A. J., YOUNG, R. J., *Fracture Behavior of Polymers*, Elsevier, New York, **1985**.
- 74 DUNCAN-HEWITT, W. C., WEATHERLY, G. C., Evaluating the fracture toughness of sucrose crystals using microindentation techniques, *Pharm. Res.* **1989**, *6*, 373–378.
- 75 SCHONERT, K., Aspects of very fine grinding, In *Challenges in Mineral Processing*, SASTRY, K. V. S., FUERSTENAU, M. C. (Eds.), Society of Mining Engineers, Littleton, CO, **1989**, pp. 155–172.
- 76 SCHONERT, K., Comminution from theory to practice, In *Proceedings of the XIX International Mineral Processing Congress*, Society of Mining Engineers, Littleton, CO, **1995**, pp. 7–14.
- 77 PLOEHN, H. J., RUSSEL, W. B., Interactions between colloidal particles and soluble polymers, *Adv. Chem. Eng.* **1990**, *15*, 137–228.
- 78 LEE, J., CHENG, Y., Critical freezing rate in freeze drying nanocrystal dispersions, *J. Controlled Rel.*, submitted.
- 79 GEDDE, U. W., *Polymer Physics*, Chapman & Hall, London, **1995**.
- 80 HANNAY, J. B., HOGARTH, J., On the solubility of solids in gases, *Proc. Roy. Soc. London* **1879**, *29*, 324.
- 81 McHUGH, M. A., KRUKONIS, V. J., *Supercritical Fluid Extraction*, Butterworth Heinemann, Boston, MA, **1994**.
- 82 TOM, J. W., DEBENEDETTI, P. G., Particle formation with supercritical

- fluids – review, *J. Aerosol Sci.* **1991**, *22*, 555–584.
- 83 SUBRAMANIAM, B., RAJEWSKI, R. A., SNAVELY, K., Pharmaceuticals processing with supercritical carbon dioxide, *J. Pharm. Sci.* **1997**, *86*, 885–890.
- 84 REVERCHON, E., Supercritical antisolvent precipitation of micro- and nano-particles, *J. Supercritical Fluids* **1999**, *15*, 1–21.
- 85 PALAKODATY, S., YORK, P., Phase behavioral effects on particle formation processes using supercritical fluids, *Pharm. Res.* **1999**, *16*, 976–985.
- 86 JUNG, J., PERRUT, M., Particle design using supercritical carbon dioxide, *J. Mater. Chem.* **2001**, *20*, 179–219.
- 87 YE, X., WAI, C. M., Making nano-materials in supercritical fluids: a review, *J. Chem. Educ.* **2003**, *80*, 198–205.
- 88 HAKUTA, Y., HAYASHI, H., ARAI, K., Fine particle formation using supercritical fluids, *Curr. Opin. Solid State Mater. Sci.* **2003**, *7*, 341–423.
- 89 KRUKONIS, V., Supercritical fluid nucleating of difficult-to-comminute solids, Presented at *Annual Meeting of the AIChE*, San Francisco, CA, **1984**.
- 90 MOHAMED, R. S., DEBENEDETTI, P. G., PRUD'HOMME, R. K., Effects of process conditions on crystals obtained from supercritical mixtures, *AIChE J.* **1989**, *325*–332.
- 91 KROBER, H., TEIPEL, U., KRAUSE, H., The formation of small organic particles using supercritical fluids, In *Proceedings (CD-ROM) of the 5th International Symposium on Supercritical Fluids*, ECKERT, C., TEJA, A. (Eds.), Atlanta, GA, **2000**.
- 92 DOMINGO, C., BERENDS, E., VAN ROSMALEN, G. M., Precipitations of ultrafine organic crystals from the rapid expansion of supercritical solutions over a capillary and a frit nozzle, *J. Supercritical Fluids* **1997**, *10*, 39–55.
- 93 FRANK, S. G., YE, C., Small particle formation and dissolution rate enhancement of relatively insoluble drugs using rapid expansion of supercritical solutions (RESS) processing, In *Proceedings (CD-ROM) of the 5th International Symposium on Supercritical Fluids*, ECKERT, C., TEJA, A. (Eds.), Atlanta, GA, **2000**.
- 94 DEBENEDETTI, P. G., TOM, J. W., YEO, S. D., LIM, G.-B., Application of supercritical fluids for the production of sustained delivery devices, *J. Controlled Rel.* **1993**, *24*, 27–44.
- 95 MISHIMA, K., MATSUYAMA, K., UCHIYAMA, H., IDE, M., Microcoating of flavones and 3-hydroxyflavone with polymer using supercritical carbon dioxide, In *Proceedings of the 4th International Symposium on Supercritical Fluids*, Sendai, Japan, **1997**, pp. 267–270.
- 96 MISHIMA, K., MATSUYAMA, K., YAMAUCHI, S., IZUMI, H., FURUDONO, D., Novel control of crystallinity and coating thickness of polymeric microcapsules of medicine by cosolvency of supercritical solution, In *Proceedings (CD-ROM) of the 5th International Symposium on Supercritical Fluids*, ECKERT, C., TEJA, A. (Eds.), Atlanta, GA, **2000**.
- 97 DEBENEDETTI, P. G., LIM, G.-B., PRUD'HOMME, R. K., Formation of protein microparticles by antisolvent precipitation, *European patent 0542314*, **1992**.
- 98 YEO, S. D., LIM, G.-B., DEBENEDETTI, P. G., BERNSTEIN, H., Formation of microparticulate protein powders using a supercritical fluid anti-solvent, *Biotechnol. Bioeng.* **1993**, *41*, 341–346.
- 99 THIERING, R., DEGHANI, F., DILLOW, A., FOSTER, N. R., The influence of operating conditions on the dense gas precipitation of model proteins, *J. Chem. Technol. Biotechnol.* **2000**, *75*, 29–41.
- 100 THIERING, R., DEGHANI, F., DILLOW, A., FOSTER, N. R., Solvent effects on the controlled dense gas precipitation of model proteins, *J. Chem. Technol. Biotechnol.* **2000**, *75*, 42–53.
- 101 WEBER, A., WEISS, C., TSCHERNJAEW, J., KUMMEL, R., Gas anti-solvent crystallization – from fundamentals to industrial applications, In *GVC-Fachausschub "High Pressure Chemical Engineering"*, Karlsruhe, Germany, **1999**, pp. 235–238.

- 102 REVERCHON, E., DE ROSA, I., DELLA PORTA, G., Effect of process parameter on the supercritical anti-solvent precipitation of microspheres of natural polymers, In *GVC-Fachauschub "High Pressure Chemical Engineering"*, Karlsruhe, Germany, 1999, pp. 251–258.
- 103 PLA-REVERCHON, E., DELLA PORTA, G., DE ROSA, I., SUBRA, P., LETOURNEUR, D., Biopolymers micronization by supercritical anti-solvent precipitation: the influence of some process parameters, In *Proceedings of the 5th Conference on Supercritical Fluids and their Applications*, Garda, 1999, pp. 473–478.
- 104 ELVASSORE, N., BERTUCCO, A., CALICETI, P., Production of protein-polymer micro-capsules by supercritical anti-solvent techniques. In *Proceedings (CD-ROM) of the 5th International Symposium on Supercritical Fluids*, ECKERT, C., TEJA, A. (Eds.), Atlanta, GA, 2000.
- 105 CHOU, Y. H., TOMASKO, D. L., GAS crystallization of polymer–pharmaceutical composite particles, In *Proceedings of the 4th International Symposium on Supercritical Fluids*, Sendai, Japan, 1997, pp. 55–57.
- 106 SOLAN, R., HOLLOWOOD, M. E., HUMPREYS, G. O., ASHRAF, P., YORK, P., Supercritical fluid processing: preparation of stable protein particles. In *Proceedings of the 5th International Symposium on Supercritical Fluids*, PERRUT, M., SUBRA, P. (Eds.), Nice, France, 1998, Vol. 1, pp. 301–306.
- 107 HANNA, M., YORK, P., Method and apparatus for the formulation of particles, *World patent WO 96/00 610*, 1996.
- 108 AMSDEN, B. G., GOOSEN, M. F. A., An examination of factors affecting the size, distribution and release characteristics of polymer microbeads made using electrostatics, *J. Controlled Rel.* 1997, 43, 183–196.
- 109 YOSHII, H., SOOTTITANTAWAT, A., LIU, X.-D., ATARASHI, T., FURUTA, T., AISHIMA, S., OHGAWARA, M., Flavor release from spray-dried maltodextrin/gum arabic or soy matrices as a function of storage relative humidity, *Inn. Food Sci. Em. Technol.* 2001, 2, 55–61.
- 110 HARDAS, N., DANVIRIYAKUL, S., FOLEY, J. L., NAWAR, W. W., CHINACHOTI, P., Accelerated stability studies of microencapsulated anhydrous milk fat, *Lebensm.-Wiss. U.-Technol.* 2000, 33, 506–511.
- 111 LEE, S. J., ROSEMBERG, M., Whey protein-based microcapsules prepared by double emulsification and heat gelation, *Lebensm.-Wiss. U.-Technol.* 2000, 33, 80–91.
- 112 LEE, Y. H., KIM, C. A., JANG, W. H., CHOI, H. J., JHON, M. S., Synthesis and electrorheological characteristics of microencapsulated polyaniline particles with melamine-formaldehyde resins, *Polymer* 2001, 42, 8277.
- 113 BURLAK, G., KOSHEVAYA, S., SANCHEZ-MONDRAGON, J., GRIMALSKY, V., Electromagnetic eigenoscillations and fields in a dielectric microsphere with multilayer spherical stack, *Opt. Commun.* 2001, 187, 91.
- 114 TAYLOR, G. I., Disintegration of water drops in an electric field, *Proc. Roy. Soc. London Ser. A* 1964, 280, 383.
- 115 CLOUPEAU, M., PRUNET-FOCH, B., Electrohydrodynamic spraying functioning modes: a critical review, *J. Aerosol Sci.* 1994, 25, 1021.
- 116 LOSCERTALES, I. G., BARRERO, A., GUERRERO, I., CORTIJO, R., MA'RQUEZ, M., GAÑÁN-CALVO, A. M., Micro/nano encapsulation via electrified coaxial liquid jets, *Science* 2002, 295, 1695.
- 117 DE LA MORA, F., LOSCERTALES, I. G., The current emitted by highly conducting Taylor cones, *J. Fluid Mech.* 1994, 260, 155.
- 118 GAÑÁN-CALVO, A. M., Generation of steady liquid microthreads and micron-sized monodisperse sprays in gas streams, *Phys. Rev. Lett.* 1997, 80, 285.
- 119 GAÑÁN-CALVO, M., Cone-jet analytical extension of Taylor's electrostatic solution and the asymptotic universal scaling laws in electro spraying, *Phys. Rev. Lett.* 1997, 79, 217.
- 120 GAÑÁN-CALVO, M., Generation of steady liquid microthreads and

- micron-sized monodisperse sprays in gas streams, *Phys. Rev. Lett.* **1998**, *80*, 285.
- 121 GAMERO-CASTANO, M., HRUBY, V., Electric measurements of charged sprays emitted by cone-jets, *J. Fluid Mech.* **2002**, *459*, 245.
- 122 LÓPEZ-HERRERA, J. M., BARRERO, A., LÓPEZ, A., LOSCERTALES, I. G., MÁRQUEZ, M., Coaxial jets generated from electrified Taylor cones-scaling laws, *J. Aerosol Sci.* **2003**, *34*, 535.
- 123 FENN, J. B., MANN, M., MENG, C. K., WONG, S. F., Electrospray ionization for mass spectrometry of large biomolecules, *Science* **1989**, *246*, 64.

10

Production of Biofunctionalized Solid Lipid Nanoparticles for Site-specific Drug Delivery

Rainer H. Müller, Eliana B. Souto, Torsten Göppert and Sven Gohla

10.1

Introduction

The concept of site-specific drug delivery using particles has greatly benefited from the fast development of nanotechnology to a stage where it is possible not only to produce such small particles (less than 1 μm) in a very narrow size distribution range, but also to modify the particle surface in order to provide site-specific delivery of drugs.

It is well known that the size of nanoparticles and their surface characteristics are crucial factors to determine the success of the particles when used *in vivo*. With regard to the particle dimensions, it has been shown that nanometer-sized particles could be used for drug targeting, especially to the mononuclear phagocyte system (MPS) and the polymorphonuclear leukocytes, a mechanism that is based on their natural tropism and their biophysical properties [1, 2]. Concerning the surface characteristics, such as hydrophobicity and electrical charge, the internalization of nanoparticles by cells other than MPS cells is severely limited by the short residence time of particles in the blood. The modification of nanoparticle surface induces alterations in cell behavior distinct from the unmodified particles, suggesting that cell response and uptake can be directed via specifically engineered particle surfaces. The surface of nanoparticles can be modified using hydrophilic chains, such as polyethylene glycol (PEG), to prolong the circulation time of those carriers in the blood by resisting protein adsorption, reducing or avoiding the natural blood opsonization process and therefore their intracellular uptake by macrophages from the liver and spleen [2, 3]. The electrical charge of the nanoparticles also affects their *in vivo* fate [4–7].

This approach has been applied to target drug substances incorporated into colloidal drug carriers such as liposomes [8] and polymeric nanoparticles [9]. However, the use of those systems had some disadvantages. In spite of being one of the most extensively investigated drug delivery systems, liposomes show some chemical and physical stability problems that can lead to aggregation and drug degradation or expulsion of drug during storage, limiting their therapeutic performance [10]. Regarding the use of polymeric nanoparticles, the cytotoxicity of polymers

and the problems with polymer chemistry, as well as the need for γ -irradiation for production of sterile formulations, which can cause decomposition of incorporated drug and/or polymer and formation of potentially carcinogenic radicals, are the main disadvantages. Several synthetic polymers, such as poly(lactic acid) (PLA), poly(β -hydroxybutyrate) (PHB) and poly(lactide-co-glycolide) (PLGA), have shown good histocompatibility and biodegradability, and their safety has been extensively documented. However, even those polymers which are accepted for use as microparticles and implants can show cytotoxic effects when delivered as nanoparticles or as very small microparticles [11].

Cytotoxic effects can occur both on the outside of the phagocytic cells or after ingestion in the interior of the cell. Therefore, both surfactants and matrix material can lead to cytotoxic degradation products [12, 13]. Furthermore, there is a lack of large-scale production methods for polymeric nanoparticles which are acceptable to the regulatory authorities and at the same time cost-effective. As a consequence – in contrast to liposomes – no polymeric nanoparticulate product is on the market (only polymeric microparticles).

In order to achieve higher viability of cells (i.e. better tolerability) and decrease the risk of toxicity, nanoparticles can be produced by using lipids which are solid both at room and at body temperature. Such systems are called solid lipid nanoparticles (SLN) [14], and they have been recently tested as site-specific carriers particularly for drugs that have a rapid metabolism and are quickly eliminated from the blood, i.e. peptide and protein-loaded SLN [15, 16]. A clear advantage of these particles is the fact that the lipid matrix is composed of physiological lipids, e.g. generally recognized as safe (“GRAS”) status, which decreases the risk of acute and chronic toxicity [17]. SLN prepared with several lipids and emulsifying agents do not exhibit any cytotoxic effects *in vitro* up to concentrations of 2.5% lipid. In fact, it has been shown that even concentrations higher than 10% of lipid phase led to a viability of 80% with human granulocytes in culture [12]. For comparison, PLA nanoparticles showed complete cell death at 0.5% [12, 18]. In addition, a high loading capacity for a broad range of drugs can be achieved, especially if they have lipophilic properties [17, 19].

Due to their physiological and biodegradable properties, SLN have been tested for several administration routes [20], such as the oral and peroral routes [21, 22], pulmonary route, ocular [23], topical, dermal and transdermal administration [24–29], as well as for gene therapy [30–32], as new adjuvants for vaccines [33], and for parenteral delivery [34–38]. Concerning the latter, SLN can accumulate in target tissues based on their natural host cell tropisms and on their biophysical properties (passive targeting). In practice, active targeting to cells other than MPS cells is often insufficient for rapid and specific accumulation in target tissues. Further improvement of tissue selectivity can be achieved by engineering the surface of SLN with hydrophilic polymers [39, 40] or coupling targeting ligands [41–43].

In the present chapter, the concept of differential protein adsorption as well as the concept of functionalization of SLN via surface modification will be defined and discussed from a practical point of view. First, a brief introduction to the concept of differential adsorption after intravenous administration will be given, fol-

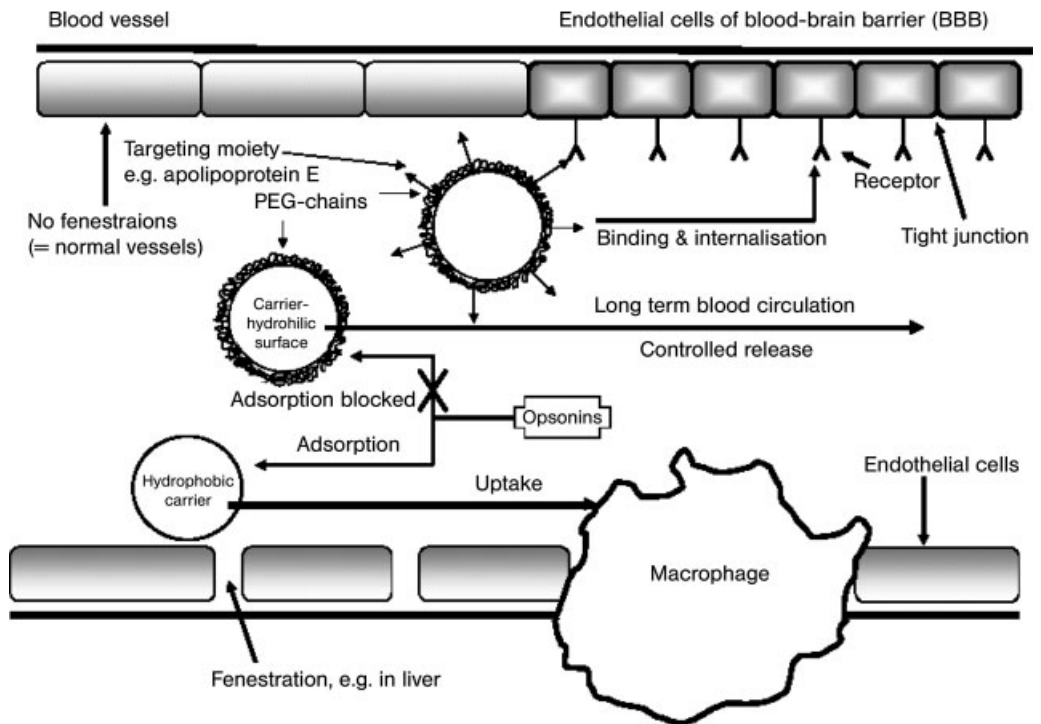


Fig. 10.1. Approaches to achieve passive targeting, long-circulating carriers for prolonged drug release and target-specific carriers (active targeting) via the intravenous route. (With permission after Ref. [80].)

lowed by a description of the methods used for the preparation of coated SLN. The last section will focus on the functionalization of SLN by modification of their surface characteristics, where some examples will be presented.

10.2 Concept of Differential Adsorption

By far the greatest attention to deliver drugs to selected sites in body has been focused on the intravenous route. Figure 10.1 reviews the main approaches to achieve both passive and active targeting. After injection, hydrophobic carriers will adsorb opsonins leading to uptake by the macrophages. In the liver, the macrophages are located in the layer of the endothelial cells. In case carriers are surface modified with hydrophilic polymers, e.g. PEG chains, the adsorption of opsonins will be minimized or avoided. Long-term blood circulation is achieved with such carriers which can be used, for example, for the controlled release of drugs. By at-

taching targeting moieties to these “stealth” carriers, location at specific cells can be achieved which carry the appropriate receptor and are accessible from the blood, e.g. the endothelial cells of the blood–brain barrier (BBB) or cells which are behind fenestrated blood vessels, such as liver or bone marrow.

Since the 1950s attempts have been made in order to correlate the organ distribution of intravenous injected drug carriers with their physicochemical properties, such as particle size [44] or electrical charge [7]. At the end of the 1980s it was realized that such a complex process like organ distribution could not be explained only by the physicochemical characteristics of the above-mentioned carriers [45]. After intravenous injection colloidal drug carriers immediately interact with plasma proteins, which are adsorbed onto the surface of the carriers. These adsorbed plasma proteins are generally accepted as the determining factor for the *in vivo* fate of the carriers. Drug carriers with different protein adsorption patterns will be recognized by different macrophage subpopulations (“concept of differential adsorption” [45, 46]), carrying proteins such as opsonins, like immunoglobulins or complement factors. When these are preferentially adsorbed onto the carriers’ surface, these carriers are immediately recognized by the MPS as foreign bodies and are therefore “cleared” from the blood. In contrast, when dysopsonins, such as hydrophilic proteins like albumin [47], are enriched on the carriers’ surface the systems will not be so easily recognized by macrophages. Such carriers are useful as circulating depots for the controlled release of drugs. Thus, in order to achieve an active drug targeting with these nonrecognizing carriers, it is important to have an additional enrichment of a protein mediating uptake into the target cells.

The decisive adsorption patterns acquired after intravenous injection depend on the physicochemical properties of the carriers [45, 48]. Therefore, there is a correlation between the physicochemical surface characteristics of the carriers, the plasma protein adsorption patterns and the resulting organ distribution (Fig. 10.2). Knowledge of this basic correlation can be exploited to develop site-specific intravenous carriers in a controlled way.

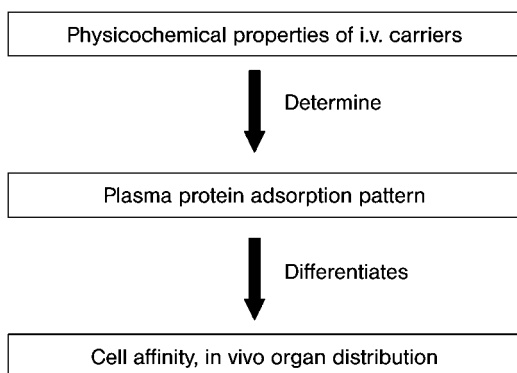


Fig. 10.2. Basic correlation exploited in the development of site-specific colloidal drug carriers (concept of “differential protein adsorption”).

In the middle of the 1990s, Kreuter et al. showed the possibility of site-specific targeting of various drugs, such as dalargin, enkephalin, tubocurarine and doxorubicin, into the brain by using polysorbate-coated poly(butyl cyanoacrylate) (PBCA)-nanoparticles [49–52]. The efficiency of drug delivery into the brain depended on the coating of those particles with polysorbate surfactants, particularly polysorbate 80, but also polysorbate 20, 40 and 60. Other surfactants such as poloxamers (e.g. poloxamer 338) led to no effects [53]. Using two-dimensional polyacrylamide gel electrophoresis (2-D PAGE), Müller et al. observed an enrichment of apolipoprotein E (apoE) on the surface of PBCA nanoparticles after incubation in human plasma. No apoE adsorption was seen after incubation with the other surfactants mentioned before [54]. ApoE seemed to play an important role in the transport of lipoproteins into the brain via the low-density lipoprotein receptor at the BBB [55]. Thus, it is possible that apoE-adsorbing drug carriers mimic lipoprotein particles leading to their brain uptake by endocytic processes. This theory was confirmed by turning the negative control in the Kreuter experiments [uncoated PBCA nanoparticles (no polysorbate adsorbed), loaded with dalargin] into a brain-specific carrier. ApoE was preadsorbed prior to injection and then the particles were able to carry dalargin across the BBB. Figure 10.3 summarizes the Kreuter experiments [49, 56].

In the experiments performed by Kreuter et al. the drug was adsorbed onto the surface, leading to a limited loading capacity. Furthermore, these polymeric nanoparticles exhibit the already mentioned toxicity problems. Due to the limited loading capacity, too much matrix material is required to deliver a sufficient amount of the drug to the brain. In addition, the *in vivo* biodegradation will be relatively slow, i.e. depending on the dose, the carrier material might accumulate in the target cell. In addition, the degradation leads to a release of toxicologically problematic formaldehyde [57], whereas it is a controversial discussion if the formaldehyde is really

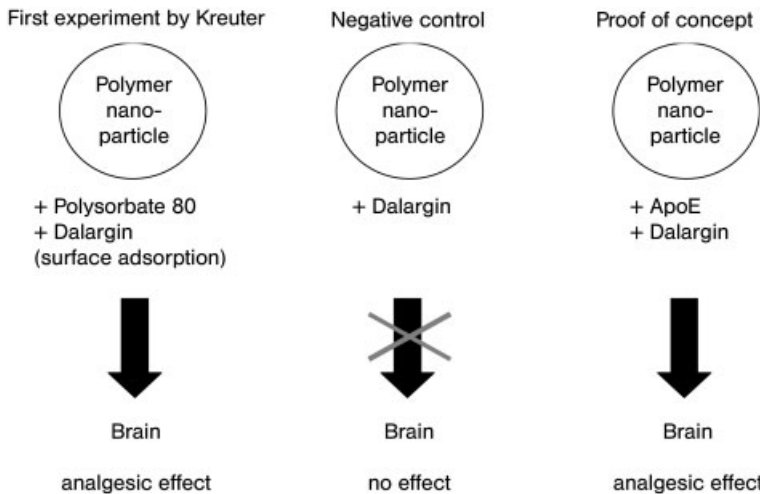


Fig. 10.3. Scheme of the experiments performed by Kreuter et al. (Modified after Ref. [56].)

a problem. Thus, the “concept of differential adsorption” and the analytical methodology to investigate the decisive adsorption patterns were transferred to the *in vivo* well tolerable SLN. Special SLN were produced using different surfactants and the influence on plasma protein adsorption patterns was investigated by 2-D PAGE.

10.3

Production of SLN

SLN of narrow size ranges can easily be produced and coated with hydrophilic polymers, providing convenient, readily targetable systems [15, 34, 36]. In order to prepare SLN with adsorbed hydrophilic polymers onto their surface, the literature describes three main production methods. These methods are the high-pressure homogenization (HPH) technique developed by Müller and Lucks [14], the microemulsion-based SLN technique developed by Gasco [58] and the solvent emulsification-evaporation technique described by Sjöström and Bergenstahl preparing SLN dispersions by solvent evaporation in oil-in-water (o/w) emulsions [59]. However, methods such as the solvent displacement and the emulsification-diffusion techniques, which have been used to prepare polymeric nanoparticles, have also been tested for SLN preparation [60].

Production of SLN by HPH can be done using either the hot or the cold homogenization technique. For both techniques, the active compound is dissolved or dispersed in the melted lipid prior to HPH [19, 20]. Concerning the hot technique, which is the most frequently applied technique, two different phases are prepared at the same temperature – the lipid phase consisting of melted lipid mixed with drug and the aqueous phase consisting of a hot solution where the hydrophilic coating polymer or protein is dissolved. Both phases are mixed by high-speed stirring or by ultrasound breaking the large droplets of the internal lipid phase into smaller ones yielding a pre-emulsion. This pre-emulsion is then passed through a high-pressure homogenizer applying, for example, a homogenization pressure of 500 bar and one to three homogenization cycles. The obtained nanoemulsion is cooled and solidifies, forming an aqueous SLN dispersion. This technique can process lipophilic and insoluble drugs. Even temperature-sensitive compounds (e.g. retinol) can be incorporated into the SLN matrix by hot HPH once the exposure time to elevated temperatures is relatively short [19]. However, this technique is not suitable for incorporating hydrophilic drugs because they will partition from the melted lipid to the water phase during the homogenization step, resulting in a too low loading capacity.

With regard to the cold technique, the drug-containing lipid melt is cooled and solidified. Dry ice or liquid nitrogen are added to increase the brittleness of the lipid and to ease the further milling procedure. The high cooling rate favors a homogeneous distribution of the drug within the lipid matrix. After solidification, the lipidic mass is ground by means of ball or mortar milling to yield lipid microparticles with a diameter between 50 and 100 μm . The lipid microparticles are then

dispersed in a cold surfactant solution by stirring, yielding a macro-suspension. This suspension is passed through a high-pressure homogenizer at/or below room temperature and the microparticles are broken down to form SLN. The cavitation and shear forces in the homogenization gap are sufficiently high to break the microparticles and to yield SLN. The cold HPH technique minimizes the thermal exposure of the sample, but does not avoid it completely due to the melting of the lipid in the initial step of the process. Therefore, this technique is recommended for extremely temperature-sensitive or hydrophilic drugs, which might partition from the liquid lipid phase to the water phase during hot HPH. SLN prepared by this procedure possess slightly higher mean particle sizes and polydispersity indices compared to those obtained by the hot HPH technique of the same lipid at identical homogenization parameters (pressure, temperature and number of homogenization cycles). To further reduce the mean particle size and to minimize the polydispersity, a higher number of homogenization cycles can be applied. The cold HPH technique can also be employed when the lipid matrix is composed by lipids with high melting points [61]. Note that this technique is less effective in dispersing the lipids. During the production process, the lipid matrix remains mainly in the solid state despite possible high (but extremely short) temperature peaks occurring in the high-pressure homogenizer. The homogenization can be performed slightly below the melting point of the lipid (e.g. 5–10 °C), which seems to lead to a softening of the lipid during the homogenization process. The softened lipid can be more easily dispersed, leading to a more uniform product of smaller mean SLN diameter. The homogenization temperature needs to be carefully selected because otherwise the loss of hydrophilic drugs to the water phase might be too high.

For the preparation of SLN using the microemulsion technique developed by Gasco, the lipid phase is melted and at the same temperature (approximately 60–70 °C) an o/w surfactant/cosurfactant-containing aqueous phase is prepared [58, 62]. Both lipid and aqueous phases are added, and mixed in such a ratio that a microemulsion results. SLN are obtained when the hot microemulsion is diluted into excess of cold water leading to a “breaking” of the microemulsion, converting it into an ultrafine nanoemulsion, which recrystallizes forming SLN. The reasons for the breaking of the emulsion are the dilution with water and the reduction of temperature narrowing the microemulsion region.

Regarding the preparation of SLN by solvent evaporation in o/w emulsions described by Sjöström and Bergenståh, the lipid phase is dissolved in a water-immiscible organic solvent, such as cyclohexane, chloroform or methylene chloride. Then the drug is dissolved or dispersed producing an organic phase containing the drug [63, 64]. This organic phase is emulsified in an o/w surfactant-containing aqueous phase by mechanical stirring. Upon evaporation of the organic solvent from the obtained o/w emulsion under mechanical stirring or reduced pressure, a nanoparticle dispersion is formed by precipitation of the lipid in the aqueous medium.

In the solvent displacement technique described Fessi et al. [65], the lipid phase is dissolved in a semipolar water-miscible solvent, such as ethanol, acetone or

methanol, where the active compound is also dissolved or dispersed. Simultaneously, an o/w surfactant-containing aqueous phase is prepared. The organic phase is injected into the aqueous phase under magnetic stirring. A violent spreading is observed because of the miscibility of both phases. Droplets of solvent of nanometer size are torn from the o/w interface. These droplets are rapidly stabilized by the surfactant molecules presented in the aqueous phase, until diffusion of the solvent is complete and lipid precipitation has occurred. Removal of solvent can be performed by distillation. SLN are formed after total evaporation of the water-miscible organic solvent.

With regard to the emulsification-diffusion methodology described by Quintanar-Gerrero and Fessi, this technique involves the use of a partially water-soluble solvent, such as benzyl alcohol [66] or tetrahydrofuran [67], which is saturated with water to ensure the initial thermodynamic equilibrium between those two liquids (water and solvent). The lipid is dissolved in the saturated solvent producing an organic phase where the drug is added. This organic phase is then emulsified, under vigorous agitation, in an aqueous solution containing a stabilizer agent obtaining an o/w emulsion. The subsequent addition of water to the system, under moderate mechanical stirring, causes solvent diffusion into the external phase and the lipid starts precipitating. Depending on its boiling point, the solvent can be eliminated by distillation or ultrafiltration. After the organic solvent is totally eliminated, an aqueous dispersion of SLN is formed.

Comparing the different methodologies described above, HPH is the most broadly used in different areas and it is also established in pharmaceutical production, e.g. the production of emulsions for parenteral nutrition (Intralipid[®] and Lipofundin[®]) [17]. This technique overcomes a major problem of other methods, i.e. large scale production. HPH also leads to nanoparticles with a relatively homogeneous size distribution, which increases the physical stability of the aqueous SLN dispersion.

The microemulsion method has the disadvantage of the dilution of the particle suspension with water, which needs to be removed. However, it avoids the collapse of the hydrophilic chains coating the surface of the particles [20]. Methods requiring solvent evaporation from o/w emulsions have the inconvenience of using organic solvents. In addition, evaporation must be fast in order to avoid collapse of the hydrophilic chains and potential aggregation.

10.4

Functionalization by Surface Modification

As already mentioned, targeting of drugs to different sites of the body via intravenous administration requires avoidance of recognition of the carrier system by macrophages of the MPS. To achieve this goal, nanoparticles were engineered by modifying the surface using nonionic surfactants such as poloxamers, poloxamines or polysorbates, reducing adsorption of proteins and blood opsonins compared to uncoated particles [68] (Fig. 10.4).

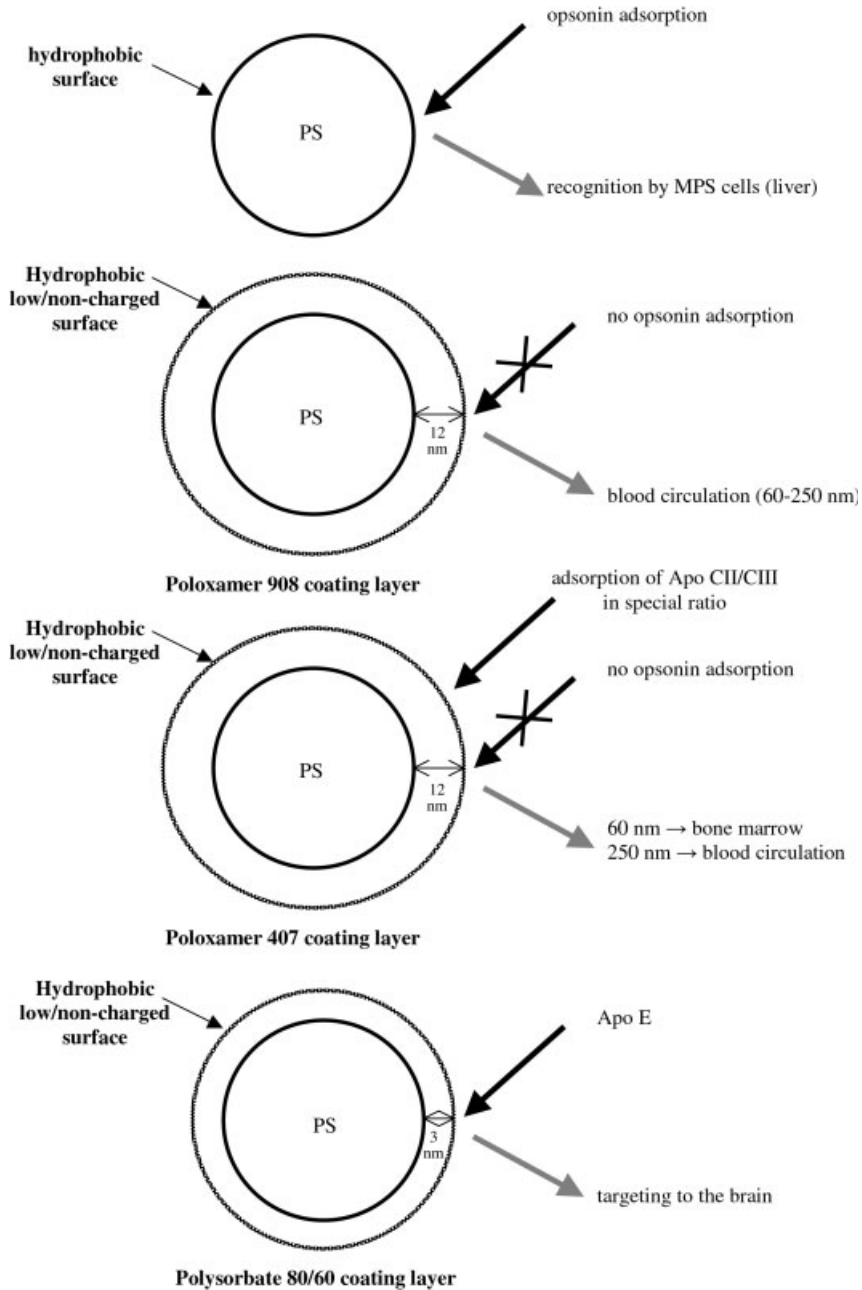


Fig. 10.4. Functionalization by surface modification of nanoparticles with poloxamer and polysorbate surfactants and resulting effects obtained *in vivo* (PS, polystyrene particle; PBCH, polybutylcyanoacrylate nanoparticle).

Once the phagocytic uptake is dependent on the surface hydrophilicity, i.e. it increases with the increase of hydrophilicity, it would be beneficial to have an enrichment of hydrophilic proteins (so-called dysopsonins) on the carriers' surface [69–71]. Such dysopsonins are, for example, albumin and apolipoproteins. Apolipoproteins are inherently adsorbed onto the surface of hydrophobic lipids such as triacylglycerols, cholesterol and cholesterol esters, forming lipoproteins in the blood. They show a relatively flexible molecular structure, which is able to change its conformation when adsorbing onto surfaces (“soft proteins”) [72]. This ability of changing its multiple α -helical segments in the interface in contact to water is the crucial property of these proteins for the efficient removal of nonpolar residues. Therefore, it has been anticipated that apolipoproteins would have a great affinity to SLN as well, because these particles also have a lipid core like lipoproteins. Indeed, a 5-min incubation of different SLN formulations with human plasma at 37 °C and subsequent 2-D PAGE analysis revealed apolipoprotein adsorption of up to 90% of the total amount of proteins adsorbed.

Figure 10.5 shows the plasma protein adsorption patterns obtained after 2-D PAGE analysis (2-D PAGE separation and subsequent silver staining) of cetyl palmitate-based SLN (10% m/m), stabilized with polysorbate 60 (PS60-SLN) and stabilized with poloxamer 338 (1.2% m/m) (PX338-SLN).

The adsorption patterns did not differ greatly with regard to the qualitative aspects of the adsorbed proteins. However, the apolipoproteins showed particularly distinct quantitative changes in the adsorbed amounts, showing the importance of the surfactant used for production of functionalized SLN.

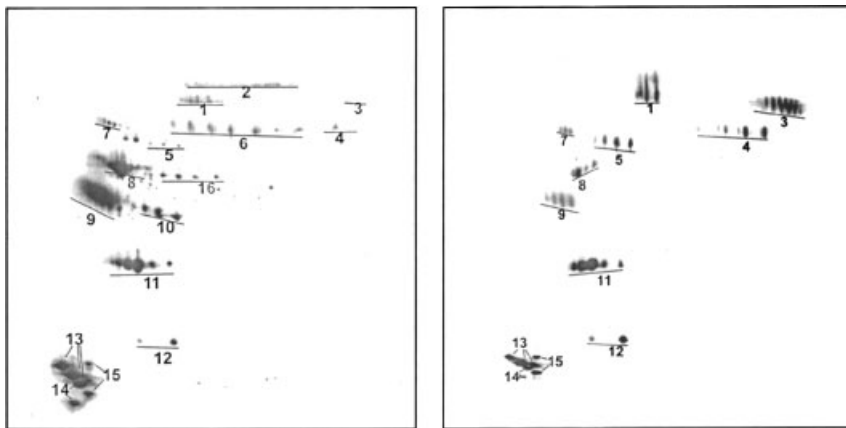


Fig. 10.5. Plasma protein adsorption patterns of PS60-SLN (left) and PX338-SLN (right) obtained after 2-D PAGE separation and silver staining. The whole 2-D gels are shown; pI 4.0–9.0 (from left to right, non-linear) molecular weight 250–60 000 Da (top to bottom, non-linear); 1, albumin; 2, IgM μ

chain; 3, fibrinogen α chain; 4, fibrinogen β chain; 5, fibrinogen γ chain; 6, apoH; 7, α_1 -antitrypsin; 8, apoA-IV; 9, apoJ; 10, apoE; 11, apoA-I; 12, transthyretin; 13, apoC-III; 14, apoC-II; 15, apoA-II; 16, haptoglobin β chain. (With permission after Ref. [46].)

Interestingly, apoE, which is hardly detectable on 2-D PAGE gels of human plasma, was enriched on the PS60-SLN (Fig. 10.5, left, spot 10), whereas no apoE could be detected on the PX338-SLN. ApoE was also adsorbed onto SLN surface, stabilized by polysorbate 20, 40 and 80 (in similar amounts). This result is in agreement with the findings documented by Müller et al., who investigated the brain specificity of PBCA nanoparticles coated with polysorbates and the lack of brain specificity of PBCA nanoparticles coated with poloxamers (e.g. poloxamer 338) [54].

The spot intensity was evaluated using special software from Bio-Rad (MELANIE III). For data evaluation it has to be taken into account that the silver-staining density is characteristic for each protein [73]. A quantitative comparison between identical protein types on different 2-D PAGE gels is valid, but not between different protein types on an identical gel. Therefore, quantitative 2-D PAGE data assessment is called "semi-quantitative". Nevertheless, it can be used for a reliable approximation of the amount of protein adsorbed.

Typical opsonins, such as immunoglobulins or complement factors, were not detected or were detected in a very low amount (below 5%) on both types of SLN. However, it must be pointed out that PX338-SLN shows higher quantities of fibrinogen adsorbed onto their surface, which has an opsonic function. However, apolipoproteins dominate the protein adsorption patterns (about 86% on PS60-SLN and about 70% on PX338-SLN). From these results, it can be concluded that both SLN types should have the potential to circulate in the blood stream for a prolonged time; in particular, PS60-SLN should be able to target drugs to the brain. The first results of *in vivo* experiments conducted with Nile Red-labeled PS60-SLN indeed nicely showed adherence of particles to the endothelial cells of the brain vessels [74, 75]. Pictures obtained by confocal laser scanning microscopy of the mouse brain tissue showed the particles adhering to the endothelium of the brain vessels, as well as the dye diffusing into the brain tissue. See Fig. 10.6.

Studying a full range of different poloxamer polymers as stabilizers for different SLN formulations revealed that apoE was preferentially adsorbed on the surface of SLN which were stabilized with a poloxamer having a low number of polyethylene oxide (PEO) units. There was an exponential relationship between adsorbed apoE and the PEO chain length, showing highest adsorption of apoE when using poloxamer 184 and poloxamer 235 [76]. These results are in good agreement with the apoE values obtained by Blunk [77] with o/w emulsions (20% w/w soya oil) stabilized with the respective poloxamers (2.5% w/w). Again, highest apoE adsorption occurred when using polymers with short PEO blocks in the molecule.

On cetyl palmitate SLN stabilized with egg lecithin, apoE was enriched up to 5% on their surface [78]. Recently, interesting accumulations in the brain were reported after intravenous injection of SLN with camptothecin [34], paclitaxel [79] and 3',5'-dioctanoyl-5-fluoro-2'-deoxyuridine [15]. All of these workgroups used lecithin as a stabilizer among other surfactants. From this, it can be assumed that apoE was also enriched on the surface of these SLN, leading to their uptake into the endothelial cells of the BBB.

According to these observations, it can be assumed that SLN are suitable car-

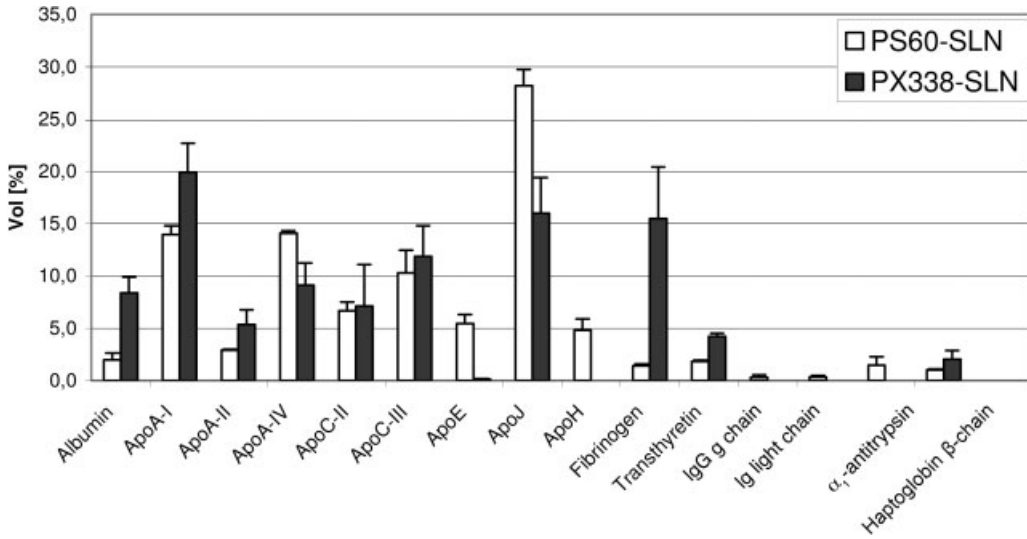


Fig. 10.6. Semiquantitative plasma protein composition on PS60-SLN and PX338-SLN expressed in percent (percentage of the overall detected protein pattern); error bars represent the standard deviation ($n = 2$). (With permission after Ref. [46].)

riers, especially when stabilized with polysorbates, to be biofunctionalized with apoE in the blood to have a high potential to deliver drugs to the brain.

10.5

Conclusions

Over recent decades, significant efforts have been made towards the surface modification of various polymeric drug carriers with PEG, not only to improve their biocompatibility and blood circulation times, but also to resist protein adsorption and to increase target cell uptake efficiency.

The surface characteristics of intravenously administered particulate drug carriers decisively influence the protein adsorption, which is regarded as a key factor for the *in vivo* fate of the carriers. It has already been shown that immobilization of PEG on nanoparticles reduces uptake by MPS cells and subsequently increases the amount of nanoparticle uptake into cancer cells in comparison to unmodified nanoparticles. For brain-targeting, substances such as the hexapeptide dalargin, loperamide and doxorubicin have been adsorbed into coated polymeric nanoparticles with a surfactant. In order to reduce toxicological problems of polymeric nanoparticles, biodegradable lipid nanoparticles such SLN can be used. This chapter has given a brief review of the state of the art of biofunctionalized SLN, as well as a brief description of the main production methods of these carriers. *In vivo* data

about achievements in targeting with SLN are summarized. The results obtained with lipid nanoparticles systems are quite promising for further developments in this research field.

References

- 1 J. KARAJGI, N. K. JAIN, S. P. VYAS, Passive vectoring of a colloidal carrier system for sodium stibogluconate: preparation, characterization and performance evaluation, *J. Drug Target.* **1993**, *3*, 197–206.
- 2 R. H. MÜLLER, *Colloidal Carriers for Controlled Drug Delivery and Targeting*, CRC Press, Boca Raton, FL, **1991**.
- 3 L. ILLUM, S. S. DAVIS, R. H. MÜLLER, E. MAK, P. WEST, The organ distribution and circulation time of intravenously injected colloidal carriers sterically stabilized with a block copolymer – poloxamine 908, *Life Sci.* **1987**, *40*, 367–374.
- 4 A. GESSNER, A. LIESKE, B. R. PAULKE, R. H. MÜLLER, Influence of surface charge density on protein adsorption on polymeric nanoparticles: analysis by two-dimensional electrophoresis, *Eur. J. Pharm. Biopharm.* **2002**, *54*, 165–170.
- 5 L. ILLUM, L. O. JACOBSEN, R. H. MÜLLER, E. MAK, S. S. DAVIS, Surface characteristics and the interaction of colloidal particles with mouse peritoneal macrophages, *Biomaterials* **1987**, *8*, 113–117.
- 6 K. LIND, M. KRESSE, R. H. MÜLLER, Comparison of protein adsorption patterns onto differently charged hydrophilic superparamagnetic iron oxide particles obtained *in vitro* and *ex vivo*, *Electrophoresis* **2001**, *22*, 3514–3521.
- 7 D. J. WILKENS, P. A. MEYERS, Studies on the relationship between the electrophoretic properties of colloids and their blood clearance and organ distribution in the rat, *Br. J. Exp. Pathol.* **1966**, *47*, 568–576.
- 8 W. E. BUCKE, S. LEITZKE, J. E. DIEDRICH, K. BORNER, H. HAHN, S. EHLERS, R. H. MÜLLER, Surface-modified amikacin-liposomes: organ distribution and interaction with plasma proteins, *J. Drug Target.* **1997**, *5*, 99–108.
- 9 P. CALVO, B. GOURITIN, H. VILLARROYA, F. ECLANCHER, C. GIANNAVOLA, C. KLEIN, J. P. ANDREUX, P. COUVREUR, Quantification and localization of PEGylated polycyanoacrylate nanoparticles in brain and spinal cord during experimental allergic encephalomyelitis in the rat, *Eur. J. Neurosci.* **2002**, *15*, 1317–1326.
- 10 G. GREGORIADES, *Liposomes as Drug Carriers*, Wiley, Chichester, **1989**.
- 11 A. SMITH, J. M. HUNNEYBALL, Evaluation of poly(lactic acid) as biodegradable drug delivery system for parenteral administration, *Int. J. Pharm.* **1986**, *30*, 215–220.
- 12 R. H. MÜLLER, S. MAASEN, H. WEYHERS, F. SPECHT, J. S. LUCKS, Cytotoxicity of magnetite-loaded polylactide, poly(lactide/glycolide) particles and solid lipid nanoparticles, *Int. J. Pharm.* **1996**, *138*, 85–94.
- 13 C. LHERM, R. H. MÜLLER, F. PUISIEUX, P. COUVREUR, Alkylcyanoacrylate drug carriers II: cytotoxicity of cyanoacrylate nanoparticles with different alkyl chain length, *Int. J. Pharm.* **1992**, *84*, 13–22.
- 14 R. H. MÜLLER, J.-S. LUCKS, Azneistoff-träger aus festen Lipidteilchen – feste Lipid Nanosphären (SLN), *European patent 0605497*, **1996**.
- 15 J.-X. WANG, X. SUN, Z.-R. ZHANG, Enhanced brain targeting by synthesis of 3'-5'-dioctanoyl-5-fluoro-2'-deoxyuridine and incorporation into solid lipid nanoparticles, *Eur. J. Pharm. Biopharm.* **2002**, *54*, 285–290.
- 16 F. Q. HU, Y. HONG, H. YUAN, Preparation and characterization of solid lipid nanoparticles containing

- peptide, *Int. J. Pharm.* **2004**, *273*, 29–35.
- 17 R. H. MÜLLER, W. MEHNERT, J.-S. LUCKS, C. SCHWARZ, A. ZUR MÜHLEN, H. WEYHERS, C. FREITAS, D. RÜHL, Solid lipid nanoparticles (SLN) – an alternative colloidal carrier system for controlled drug delivery, *Eur. J. Pharm. Biopharm.* **1995**, *41*, 62–69.
 - 18 S. MAAßEN, C. SCHWARZ, W. MEHNERT, J. S. LUCKS, F. YUNIS-SPECHT, B. W. MÜLLER, R. H. MÜLLER, Comparison of cytotoxicity between polyester nanoparticles and solid lipid nanoparticles (SLN), *Proc. Int. Symp. Controlled Rel. Bioact. Mater.* **1993**, *20*, 490–491.
 - 19 R. H. MÜLLER, K. MÄDER, S. GOHLA, Solid lipid nanoparticles (SLN) for controlled drug delivery – a review of the state of art, *Eur. J. Pharm. Biopharm.* **2000**, *50*, 161–177.
 - 20 W. MEHNERT, K. MÄDER, Solid lipid nanoparticles – production, characterization and applications, *Adv. Drug Deliv. Rev.* **2001**, *47*, 165–196.
 - 21 S. YANG, J. ZHU, Y. LU, B. LIANG, C. YANG, Body distribution of camptothecin solid lipid nanoparticles after oral administration, *Pharm. Res.* **1999**, *16*, 751–757.
 - 22 P. M. BUMMER, Physical chemical considerations of lipid-based oral drug delivery solid lipid nanoparticles, *Crit. Rev. Ther. Drug Carrier Syst.* **2004**, *21*, 1–19.
 - 23 R. H. MÜLLER, M. RADTKE, S. A. WISSING, S. A., Solid lipid nanoparticles and nanostructured lipid carriers, In *Encyclopedia of Nanoscience and Nanotechnology*, H. S. NALWA (Ed.), American Scientific Publishers, Stevenson Ranch, CA, **2004**, pp. 43–56.
 - 24 M. KALARIYA, B. K. PADHI, M. CHOUGULE, A. MISRA, Methotrexate-loaded solid lipid nanoparticles for topical treatment of psoriasis: formulation and clinical implications, *Drug Deliv. Technol.* **2004**, *4*, 64–66.
 - 25 A. ILLING, T. UNRUH, Investigation on the flow behavior of dispersions of solid triglyceride nanoparticles, *Int. J. Pharm.* **2004**, *284*, 123–131.
 - 26 M. SCHÄFER-KORTING, W. MEHNERT, Delivery of lipophilic compounds with lipid nanoparticles – applications in dermatics and for transdermal therapy, In *Lipospheres in Drug Targets and Delivery: Approach, Methods and Applications*, C. NORSTRUTTI (Ed.), CRC Press, Boca Raton, FL, **2005**, pp. 127–142.
 - 27 E. B. SOUTO, S. A. WISSING, C. M. BARBOSA, R. H. MÜLLER, Evaluation of the physical stability of SLN and NLC before and after incorporation into hydrogel formulations, *Eur. J. Pharm. Biopharm.* **2004**, *58*, 83–90.
 - 28 E. B. SOUTO, S. A. WISSING, C. M. BARBOSA, R. H. MÜLLER, Development of a controlled release formulation based on SLN and NLC for topical clotrimazole delivery, *Int. J. Pharm.* **2004**, *278*, 71–77.
 - 29 Z. MEI, H. CHEN, T. WENG, Y. YANG, X. YANG, Solid lipid nanoparticle and microemulsion for topical delivery of triptolide, *Eur. J. Pharm. Biopharm.* **2003**, *56*, 189–196.
 - 30 C. OLBRICH, K. TABATT, S. WISSING, N. SCHOELER, R. H. MUELLER, Solid lipid nanoparticles: interaction with cells, cytokine production, and enzymatic degradation, In *Lipospheres in Drug Targets and Delivery: Approach, Methods and Applications*, C. NORSTRUTTI (Ed.), CRC Press, Boca Raton, FL, **2005**, pp. 101–125.
 - 31 K. TABATT, C. KNEUER, M. SAMETI, C. OLBRICH, R. H. MÜLLER, C.-M. LEHR, U. BAKOWSKY, Transfection with different colloidal systems: comparison of solid lipid nanoparticles and liposomes, *J. Controlled Rel.* **2004**, *97*, 321–332.
 - 32 K. TABATT, M. SAMETI, C. OLBRICH, R. H. MÜLLER, C.-M. LEHR, Effect of cationic lipid and matrix lipid composition on solid lipid nanoparticle-mediated gene transfer, *Eur. J. Pharm. Biopharm.* **2004**, *57*, 155–162.
 - 33 C. OLBRICH, R. H. MÜLLER, K. TABATT, O. KAYSER, C. SCHULZE, R. SCHADE, Stable biocompatible adjuvants – a new type of adjuvant based on solid lipid nanoparticles: a

- study on cytotoxicity, compatibility and efficacy in chicken, *Altern. Lab. Anim.* **2002**, *30*, 443–458.
- 34 A. C. YANG, L. F. LU, Y. CAI, J. B. ZHU, B. W. LIANG, C. Z. YANG, Body distribution in mice of intravenously injected camptothecin solid lipid nanoparticles and targeting effect on brain, *J. Controlled Rel.* **1999**, *59*, 299–307.
 - 35 G. P. ZARA, A. BARGONI, R. CAVALLI, A. FUNDARO, D. VIGHETTO, M. R. GASCO, Pharmacokinetics and tissue distribution of idarubicin-loaded solid lipid nanoparticles after duodenal administration to rats, *J. Pharm. Sci.* **2002**, *91*, 1324–1333.
 - 36 G. P. ZARA, R. CAVALLI, A. BARGONI, A. FUNDARO, D. VIGHETTO, M. R. GASCO, Intravenous administration to rabbits of non-stealth and stealth doxorubicin-loaded solid lipid nanoparticles at increasing concentrations of stealth agent: pharmacokinetics and distribution of doxorubicin in brain and other tissues, *J. Drug Target.* **2002**, *10*, 327–335.
 - 37 A. FUNDARO, R. CAVALLI, A. BARGONI, D. VIGHETTO, G. P. ZARA, M. R. GASCO, Non-stealth and stealth solid lipid nanoparticles (SLN) carrying doxorubicin: pharmacokinetics and tissue distribution after i.v. administration to rats, *Pharmacol. Res.* **2000**, *42*, 337–343.
 - 38 S. C. YANG, J. B. ZHU, Preparation and characterization of camptothecin solid lipid nanoparticles, *Drug Dev. Ind. Pharm.* **2002**, *28*, 265–274.
 - 39 T. GÖPPERT, R. H. MÜLLER, Plasma protein adsorption of Tween 80- and Poloxamer 188-stabilized solid lipid nanoparticles, *J. Drug Target.* **2003**, *11*, 225–231.
 - 40 T. GÖPPERT, R. H. MÜLLER, Alternative sample preparation prior to two-dimensional electrophoresis protein analysis on solid lipid nanoparticles, *Electrophoresis* **2004**, *25*, 134–140.
 - 41 W. M. PARDRIDGE, Y. S. KANG, J. L. BUCIAK, J. YANG, Human insulin receptor monoclonal antibody undergoes high affinity binding to human brain capillaries *in vitro* and rapid transcytosis through the blood–brain barrier *in vivo* in the primate, *Pharm. Res.* **1995**, *12*, 807–816.
 - 42 Y. ZHANG, W. M. PARDRIDGE, Rapid transferrin efflux from brain to blood across the blood–brain barrier, *J. Neurochem.* **2001**, *76*, 1597–1600.
 - 43 B. DEHOUCK, M. P. DEHOUCK, J. C. FRUCHART, R. CECHELLI, Upregulation of the low density lipoprotein receptor at the blood–brain barrier: intercommunications between brain capillary endothelial cells and astrocytes, *J. Cell Biol.* **1994**, *126*, 465–473.
 - 44 S. S. DAVIS, Colloids as drug-delivery systems, *Pharm. Technol.* **1981**, *5*, 71–88.
 - 45 R. H. MÜLLER, S. HEINEMANN, Surface modelling of microparticles as parenteral systems with high tissue affinity, In *Bioadhesion – Possibilities and Future Trends*, R. GURNY, H. E. JUNGINGER (Eds.), Wissenschaftliche Verlagsgesellschaft, Stuttgart, **1989**, pp. 202–214.
 - 46 T. BLUNK, D. F. HOCHSTRASSER, J.-C. SANCHEZ, B. W. MÜLLER, R. H. MÜLLER, Colloidal carriers for intravenous drug targeting: plasma protein adsorption patterns on surface-modified latex particles evaluated by two-dimensional polyacrylamide gel electrophoresis, *Electrophoresis* **1993**, *14*, 1382–1387.
 - 47 D. R. ABSOLOM, Opsonins and dysopsonins: an overview, *Methods Enzymol.* **1986**, *132*, 281–318.
 - 48 J. L. BRASH, Protein adsorption at the solid-solution interface in relation to blood–material interactions, In *Proteins at Interfaces: Physicochemical and Biochemical Studies*, J. L. BRASH, T. A. HORBETT (Eds.), ACS, Washington, DC, **1987**, pp. 490–506.
 - 49 R. ALYAUDIN, D. GOTHIER, V. PETROV, D. KHARKEVICH, J. KREUTER, Analgesic activity of the hexapeptide dalargin adsorbed on the surface of polysorbate 80-coated poly(butyl cyanoacrylate) nanoparticles, *Eur. J. Pharm. Biopharm.* **1995**, *41*, 44–48.
 - 50 R. N. ALYAUDIN, E. B. TEZIKOV, P. RAMGE, D. A. KHARKEVICH, D. J.

- BEGLEY, Significant entry of tubocurarine into the brain of rats by adsorption to polysorbate 80-coated polybutylcyanoacrylate nanoparticles: an *in situ* brain perfusion study, *J. Microencapsul.* **1998**, *15*, 67–74.
- 51 A. E. GULYAEV, S. E. GELPERINA, I. N. SKIDAN, A. S. ANTROPOV, G. Y. KIVMAN, J. KREUTER, Significant transport of doxorubicin into the brain with polysorbate 80-coated nanoparticles, *Pharm. Res.* **1999**, *16*, 1564–1569.
- 52 J. KREUTER, R. N. ALYAUDIN, D. A. KHARKEVICH, A. A. IVANOV, Passage of peptides through the blood–brain barrier with colloidal polymer particles (nanoparticles), *Brain Res.* **1995**, *674*, 171–174.
- 53 J. KREUTER, V. E. PETROV, D. A. KHARKEVICH, R. N. ALYAUDIN, Influence of the type of surfactant on the analgesic effects induced by the peptide dalargin after its delivery across the blood brain barrier using surfactant-coated nanoparticles, *J. Controlled Rel.* **1997**, *49*, 81–87.
- 54 R. H. MÜLLER, M. LÜCK, J. KREUTER, Medicament excipient particles for tissue specific application of a medicament, *PCT application PCT/EP98/064299 (P53601)*, **2001**.
- 55 B. DEHOUCK, L. FENART, M. P. DEHOUCK, A. PIERCE, G. TORPIER, R. CECHELLI, A new function for the LDL receptor: transcytosis of LDL across the blood–brain barrier, *J. Controlled Rel.* **1997**, *138*, 877–889.
- 56 R. H. MÜLLER, S. SCHMIDT, PathFinder technology for the delivery of drugs to the brain, *New Drugs* **2002**, *2*, 38–42.
- 57 V. LENAERTS, P. COUVREUR, D. CHRISTIAENS-LEYH, E. JOIRIS, M. ROLAND, B. ROLLMAN, P. SPEISER, Degradation of poly(isobutyl cyanoacrylate) nanoparticles, *Biomaterials* **1984**, *5*, 65–68.
- 58 M. R. GASCO, Solid lipid nanospheres from warm micro-emulsions, *Pharm. Tech. Eur.* **1997**, *9*, 52–58.
- 59 B. SJÖSTRÖM, B. BERGENSTÅHL, Preparation of submicron drug particles in lecithin-stabilized o/w emulsions. I. Model studies of the precipitation of cholesteryl acetate, *Int. J. Pharm.* **1992**, *88*, 53–62.
- 60 E. B. SOUTO, SLN and NLC as drug carriers of clotrimazole for topical formulations, *Master thesis*, Oporto University, **2003**.
- 61 A. ZUR MÜHLEN, E. ZUR MÜHLEN, H. NIEHUS, W. MEHNERT, Atomic force microscopy studies of solid lipid nanoparticles, *Pharm. Res.* **1996**, *13*, 1411–1416.
- 62 M. R. GASCO, Method for producing solid lipid microspheres having a narrow size distribution, *US patent 5,250,236*, **1993**.
- 63 B. SJÖSTRÖM, B. BERGENSTÅHL, B. KRONBERG, A method for the preparation of submicron particles of sparingly water-soluble drugs by precipitation in oil-in-water emulsions. II: influence of the emulsifier, the solvent, and the drug substance, *J. Pharm. Sci.* **1993**, *82*, 584–589.
- 64 B. SJÖSTRÖM, B. KRONBERG, J. CARLFORS, A method for the preparation of submicron particles of sparingly water-soluble drugs by precipitation in oil-in-water emulsions. I: influence of emulsification and surfactant concentration, *J. Pharm. Sci.* **1993**, *82*, 579–583.
- 65 C. FESSI, J. P. DEVISSAGUET, F. PUISIEUX, C. THIES, C., Process for the preparation of dispersible colloidal systems of a substance in the form of nanoparticles, *US patent 5,118,528*, **1992**.
- 66 M. TROTTA, F. DEBERNARDI, O. CAPUTO, Preparation of solid lipid nanoparticles by a solvent emulsification-diffusion technique, *Int. J. Pharm.* **2003**, *257*, 153–160.
- 67 P. SHAHGALDIAN, J. GUALBERT, K. AÏSSA, A. W. COLEMAN, A study of the freeze-drying conditions of calixarene based solid lipid nanoparticles, *Eur. J. Pharm. Biopharm.* **2003**, *55*, 181–184.
- 68 S. M. MOGHIMI, I. S. MUIR, L. ILLUM, S. S. DAVIS, V. KOLB-BACHOFEN, Coating particles with a block copolymer (poloxamine-908) suppresses opsonization but permits the activity of dysopsonins in the serum, *Biochim. Biophys. Acta* **1993**, *1179*, 157–165.

- 69 S. RUDT, R. H. MÜLLER, *In vitro* phagocytosis assay of nano- and microparticles by chemiluminescence. II. Effect of surface modification by coating of particles with poloxamer on the phagocytic uptake, *J. Controlled Rel.* **1993**, *25*, 51–59.
- 70 R. H. MÜLLER, D. RÜHL, M. LÜCK, B. R. PAULKE, Influence of fluorescent labelling of polystyrene particles on phagocytic uptake, surface hydrophobicity, and plasma protein adsorption, *Pharm. Res.* **1997**, *14*, 18–24.
- 71 R. GREF, M. LÜCK, P. QUELLEC, M. MARCHAND, E. DELLACHERIE, S. HARNISCH, T. BLUNK, R. H. MÜLLER, Stealth corona-core nanoparticles surface modified by polyethylene glycol (PEG): influences of the corona (PEG chain length and surface density) and of the core composition on phagocytic uptake and plasma protein adsorption, *Colloids Surfaces B Biointerfaces* **2000**, *18*, 301–313.
- 72 D. J. GRAHAM, M. C. PHILLIPS, Proteins at liquid interfaces. I., Kinetics of adsorption and surface denaturation, *J. Colloid Interface Sci.* **1979**, *70*, 403.
- 73 H.-M. POEHLING, V. NEUHOF, Visualization of proteins with a silver “stain”: a critical analysis, *Electrophoresis* **1981**, *2*, 141–147.
- 74 C. OLBRICH, O. KAYSER, A. LAMPRECHT, C. KNEUER, C. M. LEHR, R. H. MÜLLER, Interactions of fluorescent solid lipid nanoparticles (SLN) with macrophage-like cells visualized by CLSM, Presented at *3rd World Meeting of APGI/APV*, Berlin, **2000**, pp. 331–332.
- 75 A. GESSNER, C. OLBRICH, W. SCHRÖDER, O. KAYSER, R. M. MÜLLER, The role of plasma proteins in brain targeting: species dependent protein adsorption patterns on brain-specific lipid drug conjugate (LDC) nanoparticles, *Int. J. Pharm.* **2001**, *214*, 87–91.
- 76 T. M. GÖPPERT, R. H. MÜLLER, Protein adsorption patterns on poloxamer- and poloxamine-stabilized solid lipid nanoparticles (SLN), *Eur. J. Pharm. Biopharm.* **2005**, *60*, 361–372.
- 77 T. BLUNK, *Plasmaproteinadsorption auf kolloidalen Arzneistoffträgern*, Department of Pharmacy, Christian-Albrechts-Universität zu Kiel, **1994**.
- 78 T. M. GÖPPERT, R. H. MÜLLER, Solid lipid nanoparticles (SLN) for intravenous drug targeting: comparison of plasma protein adsorption patterns on different SLN detected by two-dimensional polyacrylamide gel electrophoresis (2-D PAGE), Presented at *AAPS Annual Meeting*, Salt Lake City, UT, **2003**, M1002.
- 79 A. MIGLIETTA, R. CAVALLI, C. BOCCA, L. GABRIEL, M. R. GASCO, Cellular uptake and cytotoxicity of solid lipid nanospheres (SLN) incorporating doxorubicin or paclitaxel, *Int. J. Pharm.* **2000**, *210*, 61–67.
- 80 R. H. MÜLLER, C. M. KECK, Challenges and solutions for the delivery of biotech drugs – a review of drug nanocrystal technology and lipid nanoparticles, *J. Biotechnol.* **2004**, *113*, 151–170.

11 Biocompatible Nanoparticulate Systems for Tumor Diagnosis and Therapy

Mostafa Sadoqi, Sunil Kumar, Cesar Lau-Cam and Vishal Saxena

11.1

Introduction

Nanotechnology is the development and engineering of materials, devices and systems so small that they can be measured on a molecular scale. This emerging technological field has received considerable attention in the past two decades due to its numerous medical, pharmaceutical, environmental and military applications.

The development of nanoparticles and nanodevices capable of navigating in the bloodstream and of reaching specific destinations remains an attractive and most desirable biomedical endeavor since, for example, it can provide the clinician with an effective and powerful means for detecting and/or treating pathological abnormalities such as solid tumors. Ideally, a nanodevice suitable for diagnostic and therapeutic use should exhibit good physical stability within the biological environment it needs to travel, be fully biocompatible, and show high affinity and selectivity for its final target.

One possible way of maximizing the clinical capabilities of nanodevices is to combine nanotechnology with photonics [1]. For this purpose, nanoparticles carrying a suitable photoexcitable molecule are converted *in situ*, under the activating influence of laser radiation, to a chemical form that will make a tumor more sensitive to the action of conventional chemotherapeutic agents or emit a spectral signal with an output that can be electronically manipulated to provide information on the presence of pathological growth.

This chapter offers an overview of the different methodological approaches that can be used for the fabrication of nanoparticulate systems for medical purposes, of the ways these devices can sense changes within specific biological surroundings and of the medical applications that can be derived from the interaction of loaded nanoparticles within biological matter with laser radiation, particularly as it relates to the imaging and therapy of tumors.

Particular attention will be given to the near-infrared dye (NIR) indocyanine green (ICG), and to the potential of this dye for tumor diagnosis and therapy when administered encapsulated within polymeric nanoparticulate systems. ICG was found to be free of perceptible toxicity, to exhibit good chemical stability within polymeric nanoparticles, to be appreciably taken up by tumor cells following its

delivery as a nanoparticulate formulation and to cause singlet oxygen-induced oxidative damage in target cells when photoexcited. A discussion of the benefits of photodynamic therapy (PDT) with ICG as a means of eradicating unwanted abnormal growths such as tumors will also be presented.

11.2

Nanoscale Particulate Systems and their Building Blocks/Components

Nanoscale particulate systems are 100 to 100 000 times smaller than human cells and hair. At present, a vast choice of sensing devices are commercially available for detecting and measuring specific bacteria or hazardous chemicals, for checking acidity levels and for monitoring changes in biological and nonbiological environments. In nanomedicine, nanoscale systems can easily enter most types of cells and can move undisturbed out of blood vessels as they circulate through the body. Furthermore, biomedical nanoscale systems can interact with surface and intracellular biomolecules, can make their way into tissues through capillaries, can get through fenestrations present in epithelial linings such as those of the liver and can diffuse through the blood–brain barrier (BBB) by following openings created at tight junctions by a hyperosmotic mannitol solution [2]. As a result, they can be used to efficiently deliver both low-molecular-weight compounds, such as drugs, and macromolecules such as proteins, peptides and genes, to tissues of interest by either localized or targeted delivery.

In recent years, a great deal of effort has been devoted to the application of nanotechnology to drug delivery, molecular imaging, the assessment of therapeutic efficacy, targeted and multifunctional therapeutics, and the early detection, prevention and control of cancer. Some of the nanoparticulate formulations that have been developed for the delivery of therapeutic agents in a biocompatible form have included nanoparticles, nanocapsules (nanoshells), polymeric micellar systems, buckyballs, nanotubes, dendrimers, quantum dots and immunoconjugates.

Although this chapter will address a select few nanoscale systems, emphasis will be placed on nanoparticle systems of the type developed in our laboratory, since experiments conducted in this laboratory have been focused on the use of nanoparticles to deliver photoexcitable molecules to normal and cancer cells, allowing the study of the interaction of light with the incorporated nanoparticulates in real time and during the earliest stages of the cancer process [3]. In this way, it has been possible to determine that nanoparticles can be used to detect cancer even when the process is still limited to a few cells and that they have the potential as a better alternative to therapy with conventional drug formulations since they can reduce or even eliminate drug side-effects.

11.2.1

Dendrimers

Dendrimers are a large and complex group of highly branched polymerized macromolecules with well-defined chemical structures and exhibiting monodispersity,

i.e. having the same structure, composition and molecular weight. The three major architectural components of a dendrimer are the core, branches and end groups of the precursor monomeric units. The core is usually an amine, although ammonia, sugars and other molecules can also be used. Regardless of the type of constitutive molecule present, the core exhibits multiple and identical reaction sites. The dendrimer can start with a few branches of atoms, usually three or four, radiating from a central core, with a branch point occurring every six atoms. At each branch point, the current chain of atoms becomes two chains of atoms. As a result, a structure resembling a tree with numerous branches is formed.

In general, a dendrimer consists of layers or shells of branches, each one known as a generation (G), built around a small core molecule. As the number of generations increases to G4, the regular and highly branched architecture of a dendrimer starts to develop into a sphere, whose preferred three-dimensional structure starts to become apparent by G5. Synthetic procedures available for the fabrication of dendrimers allow for the nearly complete control of critical molecular parameters such as size, shape, interior/surface chemistry, flexibility and topology, as well as for a very easy control of the chemical composition and reactivity. Manufacture of cone-shaped, spherical or disk-like dendrimers with a size in the range of 2–12 nm is possible.

The synthesis of a dendrimer is a stepwise iterative process. In its most basic form, it is started by reacting all of the reactive groups of the core molecule with an excess of a monomeric building unit possessing different reactive groups on each end. Reaction of one end of this monomer with the core will produce the first set of branches and reaction of the second end with a different type of monomer, also having two different reactive groups at each end, will generate a second set of branches. At this point, the first shell and the first generation of the dendrimer are complete. The unreacted ends of the first shell will serve as the starting point for new branching and for the next shell.

The two main techniques for the synthesis of dendrimers with a unique combination of properties are the Starbust divergent method [4, 5] and the convergent growth method [6], but a self-assembly method [7] has also been developed. In the divergent method, the dendrimer is started from the periphery (i.e. the tips of the branches) and made to grow inwards. Two of the end tips are connected to a branched monomer to form a dendron (or dendrimer segment) and the process is repeated until a desired size is achieved. In the final step, the interconnected branches are attached to a core molecule. Since the growing dendrimer is undergoing multiple simultaneous reactions, the final product may lack uniformity. Building a dendrimer by a convergent approach requires the same number of steps as by the divergent approach, but starting with a central initiator core around which dendrimer segments are assembled. More importantly, since only two reactions take place at each step of the growing process, the resulting final product is of a high purity.

The self-assembly method, first studied with surfactant molecules in aqueous media, is now being applied to water-soluble dendrimeric polymers and their supra-molecular analogs. Taking advantage of the abundance of surface active end groups on dendrimers, nanoparticulate aggregates having micellar properties can be made

to form from dendrimers at an interface. In turn, these unimolecular micelles can serve as hosts for hydrophobic molecules to enhance solubility in water with an efficiency than may exceed that derived from a conventional surfactant such as sodium dodecylsulfate [8]. By reacting the amino end groups of poly(propylene imine) with various aliphatic acid chlorides it was possible to prepare a series of nonaggregating inverted unimolecular dendritic micelles with a compact hydrophobic shell, a hydrophilic interior and high generation numbers ($n \geq 4$). In contrast to normal micelles, these inverted unimolecular micelles were able to bind hydrophilic molecules in the interior and to solubilize the guest molecule in apolar solvents.

Dendrimers have been more commonly synthesized from polymers such as poly(amidoamine) (PAMAM dendrimers) by a divergent method initiated by ammonia or ethylenediamine as a core or from poly(propylene imine) (PPI dendrimers) by a divergent method initiated by a core of 1,4-diaminobutane, but poly(aminoalcohol), cyclotriphosphazene and phenylacetylene have also been used.

Due to the large number of active chemical groups located at the surface of each generation and to their well-defined chemical structure, dendrimers are good candidates for creating biomedically useful nanodevices. While suitable modifications of the surface properties of dendrimers will allow them to be made electrically charged into a polyelectrolyte or to be linked to biological agents, their cavities can serve as depots or be used as pumping devices for small guest molecules such as organic dyes, drugs and metal clusters [9]. In this respect, a most interesting departure from a conventional dendrimer is the so-called “core dendrimer”, which is synthesized by crosslinking the peripheral groups of the dendrimer and then removing the core by hydrolysis [10].

From a technical and commercial standpoint, some of the most interesting applications of dendrimers are in the pharmaceutical and biomedical fields. For example, sufficient flexibility exists to create dendrimers that are either biologically active or inert and of a sufficiently small size that will permit their entry into cells to deliver drugs, genetic material and organic and inorganic chemical markers without triggering an immune response. In addition, dendrimers can be used to deliver diagnostic and chemotherapeutic agents to target sites for the diagnosis, treatment and eradication of malignant tumors. Medical researchers envision that one day tecto-dendrimers will be used to carry out a five-step task when diagnosing and treating tumors: (a) the search of tumor cells throughout the body, (b) the binding to receptors on tumor cells, (c) the entry into tumor cells upon crossing the cell membranes, (d) the release of chemotherapeutic or radioactive agents inside the tumor cell and (e) the confirmation of the presence, location or death of tumor cells through the use of appropriate medical devices.

11.2.2

Buckyballs and Buckytubes

Buckyballs, also known as C_{60} , buckminsterfullerenes or fullerenes, are clusters of up to 60 carbon atoms arranged in a series of interlocking hexagons and pentagons to form a structure resembling a soccer ball [11]. In actuality, C_{60} is a “truncated

icosahedron" consisting of 20 hexagons and 12 pentagons. Buckyballs can be easily manufactured in quantity by heating graphite rods to a high temperature and passing an electric current between them. The crystals of C_{60} are separated from other carbon compounds, especially C_{70} , found in the soot fraction. It is the only molecule known to mankind to be composed of a single element and to exist in the form of a hollow spheroid. Possible ways of utilizing a buckyball for biomedical purposes would be to use its spherical structure to carry molecules with diagnostic or therapeutic value in the body after they have been added to its outer surface through chemical reaction or introduced into its cage-like interior. As a delivery system, buckyballs appear well suited because of their nanometer size, and perfectly smooth surface and round shape. In addition, they are inert, nontoxic and, due to their small size, capable of interacting with cells, proteins, and viruses.

Buckytubes, variously designated as nanotubes (NTs) or carbon nanotubes, are molecular-scale nanomaterials of pure carbon that have been prepared in a relatively efficient way by the laser vaporization of graphite in the presence of cobalt nickel catalyst in a furnace at 1200 °C. In this way, a product that can be thought of as a sheet of graphite rolled into a single-wall seamless cylinder and closed at both ends by hemispherical endcaps (SWNTs) can be obtained. In the absence of a catalyst, a group of graphite layers will coil around each other to produce a multi-wall cylinder (MWNTs). Their diameter is in nanometers, their length up to a few millimeters and, depending on their helicity, they can be either electrically conductive (metallic) or semiconductive. In addition to their unusually high strength, buckytubes are light, flexible, with good thermal stability, chemically inert, and have extraordinary electrical conductivity, heat conductivity and mechanical properties. Given their high electrical conductivity and sharpness of their tips, buckytubes are unsurpassed as field emitters, especially at low voltage, and can carry as much as 10^{13} A cm^{-2} [12].

A demonstration that single-wall buckyballs absorb light and emit it at a single wavelength in the NIR spectrum has opened the door to a new field of potential biomedically related applications for these materials [13]. For the fluorescence to be measurable, however, the buckytubes must be isolated from one another since aggregation into bundles quenches fluorescence and considerably broadens the absorption spectra due to intertube energy transfer from the semiconducting to the metallic nanotubes within each bundle [14], followed by rapid nonradiative carrier cooling in the metallic nanotubes [15]. Time-resolved spectroscopy of these buckyball bundles reveals extremely rapid excited state relaxation [14, 15].

As a result of their small size that allows them to migrate through cell walls, buckyballs could be used as optical biosensors for seeking out specific targets within the body such as tumor cells or inflamed tissues. To increase their specificity toward their targets, buckyballs could be wrapped with proteins that will serve as ligands for surface receptors on target cells. Covalently linked adducts of SWNTs with biomolecules such as biotin or DNA have great potential in biosensing and as a possible means of implementing nanoscale assembly onto selected locations on a surface [16]. By combining buckytubes of a different diameter size one could simultaneously study different target cells. A most promising application of bucky-

tubes has been the imaging of cells. SWNTs were found to be actively ingested by macrophages suspended on a growth medium through phagocytosis and to be held in phagosomes within the macrophages. Cell viability was not affected by the buckytubes and the intracellular fluorescence remained detectable in the harsh oxidizing environment of the phagosomes. These results suggest that the high-contrast NIR detection of SWNTs can lead to valuable methods for tracing the interactions of buckytubes with organisms, and may form the basis for future families of biological contrast agents and fluorescent markers.

On account of the natural fluorescence of SWNTs, and the transparency of human tissues and biological fluids in the NIR region of the spectrum, buckyballs wrapped with a molecular sheath that responds to a particular biological molecule and modulates the optical properties of the buckyball can be constructed. Based on this model, a sensor for tracking blood glucose in diabetics was built by organizing a monolayer of the enzyme glucose oxidase on the surface of SWNTs suspended in water. Reaction of glucose with the enzyme generates hydrogen peroxide which, when exposed to ferricyanide ions, increases the fluorescence emission of the sensor in direct proportion to the concentration of glucose present [17]. In view of their high resistance to degradation, it could be possible to construct buckyballs for implantation into thick tissues or biological fluids for long-term monitoring of specific body components.

11.2.3

Quantum Dots

Quantum dots, also known as nanocrystals, are tiny semiconducting inorganic crystals with unique quantum properties, typically between a nanometer and a few microns in size, and containing from one to several thousand free electrons. The size and the shape of these structures and, hence, the number of electrons they contain, can be precisely controlled. Quantum effects arise from the confinement of electrons and “holes” (an electronless region that behaves as if it were a positively charged particle) in the material. The small size also leads to changes in the electrical and nonlinear optical properties of a material relative to its bulk form. They are made of silicon, germanium, lead, zinc and cadmium salts – materials that can absorb white light and reemit it a couple of nanoseconds later at a higher frequency. The type and intensity of the color is dependent on the size of the crystal. For example, the larger the dot, the redder the light; but as the size shrinks, the wavelength of emission becomes shorter and moves toward the blue or green. Hence, a gamut of colors can be obtained by a simple change in the size of the dot. Moreover, when excited, the smaller the dot the higher the energy and intensity of the emitted light.

These particles represent a convenient alternative to fluorescent dyes in a variety of analytical, biological and biomedical applications since their emitting radiation can be measured over the entire visible spectrum, they have a broader excitation spectrum, and their fluorescence is extremely stable over time. On these bases, a mixture of quantum dots of different sizes can be excited by a light source with a

single wavelength, allowing simultaneous detection and imaging of different biological molecules simultaneously within living organisms. In contrast, the use of more than one organic dye to accomplish the same purpose might meet with difficulties since their spectra may overlap with each other because each dye emits light over a wide range of wavelengths.

The utility of quantum dot nanomaterials as a result of their optoelectronic properties can be further expanded not only by changing their size and composition, but also by incorporating them into a wide variety of polymers and material forms that will make them stable in water. Core quantum dots with fewer surface defects, improved physical stability and enhanced fluorescence brightness are already commercially available. Quantum dots represent a powerful new approach to genetic analysis, disease diagnosis and the monitoring of cell responses to certain drugs or viruses [18, 19]. However, their application to the detection of tumors, in particular, and of cancer, in general, remains to be realized because of their intrinsic toxicity and lack of biocompatibility.

11.2.4

Polymeric Micelles

Polymeric micelles are a viable form of targeted delivery system for water-insoluble and amphiphilic drugs [20, 21]. Like surfactant-based micelles, polymeric micelles are core/shell structures; however, unlike their traditional counterparts, they are physically more stable and capable of solubilizing substantial amounts of hydrophobic compounds within their inner core. Due to their hydrophilic shell and small size they may prolong the circulation of drugs in body fluids and increase drug accumulation in tissues [20]. The shell is responsible for micelle stabilization and interaction with plasma proteins and cell membranes. The hydrophobic core, usually made from a biodegradable polymer, serves as a reservoir for an insoluble drug and shields the drug from the aqueous surroundings. Polymers used for fabricating polymeric micelles have included pluronics, polyethylene glycol (PEG)-lipid conjugates and pH-sensitive poly(*N*-isopropylacrylamide)-based micelles or polyion complex micelles.

Polymeric micelles have also been used for encapsulating and delivering photosensitizing drugs and dyes. However, the biodistribution characteristics of the polymeric micelle formulations thus far investigated have not been entirely satisfactory. For example, greater selectivity and effectiveness could be gained by introducing targeting ligands and site-controlled releasing capabilities, respectively, and excessive nanoparticulate accumulation and long-term toxic effects could be reduced by utilizing biodegradable polymers with good clearance properties.

11.2.5

Liposomes

A liposome is a spherical vesicle of colloidal dimensions composed of one or more lipid or phospholipid bilayers. The size of liposomes varies from 20 nm to 100 μm,

although each lipid bilayer is about 4 nm thick. Various amphipathic molecules have been used to fabricate liposomes, especially lecithins from natural or synthetic sources. To increase mechanical stability and decrease the leakage of the contents, charged phospholipids like phosphatidylserine or phosphatidylglycerol and cholesterol can be added. Depending on its physicochemical characteristics, a drug can become trapped in the aqueous space, intercalated or dissolved within the lipid bilayer, or form ionic or hydrophobic complexes with nucleic acids and other macromolecules without physical entrapment [22]. For medical use, a liposome suspension must be precisely defined with respect to drug and lipid concentrations, size distribution, percentage of entrapped drug, pH, osmolarity, conductivity, and presence of degradation products. Specific methods exist to manufacture liposomes of a particular size, morphology and surface characteristics, parameters that together will determine the biologic fate of the liposomes [22].

Due to similarities in both structure and chemical composition to biomembranes, liposomes have been extensively investigated as carriers for enhancing the incorporation of an assortment of drug molecules into target cells [23, 24]. Through the use of liposomes one can achieve a variety of therapeutic goals, including enhanced drug uptake and reduced toxicity. Numerous studies have been conducted on the use of liposomes to deliver chemotherapeutics to tumor cells; however, in spite of some impressive results in animal models, acceptance of liposomes as a drug delivery system for human use has only been realized in a very few instances. In addition to a relatively high cost, additional shortcomings associated with this form of drug delivery are short residency time in the circulation due to rapid removal by phagocytic cells of the reticuloendothelial system (RES), physical and chemical instability on storage, and the lack of generally uniform and applicable techniques for their production on a commercial scale [23, 24].

Conventional liposomes are unstable *in vivo* and show little or no affinity towards tumors. These shortcomings have served as the impetus for the development of more complex liposomal preparations where the surface and/or composition of the structural components have undergone chemical modification. Moreover, in the case of conventional liposomes a significant fraction of the injected dose ends up in organs rich in phagocytic (monocytes, macrophages, Kupffer) cells such as the liver and spleen, which eventually sequester and, thus, reduce the amount of drug that is available for antitumor action. To counteract this situation, liposomal surfaces have been variously modified to limit irrelevant recognition and reduce the uptake of the liposomes into cells of the immune system, thus extending the half-life of drugs in the circulation. Alternatively, these liposomes can be targeted to cells expressing specific receptors by equipping them with specific surface ligands. This delivery modality has been successfully used to provide selective binding and enhanced entry into tumor cells of liposomes loaded with a photosensitizer for PDT purposes and bearing surface tumortropics with the ability to recognize specific target molecules expressed on tumor cell membranes [23, 24].

Through a combination of polymer physics, organic chemistry, biochemistry, pharmacology, ecology and anatomy, sterically stable (“stealth”) liposomes have been developed. This type of lipid-based particles is represented by polymorphic

liposomes designed to change their structure in response to a particular signal such as a change in temperature or pH in the presence of specific molecules. These reactive liposomes can be made to fuse or increase in permeability, or triggered to disintegrate to release their contents upon arrival to the target site. An important breakthrough in chemotherapy with stealth liposomes is the substantial improvement in longevity that is observed in biological systems. This stability arises from the sterile nature of the surface polymer, which limits the clearance of the liposomes from the circulation by opsonization and subsequent macrophage uptake, and by disintegration upon interactions with plasma proteins and lipoproteins. Commercial stealth liposomes of doxorubicin and daunorubicin have received approval by the FDA for the parenteral treatment of Kaposi's sarcoma and solid tumors. Apart from drugs, liposomes can be made to carry a significant load of signal molecules such as dyes, radionuclides or contrast agents for *in vitro* and *in vivo* diagnostic work.

11.3

Biodegradable Nanoparticles

In recent years, polymeric nanoparticles have received recognition as a promising type of colloidal drug carrier [25]. They have been widely used for controlled drug delivery by the intravenous, ocular and oral routes of administration. An additional positive feature of this form of drug delivery is that they have shown potential as a carrier for anticancer agents. It has been verified that the tissue distribution characteristics, specificity and pharmacokinetic properties of anticancer drugs can be better controlled upon their incorporation into nanoparticles [26, 27]. Furthermore this form of drug delivery may contribute to reducing the side-effects and toxicity normally associated with anticancer drugs, while increasing therapeutic efficacy, and can lead to drug accumulation in the solid tumor since they have been found to escape from the vasculature through the leaky endothelial tissue that surrounds a solid tumor [28, 29].

Nanoparticles can overcome the multidrug-resistance phenotype mediated by P-glycoprotein and bring about an increase in drug content inside neoplastic cells [30]. This finding is of special significance for patients with cancer undergoing treatment with paclitaxel and who, after some time, develop resistance to the drug [31]. Other important advantages derived from the use of nanoparticles include the ease of their preparation, the availability of well-defined biodegradable polymers for their manufacturing [e.g. poly(D,L-lactide-co-glycolide) (PLGA)], and their high stability in biological fluids and during storage [32]. Moreover, nanoparticles can permeate cells and tissues to become internalized and can efficiently deliver a particular drug to its target tissue without clogging the capillaries [33].

The ability of nanoparticles to improve drug diffusion through biological barriers is particularly useful for the delivery of biomarkers and photodynamic agents to the brain without the need for preliminary pharmacological intervention to overcome the BBB [34]. Some studies on nanoparticle-bound antitumor agents have in-

licated that nanoparticles can prolong the retention of the drug by tumors, reduce tumor growth and prolong the survival of tumor-bearing animals [30, 35–37].

11.3.1

Preparation of Nanoparticles

Several synthetic and natural polymers have been described for the manufacturing of biodegradable nanoparticles [38]. One advantage of synthetic polymers over natural ones is that they can yield nanoparticles with the ability to sustain the release of the encapsulated therapeutic agent over longer periods of times (days to several weeks). However, the use of synthetic polymers in nanoparticle technology is limited by the need to use often toxic organic solvents and relatively harsh formulation conditions. Synthetic polymers for formulating nanoparticles have included polylactic acid and its copolymerization with glycolic acid (PLGA), polyacrylates and polycaprolactones.

Among natural polymers, albumin, gelatin, alginate, collagen and chitosan have been evaluated [38]. Of these polymers, polylactides (PLA) and PLGA are the ones most extensively investigated for achieving controlled release of conventional drug molecules, peptides and proteins. PLGA is the most common choice in pharmaceutical formulations probably because of its good biocompatibility and biodegradability and of its approval by the FDA for use in humans [39]. These polyesters undergo hydrolysis upon implantation in body tissues to biologically compatible and metabolizable moieties (e.g. lactic acid and glycolic acid) that are eventually removed from the body by the citric acid cycle.

In addition, since the biodegradation products are formed at a very slow rate, they appear not to interfere with normal cell functions to a significant extent. Extensive testing for toxicity and safety in laboratory animals has found these polymers to be safe, and, thus, suited for use in humans as contraceptive implants [40, 41], graft materials for artificial organs and, more recently, as supporting scaffolds in tissue engineering research [42–44].

Some of the methods described for the preparation of nanoparticles from preformed biodegradable polymers are solvent evaporation [45], salting out [46], nanoprecipitation [47], extrusion [48], spray drying [49] and supercritical fluid extraction [50].

The most popular method of making nanoparticles is the emulsification-solvent evaporation method, also known as the solvent displacement techniques [51–53]. This methodological approach, schematically shown in Fig. 11.1, usually involves the following major steps: (a) emulsification of a water-immiscible organic solution of the polymer and an organic or inorganic material of interest with an aqueous phase containing stabilizers, (b) stabilization of the particles by chemical crosslinking or by heat, (c) evaporation of the organic solvent to precipitate the encapsulating polymer as nanoparticles, and (d) isolation of the nanoparticles by filtration or centrifugation [54]. This method is suitable for hydrophilic drugs since the drug dissolves in the inner water phase of the double emulsion. In most cases, a stabilizer is added to the formulation to stabilize the emulsion formed during particle

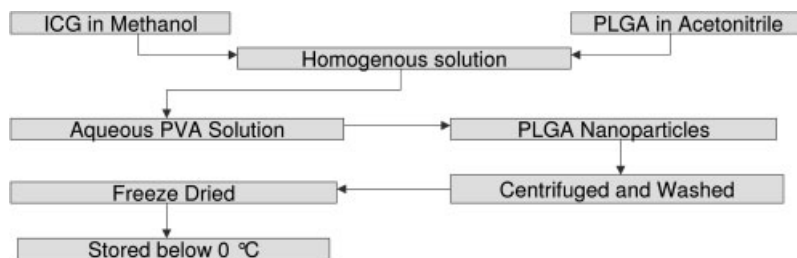


Fig. 11.1. Flow diagram of the manufacturing of ICG-loaded PLGA nanoparticles by a modified spontaneous emulsification-solvent diffusion method.

preparation. In this method, the type and concentration of the stabilizer may exert a modifying effect on the properties of the particles being formed. By occupying the boundary between the aqueous and organic phases, the stabilizer can become incorporated onto the surface of the forming particles and, in this way, influence particle properties such as the ζ potential and mucoadhesion [55, 56]. In turn, these physicochemical parameters can modify the physical stability of the formulation as well as certain biopharmaceutical properties such as drug release rate, bio-distribution and cellular uptake. Although polyvinyl alcohol (PVA) is the stabilizer most often used for the production of PLGA nanoparticles, other available choices are cellulose derivatives such as methylcellulose, hydroxyethylcellulose and hydroxypropylcellulose, gelatin types A and B, carbomer, and poloxamer [57].

One way to construct nanoparticles with long circulating characteristics is to modify their surface with the hydrophilic, flexible and nonionic polymer, PEG [58–60]. The resulting PEG-coated nanoparticles have shown good potential as a biodegradable colloidal type of formulation for the delivery of therapeutic agents to specific sites.

11.4

Biodegradable Optical Nanoparticles

11.4.1

Optical Nanoparticles as a Potential Technology for Tumor Diagnosis

Solid tumors and other forms of cancer are commonly localized inside the body by screening diagnostic methods based on imaging techniques or radiology [61–64]. Images of internal parts of the human body can be obtained by using X-rays (tomography, scan or mammography), a powerful magnetic field (magnetic resonance imaging), radioactive isotopes (nuclear scan or radionuclide imaging) and high-frequency sound waves (ultrasound) [65–68]. Examples of nuclear scanning include single-photon emission computed tomography (SPECT) and positron emission tomography (PET) scans. There are also diagnostic methods whose use

is determined by the location of the cancer (e.g. endoscopy for cancers in body openings like the mouth, anus or urethra, tests for measuring estrogen and progesterone receptors in suspected cases of breast cancer, and the Pap smear test for detecting cancers of the cervix and vagina) [69–74]. Once a tumor has been detected in the body by any of the aforementioned screening techniques, confirmatory evidence is gathered by histopathological examination of a tissue sample obtained by biopsy of the suspected area. In spite of their widespread use, these forms of tumor diagnosis suffer from serious limitations. For example, there is a strong safety concern attached to the use of harmful radioactive substances and X-rays, both of which are in themselves risk factors for cancer. Furthermore, harmful adverse reactions may develop from the use of contrast agents, the test may not be sensitive enough to detect very small tumors and the diagnostic procedure may be expensive in comparison to other laboratory medicine procedures.

Nanoparticles loaded with photosensitizer molecules can be an alternative method for tumor diagnosis as well as for drug delivery purposes. Their ability to be readily detected, to show selectivity, and to be easily transported through the blood stream is inherent to the nature of the dye, the specific agent linked to the particulate system (e.g. antibodies) and the physical as well as chemical structure of the polymer used. Nanoparticulate systems have the means to detect the cancer at an early stage and they have the potential as a better alternative to therapy with conventional drug formulations since they can greatly minimize drug side-effects.

11.4.2

Optical Nanoparticles as a Potential Technology for Tumor Treatment

After detection of a tumor, its treatment usually relies on chemotherapy with specific anticancer agents to ensure that the cancer cells have not metastasized to the other parts of the body [75–83], localized radiation therapy with ionizing radiation such as X-rays and γ -rays [84–87], biologic therapy based on the defense provided by the body's immune system [88–108], and invasive approaches for localized cancer such as surgery [109–111]. Although effective and beneficial, these therapeutic approaches are surrounded by certain drawbacks, among which the main ones are intrinsic toxicity, serious side-effects and damage to healthy tissues by the radiotherapy itself. Consequently, there is a pressing need for simpler, safer, noninvasive imaging systems and technologies than those currently available, offering the required selectivity to detect and/or destroy a tumor while sparing the surrounding areas. At the same time there is also a need for developing diagnostic and therapeutic systems and technologies based on the use of agents that are nontoxic, not requiring systemic distribution or capable of obviating the use of harmful radiation, particularly as it relates to tumors of the skin and breast.

As stated earlier, a nanoparticulate system encapsulating a dye that can be photoexcited to produce singlet oxygen will be a better system for tumor detection and therapy than conventional approaches. The uptake of these nanoparticles by tumor cells can serve as an optical indicator of the presence of the tumor, and can be used

to trigger a laser system for oxidizing and, thus, eradicating tumors or unwanted tissues from the body in a noninvasive manner. Based on these considerations, we have developed nanoparticles loaded with ICG, a photoexcitable molecule with NIR fluorescence properties, good penetrating ability into tumor cells and a long residency time within tissues. The novelty of this approach is to combine the tools and principles of optics, chemistry, physics and engineering for the development and manufacturing of a multifunctional smart nanodevice with the capability of navigating in the blood stream, looking for uptake into abnormal growths such as tumors or for specific areas where to deliver a particular drug. In turn, the drugs thus delivered can emit a measurable signal that can help to locate the abnormality or be made to eliminate the abnormality upon photoactivation with laser radiation via PDT (Fig. 11.2) [3].

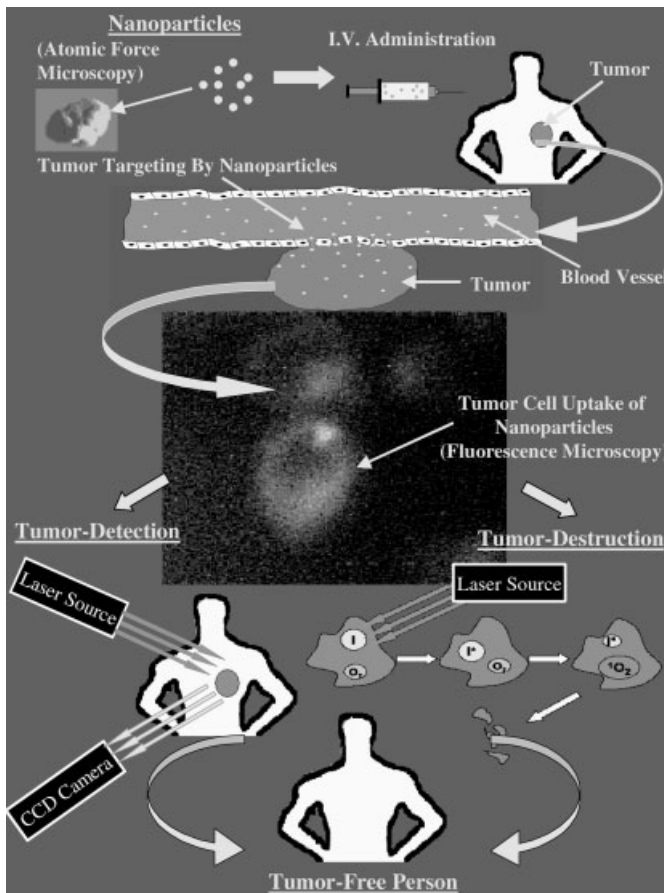


Fig. 11.2. ICG encapsulated in nanoparticles preferentially locates in tumors to allow the noninvasive imaging and destruction of superficial tumors. (from Ref. [3].)

11.5

Optical Imaging and PDT

11.5.1

Optical Imaging

Optical imaging is a form of tumor diagnosis based on the interaction between light and biological matter [112]. Two of the most salient advantages this technique can offer to the clinician over traditional diagnostic modalities are a non-reliance on both ionizing radiation and radioactive material, and the wealth of information that it can generate about the structure, dynamics and interactions in biological bulk specimens such as tissues. Optical imaging takes advantage of the spatial variation in the optical properties of a biological specimen, whether it is a cell, a tissue, an organ or an entire live organism [113]. With this diagnostic technique, an optical image is obtained by monitoring the spatial variation of light that is reflected, scattered, absorbed or emitted as fluorescence. The use of lasers as an intense and convenient light source to generate an optical response has considerably expanded the boundaries of optical imaging, particularly as it relates to tumor diagnosis [114–116].

11.5.1.1 Fluorescence-based Optical Imaging

Fluorescence is a radiative phenomenon whereby a molecule becomes excited upon absorbing light of a given wavelength and later on returns to the ground state by emitting light of a longer wavelength. The major advantages of fluorescence detection over other optical imaging techniques are high sensitivity (low signal-to-noise ratio), high speed and safety. In this instance, safety refers to the fact that the sample is neither altered nor destroyed and that no hazardous byproducts are generated in the process [117].

11.5.1.2 NIR Fluorescence Imaging

NIR fluorescence imaging is increasingly gaining importance in the diagnosis of tumors [118, 119]. The NIR region is that portion of the light spectrum extending from 700 to 900 nm. At least four main reasons are responsible for the increasing importance of this imaging technique:

- (a) Blood and other biological tissues are relatively transparent across this spectral wavelength range, thus creating an optical window [113, 119].
- (b) The excitation of chemical agents or dyes for imaging by NIR radiation produces practically no autofluorescence from any endogenous cellular components, a factor that dramatically improves the sensitivity of the detection signal detection, often limited by background autofluorescence [120].
- (c) The NIR excitation and emission wavelengths reduce scattering in tissues, and, thus, increase both the penetration depth and the efficiency of the detection signal [113, 119].

Tab. 11.1. Common NIR dyes

Name	Wavelengths of excitation/emission (nm)
Cy-3 iodoacetamide	565/590
Cy-5 N-hydroxysuccinimide	648/669
Cy-7 isothiocyanate	750/777
Rhodamine 800	680/700
Indocyanine green	782/830
Azure B	638/660
Thiazole orange	735/765
Nile Blue	638/660
Al phthalocyanine	662/680
Oxazine 1	643/658
BODIPY™	665/676

(d) Commercial NIR lasers used as exciting sources are low in cost and convenient to use because of a compact design [113].

11.5.1.3 NIR Dyes for Fluorescence Imaging

The dyes for NIR fluorescence imaging listed in Table 11.1 are either long-wavelength probes such as cyanine, rhodamine, oxazine, phthalocyanine and naphthalocyanine dyes or extended conjugated systems [119, 121–125]. The cyanines, which were initially developed for use as membrane probes, are probably the most commonly used NIR dyes. Typical examples include, in increasing order of wavelength, Cy-3, Cy-5 and Cy-7 [126].

The phthalocyanine and naphthalocyanine dyes are less popular due to their water insolubility, tendency to aggregate, lack of conjugateable forms, and environmental and photochemical instability. Among dyes categorized as extended conjugated systems, ICG has been extensively investigated for use as a long-wavelength probe. By encapsulating this dye within nanoparticles, the authors were recently able to develop a delivery system for the imaging of cancer cells that would overcome most of the problem commonly encountered with other NIR dyes used in biophotonics.

11.5.2

PDT

PDT, also referred to as photoradiation therapy, phototherapy or photochemotherapy, is a promising new form of treatment for a variety of oncological, cardiovascular, dermatological and ophthalmic diseases [127, 128]. PDT is an emerging therapy for the treatment of tumors that are accessible to light radiation such as those of the head, neck, digestive tract, skin and breast. PDT has been proposed in several studies as an alternative to overcoming “multidrug resistance phenotype” (MDR), a frequent reason for the failure of conventional chemotherapy. PDT has been approved by the FDA for the treatment of both early- and late-stage lung cancer, for certain types of esophageal cancer and for non-small cell lung cancer, and

most recently it was also approved for the treatment of actinic keratosis, a precancerous skin condition. Clinical trials are currently in progress in the US and abroad to evaluate the effectiveness of PDT in the treatment of several types of cancer and precancerous conditions [113].

PDT is a form of light-activated chemotherapy based on the activation of an exogenous chemical agent, known as the photosensitizer, by light. The photosensitizer is administered either systemically by the intravenous route or locally into the malignant growth, after which light of a specific wavelength is used to irradiate the photosensitizer in a specific part of the body. Upon absorbing light, the photosensitizer will produce reactive oxygen species (ROS) with the ability to destroy the tumor with minimal damage to the surrounding cells [129, 130].

The advantages of PDT are numerous. For example, it circumvents systemic treatment since the light is focused only on the site occupied by the tumor, thus sparing the patient from side-effects commonly associated with conventional chemotherapy such as hair loss, nausea and vomiting. It exhibits more selectivity than conventional chemotherapy and radiotherapy toward tumors because of preferential accumulation of the photosensitizing agent in tumor tissue and the spatially confined photodynamic effects achieved with light radiation. PDT will be a suitable option in patients that cannot undergo removal of a tumor by surgery, e.g. in the upper bronchi, since it can kill cancer cells without damaging adjacent collagenous tissue structures, a situation that allows for the repopulation of these structures by new normal cells. It is expected to be cost-effective and, unlike radiation therapy, amenable to be repeated as many times as deemed necessary, thus providing a way for the long-term management of cancer and the complete removal of the tumor. Additionally, in contrast to surgery, it is a noninvasive form of therapy that does not cause pain or discomfort in the patient or lead to such complications as surgery-related secondary infections.

11.5.2.1 Basis of PDT

In PDT, cytotoxicity by a photosensitizer molecule is attained when the photosensitizer, after undergoing activation by laser light energy, proceeds to return to the ground state by either radiative or nonradiative decay [131–133]. In nonradiative decay, the energy absorbed by the photoactive molecule can be converted to heat (internal conversion) that can then be transferred to nearby intracellular molecules (photooxidation type I) to cause cellular damage by raising the intracellular temperature. Alternatively, the energy absorbed by the photosensitizer can be transferred to molecular oxygen by means of a triplet state (photooxidation type II), to form reactive intermediates such as singlet oxygen that, in turn, can cause irreversible destruction of biological substrates [134, 135]. ROS such as the superoxide anion, and hydroperoxyl and hydroxyl radicals may also be involved in mediating irreversible damage to biologic components [127]. Singlet oxygen possesses a reactive distance of only 0.1 μm , so its cytotoxicity is restricted to the immediate vicinity of the photoactivated drug. When used within their standard doses, neither the photosensitizer nor the light source is active against the target when used independently of each other.

Tab. 11.2. Common photosensitizers

<i>Name</i>	<i>Chemical type</i>	<i>Absorption wavelength (nm)</i>
Photofrin®	porphyrin	630
Bonellin	chlorin	625
MTHPC	chlorin	652
SnET2	chlorin	660
Mono-L-aspartyl chlorine e6	bacteriochlorin	654
HPPH	pyropheophorbide	670
Veteroporphin	benzoporphyrin	690
Protoporphyrin IX	ala	630
Lu-TeX	texaphyrins	732
Indocyanine green	tricyanocyanine	786
AlPcS	phthalocyanine	674
Methylene blue	cationic	660
Tetrabromorhodamine	cationic	540

11.5.2.2 Photosensitizers for PDT

Photosensitizers for PDT are selected taking into account various physiological factors. In brief, an ideal photosensitizer should possess the following properties: (a) ability to selectively accumulate in the cancerous or precancerous tissue, (a) capability of absorbing light significantly in the region of maximum transparency of biological tissues and (c) minimal drug toxicity. Table 11.2 lists some of the common photosensitizers used in PDT [136–149].

11.5.3

ICG: An Ideal Photoactive Agent for Tumor Diagnosis and Treatment

Among the photosensitizing agents listed in Tables 11.1 and 11.2, ICG stands out as unique because it possesses both NIR fluorescent properties and PDT capabilities, thus becoming suited for both NIR fluorescence imaging and PDT of tumors. ICG may be more advantageous than other photoactive agents since it causes minimal toxicity, is commercially available in a very pure form, has a low cost, and, more importantly, has been approved by the FDA as a diagnostic agent for use in ophthalmology and other medical specialties. Moreover, in other countries ICG has received approval for use in PDT. On these bases, it would appear that the development of a commercial ICG-based nanoparticulate system for tumor imaging and treatment would meet fewer hurdles for obtaining federal approval for use in humans than would be possible with other related agents.

11.5.3.1 Clinical Uses of ICG

ICG is a photoactive dye approved by the FDA for medical diagnostic studies, and is widely used in the clinical setting for the evaluation of cardiac output, liver function and microcirculation of skin flaps, the visualization of the retinal and choro-

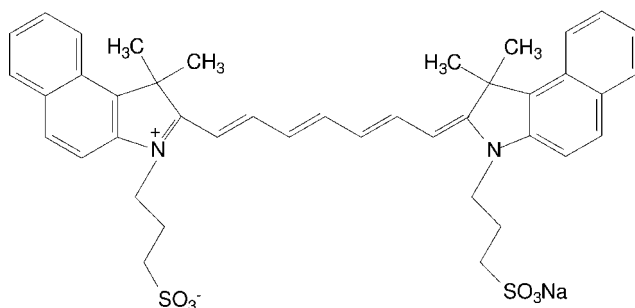


Fig. 11.3. Chemical structure of ICG.

dal vasculatures, in pharmacokinetic analysis, to localize objects within tissues, as a fluorescence probe for enzyme and proteins, and in tissue welding [150, 151].

11.5.3.2 Structure and Physicochemical Properties of ICG

Chemically ICG (FW 775) is a tricyanocyanine dye containing an extended conjugated system. The structure of ICG, shown in Fig. 11.3, is made up of two polycyclic moieties, each known as a benzoindotricarbocyanin, connected to each other by a carbon chain. While the polycyclic moieties are responsible for the lipophilic properties of ICG, the sulfate groups attached to each polycyclic component impart hydrophilicity. As a result, ICG is, overall, amphiphilic in nature and, because of its amphiphilicity, ICG is soluble in organic solvents [e.g. methanol and dimethylsulfoxide (DMSO)] and in aqueous media, including buffers.

11.5.3.3 Binding Properties of ICG

ICG binds rapidly and almost completely (98%) to most plasma proteins. Thus, in the circulation it binds to albumin, globulins and lipoproteins. Due to its amphiphilic nature, ICG can interact with both lipophilic and hydrophilic molecules. Furthermore, because of its three-dimensional structure, ICG can simultaneously bind to the lipophilic and hydrophilic parts of amphiphiles such as phospholipids.

ICG binds to human serum albumin (HSA) through its hydrophobic core. In this case, about one or two molecules of ICG become bound to one molecule of HSA [152]. ICG has also been found to bind to α_1 -lipoproteins and β -lipoproteins [153] in human serum. In general, the binding of ICG to plasma proteins will impact negatively on its potential intracellular effects since the bound form will be primarily confined to the vascular compartment and hindered from entering tumors [154–156]. Numerous reports have described the binding of ICG to phospholipids [157–159]. These binding interactions are relevant to photoimaging since the emission spectrum and fluorescence yield of ICG are influenced by the resulting quenching [158, 160–163].

Several studies have been carried out on the interactions of ICG with model membranes. It was observed that ICG is able to interact with phospholipid bilayers and that the binding takes place at the interface of the model membrane. The

physicochemical and fluorescence spectral characteristics of ICG in aqueous solution have been evaluated in the presence of micelles and liposomes [162]. ICG was found to be tensioactive, and to aggregate or become embedded at the interface of micelles and liposomes. The fluorescence of ICG was very low in the aggregated form due to quenching and very high when embedded at the interface.

11.5.3.4 Metabolism, Excretion and Pharmacokinetics of ICG

The excretion of ICG follows a hepatobiliary route in the human body. After intravenous injection, most of the circulating ICG is taken up into the liver where, rather than being metabolized, it is excreted as part of the bile into the intestinal tract. Upon reaching the intestine it is neither reabsorbed through the intestinal mucosa nor put through the enterohepatic circulation [156]. Negligible uptake of the dye occurs in the kidneys, lungs and peripheral tissues. ICG does not undergo significant renal excretion [164] and it is not detected in the cerebrospinal fluid [156].

The metabolic fate and excretion of ICG correlate well with its lipophilic characteristics. As a result, ICG is rapidly eliminated from the circulation after an intravenous injection, with the plasma half-life being about 2–4 min [164–167]. The plasma disappearance rate of ICG in healthy human subjects is from 18 to 24% min^{-1} . The normal biological half-life has been determined to be from 2.5 to 3 min, so single blood samples taken from healthy subjects 20 min after an intravenous injection should contain not more than 4% of the initial concentration of dye [168].

Spectrophotometric studies on ICG have shown the blood levels of this dye to follow a biexponential decay curve following intravenous injection. The plasma clearance of ICG is biphasic, showing a rapid initial phase with a half-life of 3–4 min and a secondary phase with a half-life of more than 1 h at low concentrations [165, 169, 170].

11.5.3.5 Toxicity of ICG

ICG produces minimal toxicity in animals and its LD_{50} after intravenous administration ranges from 50 to 80 mg kg^{-1} [171]. Although no equivalent data exists for humans, the maximum recommended human dose is 5 mg kg^{-1} . The safety of intravenous ICG in humans is well documented, with severe adverse reactions occurring in only 0.05% of recipients [172].

11.5.3.6 Tumor Imaging with ICG

ICG is rapidly gaining acceptance as a diagnostic agent for tumor imaging purposes due to its NIR fluorescence characteristics. Li et al. [173] have studied the efficiency of ICG as a sensitive contrast agent for tumor detection and localization. These authors assessed the differences in fluorescence signals of ICG between opposite tumor-bearing and tumor-free areas after the intravenous administration of a low, 80 $\mu\text{g kg}^{-1}$ body weight, dose of ICG to rats implanted with a tumor in one leg. In this way it was possible to determine that a difference in fluorescence exists between the tumor side and tumor-free side, and that the difference was detectable

even when the tumor was very small (about 0.15 cm^3). During the exponential growth phase of the tumor, the ratio of these two signals was approximately 2.5 and the ratio of the initial ICG clearance velocity in the tumor leg to that in the control leg was about 3.

Preliminary investigations with human subjects affected with breast tumors were conducted using an ICG dose of $400 \mu\text{g kg}^{-1}$ body weight. The results of this study indicated the existence of differences in the fluorescence emanating from a tumor-bearing breast and that from a tumor-free breast. Additional evidence in support of the use of ICG in the imaging of breast tumors has been gathered in dogs [174]. By using a gain-modulated, image-intensified, charge-coupled, camera these authors were able to obtain intensity-modulated fluorescence signals from canine mammary tumors. By means of a continuous wave diffuse optical tomography apparatus, Intes et al. [175] have demonstrated the usefulness of ICG as a diagnostic tool for differentiating benign from malignant pathologies in breast cancer patients.

A number of studies have also reported on the use of ICG as a fluorescence contrast imaging agent to obtain two- or three-dimensional images from experimental phantoms, rats and synthetic samples [176]. It is quite clear that a great deal of interest exists in finding new diagnostic applications for ICG by NIR imaging, optical spectroscopy and tomography, and that there is still room for improving the sensitivity, specificity and cost-effectiveness of currently available ICG-based optical techniques, especially of those intended for the detection of breast and skin tumors.

11.5.3.7 PDT with ICG

Due to its photosensitizing properties, ICG has great potential for application in PDT. An important reason for using ICG in PDT is that its strongest absorption and emission bands occur at around 800 and 820 nm, respectively [177, 178]. Since these two wavelengths are the wavelengths at which blood and other tissues are relatively transparent, and at which the penetration depth of light in biological tissue is at its maximum (5 mm or more) [179, 180], they confer ICG an advantage over comparable chemical agents that work in the visible spectral range. In addition, like other second-generation photosensitizers, ICG demonstrates those features that are considered desirable in PDT, including rapid biodistribution, low skin phototoxicity, and ease of administration and monitoring [181].

Fickweiler et al. [182] were the first to provide concrete evidence on the photodynamic action of ICG. Using HaCaT cells, an immortalized human keratinocyte cell line, they were able to examine the dose-dependent phototoxic effects of ICG *in vitro*. In their experiments, keratinocytes were incubated with 0–50 μM aqueous solutions of ICG for 24 h, after which the cells were irradiated with diode laser (805 nm) of a different energy density (0, 12, 24 and 48 J cm^{-2}). Under these conditions, photoactivated ICG demonstrated a cell killing effect at concentrations above 5 μM . In addition, the participation of ROS in the cell killing process was suggested by the results of an experiment in which sodium azide, a quencher of ROS, protected against the cytotoxicity of ICG [182].

A different approach was later used by Baumler et al. [135] to elucidate the mechanism responsible for the cytotoxicity of ICG in PDT. In their study, HT-29 cells, an immortalized human colon carcinoma cell line, were first incubated with different concentrations of ICG (10–100 μM) for 24 h and next irradiated with a continuous wave diode laser (805 nm, 30 J cm^{-2}). Apart from demonstrating light-induced cytotoxicity, these investigators also observed that the cytotoxicity increased when heavy water (D_2O) was used in place of normal water. These results were interpreted as indicative of the production and participation of singlet oxygen during laser irradiation of ICG since D_2O is known to prolong the lifetime of singlet oxygen. Moreover, evidence for the occurrence of lipid peroxidation upon the addition of D_2O was gathered from the concomitant elevation of the levels of malondialdehyde, a marker of lipid peroxidation. This line of thought was further examined with quenchers of singlet oxygen species such as sodium azide, histidine, and with specific quenchers of superoxide anion and hydroxyl radical such as mannitol. Since only sodium azide and histidine protected against the photodynamic killing effect of ICG on HT-29 cells, the participation of singlet oxygen and of lipid peroxides, but not of superoxide anion and hydroxyl radicals, was inferred. Virriale et al. [183] have also provided proof of the involvement of singlet oxygen in the photodynamic antitumor action of ICG. In photosensitization experiments performed by this research group, irradiation of U-937 human monocytes (histiocytic lymphoma, CRL-1593), a leukemia cell line, with a diode laser (805 nm) source providing a dose of radiation of 18 J cm^{-2} in the presence of 12 μM of ICG and dithiothreitol, an oxidizable substrate, caused the cells to undergo programmed cell death (apoptosis).

Urbanska et al. [184] have reported the potential utility of ICG as a photosensitizer for the treatment of melanoma, a common type of skin cancer. PDT with ICG is particularly suited to control melanoma because the melanin present in these cells absorbs the wavelength of visible light commonly used for photodynamic effect but not the NIR wavelengths at which ICG exerts its cytotoxic effects. In this study a very high photosensitizing efficiency was demonstrated for ICG upon exposing SKMEL 188 cells, a human melanoma cell line, to 100 μM of ICG followed by irradiation with a diode laser (830 nm) delivering a radiation dose of 30–100 J cm^{-2} . Costa et al. [181] have described an *in vivo* photodynamic study on ICG that demonstrated the potential utility of the dye in the occlusion of choroidal neovascularization. Using pigmented rabbits as an animal model, doses of ICG between 10–20 mg kg^{-1} and an activating light dose of 6.3 J cm^{-2} from a diode laser, ICG was shown to be effective in occluding choriocapillaries.

11.5.3.8 Limitations of ICG for Tumor Diagnosis and Treatment

The *in vivo* value of ICG in tumor imaging and treatment is severely limited by two intrinsic characteristics – a very high tendency to bind to plasma proteins (95–98%) and a rapid elimination from the body (plasma $t_{1/2} = 2\text{--}4$ min) [158, 178]. As a result, a very small amount of ICG will accumulate in tumor tissue following intravenous dosing since the dye will remain largely confined in the blood before its removal by the liver for eventual rapid elimination into the small intestinal

tract. Needless to say that for both imaging and PDT applications, it will be essential to deliver a substantially higher quantity of ICG to the tumor site than it is possible with a conventional aqueous solution and that this objective will be only realized when its limiting characteristics are appropriately minimized.

Another important factor that limits the clinical use of ICG is extreme instability in aqueous media. In addition to preventing its storage for a significant period of time, aqueous solutions of ICG are only suitable for conducting *in vivo* imaging and other types of diagnostic procedures for a short time [150, 185]. The chemical stability of ICG at ambient temperature has been found to decrease in inverse proportion to its concentration [177, 186], and it can be easily monitored by following the changes of its visible absorption spectrum over time [177, 186–188]. Light appears to be the major determining factor in the stability of ICG since degradation is much greater for samples exposed to ordinary light than for samples kept in the dark [186, 189]. A similar photodegradation has been verified with aqueous solutions of ICG that were exposed to laser radiation [185]. Since most current clinical applications of ICG are carried out with aqueous solutions, the development of a more stable preparation for parenteral use is clearly warranted.

11.5.3.9 Recent Approaches for Improving the Blood Circulation Time and Uptake of ICG by Tumors

No specific mechanism has been described for the localization of ICG in tumors [190]. Moreover, since ICG lacks tumor selectivity, its use as a diagnostic tool for differentiating among various types of tumor will not be reliable. Several approaches have been tested as ways of attaining greater tumor selectivity with ICG. One attempt has been to synthesize dye–peptide conjugates that are receptor specific [190]. The experimental results suggest that small dye–peptide conjugates are effective as contrast agents for optical imaging purposes. Even when covalently united to each other, the dye and the peptide were found to retain the native fluorescence characteristics and the affinity for peptide receptors, respectively. These newly synthesized conjugates, identified as Cytate and Cybesin, preferentially localized for over 24 h in tumors known to overexpress somatostatin and bombesin receptors, respectively. In contrast, the dye moiety was not retained in these two tumor models when they were no longer conjugated to a peptide [190]. This behavior and the lack of data on the chemical stability of dye–peptide combinations *in vitro* and *in vivo* represent a significant impediment to the potential commercialization of dye–peptide conjugates.

Devoisselle et al. [191] have developed an emulsion formulation to increase the blood circulation time of ICG. To test this formulation, Wistar rats were intravenously dosed with 7.5 mg kg⁻¹ body weight of ICG, given as either an aqueous solution or as an oil-in-water emulsion formulation. It was verified that the emulsion increased the plasma clearance time of ICG in the first 15–60 min and the residence time in the skin as compared to an equipotent dose of an aqueous solution. However, no information was given on the chemical stability of ICG in water or in an o/w emulsion *in vitro* and no experiments were conducted to determine the efficiency of an emulsion in tumor targeting under *in vivo* conditions.

11.5.3.10 Recent Approaches for ICG Stabilization *In Vitro*

An early way of ensuring the stability of ICG in solution was to substitute water by nonaqueous solvents. For this purpose, methanol, 1,2-propanediol and dimethylformamide were evaluated [192]. It was found that under ordinary conditions of illumination, ICG was more stable in methanol than in any of the other solvents. Moreover, the thermostability of ICG was greater in methanol and 1,2-propanediol than in dimethylformamide. A later study examined the photodegradation and thermodegradation of ICG in a wide variety of aqueous and organic solvents [185]. This study indicated that ICG exhibited a low photostability in water, D₂O and aqueous sodium azide (NaN₃) solutions, and a good photostability in methanol, DMSO and human plasma. In addition, the thermal stability of ICG was moderate in water, D₂O and aqueous NaN₃, and very high in human plasma, methanol and DMSO. Thus, excluding human plasma, ICG appears to remain quite stable in organic solvents. Unfortunately these results are of no value in trying to develop an appropriate photostable, thermostable and biocompatible injectable solution of ICG for use in human subjects inasmuch as they all possess intrinsic toxicity.

A different solution to improving the stability of ICG in aqueous media has been to complex the dye with water-soluble cyclodextrins [193]. The stability of ICG in water increases because the dye can fit in the torus of γ -cyclodextrin to form an inclusion complex at pH 6.0 and 25 °C that will somewhat shield the dye from the external environment. Although in this manner the stability of ICG increases in aqueous media, the effect is short-lived due to the tendency of ICG to leave the cavity of γ -cyclodextrin to form an equilibrium mixture with its complexed form. Also, complexation of ICG with a cyclodextrin will make accurate assessment of the thermostability of ICG a difficult task.

The stability of ICG in aqueous solutions has also been achieved by conjugating it noncovalently with a polymeric carrier molecule [151, 194]. The conjugate is formed by gently stirring a solution of ICG plus the anionic polymer sodium polyaspartate (PASP), added in a respective molar ratio of 1:2.6, at ambient temperature. Under ordinary conditions of illumination and ambient temperature, an aqueous solution of conjugated ICG emitted a fluorescence that remained quite stable for up to 24 days. In contrast, the fluorescence of a solution of plain ICG was only stable for 4 days. However, this gain is offset by the failure of the ICG–PASP conjugate to show a sufficiently long blood clearance rate for ICG that would allow the dye to accumulate in tumors in a therapeutically effective concentration.

A more recent attempt to prevent the photodegradation of ICG has been to place this compound in close proximity to colloidal gold [195]. Although the interaction of ICG with colloidal gold allows ICG to form a metallic conjugate with better photostability than plain ICG, the utilization of metallic nanoparticles raises concerns about the biodegradability and biocompatibility of the formulation. An additional concern is the efficiency and effectiveness of this type of conjugate under *in vivo* conditions since none of these issues has, thus far, been experimentally substantiated.

11.6

PLGA-based Nanoparticulate Delivery System for ICG

11.6.1

Rationale of Using a PLGA-based Nanoparticulate Delivery System for ICG

From the foregoing statements, it is apparent that the use of ICG in tumor diagnosis and treatment will only become a reality when its present shortcomings in terms of chemical stability in solution, circulation half-life and adequate uptake by tumor cells are solved.

One attractive and novel approach to achieving these objectives may be to encapsulate ICG within a biocompatible and biodegradable nanoparticulate system. Among possible candidates for use in the preparation of nanoparticles for drug delivery purposes, PLGA and several of its derivatives stand out since they meet the requirements of biocompatibility and biodegradability, and, in addition, have been extensively used by the pharmaceutical industry. Further advantages to be gained from the use of PLGA in nanoparticles are, among others, (a) enhanced uptake into a tumor site because of increased endocytosis and of leakiness of the vasculature permeating a tumor, i.e. they are suited for the passive targeting of tumors [196], (b) amenability to surface modification by special targeting moieties such as antibodies to enhance specificity toward a target site, i.e. active targeting [196], (c) attainment of a long circulation half-life (14 min, which is about 3–7 times that of plain ICG [197], and which can be increased further by coating the surface of the nanoparticles with specific polymers such as PEG [198]), (d) confirmation by *in vitro* studies with PLGA nanoparticles of their ability to be enter human cell lines such as arterial smooth muscle cells (HASMC) and vascular smooth muscle cells (VSMC), and accumulate at the tumor site [199, 200], (e) demonstrable stability in aqueous media for intravenous delivery and which, unlike that of micelles and liposomes, is independent of surfactant/lipid concentrations, and (f) ease of preparation which, unlike the synthesis of delivery systems based on a antibody–drug conjugate, does not entail the formation of covalent linkages. It is expected that as a result of future advances in nanotechnology, fully biocompatible and biodegradable PLGA-based nanoparticles will be engineered on an industrial scale to meet the clinical demands imposed by human tumors.

PLGA was used to entrap ICG into nanoparticles. The amount of each ingredient was varied to represent ratios of dye to polymer ranging from 1:10 to 1:800. The ICG content appeared to vary within a narrow range (0.17–0.29%) regardless of the dye to polymer ratio (Table 11.3) [201–203]. A similar trend was noted for the particle size and polydispersity of the nanoparticles (Table 11.4). The ζ potential was more negative with a dye to polymer ratio of 1:800 than with the other ratios used (Table 11.4). The surface of the nanoparticles was porous in nature (Fig. 11.4), a feature that may facilitate the fairly rapid release of the dye into an aqueous environment during the first 8 hours (Fig. 11.5). The incorporation of ICG into nanoparticles not only isolated the dye from a potentially hostile external environment, but at the same time contributed to enhance its chemical stability to the degrading

Tab. 11.3. Effect of formulation parameters on ICG entrapment efficiency, ICG content and nanoparticle recovery

Formulation number	Amount of ICG in formulation (mg)	Amount of polymer in formulation (mg)	ICG content (%)^[a]	ICG entrapment (%)^[a]	Nanoparticle recovery (%)
1	1	100	0.21 ± 0.06	9.92 ± 2.68	48.0
2	5	100	0.29 ± 0.04	2.92 ± 0.40	49.4
3	10	100	0.17 ± 0.01	1.14 ± 0.08	65.3
4	1	800	0.20 ± 0.01	74.47 ± 0.74	45.7

^a Values are given as mean ± SD for $n = 3$.

action of an aqueous medium, ambient light and heat (Figs. 11.6–11.8, and Tables 11.5 and 11.6) [202].

The uptake of PLGA nanoparticles into cells is by endocytosis and this uptake mechanism appears to take place even at low concentrations of ICG. As shown in Fig. 11.9, the amount of ICG taken up as nanoparticles into B16-F10 and C-33A cells, two types of cancer cells, increased in liner proportion to the concentration of extracellular ICG and the rate of uptake was greater into B16-F10 cells than into C-33A cells.

Figure 11.10 compares the uptake of ICG into B16-F10 and C-33A cells from aqueous solutions and from nanoparticles. For each type of formulation, the uptake of ICG was always slightly better into B16-F10 cells than into C-33A cell and the resulting uptake versus concentration profiles were virtually parallel to each other. Irrespective of the extracellular concentration of ICG used (0.0005–50 μ M), in all instances ICG was better taken up into cells as nanoparticles than in the free form [204].

The entry of a nanoencapsulated compound into the cytoplasm was investigated by fluorescence microscopy after incubating B16-F10 cells with PLGA nanoparticles loaded with coumarin 6 serving as a fluorescence probe (mean diameter 300 ± 10 nm, polydispersity index = 0.01). There were three main reasons for using coumarin 6 in place of ICG to make the nanoparticles for cell uptake studies. First, since ICG fluoresces in the NIR portion of the light spectrum, it cannot be detected using an ordinary fluorescence microscope. Second, coumarin 6 emits a

Tab. 11.4. Size and ζ potential values of various nanoparticle formulations

Formulation number	Nanoparticle size (nm)^[a]	Polydispersity	ζ potential (mV)^[a]
1	405 ± 05	0.01	-7.2 ± 1.0
2	338 ± 12	0.04	-7.8 ± 0.8
3	307 ± 08	0.02	-10.3 ± 2.1
4	357 ± 21	0.06	-16.3 ± 1.5

^a Values are given as mean ± SD for $n = 3$.

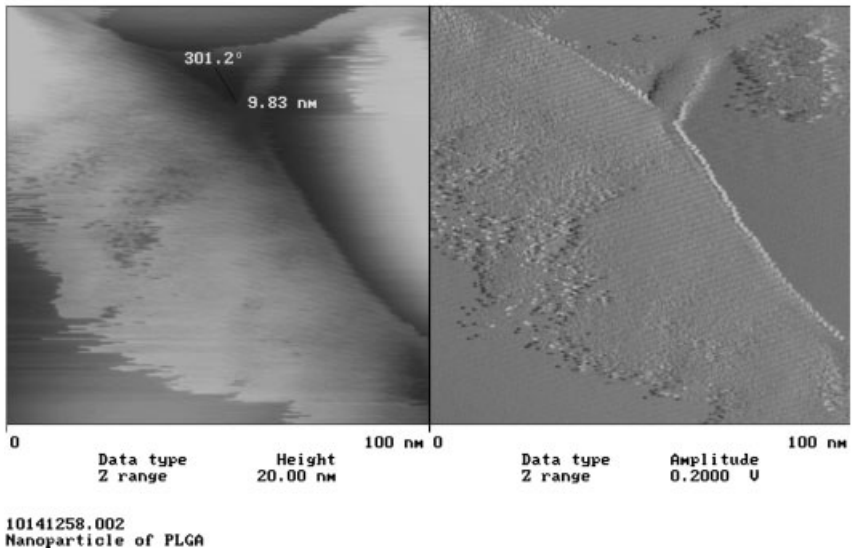
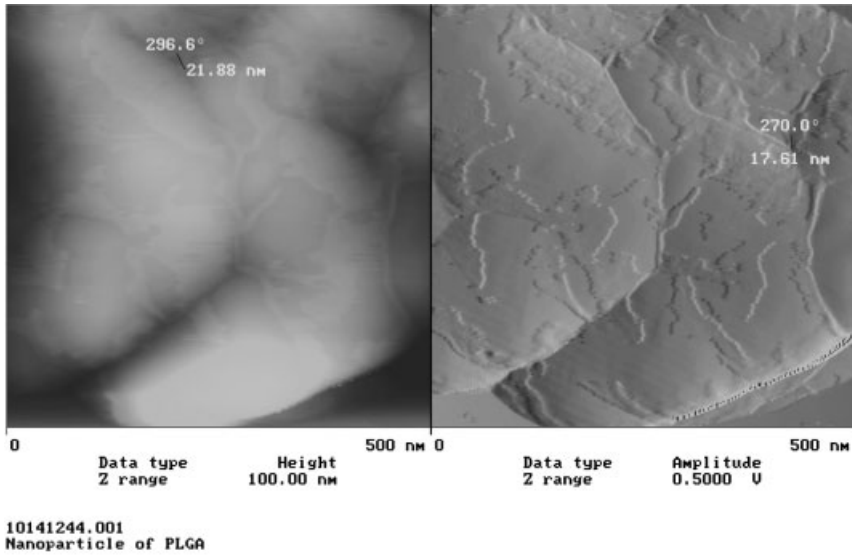


Fig. 11.4. Different views of the surface of ICG-loaded PLGA nanoparticles.

characteristic green fluorescence when excited with red light, thus becoming suited for detection by fluorescence microscopy [200]. Third, due to a higher degree of lipophilicity than ICG, coumarin 6 tends to remain longer within PLGA nanoparticles exposed to an aqueous environment than ICG [202, 205, 206]. As seen in Fig. 11.11, coumarin 6 was found to be evenly distributed throughout

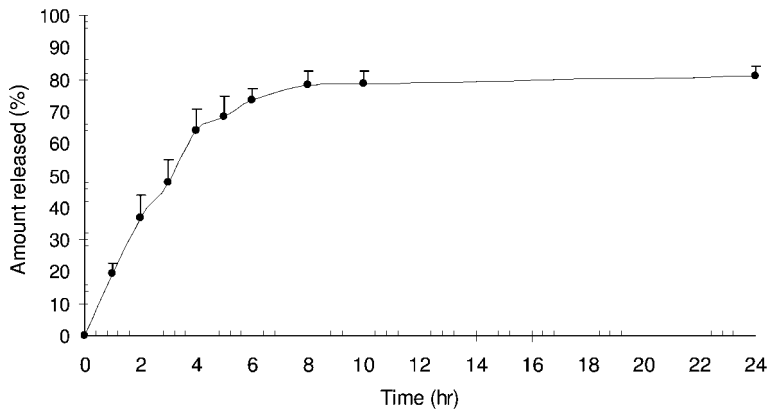


Fig. 11.5. Release profile of ICG from nanoparticles (mean \pm SD, $n = 3$).

the cytoplasm apart from the nucleus, and to bind to intracellular proteins and structures.

Incubating B16-F10 cancer cells in the dark with either ICG added as an aqueous solution or as nanoparticles was without apparent effect on cell viability at all concentrations of ICG examined (Figs. 11.12 and 11.13). Irradiating the cancer cells with a laser source emitting at 786 nm had no apparent effect on the viability of cells incubated with various doses (1–100 μ M) ICG as a solution (Fig. 11.14) or with empty nanoparticles (Fig. 11.15), but reduced viability by 22 and 24% in cells incubated with ICG nanoparticles providing 11 and 22 μ M of dye, respectively (Fig. 11.15) [205].

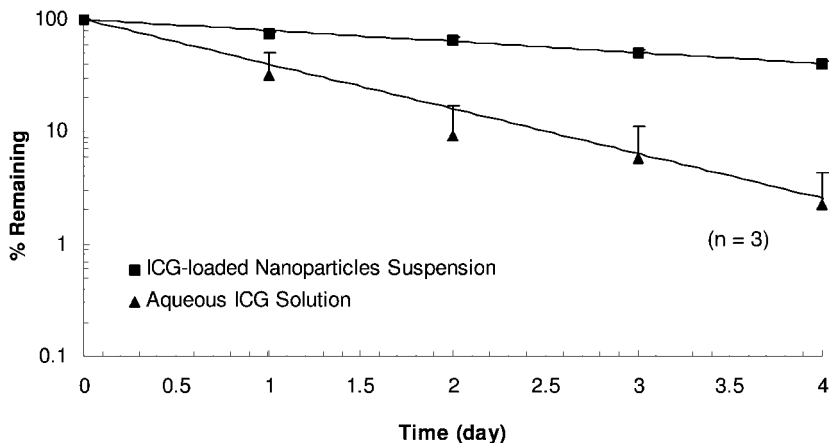


Fig. 11.6. Chemical stability of ICG in an aqueous solution and as a nanoparticle suspension in distilled water after storage at 22 $^{\circ}$ C in the dark.

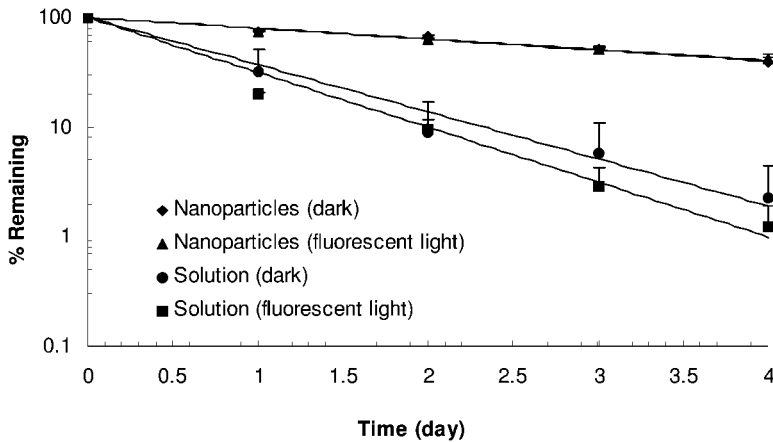


Fig. 11.7. Chemical stability of ICG in an aqueous solution and as a nanoparticle suspension in distilled water after storage at 22 °C in the dark and under fluorescent light.

11.6.2

In Vivo Pharmacokinetics of ICG Solutions and Nanoparticles

Assessment of the plasma kinetics and biodistribution of ICG following administration as an aqueous solution and as a nanoparticle suspension was conducted in mice. This type of study will also be of help in the future optimization of ICG-containing nanoparticulates in terms of dye load, and selectivity for and improved uptake into target sites.

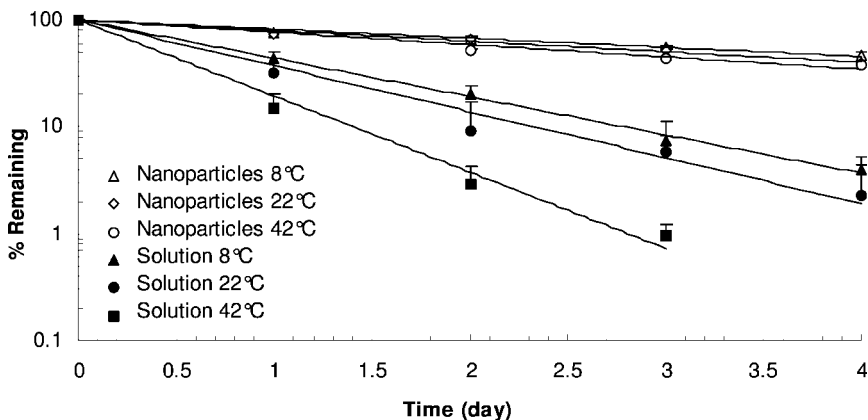


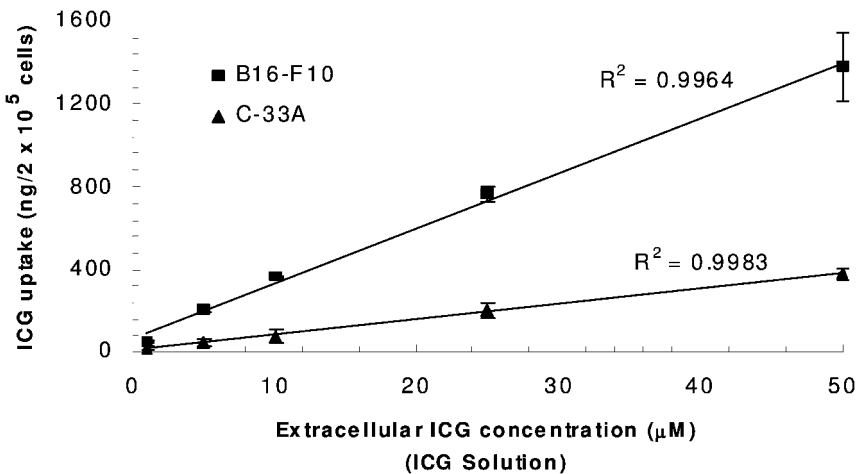
Fig. 11.8. Chemical stability of ICG in an aqueous solution and as a nanoparticle suspension in distilled water stored at different temperatures in the dark.

Tab. 11.5. Degradation rate constants, k_{obs} and degradation half-lives, $t_{1/2}$ of ICG aqueous solution and aqueous nanoparticle suspension (mean \pm SD, $n = 3$)

Formulation	Experimental conditions	k_{obs} (h^{-1})	$t_{1/2}$ (h)	R^2
ICG aqueous solution (ICG concentration $1 \mu\text{g mL}^{-1}$)	dark at 22 °C	0.0412 ± 0.0038	16.8 ± 1.5	0.972 ± 0.023
	room light at 22 °C	0.0480 ± 0.0052	14.4 ± 2.4	0.979 ± 0.016
	dark at 8 °C	0.0344 ± 0.0027	20.1 ± 1.6	0.997 ± 0.006
	dark at 42 °C	0.0684 ± 0.0043	10.1 ± 0.6	0.984 ± 0.063
ICG loaded nanoparticles aqueous suspension (ICG concentration $1 \mu\text{g mL}^{-1}$)	dark at 22 °C	0.0096 ± 0.0008	72.2 ± 6.1	0.986 ± 0.023
	room light at 22 °C	0.0094 ± 0.0009	73.7 ± 7.5	0.979 ± 0.019
	dark at 8 °C	0.0082 ± 0.0006	84.5 ± 6.3	0.981 ± 0.009
	dark at 42 °C	0.0111 ± 0.0003	62.4 ± 1.7	0.960 ± 0.011

Tab. 11.6. Extent of ICG degradation in solution and as nanoparticles after 4 days of storage under different conditions (mean \pm SD, $n = 3$)

Storage condition	ICG remaining (% of initial)	
	Aqueous solution	Nanoparticles
Darkness, 22 °C	97.8 ± 0.8	60.5 ± 3.2
Ambient light, 22 °C	98.8 ± 0.7	57.8 ± 4.1
Darkness, 8 °C	96.1 ± 1.3	53.4 ± 3.7
Darkness, 42 °C	99.2 ± 0.3	62.8 ± 0.9

**Fig. 11.9.** Effect of the extracellular concentration of ICG (1–50 μM) on the uptake of ICG into B16-F10 and C-33A cells.

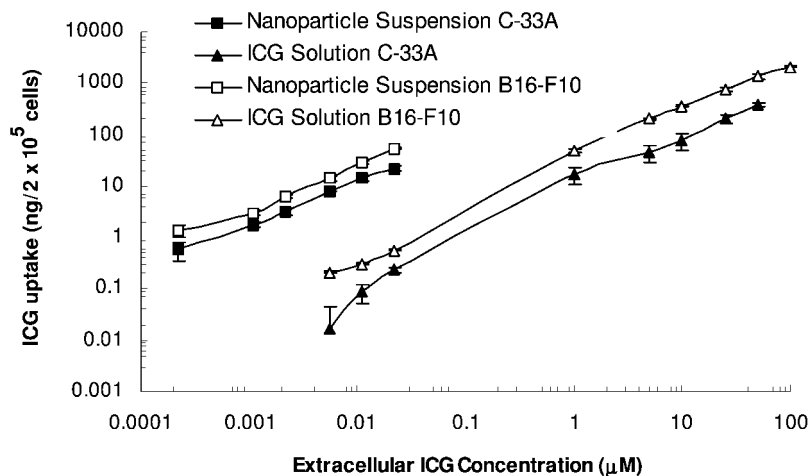


Fig. 11.10. Uptake of ICG from a solution and a suspension of nanoparticles into B16-F10 and C-33A cells (mean \pm SD, $n = 3$). Extracellular concentration of ICG: 0.0005–50 μM .

The temporal changes of ICG in plasma and in various tissues that follow a single intravenous dose of ICG (10 μg per mouse) as a solution and as nanoparticles was investigated. The results of these studies are presented in Figs. 11.16 and 11.17. For the ICG solution, the highest levels of ICG were found in the liver, followed in decreasing order in the kidney, spleen, heart and lung. These data confirm the role of the liver as the major organ for the removal of ICG from the general circulation and supports the clinical use of ICG as a test for liver function. In

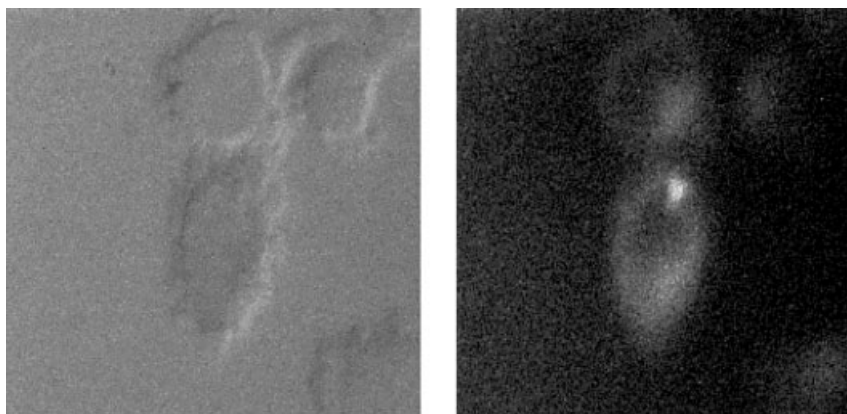


Fig. 11.11. Fluorescence microscopic images of B16-F10 cells incubated with 0.1 mg mL^{-1} coumarin-6-loaded nanoparticle suspension. Differential contrast image (left) and fluorescence image (right). A Nikon 100/1.40 oil lens was used.

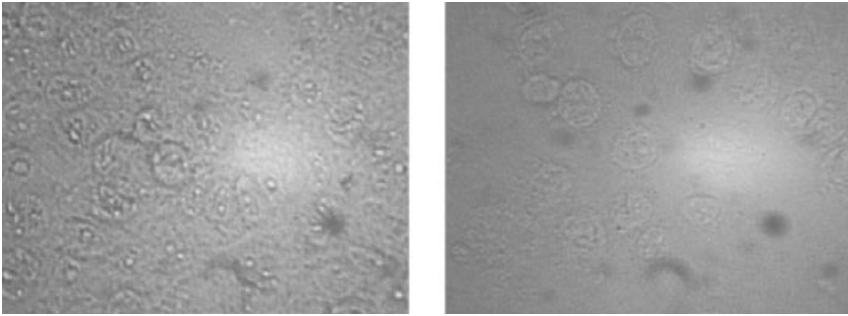


Fig. 11.12. Subcellular localization of ICG in C-33A cancer cells (using free ICG solution). Treated cells incubated with 100 μM ICG (left) and control cells without ICG (right).

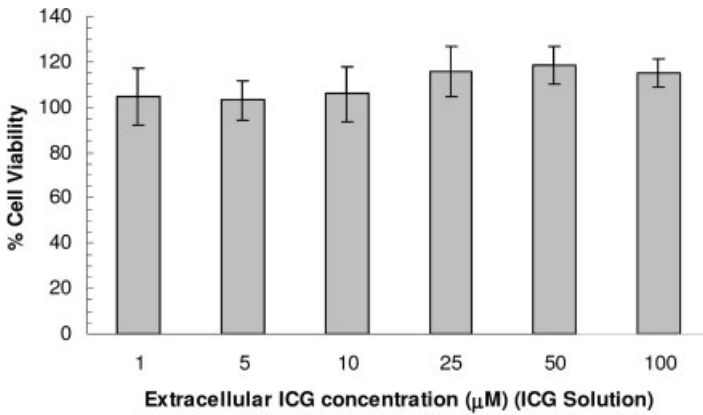


Fig. 11.13. Effect of ICG in solution on the viability of B16-F10 cells (mean \pm SD, $n = 5$). Extracellular concentration of ICG: 1–100 μM .

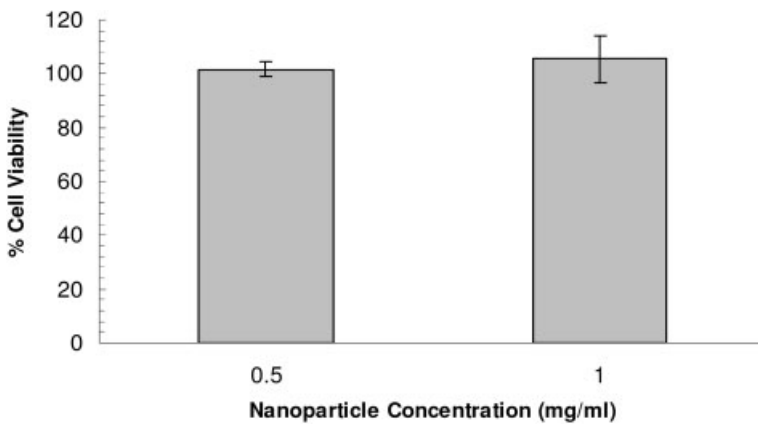


Fig. 11.14. Effect of ICG-loaded nanoparticles on the viability of B16-F10 cells (mean \pm SD, $n = 5$). Nanoparticle concentration: 0.5 and 1 mg mL^{-1} .

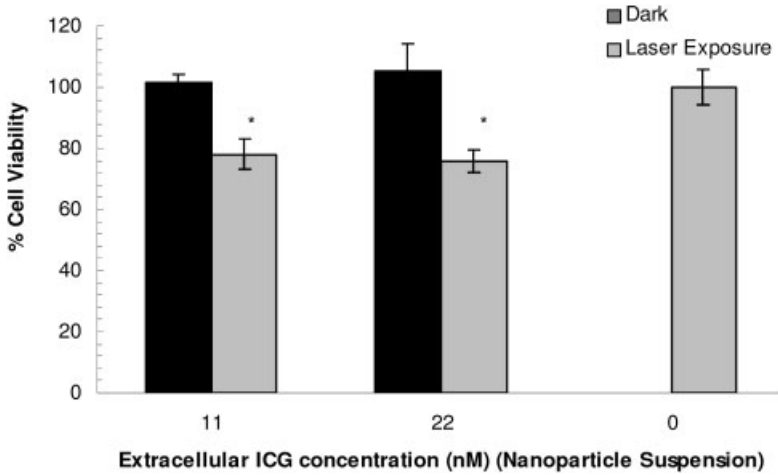


Fig. 11.15. Photodynamic activity of ICG-loaded nanoparticles on the viability of B16-F10 cells (mean \pm SD, $n = 5$). Extracellular concentration of ICG was 11 and 22 nM. *Significantly different from dark at $p < 0.05$.

the case of ICG nanoparticles, while the liver again accumulated the highest concentrations of dye, the biodistribution pattern for other organs was somewhat different than with a solution, since the concentrations decreased in the order spleen, lungs, heart and kidneys. It is evident that ICG nanoparticles are preferentially taken up into liver and spleen, two organs that form part of the RES that is responsible for the removal of foreign particles from the blood through an active phagocytic activity.

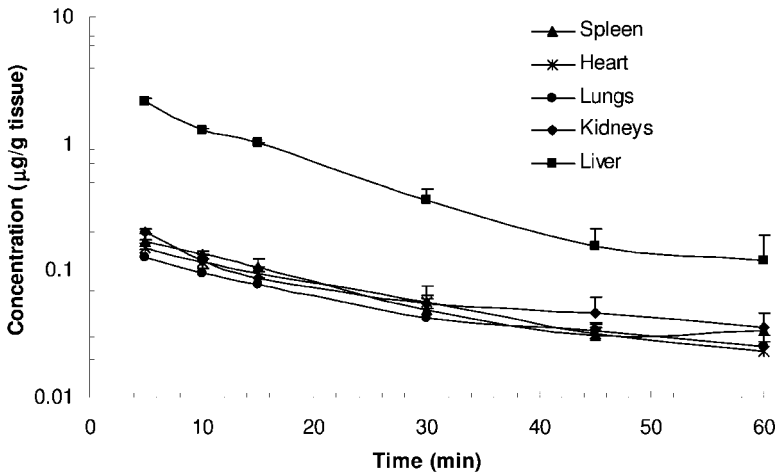


Fig. 11.16. Biodistribution of ICG (solution) in mouse tissues following an intravenous dose of ICG (10 μg per mouse).

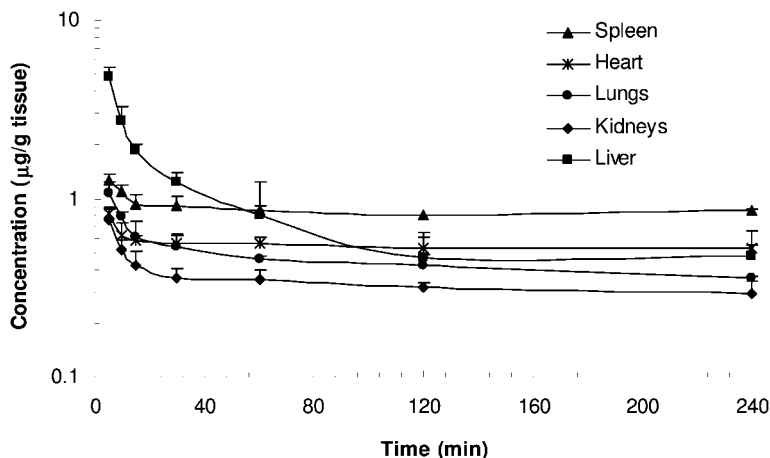


Fig. 11.17. Biodistribution of ICG (nanoparticles) in mouse tissues following an intravenous dose of ICG (10 µg per mouse).

Interestingly, the administration of ICG as a nanoparticle formulation led to a blood ICG level that was significantly higher than from a solution and which remained elevated for up to 4 h posttreatment. We believe that these results reflect the slower hepatic clearance of circulating ICG nanoparticles than of free ICG [155]. Also, nanoparticles may enhance the entry and retention of ICG into organs since the levels of ICG in organs were higher from a suspension of nanoparticles than from an equivalent aqueous solution. This feature should be of particular value in the targeting of tumors with ICG-loaded nanoparticles. In the body, the elimination of ICG appears to follow a biphasic pattern, with a rapid initial phase of maximum dye removal followed later by a slower removal phase.

11.7

Conclusions and Future Work

Nanoparticulate systems can serve as an ideal carrier system for drugs used in tumor imaging and PDT. By forming a wall around the drug they contain, nanoparticles can effectively protect the drug from the altering effects of the surrounding aqueous environment and from potential degradation by light and temperature. Taking advantage of the leaky vasculature of tumors, nanoparticles can enhance the passive uptake into and ultimate accumulation of antitumor drugs at the target site by an enhanced permeation and retention effect. Furthermore, in comparison to a drug solution, nanoparticles can provide a longer half-life and retention of a drug in the body due to their size and surface characteristics. Finally, nanoparticulates loaded with photoactive antitumor drugs can show photodynamic activity in tumor cells.

We have shown the feasibility of manufacturing PLGA nanoparticles of ICG with good potential as an agent for the diagnosis and treatment of tumors. These nanoparticles should be viewed primarily as a foundation for the development of new nanoparticles with improved pharmaceutical and therapeutic features. In pursuit of this goal, future work on this area will be addressed to, among other things, compare different types of PLGA (e.g. 25/75, 30/70, 75/25) for their suitability in manufacturing ICG nanoparticles with enhanced entrapment efficiency and dye content. Another idea worthy of a future investigation is to test polymeric materials such as albumin, chitosan, and PEGs (including PEG 2000, 5000 and 20000). In an effort to minimize the opsonization of the nanoparticles *in vivo* and, hence, to prolong the plasma half-life of ICG, the application of an external coating with a hydrophilic polymer may be warranted. Furthermore, to magnify the selectivity of the nanoparticles to particular target sites, one could explore the possibility of modifying the nanoparticle surface by the attachment of antibodies and other types of ligands with the ability to interact with specific types of tumors.

Another important aspect of nanotechnology applied to drug delivery using polymeric nanoparticles that will need to be considered is the scale-up of the production from the laboratory to an industrial scale, with particular attention to uniformity of particle size, reproducible solute entrapment efficiency and stability on storage under a variety of environmental conditions. Efforts will need to be directed to investigating the porosity characteristics of the nanoparticle surface (including pore size, pore shape and number of pores per surface area) and its relevance to solute release in a biological environment. In addition, to reduce the dose of ICG as ICG nanoparticles for applications like imaging and PDT, future developmental work on this type of formulation should concentrate in finding ways to enhance the fluorescence signal of a dye after undergoing intracellular uptake. The use of nanoparticles containing both silver ions and ICG is an attractive alternative that merits future consideration.

At the cellular level, a vast amount of work remains to be carried out with ICG nanoparticles using cell culture systems. In this regard, the use of new tumor cell lines will provide a better picture of the type of cancers that can be treated with ICG, especially cell lines of breast and skin cancers. The effectiveness of PDT for each of the cancer cell lines will only be established by evaluating the effects of critical factors such as light dose and ICG dose, which will eventually have to be optimized. A detailed investigation will have to be conducted to elucidate the mechanism of PDT activity on different tumor cell lines and the role of singlet oxygen in this process. The location of nanoparticles in the cell, their movement within the cells and the delivery of the nanoparticle contents to various cell organelles are also important subjects for future studies.

To more accurately define the biodistribution patterns and pharmacokinetic profiles of ICG delivered as nanoparticles, further investigation of this type of formulation could be done in higher animal models such as the rat and rabbit. Furthermore, testing the nanoparticles in tumor-bearing animal models will provide us with a clearer picture of the therapeutic and diagnostic effectiveness of the nanoparticles under more realistic conditions, particularly as it relates to tumor imaging

and PDT applications. Again, the results of these studies will be of great help in optimizing the test formulations.

References

- 1 SHEN, Y., FRIEND, C. S., JIANG, Y., JAKUBCZYK, J., PRASAD, P. N., Nanophotonics: interactions, materials and applications, *J. Phys. Chem.* **2000**, *104*, 7577–7587.
- 2 KROLL, R. A., PAGEL, M. A., MULDOON, L. L., ROMAN-GOLDSTEIN, S., FIAMENGO, S. A., NEUWELT, E. A., Improving drug delivery to intercerebral tumor and surrounding brain in a rodent model: a comparison of osmotic versus bradykinin modification of the blood–brain and/or blood–tumor barriers, *Neurosurgery* **1998**, *43*, 879–886.
- 3 SAXENA, V., SADOQI, M., SHAO, J., KUMAR, S., Tiny bubbles, *SPIE's OE Mag (Special Focus): Biotechnology* **2004**, *Sept*, 21–23.
- 4 TOMALIA, D. A., BAKER, H., DEWALD, J., HALL, M., KALLOS, G., MARTIN, S., ROECK, J., RYDER, J., SMITH, P., A new class of polymers: starburst-dendritic macromolecules, *Polym. J.* **1985**, *17*, 117–132.
- 5 TOMALIA, D. A., NAYLOR, A. M., GODDARD III, W. A., Starburst dendrimers: molecular-level control of size, shape, surface chemistry, topology, and flexibility from atoms to macroscopic matter, *Angew. Chem. Int. Ed.* **1990**, *29*, 138–175.
- 6 FRECHET, J. M. J., HAWKER, C. J., WOOLEY, K. L., The convergent route to globular dendritic macromolecules – a versatile approach to precisely functionalized 3-dimensional polymers and novel block-copolymers, *J. Macromol. Sci. Pure Appl. Chem.* **1994**, *A31*, 1627–1645.
- 7 ZIMMERMAN, S. C., ZENG, F., REICHERT, D. E. C., KOLOTUCHIN, S. V., Self-assembling dendrimers, *Science* **1996**, *271*, 1095–1098.
- 8 FRECHET, J. M. J., Functional polymers and dendrimers: reactivity, molecular architecture, and interfacial energy, *Science* **1994**, *263*, 1710–1715.
- 9 MEIJER, E. W., Macro-organische chemie, supramoleculaire architectuur van functionele materialen, *Chem. Mag.* **1994**, *May*, 2002–2005.
- 10 WENDLAND, M. S., ZIMMERMAN, S. C., Synthesis of cored dendrimers, *J. Am. Chem. Soc.* **1999**, *121*, 1389–1390.
- 11 WEBER, S., Application of the five-dimensional maximum entropy method to the structure refinement of decagonal Al–Mn–Pd quasicrystals, *Doctoral thesis*, University of Tsukuba, Japan, **1997**.
- 12 WEI, B. Q., VAJTAI, R., AJAYAN, P. M., Reliability and current carrying capacity of carbon nanotubes, *Appl. Phys. Lett.* **2001**, *79*, 1172.
- 13 O'CONNELL, M. J., BACHILO, S. M., HUFFMAN, C. B., MOORE, V. C., STRANO, M. S., RIALON, K. L., BOUL, P. J., NOON, W. H., KITRELL, C., MA, J. P., HAUGE, R. H., WEISMAN, R. B., SMALLEY, R. E., Band gap fluorescence from individual single-walled carbon nanotubes, *Science* **2002**, *297*, 593–596.
- 14 HERTEL, T., FASEL, R., MOOS, G., Charge-carrier dynamics in single-wall carbon nanotube bundles: a time-domain study, *Appl. Phys. A Mater. Sci. Process.* **2002**, *75*, 449–465.
- 15 LAURET, J. S., VOISIN, C., CASSABOIS, G., DELALANDE, C., ROUSSIGNOL, Ph., JOST, O., CAPES, L., Ultrafast carrier dynamics in single-wall carbon nanotubes, *Phys. Rev. Lett.* **2003**, *90*, 057404.
- 16 BAKER, S. E., LASSETER, T. L., SMITH, L. M., HAMERS, R. J., Covalently bonded adducts of deoxyribonucleic acid (DNA) oligonucleotides with single-wall carbon nanotubes: synthesis and hybridization, *Nano Lett.* **2002**, *2*, 1413–1417.
- 17 STRANO, M. S., Probing chiral selective reactions using a revised Kataura plot

- for the interpretation of single-walled carbon nanotube. *J. Am. Chem. Soc.* **2003**, *125*, 16148–53.
- 18 BALLOU, B., ERNST, L. A., WAGGONER, A. S., Fluorescence imaging of tumors *in vivo*, *Curr. Med. Chem.* **2005**, *12*, 795–805.
 - 19 VOURA, E. B., JAISWAL, J. K., MATTOUSSI, H., SIMON, S. M., Tracking metastatic tumor cell extravasation with quantum dot nanocrystals and fluorescence, emission-scanning microscope, *Nat. Med.*, **2004**, *10*, 993–998.
 - 20 JONES, M. C., LEROUX, J. C., Polymeric micelles – a new generation of colloidal drug carriers, *Eur. J. Pharm. Biopharm.* **1999**, *48*, 101–11.
 - 21 NOSTRUM, C. F., Polymeric micelles to deliver photosensitizers for photodynamic therapy, *Adv. Drug Deliv. Rev.* **2004**, *56*, 9–16.
 - 22 LASIC, D. D., Doxorubicin in sterically stabilized liposomes, *Nature* **1996**, *381*, 630–630.
 - 23 KIM, S., Liposomes as carriers of cancer chemotherapy: current status and future prospects, *Drugs* **1993**, *46*, 618–638.
 - 24 DERYCKE, A. S. L., DE WITTE, P. A. M., Liposomes for photodynamic therapy, *Adv. Drug Deliv. Rev.* **2004**, *56*, 17–30.
 - 25 SOPPIMATH, K. S., AMINABHAVI, T. M., KULKARNI, A. R., RUDZINSKI, W. E., Biodegradable polymeric nanoparticles as delivery devices, *J. Controlled Rel.* **2001**, *70*, 1–20.
 - 26 COUVREUR, P., KANTE, B., LENAERTS, V., SCAILTEUR, V., ROLAND, M., SPEISER, P., Tissue distribution of antitumor drugs associated with polyalkylcyanoacrylate nanoparticles, *J. Pharm. Sci.* **1980**, *69*, 199–202.
 - 27 ROLLAND, A., Clinical pharmacokinetics of doxorubicin in hepatoma patients after a single intravenous injection of free or nanoparticle-bound anthracycline, *Int. J. Pharm.* **1989**, *54*, 113–121.
 - 28 LEROUX, J. C., DOELKER, E., GURNY, R., The use of drug-loaded nanoparticles in cancer chemotherapy, In *Microencapsulation: Methods and Industrial Applications*, BENITA, S. (Ed.), Marcel Dekker, New York, **1996**, pp. 535–575.
 - 29 MONSKY, W. L., FUKUMURA, D., GOHONGI, T., ANCUKIEWCZ, M., WEICH, H. A., TORCHILIN, V. P., YUAN, F., JAIN, R. K., Augmentation of transvascular transport of macromolecules and nanoparticles in tumors using vascular endothelial growth factor, *Cancer Res.* **1999**, *59*, 4129–4135.
 - 30 BENNIS, S., CHAPEY, C., COUVREUR, P., ROBERT, J., Enhanced cytotoxicity of doxorubicin encapsulated in polyisohexylcyanoacrylate nanospheres against multidrug-resistant cells in culture, *Eur. J. Cancer* **1994**, *30*, 89–93.
 - 31 ROWINSKY, E. K., and DONEHOWER, R. C., Drug therapy: paclitaxel, *N. Engl. J. Med.* **1995**, *332*, 1004–1014.
 - 32 MAGENHEIM, B., and BENITA, S., Nanoparticle characterization: a comprehensive physicochemical approach, *STP Pharma Sci.* **1991**, *1*, 221–241.
 - 33 MU, L., FENG, S. S., A novel controlled release formulation for the anticancer drug paclitaxel (Taxol®): PLGA nanoparticles containing vitamin E TPGS, *J. Controlled Rel.* **2003**, *86*, 33–48.
 - 34 BRIGGER, I., DUBERNET, C., COUVREUR, P., Nanoparticles in cancer therapy and diagnosis, *Adv. Drug Deliv. Rev.* **2002**, *54*, 631–651.
 - 35 VERDUN, C., BRASSEUR, F., VRANOKX, H., COUVREUR, P., ROLAND, M., Tissue distribution of doxorubicin associated with polyisohexylcyanoacrylate nanoparticles, *Cancer Chemother. Pharmacol.* **1990**, *26*, 13–18.
 - 36 SIMEONOVA, M., ILARIONOVA, M., IVANOVA, T., KONSTANTINOV, C., TODOROV, D., Nanoparticles as drug carriers for vinblastine. Acute toxicity of vinblastine in a free form and associated to polybutylcyanoacrylate nanoparticles, *Acta Physiol. Pharmacol. Bulg.* **1991**, *17*, 43–49.
 - 37 BECK, P., KREUTER, J., RESZKA, R., FICHTNER, I., Influence of polybutylcyanoacrylate nanoparticles and liposomes on the efficacy and toxicity of the anticancer drug mitoxantrone in

- murine tumor models, *J. Microencapsul.* **1993**, *10*, 101–114.
- 38 MOGHIMI, M. S., HUNTER, C. A., MURRAY, C. J., Long-circulation and target-specific nanoparticles: theory to practice, *Pharmacol. Rev.*, **2001**, *53*, 283–318.
- 39 ANDERSON, J. M., SHIVE, M. S., Biodegradation and biocompatibility of PLA and PLGA microspheres, *Adv. Drug Deliv. Rev.* **1997**, *28*, 5–24.
- 40 HANAFUSA, S., MATSUSUE, YASUNAGA, T., YAMMAMURO, T., OKA, M., SHIKINAMI, Y., IKADA, Y., Biodegradable plate fixation of rabbit femoral shaft osteotomies. A Comparative study, *Clin. Orthop.* **1995**, *315*, 262–271.
- 41 MATSUSUE, Y., HANAFUSA, S., YAMMAMURO, T., SHIKINAMI, Y., IKADA, Y., Tissue reaction of biodegradable ultra high strength poly(L-lactide) rod. A long-term study in rabbits, *Clin. Orthop.* **1995**, *317*, 246–253.
- 42 LANGER, R., Tissue engineering: a new field and its challenges, *Pharm. Res.* **1997**, *14*, 840–841.
- 43 MOONEY, D. J., SANO, K., KAUMANN, P. M., MAJAHOD, K., SCHLOO, B., VACANTI, J. P., LANGER, R., Engraftment of hepatocytes transplanted on biodegradable polymer sponges, *J. Biomed. Mater. Res.* **1997**, *37*, 413–420.
- 44 EISELT, P., KIM, B. S., CHACKO, B., ISENBERG, B., PETERS, M. C., GREENE, K. G., ROLAND, W. D., LOEBSACK, A. B., BURG, K. J., CULBERSON, C., HALBERSTADT, C., HOLDER, W. D., MOONEY, D. J., Development of technologies aiding large-tissue engineering, *Biotechnol. Progr.* **1998**, *14*, 134–140.
- 45 GURNY, R., PEPPAS, N. A., HARRINGTON, D. D., BANKER, G. S., Development of biodegradable and injectable lattices for controlled release of potent drugs, *Drug Dev. Ind. Pharm.* **1981**, *7*, 1–25.
- 46 BINDSCHAELDER, C., LEONG, K., MATHIOWITZ, E., LANGER, R., Polyhydride microsphere formulation by solvent-extraction, *J. Pharm. Sci.* **1988**, *77*, 696–698.
- 47 FESSI, H., PUISIEUX, F., DEVISSAGUET, J. P., AMMOURY, N., BENITA, S., Nanocapsule formation by interfacial polymer deposition following solvent displacement, *Int. J. Pharm.* **1989**, *55*, R1–R4.
- 48 ZHANG, X., WISS, U. P., PICHORA, D., GOOSSEN, M. F., A mechanistic study of antibiotic release from biodegradable poly(D,L-lactide) cylinders, *J. Controlled Rel.* **1994**, *31*, 128–144.
- 49 O'HARA, P., HICKNEY, A. J., Respirable PLGA microspheres containing rifampicin for the treatment of tuberculosis: manufacture and characterization, *Pharm. Res.* **2000**, *17*, 955–961.
- 50 KOMPELLA, U. B., KOUSHIK, K., Preparation of drug delivery systems using supercritical fluid technology, *Crit. Rev. Ther. Drug. Carrier Syst.* **2001**, *18*, 2173–2199.
- 51 JAIN, R. A., The manufacturing techniques of various drug loaded biodegradable poly(lactide-co-glycolide) devices, *Biomaterials* **2000**, *21*, 2475–2490.
- 52 O'DONNELL, P. B., MCGINITY, J. W., Preparation of microspheres by the solvent evaporation technique, *Adv. Drug Deliv. Rev.* **1997**, *28*, 25–42.
- 53 MURAKAMI, H., KOBAYASI, M., TAKEUCHI, H., KAWASHIMA, Y., Preparation of poly(DL-lactide-co-glycolide) nanoparticles by modified spontaneous emulsification solvent diffusion method, *Int. J. Pharm.* **1999**, *187*, 143–152.
- 54 CLELAND, J. L., JONES, A. J. S., Stable formulations of recombinant human growth hormone and interferon-gamma for microencapsulation in biodegradable microspheres, *Pharm. Res.* **1996**, *13*, 1464–1475.
- 55 SCHOLLES, P. D., COOMBS, A. G. A., ILLUM, L., DAVIS, S. S., WATTS, J. F., USTARIZ, C., VERT, M., DAVIS, M. C., Detection and determination of surface levels of proloxamer and PVA surfactant on biodegradable nanospheres using SSIMS and XPS, *Int. J. Pharm.* **1999**, *59*, 261–278.
- 56 FENG, S., HUANG, G., Effects of emulsifiers on the controlled release

- of paclitaxel (taxol) from nanospheres of biodegradable polymers, *J. Controlled Rel.* **2001**, *71*, 53–69.
- 57 VANDERVOORT, J., LUDWIG, A., Biocompatible stabilizers in the preparation of PLGA nanoparticles: a factorial design study, *Int. J. Pharm.* **2002**, *238*, 77–92.
- 58 GREF, R., MINAMITAKE, Y., PERACCHIA, M. T., TRUBETSKOY, V., TORCHILIN, V., LANGER, R., Biodegradable long-circulating polymeric nanospheres, *Science* **1994**, *263*, 1600–1603.
- 59 STOLNIK, S., FELUMB, N. C., HEALD, C. R., GARNETT, M. C., ILLUM, L., DAVIS, S. S., Adsorption behavior and conformation of selected poly(ethylene oxide) copolymers on the surface of a model colloidal drug carrier, *Colloids Surfaces A: Physicochem. Eng. Aspects* **1997**, *122*, 151–159.
- 60 TOBIO, M., GREF, R., SANCHEZ, A., LANGER, R., ALONSO, M. J., Stealth PLA–PEG nanoparticles a protein carriers for nasal administration, *Pharm. Res.* **1998**, *1*, 270–275.
- 61 THOMAS, G. M., Improved treatment for cervical cancer – concurrent chemotherapy and radiotherapy, *N. Engl. J. Med.* **1999**, *340*, 1198–1200.
- 62 WHARTON, J. T., TORTOLERO-LUNA, G., Neoplasms of the cervix, In *Cancer Medicine*, BAST, R. C., KUFFE, D. W., POLLOCK, R. E., WEICHSELBAUM, R. R., HOLLAND, J. F., FREI, E. (Eds.), BC Decker, Hamilton, **2000**, pp. 1631–1666.
- 63 EIFEL, P. J., BEREK, J. S., THIGPEN, J. T., Cancer of the cervix, vagina, and vulva, In *Cancer: Principles and Practice of Oncology*, DeVITA, V. T., HELLMAN, S., ROSENBERG, S. A. (Eds.), Lippincott Williams & Wilkins, Philadelphia, PA, **2001**, pp. 1526–1572.
- 64 FIELDS, A. L., JONES, J. G., THOMAS, G. N., RUNOWICZ, C. D., Gynecologic cancer, In *Clinical Oncology*, LENHARD, R. E., OSTEEEN, R. T., GANSLER, T. (Eds.), American Cancer Society, Atlanta, GA, **2001**, pp. 455–496.
- 65 STECKEL, R. J., Principles of imaging, In *Cancer Medicine*, BAST, R. C., KUFFE, D. W., POLLOCK, R. E., WEICHSELBAUM, R. R., HOLLAND, J. F., FREI, E. (Eds.), BC Decker, Hamilton, **2000**, pp. 400–439.
- 66 YARBRO, C. H., FROGGE, M., GOODMAN, M., GROENWALD, S. L. (Eds.), *Cancer Nursing: Principles and Practice*, 5th edn., Jones and Bartlett, Sudbury, MA, **2000**.
- 67 COLEMAN, R. E., TESAR, R. D., Diagnostic aspects of radiopharmaceuticals. In *Radiopharmaceuticals in the Diagnosis and Treatment of Cancer, Oncol. Issues (Suppl.)* **2001**, *16*, 7–8.
- 68 FISHMAN, E. K., URBAN, B. A., Cancer diagnosis: imaging, In *Cancer: Principles and Practice of Oncology*, DeVITA, V. T., HELLMAN, S., ROSENBERG, S. A. (Eds.), Lippincott Williams & Wilkins, Philadelphia, PA, **2001**, pp. 659–720.
- 69 MORRA, M., POTTS, E., *Choices*, Avon Books, New York, **1994**.
- 70 DOLLINGER, M., ROSENBAUM, E. H., CABLE, G., *Everyone's Guide to Cancer Therapy*, 3rd edn., Somerville House Books, Toronto, **1997**.
- 71 RUNOWICZ, C. D., PETREK, J. A., GANSLER, T. S., *Women and Cancer*, Villard, New York, **1999**.
- 72 ABELOFF, M. D., ARMITAGE, J. O., LICHTER, A. S., NIEDERHUBER, J. E., *Clinical Oncology*, 2nd edn., Churchill Livingstone, Philadelphia, PA, **2000**.
- 73 DeVITA, JR. V. T., HELLMAN, S., ROSENBERG, S. A. (Eds.), *Cancer: Principles and Practice of Oncology*, Lippincott Williams & Wilkins, Philadelphia, PA, **2001**.
- 74 MURPHY, G. P., MORRIS, L. B., LANGE, D., *Informed Decisions: The Complete Book of Cancer Diagnosis, Treatment, and Recovery*, 2nd edn., American Cancer Society, Viking Press, New York, **2002**.
- 75 VARRICCHIO, C., PIERCE, M., WALTER, C. L., ADES, T. B., *A Cancer Source Book for Nurses*, 7th edn., American Cancer Society, Atlanta, GA, **1977**.
- 76 COOPER, G. M., *The Cancer Book: A Guide to Understanding The Causes, Prevention, and Treatment of Cancer*, Jones and Bartlett, Boston, MA, **1993**.

- 77 BURKE, M. B., WILKES, G. M., INGWERSEN, K., BEAN, C. K., BERG, D., A nursing process approach, In *Cancer Chemotherapy*, 2nd edn., Jones and Bartlett, Boston, MA, 1996.
- 78 GUY, J. L., INGRAM, B. A., Medical oncology: the agents, In *Cancer Nursing: A Comprehensive Textbook*, MCCORKLE, R., GRANT, M., FRANK-STROMBORG, M., BAIRD, S. B. (Eds.), Saunders, Philadelphia, PA, 1996, pp. 359–394.
- 79 CAMP-SORRELL, D., Chemotherapy: toxicity management, In *Cancer Nursing: Principles and Practice*, 4th edn., GROENWALD, S. L., FROGGE, M. H., GOODMAN, M., YARBRO, C. H. (Eds.), Jones and Bartlett, Boston, MA, 1997, pp. 387–425.
- 80 GOODMAN, M., RILEY, M. B., Chemotherapy: principles of administration, In *Cancer Nursing: Principles and Practice*, 4th edn., GROENWALD, S. L., FROGGE, M. H., GOODMAN, M., YARBRO, C. H. (Eds.), Jones and Bartlett, Boston, MA, 1997, pp. 31–386.
- 81 TROTICE, P. V., Chemotherapy: principles of therapy, In *Cancer Nursing: Principles and Practice*, 4th edn., GROENWALD, S. L., FROGGE, M. H., GOODMAN, M., YARBRO, C. H. (Eds.), Jones and Bartlett, Boston, MA, 1997, pp. 283–316.
- 82 YASKO, J. M., *Nursing Management of Symptoms Associated with Chemotherapy*, Meniscus Health Care Communications, Bala Cynwyd, PA, 1998.
- 83 LABRIOLA, D., LIVINGSTON, R., Possible interactions between dietary antioxidants and chemotherapy, *Oncology* 1999, 13, 1003–1008.
- 84 MOSS, W. T., COX, J. D., *Radiation Oncology: Rationale, Technique, Results*, Mosby, St. Louis, MO, 1994.
- 85 COIA, L., MOYLAN, D., *Introduction to Clinical Radiation Oncology*, 3rd edn., Medical Physics Publishing, Madison, WI, 1998.
- 86 PEREZ, C. A., BRADY, L. W., *Principles and Practice of Radiation Oncology*, 3rd edn., Lippincott-Raven, Philadelphia, PA, 1998.
- 87 STROHL, R., Radiation therapy, In *Oncology Nursing: Assessment & Clinical Care*, MIASKOWSKI, C., BUCHSEL, P. (Eds.), Mosby, St. Louis, MO, 1999, pp. 59–81.
- 88 RIETHMULLER, G., SCHNEIDER-GADICKE, E., SCHLIMOK, G., Randomised trial of monoclonal antibody for adjuvant therapy of resected Dukes' C colorectal carcinoma, *Lancet* 1994, 14, 1177–1183.
- 89 CANEVARI, S., STOTER, G., ARIENTI, F., Regression of advanced ovarian carcinoma by intraperitoneal treatment with autologous T lymphocytes retargeted by a bispecific monoclonal antibody, *J. Natl Cancer Inst.* 1995, 87, 1463–1469.
- 90 DISIS, M. L., GRABSTEIN, K. H., SLEATH, P. R., CHEEVER, M. A., Generation of immunity to the HER-2 *neu* oncogenic protein in patients with breast and ovarian cancer using a peptide-based vaccine, *Clin. Cancer Res.* 1999, 5, 1289–1297.
- 91 FOON, K. A., CHAKRABORTY, M., JOHN, W. J., SHERRATT, A., KOHLER, H., BHATTACHARYA-CHATTERJEE, M., Immune response to the carcino-embryonic antigen in patients treated with an anti-idiotypic antibody vaccine, *J. Clin. Invest.* 1995, 96, 334–342.
- 92 FUJITA, K., IKARASHI, H., TAKAKUWA, K., Prolonged disease-free period in patients with advanced epithelial ovarian cancer after adoptive transfer of tumor-infiltrating lymphocytes, *Clin. Cancer Res.* 1995, 501–507.
- 93 HSU, F. J., CASPAR, C. B., CZERWINSKI, D., Tumor-specific idiotype vaccines in the treatment of patients with B-cell lymphoma long-term results of a clinical trial, *Blood* 1997, 89, 3129–3135.
- 94 TOURANI, J. M., PFISTER, C., BERDAH, J. F., Outpatient treatment with subcutaneous interleukin-2 and interferon alfa administration in combination with fluorouracil in patients with metastatic renal cell carcinoma: results of a sequential nonrandomized phase II study, *J. Clin. Oncol.* 1998, 16, 2505–2513.

- 95 GEZ, E., MEKORI, T., STRUMINGER, L., T-cell subpopulation in patients with metastatic renal cell carcinoma treated by recombinant interleukin-2, recombinant interferon-alpha, 5-fluorouracil, and vinblastine, *Cancer Invest.* **1999**, *17*, 259–263.
- 96 GRETEN, T. F., JAFFEE, E. M., Cancer vaccines, *J. Clin. Oncol.* **1999**, *17*, 1047–1060.
- 97 HADDEN, J. W., The immunology and immunotherapy of breast cancer: an update, *Int. J. Immunopharmacol.* **1999**, *21*, 79–101.
- 98 HEMILLA, M. R., CHANG, A. E., Clinical implications of the new biology in the development of melanoma vaccines, *J. Surg. Oncol.* **1999**, *70*, 263–274.
- 99 HSUEH, E. C., NATHANSON, L., FOSHAG, L. J., Active specific immunotherapy with polyvalent melanoma cell vaccine for patients with in-transit melanoma metastases, *Cancer* **1999**, *85*, 2160–2169.
- 100 SANDMAIER, B. M., OPARIN, D. V., HOLMBERG, L. A., REDDISH, M. A., MACLEAN, G. D., LONGENECKER, B. M., Evidence of a cellular immune response against sialyl-Tn in breast and ovarian cancer patients after high-dose chemotherapy, stem cell rescue, and immunization with Theratope STn-KLH cancer vaccine, *J. Immunother.* **1999**, *22*, 54–66.
- 101 TJOA, B. A., SIMMONS, S. J., ELGAMAL, A., Follow-up evaluations of a phase II prostate cancer vaccine trial, *Prostate* **1999**, *40*, 125–129.
- 102 BAST, R. C., ZALUTSKY, M. R., KREITZMAN, R. J., SAUSVILLE, E. A., FRANKEL, A. R., Monoclonal serotherapy, In *Cancer Medicine*, BAST, R. C., KUFU, D. W., POLLOCK, R. E., WEICHELBAUM, R. R., HOLLAND, J. F., FREI, E. (Eds.), 5th edn., Williams & Wilkins, Baltimore, MD, **2000**, pp. 860–875.
- 103 GRIMM, E. A., Cytokines: biology and applications in cancer medicine, In *Cancer Medicine*, BAST, R. C., KUFU, D. W., POLLOCK, R. E., WEICHELBAUM, R. R., HOLLAND, J. F., FREI, E. (Eds.), 5th edn., Williams & Wilkins, Baltimore, MD, **2000**, pp. 825–834.
- 104 RAVINDRANTH, M. H., MORTON, D. L., Active specific immunotherapy with vaccines, In *Cancer Medicine*, BAST, R. C., KUFU, D. W., POLLOCK, R. E., WEICHELBAUM, R. R., HOLLAND, J. F., FREI, E. (Eds.), 5th edn., Williams & Wilkins, Baltimore, MD, **2000**, pp. 800–814.
- 105 SALGALLER, M. L., Immune adjuvants, In *Principles and Practice of the Biologic Therapy of Cancer*, ROSENBERG, S. A. (Ed.), 3rd edn., Lippincott Williams & Wilkins, Philadelphia, PA, **2000**, 584–601.
- 106 KREITZMAN, R. J., WILSON, W. H., BERGERON, K., Efficacy of the anti-CD22 recombinant immunotoxin BL22 in chemotherapy-resistant hairy-cell leukemia, *N. Engl. J. Med.* **2001**, *345*, 241–247.
- 107 RESTIFO, N. P., SZYNOL, M., OVERWIJK, W. W., Therapeutic cancer vaccines, In *Cancer: Principles and Practice of Oncology*, DeVITA, V. T., HELLMAN, S., ROSENBERG, S. A. (Eds.), Lippincott Williams & Wilkins, Philadelphia, PA, **2001**, pp. 3195–3217.
- 108 DUDLEY, M. E., WUNDERLICH, J. R., ROBBINS, P. F., YANG, J. C., HWU, P., SCHWARTZENTRUBER, D. J., TOPALIAN, S. L., SHERRY, R., RESTIFO, N. P., HUBICKI, A. M., ROBINSON, M. R., RAFFELD, M., DURAY, P., SEIPP, C. A., ROGERS-FREEZER, L., MORTON, K. E., MAVROUKAKIS, S. A., WHITE, D. E., ROSENBERG, S. A., Cancer regression and autoimmunity in patients after clonal repopulation with antitumor lymphocytes, *Science* **2002**, *298*, 850–854.
- 109 PAZDUR, R., COIA, L. R., HOSKINS, W. J., WAGMAN, L. D., *Cancer Management: A Multidisciplinary Approach, Medical Surgical and Radiation Oncology*, PRR, Huntington, NY, **1996**.
- 110 LENHARD, R. E., OSTEEN, R. T., GANSLER, T. (Eds.), *Clinical Oncology*, American Cancer Society, Atlanta, GA, **2001**.
- 111 EYRE, H. J., LANGE, D., MORRIS, L. B., *Informed Decisions*, 2nd edn.,

- American Cancer Society, Atlanta, GA, 2002.
- 112 GAYEN, S. K., ALFANO, R. R., Emerging biomedical imaging techniques, *Opt. Photon. News* **1996**, *7*, 17–22.
- 113 PRASAD, P. N., *Introduction to Biophotonics*, 1st edn., Wiley-Interscience, New York, 2003.
- 114 MITRA, K., KUMAR, S., Development and comparison of models for light pulse transport through scattering-absorbing media, *Appl. Optics* **1999**, *38*, 188–196.
- 115 GUO, Z., ABER, J., GARETZ, B., KUMAR, S., Monte Carlo Simulation and experiments of pulsed radiative transfer, *J. Quant. Spec. Radiat. Transfer* **2002**, *73*, 159–168.
- 116 WAN, S. K., GUO, Z., KUMAR, S., ABER, J., GARETZ, B. A., Noninvasive detection of inhomogeneities in turbid media with time-resolved log-slope analysis, *J. Quant. Spec. Radiat. Transfer* **2004**, *84*, 493–500.
- 117 SADOQI, M., RISEBORO, P., KUMAR, S., Analytical models for pulse laser fluorescence imaging in tissues, *Phys. Med. Biol.* **2001**, *46*, 2725–2743.
- 118 GAYEN, S. K., ZEVALLOS, M. E., AERUBAIEE, M., ALFANO, R. R., Near-infrared laser spectroscopic imaging: a step towards diagnostic optical imaging of human tissue, *Laser Life Sci.* **1999**, *98*, 187–198.
- 119 LAKOWICZ, J. R., *Principles of Fluorescence Spectroscopy*, 2nd edn., Kluwer, New York, NY, 1999.
- 120 THOMPSON, R. B., Red and near-infrared fluorometry, In *Topics in Fluorescence Spectroscopy 4: Probe Design and Chemical Sensing*, LAKOWICZ, J. R. (Ed.), Plenum Press, New York, NY, 1994, 151–222.
- 121 LEZNOFF, C. C., LEVER, A. B. P., *Phthalocyanines: Properties and Applications*, VCH, New York, NY, 1989.
- 122 MATSUOKA, M., *Infrared Absorbing Dyes*, Plenum Press, New York, NY, 1990.
- 123 RAHAVENDRAN, S. V., KARNES, H. T., Application of rhodamine 800 for reversed phase liquid chromatographic detection using visible diode laser induced fluorescence, *Anal. Chem.* **1996**, *68*, 3763–3768.
- 124 FLANAGAN, J. H., ROMERO, S. E., LEGENDRE, B. L., HAMMER, R. P., SOPER, A., Heavy-atom modified near-IR fluorescent dyes for DNA sequencing applications: synthesis and photophysical characterization, *SPIE Proc.* **1997**, *2980*, 328–337.
- 125 OWENS, C. V., DAVIDSON, Y. Y., KAR, S., SOPER, S. A., High-resolution separation of DNA restriction fragments using capillary electrophoresis with near-IR diode-based, laser-induced fluorescence detection, *Anal. Chem.* **1997**, *69*, 1256–1261.
- 126 SOUTHWICK, P. L., ERNST, L. A., TAURIELLO, E. W., PARKER, S. R., MAJUMDAR, R. B., MAJUMDAR, S. W., CLEVER, H. A., WAGGONER, A., Cyanine dye labeling reagents – carboxymethylindocyanine succinimidyl esters, *Cytometry* **1990**, *11*, 418–430.
- 127 HENDERSON, B., DOUGHERTY, T., How does photodynamic therapy work?, *J. Photochem. Photobiol. B Biol.* **1992**, *55*, 145–157.
- 128 FISHER, A. M. R., MURPHREE, A. L., GOMER, C. J., Clinical and preclinical photodynamic therapy, In *Laser Surgery and Medicine*, PULIAFITO, C. A. (Ed.), Wiley-Liss, New York, NY, 1996, pp. 339–368.
- 129 BHAWALKAR, J. D., KUMAR, N. D., ZHAO, C. F., PRASAD, P. N., Two-photodynamic therapy, *J. Clin. Laser Med. Surg.* **1997**, *15*, 201–204.
- 130 OCHSNER, M., Photophysical and photobiological processes in the photodynamic therapy of tumors, *J. Photochem. Photobiol. B Biol.* **1997**, *39*, 1–18.
- 131 SCHMIDT-ERFURTH, U., HASAN, T., Mechanisms of action of photodynamic therapy with Verteporfin for the treatment of age-related macular degeneration, *Surv. Ophthalmol.* **2000**, *45*, 195–214.
- 132 KONAN, Y. N., GURNY, R., ALLEMANN, E., State of the art in the delivery of photosensitizers for photodynamic therapy, *J. Photochem. Photobiol. B Biol.* **2001**, *66*, 89–106.

- 133 MORGAN, J., OSEROFF, A. R., Mitochondria based photodynamic anti-cancer therapy, *Adv. Drug Deliv. Rev.* **2001**, *49*, 71–86.
- 134 GORMAN, A. A., RODGERS, M. A. J., Current perspectives of singlet oxygen detection in biological environments, *J. Photochem. Photobiol. B Biol.* **1992**, *14*, 159–176.
- 135 BAUMLER, W., ABELS, C., KARRER, S., WEIB, T., MESSMANN, H., LANDTHALER, M., SZEIMIES, R. M., Photooxidative killing of human colonic cancer cells using indocyanine green and infrared light, *Br. J. Cancer* **1999**, *80*, 360–363.
- 136 JOHNSON, L. V., WALSH, M. L., BOCHUS, B. J., CHEN, L. B., Monitoring of relative mitochondrial membrane potential in living cells by fluorescence microscopy, *J. Cell Biol.* **1981**, *88*, 526–535.
- 137 DOUGHERTY, T. J., GOMER, C. J., HENDERSON, B. W., Photodynamic therapy, *J. Natl. Cancer Inst.* **1998**, *32*, 889–368.
- 138 STERNBERG, E. D., DOLPHIN, D., BROCKNER, C., Porphyrin-based photosensitizers for use in photodynamic therapy, *Tetrahedron* **1998**, *54*, 4151–4202.
- 139 MORGAN, A. R., GARBO, G. M., KECK, R. W., SELMAN, S. H., New photosensitizers for photodynamic therapy: combined effect of metallopyrin derivatives and light on transplantable bladder tumors, *Cancer Res.* **1998**, *48*, 194–198.
- 140 VOGTEL, F., Dendrimers, *Curr. Chem.* **1998**, *197*, 1–228.
- 141 COLUSSI, V. C., FEYES, D. K., MULIVHILL, J. W., Phthalocyanine 4 (Pc4) photodynamic therapy of human OVCAR-3 tumor xenografts, *Photochem. Photobiol.* **1999**, *69*, 236–241.
- 142 FISHER, M., VOGTEL, F., Dendrimers from design to applications: a progress report, *Angew. Chem. Int. Ed. Engl.* **1999**, *38*, 884–905.
- 143 HORNUNG, R., FEHR, M. K., MONTIFRAYNE, J., Highly selective targeting of ovarian cancer with the photosensitizer PEG–m-THPC in a rat model, *Photochem. Photobiol.* **1999**, *70*, 624–629.
- 144 SHARMAN, W. M., ALLEN, C. M., VAN LIER, JR. J. E., Photodynamic therapeutics, *Drug Discov. Today* **1999**, *4*, 507–517.
- 145 PANDEY, R. K., SUMLIN, A. B., CONSTANTINE, S., AOUA, M., POTTER, W. R., HENDERSON, B. W., RODGERS, M. A., DOUGHERTY, T. J., Alkyl ether analogs of chlorophyll-a derivatives, part 1: synthesis, photophysical properties and photodynamic efficacy, *Photochem. Photobiol.* **1996**, *64*, 194–204.
- 146 SESSLER, J. L., and MILLE, R. A., Texaphyrins – new drugs with diverse clinical applications in radiation and photodynamic therapy, *Biochem. Pharmacol.* **2000**, *59*, 733–739.
- 147 PIFFERI, A., TARONI, P., TORRICELLI, A., VALENTINI, G., COMELLI, D., D'ANDREA, C., ANGELINI, V., CANTI, G., Fluorescence imaging during photodynamic therapy of experimental tumors in mice sensitized with disulfonated aluminium phthalocyanine, *Photochem. Photobiol.* **2000**, *72*, 690–695.
- 148 BATTAH, S. H., CHEE, C. E., NAKANISHI, H., GERSCHER, S., MACROBERT, A. J., EDWARDS, C., Synthesis and biological studies of 5-aminolevulinic acid-containing dendrimers for photodynamic therapy, *Bioconjug. Chem.* **2001**, *12*, 980–988.
- 149 HACKBARTH, S., HORNEFFER, V., WIEHE, A., HILLENKAMP, F., and RÖDER, B., Photophysical properties of pheophorbide-a substituted diamino-butane polypropyleneamine imine dendrimer, *Chem. Phys.* **2001**, *269*, 339–346.
- 150 PHILIP, R., PENZKOFER, A., BAUMLER, W., SZEIMIES, R. M., and ABELS, C., Absorption and fluorescence spectroscopic investigation of indocyanine green, *J. Photochem. Photobiol. A Chem.* **1996**, *96*, 137–148.
- 151 MAAREK, J. M. I., HOLSCHNEIDER, D. P., HARIMOTO, J., Fluorescence of indocyanine green in blood: intensity dependence on concentration and stabilization with sodium poly-

- aspartate, *J. Photochem. Photobiol. B Biol.* **2001**, *65*, 157–164.
- 152** ZHOU, J. F., CHIN, M. P., SCHAFER, S. A., Aggregation and degradation of indocyanine green, In *Laser Surgery: Advanced Characterization, Therapeutics and Systems IV*, ANDERSON, R. (Ed.), SPIE, Bellingham, CA, **1994**, pp. 495–505.
- 153** KAMISAKA, K., YATSUJII, Y., YAMADA, H., KAMEDA, H., The binding of indocyanine green and other organic anions to serum proteins in liver diseases, *Clin. Chim. Acta* **1974**, *53*, 225–264.
- 154** BAKER, K. J., Binding of sulfobromophthalein (BSP) sodium and indocyanine green (ICG) by plasma alpha-1 lipoprotein, *Proc. Soc. Exp. Biol. Med.* **1966**, *122*, 957–963.
- 155** PAUMGARTNER, G., PROBST, P., KRAINES, R., and LEEVY, C. M., Kinetics of indocyanine green removal from the blood, *Ann. NY Acad. Sci.* **1970**, *170*, 134–147.
- 156** PAUMGARTNER, G., The handling of indocyanine green by the liver, *Schweiz. Med. Wochenschr.* **1975**, *105*, 1–30.
- 157** CHANG, A. A., MORSE, L. S., HANDA, J. T., Histologic localization of indocyanine green dye in aging primate and human ocular tissues with clinical angiographic correlation, *Ophthalmology* **1998**, *105*, 1060–1068.
- 158** MORDON, S., DEVOISSELLE, J. M., SOULIE-BEGU, S., DESMETTRE, T., Indocyanine green: physicochemical factors affecting its fluorescence *in vivo*, *Microvasc. Res.* **1998**, *55*, 146–152.
- 159** YONEYA, S., SAITO, T., KOMATSU, Y., KOYAMA, I., TAKAHASHI, K., DUVOLLYOUNG, J., Binding properties of indocyanine green in human blood, *Invest. Ophthalmol. Vis. Sci.* **1998**, *39*, 1286–1290.
- 160** YONEYA, S., NOYORI, K., Improved visualization of the choroidal circulation with indocyanine green angiography, *Arch. Ophthalmol.* **1993**, *111*, 1165–1166.
- 161** DESMETTRE, T., MORDAN, S., SOULIE, S., Shift of the fluorescence peak of Indocyanine green (ICG) after injection: *in vivo* study on a vascular model, *Invest. Ophthalmol. Vis. Sci.* **1996**, *36*, S1127.
- 162** DEVOISSELLE, J. M., MORDON, S., SOULIE, S., DESMETTRE, T., MAILLOLS, H. C., Fluorescence properties of indocyanine green, Part 1: *in vitro* study with micelles and liposomes, In *Advances in Fluorescence Sensing Technology III*, LAKOWICZ, J. R., THOMPSON, J. B. (Eds.), SPIE, Bellingham, CA, **1997**, pp. 530–537.
- 163** ITO, S., MUGURUMA, N., HAYASHI, S., Developments of agents for reinforcement of fluorescence on near-infrared ray excitation for immunohistological staining, *Bioorg. Med. Chem.* **1998**, *6*, 613–618.
- 164** CHERRICK, G. R., STEIN, S. W., LEEVY, C. M., DAVIDSON, C. S., Indocyanine green: observation on its physical properties, plasma decay and hepatic extraction, *J. Clin. Invest.* **1960**, *39*, 592–600.
- 165** HOLLINS, B., NOE, B., HENDERSON, J. M., Fluorometric determination of Indocyanine green in plasma, *Clin. Chem.* **1987**, *33*, 765–768.
- 166** McEVoy, G. K., *AHFS 97 Drug Information*, American Society of Health-System Pharmacists, Bethesda, MD, **1997**.
- 167** FLOCK, S. T., JACQUES, S. L., Thermal damage of blood vessels in a rat skin flap window chamber using ICG and a pulsed alexandrite laser: a feasibility study, *Laser Med. Sci.* **1993**, *8*, 185–196.
- 168** VILLENEUVE, J. P., HUOT, R., MARLEAU, D., HUET P. M., The estimation of hepatic blood flow with Indocyanine green: comparison between the continuous infusion and single injection methods, *Am. J. Gastroenterol.* **1982**, *77*, 233–237.
- 169** BOLLINGER, A., SAESSELL, B., HOFFMANN, U., FRANZECK, U. K., Intravital detection of skin capillary aneurysms by videomicroscopy with indocyanine green in patients with progressive systemic sclerosis and related disorders, *Circulation* **1991**, *83*, 546–551.
- 170** OTT, P., KEIDING, S., JOHNSEN, A. H.,

- Bass, L., Hepatic removal of two fractions of indocyanine green after bolus injections in anesthetized pigs, *Am. J. Physiol.* **1994**, *266*, 1108–1122.
- 171 LUTTY, G. A., The acute intravenous toxicity of biological stains, dyes, and other fluorescent substances, *Toxicol. Appl. Pharmacol.* **1978**, *44*, 225–249.
- 172 HOPE-ROSS, M., YANNUZZI, L. A., GRAGOUDAS, E. S., Adverse reactions due to indocyanine green, *Ophthalmology* **1994**, *101*, 529–533.
- 173 LI, X., BEAUVOIT, B., WHITE, R., NIOKA, S., CHANCE, B., YODH, A. G., Tumor localization using fluorescence of indocyanine green (ICG) in rat models, Abstract. Optical Tomography, Photon migration, and spectroscopy of tissue and model media theory, human studies and instrumentation, *SPIE Proc.* **1995**, *2389*, 789–797.
- 174 REYNOLDS, J. S., TROY, T. L., MAYER, R. H., THOMPSON, A. B., WATERS, D. J., CORNELL, K. K., SNYDER, P. W., SEVICK-MURACA, E. M., Imaging of spontaneous canine mammary tumors using fluorescent contrast agents, *Photochem. Photobiol.* **1999**, *70*, 87–94.
- 175 INTES, X., RIPOLL, J., CHEN, Y., NIOKA, S., YODH, A. G., CHANCE, B., *In vivo* continuous-wave optical breast imaging enhanced with ICG, *Med. Phys.* **2003**, *30*, 1039–1047.
- 176 NTZIACHRISTOS, V., CHANCE, B., Accuracy limits in the determination of absolute optical properties using time-resolved NIR spectroscopy, *Med. Phys.* **2001**, *28*, 1115–1124.
- 177 LANDSMAN, M. L., KWANT, G., MOOK, G. A., ZIJLSTRA, W. G., Light-absorbing properties, stability and spectral stabilization of indocyanine green, *J. Appl. Physiol.* **1976**, *40*, 575–583.
- 178 DESMETTRE, T., DEVOISSELLE, J. M., MORDON, S., Fluorescence properties and metabolic features of indocyanine green (ICG) as related to angiography, *Surv. Ophthalmol.* **2000**, *45*, 15–27.
- 179 ANDERSON, R., HU, J., PARRISH, J., Optical radiation transfer into human skin, In *Bioengineering and the Skin*, MARKS, R., and PAYNE, P. (Eds.), MTP, Boston, MA, **1991**, pp. 253–265.
- 180 GROSSWEINER, L., *Science of Phototherapy*, CRC Press, London, **1994**.
- 181 COSTA, R. A., FARAH, M. E., FREYMLER, E., MORALES, P. H., SMITH, R., CARDILLO, J. A., Choriocapillaries photodynamic therapy using indocyanine green, *Am. J. Ophthalmol.* **2001**, *132*, 557–565.
- 182 FICKWEILER, S., SZEIMIES, R. M., BAUMLER, W., STEINBACH, P., KARRER, S., GOETZ, A. E., ABELS, C., HOFSTADTER, F., LANDTHALER, M., Indocyanine green: intracellular uptake and phototherapeutics effects *in vitro*, *J. Photochem. Photobiol. B Biol.* **1997**, *38*, 178–183.
- 183 VARRIALE, L., CRESCENZI, E., PABA, V., DE CELSO, B. M., Selective light-induced modulation of Bcl-X_L and Bax expressions in indocyanine green-loaded U937 cells: effects of continuous or intermittent photosensitization with low IR-light using a 805-nm diode laser, *J. Photochem. Photobiol.* **2000**, *57*, 66–75.
- 184 URBANSKA, K., ROMANOWSKA-DIXON, B., MATUSZAK, Z., OSZAJCA, J., NOWAK-SLIWINSKA, P., STOCHEL, G., Indocyanine green as a prospective sensitizer for photodynamic therapy of melanomas, *Acta Biochim. Polon.* **2002**, *49*, 387–391.
- 185 HOLZER, W., MAUERER, M., PENZKOFER, A., SZEIMIES, R. M., ABELS, C., LANDTHALER, M., BAUMLER, W., Photostability and thermal stability of indocyanine green, *J. Photochem. Photobiol. B Biol.* **1998**, *47*, 155–164.
- 186 GATHJE, J., STEUER, R. R., NICHOLAS, K. R. K., Stability studies on indocyanine green dye, *J. Appl. Physiol.* **1970**, *29*, 181–185.
- 187 OWEN, V. M. J., Laboratory note: estimation of indocyanine green concentrations, *Clin. Biochem.* **1973**, *6*, 132–135.
- 188 HEINTZ, R., SVENSSON, C. K., STOECKEL, K., POWERS, G. L., Indocyanine green: pharmacokinetics in the rabbit and relevant studies of its stability and purity, *J. Pharm. Sci.* **1986**, *75*, 398–402.

- 189 SAXENA, V., SADOQI, M., SHAO, J., Degradation kinetics of indocyanine green in aqueous solution, *J. Pharm. Sci.* **2003**, *92*, 2090–2097.
- 190 BUGAJ, J. E., ACHILEFU, S., DORSHOW, R. B., RAJAGOPALAN, R., Novel fluorescent contrast agents for optical imaging of *in vivo* tumors based on a receptor-targeted dye-peptide conjugate platform, *J. Biomed. Optics* **2001**, *6*, 122–133.
- 191 DEVOISSELLE, J. M., SOULIE, S., MORDON, S., DESMETTRE, T., MAILLOLS, H., A preliminary study of the *in vivo* behavior of an emulsion formulation of indocyanine green, *Lasers Med. Sci.* **1998**, *13*, 279–282.
- 192 BJORNSSON, O. G., MURPHY, R., CHADWICK, V. S., BJORNSSON, S., Physicochemical studies on indocyanine green: molar lineic absorbance, pH tolerance, activation energy and rate of decay in various solvents, *Clin. Chem. Clin. Biochem.* **1983**, *21*, 453–458.
- 193 JEJURKAR, P., Effects of γ -cyclodextrin on stability of indocyanine green in aqueous solution, *MS thesis*, St. John's University, New York, NY, **1997**.
- 194 RAJAGOPALAN, R., UETRECHT, P., BUGAJ, J. E., ACHILEFU, S. A., DORSHOW, R. B., Stabilization of the optical tracer agent indocyanine green using noncovalent interactions, *Photochem. Photobiol.* **2000**, *7*, 347–350.
- 195 GEDDES, C. D., CAO, H., LAKOWICZ, J. R., Enhanced photostability of ICG in close proximity to gold colloids, *Spectrochim. Acta A* **2003**, *59*, 2611–2617.
- 196 PANYAM, J., LABHASETWAR, V., Biodegradable nanoparticles for drug and gene delivery to cells and tissue, *Adv. Drug Deliv. Rev.* **2003**, *55*, 329–347.
- 197 LI, Y. P., PEI, Y. Y., ZHANG, X. P., GU, Z. H., ZHOU, Z. H., YUAN, W. F., ZHOU, J. J., ZHU, J. H., GAO, X. J., PEGylated PLGA nanoparticles as protein carriers: synthesis, preparation and biodistribution in rats, *J. Controlled Rel.* **2001**, *71*, 203–211.
- 198 AVGOUSTAKIS, K., BELETSI, A., PANAGI, Z., KLEPETSANIS, P., LIVANIOU, E., EVANGELATOS, G., ITHAKISSIOS, D. S., Effect of copolymer composition on the physicochemical characteristics, *in vitro* stability, and biodistribution of PLGA-mPEG nanoparticles, *Int. J. Pharm.* **2003**, *259*, 115–127.
- 199 SAHOO, S. K., PANYAM, J., PRABHA, S., LABHASETWAR, V., Residual polyvinyl alcohol associated with poly(DL-lactide-co-glycolide) nanoparticles affects their physical properties and cellular uptake, *J. Controlled Rel.* **2002**, *82*, 105–114.
- 200 PANYAM, J., SAHOO, S. K., PRABHA, S., BARGAR, T., LABHASETWAR, V., Fluorescence and electron microscopy probes for cellular and tissue uptake of poly(D,L-lactide-co-glycolide) nanoparticles, *Int. J. Pharm.* **2003**, *262*, 1–11.
- 201 SAXENA, V., SADOQI, M., SHAO, J., Indocyanine green loaded biodegradable nanoparticles: preparation, physicochemical characterization and *in-vitro* release, *Int. J. Pharm.* **2004**, *278*, 293–301.
- 202 SAXENA, V., SADOQI, M., KUMAR, S., SHAO, J., Novel near-infrared nanoparticulate biomarker: preparation and stability studies, *SPIE Proc.* **2004**, *5329*, 269–275.
- 203 SAXENA, V., SADOQI, M., KUMAR, S., SHAO, J., Novel multifunctional near-infrared fluorescent nanoparticles: integrating nanotechnology and biophotonics, *SPIE Proc.* **2004**, *5331*, 29–35.
- 204 SAXENA, V., SADOQI, M., SHAO, J., Enhanced photo stability, thermal stability and aqueous-stability of indocyanine green in polymeric nanoparticulate systems, *J. Photochem. Photobiol. B Biol.* **2004**, *74*, 29–38.
- 205 SAXENA, V., SADOQI, M., KUMAR, S., SHAO, J., Long circulating near-infrared fluorescent nanoparticles for diagnosis and photodynamic therapy of cutaneous cancers, *SPIE Proc.* **2004**, *5312*, 41–46.
- 206 SAXENA, V., SADOQI, M., SHAO, J., Enhanced intracellular uptake of indocyanine green by polymeric nanoparticulate delivery systems, *J. Biomed. Nanotechnol.* **2005**, *1*, 168–215.

12

Nanoparticles for Crossing Biological Membranes

R. Pawar, A. Avramoff and A. J. Domb

12.1

Introduction

Membrane transport plays an important role in cellular and subcellular pathways, including multidrug resistance (MDR), cellular signaling and cell–cell communication. Membrane transport mechanisms, such as the membrane permeability and extrusion machinery, lead to accumulation of specific intracellular substances and MDR. The introduction of the polymerase chain reaction resulted in the designing of new laboratory devices and analysis of amplified DNA fragments. In addition, a number of studies have been conducted related to mimicking living systems as well as developing nanodevices such as biomolecular sensors and artificial cells. The potential of nanotechnology has been studied in health care and medicine, including the development of nanoparticles for diagnostic and screening purposes [1].

New therapeutic agents are naturally occurring compounds like peptides, proteins, carbohydrates or oligonucleotides. The main problems faced in the utilization of these compounds are efficient and targeted drug delivery. Oral, nasal, transdermal and buccal routes are generally used for the administration of protein drug delivery. In such administration, the absorption of sufficient amount of drug through a particular barrier is expected in order to achieve a pharmacological response.

In therapeutic drug delivery, drugs generally should pass through barriers like the skin, blood–brain barrier (BBB) and gastrointestinal (GI) tract via cell membranes. These barriers can be overcome by using nanoparticle drug delivery. This chapter discusses general information on cell membranes and the problems encountered by drugs when trying to cross them. To circumvent such barriers in drug delivery, nanoparticulate drug delivery is preferred through the skin, BBB and orally.

In nanoparticle drug delivery through the skin the encapsulation of hydrophobic carriers with penetration enhancers is used to increase the hydrophobicity. Encapsulation involves the entrapment of a polypeptide drug within a polymeric, phospholipid or carbohydrate particulate delivery system such as nanoparticles, micro-

spheres and liposomes [2]. The BBB acts as an insurmountable barrier for a large number of drugs like central nervous system (CNS)-active drugs and antibiotics. It is also used as a major component in the regulation of the internal environment of the brain. A number of attempts have been made to overcome such a barrier, including the osmotic opening of tight junctions and the use of prodrugs or carrier system like nanoparticles/liposomes. Prodrugs can efficiently penetrate and transport across the lipophilic endothelial barrier or the efflux pump systems [3]. The best carriers for oral administration are nanoparticles and microspheres. A wide range of polymers of different sizes have been employed to investigate particle uptake. An encapsulation technique is used for the entrapment of hydrophilic or hydrophobic fluorochromes.

Nanoparticulate drug delivery has become a popular route of administration due to its penetrating and fast-acting capacity. Nanomaterials used in drug delivery created by nanotechnology research range from 1 to 100 nm in size. Nanomaterials have the potential to solve unique biological challenges such as dealing with inorganic materials, detecting electrical changes from biological molecules and treating disease.

12.2

Cell Membranes

Cell membranes are composed of lipid bilayers, proteins and lipopolysaccharides attached to the membrane surface. Due to the amphipathic nature of the lipid molecules, the lipid bilayer has charged (phosphate) groups on the water-faced surface and hydrophilic carbon inside the chains. The membrane proteins are either partially or fully integrated into the membrane bilayer or attached to its surface. Protein-free lipid bilayers are freely permeable to water and small nonpolar molecules, such as O_2 and N_2 , but impermeable to ions. For this reason, cells have evolved special ways of transferring water-soluble molecules across the membranes [4].

Understanding membrane transport has been an important goal for more than a century because it governs many aspects of life. All membranes work as gatekeepers to cells. They are responsible for signaling in the nervous system, and for coordination of the contraction of skeletal muscle and the heart, forcing its muscle to function as a pump. Membranes contain receptors or effectors for many drugs and natural substances that control the life of cells. Some other important functions like energy storage and signal transduction are also mediated through biological pores via ion flow.

One major group of transport drugs is the ion channel proteins. The mechanism and properties of ion transport through these channel proteins are subjects of wide current interest [5–9]. These ion channels provide gates for ions like Na^+ , Cl^- , K^+ and Ca^{2+} to enter or leave the cell. The channel and carrier proteins allow solutes to cross the membrane passively in a so-called “facilitated diffusion”. These transport processes occur in the direction of a concentration gradient or according to

different transmembranal potentials [10] without requiring any cell energy. However, certain membrane proteins can also act as ion pumps, transporting ions actively against a concentration gradient using energy equivalents such as ATP. By regulating the passage through these gates, cells can maintain the desired internal ion concentrations (which are often quite different from their concentrations in the surrounding solutions).

Transport processes across membranes are experimentally studied with the patch-clamp recording technique, which has revolutionized research in this field. Transport through a single molecule of a channel protein can be studied in a small patch of membrane covering the mouth of a micropipette using this technique [4]. Patch-clamp recording enables us to observe the current flow through the channel depending on the applied voltage and voltage or transmitter-induced channel gating states.

Gap junctions are clusters of closely packed intercellular membrane channels embedded in the plasma membranes of two adjoining cells [11]. They are unique systems among ion channels because two hemi-channels are connected to span two cell membranes. They facilitate a form of intercellular communication by permitting the regulated passage of ions and small molecules from one cell to another. Intercellular communication through gap junction channels has functional roles in cell survival, development, differentiation, metabolism, morphogenesis and mutagenesis [12–15]. Gap junctions permit action potential propagation in electrically excitable synapses and help to maintain homeostasis in vascular systems, such as the lens and ovarian follicles [16]. The two hemi-channels are a structure of connexon hexamers, each consisting of six connexin proteins. They dock to form a sealed cell-to-cell passageway [17]. The interlocking of the two channels occurs extracellularly in a narrow 3.5 nm “gap” separating the junctional membranes. This channel–channel interaction is known to be selective between connexins [18]. So far, the secondary and tertiary structural organization of the connexins has been solved at 7–21 Å resolution [19]. The outer diameter of the connexon is about 70 Å and it narrows at the extracellular domains, creating a “waist” in the appearance of the intercellular channel in the gap region of an outer diameter of about 50 Å [11]. The channel pore narrows from an apparent 40 Å diameter at the cytoplasmic side to 15 Å at the extracellular side of the bilayer and then widens to 25 Å in the extracellular region. The gap junction channels can be opened and closed by various physiological stimuli and experimental treatments (gating processes). They are permeable to ions and neutral molecules up to a size of about 1 kDa or 1.5 nm diameter, including secondary messengers and metabolites. Trans-junctional voltages or those between the cytoplasm and exterior affect junctions the most [12, 16].

12.2.1

Functions of Biological Membranes

The main functions of biological membranes are to: (a) provide an enclosure for the cells, (b) allow the exchange of materials, (c) act as sites of biological reactions

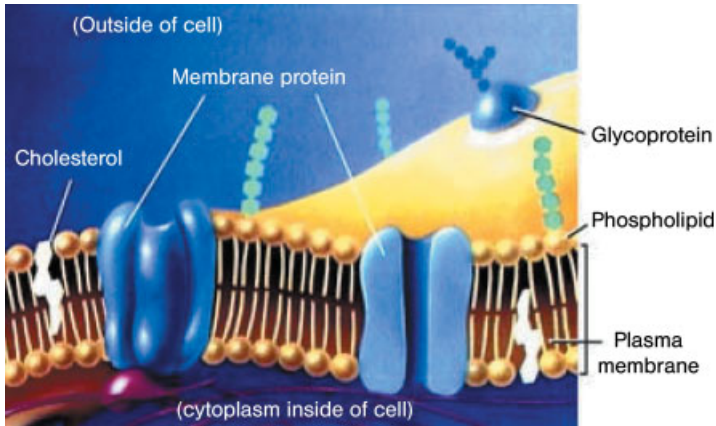


Fig. 12.1. Schematic view of a typical cell membrane [20b].

including photosynthesis, electron transfer and oxidative phosphorylation, (d) facilitate cell motion, and (e) enable recognition and cell fusion.

The biological membrane has proved to be vital in countless mechanisms necessary for cell survival. The phospholipid bilayer performs the simpler functions of compartmentalization, protection and osmoregulation. The proteins perform a wider range of functions such as extracellular interactions and metabolic processes. The carbohydrates are found in conjunction with both the lipids and proteins, and therefore enhance the properties of both. This may vary from recognition to protection.

Overall, the biological membrane is an extensive, self-sealing, fluid, asymmetric, selectively permeable and compartmental barrier essential for the correct functioning of a cell or organelles, and for a cell survival [20a]. See Fig. 12.1 for a schematic view of a typical cell membrane.

12.2.2

Kinetic and Thermodynamic Aspects of Biological Membranes

Plasma membranes of eukaryotic cells show a pronounced asymmetry with respect to the distribution of the major lipid components between the two protein monolayers. The aminophospholipids phosphatidylserine (PS) and phosphatidylethanolamine (PE) are predominantly located on the cytoplasmic leaflet, whereas the phospholipids phosphatidylcholine (PC) and sphingomyelin (SM) are mainly found on the external leaflet. Evidence for the distribution of cholesterol as another membrane component is still contradictory. Some researchers found a preference for cholesterol for the cytoplasmic layer of the red blood cell membrane, whereas other results indicated a rather symmetrical distribution.

The asymmetrical distribution of the aminophospholipids may be understood by an ATP-dependent translocation of these components from the external to the

cytoplasmic layer. The response of the membrane to this directed transport will concern not only the counter-directed movement of PS and PE, but also a redistribution of PC, SM and cholesterol. Furthermore, a change in membrane curvature may occur because of geometrical restrictions and corresponding mechanical forces caused by the coupling of the monolayer surfaces. This reasoning shows that the membrane asymmetry is determined by a multitude of processes, depending on (a) the metabolic state of the cell, (b) the mechanism of active translocation, (c) the transmembrane concentration differences of lipids and (d) mechanical forces.

Studies have attempted to gain a complete understanding of the phenomena of transbilayer lipid movement by finding an appropriate phenomenological description of the lipid fluxes. The steady-state asymmetrical lipid distribution is governed by dynamic equations. A reference simulation with a minimal set of phenomenological parameters yields qualitative restrictions to the many possible translocation mechanisms. Relations between phenomenological and kinetic model parameters serve, furthermore, as guidelines for the selection of kinetic constants in a quantitative way. It can be shown how the mechanical driving forces of the phenomenological model are to be incorporated into a kinetic model of lipid translocation.

Active transport based on a kinetic scheme involving competitive binding of PS and PE has been developed. It is clear that besides the kinetic parameters of passive translocation, mechanical forces affect those of active transport. However, the presented mechanism of active transport is not sufficient to allow for a proper treatment of mechanical effects because ATP binding, ATP hydrolysis, ADP release and lipid translocation are lumped into single irreversible translocation steps for PS and PE. Despite this, the proposed equations for active translocation are compatible with present knowledge about the kinetic properties of active lipid translocation in erythrocytes. This is particularly noted in the competition of PS and PE for the same binding site with a 10-fold higher affinity of PS on the external monolayer. The latter property results in a pronounced difference in the time constants of active transport of these two lipids.

The effect of proteins on membrane asymmetry has been taken into account in the mechanism of active translocation, in the kinetic approach and in the mechanism of facilitated lipid transport. However, possible effects of the mechanical properties of the membrane proteins have not been analyzed in detail. It may be an oversimplification that a rather high proportion of the membrane surface (around 50% for erythrocytes) is occupied by proteins. It would be straightforward to extend the mechanical energy of the monolayers by incorporating compressible protein components. Thus, the net effect of proteins on the mechanical force constants is taken into account, at least qualitatively. In addition to mechanical forces, transmembrane electric potential gradients may also affect the translocation kinetics of lipids, depending on their ionization states under physiological conditions. The present model neglects the effects of lateral organization of cell membranes that could result from specific lipid–lipid interactions, e.g. the pronounced interaction of cholesterol and SM and the protein–lipid interactions. These interactions would give rise to a more general expression for the free energy of mixing. Prelim-

inary results, based on the Bragg–Williams approximation, indicate that no qualitative changes regarding the simulation of the overall transversal lipid distributions occur, at least in the limits of that approximation [21].

12.3

Problems of Drugs Crossing through Biological Membranes

12.3.1

Through the Skin

The skin is an extremely efficient barrier that minimizes water loss from the body. Drug absorption across the skin is potentially more limiting, and the relationship between drug physiochemical properties and epidermal permeability is less ambiguous than for the mucosal barriers. The body skin surface area in humans is approximately 1.5 m^2 and represents a readily accessible surface for the application of drug delivery systems. The skin is structured in three layers: the epidermis, the dermis and the subcutaneous layer. The outer layer of the epidermis and the stratum corneum cover the entire outside of the body, and contain dead cells only, those that are strongly keratinized. For most chemicals, the stratum corneum is the rate-limiting barrier to percutaneous absorption. The skin of mammalian species is, on most parts of the body, covered with hair. At the sites where hair follicles grow, the barrier capacity of the skin differs slightly from the “normal” stratified epidermis. Most studies concerning penetration of materials into the skin have focused on whether or not drugs penetrate through the skin using different formulations containing chemicals and particulate materials as a vehicle.

The main types of particulate materials commonly used are: liposomes, inorganic compounds such as zinc and TiO_2 , polymer particulates and solid lipid nanoparticles (SLN). TiO_2 particles are often used in sunscreens to absorb UV light and therefore protect skin against sunburn or genetic damage. The micrometer-sized particles of TiO_2 penetrate through the human stratum corneum and even into some hair follicles (including their deeper parts) [22]. The observation of penetration into living layers of the skin is not considered, since this part of the follicular channel (the acroinfundibulum) is covered with a horny barrier layer. In a recent review, Kreilgaard argued that “very small TiO_2 particles (e.g. 5–20 nm) penetrate into the skin and can interact with the immune system”. Particles of $0.5\text{--}1.0 \text{ }\mu\text{m}$, in conjunction with motion, penetrate the stratum corneum of human skin, and reach the epidermis and, occasionally, the dermis. The lipid layers within the cells of the stratum corneum form a pathway through which the particles can move into the skin and be phagocytosed by the Langerhans cells [23]. The penetration of particles is limited to particle diameter of $1 \text{ }\mu\text{m}$ or less.

Penetration of nonmetallic solid materials such as biodegradable poly(D,L-lactic-co-glycolic acid) (PLGA) microparticles, $1\text{--}10 \text{ }\mu\text{m}$ with a mean diameter of $4.61 \pm 0.8 \text{ }\mu\text{m}$, was studied after application on to porcine skin. The number of microparticles in the skin decreased with the depth (measured from the airside

towards the subcutaneous layer). At 120 μm depth (where the viable dermis is present), a relatively high number of particles was found. At 400 μm depth (dermis), some microparticles were still seen. At 500 μm depth, no microparticles were found. Soil microparticles frequently of 0.4–0.5 μm and some large particles 25 μm diameter were found in the dermis of the foot in a patient with endemic elephantiasis. The particles are seen to be in the phagosomes of macrophages or in the cytoplasm of other cells. The failure to conduct lymph to the nodes produces a permanent deposit of silica in the dermal tissues (a parallel is drawn with similar deposits in the lung in pneumoconiosis). This indicates that soil particles penetrate through (damaged) skin, most probably in every individual, and are normally removed through the lymphatic system [24]. Liposomes penetrate through the skin in a size-dependent manner. Micron-sized, and even submicron-sized, liposomes do not easily penetrate into the viable epidermis, whereas liposomes with an average diameter of 272 nm can reach into the viable epidermis and some are found in the dermis. Smaller-sized liposomes of 116 and 71 nm were found in higher concentration in the dermis. Submicron emulsion particles such as liposomes and nonionic surfactant vesicles (niosomes), with a diameter of 50 nm to 1 μm , were detected in the epidermis in association with the cell membranes after application to human skin. The single molecules that make up the particles penetrate the intercellular spaces at certain regions in the stratum corneum, and are able to accumulate and reform into microspheres. The formulation used allowed the penetration of the spheres into melanoma cells, even to the nucleus [25]. The uptake of metals through the skin is difficult because of both exogenous factors (e.g. dose, vehicle, protein reactivity, valence) and endogenous factors (e.g. age of skin, anatomical site, homeostatic control). Penetration of metals through the skin still needs to be determined separately for each of metal species, either by *in vitro* or *in vivo* assays.

12.3.1.1 Mechanical Irritation of Skin

Glass and rockwool fibers are widely distributed manmade mineral fibers, and have many applications, mainly as insulation materials. They are used as a substitute for asbestos fibers. In contact with the skin, these fibers can induce dermatitis through mechanical irritation. These fibers are strong irritants and thus were not examined in detail. In occlusion with irritant patch tests in humans, rockwool fibers with a diameter of $4.20 \pm 1.96 \mu\text{m}$ were more irritating than those with a mean diameter of $3.20 \pm 1.50 \mu\text{m}$. The fact that “small” fibers can cause strong skin irritation has been known for a long time. It is also commonly accepted that some types of manmade fibers can easily induce nonallergic dermatitis. It is not clear what makes these fibers irritants. No information is available on skin irritation caused by fibers with a diameter of less than 100 nm, indicating that more research is needed on this problem [26].

12.3.1.2 Low-voltage Electroporation of the Skin

The skin is an effective barrier against toxic chemicals and pathogens. The uppermost layer of skin, the stratum corneum, is impermeable to almost all water-

soluble substances. It also constitutes a formidable obstacle to transdermal delivery of drugs and genetic material. The transdermal route, if available, provides an alternative, convenient and noninvasive pathway for local and systemic delivery of drugs, especially with respect to time release and the avoidance of degradation or metabolism in the GI tract or liver. The stratum corneum is crossed by many appendages like hair follicles and sweat glands. The lining of these appendage ducts, consisting of two layers of epithelial cells, is much less resistant than the stratum corneum for drug transport.

Many biophysical approaches have been suggested to facilitate the transport of selected chemicals across the skin barrier. The most well-known method used is iontophoresis. In this approach, a low DC voltage (normally below 5 V) is applied across the skin. Charged molecules to be delivered are placed under an appropriate electrode, and driven through the skin barrier by electrophoresis and electroosmosis [27, 28]. The electrical impedance spectra of the skin are well characterized and transport by iontophoresis has been analyzed by macroscopic theory [29].

About 20 years ago, reversible electroporation of biological membranes was recognized to deliver materials into living cells [30]. This method is based on the resilience of the cell membrane to resealing after a temporary electrical breakdown. Due to the low electric conductivity across the membrane, as compared with that of the cytoplasm and the external media, the major potential drop across the cell is concentrated across the plasma membrane “poles” facing the electric field direction. This leads to the electroporation of the membrane, whereas the rest of the cell experiences a much lower potential gradient. The same advantage applies to the electroporation of the skin barrier in which the major potential drop develops across the highly resistive stratum corneum – the target for electroporation. This was recognized recently and the technique has been applied, although sometimes in an irreversible sense, to permeabilize the skin for drug delivery.

A paradox is realized that if electroporation occurs when a potential of 1 V is applied across a cell membrane, the membranes of the epithelial cell layers lining the skin appendages are porated, as soon as the low iontophoretic voltage (above 4 V) is applied to the skin. Molecular transport by iontophoresis is considered, as there is consequence of electroporation of the epithelial layers of the skin appendages. This alternative interpretation is complicated because the potential drop along narrow hair follicles or sweat glands is taken into account in calculating the net potential drop across the epithelial cell layers at different depths from the skin surface. Furthermore, the response and resealing times of the membrane to the applied electric field are unknown. The difficulties arise in modeling the low field electroporation if a pulse or AC voltage is applied in the traditional iontophoretic setting [31].

The analysis and the experimental support given provide a broad picture of what happens when a low electric voltage is applied to the skin with appendages. The initial event, characterized by the charging of the skin capacitor and the subsequent poration of the appendage lining, is clearly depicted. It bridges the gap between the theories of iontophoresis and electroporation. This work paves the way for the future development of combined high- and low-voltage protocols

designed to enhance transdermal transport that will play an increasingly important role in drug and gene delivery [32].

12.3.2

Through the BBB

Despite enormous advances in brain research, brain and CNS disorders remain the world's leading cause of disability. More hospitalization and prolonged care is necessary in CNS disorders than almost all other diseases. The major problem in drug delivery to the brain is the presence of the BBB. Effective drugs against the CNS disease reach the brain via the blood compartment, which must pass through the BBB. It is important to understand the mechanisms involved in uptake into and efflux from the brain. Various cells present at the level of the BBB dynamically regulate the function of the BBB. This realization implies a better understanding of the relationship of transport at the BBB to drug structure and physicochemical properties. Despite successful drug delivery to the CNS, only some drugs have reached the phase where they can provide safe and effective human applications. As pharmacological strategies improve, there will be less need for invasive procedures for treating CNS diseases. Considerable advances are being made in intravascular delivery and neurosurgical invasive procedures to deliver therapeutic substances into the brain. The failure of systemically delivered drugs to effectively treat many CNS diseases can be rationalized by considering a number of barriers that inhibit drug delivery to the CNS.

The CNS consists of blood capillaries which are structurally different from the blood capillaries in other tissues. These structural differences result in a permeability barrier between the blood within brain capillaries and the extracellular fluid in brain tissue. Blood capillaries of the vertebrate brain and spinal cord lack small pores and allow rapid movement of solutes from the circulation into other organs. These capillaries are lined with a layer of special endothelial cells that lack fenestrations and are sealed with tight junctions. Tight epithelium, similar in nature to this barrier, is also found in other organs (skin, bladder, colon and lung) [33].

Ependymal cells lining the cerebral ventricles and glial cells are of three types. Astrocytes form the structural framework for the neurons and control their biochemical environment. Astrocyte foot processes or limbs spread out and meet one other, encapsulate the capillaries to form the BBB. Oligodendrocytes are responsible for the formation and maintenance of the myelin sheath, which surrounds axons and is essential for fast transmission by salutatory conduction. The tight junctions between endothelial cells result in a very high transendothelial electrical resistance of 1500–2000 $\Omega \text{ cm}^2$ compared to 3–33 $\Omega \text{ cm}^2$ of other tissues, which reduces the aqueous based paracellular diffusion observed in other organs [34, 35].

Microvessels cover an estimated 95% of the total surface area of the BBB and represent the principal route through which chemicals enter the brain. Vessels in the brain are found to have a somewhat smaller diameter and thinner wall than vessels in other organs. The mitochondrial density in brain microvessels was also

found to be higher than in other capillaries, not because of more numerous or larger mitochondria, but because of the small dimensions of the brain microvessels and, consequently, the smaller cytoplasmic area. In brain capillaries, intercellular cleft, pinocytosis and fenestrae are virtually nonexistent; transcellular exchange is preferred. Lipid-soluble solutes can only freely diffuse through the capillary endothelial membrane and may cross the BBB. In capillaries of other parts of the body, such exchange is overshadowed by other nonspecific exchanges. Despite the estimated total length of 650 km and total surface area of 12 m² of capillaries in human brain, this barrier is very efficient and makes the brain practically inaccessible for lipid-insoluble compounds such as polar molecules and small ions.

Therefore, the therapeutic value of many promising drugs is diminished and cerebral diseases have proved to be most refractory to therapeutic interventions. All drugs used for disorders of the brain are lipid soluble and readily cross the BBB following oral administration. Although antimicrobial β -lactam antibiotics, when administered intracerebroventricularly, cause severe convulsion, these antibiotics do not cause such CNS side-effects when administered intravenously or orally, due to their limited transport across the BBB. Further, in spite of being well distributed into various tissues, a lipophilic new quinolone antimicrobial agent, grepafloxacin, cannot enter the brain. It results in CNS side-effects such as headache and dizziness due to the displacement of γ -aminobutyric acid (GABA) from the GABA receptor binding sites. Benzodiazepines such as diazepam are used as sedative hypnotic agents because these lipophilic drugs readily cross the BBB. However, the BBB transport of an immunosuppressive agent, cyclosporin A, that is more lipophilic than diazepam is highly restricted. Similarly, almost all of the lipophilic anticancer agents such as doxorubicin, epipodophylotoxin and Vinca alkaloids (e.g. vincristine and vinblastine) hardly enter the brain, causing difficulty in the treatment of brain tumors. L-DOPA, used for the treatment of Parkinson's disease, is very hydrophilic and it can readily penetrate the BBB. What mechanisms underlie these diverse BBB transport characteristics of drugs that are apparently structurally and pharmacologically unrelated? Drug transport across the BBB of small-molecular drugs by carrier-mediated transport and of peptide drugs through adsorptive-mediated transcytosis is possible. The regions adjacent to the ventricles of the brain are termed circumventricular organs (CVOs). The CVOs include the choroid plexus, median eminence, neurohypophysis, pineal gland, organum vasculosum of the lamina terminalis, subfornical organ, subcommissural organ and area postrema. Although the capillaries in the CVO brain regions are more permeable to solutes, the epithelial cells of the choroid plexus and the tanycytes of other regions form tight junctions to prevent transport from the abluminal extracellular fluid (ECF) to the brain ECF. The choroid plexus is very important for the transport of peptide drugs. Although it is the major site of cerebrospinal-fluid (CSF) production, both the CSF and brain ECF are freely exchanged with each other [36]. BBB enzymes are well known and recognized for rapid degradation of almost all peptides, including naturally occurring neuropeptides. Solutes crossing the cell mem-

branes are subsequently exposed for enzyme degradation present in large numbers inside endothelial cells. These contain large densities of mitochondria and metabolically highly active organelles. The BBB is further reinforced by a high concentration of P-glycoprotein, an active drug-efflux transporter protein in the luminal membranes of the cerebral capillary endothelium. This efflux transporter actively removes a broad range of drug molecules from the endothelial cell cytoplasm before they cross into the brain parenchyma [37].

12.3.2.1 Small Drugs

The majority of drugs do not cross the brain capillary wall which forms the BBB *in vivo*. Only small molecules with high lipid solubility and a low molecular mass (M_r) below 400–500 Da cross the BBB [38]. However, only few diseases of the brain consistently respond to this category of small-molecule drugs [39, 40]. These include depression, affective disorders, chronic pain and epilepsy. In contrast, many other serious disorders of the brain do not respond to conventional lipid-soluble molecular therapeutics. These include Alzheimer's disease, stroke/neuroprotection, brain and spinal cord injury, brain cancer, HIV infection of the brain, various ataxia-producing disorders, amyotrophic lateral sclerosis, Huntington's disease, Parkinson's disease, multiple sclerosis and childhood inborn genetic errors affecting the brain. Although L-DOPA therapy has been available for decades to treat Parkinson's disease, there has been no neuroprotective drug available for Parkinson's disease that halts the inexorable neurodegeneration of this disorder. Patients with multiple sclerosis have benefited from cytokine drug therapy that acts on the peripheral immune system. However, no drug is available to stop the inevitable demyelination within the CNS caused by multiple sclerosis. Many of the CNS disorders that are refractory to small-molecule drug therapy might be treated with large-molecule drugs including recombinant proteins and gene-based medicines; however, several obstacles, both biochemical and economic, are inhibiting their development.

12.3.2.1.1 Limitations of Small Drugs

Only 12% of drugs are active in the CNS and only 1% of the total number of drugs are active in the CNS for diseases other than affective disorders [41]. The rate-limiting role of the BBB is illustrated by the small molecule histamine. Histamine, however, does not cross the BBB, but the inability of histamine to penetrate the brain is illustrated [42]. Histamine has too many hydrogen-bond-forming functional groups and the BBB penetration is inversely related to the number of hydrogen bonds that a drug forms with solvent water. Large-molecule drugs are not suitable for brain treatment because of the BBB problem. Indeed, if a large-molecule drug is found to be effective for the brain, the molecule is generally abandoned for a small-molecule peptidomimetic. However, with the exception of where the endogenous ligand itself is a small molecule, no small-molecule peptidomimetics have been discovered to date that are capable of transport across the BBB. There-

fore, the small-molecule peptidomimetics still have to be reformulated for BBB transport. The development of a small-molecule drug targeting the BBB is challenging and requires more work in this field.

12.3.2.2 Peptide Drug Delivery via SynB Vectors

Cells poorly take up a large number of hydrophilic molecules such as peptides, proteins and oligonucleotides, since they do not efficiently cross the lipid bilayer of the plasma membrane. Peptide neuromodulators failed to affect their target cells within the brain when administered peripherally. This is due to the existence of the BBB. The most important factors determining the extent to which a molecule is delivered from the blood into the CNS are lipid solubility, molecular mass and charge. Simply based on lipid solubility and molecular mass, peptide- or oligonucleotide-based neuropharmaceuticals are impeded by the BBB. To overcome the limitation in accessing the drugs to the brain, some strategies need to be developed to achieve BBB penetration [43, 44]. In the past decade, several peptides have been described such as penetratin [45, 46], a basic segment of the transcription-activating factor (Tat), and SynB vectors [44] that allow the intracellular delivery of polar, biologically active compounds *in vitro* and *in vivo*. Since the peptides penetrate into the cells by a receptor-independent nonendocytotic process, the interaction of some of them with the lipid matrix of the plasma membrane could play a key role in their cell uptake [43].

12.3.3

GI Barrier

The GI barrier plays an important role in the organism – protecting against toxic substances, and transferring nutrients and xenobiotics from the lumen to the blood. Since the oral route of administration is the most common route, the absorption and metabolism of a chemical in the intestinal mucosa is particularly important. These processes affect the bioavailability of a chemical, i.e. the fraction of an oral dose that reaches the systemic circulation [47]. Absorption across the intestinal lining includes passive diffusion across the cell membrane and cytoplasm (transcellular transport). The uptake transporters includes the sodium-dependent bile transporter, peptide transporters, the glucose transporter and organic anion transporters. Some of the export transporters includes ATP-dependent P-glycoprotein, and multi drug resistance (MDR) proteins 1 and 2 (MRP1 and MRP2). These represent well-characterized transporters in the apical membrane of the intestinal mucosal epithelium, which actively pump substrates back into the intestinal lumen after absorption into the intestinal epithelial cells [48, 49]. The current *in vitro* models of the intestinal barrier have been recently made available for investigating the principal mechanisms of absorption [50, 51]. The advantage of *in vivo* models is that they integrate all the factors that can influence chemical partitioning. The disadvantage is that it is very difficult to separate these variables during absorption. The advantage of *in vitro* models over *in vivo* models is that

it is possible to study the mechanisms of absorption *per se*, and to bypass stomach and liver metabolism. The rate and extent of drug absorption from the small intestine depends on the release of the active ingredient from a dosage form, its solubility in the liquid phase of the GI contents, and the transport of the dissolved compound or the intact dosage form from the stomach into the duodenum. In dynamic systems such as dosing to the GI tract, drug absorption is dependent on the residence time of the drug in solution at an absorption site. As such, gastric emptying and intestinal motility can be critical determinants of drug absorption.

The oral route of administration for protein and nucleic acid drugs is quite problematic because in addition to proteolysis in the stomach, the high acidity of the stomach destroys them before they can reach the intestine for absorption. Polypeptides and protein fragments, produced by the action of gastric and pancreatic enzyme, are further cleaved by exo- and endopeptidases in the intestinal brush border membrane to yield di- and tripeptides, even if proteolysis by pancreatic enzymes is avoided. Polypeptides are mostly degraded by brush border peptidases. Any peptide that survives and passes through the stomach is further metabolized in the intestinal mucosa, where the penetration barrier prevents entry into cells [52].

12.3.3.1 Intestinal Translocation and Disease

Crohn's disease is characterized by transmural inflammation of the GI tract. It is of unknown etiology, and it has been suggested that a combination of genetic predisposition and environmental factors plays a role. Particles (0.1–1.0 μm) are associated with the disease and indicated as potent adjuvants in model antigen-mediated immune responses. In a double-blind randomized study, a low particle diet (low in calcium and exogenous microparticles) alleviated the symptoms of Crohn's disease [53]. However, there is a clear association between particle exposure, their uptake and Crohn's disease. The exact role of the phagocytosis cells in the intestinal epithelium is not known. The disruption of the epithelial barrier function by apoptosis of enterocytes is a possible trigger mechanism for mucosal inflammation. Diseases other than of gut origin also have marked effects on the ability of the GI tract to translocate particles. The absorption of 2- μm polystyrene particles from the PP of rats with experimentally induced diabetes is increased up to 100-fold (10% of the administered dose) compared to normal rats [54]. However, the diabetic rat displayed a 30% decrease in the systemic distribution of the particles. The possible explanation for this discrepancy is the increased density of the basal lamina underlying the GI mucosa of diabetic rats that may impede particle translocation into deeper villous regions. This uncoupling between enhanced intestinal absorption and reduced systemic dissemination has been observed in dexamethasone-treated rats [55].

From the literature it is clear that engineered nanoparticles are taken up via the GI tract. In general, the intestinal uptake of particles is better understood and has been studied in more detail than pulmonary and skin uptake. Because of this advantage, it is possible to predict the behavior of some particles in the intestines,

with some precautions. Nanoparticles designed for food or to drug delivery via intestinal uptake needs to follow strict rules before marketing.

12.4

Nanoparticulate Drug Delivery

Drug delivery at a simplistic level has been dominated by the theme of noninjected peptide delivery. Efforts to combine peptides with novel mucoadhesive polymers and to encapsulate them in nanoparticles are being renewed. This is done by increasing intestinal permeability and increasing solubility. In last 10 years, scientists have discovered nanoparticles that favor uptake by immune surveillance systems in the intestine and in the dermis of the skin. This led to an increase in vaccine delivery research with novel antigens and adjuvants. The nanoparticles and liposomes discovered can access the brain, which has potential for targeting them to the BBB. It is worth noting that 95% of all drugs discovered for Alzheimer's disease, Parkinson's disease and stroke have poor brain-penetrating capability. There are a number of advanced transdermal systems in the research phase, including iontophoresis, sonophoresis and patches with probes. Peptide delivery via the skin is back in vogue, although the devices are simpler and cheaper. A complete range of new bioadhesive and mucoadhesive polymers is being produced, and they have unique properties to increase organ retention. Such polymers, of which the glucosamine-based chitosan was a pioneer, can lead to increased localization and retention of a conjugated drug.

Several types of nanomaterials created by nanotechnology research range are used in drug delivery, ranging in size from 1 to 100 nm:

- Fullerenes are pure carbon molecules composed of at least 60 atoms of carbon. Fullerene has a shape similar to a soccer ball or a geodesic dome (also known as a "buckyball").
- Nanotubes are a sequence of nanoscale C_{60} atoms arranged in a long, thin cylindrical structure. They are related to two other carbon crystal forms – graphite and diamonds. They often look like rolls of graphite chicken wire. However, as member of the fullerene family, they are buckyballs expanded from the center into cylinders.
- Quantum dots are nanoscale crystalline structures made up of cadmium selenide that absorb white light and then reemit it within a couple of nanoseconds later in a specific color.
- Dendrimers are synthetic, three-dimensional macromolecules formed using a nanoscale fabrication process. A dendrimer is formed from monomers, with new branches added in steps until form a tree-like structure.
- Nanoshells are concentric sphere nanoparticles consisting of a dielectric (typically gold sulfide or silica) core and a metal (gold) shell. They are a very special kind of nanoparticle because they combine IR optical activity with the uniquely biocompatible properties of gold colloids. In simple words, they are spheri-

cal glass particles with an outer shell of gold. Their size is about 100 nm in diameter.

12.4.1

Skin

Mammalian skin is a complex transport barrier with an anatomical organization and chemical structure. The important region of skin is the stratum corneum, which comprises columns of tightly packed corneocytes organized into clusters of up to a dozen cells. Mammalian stratum corneum consists of 15 corneocyte layers, with a total thickness of 0.3–0.8 μm . The corneocytes merge together with desmosomes and are sealed tightly with intercellular lipids, attached to plasma membranes. The quality and crystallinity of lipids in the stratum corneum determine the skin barrier characteristics. The fine structure of the skin and epidermal refractivity to molecular diffusion differ at different body sites [56–58].

12.4.1.1 Skin as Semipermeable Nanoporous Barrier

The skin behaves as a mechanical nanoporous barrier perforated by a large number of probably gap-like or quasi-semicircular pathways. The reported estimates for such passage widths range from 0.4 to 36 nm. Detailed information on the distribution of hydrophilic transcutaneous path widths in the skin is unavailable to date. Arguably, pore size distribution is nonsymmetrical, with a peak around 20 nm and decline on the low size side. Only one hydrophilic (circular) pathway exists between two corneocytes in the stratum corneum. The maximum number of passages through the barrier is calculated to be between 10^{10} cm^{-2} (in the case of 0.4-nm pores) and $4.5\text{--}10^8 \text{ cm}^{-2}$ (for 20-nm pores). The most likely, realistic “open pore” density in the skin is $10^8\text{--}10^9 \text{ cm}^{-2}$. Pore density of a comparable order of magnitude was determined by analyzing the results of transcutaneous electrical current (iontophoresis) and water flux (streaming potential) measurements. The funnel-like pathway shape close to the skin surface minimizes the impact of such geometrical factors. Experiments accordingly reveal that a much higher proportion of the epicutaneously applied material is transported through the skin, at least under suitable conditions [59, 60].

12.4.1.2 Hydrophilic Pathway through the Skin Barrier

The hydration and stress-dependent pathways within each cluster of cells have relatively high transport resistance, and typically lead between intercellular lipid (multi) lamellae and/or such lamellae and the proximal corneocyte envelope. In contrast, the hydrophilic pathways between clusters of corneocytes in the stratum corneum have a lower transport resistance and are sparser. The hydrophilic path between the skin cells clusters acts as a transcutaneous shunt, which is typically wider than 30 nm and permanently open. Transepidermal shunts thus cover a broad spectrum of widths, encompassing anything between a relatively wide inter-cluster gap (width greater than 5 μm), a hair follicle (width greater than 5 μm) and a cutaneous gland (width greater than 50 μm) [61].

12.4.2

Solid-Lipid Nanoparticles (SLN) Skin Delivery

The liposomal and emulsion solid particles possess several advantages like protection of incorporated active compounds from chemical degradation and flexibility in modulating the release of the compound. Liposomes and emulsions are composed of well-tolerated excipients and are used as a carrier for drug delivery. Solid-Lipid Nanoparticles (SLN) were realized simply by exchanging the liquid lipid (oil) of the emulsion by a solid lipid at room temperature. Solid-Lipid Nanoparticles (SLN) focused exclusively on pharmaceutical applications mainly for nondermal administration routes, e.g. oral and parenteral administration. In the last few years Solid-Lipid Nanoparticles (SLN) have been used in topical formulations for pharmaceutical and cosmetic products [62, 63]. In addition, generally recognized as safe (“GRAS”) substances were also used, which provide a broad variety of lipids and surfactants/polymers for the formulation of Solid-Lipid Nanoparticles (SLN) dispersions. The production of Solid-Lipid Nanoparticles (SLN) is done using hot or cold homogenization techniques. The cold homogenization technique is commonly used for extremely temperature-sensitive and hydrophilic compounds [64].

12.4.2.1 Chemical Stability of SLN

With regard to polymeric nanoparticles, the active compounds were incorporated into the solid matrix of SLN to protect them from degradation. The coenzyme Q10 incorporated in SLN composed of cetyl palmitate is stabilized with 1.2% Tego Care 450 as a surfactant [65]. Similarly, under the influence of light and oxygen, the sensitive cosmetic molecule retinol is decomposed to different epoxyretinoids. The stabilization effect of SLN on retinol was investigated using different lipids as matrix and different surfactants. The study of the stabilization effect between lipids indicates the lipids have to be selected carefully for sensitive molecules. The smallest particles with a large interface area had the most pronounced stabilization effect. Obviously, retinol located in the surface layer and an optimal surfactant showed highest stability. This indicates that the smallest particles provided the largest interfacial area for retinol and led to the highest stabilization.

The homogeneous matrix with dispersed drug molecules is present in amorphous clusters when the cold homogenization method is applied and when the lipophilic drug molecules are incorporated in SLN by the hot homogenization method. In the cold homogenization method, the bulk lipid contains the dissolved drug in dispersed form, which breaks up under high pressure and leads to nanoparticles having a homogeneous matrix structure [66]. Fast release is attained if the application of SLN to the skin should increase the drug penetration, using the occlusive effect of SLN. A core with an active compound is formed when the active compound starts precipitating and the shell has fewer drugs. This leads to a membrane-controlled release governed by the law of diffusion. It indicates that the structure of the SLN formed depends on the chemical nature of the active compounds and excipients. The release profile of SLN is often biphasic. The initial burst release is followed by a prolonged release. The burst release is high when produced at high temperature by hot homogenization.

12.4.2.2 *In Vitro* Occlusion of SLN

An adhesive effect is claimed for small-sized liposomes, forming a film on the skin after application. The occlusivity of SLN in the form of the occlusion factor has been investigated using the de Vringer model of a water beaker covered by a filter paper [67]. In this study, the particle size should be small-sized nanoparticles. Admixing of the SLN increased the occlusivity to maintain the light characters of day cream, avoiding the glossiness of occlusive night cream. Highly occlusive night cream was composed of lipid nanoparticles of high lipid concentration.

12.4.2.3 *In Vivo* SLN: Occlusion, Elasticity and Wrinkles

A study on the effect of *in vivo* SLN on skin hydration and elasticity has been performed. Using several volunteers, the cosmetic formulation was applied to one arm and the same formulation with 4% SLN was applied to other arm twice a day for 4 weeks. The addition of SLN with the commercial formulation increased the skin hydration by 32%, while in pure formulation the skin hydration increased by 24% [68]. Little or no increase in elasticity was observed in young volunteers. The effect on wrinkle depth was found effective in wrinkle treatment using established formulations with SLN. Detection of adhesive SLN on human skin was done by the Tesa strip test. The SLN were found to stick to the skin surface, forming a film and increasing the skin hydration.

12.4.2.4 Active Compound Penetration into the Skin

The penetration of active compounds into human skin involves coenzyme Q10 and retinol. SLN are found to be more efficient in promoting penetration into the stratum corneum. In cosmetic products the active compounds should stay in the skin, penetrating sufficiently deep, but not too deep so as to affect systemic availability. Penetration study with drugs in pharmaceutical dermal formulations revealed that the degree of penetration depends on the chemical composition of the formulation. The film formation, skin hydration, SLN lipids interaction and surfactants with the skin lipids are considered the factors affecting the degree of penetration [65].

Depending on the composition of SLN, different penetration profiles were obtained [69]. In the optimized formulation, a therapeutically desired enrichment in the upper layer of the skin was obtained with systemic uptake minimization.

12.4.2.5 Controlled Release of Cosmetic Compounds

Perfume was incorporated in SLN and the release study compared to a nanoemulsion of the same lipid and surfactant composition. Initially the release was same due to the presence of perfume in the outer shell of the SLN. During the follow-up period to 8 h the release from SLN was delayed. This technique is used for developing longer-lasting perfume formulations based on the prolonged release of the perfume from the solid lipid matrix [70].

Prolonged release is also desired for insect repellents, while the carrier should be also released from the adhesive SLN carrier system to stick firmly to the skin. The insect repellent DEET (*N,N*-diethyl-4methyl Benzamide) was incorporated in different SLN formulations. A loading of 10% was achieved in stearic acid SLN stabi-

lized with Tween 80 as a surfactant. The particles were physically stable for a long period when incorporated into a gel [71, 72].

12.4.2.6 Novel UV Sunscreen System Using SLN

The reduction of the ozone layer has increased the need for effective UV protection systems with minimum side-effects. The main UV protection systems are molecular UV blockers (sunscreens) and particulate compounds like TiO_2 . The molecular blockers showed side-effects such as photoallergies and phototoxic effects; therefore, the particulate blockers systems are now used. The mechanism of the protection is simply the scattering of UV rays. However, the very small TiO_2 particles penetrate into the skin and interact with the immune system [73]. The crystalline solid lipid nanoparticles also act as particulate UV blockers by scattering the light efficiently. To enhance the UV protection further, a molecular sunscreen was incorporated into the solid lipid matrix. The fixation of the molecular sunscreen inside the solid matrix minimized the side-effects due to penetration of the molecular sunscreen into the skin. Incorporation of the molecular sunscreen into the SLN matrix led to a synergetic protective effect. This means that the total amount of molecular sunscreen in the formulation was reduced with a minimization of the side-effects.

The release of the sunscreen from oil-in-water nanoemulsions and SLN dispersions was studied. A membrane-free release model used an oil phase above the aqueous nanoemulsion or aqueous SLN dispersion in a test tube. After 4 h, 6.5% of the sunscreen was released from the nanoemulsion; however, only 3.1% of the sunscreen was released from the SLN dispersion [74].

12.4.3

Polymer-based Nanoparticulate Delivery to the Skin

Poly(alkyl cyanoacrylate) (PACA) nanoparticles have been used as controlled release devices for peptide delivery after subcutaneous administration. Radiolabeled poly(isobutyl cyanoacrylate) (PIBCA) nanospheres injected subcutaneously revealed a progressive reduction of staining in muscular tissue suggesting that the nanospheres were progressively biodegraded [75a]. These nanospheres were used to release growth releasing factor in a sustained manner and to improve its bioavailability. After association with the nanospheres, the peptide was partially protected from enzymatic degradation, whereas it was very rapidly metabolized at the injection site when administered with the free drug.

A proposed mechanism for the reversion of MDR by means of doxorubicin-loaded PACA nanospheres is shown in Fig. 12.2.

12.4.4

Subcutaneous Nanoparticulate Antiepileptic Drug Delivery

Antiepileptic drugs are rarely administered subcutaneously due to their slowness and unreliability. In extraordinary circumstances such as end of life palliative

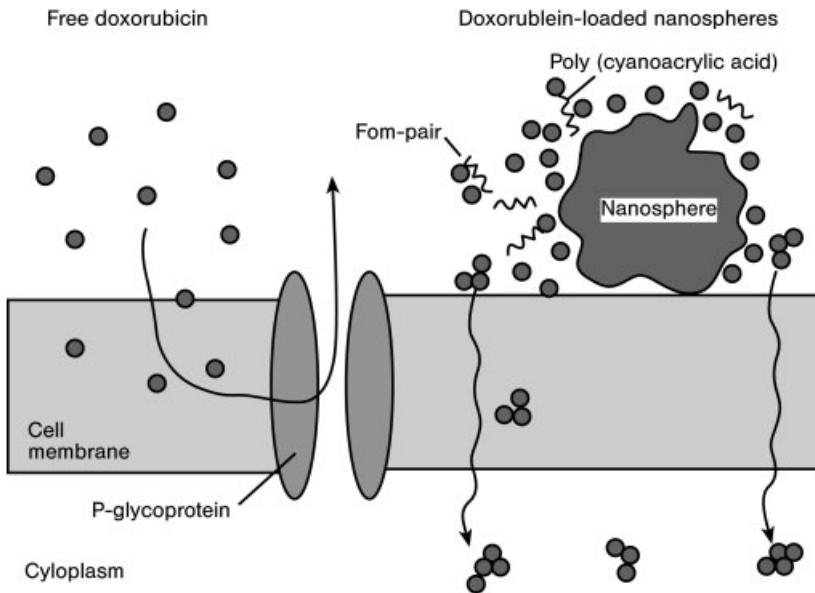


Fig. 12.2. Proposed mechanism for the reversion of MDR by means of doxorubicin-loaded PACA nanospheres. Given as free drug, doxorubicin is pumped out of the cell by P-glycoprotein (A). When given as PACA nanospheres, doxorubicin and degradation

products such as poly(cyanoacrylic acid) are released locally from the nanospheres adsorbed on the cell membrane. Together they can form ion pairs, which facilitate the penetration of doxorubicin into resistant cells [75b].

care, subcutaneous administration is advocated. Subcutaneous delivery of insulin by programmable infusion or on-demand linked to a glucose sensor has proved promising [76]. The idea of a subcutaneous antiepileptic drug implant is attractive. The low solubility, high alkaline pH in solution and low potency of most antiepileptic drugs make such implants bulky and impractical. Benzodiazepines have high potency, but exhibit tachyphylaxis with continuous use. All most all antiepileptic drugs have a relatively narrow therapeutic/toxic range, allowing for little variations in release rates from the implant. Transdermal patches are used to deliver many medications like nitroglycerine, antiemetics and nicotine. Significant transdermal penetration through the stratum corneum by medicines usually requires chemical enhancers like oxazolindiones, propylene glycol and epidermal enzymes [77]. Despite the limits of solubility and potency, antiepileptic drug patches remain an attractive option.

12.4.5

Nanoparticulate Anticancer Drug Delivery

Cancer therapy usually involves intrusive processes including application of catheters to allow chemotherapy to shrink any cancer present, surgery to then remove

the tumor followed by more chemotherapy and radiation. The purpose of the chemotherapy and radiation is to kill the tumor cells, which are more susceptible to the action of the drugs and methodologies, due to their faster growth rate than healthy cells. Current research areas include development of carriers to allow alternative dosing routes, new therapeutic targets such as blood vessels fueling tumor growth (angiogenesis) and targeted therapeutics that are more specific in their activity. The effectiveness of the treatment is directly related to the treatment's ability to target and kill the cancer cells while affecting as few healthy cells as possible. Currently, cancer patients' selectivity in their treatment is related to the inherent nature of the chemotherapeutic drugs to work on a particular type of cancer cell more intensely than on healthy cells. However, by administering bolus doses of these intense drugs systematically some side-effects will always occur and sometimes these are so intense that the patient must discontinue therapy before the drugs have a chance to eradicate the cancer [78]. Advances in the treatment of cancer are progressing quickly both in terms of new agents against cancer, and new ways of delivering both old and new agents. Some new methods for delivering therapies, both old and new, with a focus on nanoparticle formulations and ones that specifically target tumors are discussed in the following subsections.

12.4.5.1 Paclitaxel

Paclitaxel is a microtubule-stabilizing agent that promotes polymerization of tubulin causing cell death by disrupting the dynamics necessary for cell division. It has neoplastic activity against primary epithelial ovarian carcinoma, breast, colon and non-small cell lung cancers. Paclitaxel is poorly soluble in aqueous solutions, but soluble in many organic solvents such as alcohols. The currently available formulation includes Cremophor EL (polyethoxylated castor oil) and ethanol for solubilization; however, Cremophor EL is a toxic substance which shows side-effects such as hypersensitivity reactions, nephrotoxicity and neurotoxicity [79]. Biodegradable nanoparticle formulations of PLGA have been used. Paclitaxel is incorporated at very high loading efficiencies, about 100%, by a nanoprecipitation method using acetone and PLGA [80]. These nanoparticles, 117–160 nm diameter, released over half of their drug *in vitro* in the first 24 h.

12.4.5.2 Doxorubicin

It is the most potent and widely used anticancer drug and works by inhibiting the synthesis of nucleic acids within cancer cells [81]. Doxorubicin has a number of undesirable side-effects like cardiotoxicity and myelosuppression, which leads to a very narrow therapeutic index. Various researchers have studied different ways to target doxorubicin delivery to cancer tissues with minimum side-effects. Conjugates of dextran and doxorubicin have been encapsulated in chitosan nanoparticles of around 100 nm diameter. Mice injected intravenously with both dextran–doxorubicin conjugates and the conjugates encapsulated in chitosan nanoparticles showed a decrease in tumor volume. Treatment with doxorubicin alone did not decrease the tumor volume. Another method used for cancer treatment is neutron capture therapy using gadolinium [82]. *In vitro* cellular studies of chitosan-

encapsulated gadopentetic acid in nanoparticles has shown that the nanoparticles will be taken up by L929 fibroblast cells, B16F10 melanoma cells and SCC-VII squamous cell carcinoma cells through endocytosis. Doxorubicin was also conjugated with PLGA and formed nanoparticles from these conjugates [81]. Nanoparticles of 200–250 nm diameter were prepared, with *in vitro* release for up to 1 month. *In vivo* analysis of injected nanoparticles as compared with daily doxorubicin injections shows a single injection of doxorubicin–PLGA conjugate nanoparticles could suppress tumor growth for up to 12 days.

12.4.5.3 5-Fluorouracil (5-FU)

Incorporation of 5-FU is achieved using dendrimers of poly(amidoamine) modified with mPEG-500. The hydrophilicity of the 5-FU is allowed to complex with the dendrimers. Simply incubate the polymer with the drug. In *in vitro* studies, pegylated formulations showed release over 144 h (6 days), while non-pegylated formulations had completed their release within 1 day. Intravenously administered formulations in rats showed that free 5-FU was cleared from the bloodstream within 1.75 h. Those given dendrimer formulations, however, showed 5-FU clearance only after 7 h for non-pegylated systems and 13 h for pegylated systems. This confirms the formulation ability to control the 5-FU release *in vivo* and the extension of release by pegylation of the polymers in the formulation [83].

12.4.5.4 Antineoplastic Agents

Camptothecin-based drugs, specifically irinotecan (Camptosar) and topotecan (Hycamptin), have been approved by the FDA, and are used most often either in conjunction with 5-FU as first-line therapy or sometimes used alone after 5-FU has failed. Analogs of these molecules have shown up to 1000-fold higher activity, but the great challenge to their delivery is their extreme hydrophobicity [84]. Lipid-based nanoparticles of 100–375 nm diameter were prepared with the SN-38 analog of irinotecan. The weight of tumors was followed for mice injected twice weekly for 2 weeks (four doses) or daily for 10 days (10 doses) with Camptosar as compared with encapsulated SN-38 twice weekly for 2 weeks (four doses) at two different particle sizes. The longest tumor regression and survival was seen for mice injected with nanoparticles around 375 nm in diameter (65 days survival, 1.98 mg SN-38 per mouse), followed by those injected daily with Camptosar (51 days survival, 9 mg irinotecan per mouse) and those injected with nanoparticles around 100 nm diameter (48 days survival, 1.51 mg SN-38 per mouse). The control mice survival was 22 days.

12.4.5.5 Gene Delivery

Other ligands which show a selective targeting to cancer cells are transferrin (Tf) and epidermal growth factor (EGF) [85, 86]. Complexes for DNA delivery composed of poly(ethyleneimine) linked to PEG coated with either Tf or EGF were prepared with nanoparticle diameters ranging from 49 to 1200 nm. The plasmid pCMV-Luc which codes for luciferase production was incorporated into these nanoparticles and *in vivo* studies in mice showed the gene expression from admin-

istration of targeted systems was 10–100 higher in tumors than in other organs [87].

A new class of biosensors has been developed which recognizes and detects specific DNA sequences and genetic mutations in laboratory experiments. The technology could lead to a new method of cancer detection or drug development. The nanosensors, called “smart nanoparticle probes”, work by attaching short pieces of DNA (oligonucleotides) to 2.5-nm gold nanocrystals, which serve both as scaffolds and as “quenchers” for fluorescence. The oligonucleotide molecule forms into an arch-like shape labeled with a fluorescent dye at one end and a sulfur atom at the other end. The new nanoparticle probes will be more effective than conventional molecular beacons because their unique shape is better suited to binding with target molecules and their fluorescence changes very little with changes in temperature.

Nanoparticles are used to trace specific proteins in cells for early cancer diagnosis and to monitor the effectiveness of drug therapy. The nanoparticles are also used to quantify and identify gene sequences, proteins, infectious organisms and genetic disorders. The particles might be able to profile a large number of genes and proteins simultaneously, allowing physicians to individualize cancer treatments based on the molecular differences in the cancers of various patients. Because of their novel structural and optical properties, these nanobeacons open new opportunities in biomolecular sensing and bioengineering [88].

12.4.5.6 Breast Cancer

A research study used Doxil (a commercial liposomal doxorubicin formulation from Alza) in which a modified PEG conjugated to antibody F5 had been incubated to form a coupled liposome system. Comparison *in vivo* in mice treated with Doxil or F5-coupled Doxil showed a faster and greater regression in tumor volume for F5-containing Doxil over unmodified Doxil [89].

12.4.6

Nanofibers Composed of Nonbiodegradable Polymer

The incorporation of a drug into water-insoluble nonbiodegradable polyurethane has been performed to make the drug amorphous. To achieve this goal, electrostatic spinning was applied [90, 91] resulting in the formation of nanodimension fibers. The application of this technology to drug-based delivery systems has been examined only to a limited extent [92–95]. To generate drug delivery systems based on this approach, a drug is incorporated along with the polymer in the solution to be electrospun. In this process, three general variable types determine the diameter and morphology of the filaments – solution parameters, equipment-controlled parameters and environmental parameters [96, 97]. Such treatments form fibers ranging in diameter from 100 nm to several Ångstroms, which are cylindrical and uniform ranging to beaded fibers of homogeneous size. The large surface area associated with nanospun fabrics allows fast and efficient solvent evaporation, giving

limited time to recrystallize the incorporated drug for the formation of amorphous dispersions or solid solutions [92]. The electrostatic spinning of poorly water-soluble drugs in a water-insoluble nonbiodegradable polymer may generate useful delivery forms. Two drug models, itraconazole and ketanserin, were evaluated using a polyurethane carrier. Oral itraconazole is widely used for the treatment of tinea pedis and other superficial fungal infections. The compound is highly water insoluble and does not penetrate into the dermis to any significant extent after topical application to explant human skin in traditional vehicles [98, 99]. Ketanserin is a selective 5₂-serotonin antagonist which accelerates wound healing in the treatment of diabetic foot ulcers [100, 101].

12.4.6.1 Electrostatic Spinning

A high voltage Spellman DC current supply was used for the experiments in an electrostatic spinner. The voltage applied was set to 16 kV. All the experiments were done at ambient temperature and humidity. The solutions were prepared by dissolving the drug and polymer in a suitable organic solvent. The solution was fed to the glass spinneret and a high voltage was applied to the solution. On completion of the spinning nonwoven spun fabric was removed and characterized.

12.4.6.2 Scanning Electron Microscopy

The electrostatic spun fibers surface was analyzed using a scanning electron microscope. In the method of analysis the spun fibers were placed in a center of an aluminium stud. A very thin layer of gold was applied to the fibers and placed in the microscope chamber connected to a high vacuum. Surface morphology study was done at 5–10 kV mode.

12.4.6.3 Differential Scanning Calorimetry (DSC)

The Differential Scanning Calorimetry (DSC) study was done using a DSC instrument connected with a thermal analysis controller. The samples were analyzed in covered aluminum pans under dry nitrogen. Approximately 5 mg of crystalline compound was heated from 25 to 200 °C and then cooled at room temperature.

A second heating cycle was applied on the sample starting at room temperature upto 200 °C. For the electrospun materials, approximately 5 mg was weighed in the DSC pan.

12.5

Nanoparticulate Delivery to the BBB

Nanoparticles represent a tool to transport essential drugs across the BBB that are normally unable to cross this barrier. Drugs that have successfully been transported into the brain using nanoparticles include the hexapeptide dalargin, the dipeptide kytorphin, loperamide, tubocurarine, the NMDA receptor antagonist MRZ 2/576 and doxorubicin. Nanoparticles may be especially helpful for the treatment

of disseminated and very aggressive brain tumors. The first promising result in this direction was obtained in rats. The mechanism of nanoparticle-mediated transport of drugs across the BBB needs further elucidation. The most likely mechanism seems to be receptor-mediated endocytosis by the endothelial cells lining the brain blood capillaries [35], following adsorption of apolipoprotein (apo) B and E from the blood after intravenous injection.

By increasing bioavailability, nanoparticles can increase the drug development and help to treat previously untreatable conditions. Because of the BBB, many new chemical entities aimed at treating brain disorders have not proved clinically useful. In contrast, nanoparticles have been used to cross the BBB with little difficulty. Several systems have been developed, capable of reaching the brain for anesthesia (Dalargin, an analgesic), cancer drugs and other different therapeutics. There are several advantages over existing systems, including (a) no requirement to open the BBB, (b) the ability to use hydrophilic or hydrophobic drugs, and (3) the drug does not need to be modified. Researchers at the University of Texas at Austin have also described means of using nanospheres for oral drug delivery. These nanosphere carriers are derived from hydrogels – highly stable organic compounds that swell when their environment becomes more acidic. These are successfully formulated into controlled release tablets and capsules, which release active drug compounds.

12.5.1

Peptide Delivery to the BBB

Nanoparticles are used as transport vectors for peptide drugs. The nanoparticles are colloidal polymer particles of poly(butyl cyanoacrylate) with the desired peptide absorbed onto the surface and then coated with polysorbate 80. Nanoparticles are also used as a vector for delivering the hexapeptide dalargin (an enkephalin analog). Intravenous injections of the vector-dalargin produce analgesia, while dalargin alone does not [102]. Drugs successfully transported across the BBB with nanoparticles include loperamide, tubocerin and doxorubicin [103, 104]. The mechanism of nanoparticulate transport was not completely elucidated. The most probable transport pathway seems to be endocytosis by the blood capillary endothelial cells following adsorption of blood plasma components, most likely apoE after intravenous injection. These particles interact with the low-density lipoproteins (LDL) receptors on the endothelial cells and are then internalized. After internalization by the brain capillary endothelial cells, the drug is released by desorption or degradation of the nanoparticles and diffuses into the residual brain. Alternatively, transport may occur by transcytosis of the nanoparticles with the drug across the endothelial cells. The coating of nanoparticles with polysorbate led to adsorption of apoE and possibly other plasma components. This interacts with the LDL receptors of the brain endothelial cells, which could lead to their endocytosis [105]. In addition to these processes, polysorbates are capable of inhibiting the efflux pump. This inhibition could contribute to the brain transport properties of

the nanoparticles. However, the possibility of a general toxic effect is also a serious impediment.

12.5.1.1 Peptide Conjugation through a Disulfide Bond

Short peptide sequences, known as protein transduction domains (also known as cell-penetrating peptides), have become important tools to internalize impermeant molecules into cells. The transduction domain from the HIV TAT protein has been the most widely used and characterized. The ability of the TAT protein to cross the plasma membrane has since been shown to reside primarily in a highly basic region composed of nine amino acid residues.

A microanalytical instrument is used to provide quantitative data on cargo transported into the cytoplasm of living. Fluorescently labeled peptides, kinases, were conjugated to a TAT-derived peptide. Two strategies were employed to introduce a cleavage site between the TAT and the substrate cargo – a disulfide bond and a photolabile moiety. Cytosolic concentrations of the released substrates were detectable at approximate concentrations of less than 10^{-20} moles. These substrate peptides were used as probes of cytoplasmic kinase activity in single cells, with their phosphorylation providing a measure of their accessibility to cytoplasmic kinases. The percentage of phosphorylation of a TAT-loaded substrate peptide was compared to determine whether the free peptide released from the TAT conjugate was efficiently phosphorylated. The conjugated peptides were also used to determine the kinetics and temperature dependence of TAT-mediated delivery of kinase-accessible peptide to the cytosol [106].

12.5.2

Biodegradable Polymer Based Nanoparticulate Delivery to BBB

Polymeric lipid-based devices that can deliver drug molecules at defined rates for specific periods are making a tremendous impact in clinical medicine. Drug delivery to the brain interstitium using polyanhydride can circumvent the BBB. The drug is released directly to an intracranial target in a sustained fashion for an extended period of time. The fate of a drug delivered to the brain interstitium from the biodegradable polymer was predicted by a mathematical model based on (a) rates of drug transport via diffusion and fluid convection, (b) rates of elimination from the brain via degradation, metabolism and permeation through capillary networks, and (c) rates of local binding and internalization [107]. Such models are used to predict the intracranial drug concentrations, results from 1,3-bis(2-chloroethyl)-1-nitrosourea (BCNU)-loaded pCPP:SA (1,3-bis-para-carboxyphenoxypropane:sebacic acid) as well as other drug-polymer combinations, paving the way for the rational design of drugs specifically for intracranial polymeric delivery.

Conjugation of a polymerically delivered chemotherapeutic agent to a water-soluble macromolecule increases drug penetration into the brain by increasing the period of drug retention. Recently, interleukin-2-loaded biodegradable polymer microspheres were developed for local cytokine delivery to improve the immuno-

therapeutic approach to brain tumor treatment [108]. Polymeric cytokine delivery has several advantages over delivery from transduced cells, including obviating need for transecting cytokine genes, producing longer periods of cytokine release *in vivo*, yielding more reproducible cytokine release profiles and total cytokine dose. Microparticles are easily implanted by stereotaxy in discrete, precise and functional areas of the brain without damaging the surrounding tissue. This type of implantation avoids the inconvenient insertion of large implants by open surgery, which may lead to repeat operations [109]. The feasibility of polymer-mediated drug delivery by the standard chemotherapeutic agent BCNU showed local treatment of gliomas. This method is effective in animal models of intracranial tumors. Obviously, such an invasive approach is only useful in a limited number of patients; however, it does prolong survival of patients with recurrent glioblastoma multiform brain tumors. Nevertheless, because of diffusion problems the therapeutic agent is likely to reach only nearby sites.

Polymeric nanoparticles are interesting colloidal systems to enhance the therapeutic efficacy and reduces the toxicity of a large variety of drugs [110]. Nanoparticles are helpful for the treatment of the disseminated and aggressive brain tumors. Intravenously injected doxorubicin-loaded polysorbate 80-coated nanoparticles produced 40% cure in rats with intracranially transplanted glioblastomas [103]. Another study shows that pegylated PHDCA (*n*-hexadecylcyanoacrylate) nanoparticles made by pegylated amphiphilic copolymer penetrate into the brain better than all the other tested nanoparticle formulations, without inducing any modification of BBB permeability [111]. Two important requirements are necessary in design of adequate brain delivery systems – long-circulating properties of the carrier and appropriate surface characteristics to permit interactions with endothelial cells. Valproic acid-loaded nanoparticles showed reduced toxic side-effects of valproate therapy, not by reducing the therapeutically necessary dosage, but by inhibiting the formation of toxic metabolites [112]. In conclusion, the capacity of biodegradable polymer delivery methodology to deliver drugs directly to the brain interstitium is extensive.

12.5.3

Nanoparticulate Gene Delivery to the BBB

Another strategy to achieve interstitial drug delivery involves releasing drugs from biological tissues. The simplest approach to this technique is to implant into the brain a tissue which naturally secretes a desired therapeutic agent. This approach is useful in the treatment of Parkinson's disease. Transplanted tissue often did not survive due to a lack of neovascular innervation. Recently, enhanced vascularization and microvascular permeability in cell-suspension embryonic neural grafts related to solid grafts has been demonstrated [113]. An alternative for this method is to use gene therapy to develop optimized biological tissue for interstitial drug delivery. Before implantation, cells are modified genetically to synthesize and release specific therapeutic agents. The therapeutic potential of this technique in the treatment of brain tumors has been demonstrated [114]. The use of nonneuronal cells

for therapeutic protein delivery to the CNS has been recently reviewed. The survival of foreign tissue grafts may be improved by advancements in techniques for culturing distinct cell types. Co-grafted cells engineered to release neurotropic factors with cells engineered to release therapeutic proteins may enhance the survival and development of foreign tissue [115].

It is possible to perform *in vivo* genetic engineering to cause specific endogenous brain tissue to express a desired protein, circumventing the ischemic and immunogenic complications encountered with the implantation of foreign tissue grafts. One such technique that has been successfully used for the treatment of CNS malignancies involves *in vivo* tumor transduction with the herpes simplex virus thymidine kinase (HSV-tk) gene followed by the treatment with anti-herpes drug ganciclovir. It was achieved by intratumoral injection of retroviral vector-producing cells containing the HSV-tk gene, rendering the transfected tumor cells susceptible to treatment with ganciclovir [116]. Other vector systems used in CNS gene transfer studies include retroviruses, adenoviruses, adeno-associated viruses, encapsulation of plasmid DNA into cationic liposomes, and neutral and oligodendrial stem cells. Although this approach holds remarkable therapeutic potential in the treatment of CNS diseases, several obstacles hinder its efficacy – restriction to the delivery of vector systems across the BBB, inefficient transfection of host cells, nonselective expression of the transgene and deleterious regulation of the transgene by the host [117].

12.5.4

Mechanism of Nanoparticulate Drug Delivery to the BBB

The mechanism of drug delivery across the BBB has not been completely elucidated, even several possibilities are existing to explain it [103, 118]:

- (a) An increased retention of the nanoparticles in the brain blood capillaries is combined with adsorption to the capillary walls. A higher concentration gradient is responsible for enhancing the transport across the endothelial cell layer and it results in delivery to the brain.
- (b) A general surfactant effect characterized by a solubilization of the endothelial cell membrane lipids leads to membrane fluidization and enhanced drug permeability through the BBB.
- (c) The nanoparticles could lead to an opening of the tight junctions between the endothelial cells. The drug permeates through the tight junctions in free form or together with the nanoparticles.
- (d) The nanoparticles may be endocytosed by the endothelial cells followed by the release of the drugs within these cells and delivery to the brain.
- (e) The nanoparticles bound with drugs are transcytosed through the endothelial cell layer.
- (f) The polysorbate 80 used as the coating agent could inhibit the efflux system, especially P-glycoprotein.

12.5.5

Nanoparticulate Thiamine-coated Delivery to the BBB

Thiamine is a water-soluble micronutrient essential for normal cell function, growth and development. The consideration of thiamine as a cell-specific ligand for targeted delivery is rationalized since all eukaryotic cells have a specified transport mechanism for thiamine. The effectiveness of using the thiamine ligand in tumor targeting has been studied. Thiamine-coated gadolinium nanoparticles had specific association with human breast cancer cells, which expressed the thiamine transporters THTR1 and THTR2 [119]. The thiamine ligands bind to the BBB thiamine transporter and subsequently increase the number of nanoparticles at the BBB interface. Based upon BBB thiamine transport capacity and kinetics, it is referred to as a brain drug delivery vector [120]. The thiamine-coated nanoparticles (thiamine nanoparticles) specifically favor the brain uptake either by facilitating transport mechanisms or by increased passive diffusion, secondary to an increased concentration gradient of the nanoparticles located at the BBB interface due to association with the thiamine transporter. The thiamine-coated nanoparticles are engineered directly from microemulsion precursors. Brain uptake and distribution of nanoparticles with and without thiamine as a brain targeting ligand were investigated.

12.5.6

Nanoparticle Optics and Living Cell Imaging

Optical properties of silver nanoparticles depend on their size and shape and on the dielectric constant of the embedded medium [121–123]. The surface plasmon resonance of nanoparticles is excited by propagating light waves leading to the selective absorption and scattering of light. Therefore, the colors [localized SPRs (LSPRs)] of silver nanoparticles are correlated with the sizes of nanoparticles, while the shape of nanoparticles and their embedded medium remain unchanged [124, 125]. Unique size-dependent optical properties allow us to use the color index of nanoparticles (violet, blue, green, red) as nanometer-size index probes for real-time sizing of the change of living cellular membrane permeability and porosity at the nanometer scale. Individual silver nanoparticles are extremely bright under dark-field optical microscope and directly imaged by a digital or CCD camera through the dark-field microscope.

These nanoparticles do not photo-decompose and are used as probes to continuously monitor dynamics and kinetics of membrane transport in living cells for an extended time (hours). In addition, these nanoparticles are used to determine the sizes of substrates transported in and out of the living cellular membrane in real time. The scattering intensity of the nanoparticles decreases as nanoparticles enter the cell membrane and move into the cytoplasmic space. The cellular membrane and matrix absorbs the light of the microscope illuminator and reduces its intensity. The intracellular nanoparticles are surrounded by a cellular matrix (e.g. proteins, lipids) inside the cells and hence the reflection coefficient of intracellular

silver nanoparticles is smaller than the extracellular silver nanoparticles [121, 123]. The imaging system is sufficiently sensitive to detect single fluorescence dye molecules [126], and intracellular and extracellular single silver nanoparticles with diameters of 20–100 nm. Since the size of the nanoparticles and the thickness of the cellular membrane are under the optical diffraction limit (200 nm), the intracellular nanoparticles are accumulated on the membrane. However, these nanoparticles appear blurry and dimmer than extracellular nanoparticles, indicating that the blurry nanoparticles are inside the cells.

Transmission electron microscopy (TEM) is used to confirm the intracellular nanoparticles inside the cells. TEM images of ultrathin cross-sections of cells with nanoparticles unambiguously illustrate that nanoparticles up to 80 nm in diameter are observed inside the cells in the absence of chloramphenicol. The majority of nanoparticles (20–80 nm) are in the cytoplasmic space of the cells, whereas some of nanoparticles are right underneath the cellular membrane. It suggests that the outer and inner membrane of *Pseudomonas aeruginosa* permeate substrates with sizes up to 80 nm, which are 50 times larger than conventional antibiotics and detergents. Bulk cells are monitored simultaneously at single-cell resolution using single-living-cell imaging. Accumulation kinetics of nanoparticles in living cells is measured in real time using single nanoparticle optics. Even though these nanoparticles look larger than their actual sizes due to the optical diffraction limit, the sizes of nanoparticles are determined using their colors (LSPRS). As chloramphenicol concentration increases to 25 and 250 $\mu\text{g mL}^{-1}$, more nanoparticles are observed in the cells, suggesting that the membrane permeability and porosity increase. The sizes of individual intracellular nanoparticles are distinguished using their colors (LSPRS) even in the presence of 250 $\mu\text{g mL}^{-1}$ of chloramphenicol, suggesting the chloramphenicol increases membrane permeability, but does not completely disrupt the cell walls. Chloramphenicol's primary target is ribosomal peptidyl transferase, where it acts competitively to inhibit normal substrate binding and protein synthesis [127]. These new insights further demonstrate the unique advantages of using single nanoparticle as probes for the study of function of antibiotics and membrane transport.

The MexAB–OprM has a wide spectrum of substrates, such as antibiotics, dyes, detergents and chemotoxic materials, and works by using proton motive force as the energy source [128]. Therefore, it is plausible to suggest that the transport mechanism of nanoparticles through the living cellular membrane is that nanoparticles enter the cells through passive diffusion and are extruded out of the cells by the extrusion mechanism of bacteria. Even though the sizes of silver nanoparticles seem 50 times larger than the pore sizes of membrane pumps (MexAB–OprM), the substrate (nanoparticles) can induce the assembly of the pumps in real time and define the pore sizes of the pumps. Currently, the crystal structure of the membrane pump is unavailable and the extrusion mechanism of the pump is still unknown [129]. Silver nanoparticles may enter the cells and be extruded out of the cells through unidentified pathways.

Ethidium bromide (EtBr) has been widely used as a fluorescence probe for the study of membrane permeability and extrusion machinery of bacterial cells [130,

131]. EtBr emits weaker fluorescence in an aqueous environment (outside the cells), and becomes 10 times more strongly fluorescent as it enters the cells and intercalates with DNA in the cells [132]. EtBr enters the cells through passive diffusion and is extruded out of cells by efflux pumps of *P. aeruginosa* using proton motive force as an energy source. The fluorescence spectra of EtBr indicate that the emission peak at 590 nm remains unchanged after a 2-h incubation of EtBr with the living cells. The time-dependent fluorescence intensity transients also show the mutant dependence. It indicates the mutant devoid of MexAB–OprM (Δ ABM) accumulates EtBr most rapidly, whereas the mutant with overexpression of MexAB–OprM (nalB-1) accumulates EtBr most slowly. MexAB–OprM plays an important role in the accumulation of substrate (EtBr) in the cells. Taken together, accumulation kinetics measured using EtBr is consistent with those observed using single nanoparticles, eliminating the concern of the possible steric and size effects. The minimum inhibitory concentrations (MICs) of chloramphenicol in the presence of 10 μ M EtBr or 1.3 pM silver nanoparticles show mutant dependence, indicating a MIC of 12.5, 25 and 250 μ g mL⁻¹ for Δ ABM, wild-type and nalB-1, respectively [133]. See Fig. 12.3.

12.6

Oral Nanoparticulate Delivery

The oral route is the preferred route for drug delivery. However, numerous drugs remain poorly absorbed after oral administration. This can be due to (a) low mucosal permeability of a drug, (b) permeability restricted to a region of the GI tract, (c) low solubility of the compound results in low dissolution in the mucosal fluids and (d) lack of stability in the GI environment, resulting in degradation of the compound prior to its absorption (e.g. peptides, oligonucleotides). Drug delivery associated with nanoparticle systems has been investigated to overcome these problems. Several oral administration experiments are known which help to improve the pharmacokinetics of the drugs [134, 135]. See Fig. 12.4.

Orally administered drugs with nano- and microparticles follow different pathways and undergo: (a) direct transit and fecal elimination, (b) bioadhesion, and (c) oral absorption. Those pathways are important to determine an efficient drug delivery strategy. Some techniques are used for macroscopic controlled-release dosage forms for the accurate control of the drug delivery successfully transported via nanoparticles [136]. Micro- or nanoparticles orally administered in the form of a suspension diffuse into the liquid media and rapidly encounter the mucosal surface. The particles are immobilized at the intestinal surface by an adhesion mechanism referred as to as “bioadhesion”. More specifically, when adhesion is restricted to the mucus layer lining the mucosal surface, the term “mucoadhesion” is employed. The direct contact of particles with intestinal cells through a bioadhesion phase is the first step before particle absorption. The oral absorption pathway is investigated in the work of Volkheimer [137].

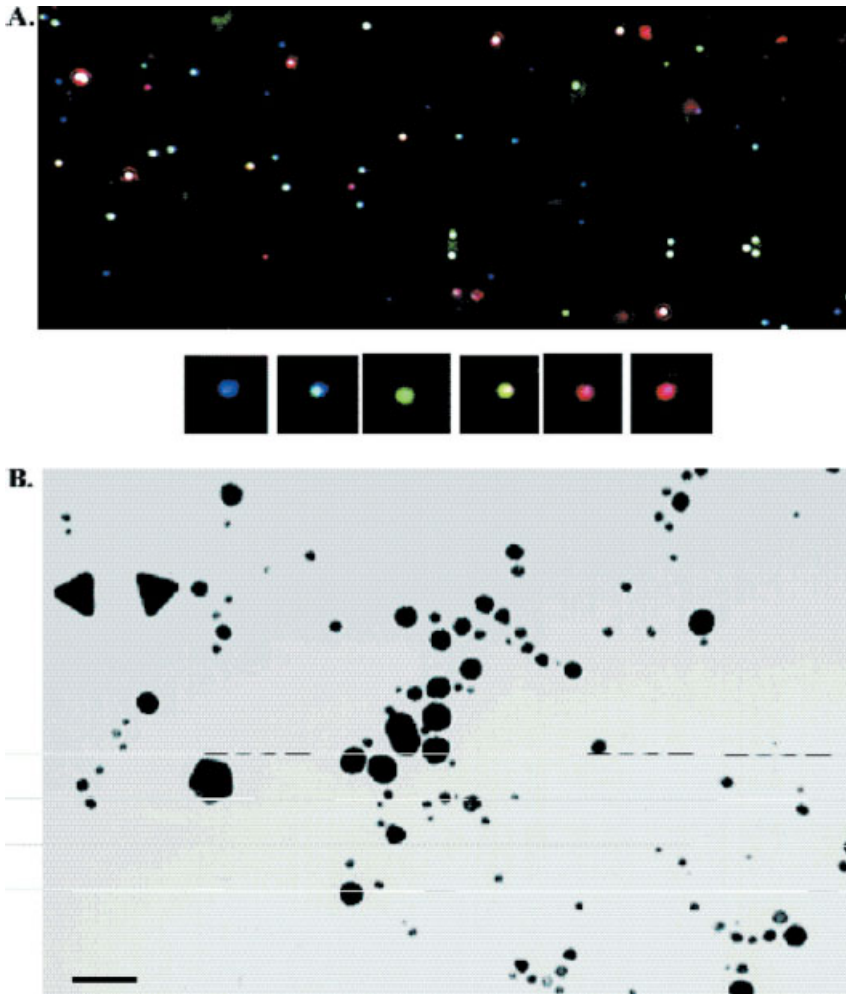


Fig. 12.3. Characterization of color index and size index of silver nanoparticles. (A) The representative full-frame optical image of silver nanoparticles taken from a 0.4-nM silver nanoparticle solution in a microchannel by a digital color camera through the dark-field optical microscope. Optical images of single silver nanoparticles selected from the full

frame image show the color index of silver nanoparticles. The optical images of nanoparticles look larger than their actual sizes because of the optical diffraction limit (200 nm). (B) Representative TEM images of silver nanoparticles from the solutions in (A) show the sizes and shapes of nanoparticles. The scale bar represents 40 nm [133].

12.6.1

Lectin-conjugated Nanoparticulate Oral Delivery

The association of ligands (i.e. lectins) with particulate systems is achieved by different procedures, including covalent linkage and adsorption processes. The ligand

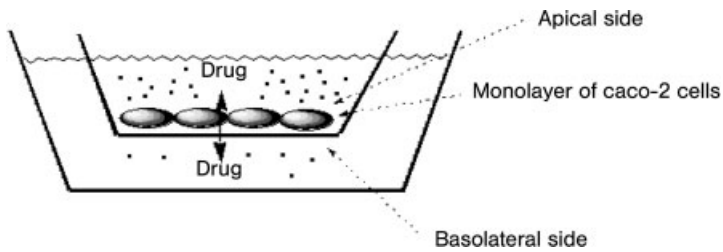


Fig. 12.4. Problems inherent in developing peptides as drugs [134b].

should be bound to particles through a covalent linkage, which is more stable than simple adsorption. It is difficult to control the amount of ligand associated, which is not sufficient to assure its efficacy [138]. Most of the conjugates have been prepared from polystyrene nanoparticles. Polystyrene latexes are interesting models from an experimental point of view, because polystyrene particles are not degradable in biological media and are easily detected by turbidimetry [139] or fluorescent labeling. However, it is probably unacceptable as a drug carrier because of the non-degradability of the polymer after a probable translocation of a fraction of the particles after administration. For conjugates based on polystyrene nanoparticles (latex), the binding procedure is by covalent attachment. Depending on the chemical nature of the functional groups located on the carrier surface, glutaraldehyde and carbodiimide, are used for lectin coupling. Recently, some lectin conjugates based on a biodegradable particulate system were described. The carbodiimide technique was successfully used for the covalent attachment of lectins to vicilin (feed vegetal protein from *Pisum sativum*) and gliadin (protein fraction from wheat gluten) nanoparticles [140]. The procedure used for the preparation of the lectin–vicilin nanoparticle conjugates is illustrated elsewhere [141, 142].

12.6.2

Oral Peptide Nanoparticulate-based Delivery

Nanospheres have a matrix-type structure, where active compounds (e.g. peptides) are adsorbed at their surface entrapped or dissolved in the matrix. The development of oral therapeutic peptide formulations with these substances is a challenging opportunity for researchers. The GI tract is designed to degrade dietary proteins and facilitate absorption of single amino acids or oligopeptides. For therapeutic compounds, however, the molecules have to remain intact when they reach the systemic circulation. Due to the presence of an acidic environment, pepsins, peptides and proteins are hydrolyzed in the stomach. In the intestine, peptides are confronted with pancreatic proteases, such as trypsin, chymotrypsin, elastase and carboxypeptidase A [143]. Furthermore, the peptides are exposed to brush border proteases and finally have to cross the epithelium. Degradation by enzymes is also possible during the absorption step. Several approaches, such as site-specific delivery systems, chemical modification of peptides (e.g. lipophilic derivatives, synthesis

of peptidomimetics), bioadhesive systems and concomitant administration of penetration enhancers or protease inhibitors, have been investigated to improve the oral delivery of peptides [143]. The use of particulate systems aims to improve the delivery of peptides by the oral route. Incorporating or encapsulating peptides in polymeric particles should have at least one effect. Depending on the nature of the particles used (type of polymer, size, adjuvant substances added), these systems enhance oral peptide absorption by other mechanisms. How the drug-loaded particulate systems are translocated from the intestinal mucosa to the systemic circulation after oral administration is still unknown [144, 145]. Many studies mention that not more than 5% of the ingested dose of submicron particles can be absorbed.

12.6.3

Polymer-Based Oral Peptide Nanoparticulate Delivery

Calcitonin is a peptide comprising 32 amino acids with high species-to-species sequence variations. It is soluble in water (1:5) and methanol (1:10), and is almost insoluble in acetone, alcohol, chloroform and ether. Calcitonin-loaded polyacrylamide nanospheres have been prepared by a reported method [146]. Particles containing hydrophilic peptide have also been prepared by interfacial polymerization, leading to the formation of nanocapsules [147, 148].

12.6.3.1 Polyacrylamide Nanospheres

Calcitonin-loaded nanospheres are prepared by the method of Birrenbach and Speiser [149]. This method involves polymerization in an inverse microemulsion (water-in-oil) method. It requires a large amount of solvent (e.g. hexane). The particles are isolated by several washings with ethanol and finally are freeze-dried. The nanospheres obtained with this technique had a size below 50 nm, but their loading efficiency remained low (5%). The peptide was immediately released from the particles after rehydration, thus impeding the protection against protease degradation.

12.6.3.2 Poly(alkyl cyanoacrylate) PACA Nanocapsules

The interfacial polymerization technique was used to encapsulate calcitonin in poly(isobutyl cyanoacrylate) PICBA nanocapsules [146]. The isobutyl cyanoacrylate (IBCA) monomers and calcitonin were dissolved in ethanol solution containing an oil (Mygliol 812). This phase was added dropwise into stirred water containing poloxamer 188. Anionic polymerization took place at the surface of the Mygliol droplets as soon as IBCA reached the oil/water interface, thus forming nanocapsules of a mean size ranging from 100 to 300 nm. Preparation additives were subsequently removed by diafiltration. Surprisingly, the calcitonin incorporated with an efficiency of 90%. The hydrophilic peptide has marked hydrophobic regions in its structure. This probably enables calcitonin to interact with the Mygliol oil. When incorporated into PIBCA nanocapsules, calcitonin was significantly more resistant to protease degradation than the free peptide [146]. However, in the pres-

ence of bile salts, the protection was significantly reduced, but still higher than a solution of free peptide. The authors suggested that calcitonin molecules diffused at the oil/water interface, together with IBCA and the poloxamer. This localization would then render the peptide susceptible to enzymes. Taking into account that peptides are highly water soluble it leads to the formation of nanocapsules with a complete inner aqueous core facilitates the incorporation of hydrophilic compounds [147, 148].

12.6.3.3 Derivatized Amino Acid Microspheres

The releasing of the peptide at a specific site of the GI tract is done using dissolved nanoparticles of substrate. Microparticles sensitive to pH were prepared by using derivatized amino acids [150, 151]. Benzoylated and phenylsulfonylated single amino acids are novel, low-molecular-weight and self-assembling molecules. At low pH, these molecules aggregate to form microspheres that dissolved readily under neutral conditions. For example, modified soybean amino acids, dissolved in water, form microparticles when poured into a 1.7 N citric acid solution containing salmon calcitonin. This technique is used for the entrapment of nearly 60% of the dissolved peptide.

12.6.4

Lymphatic Oral Nanoparticulate Delivery

The lymphatic pathway has not been investigated in many studies, possibly due to the difficulty, complexity and expense encountered in cannulating the major lymph ducts in laboratory animals. The evaluation of 80-nm solid lipid nanoparticles administered intraduodenally shows primarily their presence in the thoracic lymph duct [152]. Incorporation of the highly lipophilic drug cyclosporin in solid lipid microspheres increases lymphatic absorption 46-fold compared to conventional formulations. In another study, cyclosporin A formulated in stearic acid nanoparticles (300 nm) had a relative bioavailability of nearly 80% over the cyclosporin reference solution; however, it was unclear whether this was primarily lymphatic absorption [153]. Bioactive peptides such as insulin, calcitonin, luteinizing hormone-releasing hormone [154] and cyclosporin have been the typical peptides delivered as GI tract-labile drugs using nanoparticulate systems. Further, alteration in the physiology and metabolism of an animal is found in diseased states. In insulin-deficient streptozotocin-treated rats, the intestine is hypertrophic, and the synthesis and transport of cholesterol are increased. The increased load of cholesterol is transported through the mesenteric lymph in chylomicrons to developed oral formulations for insulin using steroidal lipids [155]. Liposome compositions of soybean sterols showed higher uptake than cholesterol, but this has been attributed to the increased stability of vesicles prepared by forming rigid liposomes [156]. All these attempts to deliver insulin orally using nanoparticles have been successful. In the oral administration of a very similar system, but dispersed in an oily phase, a 50% decrease of fasted glycemia was achieved from 2 h up to 10–13 days in rats [157]. This effect was shorter (2 days) or absent when nanospheres were dispersed in wa-

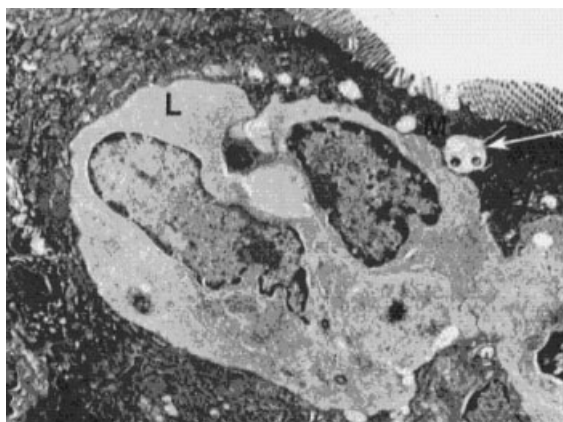


Fig. 12.5. Electron photomicrograph of semi-thin sections of rat Peyer's patch of a ligated intestinal segment after exposure to liposomes. Gold particles are indicated by the arrow. Notice the relatively small area of the M-cell apical surface sandwiched between the regular villi of the enterocytes. The presence of a large intraepithelial lymphocyte that approaches the apical surface is a conspicuous feature of the M-cell [158].

ter with and without surfactants. The results suggest primarily a lymphatic route of absorption with the nanoparticles being lodged in some way in the intestinal mucosa. A similar result has been reported for recombinant human erythro protein administered in liposomes composed of soyabean sterols. See Fig. 12.5.

12.6.5

Oral Nanosuspension Delivery

The problems to find a suitable formulation are even greater in the case of drugs that are poorly soluble in aqueous media and in organic media.

Simple examples reflecting this problem of poor solubility combined with low absorption are the experimental compound bupravaquone and the recently approved drug atovaquone (Wellvone), used for the treatment of opportunistic *Pneumocystis carinii* infections in HIV patients. Oral administration of nanosuspensions can overcome the problem of the poor solubility of drug. This is because of the high adhesiveness of drug particles, sticking on biological surfaces of the epithelial gut wall. When atovaquone formulated as a nanosuspension is given orally to *Leishmania*-infected mice, the parameter for increased absorption is related to the infectivity score of each animal or it is related to the reduction of the parasite load in the liver. In comparison to Wellvone-treated mice, containing a micronized drug, nanosuspensions of atovaquone at equivalent doses reduced infectivity from 40 to 15% at a reduced concentration of only 7.5 mg kg^{-1} [158, 159]. Another example of the effectiveness of nanosuspensions for improving bioavailability is the application of amphotericin B. When amphotericin B is given orally in approved drugs for the treatment of GI tract mycosis, the drug is not, or only to a minor ex-

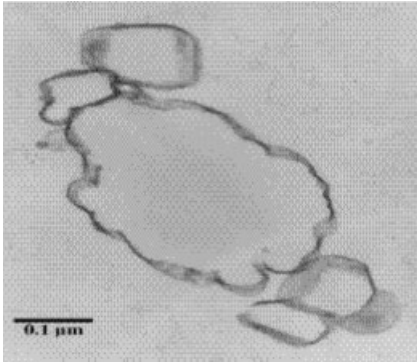


Fig. 12.6. Transmission electron micrographs of a atovaquone nanosuspension (size: 468 nm) [161].

tent, absorbed. Formulating this antimycotic and leishmanicidal drug as a nanosuspension and administering it orally, the number of *L. donovani* parasites *in vivo* was reduced significantly, indicating a high uptake of the drug in the GI tract. When given amphotericin B nanosuspensions orally, the infectivity score was determined at 25% (control = 100% parasite growth) [160]. See Fig. 12.6.

12.6.6

Mucoadhesion of Nanoparticles after Oral Administration

Considering the different phenomena occurring after oral administration of a suspension of colloidal particles via the oral route, the following general dynamic description is given. First, a suspension of particles is administered and immediately contacts the oral mucosa. From this moment on, the concentrated suspension acts as a reservoir of particles and, very rapidly, an adsorption process takes place, leading to the adsorption of a fraction of the available particles. Adsorption occurring with the mucous layer is an irreversible process. However, the luminal particle suspension transits through the intestine, progressively sweeping the whole mucosa. The simultaneous adsorption process results in a progressive covering of the intestinal mucosa by adhering particles. Finally, detachment of the particles from the mucosa begins to occur in the proximal region and is progressively extended to the distal region. Nonadhering particles from the lumen pool are detached from the mucoadherent pool and are finally eliminated in the feces. Quantitatively, particle translocation through the intestinal mucosa remains a secondary phenomenon [161].

12.6.7

Protein Nanoparticulate Oral Delivery

Protein nanoparticles are incorporated into biodegradable polymer microspheres/nanospheres as a controlled release depot or for oral delivery. In proteinaceous

therapeutics, the generation of nanoparticles is problematic. Existing practices have difficulties in achieving the desired particle size for distribution. Protein nanoparticles technology avoids most of these difficulties. The process exploits the ability of superfluids to penetrate the protein aggregates and then utilizes the expansive energy of superfluids to disaggregate protein crystals into monodisperse nanoparticles. Superfluid protein nanoparticles technology is not constrained by limited solubility in benign solvents such as ethanol [162].

References

- 1 KUBIK T., BOGUNIA K., SUGISAKA M., Nanotechnology on duty in medical applications, *Curr. Pharm. Biotechnol.* 6, 2005, 17–33.
- 2 FOLDVARI M., BECA-ESTRADA M. E., HE Z., HU J., ATTAH-POKU S., KING M., Dermal and transdermal delivery of protein pharmaceuticals: lipid-based delivery systems for interferon, *Biotechnol. Appl. Biochem.* 30, 1999, 129–137.
- 3 KREUTER J., Transport of drugs across the blood–brain barrier by nanoparticles, *Curr. Med. Chem. CNS Ag.* 2, 2002, 241–249.
- 4 ALBERTS B., BRAY D., LEWIS J., RAFF M., ROBERTS K., WATSON J. D., *Molecular Biology of the Cell*, 3rd edition, Garland Publishing, New York, 1994, pp. 195–212.
- 5 COOPER K. E., GATES P. Y., EISENBERG R. S., Surmounting barriers in ionic channels, *Q. Rev. Biophys.* 21, 1988, 331–364.
- 6 EISENBERG B., Ionic channels in biological membranes – electrostatic analysis of a natural nanotube [Review], *Contemp. Phys.* 39, 1998, 447–466.
- 7 EISENBERG R. S., From structure to function in open ionic channels, *J. Membr Biol.* 171, 1999, 1–24.
- 8 FISHMAN G. I., MORENO A. P., SPRAY D. C., LEINWAND L. A., Functional analysis of human cardiac gap junction channel mutants, *Proc. Natl Acad. Sci. USA* 88, 1991, 3525–3529.
- 9 ILLE B., ARMSTRONG C. M., MACKINNON R., Ion channels: from idea to reality, *Nat. Med.* 5, 1999, 1105–1109.
- 10 NOSSAL R., LECAR H., *Molecular and Cell Biophysics*, Addison-Wesley, San Francisco, CA, 1991.
- 11 SOSINSKY G., PERKINS G., Electron crystallographic methods for investigating gap junction structure, *Methods* 20, 2000, 140–155.
- 12 BENNETT D. L., VERSELIS V., Biophysics of gap junctions, *Semin. Cell Biol.* 3, 1992, 29–47.
- 13 DERMETZEL R., HWANG T. K., SPRAY D. S., The gap junction family: structure, function and chemistry, *Anat. Embryol. (Berl.)* 182, 1990, 517–528.
- 14 FRASER I. D., SCOTT J. D., Modulation of ion channels: a “current” view of AKAPs, *Neuron* 23, 1999, 423–426.
- 15 GILULA N. B., Topology of gap junction protein and channel function, *Ciba Found. Symp.* 125, 1987, 128–139.
- 16 BAIGENT S., STARK J., WARNER A., Modeling the effect of gap junction nonlinearities in systems of coupled cells, *J. Theor. Biol.* 186, 1997, 223–239.
- 17 UNGER V. M., KUMAR N. M., GILULA N. B., YEAGER M., Expression, two-dimensional crystallization, and electron cryo-crystallography of recombinant gap junction membrane channels, *J. Struct. Biol.* 128, 1999, 98–105.
- 18 PERKINS G., GOODENOUGH D., SOSINSKY G., Three-dimensional structure of the gap junction connexon, *Biophys. J.* 72, 1997, 533–544.
- 19 SOSINSKY G. E., PERKINS G. A.,

- Electron crystallographic methods for investigating gap junction structure. *Methods* 20, 2000, 140–155.
- 20 (a) *Studyworld Studynotes, Reports & Essays: Science – Biological, Components of Biological Membranes*. (b) <http://www.biosci.uga.edu/almanac/bio>.
 - 21 FRICKENHAUS S., HEINRICH R., Kinetic and thermodynamic aspects of lipid translocation in biological membranes, *Biophys. J.* 76, 1999, 1293–1309.
 - 22 LADEMANN J., WEIGMANN H., RICKMEYER C., BARTHELMES H., MUELLER G., STERRY W., Penetration of titanium dioxide microparticles in a sunscreen formulation into the horny layer and the follicular orifice, *Skin Pharmacol. Appl. Skin Physiol.* 12, 1999, 247–256.
 - 23 MENON G. K., ELIAS P. M., Morphologic basis for a pore-pathway in mammalian stratum corneum, *Skin Pharmacol.* 10, 1997, 235–246.
 - 24 BLUNDELL G., HENDERSON W. J., PRICE E., Soil particles in tissues of the foot in endemic elephantiasis of the lower legs, *Ann. Trop. Med. Parasitol.* 83, 1989, 381–385.
 - 25 SAUNDERS J., DAVIS H., COETZEE L., BOTHA S., KRUGER A., GROBLER A., A novel skin penetration enhancer: evaluation by membrane diffusion and confocal microscopy, *J. Pharm. Pharm. Sci.* 2, 1999, 99–107.
 - 26 HOEF F. H., HOHLFELD I. B., SALATA O. V., Nanoparticles – known and unknown health risks, *J. Nanobiotechnol.* 2, 2004, 12.
 - 27 OH S. Y., LEUNG L., BOMMANNAN D., GUY R. H., POTTS R. O., Effect of current, ionic strength and temperature on the electrical properties of skin, *J. Controlled Rel.* 27, 1993, 115–125.
 - 28 CULLANDER C., What are the pathways of iontophoretic current flow through mammalian skin?, *Adv. Drug Deliv. Rev.* 9, 1992, 119–135.
 - 29 EDWARDS D. A., LANGER R., A linear theory of transdermal transport phenomena. *J. Pharm. Sci.* 83, 1994, 1315–1334.
 - 30 CHANG D. C., CHASSY B. M., SAUNDERS J. A., SOWERS A. E. (Eds.), *Handbook of Electroporation and Electrofusion*. Academic Press, New York, 1992.
 - 31 GALLO S. A., OSEROFF A. E., JOHNSON P. G., HUI S. W., Characterization of electric pulse induced permeabilization of porcine skin using surface electrodes, *Biophys. J.* 72, 1997, 2805–2811.
 - 32 HUI S. W., Low voltage electroporation of the skin, or is it iontophoresis?, *Biophys. J.* 74, 1998, 679–680.
 - 33 CRONE C., The blood–brain barrier: a modified tight epithelium, In *The Blood–Brain Barrier in Health and Disease*, SUCKLING A. J., RUMSBY M. G., BRADBURY M. W. B. (Eds.), Ellis Harwood, Chichester, 1986, pp. 17–40.
 - 34 BRIGHTMAN M., Ultrastructure of brain endothelium, In *Physiology and Pharmacology of the Blood–Brain Barrier*, BRADBURY M. W. B. (Ed.), Springer, Berlin, 1992, pp. 1–22.
 - 35 LO E. H., SINGHAL A. B., TORCHILIN V. P., ABBOTT N. J., Drug delivery to damaged brain, *Brain. Res. Rev.* 38, 2001, 140–148.
 - 36 DAVSON H., SEGAL M. B., *Physiology of the CSF and Blood–Brain Barriers*, CRC Press, Boca Raton, FL, 1995.
 - 37 MISRA A., GANESH S., SHAHIWALA A., SHAH S. P., Drug delivery to the central nervous system: a review, *J. Pharm. Pharm. Sci.* 6, 2003, 252–273.
 - 38 PARDRIDGE W. M., *Brain Drug Targeting: The Future of Brain Drug Development*, Cambridge University Press, Cambridge, 2001.
 - 39 AJAY, BEMIS G. W., MURCKO M. A., Designing libraries with CNS activity, *J. Med. Chem.* 42, 1999, 4942–4951.
 - 40 GHOSE A. K., VISWANADHAN V. N., WENDOLOSKI J. J., A knowledge-based approach in designing combinatorial or medicinal chemistry libraries for drug discovery. 1. A qualitative and quantitative characterization of known drug databases, *J. Comb. Chem.* 1, 1999, 55–68.
 - 41 LIPINSKI C. A., Drug-like properties and the causes of poor solubility and poor permeability, *J. Pharmacol. Toxicol. Methods* 44, 2000, 235–249.

- 42 PARDRIDGE W. M., Biochemistry of the human blood–brain barrier, *Ann. Intern. Med.* 105, 1986, 82–95.
- 43 JOLLIET-RIANT P., TILLEMENT J. P., Drug transfer across the blood–brain barrier and improvement of brain delivery, *Fundam. Clin. Pharmacol.* 13, 1999, 16–26.
- 44 TEMSAMANI J., ROUSSELLE C., REES A. R., SCHERRMANN J. M., Vector-mediated drug delivery to the brain, *Expert Opin. Biol. Ther.* 1, 2001, 773–782.
- 45 LINDGREN M., HÄLLBRINK M., PROCHIANTZ A., LANGEL U., Cell-penetrating peptides, *Trends Pharmacol. Sci.* 21, 2000, 99–103.
- 46 LANGEL U., *Cell Penetrating Peptides: Processes and Applications*, CRC Press, New York, 2002.
- 47 STANLEY S. D., WILDING I. R., Oral drug absorption studies: the test model for man is man, *Drug Discov. Today* 6, 2001, 127–128.
- 48 AYRTON A., MORGAN P., Role of transport proteins in drug absorption, distribution and excretion, *Xenobiotica* 31, 2001, 469–470.
- 49 LI A. P., Screening for human ADME/Tox drug proteins in drug discovery, *Drug Discov. Today* 6, 2001, 357–366.
- 50 UNGELL A. L., *In vitro* absorption studies and their relevance to absorption from the GI tract, *Drug Dev. Ind. Pharm.* 23, 1997, 879–892.
- 51 LENNERNAS H., Human intestinal permeability, *J. Pharm. Sci.* 87, 1998, 403–410.
- 52 MAHATOO R., Biological membranes and barriers, In *Biomaterials for Delivery and Targeting of Proteins and Nucleic acids*, CRC Press, New York, 2005.
- 53 LOMER M. C., THOMPSON R. P., POWELL J. J., Fine and ultrafine particles of the diet: influence on the mucosal immune response and association with Crohn's disease, *Proc. Nutr. Soc.* 61, 2002, 123–130.
- 54 MCMINN L. H., HODGES G. M., CARR K. E., Gastrointestinal uptake and translocation of microparticles in the streptozotocin-diabetic rat, *J. Anat.* 189, 1996, 553–559.
- 55 LIMPANUSSORN J., SIMON L., DAYAN A. D., Intestinal uptake of particulate material by dexamethasone-treated rats: use of a novel technique to avoid intestinal mucosal contamination, *J. Pharm. Pharmacol.* 50, 1998, 745–751.
- 56 BODERKE P., SCHITTKOWSKI K., WOLF M., MERKLE H. P., Modeling of diffusion and concurrent metabolism in cutaneous tissue, *J. Theor. Biol.* 204, 2000, 393–407.
- 57 JOHNSON M., BLANKSCHTEIN D., LANGER R., Evaluation of solute permeation through the stratum corneum: lateral bilayer diffusion as the primary transport mechanism, *J. Pharm. Sci.* 86, 1997, 1162–1172.
- 58 DOUCETO G. N., ROSDY M., FARTASCH M., ZASTROW L., Critical events in the barrier development of reconstructed epidermis, *Perspect. Percutaneous Penetration* 5, 1997, 141–144.
- 59 FARTASCH I. D., BASSUKAS T. L., SCHÄTZLEIN A., CEVC G., Non-uniform cellular packing of the stratum corneum and permeability barrier function of intact skin: a high-resolution confocal laser scanning microscopy study using highly deformable vesicles (Transfersomes), *Br. J. Dermatol.* 138, 1998, 583–592.
- 60 VAN DEN BERGH, B. A. I., VROOM J., GERRITSEN H., JUNGINGER H. E., BOUWSTRA J. A., Interactions of elastic and rigid vesicles with human skin *in vitro*: electron microscopy, *Biochim. Biophys. Acta* 1461, 1999, 155–173.
- 61 ZHAI H., MAIBACH H. I., Effects of skin occlusion on percutaneous absorption: an overview, *Skin Pharmacol. Appl. Skin Physiol.* 14, 2001, 1–10.
- 62 MULLER R. H., MEHNERT W., LUCKS J. S., SCHWARZ C., ZUR MUHLEN A., WEYHERS H., FREITAS C., RUHL D., Solid lipid nanoparticles (SLN) – an alternative colloidal carrier system for controlled drug delivery, *Eur. J. Pharm. Biopharm.* 41, 1995, 62–69.
- 63 MULLER R. H., MADER K., GOHLA S., Solid lipid nanoparticles (SLN) for controlled drug delivery – a review of the state of the art, *Eur. J. Pharm. Biopharm.* 50, 2000, 161–177.

- 64 WEYHERS H., Feste Lipid-Nanopartikel (SLN) für die gewebsspezifische Arzneistoffapplikation, *PhD thesis*, Free University of Berlin, 1995.
- 65 MULLER R. H., DINGLER A., Feste Lipid-Nanopartikel (Lipopearls) als neuartiger Carrier für kosmetische und dermatologische Wirkstoffe, *PZ Wiss.* 49, 1998, 11–15.
- 66 ZUR MUHLEN A., MEHNERT W., Drug release and release mechanism of prednisolone loaded solid lipid nanoparticles, *Pharmazie* 53, 1998, 552.
- 67 DE VRINGER T., Topical preparation containing a suspension of solid lipid particles, *European patent application EP 0506197 A1*, 1992.
- 68 WISSING S. A., MULLER R. H., The influence of solid lipid nanoparticles (SLN) on skin hydration and viscoelasticity: *in vivo* study, *Eur. J. Pharm. Biopharm.* 2002, submitted.
- 69 SANTOS MAIA C., MEHNERT W., SCHAFER-KORTING M., Solid lipid nanoparticles as drug carriers for topical glucocorticoids, *Int. J. Pharm.* 196, 2000, 165–167.
- 70 WISSING S. A., MADER K., MULLER R. H., Solid lipid nanoparticles (SLN) as novel carrier system offering prolonged release of the perfume Allure (Chanel), *Int. Symp. Controlled Rel. Bioact Mater.* 27, 2000, 311–312.
- 71 YAZIKSIZ-ISCAN Y., HEKIMOGLU S., SARGON M. F., KAS S., HINCAL A. A., *In vitro* release and skin permeation of DEET incorporated solid lipid particles in various vehicles, In *Proceedings of the 4th World Meeting, ADRITELF/APGI/APV*, 2002, 1183–1184.
- 72 YAZIKSIZ-ISCAN Y., WISSING S. A., MULLER R. H., HEKIMOGLU S., Different production methods for solid lipid nanoparticles (SLN) containing the insect repellent DEET, In *Proceedings of the 4th World Meeting, ADRITELF/APGI/APV*, 2002, 789–790.
- 73 HAGEDORN-LEWEKE U., LIPPOLD B. C., Accumulation of sunscreens and other compounds in keratinous substrates, *Eur. J. Pharm. Biopharm.* 46, 1998, 215–221.
- 74 WISSING S. A., MULLER R. H., Solid lipid nanoparticles as carrier for sunscreens: *in vitro* release and *in vivo* skin penetration, *J. Controlled Rel.* 2002, 81 (3), 225–233.
- 75 (a) GAUTIER J. C., GRANGIER J. L., BARBIER A., DUNPONT P., DUSSOSSY D., PASTOR G., COUVREUR P., Biodegradable nanoparticles for subcutaneous administration of growth hormone releasing factor (hGRF), *J. Controlled Rel.* 3, 1992, 205–210. (b) DE VERDIERE A. C., DUBERNET C., NEMATI F., SOMA E., APPEL M., FERTE J., BERNARD S., PUISIEUX F., COUVREUR P., Reversion of multidrug resistance with poly-alkylcyanoacrylate nanoparticles: towards a mechanism of action, *Br. J. Cancer* 76, 1997, 198–205.
- 76 MANIATIS A. K., KLIGENSMITH G. J., SLOVER R. H., Continuous subcutaneous insulin infusion therapy for children and adolescents: an option for routine diabetes care, *Pediatrics* 107, 2001, 351–356.
- 77 ASBILL C. S., EL-KATTAN A. F., MICHNAIK B., Enhancement of transdermal drug delivery: chemical and physical approaches, *Crit. Rev. Ther. Drug Carrier Syst.* 17, 2000, 621–625.
- 78 FENG S. S., CHIEN S., Chemotherapeutic engineering: application and further development of chemical engineering principles for chemotherapy of cancer and other diseases, *Chem. Eng. Sci.* 58, 2003, 4087–4114.
- 79 SINGLA A. K., GARG A., AGGARWAL D., Paclitaxel and its formulations, *Int. J. Pharm.* 235, 2002, 179–192.
- 80 FONSECA C., SIMÕES S., GASPARI R., Paclitaxel-loaded PLGA nanoparticles: preparation, physicochemical characterization and *in vitro* anti-tumoral activity, *J. Controlled Rel.* 83, 2002, 273–286.
- 81 YOO H. S., PARK T. G., *In vitro* and *in vivo* anti-tumor activities of nanoparticles based on doxorubicin-PLGA conjugates, *Polym. Prep.* 41, 2000, 992–993.
- 82 SHIKATA F., TOKUMITSU H., ICHIKAWA H., FUKUMORI Y., *In vitro* cellular

- accumulation of gadolinium incorporated into chitosan nanoparticles designed for neutron-capture therapy of cancer, *Eur. J. Pharm. Biopharm.* 53, 2002, 57–63.
- 83 BHADRA D., BHADRA S., JAIN S., JAIN N. K., A PEGylated dendritic nanoparticulate carrier of fluorouracil, *Int. J. Pharm.* 257, 2003, 111–124.
- 84 WILLIAMS J., LANSDOWN R., SWEITZER R., ROMANOWSKI M., LABELL R., RAMASWAMI R., UNGER E., Nanoparticle drug delivery system for intravenous delivery of topoisomerase inhibitors, *J. Controlled Rel.* 91, 2003, 167–172.
- 85 KIRCHEIS R., KICHLER A., WALLNER G., KURSA M., OGRIS M., FELZMANN T., BUCHBERGER M., WAGNER W., Coupling of cell-binding ligands to polyethylenimine for targeted gene transfer, *Gene Ther.* 4, 1997, 409–418.
- 86 OGRIS M., STEINLEIN P., CAROTTA S., BRUNNER S., WAGNER E., DNA/polyethylenimine transfection particles: influence of ligands, polymer size, and PEGylation on internalization and gene expression, *AAPS PharmSciTech.* 3, 2001, 21.
- 87 OGRIS M., WALKER G., BLESSING T., KIRCHEIS R., WOLSHEK M., WAGNER E., Tumor-targeted gene therapy: strategies for the preparation of ligand-polyethylene glycol-polyethyleneimine/DNA complexes, *J. Controlled Rel.* 91, 2003, 173–181.
- 88 HOLLY K., Biomedical engineer constructs illuminating nanoparticles for medical imaging and gene detection, Emory University Health Sciences Center. Public release date: 27 March 2003.
- 89 NIELSEN U. B., KIRPOTIN D. B., PICKERING E. M., HONG K., PARK J. W., SHALABY M. R., SHAO Y., BENZ C. C., MARKS J. D., Therapeutic efficacy of anti-ErbB2 immunoliposomes targeted by a phage antibody selected for cellular endocytosis, *Biochim. Biophys. Acta* 1591, 2002, 109–118.
- 90 RENEKER D. H., CHUN I., Nanometre diameter of polymer, produced by electrospinning, *Nanotechnology* 7, 1996, 216–223.
- 91 DOSHI J., RENEKER D. H., Electrospinning process and applications of electrospun fibers, *J. Electrostat.* 35, 1995, 151–160.
- 92 VERRECK G., CHUN I., PEETERS J., ROSENBLATT J., BREWSTER M. E., Preparation and characterization of nanofibers containing amorphous drug dispersion generated by electrostatic spinning, *Pharm. Res.* 20, 2003, 810–817.
- 93 KENAWY E. R., BOWLIN G. L., MANSFIELD K., LAYMAN J., SIMPSON D. G., SANDERS E. H., WNEK G. E., Release of tetracycline hydrochloride from electrospun poly(ethylene-co-vinylacetate), poly(lactic acid), and a blend, *J. Controlled Rel.* 81, 2002, 57–64.
- 94 IGNATIOUS F., BALDONI J. M., Electrospun pharmaceutical compositions, *WO 0154667*, 2001.
- 95 ZONG X., KIM K., FANG D., RAN S., HSIAO B. S., CHU B., Structure and process relationship of electrospun bioabsorbable nanofiber membranes, *Polymer* 43, 2002, 4403–4412.
- 96 LEE K. H., KIM H. Y., KHIL M. S., RA Y. M., LEE D. R., Characterization of nano-structured poly(ϵ -caprolactone) nonwoven mats via electrospinning, *Polymer* 44, 2003, 1287–1294.
- 97 SHIN Y. M., HOHMAN M. M., BRENNER M. P., RUTLEDGE G. C., Experimental characterization of electrospinning: the electrically forced jet and instabilities, *Polymer* 42, 2001, 9955–9967.
- 98 PEETERS J., NEESKENS P., TOLLENAERE J. P., VAN REMOORTERE P., BREWSTER M. E., Characterization of the interaction of 2-hydroxypropyl-hydroxyethylcyclodextrin with itraconazole at pH 2, 4 and 7, *J. Pharm. Sci.* 91, 2002, 1414–1422.
- 99 MEIS J. F. G. M., VERWEIJ P. E., Current management of fungal infections, *Drugs* 61, 2001, 13–25.
- 100 MARTINEZ-DE JESUS F. R., MORALES-GUZMAN M., CASTANEDA M., PEREZ-MORALES A., GARCIA-ALONSO J., MEDIOLA-SEGURA I., Randomized

- single-blind trial of topical ketanserin for healing acceleration of diabetic foot ulcers, *Arch. Med. Res.* 28, 1997, 95–99.
- 101 APELQVIST J., CASTENFORS J., LARSSON J., STENSTROM A., PERSSON G., Ketanserin in the treatment of diabetic foot ulcer with severe peripheral vascular disease, *Int. Angiol.* 9, 1990, 120–124.
- 102 KREUTER J., ALYAUTDIN R. N., KHARKEVICH D. A., IVANOV A. A., Passage of peptides through the blood–brain barrier with colloidal polymer particles (nanoparticles). *Brain Res.* 674, 1995, 171–174.
- 103 KREUTER J., Nanoparticulate systems for brain delivery of drugs, *Adv. Drug. Deliv. Rev.* 47, 2001, 65–81.
- 104 KREUTER J., Transport of drugs across the blood–brain barrier by nanoparticles, *Curr. Med. Chem.* 2, 2002, 241–249.
- 105 LUCK M., Plasma protein adsorption als Moglicher Schlusselfaktor fur eine kontrollierte Arzneistoffapplikation mit partikularen Tragern, *PhD thesis*, Freie Universitat Berlin, 1997.
- 106 SOUGHAYER J. S., WANG Y., LI H., CHEUNG S., ROSSI F. M., STANBRIDGE E. J., SIMS C. E., ALLBRITTON N. L., Characterization of TAT-mediated transport of detachable kinase substrates, *Biochemistry* 43, 2004, 8528–8540.
- 107 FUNG L. K., EWEND M. G., SILLS A., SIPOS E. P., THOMPSON R., WATTS M., COLVIN O. M., BREM H., SALTZMAN W. M., Pharmacokinetics of interstitial delivery of carmustine, 4-hydroperoxycyclophosphamide and paclitaxel from a biodegradable polymer implant in the monkey brain, *Cancer Res.* 58, 1998, 672–684.
- 108 HANES J., BATYCKY R. P., LANGER R., EDWARDS D. A., A theoretical model of erosion and macromolecular drug release from biodegrading microspheres, *J. Pharm. Sci.* 86, 1997, 1464–1477.
- 109 JEAN-PIERRE B., NATHALIE F., MARIE-CLAIRE V. J., PHILIPPE M., Development of microspheres for neurological disorders: from basics to clinical applications, *J. Controlled Rel.* 65, 2000, 285–296.
- 110 COUVREUR P., DUBERNET C., PUISIEUX F., Controlled drug delivery with nanoparticles: current possibilities and future trends, *Eur. J. Pharm. Biopharm.* 41, 1995, 2–13.
- 111 PILAR C., BRUNO G., HELENE C., DIDIER D., JEAN A., JENE-PIERRE N., DOMINIQUE G., ELIAS F., JEAN A. P., PATRICK C., Long-circulating PEGylated polycyanoacrylate nanoparticles as new drug carrier for brain delivery, *Pharm. Res.* 18, 2001, 1157–1166.
- 112 JOERG D., FRANK M. P., BERNHARD S. A., ULRIKE S., Influence of nanoparticles on the brain-to-serum distribution and the metabolism of valproic acid in mice, *J. Pharm. Pharmacol.* 562, 2000, 1043–1047.
- 113 LEIGH K., ELISEVICH K., ROGERS K. A., Vascularization and microvascular permeability in solid versus cell-suspension embryonic neural grafts, *J. Neurosurg.* 81, 1994, 272–283.
- 114 LAL B., INDURTI R. R., COURAUD P. O., GOLDSTEIN G. W., LATERRA J., Endothelial cell implantation and survival within experimental gliomas, *Proc. Natl Acad. Sci. USA* 91, 1994, 9695–9699.
- 115 YUREK D. M., SLADEK J. R., Dopamine cell replacement: Parkinson's disease, *Annu. Rev. Neurosci.* 13, 1990, 415–440.
- 116 RAFFEL C., CULER K., KOHN D., NELSON M., SIEGEL S., GILLIS F., LINK C. J., VILLABLANCA J. G., ANDERSON W. F., Gene therapy for the treatment of recurrent pediatric malignant astrocytomas with *in-vivo* tumor transduction with the herpes simplex thymidine kinase gene/ganciclovir system, *Hum. Gene Ther.* 5, 1994, 863–890.
- 117 ZLOKOVIC B. V., APUZZO M. L., Cellular and molecular neurosurgery: pathways from concept to reality – part II: vector systems and delivery methodologies for gene therapy of the central nervous system, *Neurosurgery* 40, 1997, 805–812.
- 118 KREUTER J., SHAMENKOV D., PETROV

- V., RAMGE P., CYCHUTEK K., KOCH-BRANDT C., ALYAUTDIN R., Apolipoprotein-mediated transport of nanoparticle-bound drugs across the blood-brain barrier, *J. Drug Target.* **10**, **2002**, 317–325.
- 119 OYEWUMI M. O., LIU S., MOSCOW J. A., MUMPER R. J., Specific association of thiamine-coated gadolinium nanoparticles with human breast cancer cells expressing thiamine transporters, *Bioconjug. Chem.* **14**, **2003**, 404–411.
- 120 SMITH Q. R., Drug delivery to the brain and the role of carrier mediated transport, In *Frontiers in Cerebral Vascular Biology: Transport and its Regulation*, DREWES L. R., BETZ A. L. (Eds.), Plenum, New York, **1993**, pp. 83–93.
- 121 KREIBIG U., VOLLMER M., *Optical Properties of Metal Clusters*, Springer, Berlin, **1995**.
- 122 HAYNES C., VAN DUYN R., Nanosphere lithography: a versatile nanofabrication tool for studies of size-dependent nanoparticle optics, *J. Phys. Chem. B* **105**, **2001**, 5599–5611.
- 123 MIE G., Beitrag zur optik trüber medien, speziell kolloidaler metrallösungen, *Ann. Phys.* **25**, **1908**, 377–445.
- 124 KYRIACOU S. V., BROWNLOW W., XU X.-H. N., Nanoparticle optics for direct observation of functions of antimicrobial agents in single live bacterial cells, *Biochemistry* **43**, **2004**, 140–147.
- 125 XU X.-H. N., CHEN J., JEFFERS R., KYRIACOU S., Direct measurement of sizes and dynamics of single living membrane transporters using nano-optics, *Nano Lett.* **2**, **2002**, 175–182.
- 126 STEEL C., WAN Q., XU X.-H. N., Single living cell imaging of chromosomes in chloramphenicol-induced filamentous *P. aeruginosa*, *Biochemistry* **43**, **2004**, 175–182.
- 127 GREENWOOD D., Modes of action in antibiotic and chemotherapy, In *Antibiotic and Chemotherapy: Anti-infective Agents and Their Use in Therapy*, O'GRADY F., LAMBERT H. P., FINCH R. G., GREENWOOD D. (Eds.), 7th edn., Churchill Livingstone, New York, **1997**, pp. 10–21.
- 128 MASEDA H., YONEYAMA H., NAKAE T., Assignment of the substrate-selective subunits of the MexEF–OprN multi-drug efflux pump of *Pseudomonas aeruginosa*, *Antimicrob. Ag. Chemother.* **44**, **2000**, 658–664.
- 129 RYAN B. M., DOUGHERTY T. J., BEAULIEU D., CHUANG J., DOUGHERTY B. A., BARRETT J. F., Efflux in bacteria: what do we really know about it?, *Expert Opin. Invest. Drugs* **10**, **2001**, 1409–1422.
- 130 YONEYAMA H., MASEDA H., KAMIGUCHI H., NAKAE T., Function of the membrane fusion protein, MexA, of the MexA,B–OprM efflux pump in *Pseudomonas aeruginosa* without an anchoring membrane, *J. Biol. Chem.* **275**, **2000**, 4628–4634.
- 131 XU X. H., WAN Q., KYRIACOU S., BROWNLOW W., NOWAK M., Direct observation of substrate induction of resistance mechanism in *Pseudomonas aeruginosa* using single live cell imaging, *Biochem. Biophys. Res. Commun.* **305**, **2003**, 941–949.
- 132 MORGAN A. R., LEE J. S., PULLEYBLANK D. E., MURRAY N. L., EVANS D. H., Review: ethidium fluorescence assays. Part 1. Physicochemical studies, *Nucleic Acids Res.* **7**, **1979**, 547–569.
- 133 XU X. H., BROWNLOW W. J., KYRIACOU S. V., WAN Q., VIOLA J. J., Real-time probing of membrane transport in living microbial cells using single nanoparticle optics and living cell imaging, *Biochemistry* **43**, **2004**, 10400–10413.
- 134 (a) DAMGE C., MICHEL C., APRAHAMIAN M., COUVREUR P., DEVISSAGUET J. P., Nanocapsules as carriers for oral peptide delivery, *J. Controlled Rel.* **13**, **1990**, 233–239. (b) PAULETTI G. M., GANGWAR S., SIAHAAN T. J., AUBÉ J., BORCHARDT R. T., Improvement of oral peptide bioavailability: peptidomimetics and prodrug strategies, *Adv. Drug Deliv. Rev.* **27**, **1997**, 235–256.
- 135 AMMOURY N., FESSI H., DEVISSAGUET J. P., DUBRASQUET M., BENITA S.,

- Jejunal absorption, pharmacological activity, and pharmacokinetic evaluation of indomethacin-loaded poly(D,L-lactide) and poly(isobutylcyanoacrylate) nanocapsules in rats, *Pharm. Res.* 8, 1991, 101–105.
- 136 LEROUX J. C., COZENS R., ROESEL J. L., GALLI B., KUBEL F., DOELKER E., GURNY R., Pharmacokinetics of a novel HIV-1 protease inhibitor incorporated into biodegradable enteric nanoparticles following intravenous and oral administration to mice, *J. Pharm. Sci.* 84, 1996, 1387–1391.
- 137 VOLKHEIMER G., SCHULZ F. H., The phenomenon of persorption, *Digestion* 1, 1968, 213–218.
- 138 BETAGERI G. V., BLACK C. D., SZEBENI J., WAHL L. M., WEINSTEIN J. N., Fc-receptor-mediated targeting of antibody-bearing liposomes containing dideoxycytidine triphosphate to human monocyte/macrophages, *J. Pharm. Pharmacol.* 45, 1993, 48–53.
- 139 IRACHE J. M., DURRER C., PONCHEL G., DUCHENE D., Determination of particle concentration in latexes by turbidimetry, *Int. J. Pharm.* 90, 1993, R9–R12.
- 140 EZPELETA I., Potentialites de proteines vegetales comme materiau pour la fabrication de vecteurs particulaires, *These*, l'Universite de Rouen, 1996.
- 141 EZPELETA I., IRACHE J. M., STAINMESSE S., CHABENAT C., GUEGUEN J., ORECCHIONI A. M., Preparation of lectin–vicilin nanoparticle conjugates using the carbodiimide coupling technique, *Int. J. Pharm.* 142, 1996, 227–233.
- 142 EZPELETA I., IRACHE J. M., STAINMESSE S., GUEGUEN J., ORECCHIONI A. M., Preparation of small-sized particles from vicilin (vegetal protein from *Pisum sativum* L.) by coacervation, *Eur. J. Pharm. Biopharm.* 42, 1996, 36–41.
- 143 BANGA A. K., *Therapeutic Peptides and Proteins*, Technomic, Lancaster, 1995.
- 144 FLORENCE A. T., HILLERY A. M., HUSSAIN N., JANI P. U., Nanoparticles as carriers for oral peptide absorption: studies on particle uptake and fate, *J. Controlled Rel.* 36, 1995, 39–46.
- 145 DESAI M. P., LABHASETWAR V. D., AMIDON G. L., LEVY R. J., Gastrointestinal uptake of biodegradable micro-particles: effect of particle size, *Pharm. Res.* 13, 1996, 838–1845.
- 146 LOWE P. J., TEMPLE C. S., Calcitonin and insulin in isobutylcyanoacrylate nanocapsules: protection against proteases and effect on intestinal absorption in rats, *J. Pharm. Pharmacol.* 46, 1994, 547–552.
- 147 VRANCKX H., DEMOUSTIER M., DELEERS M., A new formulation with hydrophilic core: application to the oral administration of salmon calcitonin, *Eur. J. Pharm. Bionanocapsules Pharm.* 42, 1996, 345–347.
- 148 VRANCKX H., DEMOUSTIER M., DELEERS M., Pharmaceutical compositions containing nanocapsules, *US patent* 5,500,224, 1996.
- 149 BIRRENBAACH G., SPEISER P. P., Polymerized micelles and their use as adjuvants in immunology, *J. Pharm. Sci.* 65, 1976, 1763–1766.
- 150 LEONE-BAY A., MCINNIS C., WANG N., DEMORIN F., ACHAN D., LERCARA C., SARUBBI D., HAAS S., PRESS J., BARANTSEVICH E., O'BROIN B., MILSTEIN S., PATON D., Microsphere formation in a series of derivatized alpha-Amino acids: properties, molecular modeling, and oral delivery of salmon calcitonin, *J. Med. Chem.* 38, 1995, 4257–4262.
- 151 MILSTEIN S. J., BARANTSEVICH E. N., GRECHANOVSKI V. A., SARUBBI D. J., pH-dependent microspheres from modified soybean protein hydrolysate, *J. Microencapsul.* 13, 1996, 651–665.
- 152 BARGONI A., CAVALLI R., CAPUTO O., FUNDARO A., GASCO M. R., ZARA G. P., Solid lipid nanoparticles in lymph and plasma after duodenal administration to rats, *Pharm. Res.* 15, 1998, 745–750.
- 153 ZHANG Q., YIE G., LI Y., YANG Q., NAGAI T., Studies on the cyclosporin A loaded stearic acid nanoparticles, *Int. J. Pharm.* 200, 2000, 153–159.
- 154 HILLERY A. M., TOTH I., FLORENCE A. T., Biological activity of luteinizing hormone releasing hormone after oral dosing with a novel nanoparticulate

- delivery system: co-polymerised peptide particles, *Pharm. Sci.* 2, **1996**, 281–283.
- 155 MARTINS J., SAINSBURY A. J., MAMO J. C., REDGRAVE T. G., Lipid and apolipoprotein B48 transport in mesenteric lymph and the effect of hyperphagia on the clearance of chylomicron-like emulsions in insulin-deficient rats. *Diabetologia* 37, **1994**, 238–246.
- 156 MURAMATSU K., MAITANI Y., NAGAI T., Dipalmitoylphos phatidylcholine liposomes with soybean-derived sterols and cholesterol as a carrier for the oral administration of insulin in rats, *Biol. Pharm. Bull.* 19, **1996**, 1055–1058.
- 157 (a) MICHEL C., APRAHAMIAN M., DEFONTAINE L., COUVREUR P., DAMGE C., The effect of site of administration in the gastrointestinal tract on the absorption of insulin from nano-capsules in diabetic rats. *J. Pharm. Pharmacol.* 43, **1991**, 1–5. (b) HUSSAIN N., JAITLEY V., FLORENCE A. T., Recent advances in the understanding of uptake of microparticulates across the gastrointestinal lymphatics, *Adv. Drug Deliv. Rev.* 50, **2001**, 107–142.
- 158 MULLER R. H., BECKER R., KRUSS B., PETERS K., Pharmaceutical nano-suspensions for medicament administration as system of increased saturation solubility and rate of solution, *US patent* 5,858,410, **1998**.
- 159 KAYSER O., WATER R. W., UPTON S. J., JACOBS C., KEITHLY J. S., Anticryptosporidial activity of bupravaquone and development of a mucoadhesive drug delivery system for improving its *in vivo* efficacy. *J. Drug Target.* **2000**, submitted.
- 160 MULLER R. H., JACOBS C., KAYSER O., Nanosuspensions as particulate drug formulations in therapy: rationale for development and what we can expect for the future. *Adv. Drug Deliv. Rev.* 47, **2001**, 3–19.
- 161 PONCHEL G., MONTISCI M. J., DEMBERI A., DURRER C., DUCHENE D., Mucoadhesion of colloidal particulate systems in the gastrointestinal tract, *Eur. J. Pharm. Biopharm.* 44, **1997**, 25–31.
- 162 CASTOR T. P., Protein Nanoparticles, *NSTI Nanotechnology Conference of Trade Show*, **2005**.

Index

a

- acetylation, effect on chitosan transfection
 - efficiency 79–80
- acroinfundibulum 354
- active compound penetration, skin 365
- active drug targeting 163–164
- active pharmaceutical ingredients (API) 255
 - carriers 258
- active targeting 289
- adhesive capacity, gliadin nanoparticles 133
- adhesive interactions, gliadin nanoparticles 130
- adsorption, association of ligands with nanoparticles 127
- adsorption equilibrium 130
- AFM *see* atomic force microscopy
- agarose gel electrophoresis
 - (C₁₄CO)₂–plasmid complexes 35
 - DNA anchor 44–45
- aggregation
 - lipoplexes 57
 - modified chitosans 80
- aggregation concentration, critical 35–36
- albumin
 - clinical indication 185
 - nanoparticle preparation 154
 - principal function 187
- albumin microspheres 151
 - hormone-containing 175
- albumin nanoparticles 185–218
 - biodistribution 196–198
 - carrier system 173
 - chemical stabilization 195
 - conventional 187–193
 - diagnostic purposes 198–200
 - distribution 199–201
 - drug encapsulation 194–196
 - emulsification 192–193
 - immunochemical detection 207
 - magnetic 204
 - ocular drug delivery 205–207
 - preparation 187, 189–193
 - protective effect 201
 - Scanning electron microscope image 188
 - surface-modified 193–196
 - three-step procedure 190
 - toxicity 206
- Albunex 173
 - immune response 176
- alkyl cyanoacrylate) nanocapsules 381–382
- all-*trans* retinoic acid (RA) 124–125
- amino acid microspheres 382
- amino groups
 - interaction of chitosan amino group with DNA 75
 - N-chitosan 72
 - trimethylation (quaternization) 80
- γ-aminobutyric acid (GABA) 358
- amphiphilic drug encapsulation 126–127
- antibody, variable domain of the light chain 235
- antibody response, nanoparticle preparation 170
- anticancer agent, mercaptopurine 149
- antiepileptic drug delivery 366–367
- antimucous polyclonal antibodies 166
- antineoplastic agents 369
- antisense oligonucleotides 199–201
- API *see* active pharmaceutical ingredients
- apoE *see* apolipoprotein E
- apolipoprotein E, enrichment 291
- array structure, DNA nanotubes 10
- artificial lipid vesicles, liposomes 239
- ASGP-R *see* asialoglycoprotein receptor
- asialoglycoprotein receptor (ASGP-R) 81–82
- atomic force microscopy (AFM)
 - chitosan–DNA complexes 75
 - DNA nanotubes 7, 12–14

- atovaquone 383
 azidothymidine (AZT) 157
 AZT *see* azidothymidine
- b**
- B16-F10 cells
 – fluorescence microscopic images 333
 – viability 334
 BALB/c mice 96
 ball milling 265
 BBB, crossing 357
 BBD *see* *Bordetella bronchiseptica* dermonecrotin
 benzalkonium chloride (BZC), amphiphilic model 126–127
 betamethasone disodium phosphate (BTM), included in chitosan microspheres 89
 bifunctional crosslinkers 168
 – structure 169
 bilayer undulations, lamellar lipoplexes 55–56
 bioadhesion 129
 bioadhesive properties, gliadin nanoparticles 129–135
 bioavailability, drug particle size dependence 256
 biocompatibility, chitosan 71
 biocompatible nanoparticulate systems for tumor diagnosis 304–348
 biodegradable, plant protein-based nanoparticles 117
 biodegradable nanoparticles 312–314
 biodegradable polymer, delivery to BBB 373–374
 biodegradation, chitosan 71
 biodistribution
 – albumin nanoparticles 196
 – in vivo 26–27
 biofunctionalized solid lipid nanoparticles, production 287–303
 biological membranes
 – asymmetry 353
 – crossing by nanoparticles 349–393
 – drugs crossing problems 354–362
 – functions 351–352
 – kinetics 352–354
 – lipid bilayer structure 260
 – thermodynamics 352–354
 – *see also* cell membrane
 biomembranes *see* biological membranes
 bionanomachines 19
 1,6-bis-maleinimidohexane (BMH) 168
 blood circulation time, ICG 325
 blood opsonization process, reduction 287
 blood–brain barrier
 – crossing of albumin nanoparticles 197
 – diffusion of nanoparticles 305
 bloodstream, surviving of chitosan–DNA nanoparticles 80
 BMH *see* 1,6-bis-maleinimidohexane
 body distribution
 – drug carrier systems 163
 – peroral administration 175
Bordetella bronchiseptica dermonecrotin (BBD) 87
 bovine serum albumin *see* BSA
 breast cancer 370
 bromocriptine mesylate, drug-loaded gelatin microspheres 152
 BSA (bovine serum albumin) 187
 – incorporated in hydrophobic PLGA microspheres 148
 – nanoencapsulation 153
 – release from chitosan nanoparticles 95
 BTM *see* betamethasone disodium phosphate
 buckyballs 307–309
 buckytubes 307–309
 building blocks, nanoscale particulate systems 305–312
 burst effect, in chitosan microsphere DNA release 95
 2,3-butadione, albumin nanoparticles chemical stabilization 189
 BZC *see* benzalkonium chloride
- c**
- C₁₀CysG+ 29–30
 – structure 31, 34
 C₁₄CO, structure 34
 C₁₄CSper, structure 34
 (C₁₄CO)₂–plasmid complexes, mobility 35
 cancer treatment, albumin nanoparticles 201–204
 capillary endothelial cells, lipoplex uptake 60
 carbazole, hydrophobic fluorescent molecule 130–132, 134
 carbodiimide (CDI)
 – crosslinked with gliadin nanoparticles 133
 – preparation of ligand–gliadin nanoparticle conjugates 128
 carbohydrate-binding, S-layer 223–224
 carbon nanotubes 308
 carcinogenic radicals 288
 carriers
 – albumin nanoparticles 199
 – DNA 69–79
 cationic lipidmediated nucleic acid delivery *see* lipofection

- cationic lipids 51–53
- cationic liposomes, interactions with DNA 56
- cationic surfactants, structure 34
- caveolae-mediated endocytosis 58
- CDI *see* carbodiimide
- cell internalization elements, DNA nanoparticles 43–46
- cell-mediated response, legumin nanoparticles 137
- cell membrane 350–354
 - fusion with lipoplexes 57
 - *see also* biological membranes
- cell membrane crossing, DNA-nanoparticles 77
- cell recognition, DNA nanoparticles 43–47
- cell surface receptors, mediation of gene carrier targeting 81–83
- cellular trafficking studies 38
- CFTR *see* cystic fibrosis transport regulator
- cGMP *see* pharmaceutical current good manufacturing practice
- charge density, effect on chitosan transfection efficiency 79–80
- chemical crosslinking, chitosan nanoparticle preparation 86
- chimeric proteins 43
- chitin 68
 - structure 69
- chitosan 258
 - *N*-dodecylated chitosan (CS-12) 83–84
 - biocompatibility 71
 - carrier for gene therapy 69–79
 - chemistry 69–71
 - deoxycholic acid-modified chitosan (DAMC) 84
 - DNA–chitosan nanoparticles 68–99
 - galactosylated chitosan (GC) 81–82
 - GCPVP 81
 - genipin-crosslinked microspheres 88
 - heparin–chitosan complex 90
 - hydrophobic modification 83–84
 - pK_a 70
 - proposed applications 74
 - schematic gene therapy mechanism 79
 - structure 69
 - *see also* modified chitosan, unmodified chitosan
- chitosan nanoparticles
 - chemical crosslinking 86
 - complex coacervation 84–86
 - DNA loading 91–93
 - DNA release and release kinetics 93–95
 - emulsion crosslinking 87–88
 - emulsion droplet coalescence 90
 - ionic crosslinking/gelation 86–87
 - preparation methods 84–91
 - release of bovine serum albumin 95
 - reverse micellar method 89
 - sieving method 91
 - spray drying 88–89
- chitosan–DNA complex
 - atomic force microscopy (AFM) 75
 - incorporation by inhaled powder 98
 - potential clinical applications 97–98
 - preclinical evidence of efficacy 95–97
 - therapy of respiratory syncytial virus infection 97
- chitosan–DNA interactions 71
- cholester, structure 53
- circular dichroism (CD) measurements, S-layers 221
- circumventricular organs (CVO) 358
- clathrin-mediated endocytosis 58
- clinical studies, protein-based particles 172
- clinical uses, ICG 320–321
- coacervation, albumin nanoparticles 187, 189–192
 - nanoparticle preparation 120, 154–159
- coacervation techniques
 - complex 154–155
 - simple 155–159
- cochleate cylinders 265
- cochleates, lipid 263
- colloidal carriers 117
- colloidal drug carriers 287
- comminution
 - pharmaceutical nanoparticle processing 265–266
 - wet 266–267
- compaction, of DNA by highly charged chitosan 76
- complex coacervation, chitosan nanoparticle preparation 84–86
- condensation, DNA polymer 27–28
- condensed lamellar phase, lipoplexes 52–54
- conductivity, self-assembled 1-D nanotubes 18
- confocal microscopy, nanoparticle internalization 46
- connexin proteins, gap junctions 351
- connexon hexamers, gap junctions 351
- contrast enhancement, gas-filled microspheres 173
- convergent growth method, dendrimer synthesis 306
- copolymer grafted HSA 165
- core dendrimer 307
- core/shell nanoparticles 278

- cosmetic compounds, controlled release 365–366
- covalent linkage, association of ligands with nanoparticles 127
- coxsackievirus B3 (CVB3) 97–98
- CP *see* critical point
- Cremophor 202
- Cremophor EL 173, 368
- Crick, F. H. C. 23
- critical aggregation concentration 35–36
- critical point (CP) 270
- Crohn's disease 361
- crosslinkage, protein nanoparticles 122
- crosslinking, HSA (Human serum albumin) 150
- crosslinking agent, tripolyphosphate 258
- crustaceans 69
- crystalline bacterial cell surface layer *see* S-layer
- crystalline phases, liquid 260–261
- CS-12 (*N*-dodecylated chitosan) 83–84
- CTAB 36
- structure 34
- cubosomes 262–263
- curvature elastic energy, lipids 259–260
- CVB3 *see* coxsackievirus B3
- CVO *see* circumventricular organs
- Cybesin 325
- cyclosporin 382
- cystic fibrosis transport regulator (CFTR) 171
- Cytate 325
- cytokine, secretion in presence of nanoparticles 73
- cytotoxicity
- chitosan–DNA nanoparticles 99
- decrease 156
- galactosylated chitosan (GC) 82
- ICG 323–324
- photosensitizer molecule 319
- d**
- DAE, DNA structure 4–10
- Dalargin 372
- DAMC *see* deoxycholic acid-modified chitosan
- DAO, DNA structure 4, 9–10
- daunorubicin, hydrophilic drug 150
- DBA *see Dolichus biflorus* lectin
- DBA–gliadin nanoparticle conjugates 131
- DC-Chol, structure 53
- DDC *see* dideoxycytidine
- deacetylation, in chitosan production 69
- DEET (*N,N*-diethyl-4methyl benzamide) 365
- dendrimers 305–307, 362
- synthesis 306
- deoxycholic acid-modified chitosan (DAMC) 84
- derivatives
- *N*-chitosan *see* *N*-chitosan derivatives
- *O*-chitosan *see* *O*-chitosan derivatives
- PEG *see* PEG derivatives
- derivatized amino acid microspheres 382
- Dervan, Peter 39
- desolvation 155–159
- albumin nanoparticles 189–192
- gliadin nanoparticles 122
- protein nanoparticles 121
- detergent, C₁₀CysG+ 29–31, 36
- C₁₄CO 33, 36, 45
- cationic 27–29, 33
- lipid-based 44
- dextranox-MPEG *see* methyl polyethylene glycol (PEG)-modified oxidized dextran
- diagnostics
- albumin nanoparticles 198–200
- protein-based nanoparticles 169–175
- dideoxycytidine (ddC) 157
- diethylenetriaminopentaacetic acid (DTPA) 206
- differential adsorption 289–292
- differential scanning calorimetry 371
- direct microinjection
- lipoplexes 59
- ODN lipoplexes 62
- distamycin 38
- anchorage in minor groove 44
- disuccinimidyl tartrate (DST) 168
- disulfide bond, peptide conjugation 373–374
- DMRIE, structure 53
- DNA
- carriers 199
- chemical structure 24
- interactions with chitosan 71
- interactions with cationic liposomes 56
- interactions with fusion proteins 42–43
- DNA anchor 1, structure 44
- DNA based nanomaterials 1–99
- DNA binding intercalator 39
- DNA compaction, by highly charged chitosan 76
- DNA functionalization 37–43
- strategies 37–38
- DNA lipoplexes 51–60
- DNA loading, in chitosan micro- and nanoparticles 91–93
- DNA nanoparticles 43–47
- transfection efficiency 46
- DNA nanotubes, persistence length and stiffness 8

- DNA plasmid, size in comparison to virus and cell 27
 - DNA polymer, condensation 27–28
 - DNA recognition
 - by molecules 38
 - major groove 40
 - minor groove 43
 - DNA release, burst effect 95
 - DNA–chitosan nanoparticles 93–95
 - gene therapy 68–99
 - DNA–transferrin conjugate complexes 39
 - N*-dodecylated chitosan (CS-12) 83–84
 - Dolichus biflorus* lectin (DBA) 128
 - DOPC, structure 53
 - DOPE 28, 47
 - structure 53
 - DOSPA, structure 53
 - DOTAP, structure 53
 - DOTAP/DOPC/DNA lipoplex 56
 - DOTAP/ODN lipoplex, Cryo-TEM 61
 - DOTAP–DNA lipoplexes 80
 - Doxil 258
 - doxorubicin 368–369
 - drug carrier system 153
 - droplet size, electrical field 275–277
 - drug binding, in drug carrier systems 146
 - drug candidates, investigations. 255
 - drug carrier systems, drug binding in 146
 - drug carriers
 - colloidal 287
 - doxorubicin 153
 - protein-based nanoparticles 169–175
 - drug delivery 205–207
 - anticancer 367–370
 - antiepileptic 366–367
 - nanoparticulate 367
 - peptide 360
 - solid lipid nanoparticles 287–303
 - topical 205
 - drug delivery systems, lipid-based 258
 - drug encapsulation
 - albumin nanoparticles 194–196
 - characteristics in gliadin nanoparticles 127
 - in plant protein nanoparticles 124–127
 - drug nanoparticles
 - preparation 255–286
 - structures 257
 - drug particles, mean size 267
 - drug targeting
 - active 163–164
 - nanoparticles 161–169
 - passive 163
 - drug-targeting ligands, surface modification 166
 - drugloading efficiency, albumin nanoparticles 194
 - drugs crossing biological membranes, problems 354–362
 - DSC 371
 - DST *see* disuccinimidyl tartrate
 - DTPA *see* diethylenetriaminepentaacetic acid
 - DUV, deep ultraviolet light 241
 - DX tile nanotubes 4–10
 - dye, encapsulated 315
 - dysopsonins 290, 296
- e**
- ECF 358
 - echo-contrast agents, albumin nanoparticles 199
 - EDC *see* 1-ethyl-3-(3-dimethylaminopropyl) carbodiimide
 - EGF *see* epidermal growth factor
 - EGFP *see* enhanced green fluorescent protein
 - electrical field, droplet size 275
 - electroless chemical deposition 18
 - electron microscopy, heterotetramers 232
 - electronic nanodevices 18
 - electroporation, low-voltage 355–357
 - electrospraying 277
 - coaxial 279
 - stages 276, 278
 - electrostatic approaches, nanoformulation 275
 - electrostatic spinning 371
 - emission spectrum
 - rEGFP 240
 - rSbpA_{31a1068}/EGFP 240
 - emulsification, albumin nanoparticles 187, 192–193
 - emulsification-diffusion, SLN production 294
 - emulsion crosslinking, chitosan nanoparticle preparation 87–88
 - emulsion droplet coalescence, chitosan nanoparticle preparation 90
 - emulsion technique 151–154
 - flowchart 149
 - nanoparticle preparation 148–154
 - emulsions
 - drug carriers 258
 - oil-in-water-type 261
 - encapsulation efficiency, chitosan nanoparticle preparation 92–93
 - endocytosis
 - lipofection 57–58
 - ODN lipoplexes 62
 - receptor-mediated 38, 372

- endosomal escape, gene carriers 78
 endosomal membrane 59
 energy of bending, lipids 259
 enhanced green fluorescent protein (EGFP)
 239–240
 ependymal cells, cerebral ventricles 357
 epidermal growth factor (EGF) 369
 equilibrium structure, lipoplexes 52–55
Escherichia coli 77
 EtBr *see* ethidium bromide
 ethidium bromide (EtBr) 377
 1-ethyl-3-(3-dimethylaminopropyl)
 carbodiimide (EDC) 155
 extracellular barriers, lipofection 59
 extracellular fluid 358
 extracellular trafficking 79
- f**
- FAM-labeled strands, DNA nanotubes 7–8
 fibrous proteins, characteristics 118
 fluorescein labeled strands, DNA nanotubes
 7–8
 fluorescence
 – FAM 7–8
 – YOYO 36, 46
 fluorescence excitation
 – rEGFP 240
 – rSbpA_{31a1068}/EGFP 240
 fluorescence imaging, NIR 317–318
 fluorescence microscopy, DNA nanotubes
 7–8
 fluorescent molecules, carbazole 130–132
 fluorescently labeled albumin nanoparticles
 197
 5-Fluorouracil 369
 Fluorouracil delivery 201–202
 folate receptor (FR) 83, 97
 folate–peg-coated nanoparticles, biomedical
 applications 46
 folic acid receptor 83
 formaldehyde, albumin nanoparticles chemical
 stabilization 189
 FR *see* folate receptor
 freeze drying, nanoparticles 269
 5-FU *see* 5-Fluorouracil
 5-FU-loaded albumin 201
 fullerenes 362
 functional domains, Binding of Molecules and
 Nanoparticles 242–243
 functionalization, DNA 37–43
 fusion, lipoplexes with cell membrane 57
 fusion proteins, interactions with DNA 42–
 43
 fusogenic peptides 47
- g**
- G *see* generation
 γ -aminobutyric acid (GABA) 358
 GABA *see* g-aminobutyric acid
 β -galactosidase assay 77
 galactosylated chitosan (GC) 81–82
 β -Gal gene, vivo release 96
 ganciclovir (GCV) 156, 195
 – cancer treatment 203
 gap junctions 351
 gastrointestinal mucosal segments
 – *ex vivo* studies of drug carriers 130–131
 – *in vivo* studies of drug carriers 132–135
 gastrointestinal transit profile, gliadin
 nanoparticles 132
 GC *see* galactosylated chitosan
 GCPVP 81
 GCV *see* ganciclovir
 gel electrophoresis, agarose 35, 44–45
 gel-shift assay, SDS 230
 gelatin A, amino acid composition 152
 gelatin-based microspheres
 – drug-loaded 152
 – emulsion technique 151–153
 gelatin–DNA nanospheres 171
 gene carrier targeting, mediation by cell
 surface receptors 81–83
 gene carriers, endosomal escape 78
 gene delivery 369–370
 – BBB 374–375
 gene delivery system, inhaled powder 98
 gene expression 26
 – blocked by ODN 60
 gene therapy
 – DNA–chitosan nanoparticles 68–99
 – potential clinical applications of chitosan–
 DNA complex 97–98
 – protein-based nanoparticles 170–172
 – use of surfactants 36
 – viral vectors 51
in vivo gene transfer 88
 gene-vector complexation 79
 generation (G), dendrimers 306
 genipin-crosslinked chitosan microspheres
 88
 GFP *see* green fluorescent protein
 GI Barrier 360–362
 Gibbs equation, including nanoparticles 256
 Gibbs free energy, drug particles 256
 GlcNAc, N-acetyl glucosamine 227
 gliadin, wheat proteins 120
 gliadin nanoparticles
 – *ex vivo* studies of bioadhesive properties
 130–131

- gliadin nanoparticles (*cont.*)
 - *in vivo* studies of bioadhesive properties 132–135
 - adhesive interactions 130
 - bioadhesive properties 129–135
 - gastrointestinal transit profile 132
 - ligand–gliadin nanoparticle conjugates 127–129
 - particle size optimization 135–136
 - preparation 122–124
 - RA encapsulation 124–125
 - scanning electron micrograph 123
 - VE encapsulation 125–126
 - globular assembly, plasmid 30
 - globular proteins, characteristics 118
 - globulins
 - characteristics 118
 - pea seed proteins 119
 - glutaraldehyde, albumin nanoparticles
 - chemical stabilization 189
 - glutaraldehyde, crosslinking 155
 - glutelins, characteristics 118
 - gluten, wheat proteins 120
 - glutenin, wheat proteins 120
 - glycolic acid, nanoparticle preparation 313
 - glycoprotein, S-layer 219
 - gold chips 233
 - GRAS, safe substances 364
 - green fluorescent protein 42
 - guanidine hydrochloride 220
- h**
- H_{II}C-phase, lipoplexes 52–54
 - HCMV *see* Human CMV
 - head groups, lipids 259
 - heat-induced plasmid denaturation 42
 - heavy water, cytotoxicity of ICG 324
 - HEK 293 cells 78–83, 96, 170–172
 - HeLa cells 78–83, 96, 171, 240
 - Hélène, Claude 39
 - helper lipids 52–53
 - hemispherical endcaps nanotubes 308
 - heparin, nanoparticle preparation 154
 - heparin–chitosan complex, emulsion droplet coalescence 90
 - HepG2 cells 82, 88
 - herpes virus thymidine kinase (HSV-tk), cancer treatment 203
 - heterotetramers
 - functional 229
 - fusion protein 230
 - rSbpA 232, 234
 - SbsB 231
 - hexosomes 262–263
 - high-molecular-weight (HMW) chitosan 76, 92, 95
 - high-pressure homogenization (HPH), SLN production 292–294
 - Hildebrand theory, solubility parameter of gliadin 123
 - HIV-infection, potential therapy 157
 - HMW chitosan *see* high-molecular-weight chitosan
 - Hoechst 33258 38
 - anchorage in minor groove 44
 - homotetramers, streptavidin 229
 - “honeycomb” phase, lipoplexes 52–54
 - Hoogsteen base pairs 40
 - HPH *see* high-pressure homogenization
 - HSA 187
 - acid solution 155
 - copolymer grafted 165
 - ICG binding 321
 - microsphere and nanoparticle material 148
 - quantitative amino acid composition 150
 - HSA nanoparticles, morphology 161–162
 - HSA system, ammonium sulfate coacervated 156
 - HSA–PAA–PEG 194
 - HSA–PTAAC–PEG 194
 - HSV-tk *see* herpes virus thymidine kinase
 - human CMV, pathology 206
 - human rIL-2, included in chitosan microspheres 94
 - human serum albumin *see* HSA
 - humoral responses, legumin nanoparticles 136
 - hydrated lipids, liquid crystalline phases 260–261
 - hydrocarbon chains, lipids 259
 - hydrocortisone 195
 - included in chitosan microspheres 89
 - hydrophilic compounds, surface modification 164–165
 - hydrophilic drug encapsulation 126–127
 - hydrophilic pathway, skin barrier 363
 - hydrophobic, carbazole 130–132
 - hydrophobic modification, chitosan 83–84
 - hydrophobic PLGA microspheres 148
 - hydroxypropylcellulose, thickening agent 192
- i**
- ICG 304, 320
 - binding properties 321–322
 - biodistribution 335
 - blood circulation time 325
 - chemical stability in aqueous solution 330–331

- degradation 332
 - encapsulated in nanoparticles 316
 - excretion 322
 - metabolism 322
 - nanoparticle pharmacokinetics 331–336
 - nanoparticulate delivery system 327–336
 - pharmacokinetics 322
 - physicochemical properties 321
 - release profile 330
 - solution pharmacokinetics 331–336
 - stabilization *in vitro* 326
 - structure 321
 - subcellular localization 334
 - tumor imaging 322–323
 - uptake 333
 - uptake by tumors 325
 - ICG-loaded nanoparticles, photodynamic activity 335
 - ICG-loaded PLGA nanoparticles
 - manufacturing 314
 - surface views 329
 - IgC antibodies, *Camelidae* 235
 - IL-2, expression plasmid 86, 93–95
 - included in chitosan microspheres 94
 - immunization in animals, legumin nanoparticles 136–137
 - immunological reactions, protein-based microspheres 175–177
 - immunotherapy, type I allergy 239
 - in situ* synthesis, nanoparticles 244–244
 - in vivo* biodistribution 26–27
 - indocyanine green 304
 - *see also* ICG
 - inhaled powder, gene delivery system 98
 - intercalating dye, YOYO 36, 46
 - intercalation 38–39
 - intercalator, DNA binding 39
 - interfaces, lipids 260–261
 - interfacial energy, nanoparticles 257
 - interfacial tension 275
 - interferon- γ 195
 - interlayer DNA correlations, lamellar lipoplexes 55–56
 - interleukin *see also* cytokine, IL2, 239, 373
 - secretion in presence of nanoparticles 73
 - internalization
 - chitosan–DNA complexes 83–84
 - DNA nanoparticles 43–47
 - intestinal disease 361–362
 - intestinal translocation 361–362
 - intracellular trafficking 79
 - intracytoplasmic trafficking 26–27
 - intravitreal drug delivery 205–207
 - inverse hexagonal phase, lipoplexes 52–54
 - ion channel proteins 350
 - ionic crosslinking, chitosan nanoparticle preparation 86–87
 - ionic gelation, chitosan nanoparticle preparation 86–87
 - iontophoresis 356
 - Irwin's equation 267
- k**
- Katchalsky's equation 70
 - ketoprofen 87
 - kinetic approaches, nanoparticle preparation 257
 - KNOB protein 83, 96
- l**
- L-DOPA 359
 - (L α C)-phase, lipoplexes 52–54
 - lamellar lipoplexes, formation 55
 - Langmuir adsorption, oligonucleotides 234
 - lateral stress profile, lipid monolayer 259
 - lectin-conjugated nanoparticles, oral delivery 379–380
 - legumin, pea seed proteins 119
 - legumin nanoparticles
 - cell-mediated response 137
 - humoral responses 136
 - immunization in animals 136–137
 - preparation 121–122
 - leguminosae, source of plant proteins 119
 - ligand–gliadin nanoparticle conjugates, preparation 127–129
 - light chain antibody, variable domain 235
 - linalool–linalyl acetate (LLA) 124
 - hydrophilic model 126–127
 - lipid-based pharmaceutical nanoparticles 258–259
 - lipid emulsion, oil-in-water-type 261
 - lipid nanoparticles, site-specific drug delivery 287–303
 - lipid tubules 264
 - lipids
 - cationic 51–52
 - definition 259–260
 - hydrated 260–261
 - lipofection 51
 - direct microinjection 59
 - efficiency 57–60
 - endocytosis 57–58
 - extracellular barriers 59
 - most likely mechanism 58
 - tumor tissue 60
 - *in vitro* lipofection 57–59
 - *in vivo* lipofection 59–60

- lipophilic drug encapsulation 126–127
 - lipoplexes 51–62
 - composition 51–52
 - DOTAP–DNA 80
 - equilibrium structure 52–55
 - formation 54–55
 - fusion with cell membrane 57
 - nonequilibrium structure 55–57
 - polymorphous 56
 - size 57
 - liposomes 52, 239, 261–262, 310–312
 - conventional 262
 - drug carriers 258
 - stealth 262
 - liquid crystalline phases 260–261
 - lamellar 260
 - liquid nanodispersions, drying 267–270
 - liquid solution droplet, supercritical fluids 273
 - liver cancer, magnetic treatment 204
 - living cell imaging 376–378
 - LLA *see* linalool–linalyl acetate
 - LMW chitosan *see* low-molecular weight chitosan
 - localized SPRs, living cell imaging 376
 - low-density lipoproteins receptors 372
 - low-molecular weight (LMW) chitosan 77, 82, 92
 - low-voltage electroporation, skin 355–357
 - luciferase 170
 - lymphatic oral nanoparticulate delivery 382–384
- m**
- m-maleimidobenzoyl-N-hydroxysulfosuccinimide ester 168
 - magnetic albumin nanoparticles 204
 - major groove, DNA recognition 40
 - ManNAc, N-acetyl mannosamine 227
 - MDR *see* multi drug resistance
 - MDS *see* microsphere-based detoxification system
 - mechanical approaches 264–270
 - mechanical irritation, skin 355
 - membranes *see* biological membranes
 - mercaptapurine, anticancer agent 149
 - messenger RNA 60
 - metabolizable plant protein-based nanoparticles 117
 - metallization
 - 4 × 4 nanoribbons 18
 - TX tile nanotubes 11
 - metastable morphology, lipoplexes 55
 - metastatic breast cancer, albumin nanoparticles 202
 - Methanothermus fervidus*
 - Methotrexate delivery 201–202
 - methyl polyethylene glycol (PEG)-modified oxidized Dextran 165
 - albumin nanoparticles chemical stabilization 189
 - MexAB–OprM 377
 - MG63 cells 96
 - mica, interaction with nanotubes 7–8
 - micelle–DNA complexes, stabilized 37
 - microbeads 238
 - microcylinder, lipid 263
 - microemulsion technique, SLN production 293
 - microscopic techniques, nanoparticle size 160
 - microspheres
 - casein-based 153–154
 - gelatin-based 151–153
 - stability 153
 - uniform 151
 - microsphere-based detoxification system 237–238
 - microstructure, lipoplexes 52–55
 - microtubules, lipid 263
 - milling 265
 - minor groove
 - agents binding to 43
 - anchorage 44
 - MLV *see* multilamellar vesicles
 - MMP-9, secretion in presence of nanoparticles 73
 - modified chitosan 71
 - targeting mediated by cell surface receptors 81–83
 - transfection efficiency 79–74
 - monomolecular DNA condensation 45
 - mononuclear phagocytic system (MPS) 81
 - MPS *see* mononuclear phagocytic system
 - mucoadhesion, nanoparticles 384–385
 - multi drug resistance (MDR) proteins 360
 - reversion 367
 - multicomponent delivery vectors 47
 - multilamellar vesicles (MLV) 261
 - multiple sclerosis, pathogenesis 197
 - multiwall cylinder nanotubes (MWNT) 308
 - MWNT *see* multiwall cylinder nanotubes
- n**
- N-chitosan derivatives
 - proposed applications 74
 - structure 72
 - nanodispersions, drying 267–270
 - nanoelectronic devices 18

- nanofibers 370–371
 - nanoformulation, drug candidates 255
 - nanomaterials
 - DNA based 1–99
 - plant protein-based 117–137
 - protein-/peptide-based 115–245
 - nanoparticle crosslinkage, physico-chemical 122
 - nanoparticle optics 376–378
 - nanoparticle preparation 313–314
 - coacervation 154–159
 - mechanical energy input 264–265
 - methods 148–159
 - simple coacervation (desolvation) techniques 155–159
 - starting materials 146
 - thermodynamic approaches 257–264
 - nanoparticles
 - biodegradable 312–314
 - casein-based 153–154
 - coacervation techniques 154–155
 - crossing biological membranes 349–393
 - desolvation yield 191
 - DNA–chitosan 68–99
 - drug targeting 161–169
 - drying 268
 - gelatin-based 151–153
 - nucleic acid 23–50
 - peptide 159–161
 - peptide-based 145–176
 - pharmaceutical 258–259
 - protein-based 164
 - nanoparticulate drug delivery 362
 - anticancer 367–370
 - BBB 371–378
 - mechanisms 375
 - PLGA-based 327–336
 - skin 366
 - subcutaneous 366–367
 - nanoparticulate systems, tumor diagnosis 304
 - nanoporous barrier, semipermeable 363
 - 4 × 4 nanoribbons 18–19
 - metallization 18
 - nanoscale particulate systems, components 305–312
 - nanosensors 370
 - nanoshells 362
 - nanostructure, lipoplexes 52–55
 - nanosuspension delivery, oral 383–384
 - nanotubes (NT) 308, 362
 - self-assembled 3–22
 - nanowires 18
 - naphthalocyanine dyes, fluorescence imaging 318
 - natural self-assembly system, nanoscale patterning of S-layer proteins 219–252
 - NHS-PEG3400-Ma, PEG-based crosslinker 167
 - NIR dyes 318
 - NIR fluorescence imaging 317–318
 - NLS peptide 27
 - fusion with TetR protein 43
 - NLS peptide conjugation, triple helix formation 41
 - nonbiodegradable polymer 370–371
 - nonequilibrium structure, lipoplexes 55–57
 - NPC *see* nuclear pore complexes
 - NT *see* nanotubes
 - nuclear localization signal peptide *see* NLS peptide
 - nuclear pore complexes (NPC) 26
 - nucleic acid drugs, oral route 361
 - nucleic acid nanoparticles 23–50
 - synthesis 27–31
 - nucleus, gene expression 26
- o**
- O-chitosan derivatives
 - proposed applications 74
 - structure 73
 - ocular drug delivery, albumin nanoparticles 205–207
 - ODN
 - antisense 60–61
 - monolayers 61
 - triple helix formation 39–41
 - ODN lipoplexes 60–62
 - ODN–lipid lamellar phase 61
 - oligodeoxyribonucleotides *see* ODN
 - oligomeric chitosans 75
 - oligonucleotides
 - carriers 199
 - PNAs 41
 - optical imaging 317–326
 - fluorescence-based 317
 - optical nanoparticles, biodegradable 314–316
 - oral delivery, lectin-conjugated nanoparticles 379–380
 - oral nanoparticulate delivery 378–385
 - oral nanosuspension delivery 383
 - oral route, nucleic acid drugs 361
 - oral vaccination, protein microspheres 175
 - oxidation, C₁₀CysG+ 31
- p**
- pK_a, chitosan 70
 - PACA *see* poly(alkyl cyanoacrylate)

- paclitaxel 368
- albumin nanoparticles 202–203
- carrier system 173
- PAMAM *see* poly(amidoamine) dendrimers
- parenteral application route 172–174
- parenteral lipid emulsion 258
- particle size
 - reduction 266
 - surface energy 256
 - wet comminution 266
- particle size distribution, gliadin nanoparticles 123
- particle size optimization, gliadin nanoparticles 135–136
- particle systems
 - active drug targeting 163–164
 - passive drug targeting 163
- particulate systems, nanoscale 305–312
- PASP *see* sodium polyaspartate
- passive drug targeting 163
- passive targeting 289
- patch–clamp recording technique, cell transport 351
- patterning, S-layer proteins 219–252
- PBCA 290–291
- PBCA nanoparticles, brain specificity 297
- PC *see* phosphatidylcholine
- PCF *see* polycationic ferritin
- PCS *see* photon correlation spectroscopy
- pDNA:PLL complexes, included in chitosan microspheres 93
- PDT 317–326
 - ICG 323
 - photosensitizers 320
- PE *see* phosphatidylethanolamine
- pea seed proteins 119
- PEG 28, 82–83, 262
 - lipoplex coating 60
 - nanoparticle surface modification 287
 - protective coat 44–46, 60
- PEG derivatives, surface modification 165–166
- PEG–HSA conjugates 165
- PEG–lipid conjugates, polymeric micelles 310
- pegylation, albumin nanoparticles 193
- PEI *see* polyethylenimine
- PEO *see* polyethylene oxide
- peptide-based nanomaterials 115–245
- peptide conjugation 373–374
- peptide delivery, BBB 372–373
- peptide drug delivery 360
- peptide nanoparticles
 - oral delivery 380–381
 - polymer-based 381
- peptide nanoparticles 145–176
 - characterization techniques 159–161
- peptide nucleic acids *see* PNAs
- peptides
 - fusogenic 47
 - nanoparticles 145–176
 - NLS 27, 43
- peroral administration, body distribution 175
- peroral application, protein-based particles 175
- persistence length, DNA nanotubes 8
- Peyer's patch, electron photomicrograph 383
- PGA *see* polyglycolic acid
- pharmaceutical applications, albumin nanoparticles 198–207
- pharmaceutical current good manufacturing practice (cGMP) 270
- pharmaceutical nanoparticles
 - comminution 265
 - lipid-based 258–259, 263
 - monodisperse 277
- pharmacokinetics
 - gliadin nanoparticles 132
 - ICG 322, 331–336
- phase behavior, lipids 259–261
- phase separation phenomena, nanoparticle preparation 258
- phosphatidylcholine (PC) 352
- phosphatidylethanolamine (PE) 352
- phosphatidylglycerol, liposomes 310
- phosphatidylserine (PS) 352
 - liposomes 310
- photoactive agent, ICG 320
- photodegradation, ICG 326
- photon correlation spectroscopy (PCS), particle size 159
- photoradiation therapy (PDT) 318
- photosensitizer molecules 314
- photosensitizers, PDT 320
- phthalocyanine dyes, fluorescence imaging 318
- physicochemical characteristics, gliadin nanoparticles 133
- PIBCA *see* poly(isobutyl cyanoacrylate)
- PicoGreen assay 92
- pilocarpine, ophthalmic administration 174
- pilocarpine-coated albumin nanoparticles, topical drug delivery 205
- pilocarpine nitrate 195
- pinocytosis 77, 95–96, 358
- plant protein-based nanoparticles 117–137
 - drug encapsulation 124–127
- plant proteins, characteristics 118–120

- plasma protein composition 298
 - plasmid DNA, incorporation 155
 - plasmids
 - globular assembly 30
 - heat-induced denaturation 42
 - size in comparison to virus and cell 27
 - plasmid–transferrin–PNA complex 42
 - PLGA, structure 147
 - PLGA microspheres, hydrophobic 148
 - PLGA nanoparticles, uptake 328
 - PNAs 41–42
 - plasmid–transferrin–PNA complex 42
 - size in comparison to natural DNA 42
 - poloxamer 338 296
 - poly(alkyl cyanoacrylates) 366
 - structure 147
 - poly(alkyl methacrylates), structure 147
 - poly(amidoamine) dendrimers 307
 - poly(D,L lactic-co-glycolic acid) 354
 - poly(D,L-lactide-co-glycolide) 312
 - poly(isobutyl cyanoacrylate) 366
 - poly(N-isopropylacrylamide), polymeric micelles 310
 - poly(propylene imine) dendrimers 307
 - poly(thioetheramido acid)–PEG copolymer-grafted HSA 194
 - poly(vinyl pyrrolidone) 81
 - polyacrylamide nanospheres 381
 - polycationic ferritin (PCF) 242–243
 - polyclonal antibodies 166
 - polyethylene glycol *see* PEG
 - polyethylene oxide (PEO) 297
 - polyethylenimine (PEI) 196
 - polyglycolic acid (PGA), structure 147
 - polylactic acid, nanoparticle preparation 313
 - polylactic-co-glycolic acid *see* PLGA
 - polymer-based nanoparticulate delivery, skin 366
 - polymer erosion, DNA release 93–94
 - polymer nanoparticles, albumin coating 196
 - polymeric micelles 310
 - polymeric stabilizers 267
 - polymers
 - nonbiodegradable 370–371
 - stabilization ability 257
 - polymorphous lipoplex 56
 - polysaccharide 68
 - polysorbate 60 296
 - polysorbate 80 372
 - polysorbate-coated poly(butyl cyanoacrylate) *see* PBCA
 - PPI *see* poly(propylene imine) dendrimers
 - precipitation technique, chitosan nanoparticle preparation 94
 - preclinical studies, protein-based particles 172
 - processability, drug particle size dependence 256
 - progesterone, drug delivery system 175
 - prolamins, characteristics 118
 - protective coat, DNA nanoparticles 43–46
 - protein, KNOB 83
 - protein-based microspheres, immunological reactions 175–177
 - protein-based nanomaterials 115–245
 - protein-based nanoparticles
 - preparation 120–124
 - surface modifications 164
 - protein-based particles
 - clinical studies 172
 - oral delivery 384–385
 - peroral application 175
 - preclinical studies 172
 - topical application 174–175
 - protein desolvation 158
 - proteins, chimeric 43
 - PS *see* phosphatidylserine
 - PS60-SLN 296
 - Pseudomonas aeruginosa* 377–378
 - psoralen–DNA–peptide conjugate 41
 - P–T diagram, pure substance 271
 - pure pharmaceutical components, atomization 273
 - purification, nanoparticles 154, 191
 - PVP (Poly(vinyl pyrrolidone)) 81
 - PX338-SLN 296
- q**
- quantum dots 309–310, 362
 - quaternization, chitosan amino groups 80
- r**
- RA (all-*trans* retinoic acid, vitamin A) 124–125
 - RA encapsulation, gliadin nanoparticles 124–125
 - rabbit serum albumin 149
 - radioactive tracers 198
 - radionuclide ⁶⁷Gd, attachment to nanoparticles 164
 - radiopharmaceuticals 198
 - rapid expansion of supercritical solution 272–273
 - re-dispersibility, dried nanoparticles 269
 - reactive groups, albumin microspheres 165
 - reactive oxygen species (ROS) 319
 - receptor
 - asialoglycoprotein 81–82
 - folic acid 83

- receptor-mediated endocytosis 38
- release kinetics, chitosan nanoparticles 93–95
- remote loading technology, drug trapping 262
- RES 262
- RES uptake, modified chitosans 80
- respiratory syncytial virus infection, gene therapy with chitosan–DNA complex 97
- RESS *see* rapid expansion of supercritical solution
- reticuloendothelial system *see* RES
- retinitis, HCMV 206
- reverse Hoogsteen base pairs 40
- reverse micellar method, chitosan nanoparticle preparation 89
- ribbon structure, DNA nanotubes 10
- ROS *see* reactive oxygen species
- s**
- S-layer fusion proteins 228–240
 - rSbpA_{31a1068} 239
 - rSbpA_{31a1068}/cAb-Lys3 235
 - rSbpA_{31a1068}/cAb-PSA-N7 236
- S-layer lattices, thickness 220
- S-layer proteins
 - archaea 219
 - bacteria 219
 - immobilization 225–226
 - nanoscale patterning 219–252
 - properties 220–225
 - SbsA 226–227
 - SbsB 227–228
 - SbsC 228–229
 - S-layer homology (SLH) motifs 222
 - S-layer reassembly, spatial control 241–241
 - S-layer streptadivin *see* streptadivin
 - S-layer variation 223
- S-layers
 - carbohydrate-binding 223–224
 - chemistry and molecular biology 221–223
 - formation of regularly arranged nanoparticles 242–244
 - glycoprotein 219
 - glycosylation 221
 - heterogeneous ligand model 223–224
 - isoelectric point 221
 - isolation 220–221
 - monomolecular protein lattices 219
 - nanoparticles on 244–244
 - recrystallization 220–221
 - recrystallization experiments 229
 - symmetry 220
 - S-liposomes, S-layer-coated liposomes 239
 - “sandwich” phase, lipoplexes 52–54
- SAS *see* supercritical antisolvent
- scanning electron micrograph
 - gliadin nanoparticles 123
 - vicilin nanoparticles 121
- scanning electron microscopy (SEM) 89, 371
- SCF
 - approaches 270–275
 - characteristics 270–271
 - particle formation 271–272
- SCWP
 - biomimetic linkers 224
 - formation from 3 SLH motifs 222
 - secondary cell wall polymer 222
 - thiolated SCWP 224
- secondary cell wall polymer *see* SCWP
- SEDS *see* solution-enhanced dispersion by SCFs
- self-assembled DNA nanotubes 3–22
- self-assembly, DAE-O tiles 9
- self-assembly method, dendrimer synthesis 306
- self-assembly system, nanoscale patterning of S-layer proteins 219–252
- semipermeable nanoporous barrier, skin 363
- serum albumin 187–196
 - three-domain model 187
- SFM
 - heterotetramers 230
 - surface topography of S-layers 220
- side-effects, doxorubicin 368
- sieving method, chitosan nanoparticle preparation 91
- silver nanoparticles, color index 379
- simple coacervation 155–159
- siRNA lipoplexes 62
- site-specific drug delivery, solid lipid nanoparticles 287–303
- skin 363
 - drugs crossing problems 354–357
 - low-voltage electroporation 355–357
 - mechanical irritation 355
- SLH, S-layer homology 222
- SLN *see* solid lipid nanoparticles
- SM *see* sphingomyelin
- small drugs, BBB crossing 359
- small unilamellar vesicles (SUV) 261
- smart nanoparticle probes 370
- sodium alginate–BSA nanoparticles 201
- sodium azide, cytotoxicity of ICG 323
- sodium polyaspartate (PASP), ICG stabilization 326
- sodium sulfate, use in ionic crosslinking 87
- sodium tripolyphosphate (PSTP), use in ionic crosslinking 87
- solid-lipid nanoparticles (SLN) 288, 354

- *in vitro* occlusion 365
 - *in vivo* elasticity 365
 - *in vivo* occlusion 365
 - *in vivo* wrinkles 365
 - biofunctionalized 287–303
 - chemical stability 364
 - production 292–294
 - skin delivery 364
 - UV sunscreen 366
 - solubility
 - chitosan 70
 - effect on chitosan transfection efficiency 79–80
 - solubility parameter of gliadin, Hildebrand theory 123
 - solution-enhanced dispersion by SCFs (SEDS) 274–275
 - nozzle system 274
 - sonochemical method, albumin nanoparticles 193
 - “spaghetti” tubule structures, lipoplexes 57
 - sphingomyelin (SM) 352
 - SPR-spectroscopy, SCWP
 - spray drying, chitosan nanoparticle preparation 88–89
 - stabilization
 - albumin coacervates 191
 - albumin nanoparticles 187
 - ICG 326
 - stabilization ability, polymers 257
 - stabilizers, polymeric 267
 - starburst divergent method, dendrimer synthesis 306
 - starting materials, nanoparticle preparation 146
 - stealth carriers 290
 - stealth liposomes 262
 - sticky ends 5
 - stiffness, DNA nanotubes 8
 - Stokes’ diameter, nanoparticles 159
 - stomach mucosa, bioadhesion of gliadin nanoparticles 132–135
 - storage proteins, characteristics 118
 - streptavidin 229
 - biotin-binding properties 233
 - suicide gene therapy, albumin nanoparticles 203–204
 - sulfo-MBS 168
 - sulfo-SMCC 168
 - sulfosuccinimidyl-4-N-maleimidomethylcyclohexane-1-carboxylate (sulfo-SMCC) 168
 - supercritical antisolvent 273–274
 - supercritical fluids *see* SCF
 - supercritical nanoparticles 270
 - surface energy, drug particles 256
 - surface modification
 - drug-targeting ligands 166
 - functionalization 294–298
 - hydrophilic compounds 164–165
 - polyethylene glycol 165–166
 - protein-based nanoparticles 164
 - strategies 168–169
 - surfactants 295
 - surface plasmon resonance spectroscopy *see* SPR-spectroscopy
 - surfactant–DNA complexes 34
 - biomedical applications 36
 - organization 35
 - stability 35–37
 - ultrastructure 35
 - surfactant–plasmid complexes, morphology 36
 - surfactants
 - cationic 34
 - CTAB 36
 - reverse micellar method 89
 - stabilization ability 257
 - surface modification 295
 - synthesis 31–35
 - SUV *see* small unilamellar vesicles
 - SWNT *see* hemispherical endcaps nanotubes
 - SynB vectors, peptide drug delivery 360
 - synthesis
 - nanoparticles 244–244
 - nucleic acid nanoparticles 27–31
 - surfactants 31–35
- t**
- TAO, DNA structure 4
 - TAPP-Br, drug-loaded gelatin microspheres 152
 - target specific carriers 289
 - TAT protein 373
 - Taxol 173
 - TEM *see* transmission electron microscopy
 - TetR protein, fusion with NLS peptide 43
 - Tf *see* transferrin
 - therapeutic DNA, chemical and physical properties 25–27
 - therapy, magnetically targeted 204
 - thermodegradation, ICG 326
 - thermodynamic approaches, nanoparticle preparation 257–264
 - thiamine-coated delivery, BBB 376
 - thickening agent, albumin emulsification 192
 - three-domain model, serum albumin 187
 - 4 × 4 tile nanotubes 14–15

- 6HB tile nanotubes 16–17
- TNBS *see* 2,4,6-trinitrobenzenesulfonic acid
- α -tocopherol (vitamin E, VE) 124–125
- lipophilic model 126–127
- toxicity, ICG 322
- TP *see* triple point
- trafficking, intracytoplasmic 26–27
- transbilayer lipid movement 353
- transfection efficiency
- chitosan 76
- DNA nanoparticles 46
- modified chitosans 79–84
- unmodified chitosan 71
- transfection reagents, commercially available 172
- transferrin (Tf) 38–39, 82, 96, 369
- plasmid–transferrin–PNA complex 42
- transmission electron microscopy (TEM)
- DNA nanotubes 10
- mass distribution of S-layers 220
- monomolecular DNA condensation 45
- trastuzumab 167
- 2,4,6-trinitrobenzenesulfonic acid, nanoparticle surfaces 168
- trimethylation, chitosan amino groups 80
- triple helix formation 41
- with oligodeoxyribonucleotides 39–41
- triple point (TP) 270
- tripolyphosphate, crosslinking agent 258
- tubules, lipid 264
- tumor diagnosis 304
- ICG 320
- ICG limitations 324–325
- optical nanoparticles 314–315
- tumor imaging, ICG 322–323
- tumor necrosis factor- α , secretion in presence of nanoparticles 73
- tumor tissue, lipofection 60
- tumor treatment
- ICG 320
- ICG limitations 324–325
- optical nanoparticles 315–316
- TX tile nanotubes 11–13
- metallization 11
- u**
- UA (urocanic acid), coupled with water-soluble chitosan 78
- ultrastructure, surfactant–DNA complexes 35
- unmodified chitosan, schematic gene therapy mechanism 79
- uptake by tumors, ICG 325
- urocanic acid (UA), coupled with water-soluble chitosan 78
- urokinase 195
- UV sunscreen, solid-lipid nanoparticles 366
- v**
- K_d values 224
- variable domain, light chain antibody 235
- VE (α -tocopherol, vitamin E) 124–125
- lipophilic model 126–127
- VE encapsulation, gliadin nanoparticles 125–126
- vectors
- multicomponent delivery 47
- viral 170
- vegetable albumins, characteristics 118
- VH 235
- VHH, antibody isotype 233
- vicilin, pea seed proteins 119
- vicilin nanoparticles
- preparation 121–122
- scanning electron micrograph 121
- viral vectors, gene therapy 51
- virus infection, respiratory syncytial 97
- vitamin A (all-*trans* retinoic acid, RA) 124–125
- vitamin E (α -tocopherol, VE) 124–125
- lipophilic model 126–127
- VL 235
- w**
- w/o *see* water-in-oil emulsion
- water-in-oil emulsion (w/o) 87
- water-soluble chitosan 78
- water soluble polymers 258
- Watson, J. D. 23
- weakly overlapping mushroom regime, DNA nanoparticle protection 45
- wet comminution 266–267
- wheat proteins 119–120
- wrapping vector 10
- y**
- yield, nanoparticles 191
- YOYO, intercalating dye 36, 46
- z**
- zona pellucida (ZP) 98
- ZP *see* zona pellucida